DISSERTATION RC 14-3505

BEHAVIOR OF REINFORCED CONCRETE COLUMNS RETROFITTED BY EXTERNAL STEEL ANGLE COLLARS UNDER AXIAL COMPRESSION AND COMBINED AXIAL COMPRESSION AND REVERSED CYCLIC LOADING

NAME : PAMUDA PUDJISURYADI
ID NO. : 311 030 1005

SUPERVISOR   : PROF. TAVIO, S.T. M.T. PH.D.
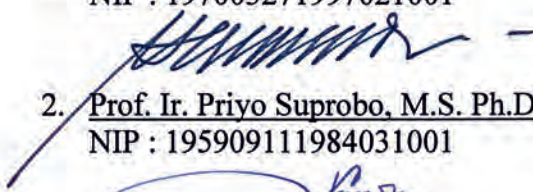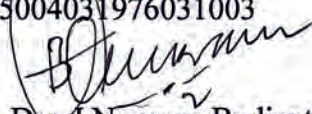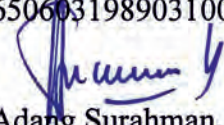CO-SUPERVISOR : PROF. IR. PRIYO SUPROBO, M.S. PH.D.

GRADUATE DIVISION
STRUCTURAL ENGINEERING PROGRAM
DEPARTMENT OF CIVIL ENGINEERING
FACULTY OF CIVIL ENGINEERING AND PLANNING
SEPULUH NOPEMBER INSTITUTE OF TECHNOLOGY
SURABAYA - INDONESIA
2017

Behavior of Reinforced Concrete Columns Retrofitted by External Steel Angle Collars under Axial Compression and Combined Axial Compression and Reversed Cyclic Loading

by

Pamuda Pudjisuryadi

311 030 1005

A dissertation submitted in partial satisfaction in the requirements for the doctoral degree in Civil Engineering
in the GRADUATE DIVISION
of the SEPULUH NOPEMBER INSTITUTE OF TECHNOLOGY

Examination Date : August 9th, 2016
Graduation Period : March 2017

1. Prof. Tavio, S.T. M.T. Ph.D.   (Supervisor)
   NIP : 197003271997021001

2. Prof. Ir. Priyo Suprobo, M.S. Ph.D.   (Co-Supervisor)
   NIP : 195909111984031001

3. Prof. Dr. Ir. I Gusti Putu Raka   (Internal Examiner)
   NIP : 195004031976031003

4. Prof. Dr. Drs. I Nyoman Budiantara, M.S.   (Internal Examiner)
   NIP : 196506031989031003

5. Prof. Ir. Adang Surahman, M.Sc. Ph.D.   (External Examiner)
   NIP : 195409071986021001

an. Direktur Program Pascasarjana   Director of Graduate Division
Asisten Direktur

Prof. Dr. Ir. Tri Widjaja, M.Eng.
NIP. 19611021 198603 1 001

Prof. Ir. Djauhar Manfaat, M.Sc. Ph.D.
NIP: 19601202 198701 1 001

ii

BEHAVIOR OF REINFORCED CONCRETE COLUMNS RETROFITTED BY EXTERNAL STEEL ANGLE COLLARS UNDER AXIAL COMPRESSION AND COMBINED AXIAL COMPRESSION AND REVERSED CYCLIC LOADING

Name   : Pamuda Pudjisuryadi
ID No.   : 3110 301 005
Supervisor   : Prof. Tavio, S.T. M.T. Ph.D.
Co-Supervisor : Prof. Ir. Priyo Suprobo, M.S. Ph.D

ABSTRACT

In reinforced concrete (RC) buildings, damages in columns should be avoided during the earthquakes since they have less ductile inelastic behavior which can lead to proggressive damages and collapse of the structure. Researchers have developed several retrofitting techniques to improve the performance or ductility of RC columns. Concrete jacketing, steel jacketing, external strand prestressing, Fiber Reinforced Polymer (FRP) jacketing, and steel collar jacketing to name a few are among the developed retrofit approaches. In this study, a new retrofitting technique utilizing steel collars as external confinement is proposed. The aim of the study is to develop an effective, yet economical, and practical method to retrofit square, and rectangular, or even elongated RC column sections. Steel angle or L-shapep sections were used as collar elements, which were mounted externally at spacing surrounding the perimeter of the column to enhance the column's strength, particularly its ductility. To achieve this objective, two phases of experimental program were carried out.

In the first phase of the experimental program, fourteen concrete column specimens were built and tested under monotonic axial compressive load in order to study the impact of the proposed external retrofitting method to the strength and most importantly to the ductility enhancement of the columns. To study this effect, volumetric ratio of confining elements was set as the main parameter. Some stiffening techniques of the collars were also investigated to further examine the potential of the proposed method. The results indicated that the strength, and strain ductility of the retrofitted specimens were enhanced. An analytical model to predict the actual stress-strain curve of the columns confined by external steel angle collars was developed and verified against the experimental stress-strain data. The predictions were in good agreement with the experimental results. The peak stress, strain at peak stress and strains at 50 and 80 percent of the peak stress can be predictied reasonably well.

A proposed calculation procedure for retrofit work is also introduced. It provides the need of additional external steel collars in order to meet the target of the column's strength. The idea is to combine the confining stresses provided by internal confinement and external steel collars by taking the average proportionally to the influenced area. Comparisons with experimental data

indicated that the proposed approach can predict with reasonable margins on the conservative side.

In the second phase, five concrete column specimens were cast, and tested under combined axial compression, and quasi-static reversed cyclic lateral load. These tests were intended to investigate the performance of the retrofitted specimens under simulated earthquake load. The enhancement of strength, and ductility which lead to larger energy dissipation capacity are clearly identified. The acceptance criteria set by ACI 374.1-05 is also satisfied. Additionally, a proposed design procedure is also developed based on the limited data obtained from the second phase of the experimental program. The step-by-step design procedure accommodates the need of additional external steel angle collars to retrofit the existing column to improve its ductility. In conclusion, the proposed retrofitting method can be applied as an alternative solution on rehabilitation of seismically deficient square RC columns.

Keywords : earthquake, external confinement, retrofit, steel collar, square RC column, stress-strain relationship.

PERILAKU KOLOM BETON BERTULANG YANG DIRETROTIT SECARA EKSTERNAL DENGAN SABUK BAJA SIKU YANG DIBEBANI AKSIAL TEKAN DAN KOMBINASI BEBAN AKSIAL TEKAN DAN BEBAN LATERAL SIKLIK

Nama : Pamuda Pudjisuryadi
NRP : 3110 301 005
Pembimbing : Prof. Tavio, S.T. M.T. Ph.D.
Ko-Pembimbing: Prof. Ir. Priyo Suprobo, M.S. Ph.D.

ABSTRAK

Pada bangunan beton bertulang (BB), kerusakan kolom sebaiknya dihindari saat gempa karena perilaku in-elastis yang kurang daktail pada kolom dapat menyebabkan kerusakan progresif, dan keruntuhan struktur. Para peneliti telah mengembangkan banyak teknik retrofit untuk memperbaiki kinerja atau daktilitas kolom BB. Pembesaran penampang beton, penambahan baja lembaran / cincin, stran eksternal prategang, Fiber Reinforced Polymer (FRP), dan sabuk baja merupakan beberapa metode retrofit yang dikembangkan. Pada penelitian ini, diusulkan sebuah teknik baru menggunakan sabuk baja sebagai pengekang eksternal. Tujuan dari penelitian ini adalah untuk mengembangkan metode retrofit untuk kolom BB bujursangkar, atau bahkan persegi panjang yang efektif, tapi ekonomis, dan praktis / mudah dilaksanakan. Profil baja siku atau L digunakan sebagai elemen sabuk, yang diaplikasikan secara eksternal mengelilingi keliling kolom BB dengan spasi tertentu untuk meningkatkan kekuatan, dan daktilitasnya. Untuk mencapai tujuan ini, dua fase ekperimen dilakukan.

Pada fase pertama dari eksperimen, empat belas spesimen kolom beton dibuat dan, diuji tekan monotonik untuk menyelidiki pengaruh dari metode retrofit eksternal yang diusulkan pada peningkatan kekuatan, dan lebih penting lagi, terhadap peningkatan daktilitas dari kolom. Untuk mempelajari efek ini, rasio volumetrik dari elemen pengekang digunakan sebagai parameter utamanya. Beberapa teknik pengakuan sabuk baja juga dilakukan, untuk menyelidiki lebih jauh potensi dari metode ini. Hasil menunjukkan adanya peningkatkan kekuatan, dan daktilitas dari spesimen yang diretrofit. Sebuah metode analitis untuk memprediksi kurva hubungan tegangan-regangan aktual dari kolom yang dikekang secara eksternal oleh sabuk baja, dikembangkan dan diverifikasi terhadap data tegangan-regangan dari eksperimen. Hasil menunjukkan prediksi yang baik. Tegangan puncak, regangan pada regangan puncak, dan regangan-regangan pada 50 dan 80 persen tegangan puncak dapat diprediksi dengan baik.

Sebuah prosedur perhitungan untuk pekerjaan retrofit juga diperkenalkan. Prosedur ini memberikan kebutuhan dari tambahan sabuk baja eksternal untuk memenuhi target kekuatan kolom. Idenya adalah dengan mengkombinasikan tegangan-tegangan kekang yang disumbangkan oleh pengekang internal maupun eksternal dengan merata-ratakan nilainya secara proposional terhadap daerah

yang dipengaruhi masing-masing. Perbandingan dengan data eksperimen mengindikasikan bahwa pendekatan yang diusulkan dapat memprediksi dengan marjin yang baik pada kecenderungan yang konservatif.

Pada fase kedua, lima spesimen kolom beton dibuat dan diuji dengan kombinasi beban aksial dan lateral siklik bolak-balik quasi-static. *Uji ini dilakukan untuk menyelidiki kinerja spesimen yang diretrofit terhadap simulasi beban gempa. Peningkatan kekuatan dan daktilitas yang berujung pada lebih besarnya kapasistas disipasi energi terlihat dengan jelas. Kriteria penerimaan dari ACI 374.1-05 juga terpenuhi. Sebagai tambahan, prosedur perencanaan juga dikembangkan berdasarkan data terbatas yang diperoleh dari eksperimen fase kedua. Prosedur perencanan langkah demi langkah mengakomodasi kebutuhan tambahan sabuk siku baja eksternal dalam meretrofit kolom untuk meningkatkan daktilitasnya. Pada akhirnya, dapat disimpulkan bahwa metode retrofit yang diusulkan dapat dipakai sebagai solusi alternatif pada rehabilitasi kolom BB yang tidak memenuhi persyaratan gempa.*

Kata Kunci : gempa, hubungan tegangan-regangan, kolom BB persegi, pengekangan eksternal, retrofit, sabuk baja.

ACKNOWLEDGEMENT

TABLE OF CONTENT

LIST OF TABLES

LIST OF FIGURES

xvi

xxii

LIST OF NOTATIONS

A_c : gross area of confined concrete core (for proposed method)

A_{cc} : net area of confined concrete core

A_{ce} : gross area of confined concrete core influenced by external confinement

A_{ci} : gross area of confined concrete core influenced by internal confinement

A_{cce} : net area of confined concrete core influenced by external confinement

A_{cci} : net area of confined concrete core influenced by internal confinement

A_{ch} : cross section area of column measured from the outside edges of transverse reinforcement

A_e : area of effectively confined concrete core (for proposed method, and Mander et al., 1988a, 1988b)

A_{ee} : area of effectively confined concrete core influenced by external confinement

A_{ei} : area of effectively confined concrete core influenced by internal confinement

A_g : gross area of concrete column section

A_l : total area of longitudinal bars

A_{par} : ineffectively confined area (for proposed method)

A_s : area of spiral confinement steel in circular concrete column (for Mander et al., 1988a, 1988b)

A_{sh} : minimum area of confinement steel (for SNI 2847 : 2013)

$A_{sx/y}$: area of confinement steel in x/y direction in rectangular concrete column

$A_{v\min}$: minimum area of stirrups

A_{sc} : area of steel angle section

B : dimension of rectangular concrete column (for Lee et al., 2010)

b : dimension of square concrete column (for proposed method); length of flat side of camfered rectangular concrete column (for Lee et al., 2010)

b_c : larger dimension of rectangular concrete column core (for Mander et al., 1988a, 1988b); diameter of circular concrete column core (for Saatcioglu et al., 1992); dimension of confined concrete core (SNI 2847 : 2013)

b_w : width of concrete element

$c_{1,2}$: coefficients (for proposed method)

c_y : core dimension (for Paultre and Legeron, 2008)

C_d : coefficient which depends on ductility level of the moment resisting frame system (International Building Code 2000)

C_i : size of WWF cell (for Kusuma and Tavio, 2007)

d : diameter of column (for Saafi et al., 1999)

d_c : smaller dimension of rectangular concrete column core (for Mander et al., 1988a, 1988b)

d_{cover} : concrete cover thickness

d_s : diameter of circular concrete column core (for Mander et al., 1988a, 1988b)

d_t : diameter of WWF reinforcement (for Kusuma and Tavio, 2007)

E_{ac} : actual dissipation energy

E_{id} : ideal dissipation energy

E_c : modulus of elasticiy of concrete

E_{des} : deterioration rate of descending branch of stress-strain realtionship curve

E_n : lateral resistance

E_{sec} : secant modulus of elasticity of confined concrete

E_{sece} : secant stiffness of concrete due to external confinement

E_{seci} : secant stiffness of concrete due to internal confinement

f_0 : peak stress of confined concrete (for Azizinamini et al., 1994)

f_c : compressive strength of concrete

f_{ce} : compressive strength of concrete do to external confinement

f_{ci} : compressive strength of concrete do to internal confinement

$f_{c.uc}$: axial stress of uneffectice confined area (for Lee et al., 2010)

$f_{cc.e}$: axial stress of effectice confined area (for Lee et al., 2010)

f_{com} : tensile strength of FRP

f_h : stress at transverse steel (for Legeron and Paultre, 2003)

f_h : average lateral confining pressure

f_{lcomb} : uniform lateral confining pressure due to combined internal and external confinement

f_{le} : equivalent uniform lateral confining pressure due to external confinement

f_{li} : uniform lateral confining pressure due to internal confinement

$f_{lx,y}$: average lateral confining pressure in x,y directions

f_s : stress in steel (for King et al., 1986)

f_{su} : ultimate stress in steel (King et al., 1986)

f_y : yield strength of longitudinal steel

f_{yh} : yield strength of transversal steel (for Hoshikusuma et al., 1997)

f_{ysc} : yield strength of steel angle section

f_{yt} : yield strength of transversal steel

f'_c : compressive strength of standard concrete cylinder

f'_{c0} : compressive strength of unconfined concrete

f'_{cc} : compressive strength of confined concrete

f'_{cccomb} : compressive strength of confined concrete due to combined internal and external confinement

f'_{cce} : compressive strength of confined concrete due to external confinement

f'_{cci} : compressive strength of confined concrete due to internal confinement

f'_h : effective stress at transverse steel (for Paultre and Legeron, 2008)

f'_l : effective lateral confining pressure

f'_t : tensile strength of concrete

f_{cc}^{CPC} : strength of confined plain concrete (for Barros et al., 2008)

h : dimension of rectangular concrete column

h'' : width of confined core (for Yong et al., 1988)

h_{sc} : height of steel angle section

h_x : smallest center to center distance of stirrups legs

H : dimension of rectangular concrete column (for Lee et al., 2010)

I'_e : effective confinement index

k : effective length factor

$k_{1,2,3,4}$: coefficients (for Razvi and Saatcioglu, 1999)

k_e : confinement effectiveness factor

k_f : coefficient (for Paultre and Legeron, 2008)

k_{ee} : confinement effectiveness factor due to external confinement

k_{ei} : confinement effectiveness factor due to internal confinement

k_n : coefficient (for Paultre and Legeron, 2008)

k_p : ratio of applied axial load with respect to nominal axial capacity of column

$K+$: initial stiffness of hysteretic loop (push mode)

$K-$: initial stiffness of hysteretic loop (pull mode)

K_e : initial effective stiffness

K_h : coefficient of effectiveness factor in horizontal direction

$K_{sec}+$: secant stiffness of hysteretic loop (push mode)

$K_{sec}-$: secant stiffness of hysteretic loop (pull mode)

K_v : coefficient of effectiveness factor in vertical direction

L_u : unbraced length of column

m : bending moment of steel collar (for proposed method), coefficient (for Tabsh, 2007), coefficient (for King et al., 1986)

m_n : nominal bending moment capacity of steel collar (proposed method)

M_{max} : maximum bending moment resistance

n : number of longitudinal bars (for Yong et al., 1988), coefficient (for Hoshikusuma, 1997)

n_l : number of longitudinal bars (for proposed method)

N_Δ : cumulative displacement ductility factor

N_φ : cumulative curvature ductility factor

p : axial force of steel collar (for proposed method)

p_n : nominal axial force capacity of steel collar (proposed method)

P_0 : theoretical nominal axial capacity

P_{0c} : theoretical nominal axial capacity contributed by concrete

P_{0cc} : theoretical nominal axial capacity contributed by concrete core

P_{cmax} : maximum axial resistance contributed by concrete

P_{max} : maximum axial resistance; maximum lateral resistance

Q_y : maximum strength (ACI 374.2R-13)

R : radius of concrete cylinder

r : radius of camfered corner of rectangular concrete column (for Lee et al., 2010), coefficient (for Mander et al., 1988), radius of gyration, coefficient (for King et al., 1986)

r_{comb} : coefficient for generating axial stress-strain curve due to combined internal and external confinement

r_e : coefficient for generating axial stress-strain curve due to external confinement

r_i : coefficient for generating axial stress-strain curve due to internal confinement

s : center-to-center spacing of stirrups

s' : clear spacing of stirrups

s_{sc} : center-to-center spacing of steel collar (for proposed method)

s_{scc} : clear spacing of steel collar (for proposed method)

TE_f : total cumulative energy up to failure of specimen

TE_{80} : total cumulative energy up to 20 percent decay of strength

TE_N : TE_{80} normalized by ideal elastoplastic energy

t : thickness of Fibre Reinforced Polymer (FRP)

t_{sc} : thickness of steel angle section

u_R : radial displacement

w_c : unit weight of concrete (kgf/m^3)

w_{sc} : width of steel angle section

w_i' : clear spacing of stirrups legs (for Mander et al., 1988a, 1988b)

x_1 : $K_e \rho_s f_{yh}$ (for Tavio et al., 2008a)

$x_2 \, \& \, x_3$: effective capacity of transverse reinforcement $= K_e \omega_w$ (for Tavio et al., 2008a)

$\hat{y}_1$: strength gain $\left(f'_{cc} - f'_{c0} \right)$ (for Tavio et al., 2008a)

$\hat{y}_2$: $\left(\varepsilon_{cc} / \varepsilon_{c0} \right) - 1$ (for Tavio et al., 2008a)

$\hat{y}_3$: $\varepsilon_{c50c} / \varepsilon_{c0}$ (for Tavio et al., 2008a)

Z_{sc} : plastic modulus of steel angle section

α : coefficient (for Hoshikusuma, 1997)

β : coefficient (for Hoshikusuma, 1997)

Δ_a : allowable displacement

Δ_{max} : maximum lateral displacement

Δ_y : yield axial displacement; yield lateral displacement

Δ_u : ultimate axial displacement; ultimate lateral displacement

ε_0 : strain corresponding to f_0 (for Azizinamini et al., 1994)

ε_{01} : axial strain corresponding to f'_{c0}

ε_1 : strain corresponding to f'_{cc} (for Saatcioglu and Razvi, 1992)

ε_{85} : axial strain at 0.85 f'_{cc} on descending branch

ε_b : strain of concrete (for Sargin, 1971)

ε_c : strain of concrete

ε_{c0} : axial strain corresponding to f'_{c0}

ε_{c50c} : axial strain at 0.50 f'_{cc} on descending branch (for Tavio et al., 2008a)

ε_{com} : ultimate strain of FRP

ε_{ct} : strain at transition zone of carbon FRP (for Barros et al. 2008)

ε_{cu} : ultimate compressive strain of concrete

ε_{f50} : axial strain at 0.50 f'_{cc} on descending branch

ε_{f80} : axial strain at 0.80 f'_{cc} on descending branch

ε_{f85} : axial strain at 0.85 f'_{cc} on descending branch

ε_h : strain of transverse steel

ε_s : strain of steel (for King et al., 1986)

ε_{sh} : strain at start of steel hardening (for King et al., 1986)

ε_{spall} : strain at concrete start spalling

ε_{su} : ultimate strain of steel (for King et al., 1986)

ε_t : ultimate tensile strain of concrete

ε_{Pmax} : strain of concrete corresponding to P_{max}

ε'_{cc} : strain corresponding to f'_{cc}

ε'_{cccomb} : strain corresponding to f'_{cccomb}

ε'_{cce} : strain corresponding to f'_{cce}

ε'_{cci} : strain corresponding to f'_{cci}

ε_{cc}^{CPC} : ultimate strain of confined plain concrete (for Barros et al., 2008)

ϕ : reduction factor (proposed method)

ϕ_l : diameter of longitudinal steel

ϕ_s : diameter of lateral steel

φ : curvature

φ_{max} : maximum curvature

φ_y : yield curvature

φ_u : ultimate curvature

λ : ratio of column nominal bending capacity with respect to beam nomimal bending capacity

μ_Δ : displacement ductility factor

μ_ε : axial strain ductility factor

$\mu_{\varepsilon a}$: absolute axial strain ductility factor

μ_φ : curvature ductility; ductility demand

υ_c : Poisson's ratio of concrete

υ_s : Poisson's ratio of FRP

ρ : ratio of longitudinal bars with respect to gross concrete area

ρ_c : area ratio of lateral steel

ρ_f : volumetric ratio of carbon FRP (for Barros et al., 2008)

ρ_s : volumetric ratio of lateral steel

σ_R : radial pressure

σ_s : hoop stress of FRP tube

= This Page is Intentionally Left Blank =

CHAPTER 1.   INTRODUCTION

1.1   BACKGROUND

With the development of knowledge on seismic action (resulting in codes specifying higher seismic demand), many existing reinforced concrete (RC) structures are in need of strengthening and retrofitting. Typically, according to Liu et al. (2008), the resulting deficiencies that often characterize old existing RC frame structures include: (1) insufficient transverse reinforcement to confine the column core and to restrain buckling of longitudinal reinforcement; (2) inadequate lap splices located immediately above floor levels where inelastic actions may be concentrated with large flexural demand; (3) insufficient shear strength to develop the column flexural capacity, or the potential degradation of column shear strength with increasing flexural ductility demand; (4) inadequate column strength to develop a strong-column weak-beam mechanism, and (5) deficient beam-to-column joint dimensions and details. These situations are worsen when combined with the existing RC structure conditions that were designed and built with no technical assistance (non-engineered buildings) commonly found in most residential houses in Indonesia. Thus, strengthening and retrofitting of existing RC structures has urgently become a national demand.

For most framed structures, it is more economical to design for dissipating seismic energy in a flexural mode by forming plastic ductile hinges in beams rather than in columns (Shiekh et al., 1986). Columns are critical elements in any structural building system and their performances during a seismic event can dominate the overall performance of the structure since single column failure can lead to additional failures and potentially result in total building collapse (Liu et al., 2008). Other research (Sakai and Sheikh, 1989) also highlighted that effectiveness of the design approach involving strong column weak beam concept is still a controverting matter, thus it will be dangerous to design the structure without considering the possibility of plastic hinge formations in columns. Recent earthquakes have highlighted the catastrophic effect of these columns' failures. Figure 1-1 shows the soft story effect in a typical commercial building during the 2005 Nias Earthquake. Figure 1-2 shows the brittle failure of a column due to

inadequate transverse reinforcement during the 2006 Yogyakarta Earthquake. Figure 1-3 shows the joints in RC structures which were not designed properly leading to the plastic hinge formations in columns instead of beams (Padang Earthquake, 2009).

Figure 1-1 Soft story effect in a typical commercial building (Nias Earthquake, 2005)

Figure 1-2 Inadequate transverse reinforcement in RC column (Yogyakarta Earthquake, 2006)

Figure 1-3 Inadequate columns' strength in joints (Padang Earthquake, 2009)

Mander et al. (1988a, 1988b) mentioned that the most important thing in plastic hinge design of reinforced concrete columns is the availability of sufficient transverse reinforcement for confining the concrete, preventing the buckling of longitudinal reinforcement, and avoiding brittle shear failure. In order to provide such requirement in existing deficient RC columns, retrofitting purpose should be introduced.

1.2 RETROFITTING METHODS

RC columns are arguably the most critical component of many structures and should be aimed for retrofit purpose. It is well known fact that lateral confinement enhances the strength and, more importantly, ductility of RC columns (Nesheli et al., 2004). In order to upgrade deficient columns so that they can reach their designated performance level, retrofittings are usually introduced. Some concrete column retrofitting methods that have been developed include concrete jacketing, steel sheet jacketing (Chai et al., 1994; Choi et al., 2010; Guo et al., 2006; Priestley et al., 1994; Xiao et al., 2003), fiber-reinforced polymer (FRP) composite jacketing (Barros et al., 2008; Carey and Harries, 2005; Fam and Rizkalla, 2001; Lee et al., 2010; Nesheli et al., 2004; Saafi et al., 1999; Tegola

and Manni, 1999), or steel collar jacketing (Chapman and Driver, 2006; Hussain and Driver, 2005; Liu et al., 2008). All methods except concrete jacketing can also be improved by applying external prestressing force (Choi et al., 2010; Guo et al., 2006; Nesheli et al., 2004; Saatcioglu et al., 2003).

Ideally, an effective retrofitting technique shall possess such characteristics as being easy to implement, minimizing disruption to the use of the structure, not requiring highly specialized skills, minimizing labour costs, and resulting in efficient performance (Liu et al., 2008). Concrete and steel jacket are very effective but inconvenient to install, because doing so requires using scaffolds for curing the concrete or grout (Choi et al., 2010). FRP jackets have several advantages over the steel and concrete jackets: (1) ease of installation; (2) no increment of the cross section; and (3) no increment of the flexural or shear stiffness of the structure. However, FRP jacketing is generally uneconomical compared with the concrete and steel jacketings (Choi et al., 2010). Chapman and Driver (2006) developed a retrofitting technique by using steel collars cut from steel plates which were installed with high strength bolts. The method has been proven to be quite effective. The ease of installation which does not require any grouting or welding effort has made the method very promising for further research.

In this study, a more economical yet promising to be effective and more practical retrofitting method for square RC columns is proposed. The proposed method is providing additional confinement externally by installing uniformly spaced steel collars made from angle or L-shaped sections. Beside the minor welding work required, only common bolt-nut connection at the corners is needed to complete the steel collar module. The steel collar module is installed by simply fastening the bolt-nut connection at the four corners. The method is indeed very practical since it does not require any grouting. The contact between steel collar and the concrete is expected to be effective as passive confinement when the column experiences large lateral expansion. The results of this study show that the proposed method works with satisfactory results. Strength and ductility enhancement are evident in retrofitted specimens, both in monotonic compressive

4

test and quasi static combined compressive and reversed cyclic loading test. An analytical model to predict axial compressive stress-strain relationship and a retrofit design procedure are also developed with very good comparisons with the experimental results.

1.3 PROBLEM STATEMENT

The current study is aimed to further investigate the feasibility of steel collar jacketing method for retrofitting seismically deficient square RC columns. Instead of heavier steel sections (hollow square sections and relatively thick plates used in previous researches by others), the economical and very light angle section commonly used for roof truss structures is chosen for making the steel collar module. Due to the lighter and relatively weaker steel angle sections, some issues that may arise and need to be investigated are as follows:

- How is the effectiveness of the proposed external retrofit method for RC columns by using steel angle collars in terms of strength and ductility enhancements ?
- How to analytically predicts the axial stress-strain relationship of square RC columns retrofitted with the steel angle collars ?
- How is the retrofit design approach of existing deficient square RC columns retrofitted by the steel angle collars ?

1.4 RESEARCH OBJECTIVES

The overall goal of the study is to investigate the feasibility of the proposed retrofitting method for seismic deficient square RC columns. In general, it is expected to contribute in solving the national demand on strengthening and retrofitting the old and existing seismic deficient or non-seismic designed RC structures. The specific objectives ofn the study are as follows:

- To investigate the strength and ductility enhancements in square RC columns retrofitted by the proposed method.

- To provide a proposed analytical method in predicting the axial stress-strain relationship of square RC columns retrofitted with the external steel collars.
- To come up with a proposed design procedure for retrofitting the existing seismic deficient or non-seismic designed square RC columns.

1.5   SCOPE OF RESEARCH

In order to effectively achieve the objectives, the scope of research should be determined. The followings are the items listed as the scope of research:

- Among available retrofitting techniques, external retrofit is selected due to its practical application.
- In order to rule out the possible effect of slenderness, the experiment is mainly focused on non-slender columns (column specimens were all set to have the shear span to depth ratio not greater than 3.0).
- Steel angle section is selected for the steel collar confinement elements due to its economical value and high availability in the market.
- The study only focuses on retrofitting square concrete columns.
- Normal strength concrete is used for representing widely used concrete strength in Indonesia, particularly in the past when high strength concrete was not yet used for non-seismic designed (seimic deficient) building structures.
- The experimental tests are limited to: (1) monotonic static compression loading; and (2) combined quasi-static axial compression and reversed cyclic lateral loading.
- The external steel collars used for retrofit are installed at zero stress state of the specimens.
- The term "retrofit" in this dissertation is meant only for strengthening and retrofitting non-damaged existing seismic deficient RC columns. The term "retrofit" is not intended for rehabilitation of damaged post-earthquake RC columns.

- Enhancement in strength and ductility are defined as the performance of the proposed method.
- Volumetric ratio of steel angle collars with respect to concrete or spacing of steel angle collars (since only one section size is used in the study) and stiffeners of steel angle collars (web stiffeners and strucutral bolts) are the independent variables in the study.

1.6   RESEARCH SIGNIFICANCE

The research will have significant contributions in:
- Enriching retrofit methods of square RC columns.
- Solving a national demand by providing an economical, efficient, and practical alternative solutions for retrofitting the existing seismic deficient or non-seismic designed square RC columns.

1.7   STATE OF THE ART

The research on seismic rehabilitation of RC structures has been conducted worldwide. The rehabilitation techniques fall under two main categories: structural system-level, and member-level approaches. The former approach includes the installation of structural systems, such as adding structural walls, damping devices, base isolators, steel braces, or steel shear plates. This approach has an impact on the overall structural response to earthquake (Liu et al., 2008). On the other hand, the member-level approach is focused on enhancing performance in only deficient components. The conventional method of this approach is by installing additional reinforcements which are later be covered by the concrete jacketing method. More recent methods of this approach are by the applications of external materials to provide confinement elements. The studies of these methods conducted by several researches as well as the proposed method in the study can be classified in Table 1-1.

7

Table 1-1 Research on external confinement for retrofitting RC columns

Confinement Method	Circular Column	Square / Rectangular Column	External Prestressing	Axial Load	Combined Axial and Lateral Loads
Prestressing Cable	Saatcioglu et al., 2003	Saatcioglu et al., 2003	Saatcioglu et al., 2003	Saatcioglu et al., 2003	Saatcioglu et al., 2003
Steel Sheet Jacketing	Chai et al., 1994; Priestley et al., 1994; Choi et al., 2010	Priestley et al., 1994; Xiao et al., 2003; Guo et al., 2006	Guo et al., 2006; Choi et al., 2010	Chai et al., 1994; Priestley et al., 1994; Xiao et al., 2003; Guo et al., 2006; Choi et al., 2010	Chai et al., 1994; Priestley et al., 1994; Xiao et al., 2003; Guo et al., 2006; Choi et al., 2010
Fiber Reinforced Polymer (FRP) Jacketing	Tegola et al., 1998; Saafi et al., 1999; Carey et al., 2005; Barros et al., 2008	Nesheli et al., 2004; Lee et al., 2010	Nesheli et al., 2004	Nesheli et al., 2004; Tegola et al., 1998; Saafi et al., 1999; Carey et al., 2005; Barros et al., 2008; Lee et al., 2010	Nesheli et al., 2004
Steel Collar Jacketing		Hussain et al., 2005; Chapman et al., 2006; Liu et al., 2008; **Pudjisuryadi et al., 2014, 2015, and 2016**	Liu et al., 2008	Hussain et al., 2005; Chapman et al., 2006; Liu et al., 2008; **Pudjisuryadi et al., 2014, 2015, and 2016**	Chapman et al., 2006; Liu et al., 2008; **Pudjisuryadi et al., 2014, 2015, and 2016**

The proposed method have several advantages over the others, as follows :

a. Ecomonical value

The use of lighter steel angle sections over heavier elements used by other researchers (e.g. thick steel plates, hollow square sections) provides more economical alternative solution. The practical preparation and implementation can save time and also cut the cost.

b. Easy to prepare and apply

Steel angle section is a commonly used for roof truss in Indonesia. It can be easily found and available in the market with relatively low in price. Only minor cutting, drilling, and welding works are required to prepare the steel collar modules. Regular bolt-nut system is used and fastened at four corners to form a steel collar from the modules. The application of the

proposed system does not require any special labor skill and devices, or even grouting material.

The proposed study is expected to contribute an alternative external retrofitting method (member-level approach). The primary difference of the proposed method compared to available steel collar jacketing method is in term of the steel section used. Available angle steel section in the market is used instead of manually fabricated from thick steel plates. All of these improve the applicability and practicability of the proposed method.

1.8   HYPOTHESIS

Some parameters should be given extra attentions, in order to gain the optimum effectiveness of the proposed method. The connections between steel collar elements at the corners should have good strength and the interactions between the surface of concrete and steel angle collars should be effectively in full contact. If developed properly, the proposed external retrofitting method using steel angle collars should provide sufficient confinement effect which leads to the enhancement of strength and ductility of seismic deficient square RC columns.

1.9   ORGANIZATION OF DISSERTATION

The dissertation is organized into seven chapters. Chapter 1, the introduction discusses the rationale of the research. The background, problem statement, research objectives, scope of research, research significance, state of the art, and the hypothesis are presented. Chapter 2 presents the detailed theoretical background and literature review. The previous works by others covering the effect of confinement in RC columns, the analytical models developed, and other retrofiting techniques are discussed. Chapter 3 presents the design and details of the experimental programs. Parameters of the design specimens are explained in this chapter. Specimen construction, laboratory equipment, and test setup are also presented. Chapter 4 presents the results of monotonic compressive test. The observed behavior of the specimens during the test are discussed. Chapter 5 presents the results of quasi-static combined axial

and cyclic lateral load test. The observed behavior during the test, and discussions of the results are covered in this chapter. Chapter 6 presents the proposed analytical model and retrofit design approach. Based on experimental results, an analytical model was developed to predict the axial stress-strain relationship of the externally confined specimens. Further, the combined confinement effect of conventional internal stirrups and external steel collars was also proposed for retrofit design. Expressions for minimum confining requirement were also derived in this chapter. Some calculation examples are also provided. Chapter 7 summarizes the conclusions of the works done and recommendations for potential future research.

CHAPTER 2.   THEORETICAL BACKGROUND AND LITERATURE REVIEW

2.1   GENERAL

For most framed structures to survive a major earthquake, they must undergo large inelastic deformations and thus dissipate energy by ductile behavior of their structural members. It is more economical to design for dissipating seismic energy in a flexural mode by forming plastic ductile hinges in beams rather than in columns. The difficulty of preventing plastic hinges from forming in columns makes it important to insure that columns are capable of behaving in ductile manner (Sheikh et al., 1986). Non-ductile behavior of column hinges should be avoided since it can lead to failures of other members and potentially result in total building collapse. In members which behavior is dominated by axial compression (columns), brittle failure as result of inelastic deformation can be avoided only if the concrete is made to behave in a ductile manner with the help of confinement provided by lateral and longitudinal steel, and if the longitudinal reinforcement is retrained adequately against premature buckling (Sheikh et al., 1993). Other research (Sakai and Sheikh, 1989) also highlighted that effectiveness of the design approach involving strong column weak beam concept is still a controverting matter, thus it will be dangerous to design the structure without considering the possibility of plastic hinges formations in columns. Mander et al. (1988a) also mentioned that the most important thing in plastic hinge design of reinforced concrete columns is the availability of sufficient transverse reinforcement for confining the concrete, preventing the buckling of longitudinal reinforcement, and avoiding brittle shear failure. The following sections of this Chapter summarize researches on the effects of confinement of reinforced concrete columns.

2.2 EFFECT OF CONFINEMENT IN REINFORCED CONCRETE COLUMNS

In columns, the compressive axial strain causes tensile strain in the transverse direction (Poisson's effect). In a confined concrete section, this transverse strain is restrained by lateral pressure from confinement. This confinement causes the concrete to enter a triaxial stress state which enhances both the strength and ductility. Many researches all over the world have confirmed such phenomenon (Azizinamini et al., 1994; Cusson and Paultre, 1995; Hoshikusuma et al., 1997; Kusuma and Tavio, 2007, 2008, 2009; Kusuma et al., 2011a, 2011b, 2015a, 2015b; Legeron and Paultre, 2003; Paultre and Legeron, 2008; Mander et al., 1988a, 1988b; Muruguma et al., 1993; Pudjisuryadi and Tavio, 2013; Pudjisuryadi et al, 2011, 2014, 2015, 2016; Razvi and Saatcioglu, 1994, 1999; Saatcioglu and Razvi, 1992; Sheikh and Uzumeri, 1980; Sheikh, 1982; Sheikh and Yeh, 1986; Tabsh, 2007; Tavio et al., 2008a, 2008b, 2011, 2012; Tavio and Kusuma, 2009 2014, 2015; Yong et al, 1988).

In a circular section, the concrete is confined uniformly. This is not the case for rectangular or square sections. The confined region is highly affected by configuration of reinforcement as illustrated by Sheikh and Yeh (1986). Closer spacing of both longitudinal and lateral reinforcement results in a higher proportion of the effectively confined area as shown in Figure 2-1.
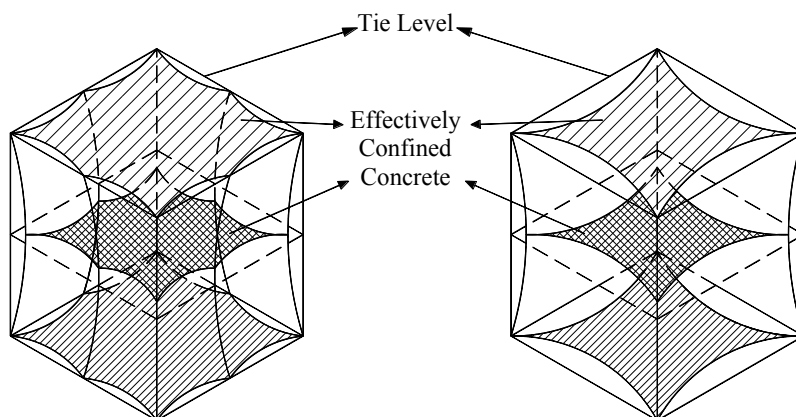
Figure 2-1 Effectively confined concrete area (adopted from Sheikh and Yeh, 1986)

The confinement can be provided through such mechanisms as conventional internal reinforcement, external reinforcement, external jackets (made of concrete, steel, or fiber reinforced polymer, etc.), or external prestressing (Liu et al., 2008). There are some general agreements on the differences of stress-strain relationship of confined concrete compared to that of plain concrete. These main differences are: (1) increment of the compressive strength; (2) flatter post peak descending branch of the curve; and (3) increment of ultimate compressive strain. These improved stress-strain relationships results in more ductile behavior which leads to higher energy absorbing capacity. It is clear that confinement elements and their resulting confining stress distribution play important part in the improved behavior. Reviews of some confinement studies from the literature are presented in the following sections.

2.3 STRESS-STRAIN RELATIONSHIP MODEL OF CONFINED CONCRETE

In an unconfined concrete under pressure uniaxial stress state is experienced. The axial strain causes tensile strain in the transverse direction (Poisson's effect) which can lead to vertical crack. In a confined concrete, this transvere strain is restrained by lateral pressure from confining reinforcement. This causes the concrete to enter a triaxial stress state which enhances the strength (Saatcioglu et al., 1992). The more confined core area, the stronger the confined concrete will be. Thus, it is important to know how this confinement affects the stress-strain behavior of the concrete. In this section, some stress-strain relationship models of confined concrete are discussed. Some models are elaborated more due to their relevance to this study, while other models are briefly discussed to give general idea of what have been done by others on this research area.

2.3.1 Sheikh and Uzumeri (1980, 1982)

Sheikh and Uzumeri (1980) studied some stress-strain models of previous researchers. There was a general agreement that the amount of confinement steel is the main parameter which affects the concrete properties enhancement. Chan et

al. (1955) suggested trilinear stress-strain curve for unconfined and confined concrete as shown in Figure 2-2. The variable used to define the curve was only volumetric ratio of tie steel to concrete core.
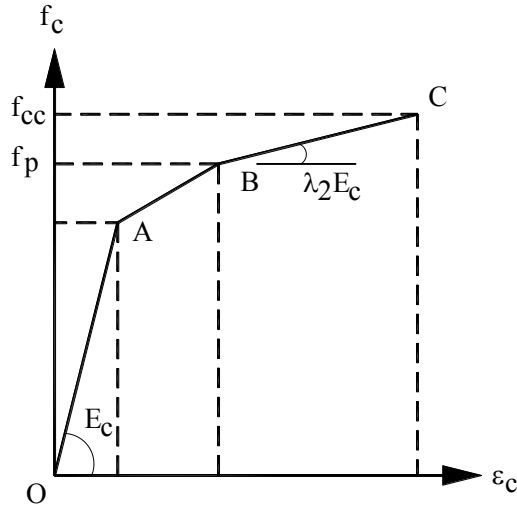
Figure 2-2 Stress-strain curve proposed by Chan (adopted from Chan et al., 1955)

Roy and Sozen (1965) suggested bilinear curve of stress strain relationship as shown in Figure 2-3. The variable used to define the curve were volumetric ratio of tie steel to concrete core, and ratio of section dimension to tie spacing.
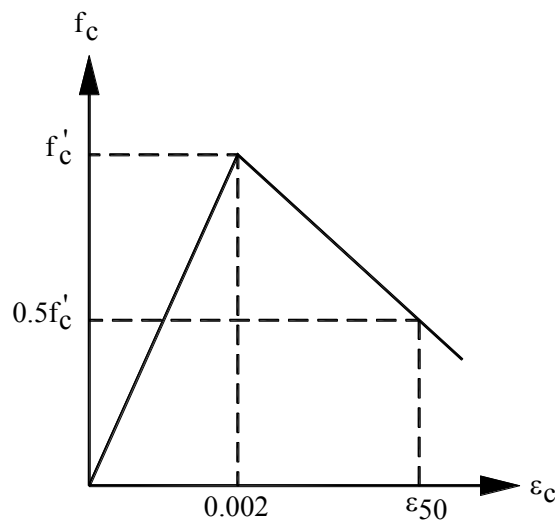
Figure 2-3 Stress-strain curve proposed by Roy and Sozen (adopted from Roy and Sozen, 1965)

Soliman and Yu (1967) suggested stress strain curve as shown in Figure 2-4. The variable used to define the curve were area of tie steel bar, tie spacing, and section geometry.

14
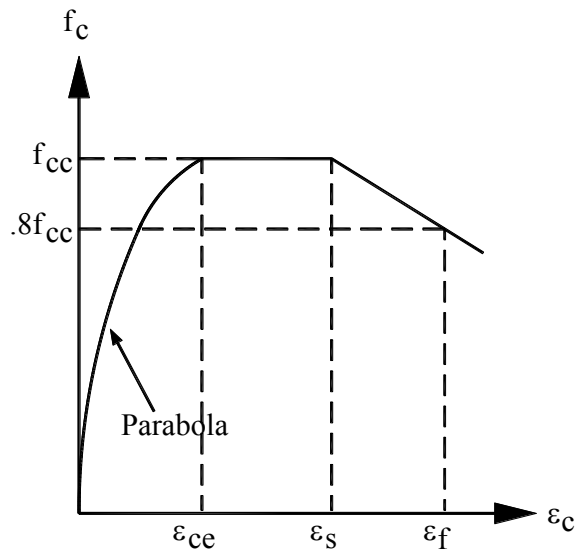
Figure 2-4 Stress-strain curve proposed by Soliman and Yu (adopted from Soliman and Yu, 1967)

Sargin (1971) suggested stress strain curve as shown in Figure 2-5. The variable used to define the curve were volumetric ratio of lateral steel to concrete core, ratio of width of concrete core to tie spacing, steel strength, and strength of plain concrete.
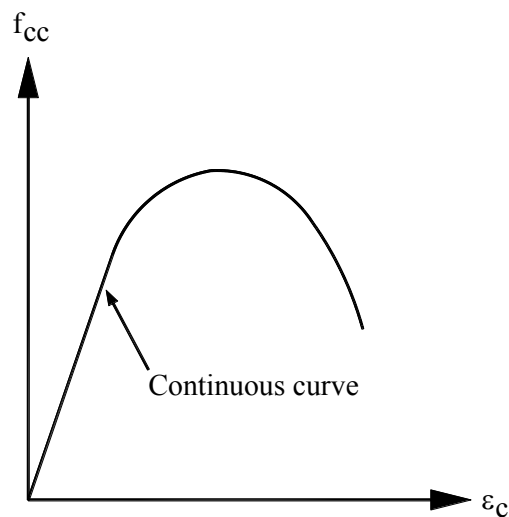
Figure 2-5 Stress-strain curve proposed by Sargin (adopted from Sargin, 1971)

Kent and Park (1971) suggested stress strain curve as shown in Figure 2-6. The variable used to define the curve were volumetric ratio of lateral steel to concrete core, ratio of width of concrete core to tie spacing, and strength of plain concrete.
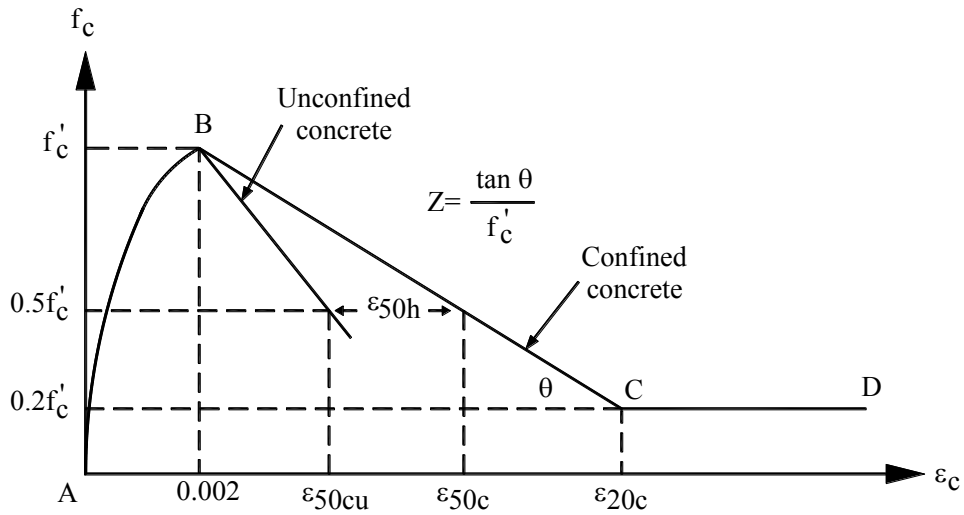
Figure 2-6 Stress-strain curve proposed by Kent and Park (adopted from Kent and Park, 1971)

Vallenas et al. (1977) suggested stress strain curve as shown in Figure 2-7. The variable used to define the curve were volumetric ratio of lateral steel to concrete core, ratio of area of longitudinal steel to area of cross section, sizes of tie bar and longitudinal bar, ratio of core dimension to tie spacing, steel strength, and strength of plain concrete.
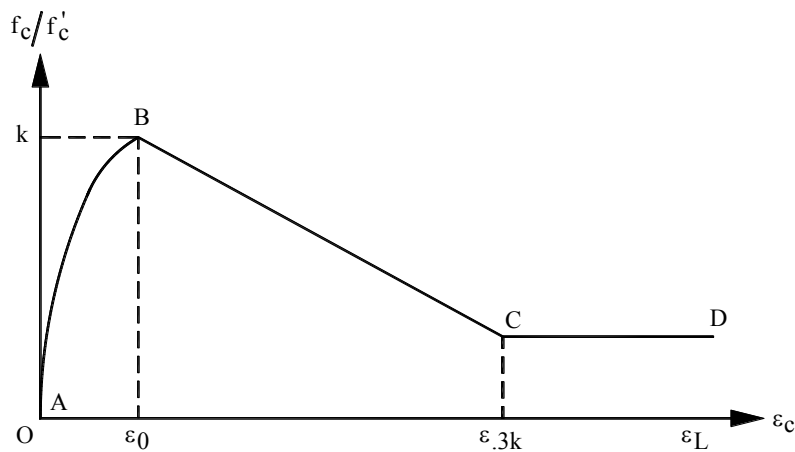
Figure 2-7 Stress-strain curve proposed by Vallenas et al. (adopted from Vallenas et al., 1977)

Sheikh and Uzumeri (1980) themselves suggested stress strain curve as shown in Figure 2-8. The variable used to define the curve were volumetric ratio of lateral steel to concrete core, distribution of longitudinal steel around the core

perimeter and the resulting tie configuration, tie spacing, characteristics of lateral steel, and strength of plain concrete.
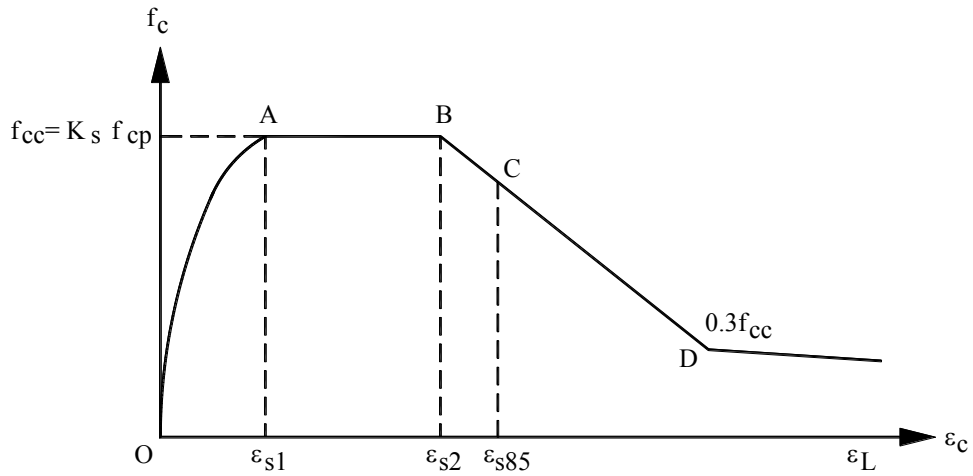
Figure 2-8 Stress-strain curve proposed by Sheikh and Uzumeri (adopted from Sheikh and Uzumeri, 1980)

These models were compared and applied to the specimens tested by Sheikh (1982) as well as by other investigators to predict the results. The loads considered were both axial as well as combined axial and bending. The model proposed by Sheikh and Uzumeri predicted test results better than the other models studied, both for axial load only and for combined axial and flexural loads. This was the only model that considered the distribution of longitudinal steel and the resulting tie configuration as a variable affecting the mechanism of confinement. Envelope of moment-curvature curve for reinforced concrete section under cyclic bending could be determined with reasonable accuracy by using Sheikh and Uzumeri stress-strain relationship for confined concrete.

2.3.2 Mander et al. (1988a)

Mander et al. (1988a) proposed stress-strain curve of unconfined and confined concrete as shown in Figure 2-9. The strength of confined concrete and its corresponding strain were expressed in Equations 2-1 and 2-2.

$$ f_{cc}' = f_{c0}' \left(-1.254 + 2.254\sqrt{1 + \frac{7.94 f_l'}{f_{c0}'}} - 2\frac{f_l'}{f_{c0}'} \right) \qquad (2\text{-}1) $$

17

$$\varepsilon_{cc} = \varepsilon_{c0}\left(1 + \left(5\frac{f'_{cc}}{f'_{c0}} - 1\right)\right) \tag{2-2}$$

f'_{cc} and f'_{c0} are the compressive strength of confined and unconfined concrete; ε_{cc} and ε_{c0} are the strains corresponding to f'_{cc} and f'_{c0} respectively; f'_l is the effective lateral confining pressure. Mander proposed a single function for entire stress-strain relationship as seen in Equation 2-3 to Equation 2-6.

$$f_c = \frac{f'_{cc}xr}{r - 1 + x^r} \tag{2-3}$$

$$x = \frac{\varepsilon_c}{\varepsilon_{cc}} \tag{2-4}$$

$$r = \frac{E_c}{E_c - E_{sec}} \tag{2-5}$$

$$E_{sec} = \frac{f'_{cc}}{\varepsilon_{cc}} \tag{2-6}$$

f_c and ε_c represent a point in the curve which expresses compressive strength and the corresponding strain; E_c is the modulus of elasticity of the concrete.
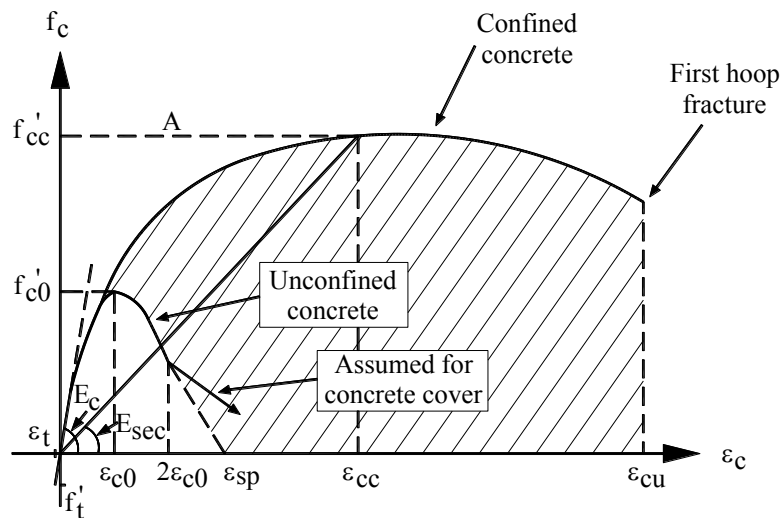
Figure 2-9 Stress-strain relationship model for plain and confined concrete subjected to monotonic loading with low strain rate (adopted from Mander et al., 1988a)

18

In order to generate complete stress-strain relationship, accurate effective confining pressure prediction is needed. Mander used similar approach used by Sheikh and Uzumeri (1980) to determine this effective lateral confining pressure. The effective lateral confining pressure, f_l' was modified from lateral confining pressure, f_l by introducing confinement effectiveness factor, k_e as shown in Equation 2-7.

$$f_l' = k_e f_l \qquad\qquad (2\text{-}7)$$

The confinement effectiveness factor, k_e is defined as the ratio of effectively confined concrete core area, A_e with respect to net concrete core area (concrete core area reduced by longitudinal reinforcement area), A_{cc} as shown in Equation 2-8.

$$k_e = \frac{A_e}{A_{cc}} \qquad\qquad (2\text{-}8)$$

The effectively confined concrete core area was determined by assuming the presence of ineffective regions in the shape of second degree parabola with initial tangent slope of 45 degree, as seen in Figures 2-10 and 2-11 for circular and rectangular sections respectively. Based on the assumption, the effectively confined concrete core area could be expressed in Equations 2-9 and 2-10 for circular and rectangular sections.

$$A_e = \frac{\pi}{4} d_s^2 \left(1 - \frac{s'}{2d_s}\right)^2 \qquad\qquad (2\text{-}9)$$

$$A_e = \left(b_c d_c - \sum \frac{(w_i')^2}{6}\right)\left(1 - \frac{s'}{2b_c}\right)\left(1 - \frac{s'}{2d_c}\right) \qquad\qquad (2\text{-}10)$$
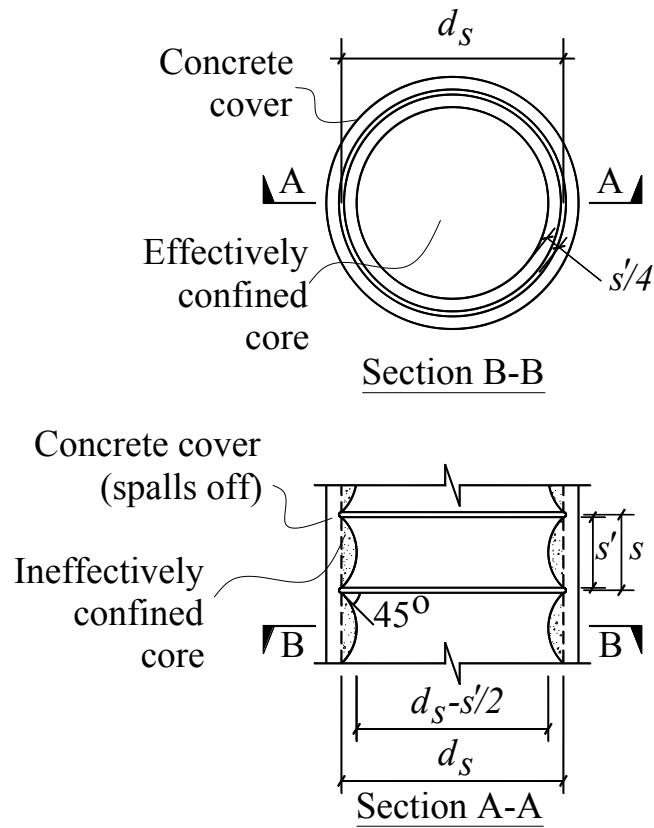
Figure 2-10 Core area in circular section (adopted from Mander et al., 1988a)
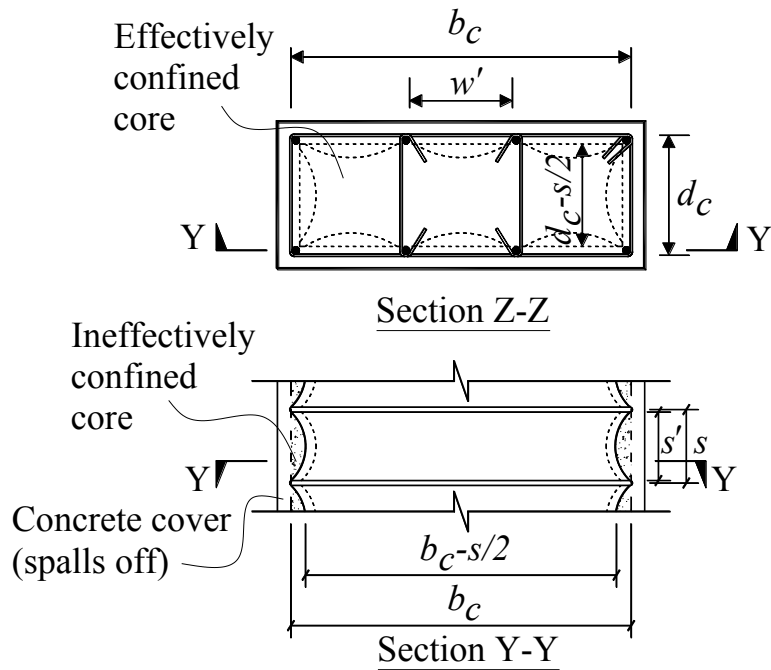
Figure 2-11 Core area in rectangular section (adopted from Mander et al., 1988a)

20

The lateral confining pressure in circular section could be shown by the half body confined by spiral hoop (see Figure 2-12). If the area of spiral reinforcement was given as A_s, and with the state of yielding at its strength f_{yt}, the lateral confining pressure could be determined as in Equation 2-11.

$$f_l = \frac{2 f_{yt} A_s}{s b_c} \tag{2-11}$$
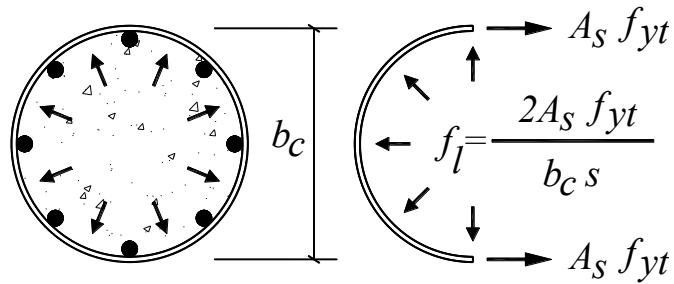
Figure 2-12 Lateral stress in a circular section due to confinement (adopted from Saatcioglu and Razvi, 1992)

Similarly, by considering half body of each direction, the lateral confining pressures in rectangular sections could be obtained. With total area of lateral reinforcement in x and y directions expressed as A_{sx} and A_{sy}, the lateral confining pressures in x and y directions were determined as in Equations 2-12 and 2-13.

$$f_{lx} = \frac{f_{yt} A_{sx}}{s d_c} \tag{2-12}$$

$$f_{ly} = \frac{f_{yt} A_{sy}}{s b_c} \tag{2-13}$$

It is possible, in general, that the confining pressure in both directions were different. Mander et al. (1988a) did not explicitly suggest which value to be used. Later, other study (Saatcioglu and Razvi, 1992) suggested that these value should be averaged proportionally to the dimensions in both directions.

2.3.3 Yong et al. (1988)

Yong et al. (1988) proposed compressive stress-strain relationship of high-strength concrete as shown in Figure 2-13. The expressions for ascending and

descending branches of the curve depended on modulus of elasticity of concrete E_c, strength of confined concrete f_{cc}' and its corresponding strain ε_{cc}, and pairs of stress and strain on the descending branch ε_i, f_i, ε_{2i}, and f_{2i} (see Figure 2-13). Detail expressions of those parameters can be seen in the original publication (Yong et al., 1988). Only strength of confined concrete f_{cc}' and its corresponding strain ε_{cc}' were presented here in Equations 2-14 and 2-15.

$$f_{cc}' = K_s f_c' = \left[1 + 0.11\left(1 - \frac{0.254s}{h''}\right)\left(\rho_s + \frac{n\phi_s\rho}{0.3149s\phi_l}\right)\frac{f_{yh}}{\sqrt{f_c'}}\right]f_c' \qquad (2\text{-}14)$$

$$\varepsilon_{cc}' = 0.00265\left[\frac{0.0035\left(1 - \frac{0.734s}{h''}\right)\left(145\rho_s f_{yh}\right)^{2/3}}{\sqrt{145f_c'}}\right] \qquad (2\text{-}15)$$

h'' is the width of confined core; n is the number of longitudinal bars; ϕ_s and ϕ_l are the diameter of lateral and longitudinal bars, respectively; ρ_s is the volumetric ratio of lateral steels; and ρ is the ratio of longitudinal bars area with respect to gross concrete area in a section.
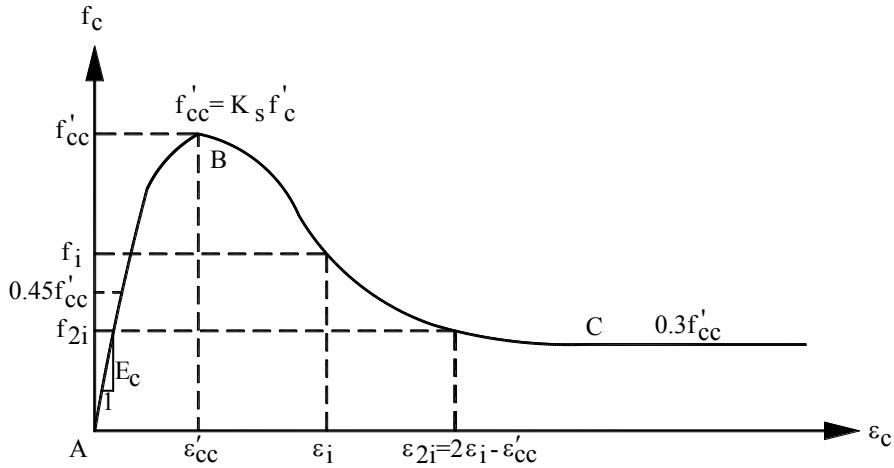
Figure 2-13 Stress-strain relationship of high-strength concrete proposed by Yong et al. (adopted from Yong et al., 1988)

22

2.3.4 Saatcioglu and Razvi (1992); Razvi and Saatcioglu (1999)

Saatcioglu and Razvi (1992) proposed stress-strain curve of unconfined and confined concrete as shown in Figure 2-14. This model was originally developed to cover only normal strength concrete. Later, the original formulation was expanded to cover high-strength concrete as well (Razvi and Saatcioglu 1999). The concept was developed on the basis of equivalent uniform confining pressure (unlike Mander et al., 1998a which used effectively confined concrete core area). It was assumed that the confining stress concentrated on tie locations which have relatively large axial ridigity, as seen in Figure 2-15. Since uniform lateral pressure was used as the basis of the formulation, a coefficient k_2 was introduced in Equation 2-16 (see Figure 2-16) to get equivalent uniform lateral pressure f_{le} (MPa) from average lateral pressure f_l (MPa).

$$f_{le} = k_2 f_l \qquad (2\text{-}16)$$

In circular section with spiral hoop, this process was not necessary since the lateral confining pressure was already uniform. In Equation 2-16, the average lateral confining pressure f_l was identical with model proposed by Mander et al. (1988a) as expressed in Equations 2-11 to 2-13.
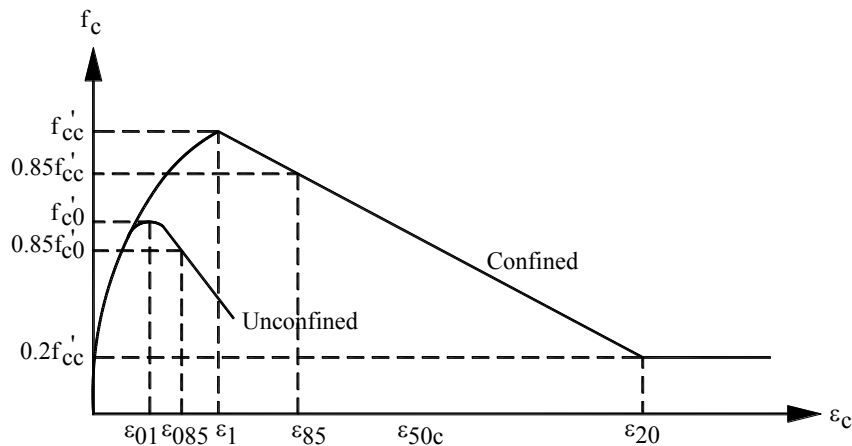
Figure 2-14 Stress-strain curve proposed by Saatcioglu (adopted from Saatcioglu and Razvi, 1992)

23
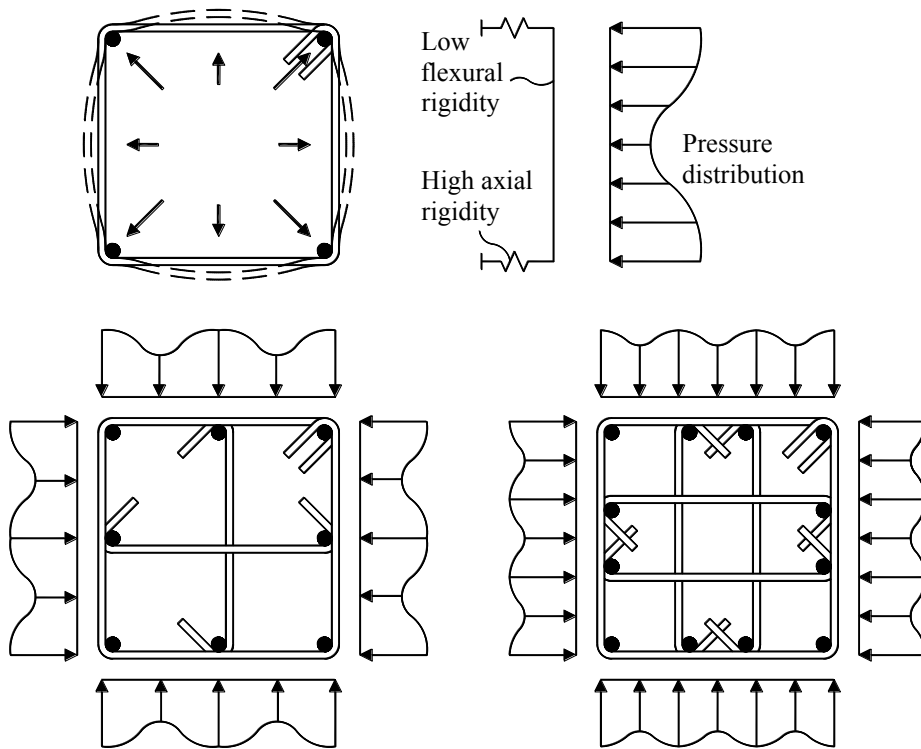
Figure 2-15 Non-unfinorm confining pressure assumed (Modified from Razvi and Saatcioglu, 1999)
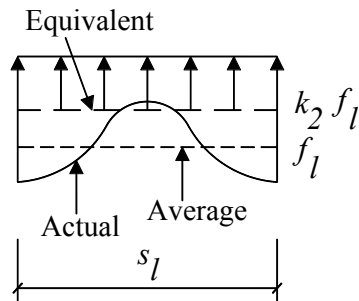
Figure 2-16 Actual, average, and equivalent confining pressure (adopted from Razvi and Saatcioglu, 1999)

However, it should be noted that the stress in transverse steel did not always reach its yield strength if higher grade of steel is used. Razvi and Saatcioglu (1999) suggested that actual steel stress be used in the expressions. The coefficient k_2 was determined empirically by Razvi and Saatcioglu (1999) which applied on both normal and high-strength concrete as shown in Equation 2-17.

$$k_2 = 0.15\sqrt{\left(\frac{b_c}{s}\right)\left(\frac{b_c}{s_l}\right)\left(\frac{1}{f_l}\right)} \leq 1.0 \tag{2-17}$$

b_c, s, s_l are the core dimension (measured from center-to-center of outermost lateral steels), spacing of lateral steels, and spacing of longitudinal bars, respectively. Once the equivalent uniform confining pressure determined, the peak strength f'_{cc} (MPa) could be determined by using Equations 2-18 and 2-19.

$$f'_{cc} = f'_{c0} + k_1 f_{le} \tag{2-18}$$

$$k_1 = 6.7\left(f_{le}\right)^{-0.17} \tag{2-19}$$

f'_{c0} (MPa) is the unconfined concrete strength. In order to complete key points in the stress-strain relationship curve, Equations 2-20 to 2-26 were used.

$$\varepsilon_1 = \varepsilon_{01}(1 + 5k_3 K) \tag{2-20}$$

$$\varepsilon_{85} = \varepsilon_{085} + 260k_3\rho_c\varepsilon_1\left(1 + 0.5k_2(k_4 - 1)\right) \tag{2-21}$$

$$k_2 = \frac{40}{f'_{c0}} \leq 1.0 \tag{2-22}$$

$$k_4 = \frac{f_{yt}}{500} \geq 1.0 \tag{2-23}$$

$$K = \frac{k_1 f_{le}}{f'_{c0}} \tag{2-24}$$

$$\varepsilon_{01} = 0.0028 - 0.0008k_3 \tag{2-25}$$

$$\varepsilon_{085} = \varepsilon_{01} + 0.0018k_3^2 \tag{2-26}$$

Finally, the ascending branch of the curve could be generated by adopting the expression proposed by Mander et al. (1988a) in Equations 2-3 to 2-6. It should be noted that notation ε_{cc} in those equations is identical to ε_1 in Equation 2-20. ρ_c is the area ratio of confining element with respect to concrete in both directions.

2.3.5   Azizinamini et al. (1994)

Azizinamini et al. (1994) proposed simple bi-linear stress-strain relationship for High-Strength confined concrete. The shape of the proposed model can be seen in Figure 2-17. The peak stress, f_0, and its corresponding strain, ε_0, were adopted from Yong et al. (1988) as in Equations 2-14 and 2-15. The whole axial stress-strain model depended on the strength of unconfined and confined conrete, tie spacing, volumetric ratio of lateral steel, area ratio of longitudinal steel, yield strength of lateral steel, and strain corresponding to peak confined stress. This model showed good agreement against experimental data presented by Yong et al. (1988).
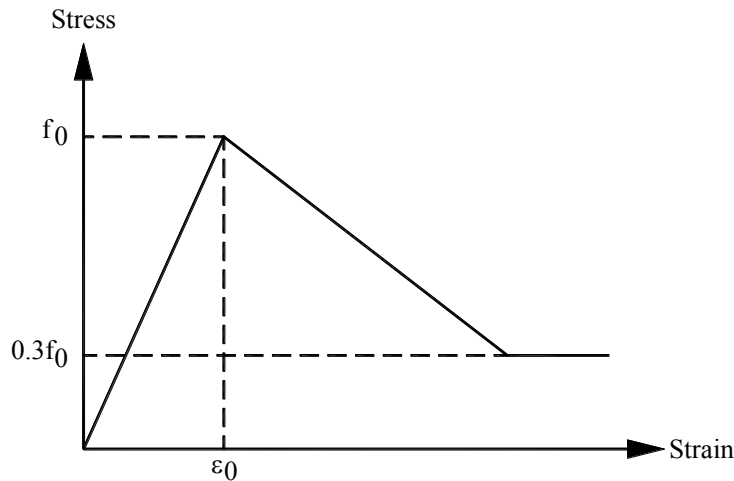
Figure 2-17 Stress-strain relationship proposed by Azizinamini et al. (adopted from Azizinamini et al., 1994)

2.3.6   Hoshikusuma et al. (1997)

Hoshikusuma et al. (1997) proposed a stress-strain model for confined concrete which covers circular as well as rectangular sections. Three parameters were identified as significant factors affecting the curve, namely the peak stress, strain at peak stress, and deteriorating rate of the descending branch. The model consisted of 2nd degree parabolic ascending branch, and linear descending branch which was shown in Figure 2-18. The peak stress, f'_{cc}, and strain at peak stress, ε'_{cc}, were given in Equations 2-27 and 2-28.

26

$$f'_{cc} = f_{c0} \left(1.0 + 3.8\alpha \frac{\rho_s f_{yh}}{f_{c0}} \right)$$ (2-27)

$$\varepsilon'_{cc} = 0.002 + 0.033\beta \frac{\rho_s f_{yh}}{f_{c0}}$$ (2-28)

f_{c0} is strength of unconfined concrete; ρ_s is volumetric ratio of lateral reinforcement; f_{yh} is yield strength of lateral reinforcement; α and β are coefficients which equal to 1.0 for circular sections, and 0.2 and 0.4 for rectangular sections, respectively. The parabolic ascending and linear descending branches were given in Equations 2-29 and 2-30.

$$f_c = E_c \varepsilon_c \left(1.0 - \frac{1}{n} \left(\frac{\varepsilon_c}{\varepsilon'_{cc}} \right)^{n-1} \right)$$ (2-29)

$$f_c = f'_{cc} - E_{des}(\varepsilon_c - \varepsilon'_{cc})$$ (2-30)

n is coefficient which depends on elastic modulus E_c, f'_{cc} is the peak stress and ε'_{cc} is the strain corresponding to the peak stress; E_{des} is deterioration rate of descending branch. This rate was developed from regression analysis of experimental data ranged from peak stress to half of the peak stress, which resulted in Equation 2-31.

$$E_{des} = \frac{11.2 f_{c0}^2}{\rho_s f_{yh}}$$ (2-31)
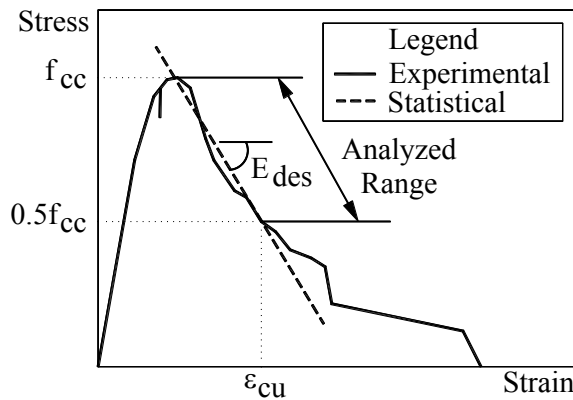
Figure 2-18 Stress-strain relationship proposed by Hoshikusuma et al. (adopted from Hoshikusuma et al., 1997)

2.3.7 Legeron and Paultre (2003)

Legeron and Paultre presented a new confinement model based on strain compatibility and transverse force equilibrium. This model was capable of predicting behavior of High-Strength Concrete confined with high-yield strength steel. Since the stress in high yield strength transverse steel might not reach its yield strength, this approach introduced step by step incremental method. In each step, due to different confinement level, the parameters corresponding to this confinement level should be recalculated. The basic shape of the model was still adopted from previous study (Cusson and Paultre, 1995) as seen in Figure 2-19.
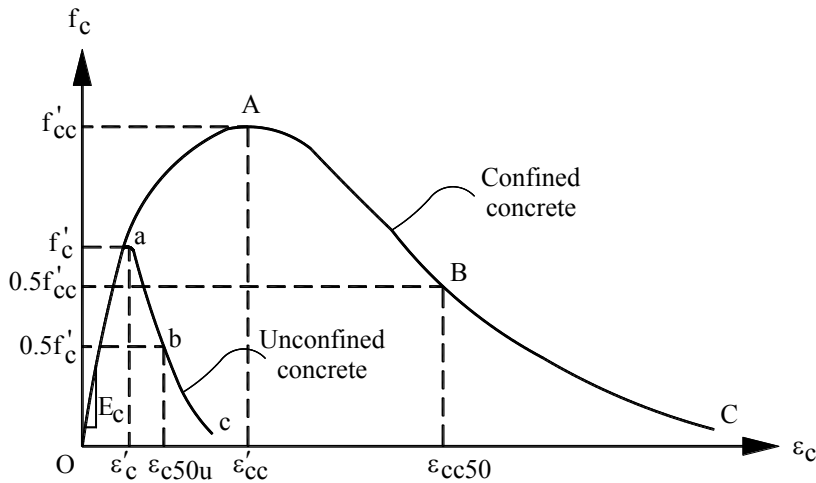
Figure 2-19 Stress-strain relationship proposed by Cusson and Paultre (adopted from Cusson and Paultre, 1995)

The step by step incremental approach was begun by choosing any initial strain value, ε_c. Secondly, the stress at transverse steel, f_h, was initially assumed as its yield strength, f_{yh}. The lateral confining stress, f_{le}, could be determined by using Equations 2-11 to 2-13 (yield stress of transverse steel are substituted with f_h). Further, expressions in determining the peak strengh, f'_{cc}, strain at peak stress, ε'_{cc}, as well as calculated strain of the transverse steel, ε_h, (of this step) can be found in the original paper. At the end of the iteration, the updated transverse steel stress, f_h, could be calculated by using its material properties. This updated value should be used to replace initial assumption, and the whole steps must be

28

repeated for convergence. Finally, once the convergence was obtained for the current step, the strain, ε_c, was increased for the next step to obtain next point in the curve. The whole process was repeated to generate complete stress-strain relationship curve in Figure 2-19.

2.3.8 Tabsh (2007)

Tabsh (2007) proposed stress-strain relationship model for High-Strength Concrete confined by Welded Wire Fabric. The model was verified against experimental data, and compared to models suggested by others. Typical comparison of the stress-strain relationship can be seen in Figure 2-20. Where previous models poorly predicted the ductility of such columns, Tabsh model showed very reasonable agreement. It should be noted, that experimental data used for comparison only consisted of specimens with confinement volumetric ratio ρ_s ranged from 3.5 to 5.0 percent. In the model, the peak stress, f_{cc}', and strain at peak stress, ε_{cc}', were empirically given as expressed in Equations 2-32 to 2-35.

$$f_{cc}' = f_c'(1.0+7\rho_s) \tag{2-32}$$

$$\varepsilon_{cc}' = \varepsilon_{c0}(650000\rho_s^{3.8}) \tag{2-33}$$

$$\varepsilon_{c0} = \left(\frac{f_c'}{E_c}\right)\left(\frac{m}{m-1}\right) \tag{2-34}$$

$$m = \frac{f_c'}{17}+0.8 \tag{2-35}$$

E_c is the concrete elastic modulus and all unit are in MPa. The ascending branch was adopted from Mander et al. (1988a), while the descending branch was adopted from ascending part of Hoshikusuma et al. (1997).
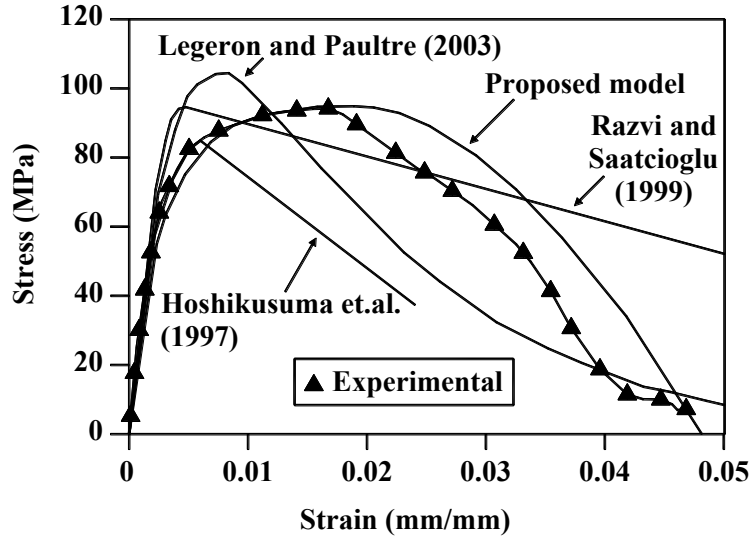
Figure 2-20 Stress-strain relationship proposed by Tabsh compared to experimental data and other models (adopted from Tabsh, 2007)

2.3.9   Kusuma and Tavio (2007)

Similar to Tabsh (2007), Kusuma and Tavio proposed stress-strain relationship model for High-Strength Concrete confined by Welded Wire Fabric (WWF). By using experimental data from Tabsh (2007), some new empirical expressions were proposed. The illustration of the model can be seen in Figure 2-21. The peak stress, f'_{cc}, and strain at peak stress, ε'_{cc}, were expressed in Equations 2-36 to 2-40.

$$f'_{cc} = f'_c(1.324 f_L^{0.13})$$ (2-36)

$$\varepsilon'_{cc} = \varepsilon_{c0}(1 + 3273\alpha w_L^{4.1})$$ (2-37)

$$f_L = \left(\frac{d_t}{C_i}\right)\alpha\rho_s f_{yh}$$ (2-38)

$$\alpha = \left(1 - \frac{\sum C_i}{6b_c d_c}\right)\left(1 - \frac{s}{2b_c}\right)\left(1 - \frac{s}{2d_c}\right)$$ (2-39)

$$w_L = \frac{\rho_s f_{yh}}{f'_c}$$ (2-40)

f'_c is the unconfined concrete strength; ε_{c0} is the strain at unconfined concrete strength (adopted from Tabsh 2007, Equations 2-34 and 2-35); d_t is the diameter

30

of WWF reinforcement; C_i is the size of WWF cell; ρ_s and f_{yh} are the volumetric ratio and yield strength of WWF, respectively; s is the spacing of WWF; b_c and d_c are the core dimensions in both orthogonal directions. Kusuma and Tavio adopted Mander model for the ascending part (Equations 2-3 to 2-6), and modified parabolic expression of Muruguma (1993) model as descending part, as shown in Equations 2-41 and 2-42.

$$f_{cc} = \frac{-0.5 f'_{cc}}{\left(\varepsilon_{cc50} - \varepsilon'_{cc}\right)^2}\left(\varepsilon_c - \varepsilon'_{cc}\right)^2 + f'_{cc} \tag{2-41}$$

$$\varepsilon_{cc50} = \varepsilon_{c0} + 2.9\alpha w_L^{3.1} \tag{2-42}$$
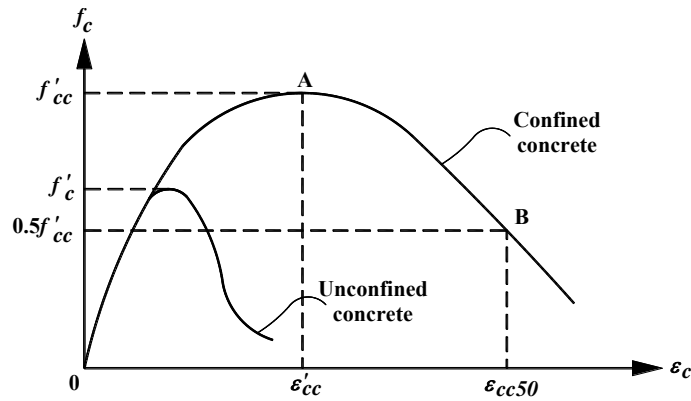
Figure 2-21 Stress-strain relationship proposed by Kusuma and Tavio (adopted from Kusuma and Tavio, 2007)

2.3.10 Kusuma and Tavio (2008)

Kusuma and Tavio (2008) proposed a unified stress-strain model for confined concrete. This model based on extensive experimental data that covered normal and high-strength concretes and steels. The complete stress-strain curve can be seen in Figure 2-22. The ascending branch was adopted from Sargin model (Sargin, 1971), given as in Equations 2-43 and 2-44:

$$f_c = f'_{cc}\left(\frac{K_b \varepsilon_b - \varepsilon_b^2}{1 + \left(K_b - 2\right)\varepsilon_b}\right) \tag{2-43}$$

31

$$f'_{cc} = f'_c \left(1 + 3.7 \frac{f_{le}}{f'_c} \right) \qquad (2\text{-}44)$$

where :

$$K_b = \frac{E_c \varepsilon'_{cc}}{f'_{cc}} \; ; \quad \varepsilon_b = \frac{\varepsilon_c}{\varepsilon'_{cc}} \; ; \quad E_c = 0.043 w_c^{1.5} \sqrt{f'_c} \; ; \quad f_{le} = \frac{1}{2} \mathrm{k}_e \, \rho_s f_{yh}$$

and f'_c is the unconfined concrete strength (MPa); w_c is the unit weigth of concrete (kgf/m^3); ρ_s is the volumetric ratio of confinement steel; f_{yh} is the confinement steel yield strength; k_e is the confinement effectiveness factor which depend on sectional shape, core dimensions, transverse and longitudinal bar spacings (see original literature). The descending branch was defined by Equations 2-45 to 2-47.

$$f_c = f'_{cc} - E_{des} \left(\varepsilon_c - \varepsilon'_{cc} \right) \qquad (2\text{-}45)$$

$$\varepsilon'_{cc} = 0.0029 + 0.055 \left(\frac{f_{le}}{f'_c} \right) \qquad (2\text{-}46)$$

$$E_{des} = \frac{12.2 f'^2_c}{\rho_s f_{yh}} \qquad (2\text{-}47)$$
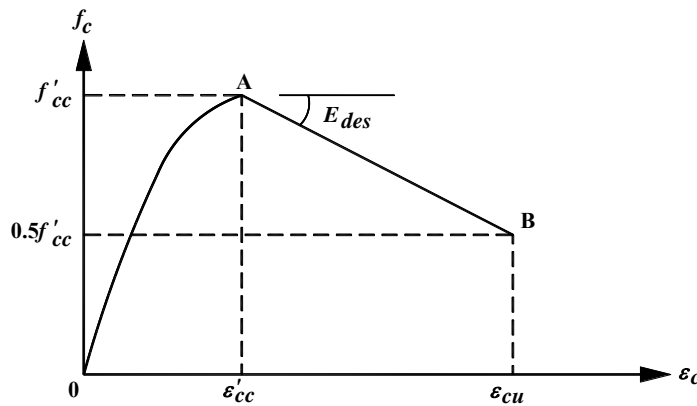
Figure 2-22 Stress-strain relationship proposed by Kusuma and Tavio (adopted from Kusuma and Tavio, 2008)

32

2.3.11 Tavio et al. (2008b)

Tavio et al. (2008b) proposed stress-strain relationship of confined High Strength Concrete with High Strength lateral steels. The stress-strain model consisted of parabolic ascending branch (which adopted Mander et al., 1998a, Equations 2-3 to 2-6), and linear descending branch, and residual strength equal to 30 percent of the peak confined strength. The expressions of descending branch were given by Equations 2-48 to 2-52:

$$f_c = f'_{cc}\left[1 - 0.85\left(\frac{\varepsilon_c - \varepsilon'_{cc}}{\varepsilon_{cc85} - \varepsilon'_{cc}}\right)\right] \tag{2-48}$$

$$f'_{cc} = f'_c\left(1 + 0.626\left(\frac{f_{le}}{f'_c}\right)\right) \tag{2-49}$$

$$\varepsilon'_{cc} = \varepsilon_{c0}(1 + 363(k_3 K)^{1.06}) \tag{2-50}$$

$$\varepsilon_{cc85} = \varepsilon_{c0}\left(1 + 23.79\left(k_3 \frac{\rho_s f_{yh}}{f'_c}\right)\right) \tag{2-51}$$

$$\varepsilon_{c0} = 0.0028 - 0.0008k_3 \tag{2-52}$$

where ε_c is the concrete strain; f_{le} is the effective lateral pressure (adopted from Mander model, Equation 2-7); f'_c is the unconfined concrete strength; ρ_s is the volumetric ratio of confinement steel; f_{yh} is the confinement steel yield strength; k_3 and K are the coefficients adopted from Razvi and Saatcioglu (1999) which depend on effective lateral presssure, unconfined concrete strength, volumetric ratio of confinement and steel.

2.3.12 Tavio et al. (2008a)

Due to enormous uncertainties in confinement models associated with the maximum compressive strength and ductility of concrete confined by rectilinear ties, Tavio et al. (2008a) implemented a spline nonparametric regression analysis as an alternative approach. The statistical evaluation was carried out based on 128 large-scale column specimens of either normal or high strength concrete tested

under uniaxial compression. The main advantage of this kind of analysis was that it can be applied when the trend of relation between predictor and response variable were not obvious. The error in the analysis could be minimized so that it did not depend on the assumption of a particular shape of the curve. This provided higher flexibility in the application. The developed empirical equations could be summarized in Equations 2-53 to 2-55:

$$\hat{y}_1 = 2.52 + 2.63x_1 - 0.06x_1^2 + 0.05\left(x_1 - 13.5\right)_+^2 \qquad (2\text{-}53)$$

$$\hat{y}_2 = 0.94 - 12.1x_2 + 164.68x_2^2 - 142.28\left(x_2 - 0.07\right)_+^2 \qquad (2\text{-}54)$$

$$\hat{y}_3 = -0.005 + 0.26x_3 - 0.66x_3^2 + 0.71\left(x_3 - 0.16\right)_+^2 \qquad (2\text{-}55)$$

where $\hat{y}_1 = f'_{cc} - f'_{c0}$ is the strength gain; $x_1 = K_e\rho_s f_{yh}$; $\hat{y}_2 = \left(\varepsilon_{cc}/\varepsilon_{c0}\right) - 1$; $x_2 = K_e\omega_w$; $\hat{y}_3 = \varepsilon_{c50c} - \varepsilon_{c0}$; and $x_3 = K_e\omega_w$. The results of the statistical analysis indicated that the stress-strain curves of confined concrete obtained from the spline nonparametric regression analysis were in good agreement with the experimental curves (Figure 2-23).
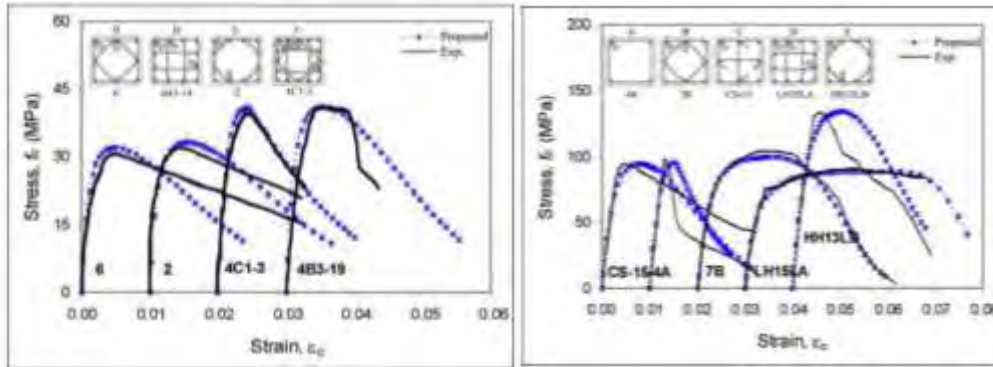
(a)   (b)

Figure 2-23 Comparison of proposed and experimental stress-strain relationship of: (a) normal concrete; and (b) high strength concrete (Tavio et al., 2008a)

2.4 EXTERNAL CONFINEMENT TECHNIQUES OF REINFORCED CONCRETE COLUMNS

2.4.1 General

As described in previous chapter, RC columns are critical members in most framed structures. Their commonly brittle failures (due to high axial loads) can lead to overall structure collapse. Retrofitting efforts have been done to prevent brittle (usually shear) failures in RC columns. Early efforts involved the installment of additional longitudinal as well as transversal bars covered by new concrete jacketing. Although proven to be effective in enhancing the performance of RC columns, this technique was found labor-intensive and time-consuming. Moreover, the larger dimension (due to application of concrete jacket) increases the stiffness, and in turn will attract larger earthquake induced inertia forces. To lessen those problems, recent researches have been done to develop alternative retrofit techniques such as steel jacketing, fiber reinforced polymer (FRP) jacketing, external strand prestressing, and steel collar jacketing. Some researches on these techniques are described in the following sections.

2.4.2 Steel Jacketing

After San Fernando Earthquake in 1971, many bridge piers were retrofitted due to the lack of confinement. Typically, the ratio of transverse reinforcement was only 0.1 to 0.2 percent, which was lower than one fifth of the required amount specified by Caltrans (California Department of Transportation) code that time. The most commonly used retrofit approach was the steel shell jacketing. Steel shell jacket was made with dimension slightly larger than the column. Gap between the jacket and concrete was filled with grout. Many research had proven that this system was effective in enhancing concrete compressive strength, ductility, and concrete shear strength of columns. Chai et al. (1994) showed that steel jacket with volumetric ratio of 3.1 percent could provide good ductility (as large as 7), and drift ratio of 5 percent. The bond failure of circular columns due to the lack of lap splice length of longitudinal reinforcements could be prevented by this steel jacket. However, in non-circular

section, this approach included a modification of the sections into elliptical shapes. The illustration of the steel jacket and enhancement of the hysteretic performance of retrofitted columns could be seen in Figures 2-24 and 2-25.
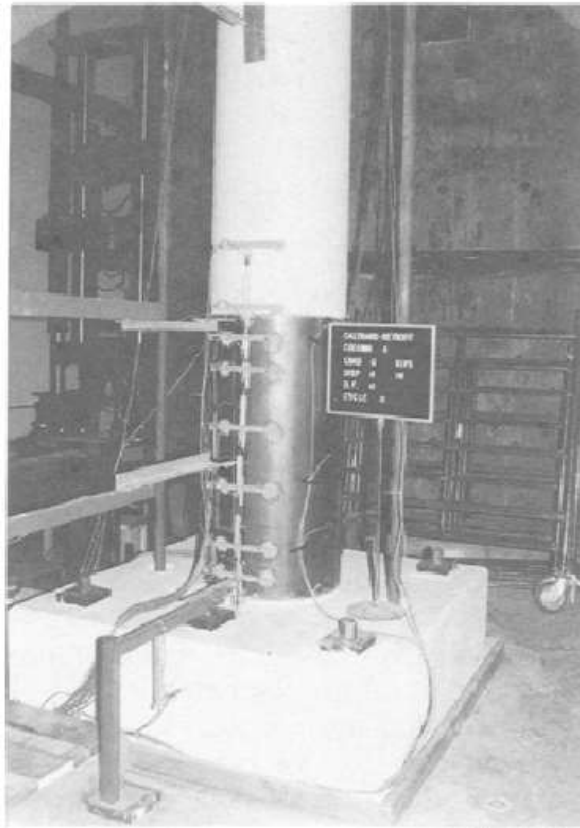
Figure 2-24 Steel jacket used to retrofit column (courtesy of Chai et al., 1994)
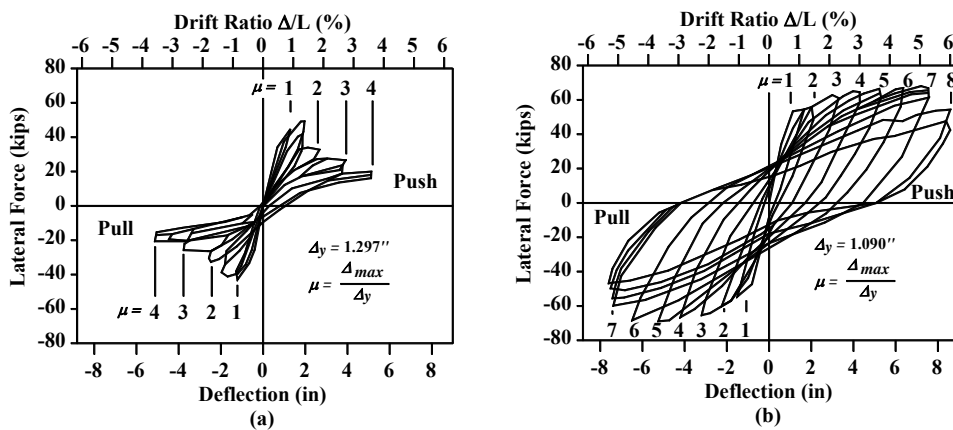
Figure 2-25 Comparison of hysteretic responses: (a) original column and (b) retrofitted column (adopted from Chai et al., 1994)

However, the enhancement of the performance of retrofitted columns was accompanied by increment of the flexural stiffness. The increase of the stiffness

36

depended on the dimension of steel jacket used, and bond strength between the steel jacket and the grout. This stiffness increment, typically would generate more inertia force due to the shifting of natural period as seen in Figure 2-26. Chai et al. (1994) mentioned that installation of steel jacket with width equal to twice of column's diameter would improve the flexural stiffness as much as 10-15 percent.
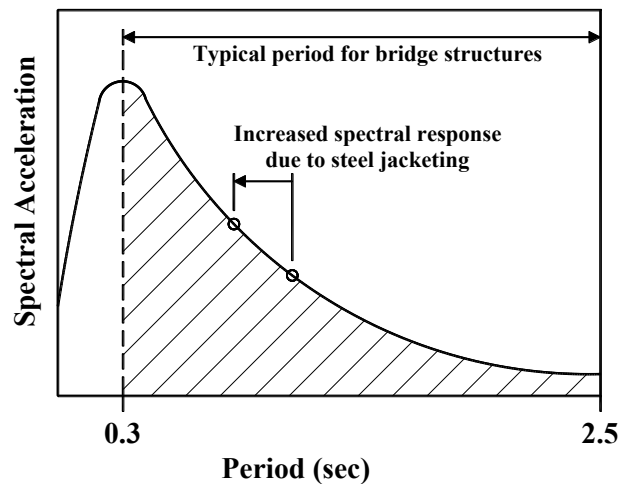
Figure 2-26 The increase of inertia force due to steel jacket retrofitting method (adopted from Chai et al., 1994)

Priestley et al. (1994) used circular cylindrical and elliptical steel jackets to retrofit circular and rectangular columns. Fourteen column specimens were tested under cyclic lateral displacement to study the proposed model (Priestley et al., 1994). The parameters included in the test were longitudinal steel strength, aspect ratio, and sectional shapes. Four unretrofitted circular columns showed shear failure at displacement ductility less than 3, while the four retrofitted ones showed ductile behavior with ductility value more than 8, and drift more than 4 percent. Damage in unretrofitted columns was initiated by horizontal flexural cracks, followed by inclined shear cracks. In retrofitted columns, after removal of the steel jackets, no significant damage was found. Spalling of concrete cover only occurred as much as 10 cm from the critical section. Three unretrofitted square columns suffered brittle low ductility shear failure with pattern similar to that of circular columns. The maximum displacement ductility reached was not more than 3. Three retrofitted square columns, modified to elliptical sections and confined by elliptical steel jackets, showed flexural behavior with high ductility.

37

The average value of over-strength in retrofitted columns was about 1.29. The capacity of energy absorbtion of retrofitted columns was about 150 times larger than that of the unretrofitted columns. This high energy absorbtion capacity indicated that steel jacket retrofitting method had excellent performance during large long duration earthquakes. It was also found that degradation of response was inevitable for rectangular columns confined by rectangular jackets, even when very thick jackets were used. This was primarily due to inadequate confinement of concrete in the flexural plastic hinge region, rather than due to inadequate shear performance (see Figure 2-27).
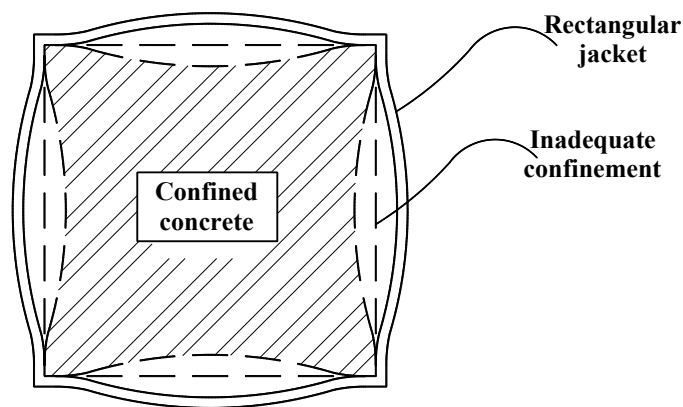
Figure 2-27 Inadequate confinement by rectangular jacket (adopted from Priestley et al., 1994)

Xiao et al. (2003) mentioned that the use of elliptical jackets to enhance the shear strength of rectangular columns increased the section of the columns substantially, thus, it might not be desirable. In the research, another improved jacketing method to retrofit square columns using welded rectilinear steel jacket and stiffners was developed. Five reinforced concrete column models were identically designed and constructed. The reinforcement details simulated existing columns designed and built based on pre-1971 codes. Four of them were retrofitted as seen in Figure 2-28. All four specimens were retrofitted with a rectilinear steel jacket for shear enhancement only. The steel jacket was designed to provide the required shear strength for retrofit. Three of the four retrofitted specimens were further retrofitted with stiffeners in the potential plastic hinge regions. The three stiffner types were thick steel plates, angles, and square tube.
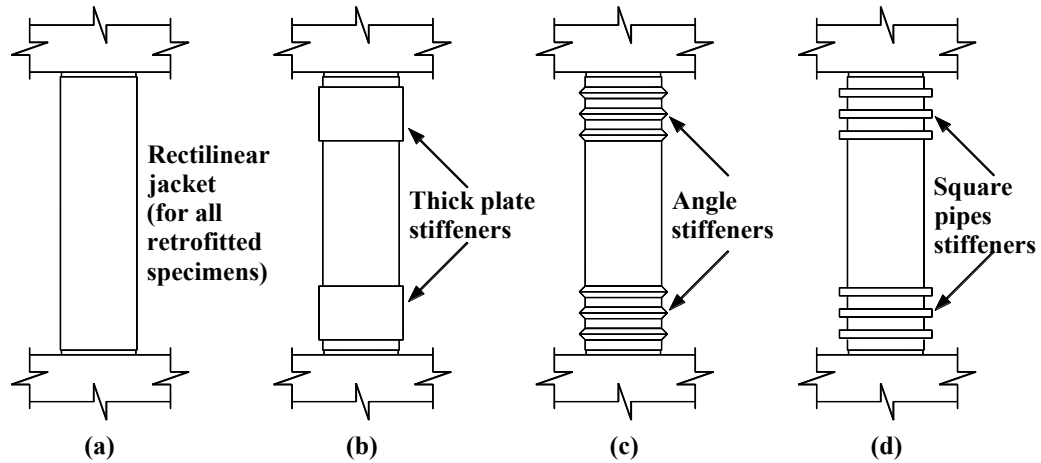
Figure 2-28 Detail of retrofitted specimens (adopted from Xiao et al., 2003)

The specimens were tested under constant axial load (30 percent of $A_g f_c'$) and lateral cyclic load based on displacement control. As built specimens (without retrofit) suffered brittle shear failure. The force-displacement hysteretic relationship was characterized by severe degradation. Slight improvement had been shown by specimen retrofitted with rectilinear steel jacket only. Because of inadequate confinement of concrete, degradation of response was inevitable at large displacement. The jacket provided enough additional shear strength to enable the development of the flexural capacity and the limited ductility. But the stiffness of the thin jacket out of plane direction was insufficient to effetively confine concrete. It could be seen by the bulging-out of the steel jacket near column ends followed by rupture at welded corners. Thus retrofitting by using the rectilinear steel jacket alone was not sufficient for achieving a ductile response. The three specimens retrofitted by rectilinear steel jacket stiffned by confinement elements showed greatly improved behaviour. The brittle shear failure was completely prevented. Significantly increased ductility and stable hysteretic behaviour was observed, with ultimate drift ratio exceeding 8 percent.

Guo et al. (2006) conducted experimental study on retrofitted RC columns by prestressed steel jacket (Figure 2-29). The Prestressed Steel Jacket (PSJ) was composed of two part of U-shape steel straps. A gap was intentionally remained between the steel straps for the purpose of prestressing the steel jacket. The prestressed force was applied by screwing two high strength bolts on the two suits

39

of strengthened plate of a PSJ simultaneously with two spanners. To lubricate the stress transmission in different side of a steel jacket during prestressing, the four corners of a specimen column were chamfered, and four arc-shape steel plates were glued to each corner of the column by structural adhesive. Six half-scale RC columns were designed seismically deficient and a shear failure rather than flexural failure would be expected. Five of them were retrofitted with main variables included the prestressed level (ratio of the prestressed jacket strain to its yield strain) and the axial compressive strain. A predetermined axial load was applied to the column, and the transverse load was applied. The whole loading procedure finished when the bearing capacity of the specimen was reduced to 85 percent of the maximum load or the hysteretic curves appeared distinctly unstable. It was observed that shear cracks in retrofitted specimens were suspended, especially in specimens with more prestressed level of SJ. In specimen with low prestressed level (0.15), the steel jacket attained its yield strain at a displacement ductility of 4.0. On the other hand, in specimens with high prestressed level (>0.35), the steel jacket remained elastic when they reached ultimate failure because the concrete core of the columns were all effectively confined by PSJ, and no obvious transverse deformation was observed. Hysteretic character showed that those retrofitted specimens experience longer plastic phase and show much better ductility than that of unretrofitted specimen. The ultimate deformation and displacement ductility of the retrofitted specimens increased over 3 times than that of the unretrofitted specimen.

(a) Chamfering   (b)Strengthening column corners   (c) Specimen after being prestressed
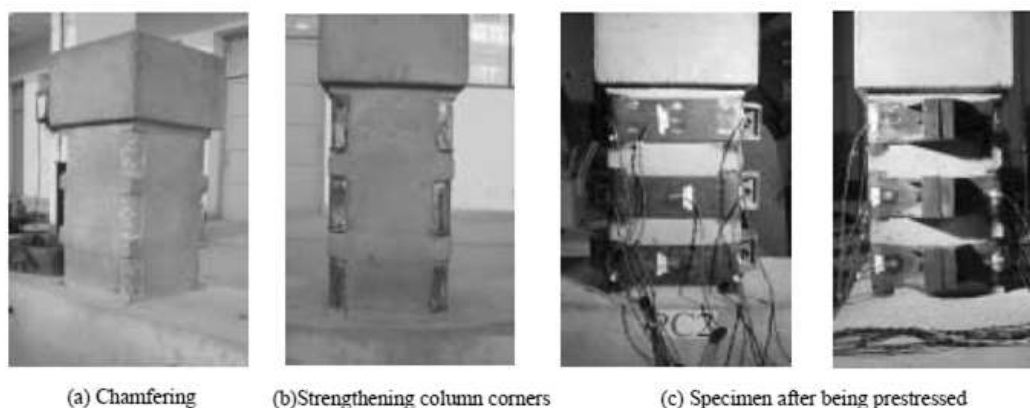
Figure 2-29 Prestressed steel jacketing (courtesy of Guo et al., 2006)

Choi et al. (2010) proposed a new steel-jacketing method that used external application of lateral pressure to attach steel sheet jacket. It did not require the application of grout between steel sheet jackets and the concrete surface. Composite behavior was not expected between the concrete and steel sheet jacket thus solved the problem of increasing the lateral stiffness of the columns. The new method offered the following advantages: (1) non increase in the cross section of RC columns; (2) no use of adhesive, such as epoxy; and (3) allows for installation of steel jackets at any position of a column. The proposed method can be seen in Figure 2-30. The new jacketing procedure was as follows: (1) wrap the jacket around the cylinder; (2) press the jacket with clamps; (3) weld the overlap line; and (4) weld lateral strip bands crossing the welding line. The thickness of the jackets were 1.0, 1.5, and 2 x 1.0 mm. Results showed that the compressive strength and ductility of specimens retrofitted by the jacket increased greatly. The correlation of jacket thickness and the increased compressive strength was nearly perfect linear. Thus, the result proved that the double-layered jacket worked as a single jacket with the same total thickness. The vertical strains of the steel jackets were almost undeveloped which meant that the steel jacket did not behave compositely with the concrete. The vertical strains of the steel jackets (developed after axial specimen strain reaches 0.0045) were not from the compression but from the bulge of the concrete.
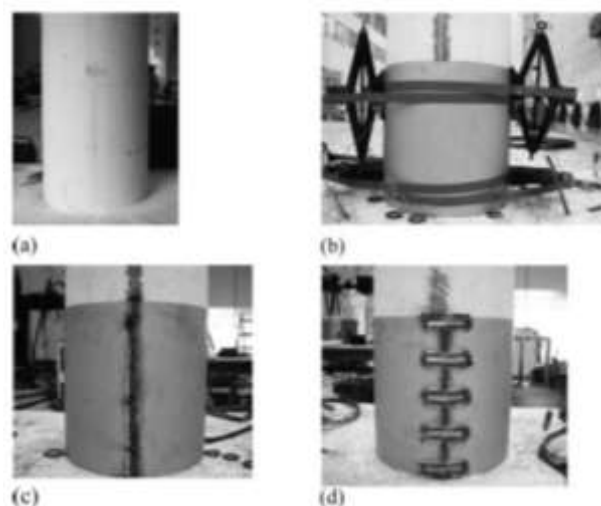
Figure 2-30 Steel sheet jacketing procedure: (a) as-built RC column; (b) apply external pressure on steel sheet jacket; (c) weld overlap line; and (d) weld lateral strip bands (courtesy of Choi et al., 2010)

2.4.3 Fiber Reinforced Polymer (FRP)

Recently, among the existing external confinement techniques for concrete columns, fibre reinforced polymer (FRP) materials have been increasingly considered for use as wraps / jackets / casings, due to their high strength-to-weight and stiffness-to-weight ratios, corrosion, and fatigue-resistance, and overall durability. In most cases, in which premature local failure of fibre due to stress concentration can be prevented, the concrete crushing occurs before the FRP sheet is fully utilized. Thus, it is natural to hope that a more efficient use can be achieved by prestressing the FRP. The FRP jackets are applied to the specimens by using adhesive epoxy or mechanic coupling. Typical illustration of FRP jacketing can be seen in Figure 2-31.
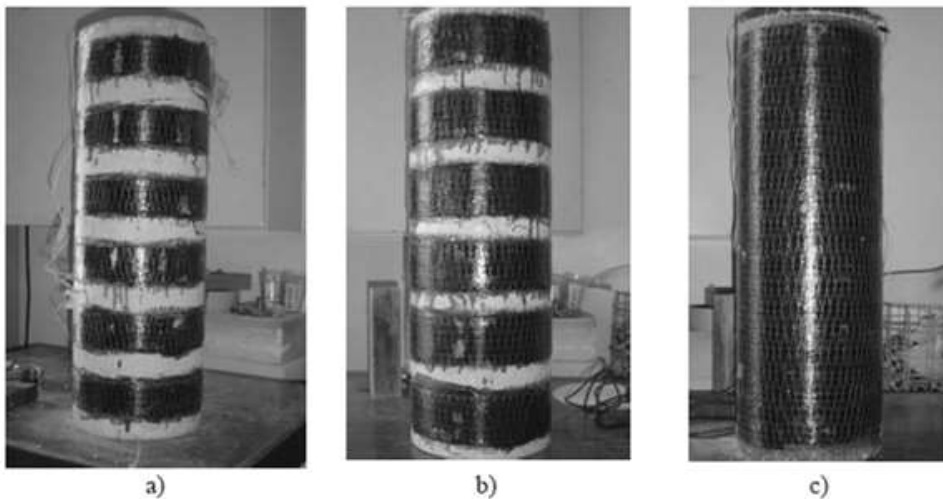
Figure 2-31 FRP sheet jacketing: (a) and (b) apply as strips at certain spacing; (c) apply as continuous sheet (courtesy of Barros et al., 2008)

Tegola et al. (1998) investigated ten standard concrete cylinders confined by filament-wound epoxy-glass tubes. With FRP ratio ranged from 8.9 percent to 13.4 percent, it was found that the compressive strength increased about 3 to 4 times. The ultimate strain significantly increased about 17 to 20 times higher than unconfined cylinder strength.

Saafi et al. (1999) observed axial compression test of 18 concrete filled FRP tubes. Test variables included the type of FRP material (glass and carbon), and their thickness (0.8 mm, 1.6 mm, and 2.4 mm). The test showed increment on

compressive strength as much as 51 to 137 percent and 57 to 177 percent for glass and carbon FRP respectively. The ultimate strain increased about 660 to 1100 percent and 300 to 788 percent for glass and carbon FRP respectively. Typical failure was indicated by fracture of glass FRP along the midheight of the specimens, while a more sudden catastrophic simultaneous failure of both tube and concrete was observed on carbon FRP specimens (Figure 2-32).
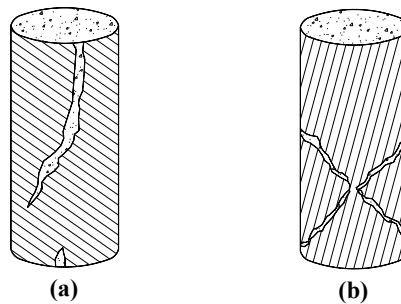
Figure 2-32 Failure mechanim of concrete filled: (a) glass FRP tubes; and (b) carbon FRP tubes (adopted from Saafi et al., 1999)

Nesheli et al. (2004) observed the effect of active confinement provided by prestressing the FRP in comparison with that of passive confinement. Five column specimens were tested in this study. One was left unretrofitted, the other four were retrofitted by using belts of FRP with the variation of FRP meterial used and level of prestressing, while keeping the same lateral stiffness. The prestressing method proposed could be manually done by a simple wrench. A metallic devices with threaded holes were attached at each end of each belt. The prestressing force could be applied by manually screw driving the bolts of the devices (see Figure 2-33). Axial force was applied and kept constant at 0.2 of the concrete cylindrical strength. Lateral loading cycles included three successive cycles at each drift angle range of 0.5, 1.0, 1.5, 2.0, 2.5, and 3.0 percent. To investigate the behavior under large deflections, the loading test continued for larger drifts of 4, 5, and 6 percent, etc. with one cycle for each. Results showed that the unretrofitted specimen failed in a brittle shear mode. The capacity of this column suddenly dropped when a diagonal crack widened at a drift angle of about 3 percent. The specimen retrofitted by non-prestressed carbon belts showed increased maximum lateral strength, and deformation ability. The specimen could mantain its lateral capacity up to about drift ratio of 7.0 percent wih no drop. The specimen

retrofitted with carbon belt prestressed up to 1/6 of ultimate strain did not show considerable difference to the one without initial prestressing. The only difference was the level of damage at final stage. It seemed that active confinement could limit the widening of the cracks once they appear.

Figure 2-33 FRP jacketing method (courtesy of Nesheli et al., 2004)

Carey and Harries (2005) conducted experiment to investigate the behavior of small, medium, and large scale circular concrete column section confined with FRP jackets (see Figure 2-34).
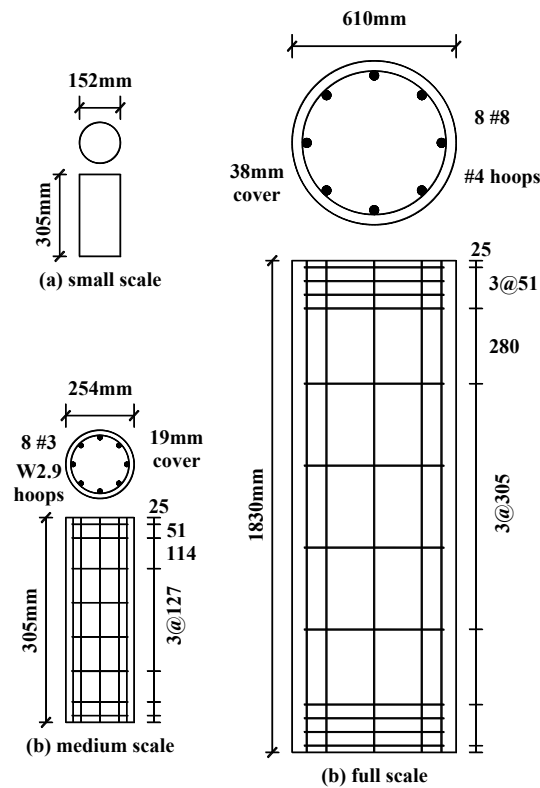
Figure 2-34 Columns dimension tested by Carey and Harries (adopted from Carey and Harries, 2005)

All specimens were tested according to ASTM C39 in a 2224 kN capacity testing machine. Linear displacement transducers were used to measure the axial and hoop strain of the specimens. In comparison with unconfined concrete strength, experiment results showed increment up to about 1.49 and 5.36 times for strength and ultimate strain respectively.

Barros et al. (2008) conducted an experiment to investigate CFRP Reinforced concrete elements subjected by cyclic compressive loading. The experimental included some wrapping arrangements of CFRP reinforcement as seen in Figure 2-31. Strain gauges were installed along the height to measure axial strains. With the basis of unconfined concrete as comparison, the test result showed significant increase in compressive strength (from 1.5 to 2.7 times). The ultimate strains also increased by scale of about 7 to 10 times. As expected, the fully confined specimens showed best results. Complete results can be seen in the original literature. Failure modes of the specimens can be seen in Figure 2-35.

W60L5_c   W60L5_m   W600L3_c   W600L3_m
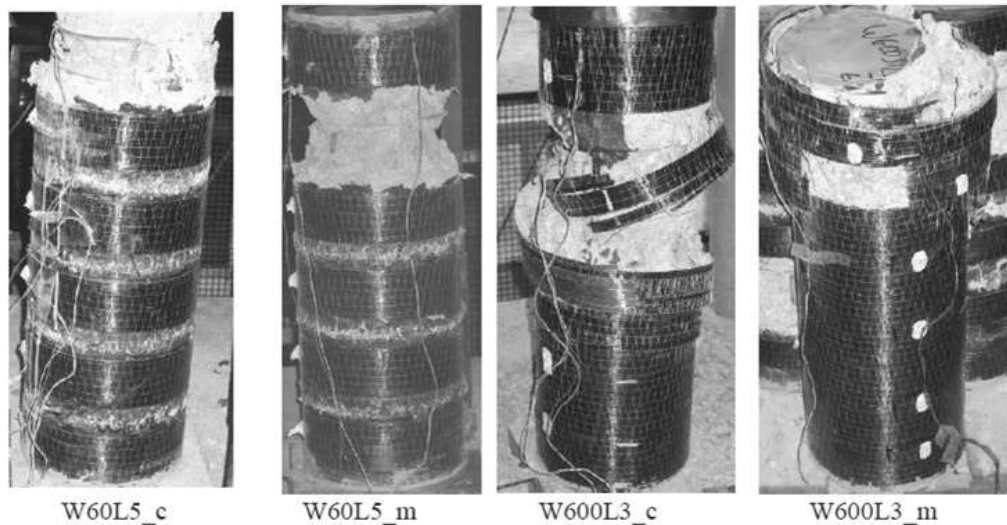
Figure 2-35 Failure modes of the tested specimens (courtesy of Barros et al., 2008)

2.4.4   External Strand Prestressing

Saatcioglu and Yalcin (2003) proposed a method to retrofit RC columns by prestressing external strands. Seven full-scale reinforced concrete bridge columns were tested under constant axial compression and incrementally increasing lateral deformation reversals. They were designed to represent pre-

1970s design practice. Two columns were tested without any retrofit and were used as reference columns. One square and four circular columns were retrofitted by external prestressing prior to testing. Figure 2-36 illustrates the overall geometry of the test specimens. Test variables included the type, spacing, and shape of prestressing hoops, as well as the amount of initial prestressing. For square specimens, semicircular discs (pulleys) were welded on hollow structural sections (HSS) sections at three locations per column side to raise the prestressing strands from the column surface so that the appropriate perpendicular force components could be developed. Illustration of the hardware used to retrofit circular and square columns are presented in Figures 2-37 and 2-38, respectively. From the test, it could be seen that the external retrofitting changed the mode of behavior from diagonal tension to flexure, and the columns failed in flexure. Application of more prestressing and closer spacing enhanced the deformability.
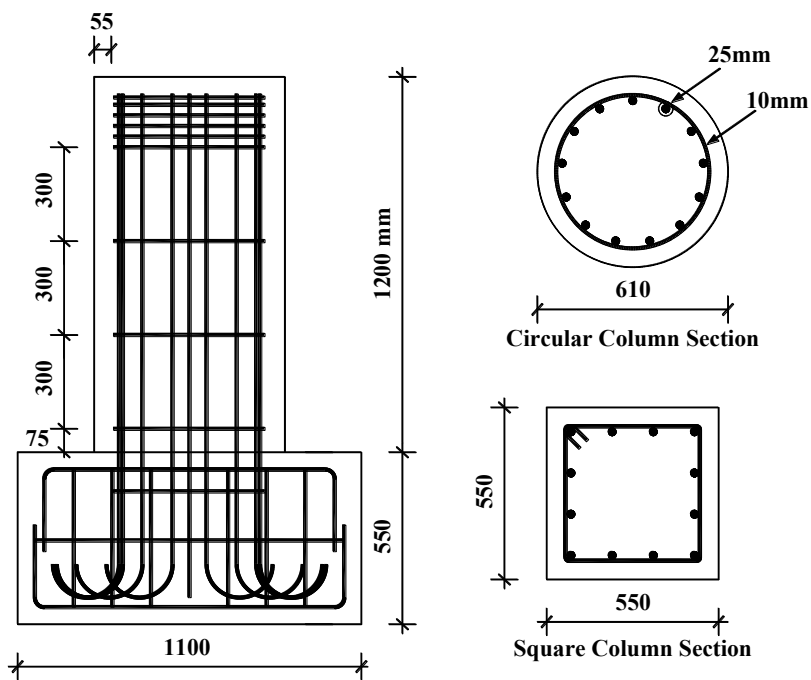
Figure 2-36 Geometry of the test specimens (adopted from Saatcioglu and Yalcin, 2003)
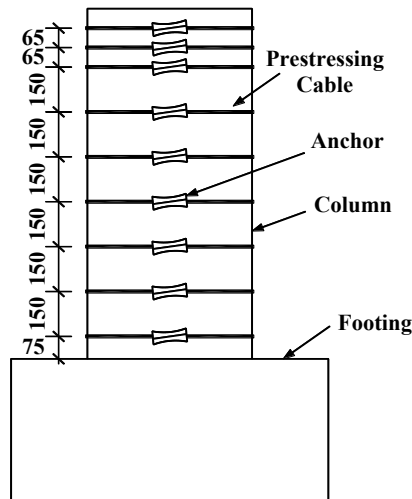
Figure 2-37 Hardware used for retrofitting circular columns (adopted from Saatcioglu and Yalcin, 2003)
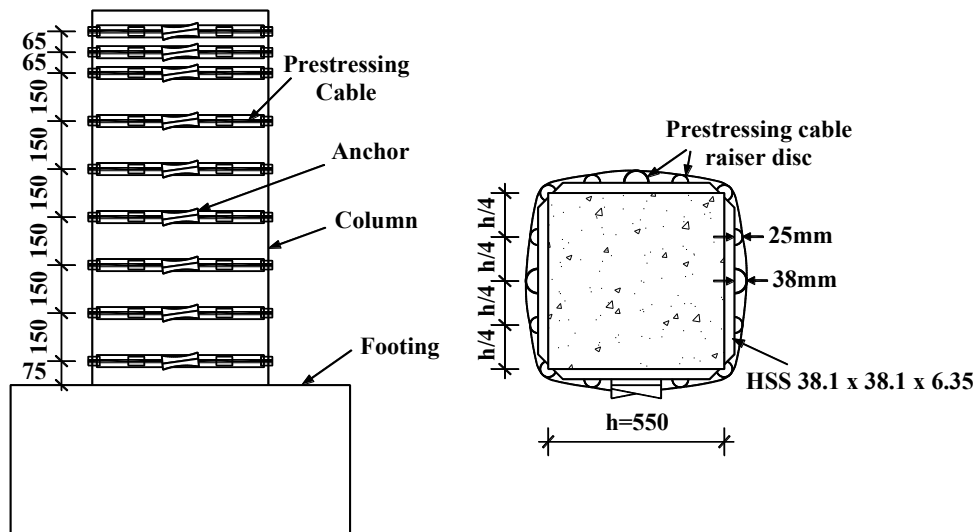
Figure 2-38 Hardware used for retrofitting square columns (adopted from Saatcioglu and Yalcin, 2003)

2.4.5   Steel Collar Jacketing

Hussain and Driver (2005) conducted research on collared columns under concentric axial loading, as well as under combined axial and lateral loading where the flexural behavior was the focus. The confinement method was shown to be effective rehabilitation method. Benefits in both strength and ductility were demonstrated (peak load of most heavily retrofitted column was enhanced almost 2 times of the control column). The external steel collars used in the research were

cut from steel hollow structural sections (HSS), as shown in Figure 2-39. Bolted and welded connections were used to assemble into steel collars.
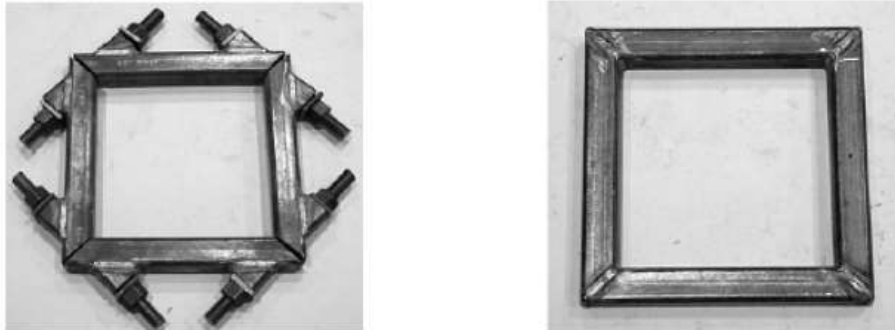
Figure 2-39 Bolted and welded steel HSS collars (courtesy of Hussain and Driver, 2005)

The test experiment done by Hussain and Driver (2005) can be seen in Table 2-1. Results showed that specimens gain increment in both strength and ductility (see Figure 2-40). The welding work was needed in the fabrication and assembly of the collars, which made the process complicated, time consuming, and costly. Hence, a relatively simple, economical alternative was developed as a solid steel collar cut from thick steel plates that requires no welding, as shown in Figure 2-41. Liu et al. (2008) studied RC columns rehabilitated with this solid steel collars under concentric and eccentric axial loading and reported significant enhancement in both the strength and ductility. It was recorded that the specimen could sustain horizontal displacement ductility of 8.0, and ultimate lateral drift of 10.6 percent.

Table 2-1 Data of collared column specimens (Hussain and Driver, 2005)

| Specimen | Transverse Steel | | | | | |
	Type	Size (mm)	Spacing on centers (mm)	Type of corner connection	Cross sectional area (mm2)	Volumetric ratio (%)
C00A	Conventional	$\phi 10$	267	-	100	0.70
C00B	reinforcing bars	$\phi 15$	70	-	200	5.19
C01	Collars made from hollow structural sections (HSS)	HSS 51 x 51 x 6.35	122	Bolted	375*	4.81*
C02		HSS 76 x 51 x 6.35	122	Bolted	375*	5.15*
C03		HSS 76 x 51 x 6.35	122	Bolted	375*	5.15*
C04		HSS 76 x 51 x 6.35	170	Bolted	375*	3.68*
C05		HSS 76 x 51 x 6.35	95	Bolted	375*	6.63*
C06		HSS 51 x 51 x 6.35	122	Welded	1085	13.92
C07		HSS 76 x 51 x 6.35	122	Welded	1375	18.90
C08		HSS 102 x 51 x 6.35	122	Welded	1734	25.48
C09		HSS 76 x 51 x 6.35	170	Welded	1375	13.50

* based on bolts
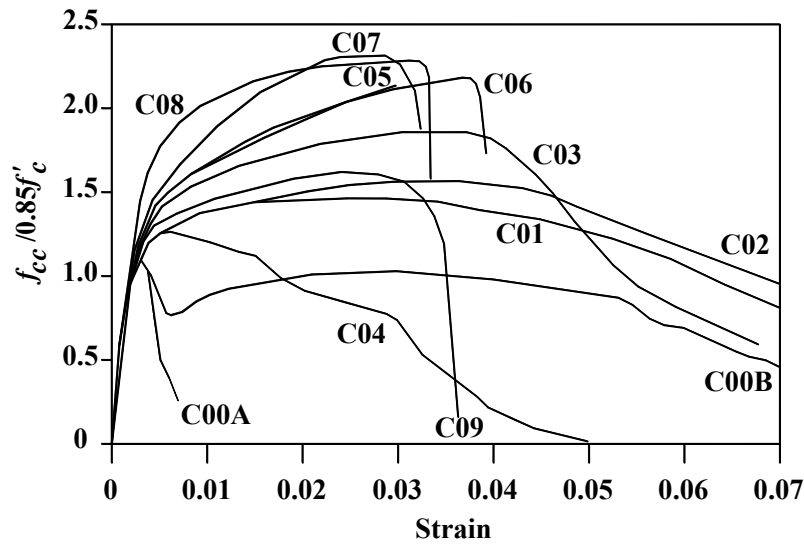
Figure 2-40 Normalized stress-strain of the specimens (adopted from Hussain and Driver, 2005)
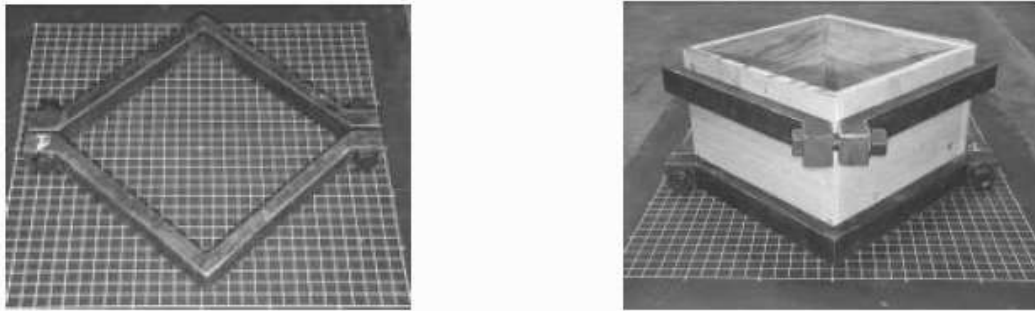
Figure 2-41 Plan and elevation view of bolted solid steel collars (courtesy of Liu et al., 2008)

2.5 STRESS-STRAIN RELATIONSHIP MODEL OF EXTERNALLY CONFINED CONCRETE

The same as conventionally confined concrete, the behavior of stress-strain relationship of externally confined concrete columns attracts the interest of researchers. Some models developed based on conventionally confined concrete model due to its similarity, while some other researchers proposed new approaches. The following sub-sections discusses some analytical models proposed by different researchers.

49

2.5.1   Saafi et al. (1999)

Saafi et al. (1999) studied the behavior of concrete columns confined with FRP tubes. Experimental tests were conducted, and an analytical model fro stress-strain relationship was developed. It was found that stress-strain relationship models developed for steel element confinement showed poor comparison with the test. This poor prediction was caused by different characteristic of FRP and steel. The FRP exhibit linear stress/strain behavior up to failure, and the stress at maximum strain was much higher than typical yield stress of steel (Saafi et al. 1999). This character resulted in bilinear stress-strain behavior (Figure 2-42) without descending branch as typically seen in concrete with steel confinement.
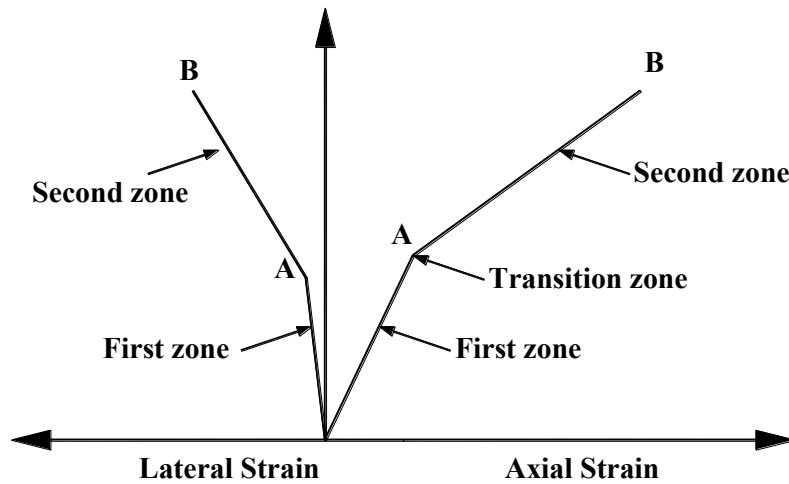
Figure 2-42 Simplified stress-strain curves of FRP-encased Concrete (adopted from Saafi et al., 1999)

In the first zone of Figure 2-42, the concrete primarily took the axial load. The slope of first zone was the same as the slope of unconfined concrete. At this early stage, the Poission's ratio of concrete was lower than FRP which caused no confinement mechanism. The second zone started when the axial stress reached the unconfined concrete axial strength, f'_{c0}. In this point, the concrete started to crack, and FRP started to show its confining characteristic. Thus, point A $\left(\varepsilon'_{c0}, f'_{c0}\right)$ was completely defined by unconfined concrete behavior. For the second zone, Saafi et al. (1999) proposed empirical formula for analytical model as in Equations 2-56 to 2-57:

50

$$f'_{cc} = f'_{c0} \left(1 + 22 \left(\frac{2tf_{com}}{df'_{c0}} \right)^{0.84} \right) \qquad (2\text{-}56)$$

$$\varepsilon'_{cc} = \varepsilon'_{c0} \left(1 + \left(5.37\varepsilon_{com} + 2.6 \right) \left(\frac{f'_{cc}}{f'_{c0}} - 1 \right) \right) \qquad (2\text{-}57)$$

where f'_{cc} and ε'_{cc} are the confined concrete strength and its corresponding strain, respectively which define point B in Figure 2-42; t is the thickness of FRP; f_{com} is the tensile strength of FRP; ε_{com} is the ultimate strain of FRP; and d is the diameter of column.

2.5.2 Fam and Rizkalla (2001)

Fam and Rizkalla (2001) also investigated concrete columns confined with circular FRP tubes. An analytical model of axial stress-strain relationship was proposed. The model was based on equilibrium, compatibility conditions, and the biaxial strength failure condition of the FRP tubes. The assumptions of contact condition as well as confining pressure for an axial load level resulting axial strain of ε_{cc} can be seen in Figure 2-43. This axial strain would generate free radial displacement u_R (Figure 2-43a) as expressed in Equation 2-58:

$$u_R = R\varepsilon_R = R\upsilon_c\varepsilon_{cc} \qquad (2\text{-}58)$$

where υ_c is the Poission's ratio of the concrete; and R is the radius of concrete cylinder. If the concrete confined by radial pressure σ_R (Figure 2-43b), it would shorten as determined in Equation 2-59:

$$u_R = R\varepsilon_R = R\frac{\left(\sigma_R - \upsilon_c\sigma_R \right)}{E_c} = \frac{\left(1 - \upsilon_c \right)}{E_c} R\sigma_R \qquad (2\text{-}59)$$

where E_c is the elastic modulus of the concrete. At the same time, the FRP tube was subjected to the same outward radial stress σ_R (Figure 2-43c). Analyzing half circular confined concrete (similar to condition illustrated in Figure 2-12), the hoop stress of FRP tubes, σ_s, could be expressed in Equation 2-60. In this

condition, the perimeter length of FRP tube increased from $P_0 = 2\pi R$ to $P_1 = 2\pi R_1$. The perimeter length increment $(P_1 - P_0)$ could also be expressed as the product of hoop strain $(\varepsilon_s = \sigma_s / E_s)$ and initial perimeter length, P_0. Equating these two expressions could lead to radial displacement of the FRP tube as seen in Equation 2-61.

$$f_l = \frac{2A_s f_{yt}}{b_c s} \cong \sigma_R = \frac{2ts\sigma_s}{2Rs} \rightarrow \sigma_s = \frac{R\sigma_R}{t} \tag{2-60}$$

$$P_1 - P_0 = \frac{\sigma_s}{E_e} P_0 \rightarrow R_1 - R = \frac{\sigma_s}{E_s} R \rightarrow u_R = \frac{R^2 \sigma_R}{E_s t} \tag{2-61}$$
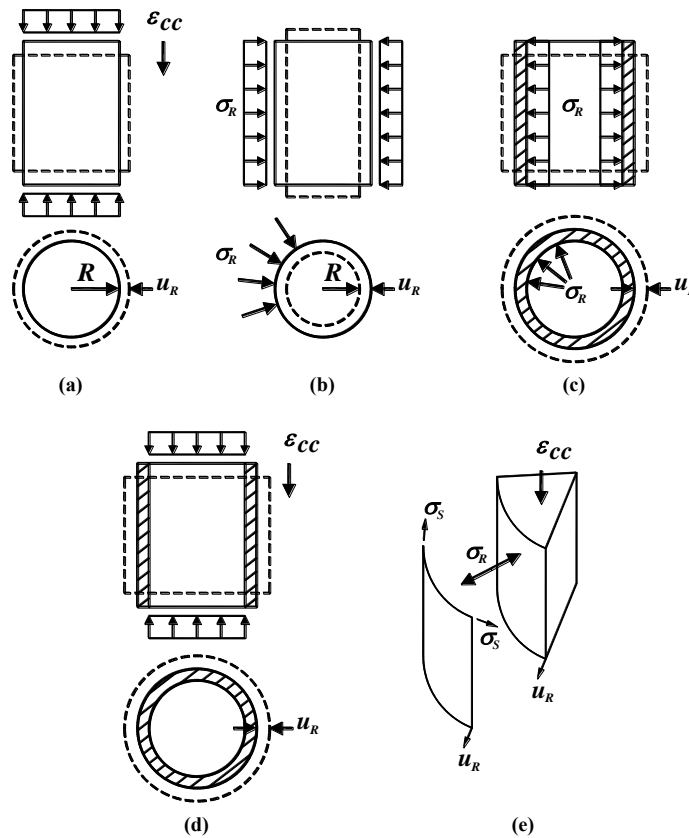
Figure 2-43 Solid concrete cylinder and thin FRP tubes under axial load (adopted from Fam and Rizkala 2001)

Beside the radial displacement as explained in Equation 2-61, there were cases when the same FRP tube was also experienced axial strain, ε_{cc}, which caused the FRP to expand as large as:

$$u_R = R\varepsilon_R = R\upsilon_s\varepsilon_{cc} \qquad\qquad (2\text{-}62)$$

where υ_s is the Poission's ratio of the FRP tube. Depends on the case, with radial displacement compatibility, it could be shown (see original literature) that the radial stress, σ_R, was a function of single unknown variable ε_{cc} (the axial strain).

At this stage, Fam and Rizkalla (2001) adopted expressions from Mander model (Mander et al., 1988a) for axial stress-strain relationship of the confined concrete. A piecewise method was applied, since the radial stress σ_R (which govern the peak strength f'_{cc}) was no longer constant as approaches done for steel confinement elements. The piecewise incremental procedure started with initial small value of axial strain, ε_{cc}. With this axial strain given, concrete's elastic modulus (E_c), concrete's Poisson's ratio (υ_c), hoop stress of FRP (σ_s), and radial confining pressure (σ_R) could be determined. In turn, with lateral confining pressure (σ_R) given, by using Mander model, the concrete peak strength (f'_{cc}), and its corresponding strain (ε'_{cc}), as well as the confined concrete stress corresponding to current axial strain $(f_{cc}(\varepsilon_{cc}))$ could be calculated. This confined concrete stress would result in one particular point in the stress-strain diagram model $(\varepsilon_{cc}, f_{cc}(\varepsilon_{cc}))$. The same procedure was iterated with increased value of axial strain ε_{cc} to obtain the next point and finally the complete stress-strain relationship. The iteration was stopped when the FRP hoop stress (σ_s) exceeded the FRP tensile strength (fracture of FRP tube). The flowchart of this method can be seen in the original literature (Fam and Rizkalla, 2001). The typical result of axial stress-strain behavior was similar to Saafi model (Saafi et al., 1999). No descending branch was observed, but Fam and Rizkalla model showed smoother transition between first and second zones (see Figure 2-44).
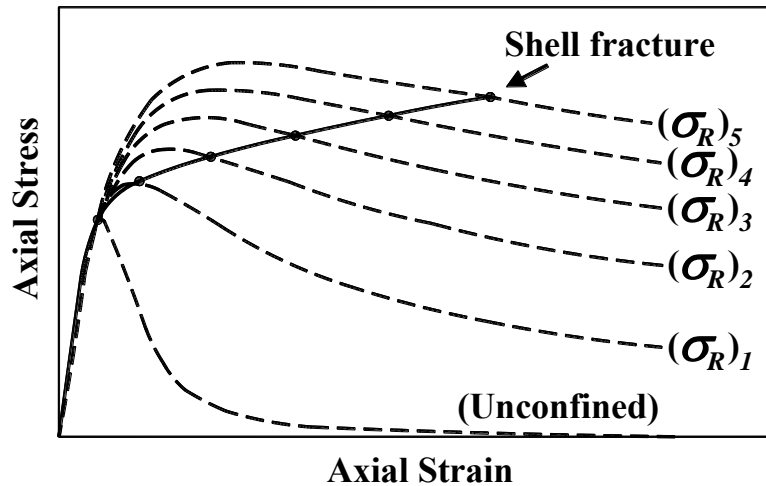
Figure 2-44 Typical stress-strain relationship of confined concrete (adopted from Fam and Rizkala 2001)

2.5.3 Carey and Harries (2005)

Carrey and Harries (2005) recommended analytical model for circular concrete column confined be FRP tubes. Their approach was similar to Saafi et al. (1999) in determining the confining pressure, adopting expressions from steel confinement models (Equation 2-11). The FRP was also assumed to be linear elastic up to rupture. In generating stress-strain curve, piecewise incremental strain method was used (similar to approach by Fam and Rizkalla, 2001). Only details of calculations were different (see original literature), since some new empirical coeffients were used in the proposed model.

2.5.4 Barros et al. (2008)

Barros et al. (2008) conducted experiments on Carbon Fiber Reinforced Polymer (CFRP) confined concrete subjected to cyclic axial loading. Based on the observation, an empiric analytical model for axial CFRP confined concrete was developed. The typical stress-strain model was similar to other researches which contains two zones of approximately linear shapes (see Figure 2-45). The envelope of stress-strain relationship could be described as follows:

$$f_c\left(\varepsilon_c\right) = E_c \varepsilon_c - \frac{\left(E_c - E_{c2}\right)^2}{4 f_{c0}} \varepsilon_c^{\ 2} \qquad \text{for} \qquad 0 \leq \varepsilon_c \leq \varepsilon_{ct} \qquad (2\text{-}63)$$

$$f_c\left(\varepsilon_c\right)=f_{c0}+E_{c2}\varepsilon_c \qquad\qquad \text{for} \qquad \varepsilon_{ct}\leq\varepsilon_c\leq\varepsilon_{cc}^{CPC} \qquad (2\text{-}64)$$

where f_{c0} is the unconfined concrete strength; E_c is the initial elastic modulus of concrete; $\varepsilon_{ct}=\left(2f_{c0}\right)/\left(E_c-E_{c2}\right)$ is the strain at transition zone; and ε_{cc}^{CPC} is the ultimate strain; $E_{c2}=\left(f_{cc}^{CPC}-f_{c0}\right)/\varepsilon_{cc}^{CPC}$ is the tangential Young's modulus. From experimental results, the confined plain concrete strength $\left(f_{cc}^{CPC}\right)$ and its corresponding strain $\left(\varepsilon_{cc}^{CPC}\right)$ were empirically determined as follows:

$$f_{cc}^{CPC}=\left(1.8244\rho_f+0.9431\right)f_{c0} \qquad\qquad (2\text{-}65)$$

$$\varepsilon_{cc}^{CPC}=\left(-14.696\rho_f{}^2+23.691\rho_f-2.0105\right)\varepsilon_{c0} \qquad (2\text{-}66)$$

where ε_{c0} is the strain corresponding unconfined concrete strength $\left(f_0\right)$; and ρ_f is the CFRP volumetric ratio.
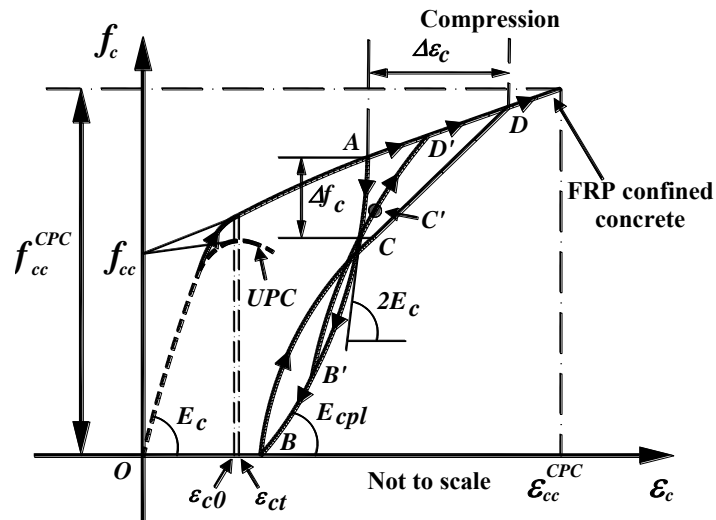
Figure 2-45 Typical stress-strain relationship of CFRP confined concrete (adopted from Barros et al., 2008)

2.5.5   Lee et al. (2010)

Lee et al. (2010) proposed an analytical model for FRP jacketed square concrete column in axial compression. Similar to steel confinement model, FRP confinement model on square concrete section also experiences non-uniform

55

confining pressure. It had high confining stress at corners due to stiff membrane action, and decreases to minimum at the mid-side due to weak flexural rigidity. To minimize the problem, it was suggested to round the corners of the square section, but still, the effectively confined area should be defined (see Figure 2-46). The unconfined areas were assumed as two degree paraobola with initial tangent slope of 45°. Based on this assumption, the effective confined area A_e could be calculated by:

$$A_e = \frac{b^2}{3} + 4br + \pi r^2 \qquad (2\text{-}67)$$

where b is the length of flat side ($B - 2r = H - 2r$ for square section).
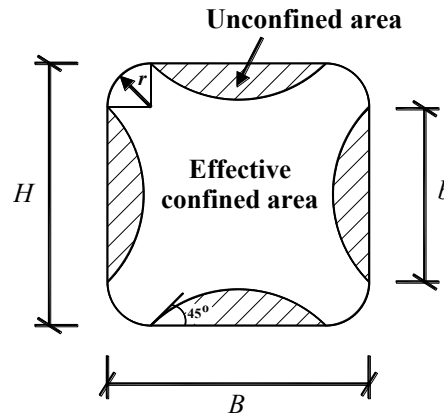
Figure 2-46 Typical assumed effective confined area (adopted from Lee et al., 2010)

In the analytical model proposed, response of whole section was devided to response of confined and unconfined area. In order to generate the axial stress-strain curve, an incremental algorithm was proposed. At any stage (i) of axial concrete strain $(\varepsilon_{c(i)})$, Lee et al. (2010) gave procedure to calculate axial stress of effective confined area $(f_{cc,e(i)})$ and uneffective confined area $(f_{c,uc(i)})$. The procedure involved lengthy mathematical expressions which can be seen in original literature. In order to obtain axial stress of the whole section $(f_{cc(i)})$, Lee et al. (2010) combined both stresses proportional to their area as follows:

$$f_{cc(i)} = f_{cc,e(i)} \frac{A_e}{A_g} + f_{c,uc(i)} \left(1 - \frac{A_e}{A_g}\right)$$ (2-68)

where A_g is the gross area of the section. The point coordinate in stress-strain curve corresponding to this incremental stage (i) was defined by $\left(\varepsilon_{c(i)}, f_{cc(i)}\right)$. To generate the whole curve, the axial strain was increased to the next subsequent steps, up to failure (stage at which the strain of FRP hoop exceeded its ultimate strain).

2.5.6 Pudjisuryadi and Tavio (2013)

A preliminary experiment was conducted Pudjisuryadi and Tavio (2013) to investigate the effect of external confinement on the strength of RC column. Three plain concrete column specimens were externally retrofitted by three different configurations of steel angle collars as seen in Figure 2-47. Description of each column and the steel collars can be seen in Table 2-2. The concrete cylinder strength $\left(f_c'\right)$ from the same concrete mix as the column specimens was 24.6 MPa. All of the specimens were tested under static concentric compression load to observe the peak strength. These results as well as the corresponding analytical predictions can be seen in Table 2-3.

In order to observe the effect of confinement, it was necessary to normalize the concrete strength with respect to their unconfined strength $\left(f_{c0}'\right)$, taken as $0.85 f_c'$ (equal to 20.9 MPa) which commonly used to relate in-place strength to standard cylinder strength (Hussain and Driver, 2005). The enhancements of the strengths were then presented relative to this in-place strength. The specimens observed strengths showed good pattern, with most confined specimen (Column C) reached the highest strength of 26.8 MPa. This meant that external steel collar confinement with 25.7 percent of volumetric ratio achieved compressive strength enhancement about 28.4 percent. Column A (the least confined specimen) and B achieved 12.6 and 18.2 percent of the strength enhancement, respectively. A proposed analytical model to predict the peak

strength was also presented. The idea of the model was determining the effective confining stress through the combined axial and bending actions of the steel collars rather than axial action only as in the case of conventional stirrups.

Errors of peak strength predictions of three specimens were all below 1 percent. Figure 2-48 gave a view of the damage pattern of each column. It could be seen that the application of steel collars can effectively reduce the damage. The locations of removed steel collar were marked with parallel lines with texts in between. Damages parts were seen more severe in regions outside the steel collars locations. This was expected since the confinements in these regions were not as effective as the collared regions. It should be noted that corner bolts were fastened with minimum force that it did not generate significant pretension force, and no grouting material was used.

(a) Column A   (b) Column B   (c) Column C

Figure 2-47 Column with (a) 4.82 percent, (b) 12.9 percent, and (c) 25.5 percent volumetric ratio of steel collars

| (a) | (b) | (c) |
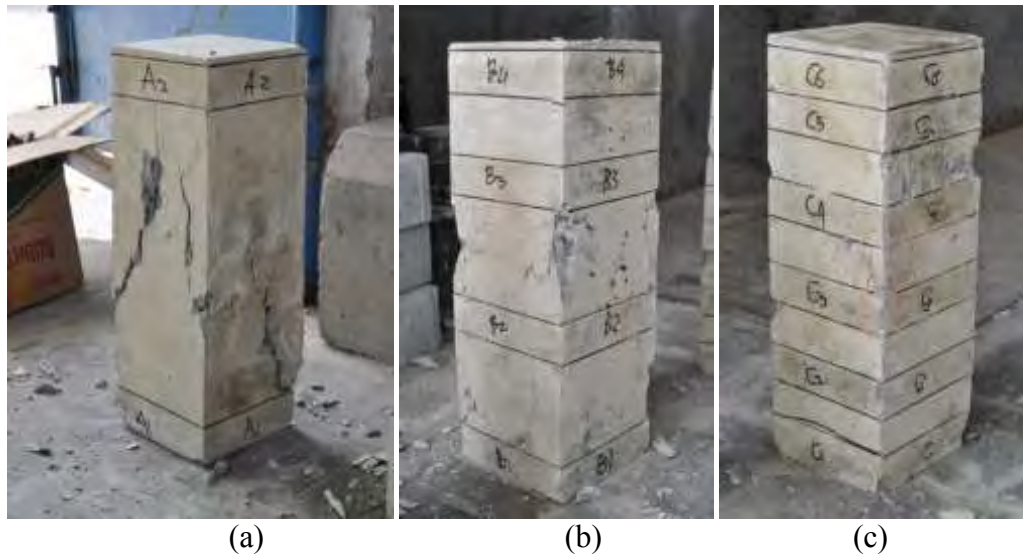
Figure 2-48 The damage patter of: (a) Column A, (b) Column B, and (c) Column C

Table 2-2 Data of the column specimens

Specimen	Column A	Column B	Column C
Cross section – height (mm)	150×150 - 450		
Steel Collar	Angle 38×38×3.8		
Yield strength (MPa)	240		
Spacing of Steel Collars (mm)	400	150	75
Volumetric ratio of steel collars (%)	4.82	12.9	25.7

Table 2-3 Compressive strength of the specimens

Specimen	Column A	Column B	Column C
In-place strength f'_{c0} (MPa)	20.9		
Experimental, f'_{cc}-ex (MPa)	23.56	24.71	26.84
Analytical, f'_{cc}-an (MPa)	23.59	24.48	27.05
Error of f'_{cc} prediction (%)	0.13	0.93	0.78
f'_{cc}-ex/ f'_{c0} (%)	12.6	18.2	28.4
f'_{cc}-an/ f'_{c0} (%)	12.8	17.1	29.3

2.5.7 Pudjisuryadi et al. (2014)

Pudjisuryadi et al. (2014) proposed an analytical model to generate complete axial stress strain curve of rectangular RC columns retrofitted by steel angle collars. Expressions to calculate confining stress and resulting peak strength were proposed in previous research (Pudjisuryadi and Tavio, 2013). The complete stress strain was then generated by adopting expressions given in Tabsh model.

Results of experiment by other authors were used to verify the analytical models. Hussain and Driver (2005) conducted a compression test of square columns externally retrofitted by Hollow Square Section (HSS) steel collars as presented in Chapter 2. Figure 2-49 showed the typical specimens and the HSS steel collars used. Normalized analytical stress-strain curves were plotted against the experimental results. Typical comparison of proposed analytical and experimental results was presented in Figure 2-50.

It could be seen that peak strength can be predicted quite well by all analytical model. But predicting peak strain was proven to be more difficult task. Both Mander and Saatcioglu models predicted the peak strain too small. The rate of strength degradation in both models also did not match the experimental results. Meanwhile, Tabsh model predicted the peak strain too large, that the rate of degradation still could not be observed. But by modifying the value of peak strain of Tabsh method (proposed), it could be seen the prediction can be slightly better than other models. It was clear that more verifications were needed to investigate the post peak behavior of this kind of retrofit method.
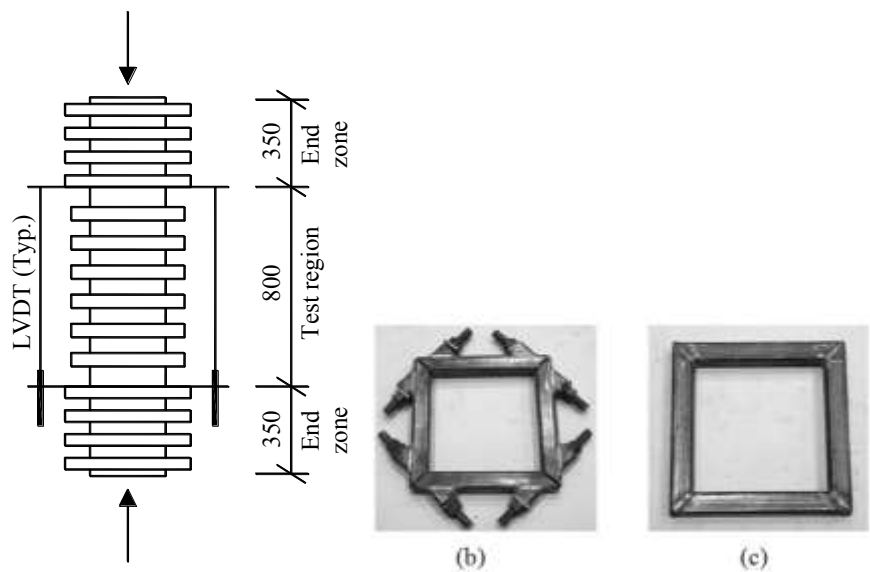
Figure 2-49 Typical specimen : (a) elevation view, (b) bolted collar, and (c) welded collar (courtesy of Hussain and Driver, 2005)

60
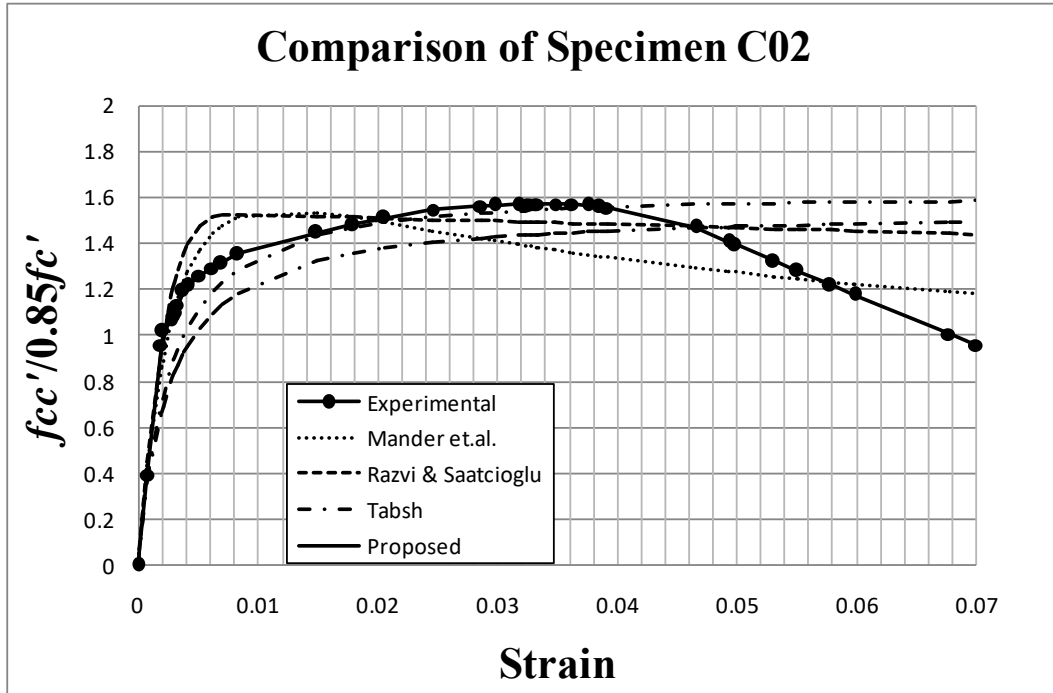
Figure 2-50 Comparison of normalized stress-strain curves for Specimen C02

2.6   STRESS STRAIN RELATIONSHIP OF STEEL

The stress and strain relationship of the steel used in this study is the model proposed by King et al. (1986), as seen in Figure 2-51.
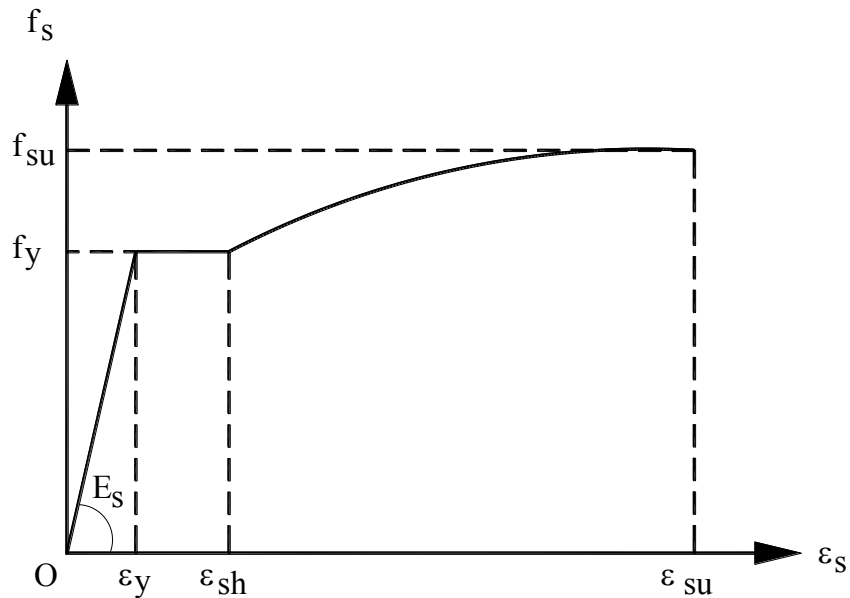
Figure 2-51 Stress strain relationship of steel (adopted from King et al., 1986)

The constitutive model of the steel is described in Equations 2-69 to 2-73:

$$f_s = E_s \varepsilon_s \qquad\qquad \text{for} \quad \varepsilon_s \leq \varepsilon_y \qquad (2\text{-}69)$$

$$f_s = f_y \qquad\qquad \text{for} \quad \varepsilon_y < \varepsilon_s \leq \varepsilon_{sh} \qquad (2\text{-}70)$$

$$f_s = f_y \left[\frac{m(\varepsilon_s - \varepsilon_{sh}) + 2}{60(\varepsilon_s - \varepsilon_{sh}) + 2} + \frac{(\varepsilon_s - \varepsilon_{sh})(60 - m)}{2(30r + 1)^2} \right] \quad \text{for} \ \varepsilon_{sh} < \varepsilon_s \leq \varepsilon_{su} \quad (2\text{-}71)$$

where:

$$m = \frac{f_{su}/f_y \left(30r^2 + 1\right)^2 - 60r - 1}{15r^2} \qquad (2\text{-}72)$$

$$r = \varepsilon_{su} - \varepsilon_s \qquad (2\text{-}73)$$

2.7 DUCTILITY

In seismic design, the ductility is usually expressed as the ratio of ultimate deformation to the deformation at first yield. This ductility represents the ability of a member to deform beyond its yielding point. In this study, the calculation of the ductility is adopted from literatures. For monotonic compression loading test, the strain ductility factor (μ_ε) is determined as the ratio of axial strain of confined concrete at 85 percent of the peak strength on the descending branch (ε_{85}) to the strain of unconfined specimen corresponding to the peak stress (ε_{01}), as expressed in Equation 2-74 (Razvi and Saatcioglu 1994). This strain ductility factor is a kind of relative ductility ratio, since the ductility of each specimen is devided by the strain of unconfined specimen. For comparison, the absolute strain ductility factors are also calculated (see Equation 2-75).

$$\mu_\varepsilon = \frac{\varepsilon_{85}}{\varepsilon_{01}} \qquad (2\text{-}74)$$

$$\mu_{\varepsilon a} = \frac{\varepsilon_{85}}{\varepsilon_{cc}'} \qquad (2\text{-}75)$$

For slowly applied simulated seismic load test, the displacement ductility factor (μ_Δ) is determined as the ratio of ultimate displacement (Δ_u) to the yield displacement (Δ_y), as expressed in Equation 2-76. The determination of yield displacement (Δ_y) is adopted from ACI 374.2R-13 as seen in Figure 2-52. In this study, α is taken as 0.70 (mid value of suggested range 0.65 to 0.75), while Q_y is taken as the maximum strength. The ultimate displacement (Δ_u) is defined as displacement corresponding to strength decay of 20 percent of the measured peak strength (ACI 374.2R-13). K_e is the initial effective stiffness. In order to capture the overall deformability, the cumulative ductility factor (N_Δ) should also be determined as expressed in Equation 2-77. In every cycle of the test, the displacement ductility is calculated and then cumulated. The average of maximum displacement in push and pull mode (Δ_i) is used to substitute ultimate displacement (Δ_u) in Equation 2-76. The yield displacement used for devider (in Equation 2-76) is also averaged from push and pull mode of the test. The concept is illustrated in Figure 2-53. The curvature ductility (μ_φ) and cumulative curvature ductility (N_φ) can be determined with the same approaches as explained in Equations 2-76, and 2-77, respectively.

$$\mu_\Delta = \frac{\Delta_u}{\Delta_y} \qquad (2\text{-}76)$$

$$N_\Delta = \sum \frac{\Delta_i}{\Delta_y} \qquad (2\text{-}77)$$

63
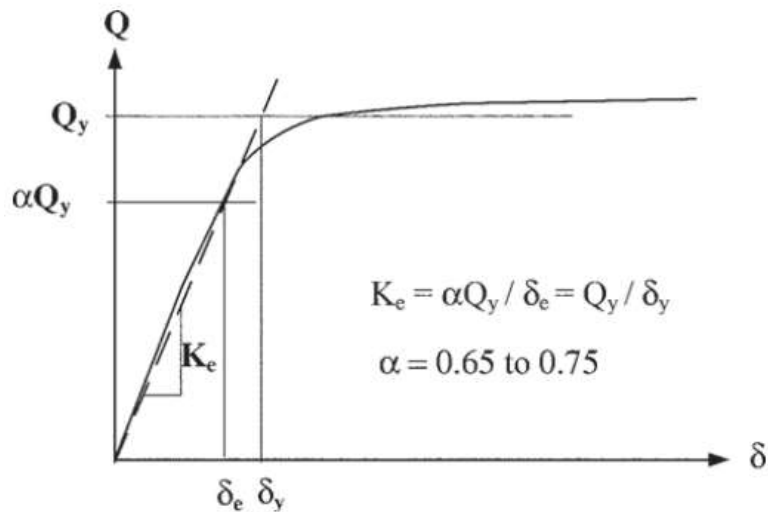
Figure 2-52 Determination of yield values Q_y and Δ_y (ACI 374.2R-13)

$$K_e = \alpha Q_y / \delta_e = Q_y / \delta_y$$

$$\alpha = 0.65 \text{ to } 0.75$$

$$\Delta y = 0.5[(\Delta y+)+(\Delta y-)]$$
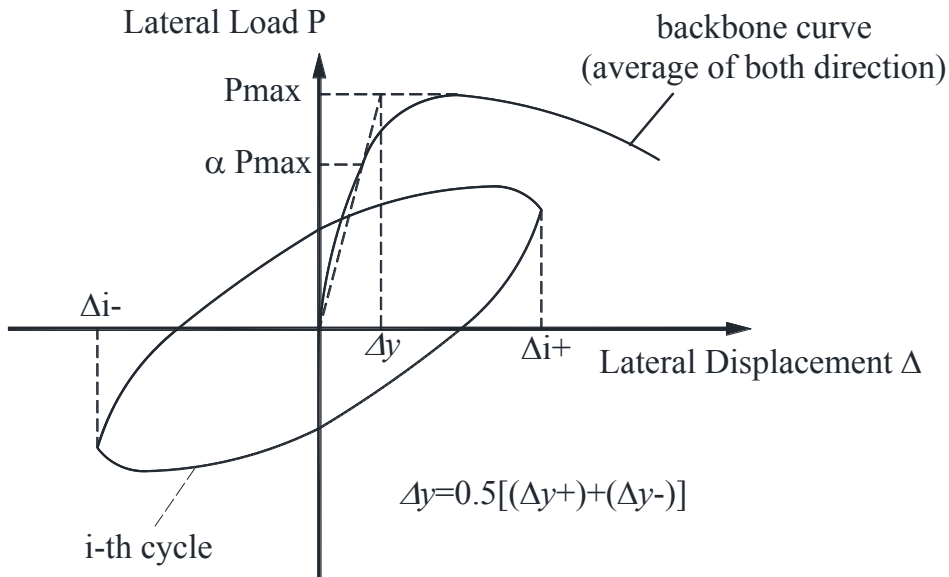
Figure 2-53 Cumulative displacement ductility

Moreover, ideal elastoplastic energy is usually used to normalize cumulative energy to get a dimensionless value. The ideal elastoplastic energy is illustrated by the shaded area in Figure 2-54.
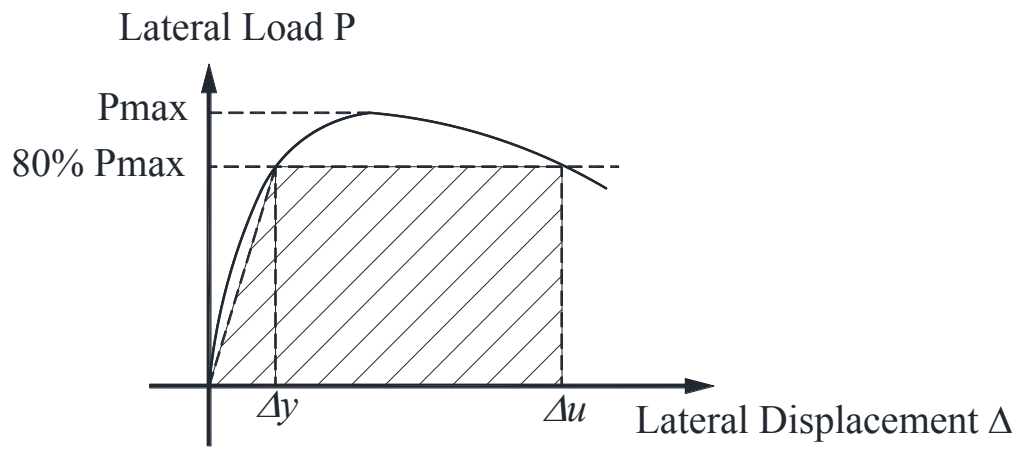
Figure 2-54 Ideal Elastoplastic Energy

= This Page is Intentionally Left Blank =

CHAPTER 3.   EXPERIMENTAL PROGRAM

3.1   INTRODUCTION

In order to achieve the objectives of the study, two phases of experimental programs were conducted. The first phase focused on the investigation of the behavior of square RC columns retrofitted externally by steel angle collars under mononotic axial compressive loading, whereas the second phase studied further on the behavior of such specimens under combined axial compressive and reversed cyclic lateral loading. All test specimens were instrumented such that the force resistances and deformations could be measured. Details of test specimens, test set up, and instrumentation are described in this Chapter.

3.2   DESIGN AND DETAILS OF SPECIMENS FOR MONOTONIC - STATIC - AXIAL COMPRESSIVE TEST

The objectives of conducting the monotonic-static- axial compressive test are (1) to obtain the axial stress-strain relationship curve; (2) to study the effect of external steel collars alone; (3) to study the effect of steel collar in combination with the internal stirrups confinement; and (4) to develop the stress-strain relationship model / method / equations. A set of physical specimens to be experimentaly tested were designed to investigate the proposed method for possible retrofitting technique of inadequately confined concrete columns. Normal strength concrete (f'_c = 20 MPa) was used for all test specimens. The cross sections, and heights of all specimens were set equal to 200×200 mm^2, and 600 mm, respectively. The clear concrete cover used was 20 mm thick. The specimens were set to have a 400 mm middle test region, and two 100 mm non-test regions at both ends. The specimens were reinforced with deformed bars for both longitudinal (f_y = 400 MPa) and transverse reinforcements (f_{yt} = 400 MPa). The non-test regions were designed to have denser confinement than the test region. Thus, no failure was expected in these regions. At 28 days after casting, the specimens were then externally confined with the steel angle collars. With this set

up kept constant, the following sub-sections describe the variations of the specimens and parameters in the study.

3.2.1 Control Specimens CS01, CS02a, and CS03a

Three Specimens CS01, CS02a, and CS03a were set as control specimens as illustrated in Figure 3-1. These control specimens were intended to study the behavior of conventionally confined concrete column specimens under axial compressive load. CS01 was constructed without any confinement within the test region, and only 4-D10 (four 10-mm diameter of deformed steel bars) longitudinal reinforcements were used. The specimen ID consisted of letters CS followed by two digits number. The letters "C", and "S" refered to "Control", and "Specimen" words, respectively. The number "0" indicated the monotonic axial compressive load test, while the last numbers are simply the sequential numbering of the specimens. The small letter "a" behind Specimens CS02, and CS03 was meant to mark variations of longitudinal bars intalled in the specimen. Letters "a", and "b" were originally meant to mark the use of four and eight longitudinal bars. It can be seen in Figure 3-1 that each side of the specimen marked with number "1" to "4" with clockwise sequence. Strain gauges attached on longintudinal bars, and strirrups are coded with letter "L", and "S", respectively. The two digit numbers (XY) following letter L were meant to identify that they were attached on the corners of sides X, and Y. While the two digit numbers (M-N) following letter S were meant to identify that they were attached on stirrups number M (counted bottom up) in the test region, at side N of the specimens.

CS02a was designed to represent the condition of columns that did not conform the seismic confinement requirement. The transverse reinforcement only satisfied the minimum shear requirement. The minimum shear requirement according to SNI 2847 : 2013, Section 11.4.6.3 is :

$$A_{vmin} = \frac{75\sqrt{f_c'}b_w s}{1200 f_{yt}} \geq \frac{1}{3}\frac{b_w s}{f_{yt}} \qquad (3\text{-}1)$$

where :

A_{vmin} = minimum area of stirrups (mm^2)

b_w = width of concrete element (mm)

f_c' = concrete strength (MPa)

s = spacing of stirrups (mm)

f_{yt} = yield strength of stirrups steel (MPa)

Elevation Views

Cross Sections
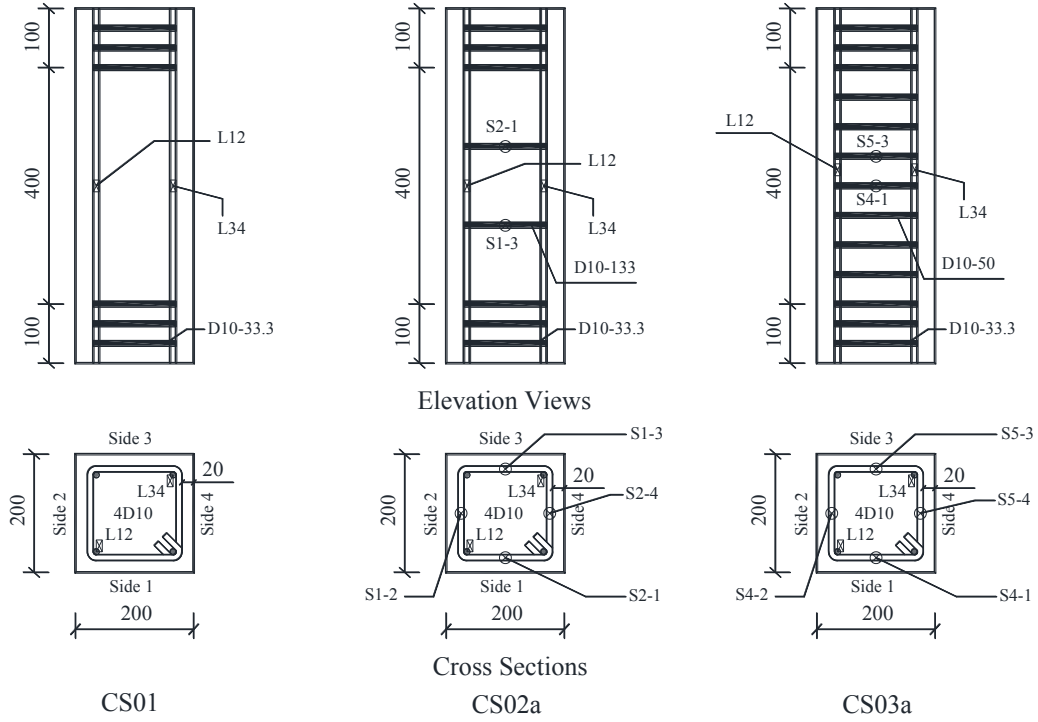
CS01   CS02a   CS03a

Note: all dimensional units are in mm

Figure 3-1 Elevation view and cross section of Specimens CS01, CS02a, and CS03a

Noting the data described in Section 3.2, the calculation of this minimum shear requirements is presented below :

b_w = 200 mm ; f_c' = 20 MPa ; f_{yt} = 400 MPa

$$\frac{A_{vmin}}{s} = \frac{75\sqrt{f_c'}b_w}{1200 f_{yt}} = \frac{75\sqrt{(20)}\,200}{1200(400)} = 0.14 \text{ mm}^2/\text{mm, and should be greater than}$$

$$\frac{A_{vmin}}{s} = \frac{1}{3}\frac{b_w}{f_{yt}} = \frac{1}{3}\frac{200}{400} = 0.17 \text{ mm}^2/\text{mm.}$$

Moreover, the selected confinement spacing should not exceed the maximum shear reinforcement spacing, which is the smaller of these followings (SNI 2847 : 2013, Section 7.10.5.2):

    a) 16 times the diameter of longitudinal reinforcement ($16\phi_l$)

    b) 48 times the diameter of transverse reinforcement ($48\phi_s$)

    c) the smaller dimensions of the column (b_w)

With D10 used for both longitudinal (ϕ_l = 10 mm), and transverse reinforcements (ϕ_s = 10 mm), the maximum shear reinforcement spacing requirements is the smallest of :

a) $16\phi_l = 16(10) = 160$ mm $\rightarrow$ maximum spacing allowed

b) $48\phi_s = 48(10) = 480$ mm

c) $b_w = 200$ mm

To meet the requirements, the 400-mm length test region was devided with three equally spaced confinement steel of D10-133. The selected confinement had the amount of confinement, and volumetric ratio (ρ_s) as followings :

$$\frac{A_v}{s} = \frac{2 \times 0.25\pi\left(10^2\right)}{133} = 1.18\,\text{mm}^2/\text{mm}$$

$$\rho_s = \frac{\text{vol. of steel}}{\text{vol. of concrete}} = \frac{4 \times (b_w - 2d_c - \phi_s) \times 0.25\pi\phi_s^2}{b_w^{\,2}s}$$

$$= \frac{4 \times (200 - 2(20) - 10) \times 0.25\pi 10^2}{200^2(133)} = 0.89\%$$

By definition, the volume of confined concrete is used for the calculation of volumetric ratio. In this study, there are two types of confinement which are the conventional internal stirrups and the proposed external steel collars. Both confinements influence different confined concrete volume. For the sake of comparison in this study, the concrete volume used for the calculation of volumetric ratio is based on the gross dimension.

CS03a was designed to represent the condition of columns confined with seismic confinement requirement. The seismic confinement requirements according to SNI 2847 : 2013, Section 21.6.4.4, are as follows:

$$A_{sh1} = 0.09\left(sb_c \frac{f'_c}{f_{yt}} \right)$$

(3-2)

or :

$$A_{sh2} = 0.3\left(sb_c \frac{f'_c}{f_{yt}} \right)\left(\frac{A_g}{A_{ch}} - 1 \right)$$

(3-3)

where b_c, A_g, and A_{ch} are the dimension of confined concrete core, gross sectional area, and confined core sectional area, respectively. The calculation of these seismic confinement requirements is presented as followings :

$$\frac{A_{sh1}}{s} = 0.09\left(b_c \frac{f'_c}{f_{yt}} \right) = 0.09\left((200 - 2(20) - 10)\frac{20}{400} \right) = 0.675 \text{ mm}^2/\text{mm}$$

$$\frac{A_{sh2}}{s} = 0.3\left(sb_c \frac{f'_c}{f_{yt}} \right)\left(\frac{A_g}{A_{ch}} - 1 \right)$$

$$= 0.3\left((200 - 2(20) - 10)\frac{20}{400} \right)\left(\frac{200^2}{(200 - 2(20) - 10)^2} - 1 \right) = 1.75 \text{ mm}^2/\text{mm}$$

These requirement must be accompanied with maximum transverse reinforcement spacing for member under combined axial and bending forces in seismec region specified in SNI 2847 : 2013 Section 21.6.4.3, which is the smallest value of these following expressions:

a) one quarter of smallest dimensions of column ($0.25 b_w$)

b) six times the diameter of longitudinal bars ($6\phi_l$)

c) $100 < 100 + (350 - h_x)/3 < 150$mm (where h_x is the maximum center to center distance of crossties or hoop legs)

The maximum transverse reinforcement spacing is the smallest of :

a) $0.25 b_w = 0.25(200) = 50$ mm → maximum spacing allowed

71

b) $6\phi_l = 6(10) = 60$ mm

c) $100 < 100 + (350 - h_x)/3 < 150$

$100 < 100 + (350 - (200 - 2(20) - 10))/3 < 150$

$100 < 66.7 < 150 \rightarrow 100\,\text{mm}$

To meet the requirements, reinforcing confinement steels of D10-50 was selected for this specimen. The corresponding amount of confinement, and volumetric ratio (ρ_s) are :

$$\frac{A_v}{s} = \frac{2 \times 0.25\pi(10^2)}{50} = 3.14\,\text{mm}^2/\text{mm}$$

$$\rho_s = \frac{\text{vol. of steel}}{\text{vol. of concrete}} = \frac{4 \times (b_w - 2d_c - \phi_s) \times 0.25\pi\phi_s^2}{b_w^2 s}$$

$$= \frac{4 \times (200 - 2(20) - 10) \times 0.25\pi 10^2}{200^2 (50)} = 2.36\%$$

3.2.2 Specimens S01, S02, S03, S04, and S05

Specimens S01 to S05 were developed further from five typical specimens which had identical sizes and details with Specimen CS01. The specimens were confined externally within their test region by using steel angle collars. S01, and S05 were specimens with the lowest and highest volumetric ratio of confinement collars, respectively. The specimens can be seen in Figures 3-2 to 3-6. All remarks in the figure had the same explanation as the control specimens, except the additional coding for strain gauges attached on the steel collars (started with letter "C"). These strain gauges were marked with code P-Q-(L/B) behind letter C which were meant to identify that the strain gauges were installed at steel collar number P (counted bottom up) in the test region, at side Q of the specimen. L or B were meant to identify that the strain gauges were attached at the leg or at the back of steel angle collar, respectively. Special case for Specimen S01, there was another code behind L/B. This code was either M or E, which meant that the strain gauge was located either at the middle or at the edge of the steel collar. The

72

volumetric ratios designed for these specimens were 3.84, 5.77, 7.68, 9.60, and 11.46 percent for S01, S02, S03, S04, and S05, respectively. For example, the ρ_s calculation of specimen S01 is presented.

Dimension of steel collar

width = height = 40 mm ; thickness = 4 mm

area, $A_{sc} = (\text{width+height}) \times \text{thickness} = (40+40) \times 4 = 320 \, \text{mm}^2$

length $= 4 \times (b_w + \text{width}) = 4 \times (200+40) = 960 \, \text{mm}^2$

$$\rho_s = \frac{\text{vol. of steel collar}}{\text{vol. of concrete}} = \frac{\text{length} \times \text{area of steel collar}}{b_w^2 s_{sc}} = \frac{960 \times 320}{200^2 (200)} = 3.84\%$$
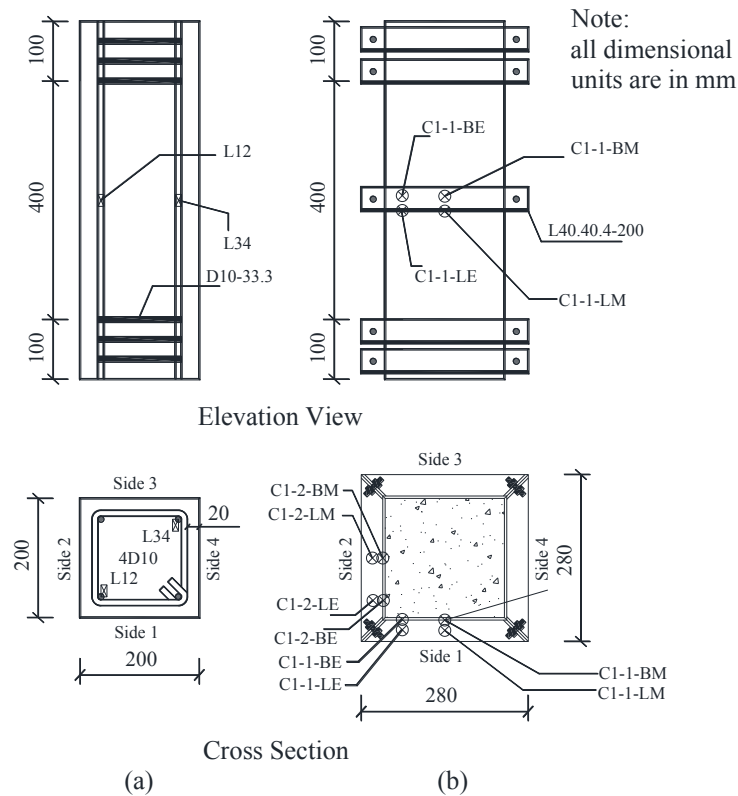
Figure 3-2 Elevation view and cross section of Specimen S01 : (a) reinforcement details ; and (b) external steel collars
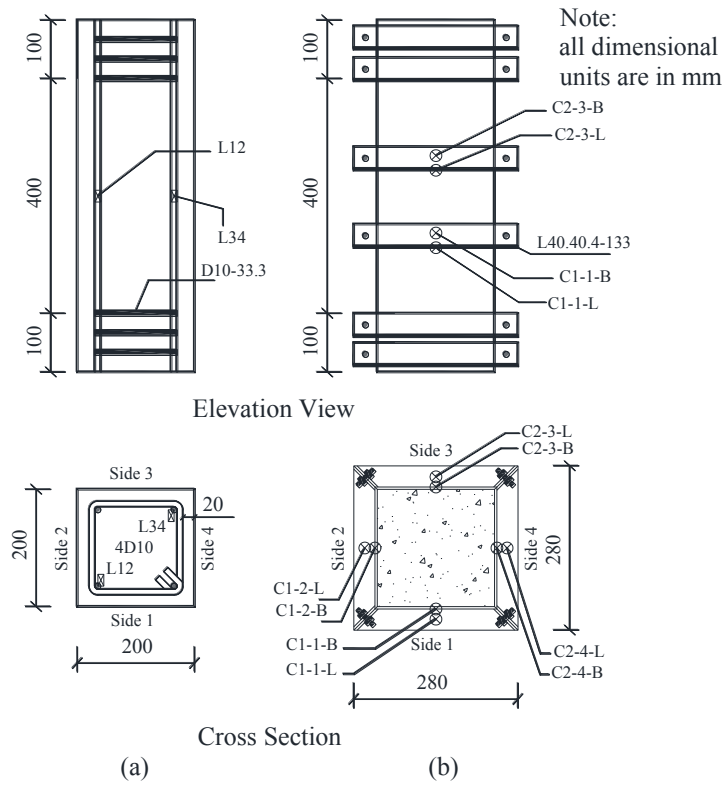
Figure 3-3 Elevation view and cross section of Specimen S02 : (a) reinforcement details ; and (b) external steel collars
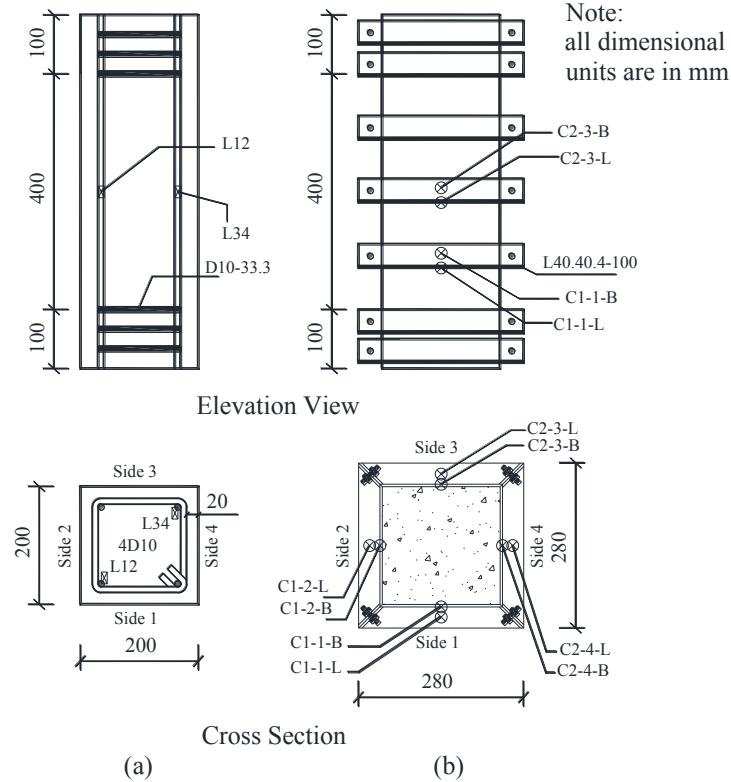
Figure 3-4 Elevation view and cross section of Specimen S03 : (a) reinforcement details ; and (b) external steel collars

74
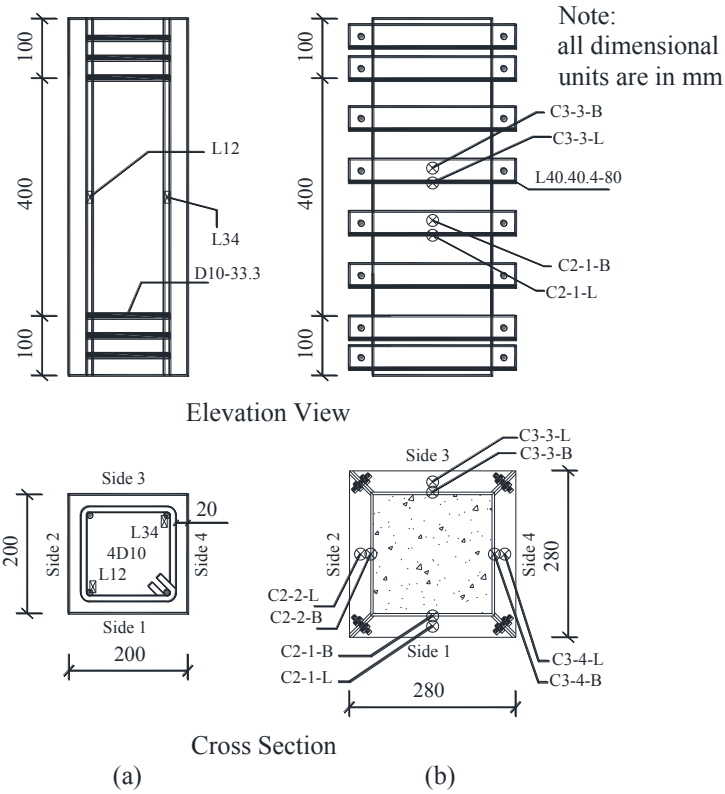
Figure 3-5 Elevation view and cross section of Specimen S04 : (a) reinforcement details ; and (b) external steel collars
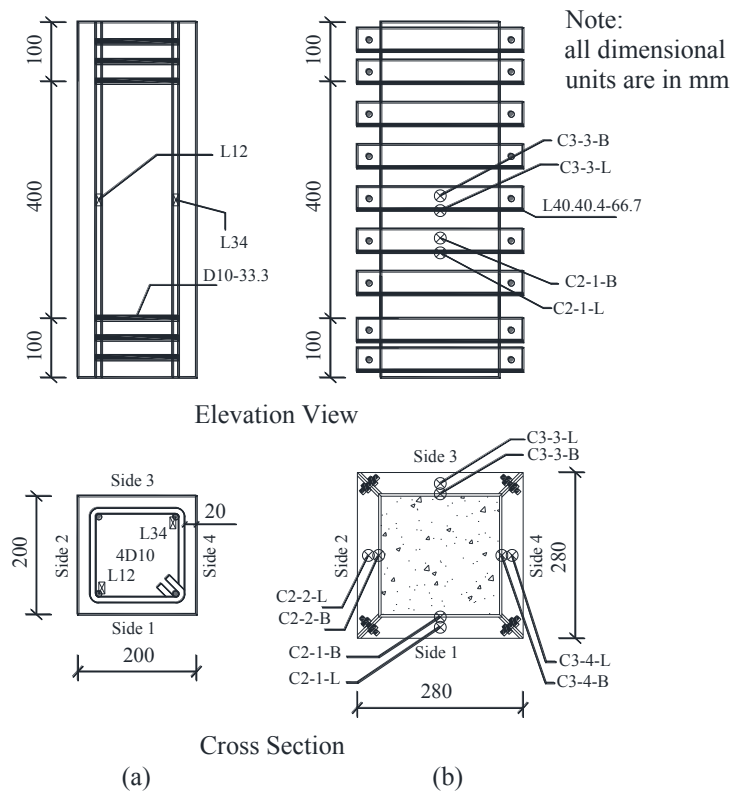
Figure 3-6 Elevation view and cross section of Specimen S05 : (a) reinforcement details ; and (b) external steel collars

75

3.2.3   Specimens S04a, and S04b

Specimens S04a and S04b had the same external confinement as Specimen
S04. However, they had internal confinement in their test regions. Specimen S04a
was designed so that the external and internal confinments having the same
spacing and location over the test region as shown in Figure 3-7. Specimen S04b
was also designed to have equal spacing of external and internal confinements,
but the external steel collars were located at the mid-spacing of the internal
confinement as can be seen in Figure 3-8. The aim of these different placement is
to study the effect of variational placement of external steel collars with respect to
the location of the internal stirrups in the existing columns.
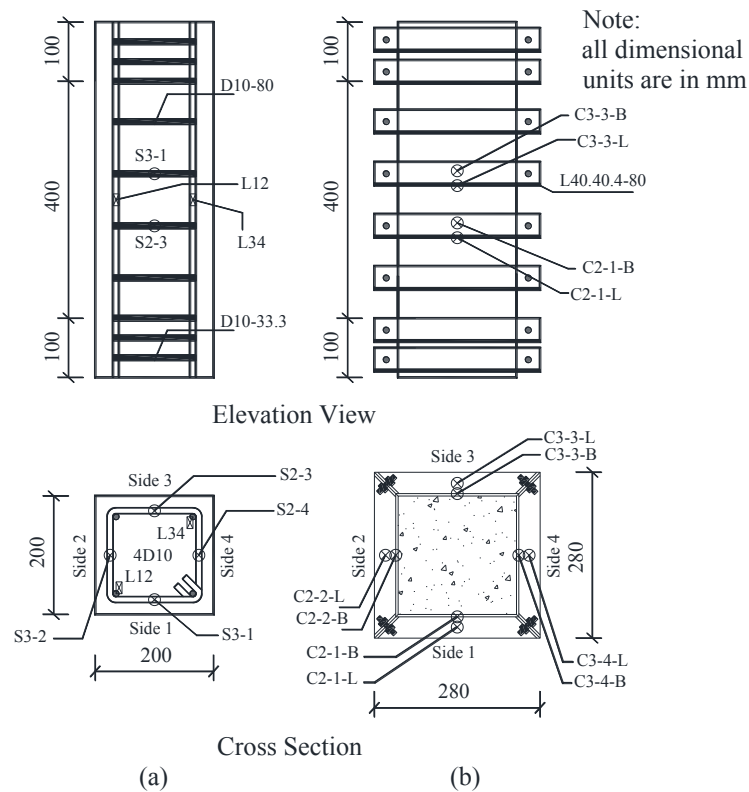
**Figure 3-7 Elevation view and cross section of Specimen S04a : (a) reinforcement
details ; and (b) external steel collars**
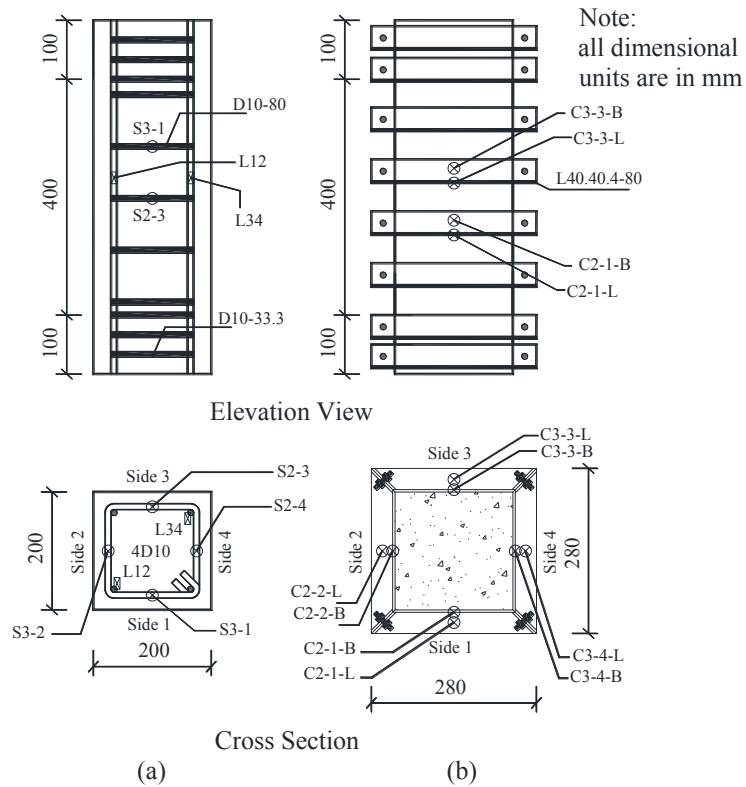
Figure 3-8 Elevation view and cross section of Specimen S04b : (a) reinforcement details ; and (b) external steel collars

3.2.4 Specimens S04c, and S04d

Specimens S04c and S04d were developed with identical data of Specimen S04, except that the steel angle collars were strengthened by a few web stiffeners. In each steel collar, one and two web stiffneres were installed for Specimens S04c and S04d respectively (see Figures 3-9 and 3-10). These specimens were used to investigate if local instability existed in standar collars. If it existed, this strengthening should improve the confining performance.
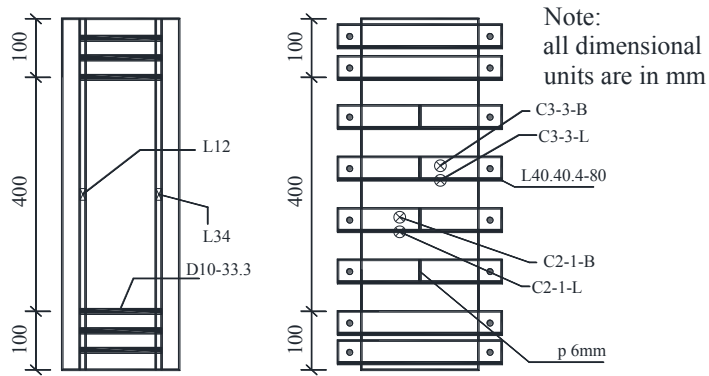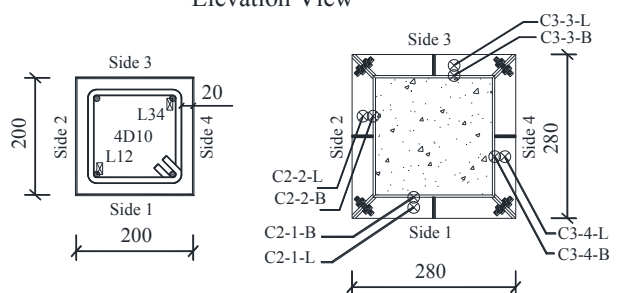
Figure 3-9 Elevation view and cross section of Specimen S04c : (a) reinforcement details ; and (b) external steel collars
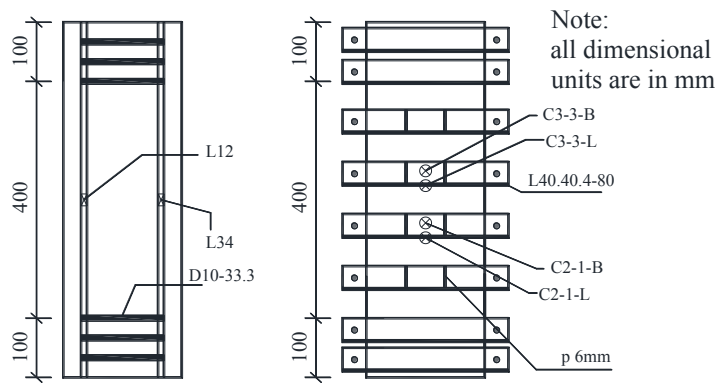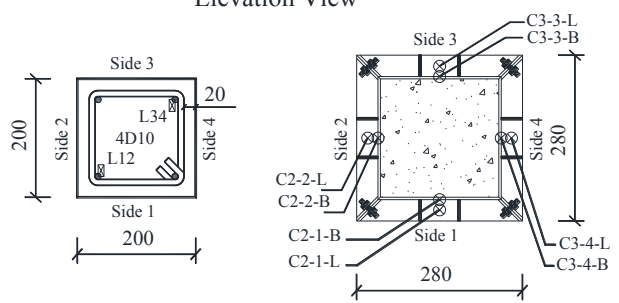
Figure 3-10 Elevation view and cross section of Specimen S04d : (a) reinforcement details ; and (b) external steel collars

3.2.5 Specimens S04e, and S04f

With the identical data as Specipen S04, the external steel collars installation of Specimens S04e and S04f were strengthened by a few bolts to the concrete. This was to ensure a better contact between the steel collars and the column specimens. In each steel collar, one and two dyna bolts were used for Specimens S04e and S04f respectively (see Figures 3-11 and 3-12). These specimens were used to investigate further the role of steel collars bending stiffness by reducing the effective flexural length.
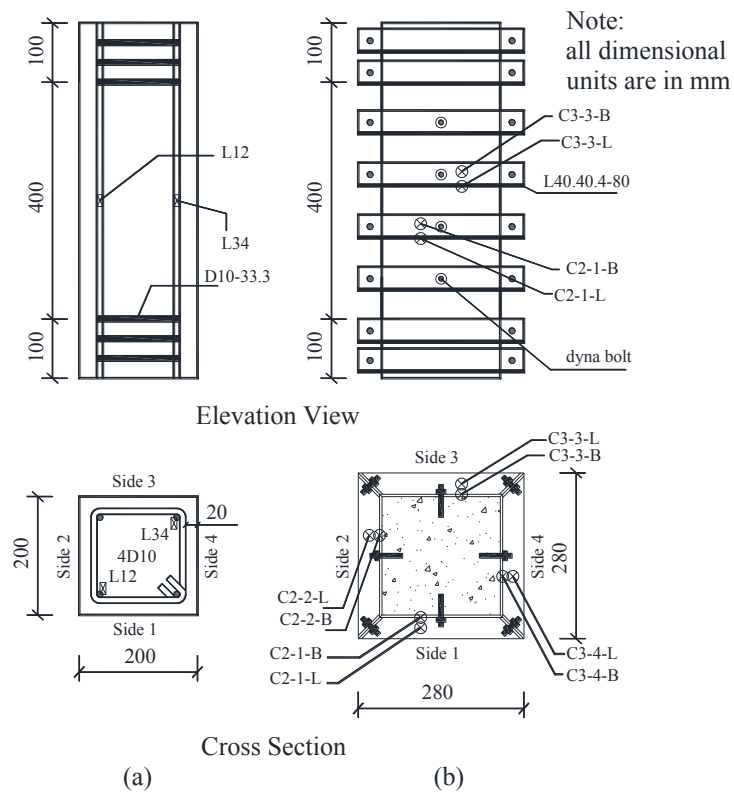
Figure 3-11 Elevation view and cross section of Specimen S04e : (a) reinforcement details ; and (b) external steel collars
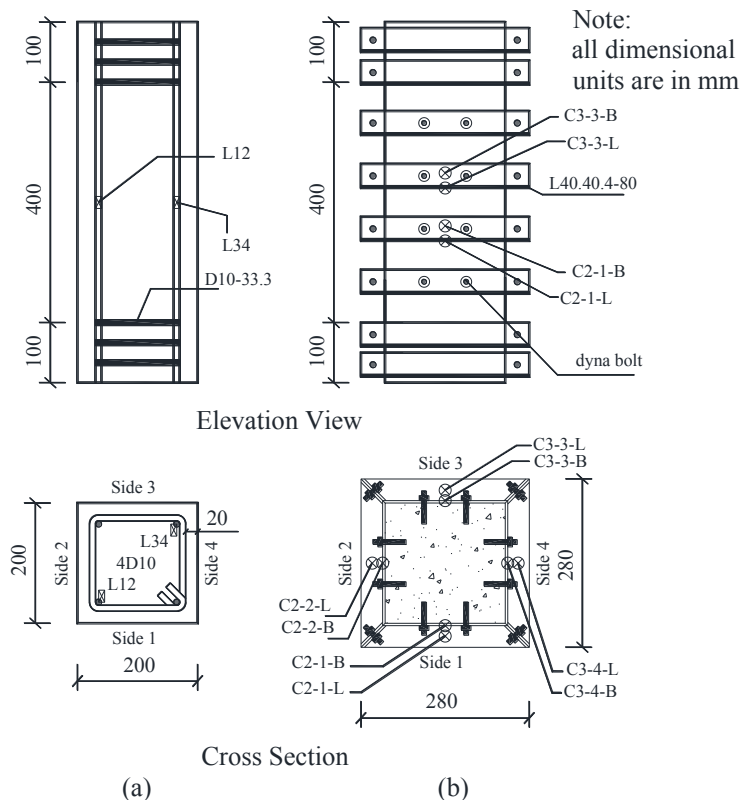
Figure 3-12 Elevation view and cross section of Specimen S04f : (a) reinforcement details ; and (b) external steel collars

3.2.6 Summary of the specimens

All specimens details for monotonic axial compressive test are summarized in Table 3-1. Three dimensional illustrations of externally collared Specimen S03 are shown in Figures 3-13 to 3-16. The two pairs of rods are intended to set the gauge length of the specimens during the tests. The other specimens also had the same illustrations as Figures 3-13 to 3-16 except the external steel collars numbers are different (see Table 3-1). Since only one specimen built for each variant, the consistent material, workmanship, and condition must be kept as constant as possible throughout the making of the specimens. To minimize the deviation in quality, the materials (cement, crushed stone, and sand) were provided from a single batch. All specimens were designed to have 4-D10 (four 10 mm-diameter) longitudinal deformed bars. The steel angle sections used for the collars, L40 had 40 mm width and 4 mm plate thickness. With variation of confinement volumetric ratio, a clear behavior pattern is expected.

Table 3-1 Confinement data of experimental specimens (compressive test)

No.	Specimen ID	Internal Confinement / Stirrups	External Confinement / Steel Collars	Notes
1	CS01	None	None	None
2	CS02a	D10-133 (VR = 0.89 %)	None	None
3	CS03a	D10-50 (VR = 2.36 %)	None	None
4	S01	None	L40 - 200 (VR = 3.84%)	None
5	S02	None	L40 - 133 (VR = 5.77%)	None
6	S03	None	L40 - 100 (VR = 7.68%)	None
7	S04	None	L40 - 80 (VR = 9.60%)	None
8	S05	None	L40 - 67 (VR = 11.46%)	None
9	S04a	D10 – 80 (VR = 1.48 %)	L40 - 80 (VR = 9.60%)	equal location of stirrups and steel collars
10	S04b	D10 – 80 (VR = 1.48 %)	L40 - 80 (VR = 9.60%)	steel collars at mid-spacing of stirrups
11	S04c	None	L40 - 80 (VR = 9.60%)	+ one web stiffner at each side of steel collar
12	S04d	None	L40 - 80 (VR = 9.60%)	+ two web stiffners at each side of steel collars
13	S04e	None	L40 - 80 (VR = 9.60%)	+ one bolt to attach each side of steel collar
14	S04f	None	L40 - 80 (VR = 9.60%)	+ two bolts to attach each side of steel collar
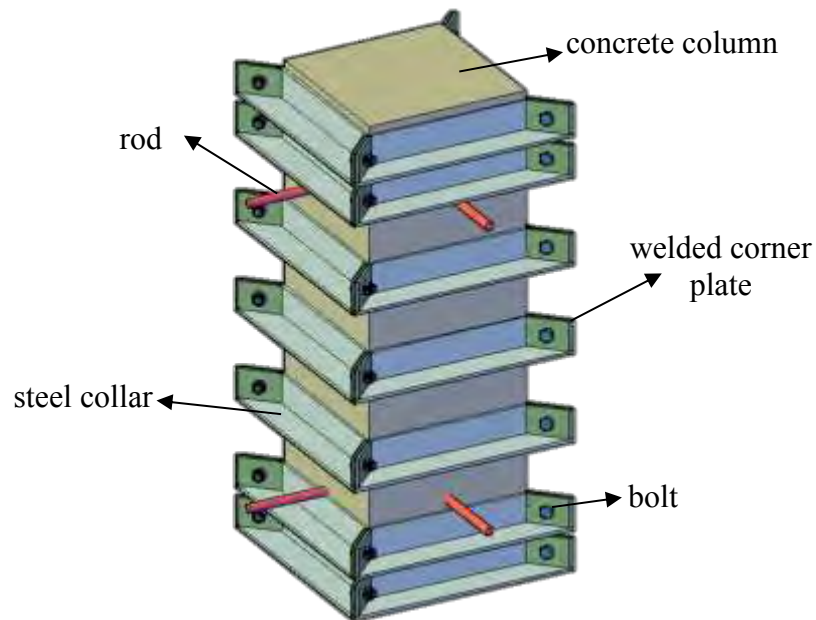
Figure 3-13 Three dimensional illustration of Specimen S03

concrete column

steel collar

welded corner plate

bolt

rod
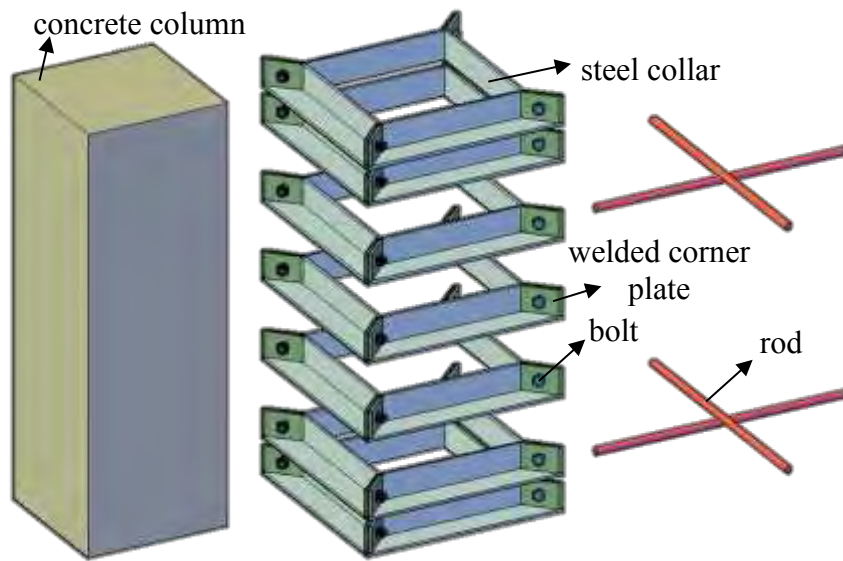
Figure 3-14 Exploded view of Specimen S03

concrete column

steel collar

rod

60

200

280

400

10
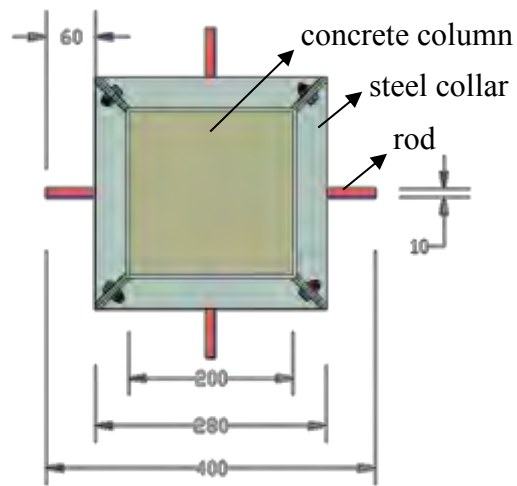
Figure 3-15 Top view of Specimen S03
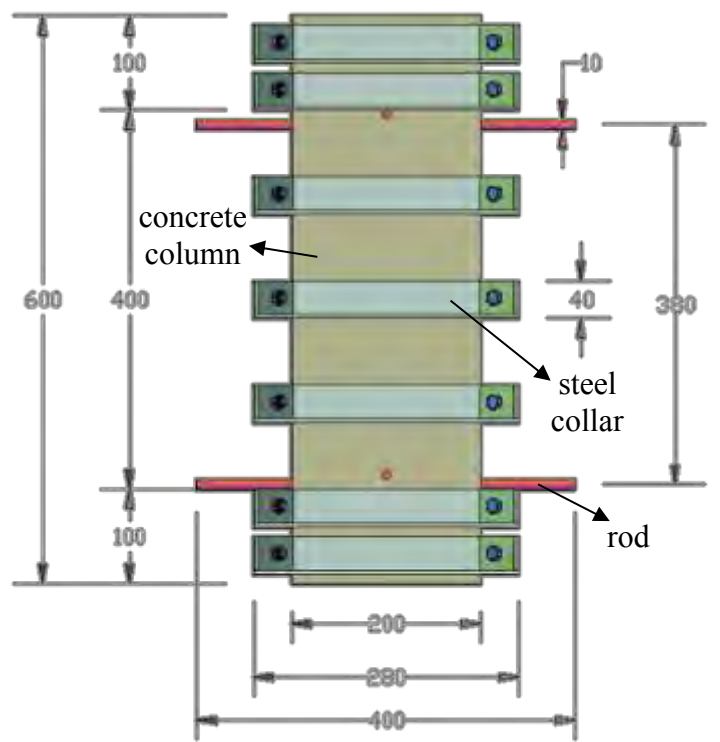
Figure 3-16 Elevation view of Specimen S03

3.3 DESIGN AND DETAILS OF SPECIMENS FOR COMBINED AXIAL COMPRESSIVE AND REVERSED CYCLIC LATERAL LOADING TEST

In order to further study the proposed method, a set of specimens under combined axial compressive and reversed cyclic lateral loading test was also designed. This test was conducted to investigate the behavior of the specimen during simulated earthquake load. The specimens consisted of columns fixed on top of solid footing foundations. The footing were massively designed (had a dimension of $700 \times 1200 \times 500$ mm^3) and heavily reinforced such that no failure was expected during the test. The cross section, and height of the columns were set equal to 200×200 mm^2, and 725 mm respectively. The clear concrete cover used was 20 mm thick. The ratio of longitudinal reinforcements (1.00 percent < ρ < 6.00 percent) installed were set to meet the amount specifed by the standard (SNI 2847 : 2013) for members under combined axial and bending forces. To ensure that the capacity of lateral hydraulic actuator is adequate to conduct the test, a relatively small amount longitudinal reinforcement of 4-D13 (four 13 mm –

83

diameter of deformed bars) was selected (ρ = 1.33 percent). The top 250 mm is defined as a non-test region and it was heavily confined so that it would not be damaged during the test. In the middle of this non-test region (600 mm from the bottom fixity) was the application point of the lateral force from the horizontal hydraulic actuator. This set up leads to shear span to depth ratio of 3.0, calculated from the height of lateral load (600 mm) devided by the dimension of the column (200 mm). This setup results in slenderness ratio $\left(kL_u/r\right)$ of 20.78, which was smaller than 22, indicating short column behavior (SNI 2847 Committee, 2013). With this set up kept constant, the following sections describes the variations of the specimens and the parameters aimed to study.

3.3.1 Control Specimens CS11, and CS12

These control specimens were intended to study the behavior of conventionally confined column specimens under combined axial compressive and reversed cyclic lateral load. The confining reinforcement in the test region of Specimens CS11 and CS12 were designed to meet the shear reinforcement requirement (D10-150), and seismic confinement requirements (D10-50), respectively as explained in Phase 1 experiment. The first number "1" indicated the specimen for for this combined axial compressive and reversed cyclic lateral load test. The detail of the specimens can be seen in Figures 3-17 and 3-18.
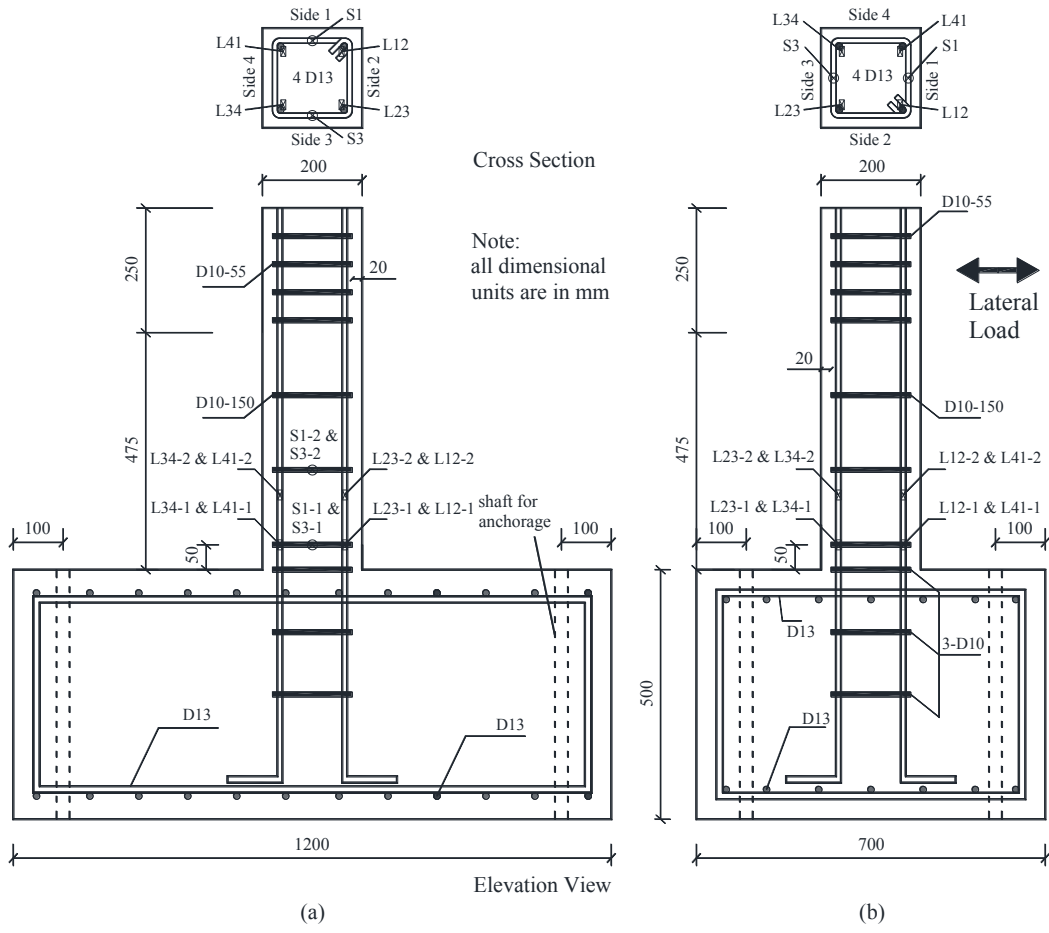
Figure 3-17 Elevation view and cross section of Specimen CS11 : (a) transverse to lateral load direction ; (b) in lateral load direction
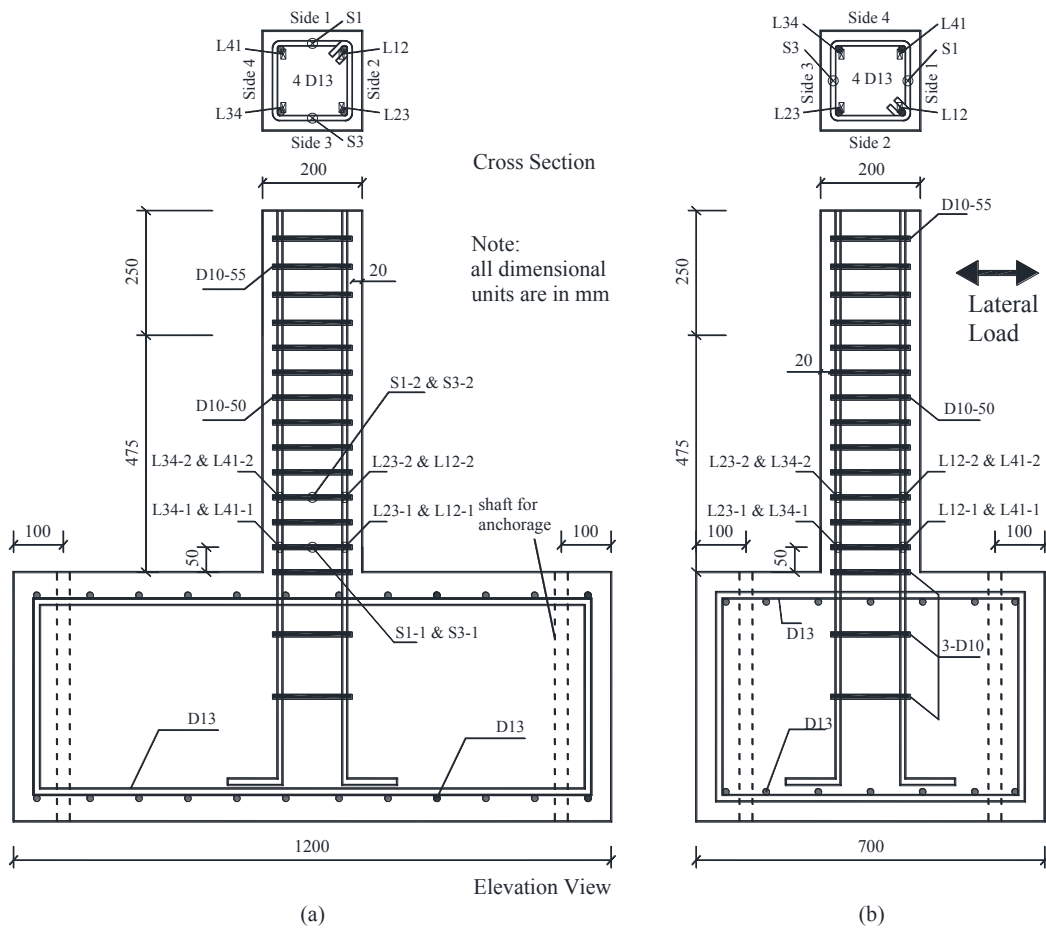
Figure 3-18 Elevation view and cross section of Specimen CS12 : (a) transverse to lateral load direction ; (b) in lateral load direction

3.3.2 Specimens S13, S14, and S15

The test regions of these specimens were only confined externally by using steel angle collars. The same steel angle collars as used in Phase 1 experiment were uniformly distributed in the 475 mm test region. The least external confinement was set with max spacing not exceeding the column dimension, which result in Specimen S13. The last number "3" indicated the number of steel collars installed in the test region. The other two Specimens S14 and S15 were confined more heavily by adding one and two steel collars, respectively. The volumetric ratio $\left(\rho_s\right)$ set for these specimens were 4.27, 6.40, and 8.53 percent for S13, S14, and S15, respectively. The specimens can be seen in Figures 3-19 to 3-21. The summary of the specimens data can be seen in Table 3-2.
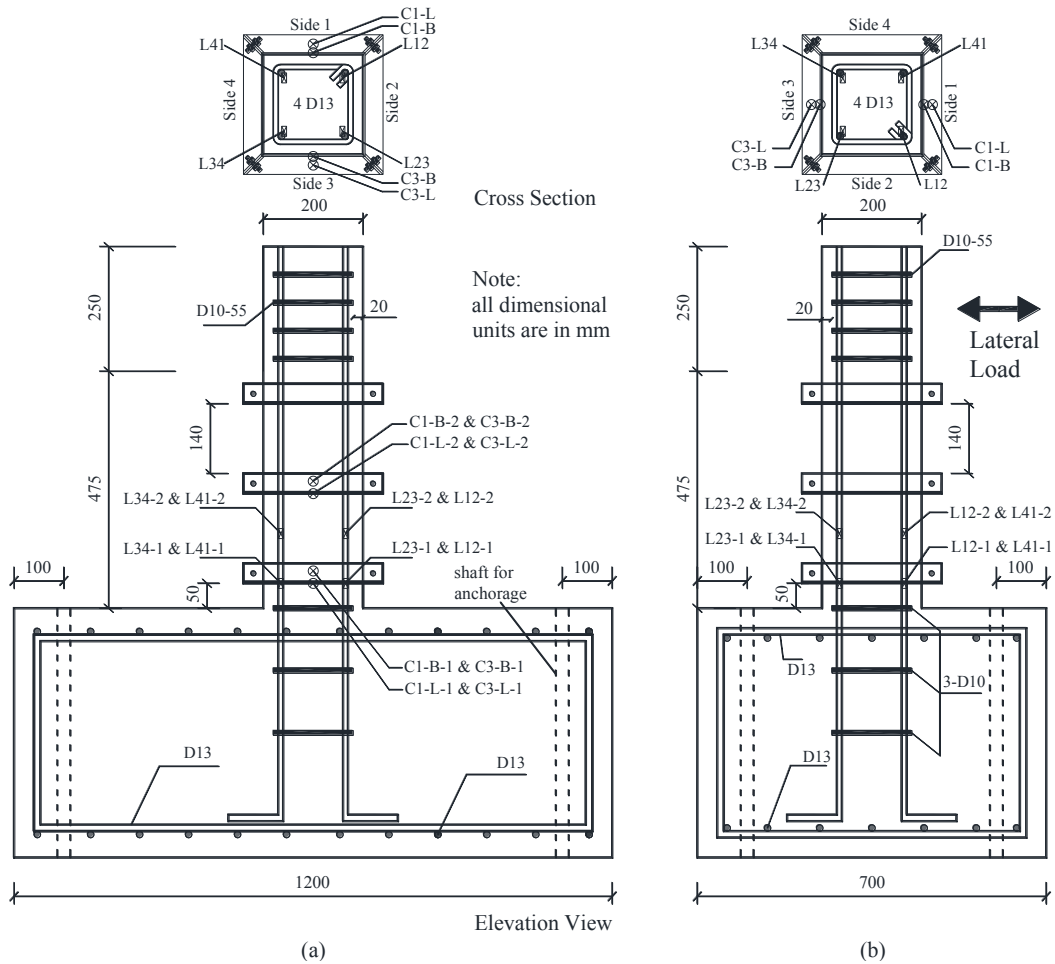
Figure 3-19 Elevation view and cross section of Specimen S13 : (a) transverse to lateral load direction ; (b) in lateral load direction
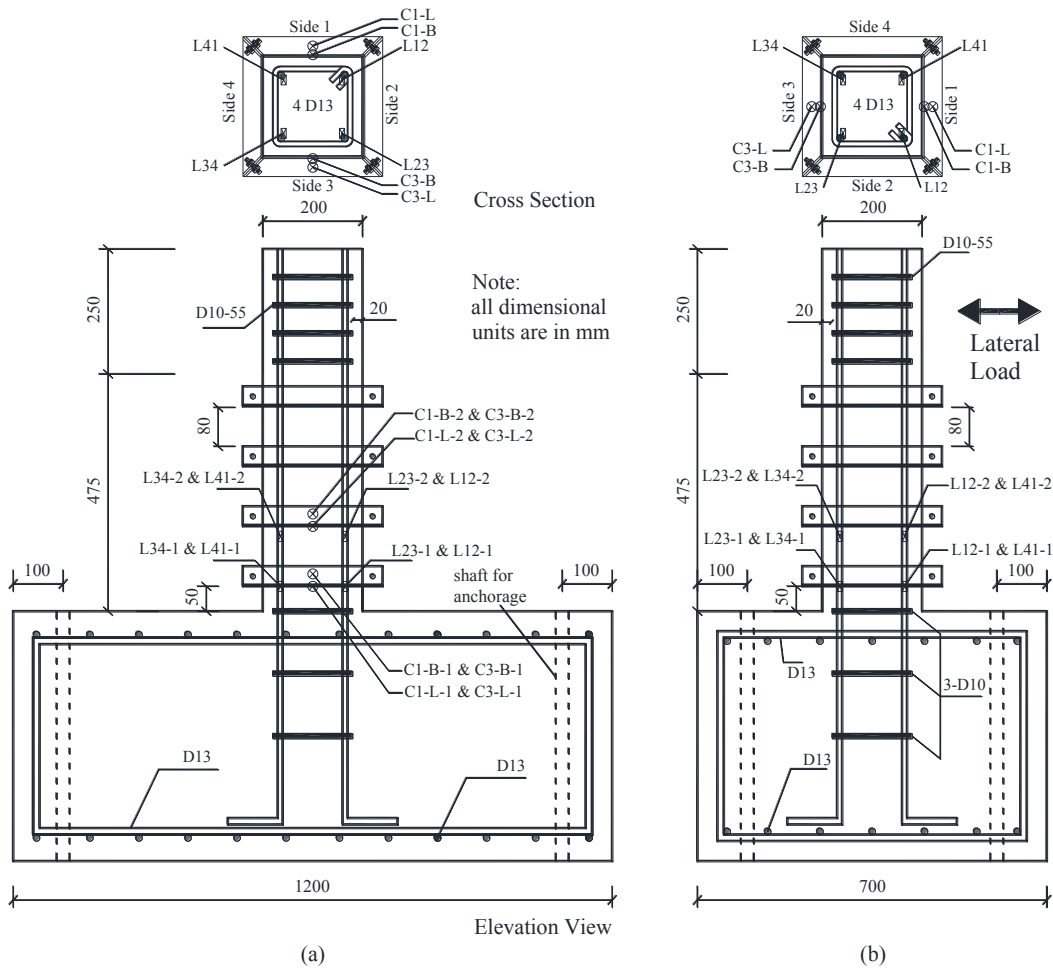
Figure 3-20 Elevation view and cross section of Specimen S14 : (a) transverse to lateral load direction ; (b) in lateral load direction

88
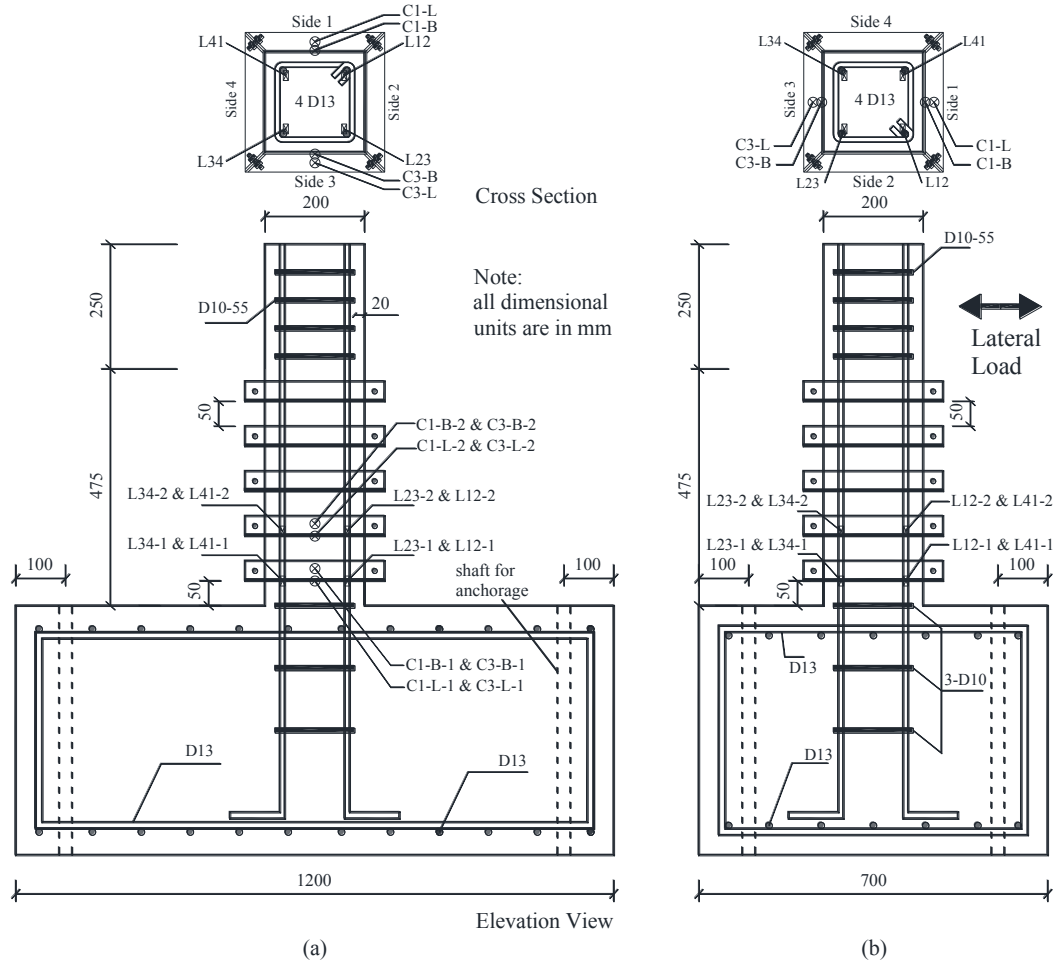
Figure 3-21 Elevation view and cross section of Specimen S15 : (a) transverse to lateral load direction ; (b) in lateral load direction

Table 3-2 The data of experimental specimens (combined lateral and compressive test)

No.	Specimen ID	Internal Confinement / Stirrups	External Confinement / Steel Collars
1	CS11	D10-150 (VR = 0.785 %)	None
2	CS12	D10-50 (VR = 2.36 %)	None
3	S13	None	L40 - 180 (VR = 4.27 %)
4	S14	None	L40 - 120 (VR = 6.40 %)
5	S15	None	L40 - 90 (VR = 8.53 %)

3.4   MATERIAL MECHANICAL PROPERTIES

3.4.1   Monotonic axial compressive loading test (Phase 1)

The mechanical properties of the concrete used in the specimens were obtained from standard cylinders (150 mm x 300 mm). The cylinder tests were conducted the same days as the columns tests (at 196 to 198 days of age). One

89

cylinder (out of twelve) was considered as an outlier since it only had around 12 MPa in strength. The average strength of the other eleven cylinders was 23.93 MPa (f_c') with a standard deviation of 2.01 MPa.

Tension tests were conducted to obtain the mechanical properties of steel bars as well as steel angle collars. The average yield strength $\left(f_y\right)$ of deformed bars (D10) used in the specimen (with nominal diameter of 9.5mm) was 317 MPa with 5.9 MPa standard deviation with three samples. The corresponding mean tensile strength was 486 MPa with 3.8 MPa standard deviation. Tension test of a strip plate, cut from the steel angle section, showed a yield strength $\left(f_{ysc}\right)$ of 285 MPa.

3.4.2 Combined axial compressive and reversed cyclich lateral loading test (Phase 2)

The physical properties of the material used for Phase 2 experiment were also obtained from standard tests. The average strength of 3 concrete cylinders was 16.7 MPa $\left(f_c'\right)$ with 0.56 MPa standard deviation.

The average yield strength $\left(f_y\right)$ and tensile strength $\left(f_u\right)$ of deformed bar (D10) used for the stirrups were 388 MPa and 519 MPa, respectively. While the average yield strength $\left(f_y\right)$ and tensile strength $\left(f_u\right)$ of deformed bar (D13) used for the longitudinal bars were 542 MPa and 658 MPa, respectively. The steel angle collars used were the same as Phase 1 experiment $\left(f_{ysc} = 285 \text{ MPa}\right)$.

3.5 CONSTRUCTION OF PHASE 1 SPECIMENS

In this section, preparations and construction of the specimens are described. These cover application of strain gauges, concreting of specimens, curing of specimens, and installment of steel collars.

3.5.1 Application of Strain Gauges

To measure the strains of the stee bars, and collars during experiment, strain gauges from Tokyo Sokki Kenkyujo Co., Ltd. were used. The type of the strain gauges was YEFLA-5-3L, which was indicated as single 5-mm post yield foil gauge with 3-m long wire. It is applicable for mild steel, stainless steel, copper alloy, aluminium, and other metals. It is designed to measure long strains (elongations) with capacity ranges from 10 to 15 percent. It has working temperature ranges from -20º to +80ºC. With these specifications, the requirements for the tests were served well as needed. The package as well as a sample of strain gauge used are shown in Figure 3-22.

Figure 3-22 The packing and strain gauge used

The strain gauges were attached to steel angle collars, longitudinal, and transversal bars. The face of the steel for mounting the strain gauge must be flat and smooth, and free from any dirt or grease that may cause ineffective adhesion. The flattened, and smoothened surfaces are shown in Figure 3-23.

Figure 3-23 Flattened and smoothened surface of bars prior to the attachment of strain gauges

Figure 3-24 The strain gauges attached to the bars by using provided adhesive

Figure 3-25 The strain gauges were protected by provided coating

The strain gauges were then attached by using adhesive and protected by coating provided by the same manufacturer (see Figures 3-24 and 3-25). On longitudinal bars, the strain gauges were placed on two corners of opposite sides. On transverse bars, again the strain gauges were placed on two layers of bar with two points of application, covering all sides of the specimens. These were to anticipate unexpected eccentricity during test, if any (see Figure 3-26). With the same consideration, strain gauges were also attached on steel angle collars, such that all sides of the specimen can be covered (see Figure 3-27).

Figure 3-26 Typical placing of strain gauges on longitudinal and transversal bars in the test region

Figure 3-27 Typical placing of strain gauges on steel angle collars

3.5.2   Concreting of Specimens

In making the specimens, a good shape and stiff formworks were necessary. Formworks constructed from 12-mm thick multiplex were used, and clamped by several bolted wooden ribs, as shown in Figure 3-28. Inside the formworks were reinforcement cage and well coded strain gauges. Samples of reinforcement cage for specimens without internal confinement in the test region (e.g. Specimen S04), and the coded strain gauges of the stirrups (e.g. Specimen CS02a) are shown in Figures 3-29 and 3-30. Two pairs of rods were also installed to mark the gauge length used in the test (see Figure 3-31). Concrete was mixed from Pozzolanic Portland Cement (PPC), well selected sand and crushed stone, and potable, clean, and fresh water (see Figures 3-32 to 3-34). Concrete mixing, placing, and compacting can be seen in Figures 3-35 to 3-37. The in place concrete for specimens as well as standard cylinder are shown in Figure 3-38.

Figure 3-28 Formworks used for the specimens

Figure 3-29 A sample of reinforcement cage (e.g. Specimen S04)

Figure 3-30 A sample of reinforcement cage with installed coded strain gauges (e.g. Specimen CS02a)

Figure 3-31 Typical rods installment for gauge length marking (e.g. Specimen S02)

Figure 3-32 Pozzolanic Portland Cement

Figure 3-33 Lumajang sand used in the concrete mix

Figure 3-34 Coarse aggregate (crushed stones) used in the concrete mix

Figure 3-35 Concrete mixing process

Figure 3-36 Concrete placing by using hand shovel

Figure 3-37 Vibrated concrete to minimize trapped bubbles

Figure 3-38 Molded specimens and standard cylinders

3.5.3   Curing of Specimens

Curing was started for specimens after the removal of the molding, that is one day after the casting process. In this experiment, the standard cylinder concretes were submerged into curing tank up to 28 days old. The specimens were protected from direct sunlight, and watered daily to maintain the moisture level (see Figures 3-39 and 3-40).

Figure 3-39 Curing of standard cylinders

Figure 3-40 Cover of specimens to prevent direct sunlight

3.5.4 Installment of steel angle collars

The curing process was conducted until the concrete reached 28 days of age. After the curing, specimens were white painted so that any crack during the test could be easily observed. The steel collars were also painted to prevent corrosions. The externally collared column specimens can be seen in Figure 3-41. All specimens were then transported to the Structural Laboratory of Research Center for Human Settlement to be tested.

Figure 3-41 Externally collared column specimens

3.6 CONSTRUCTION OF PHASE 2 SPECIMENS

In this section, preparation of the quasi-static combined axial and cyclic lateral load test is covered. The strain gauges used in the specimens were the same as those used in the monotonic compressive test. The steel reinforcement and the formwork were prepared as design and presented in Figures 3-42 to 3-44. The concrete was provided by a readymix. The foundations (footings) of all five specimens were casted first and the five columns were casted shortly after (Figures 3-45 to 3-47). This was done to minimize the variation of concrete grade in the five column specimens (which were casted with minimum time interval). During the casting, standard cylinder specimens were also made to identify the concrete strength at various stages (Figure 3-48). Finally, after the casting of columns, steel plates were anchored to the heads of columns. These plates were intended to uniformly distribute the axial load during the test (Figure 3-49).

Figure 3-42 Prepared formworks and reinforcements of the specimens

Figure 3-43 Reinforcement of typical footing of the specimens

Figure 3-44 Reinforcement of column head

Figure 3-45 Concrete casting of foundation

Figure 3-46 Concrete compacting of foundation

Figure 3-47 Concrete compacting of column

Figure 3-48 Concrete casting of standar cylinder

Figure 3-49 Steel plate of column head

After a few days of casting, the formworks were dismantled. The same curing method was applied to column specimens and standard cylinders. They were placed inside the laboratory building to avoid direct sunlight, and were covered with wet gunny sacks (burlaps) to maintain good moisture. After approximately three weeks of age, the specimens were dried in the room condition

for a week. White paint was then applied, and the external steel angle collars were installed (Figure 3-50), and the specimens were ready to be tested.

Figure 3-50 The five column specimens for quasi-static combined axial and cyclic lateral load test

3.7 TEST SETUP AND TESTING PROCEDURE

In this section, experimental test set up for the specimens as well as loading procedure are described. The experimental tests were conducted in the Structural Laboratory of Research Center for Human Settlement (Puslitbang Permukiman). This research center has several laboratories. This study took place in the Structure and Building Construction laboratory.

3.7.1 Monontonic compressive axial load (Phase 1)

This section describes the experimental setup in order to obtain the desired data. Load cells to measure vertical load and four LVDTs to measure the axial displacement that were used for compression tests. The illustration of load cells and LVDTs used is shown in Figure 3-51. Four load cells with capacity of 50 tons each were installed under the specimens (Figure 3-52). Three 60-mm thick plates were placed on these load cells to ensure uniform load distributions (see Figure 3-53). The column specimens were place on the plates with the columns' axis must be coincide with the center of four load cell configuration. One Linear

Variable Differential Transducer (LVDT) was installed at each side of the column specimen to measure the axial deformation during the test (see Figure 3-53). All load cells, LVDTs, and strain gauges were then connected to a data logger. On screen real time measurements could be seen from a computer connected to the system (Figure 3-54). All specimens were tested in a universal testing machine with the capacity of 5000 kN. The specimens were tested under incremental axial concentric loading. The strain rate was slow enough to be considered quasi-static.
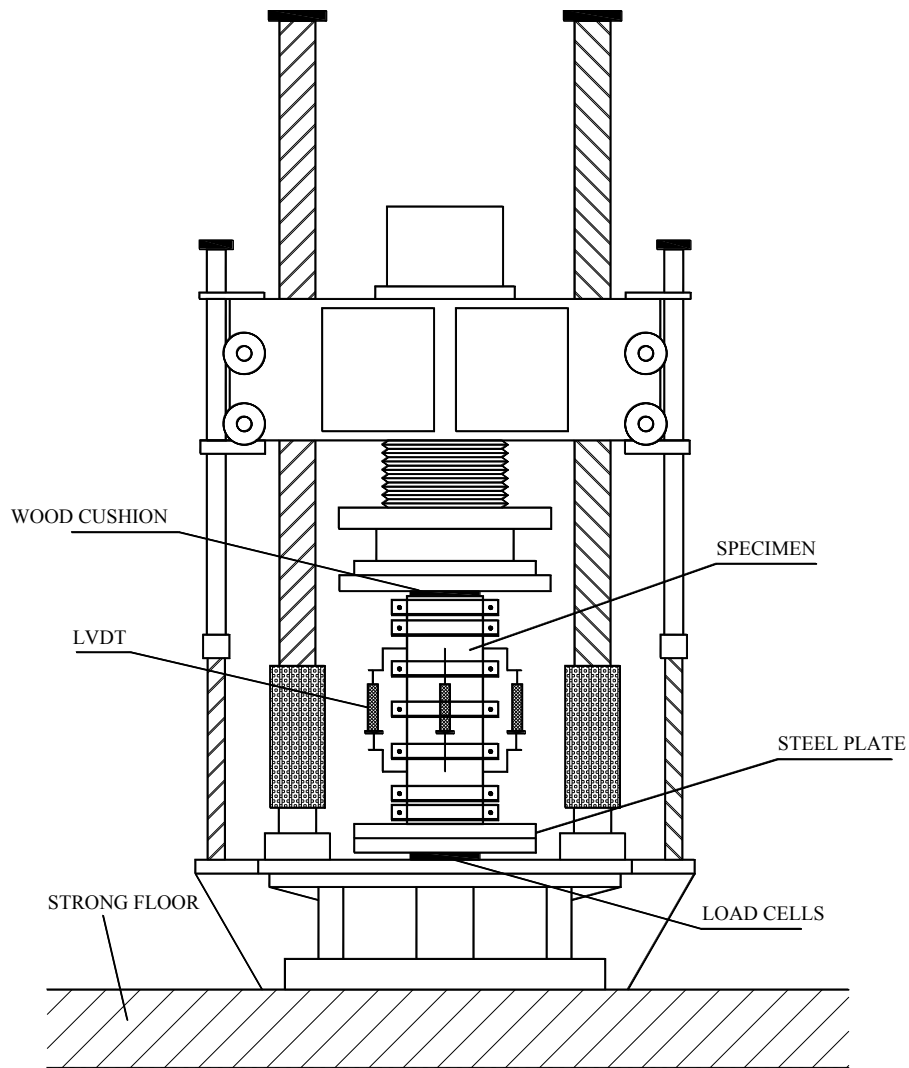
Figure 3-51 Compression test setup (static monotonic)

105

Figure 3-52 Four load cells with 50 ton capacity each

Figure 3-53 Typical axial compressive test set-up
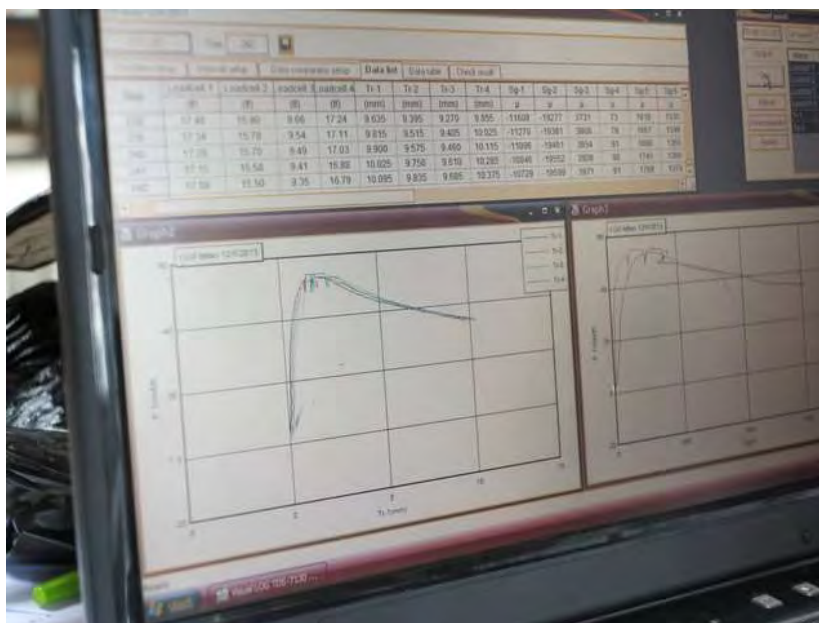
Figure 3-54 Real time on screen display during the test

3.7.2 Combined axial compressive and reversed cyclic loading (Phase 2)

For the combined axial compressive and reversed cyclic loading, all specimens were initially loaded to achieve the desired axial load of approximately $0.3A_g f_c'$, and kept constant throughout the test (Figure 3-55). Than a sequence of cyclic lateral load (according to ACI 374.1-05) was applied to the column specimens (see Figure 3-56). The lateral load was applied under displacement control, with series of 3 cycles of constant drifts until the column specimens failure (or the resistance of lateral load dropped below 50 percent of its peak). To illustrate the test setup further, Specimens S14 is taken as an example. It can be seen in Figure 3-57, the specimen was fixed to the strong floor by using six anchors. A vertical hydraulic jack was positioned on top of the column head, and was supported by stiff steel frame. A pair of clamping steel plates were installed at the column head providing attachment point of a horizontal jack which was supported by a strong wall. Besides the strain gauges, several LVDTs were set to measure various deformation of the specimen during the test. All strain gauges and LVDTs were connected to a data logger and computer to record all data during the test. The codes, and locations of each measuring device were taken carefully as shown in Figures 3-58 and 3-59. Necessary notes of the measuring

107

device were listed in Table 3-3. The overall data of measuring devices of all specimens are presented in Appendix A.
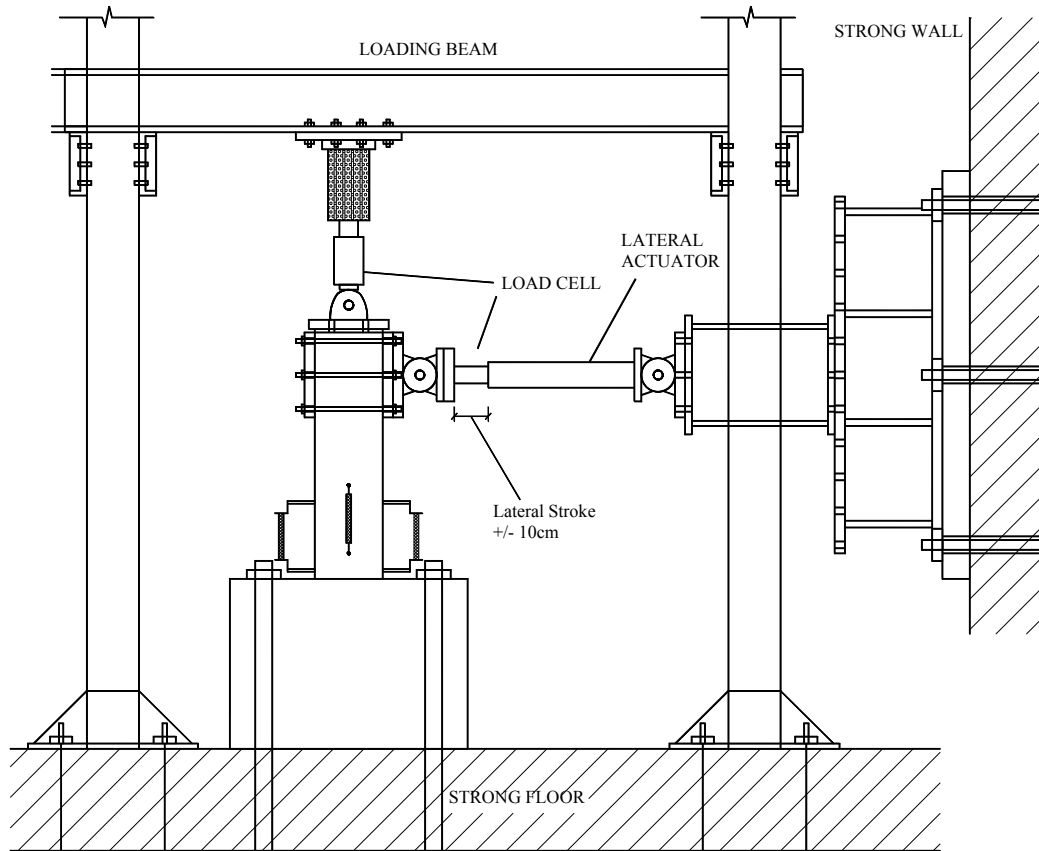
Figure 3-55 Combined axial compressive and reversed cyclic lateral load test
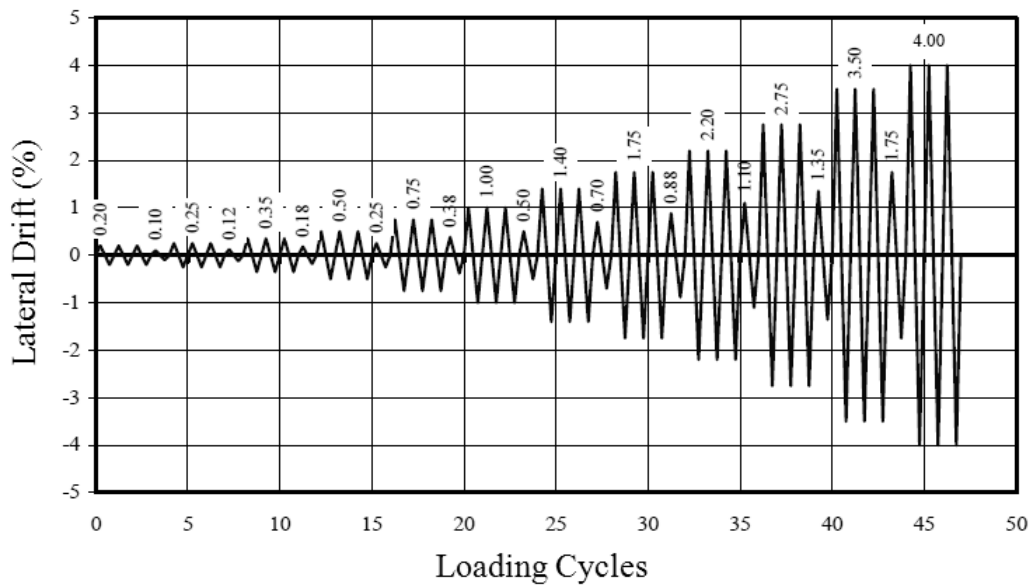
Figure 3-56 Sequence of lateral displacement used in the test (ACI 374.1-05)

108

Figure 3-57 Typical setup for combined axial compressive and reversed cyclic lateral load test
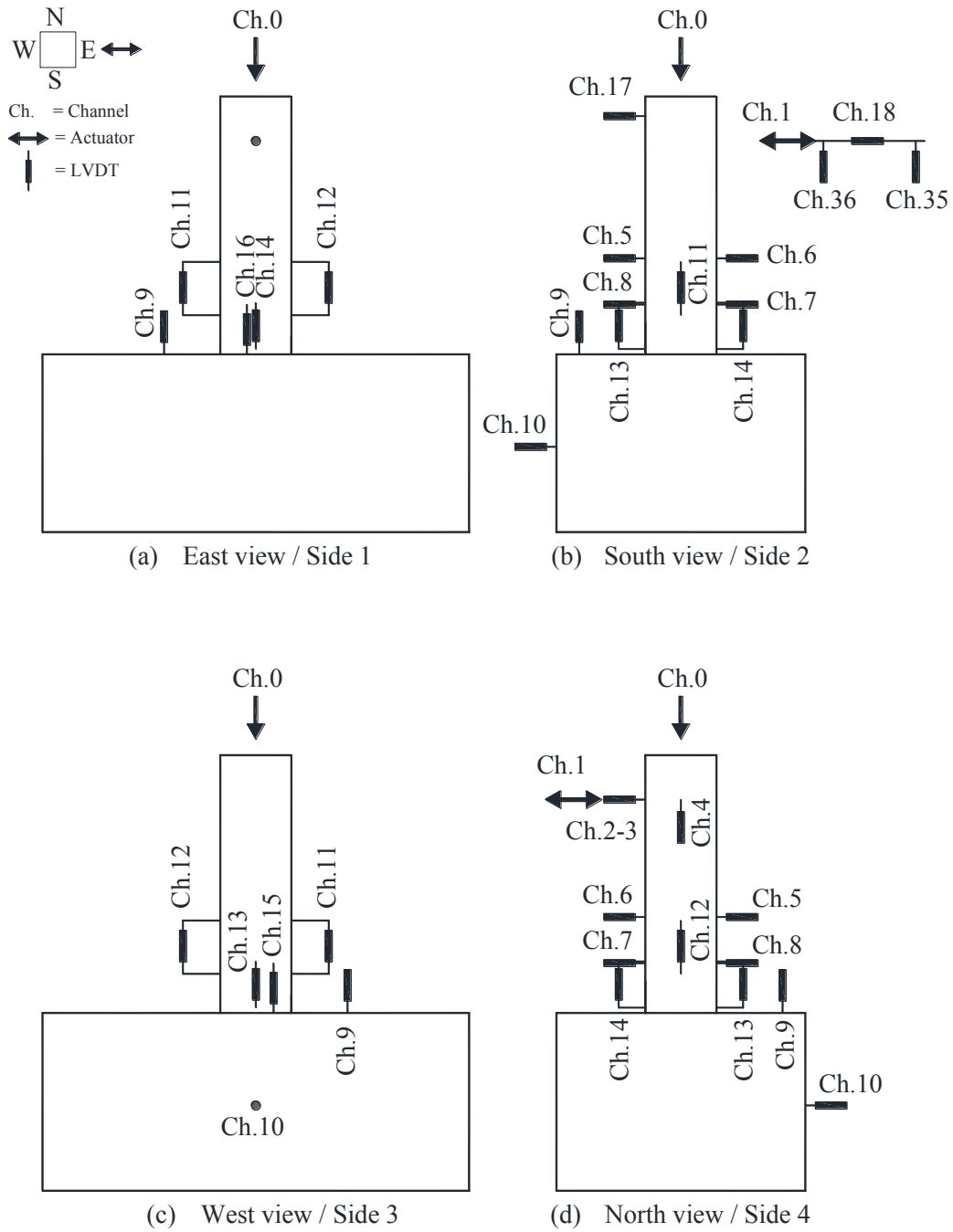
Figure 3-58 Data logger channel numbers : (a) East view / Side 1; (b) South view / Side 2; (c) West view / Side 3; and (d) North view / Side 4

110
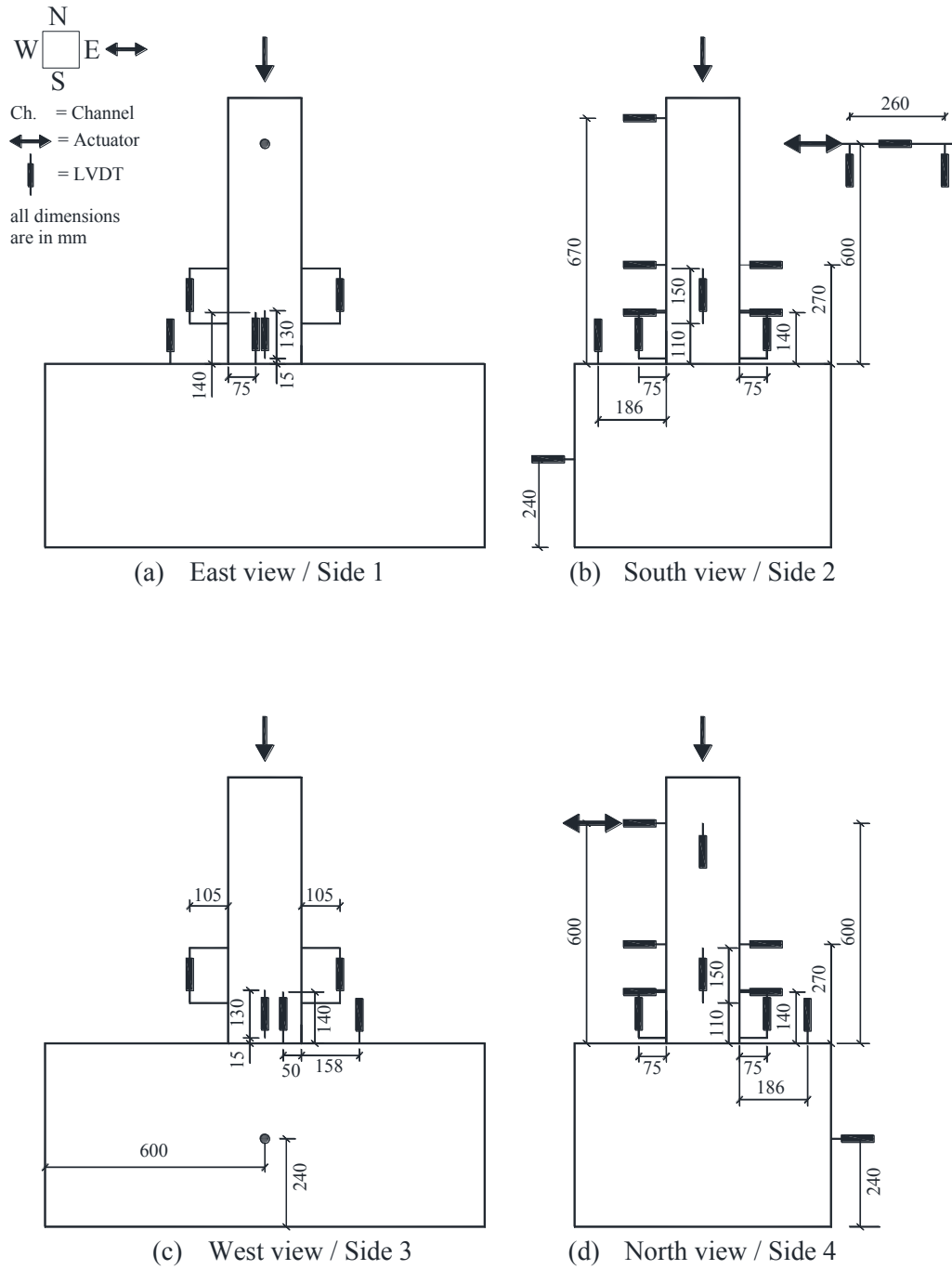
Figure 3-59 Locations of each data logger channel : (a) East view / Side 1; (b) South view / Side 2; (c) West view / Side 3; and (d) North view / Side 4

Table 3-3 Channel numbers data

Channel	TR/SG	Note
0	A	Vertical Load
1	V	Horizontal Load
2	WR/TR-1	dH, hz jack (wire), H=60cm
3	TR-2	dH, hz jack, H=60cm
4	TR-3	dV, side 4, H=60cm
5	TR-4	dH, side 3, H=27cm
6	TR-5	dH, side 1, H=27cm
7	TR-6	dH, side 1, H=14cm
8	TR-7	dH, side 3, H=14cm
9	TR-8	dV, footing, side 3
10	TR-9	dH, footing, side 3 (H=24cm)
11	TR-10	dV, side 2, L0=15 cm (H1=11cm, H2=26cm)
12	TR-11	dV, side 4, L0=15 cm (H1=11cm, H2=26cm)
13	TR-12	dV, side 3, L0=13 cm (H1=1.5cm, H2=14.5cm)
14	TR-13	dV, side 1, L0=13 cm (H1=1.5cm, H2=14.5cm)
15	TR-14	dV, side 3, H=14cm
16	TR-15	dV, side 1, H=14cm
17	TR-16	dH, side 3, H=67cm
18	WR/TR-17	dH, hz jack (wire), H=60cm
19	SG-1	L12-1 (longitudinal bar, corner 12, H=5cm)
20	SG-2	L23-1 (longitudinal bar, corner 23, H=5cm)
21	SG-3	L12-2 (longitudinal bar, corner 12, H=15cm)
22	SG-4	L23-2 (longitudinal bar, corner 23, H=15cm)
23	SG-5	L41-1 (longitudinal bar, corner 41, H=5cm)
24	SG-6	L34-1 (longitudinal bar, corner 34, H=5cm)
25	SG-7	L41-2 (longitudinal bar, corner 41, H=15cm)
26	SG-8	L34-2 (longitudinal bar, corner 34, H=15cm)
27	SG-9	C1-L-1 (collar side 1, Leg/hz, hb=5cm)
28	SG-10	C3-L-1 (collar side 3, Leg/hz, hb=5cm)
29	SG-11	C1-B-1 (collar side 1, Back/vt, hb=5cm)
30	SG-12	C3-B-1 (collar side 3, Back/vt, hb=5cm)
31	SG-13	C1-L-2 (collar side 1, Leg/hz, hb=17cm)
32	SG-14	C3-L-2 (collar side 3, Leg/hz, hb=17cm)
33	SG-15	C1-B-2 (collar side 1, Back/vt, hb=17cm)
34	SG-16	C3-B-2 (collar side 3, Back/vt, hb=17cm)
35	TR-18	dV, hz jack, point 1 (near support), D12=26cm
36	TR-19	dv, hz jack, point 2 (near hinge), D12=26cm

3.8   SUMMARY

In this Chapter, the design and preparation of the specimens are described. The experimental programs consisted of two phases which were monotonic axial compression test, and combined axial compression and reversed lateral loading test. The test setup as well as the loading procedures were also presented.

= This Page is Intentionally Left Blank =

CHAPTER 4. MONOTONIC AXIAL COMPRESSION TEST (PHASE 1)

In this Chapter, the results of monotonic axial compression test is presented and discussed as Phase 1 of the experimental program.

4.1 RESULTS OF THE TEST (PART 1)

The first set of monotonic axial compression tests was conducted on eight specimens. The control specimens cover columns with no stirrups in the test region (CS01), minimum stirrups for shear requirement (CS02a), and stirrups requiered by seismic provisions (CS03a) as previously explained in Chapter 3. The other five Specimens S01, S02, S03, S04, and S05 are only externally confined with the steel collars. Axial displacements were controlled by using LVDTs during the test and the axial resistance of the columns were recorded by using load cells. The tests were stopped if one of the following criteria was found: (1) failure of specimen; (2) resistance drops below 50 percent of the peak strength; or (3) limitation of LVDT capacity. The main parameter recorded and calculated for all specimens are listed in Table 4-1. From control Specimen CS01, it was found that the concrete strength was equal to 17.02 MPa $\left(f'_{c0} = P_{cmax} \big/ \left(A_g - A_s \right) \right)$. The ratio of this peak strength with respect to the cylinder strength $\left(f'_{c0} / f'_c \right)$ was equal to 0.711, with peak strain $\left(\varepsilon'_{cc} \right)$ and ultimate strain $\left(\varepsilon'_{ccu} = \varepsilon_{f50} \right)$ were equal to 0.23 and 1.37 percent, respectively. The commonly used parameters to identify the ductility for axially loaded specimens is the relative strain ducitily ratio $\left(\mu_\varepsilon = \varepsilon_{f85} / \varepsilon_{01} \right)$. The absolute strain ductility ratio $\left(\mu_{\varepsilon a} = \varepsilon_{f85} / \varepsilon'_{cc} \right)$ was also listed in Table 4-1 for consideration.

Table 4-1 Summary of compression test results of Specimens CS01 to S05

Parameters	CS01	CS02a	CS03a	S01	S02	S03	S04	S05
P_{max} - kN	762.92	734.57	905.07	822.86	985.41	906.93	922.73	1051.04
P_{cmax} - kN	675.80	644.69	815.19	732.98	895.54	817.06	832.85	961.16
P_0 - kN	897.73	897.73	897.73	897.73	897.73	897.73	897.73	897.73
P_{0c} - kN	807.85	807.85	807.85	807.85	807.85	807.85	807.85	807.85
P_{0cc} - kN	457.66	457.66	457.66	807.85	807.85	807.85	807.85	807.85
P_{max}/P_0	0.85	0.82	1.01	0.92	1.10	1.01	1.03	1.17
P_{cmax}/P_{0c}	0.84	0.80	1.01	0.91	1.11	1.01	1.03	1.19
P_{cmax}/P_{0cc}	1.48	1.41	1.78	0.91	1.11	1.01	1.03	1.19
ε_{pmax} (%)	0.23	0.38	1.75	0.26	0.45	0.57	0.33	1.83
ε_{cc} (%)	0.23	0.38	1.75	0.26	0.45	0.57	0.33	1.83
$\varepsilon_{01}=\varepsilon_{cc}$ CS01 (%)	0.23	0.23	0.23	0.23	0.23	0.23	0.23	0.23
ε_{f85} (%)	0.38	0.76	3.61	0.53	1.12	1.89	0.80	6.07
ε_{f80} (%)	0.43	0.85	4.22	0.60	1.34	2.42	1.26	7.20
ε_{f50} (%)	1.37	1.57	10.90	1.86	3.76	8.97	3.89	10.80
$\mu_{\varepsilon a}=\varepsilon_{f85}/\varepsilon_{cc}$	1.63	2.02	2.06	2.02	2.47	3.30	2.45	3.32
$\mu_{\varepsilon}=\varepsilon_{f85}/\varepsilon_{01}$	1.63	3.27	15.55	2.30	4.84	8.15	3.46	26.16
ε_{spall} theoretically (%)	0.30	0.30	0.30	0.30	0.30	0.30	0.30	0.30
ε_{spall} observed (%)	brittle	0.19	0.32	0.39	0.49	0.36	0.25	0.40

Notes:

P_{max} is the maximum axial resistance of the specimen

P_{cmax} is the maximum axial resistance of the specimen contributed by concrete

P_0 is the theoretical nominal axial capacity $\left(=0.85 f_c'\left(A_g - A_s\right)+f_y A_s\right)$

P_{0c} is the theoretical concrete nominal axial capacity $\left(=0.85 f_c'\left(A_g - A_s\right)\right)$

P_{0cc} is the confined core nominal axial capacity $\left(=0.85 f_c' A_{cc}\right)$

ε_{Pmax} is the axial strain corresponding to P_{max}

ε_{cc} is the axial strain corresponding to P_{cmax}

ε_{01} is the ε_{cc} of unconfined Specimen CS01

ε_{f85} is the strain corresponding to 0.85 P_{cmax} on the descending curve

ε_{f80} is the strain corresponding to 0.80 P_{cmax} on the descending curve

ε_{f50} is the strain corresponding to 0.50 P_{cmax} on the descending curve

ε_{spall} theoretically is the theoretical strain at the start of concrete spalling

116

ε_{spall} observed is the observed strain at the start of concrete spalling

$\mu_{\varepsilon a}$ is the absolute strain ductility ratio $\left(= \varepsilon_{f85}/\varepsilon'_{cc}\right)$

μ_{ε} is the relative strain ductility ratio $\left(= \varepsilon_{f85}/\varepsilon_{01}\right)$

f'_c is the concrete compressive strength

A_g is the gross sectional area

A_s is the longitudinal steel area

f_y is the yield strength of longitudinal steel

A_{cc} is the area of confined concrete

It can be seen that CS01 and CS02a showed very brittle behaviors, that the strength decreased rapidly after reaching the peak strength ($\mu_{\varepsilon} = 1.63$ and 3.27, respectively). S01 showed rather similar behavior except that it had late post-peak ductility response ($\mu_{\varepsilon} = 2.30$). CS03a showed good ductility ($\mu_{\varepsilon} = 15.55$) until it finally lost the strength at about 10 percent axial strain. For collared column specimens with higher volumetric ratios, better ductility patterns were observed except for Specimen S04 which suffered early steel collar failure. Specimens S02, S03, and S05 indicated μ_{ε} of 4.84, 8.15, and 26.16, respectively, whereas Specimen S04 only showed μ_{ε} of 3.46. In terms of strain ductility ratio, the proposed retrofitting method had demonstrated that it could get comparable value as the conventionally confined Specimen CS03a with minimum stirrups required by the seismic provisions. The onset of concrete spalling during the test were slightly difficult to detect since the load-displacement curve did not reveal particular signs or indication. For specimens characterized by sudden brittle failure, the onset of spalling and total failure might occur almost instantly. Theoretically, when the concrete reached ultimate compression strain (approximately 0.30 percent), the concrete crack and spalling would occur. It should be noted that this crack is not caused by direct tension, however it is caused by large lateral expansion due to the axial compression. Thus, the observed strains at spalling are determined at the first crack of the concrete detected during the tests. The onset of cracking could not be detected only for Control Specimen

CS01 since it failed in brittle manner. The other specimens (CS02a, CS03a, S01, S02, S03, S04, S05, S04a, S04b, S04c, S04d, S04e, and S04f) showed initial spalling at strain range of about 0.19 to 0.49 percent.

The peak strength of CS01 $\left(f'_{c0} \right)$ represents the unconfined strength of the concrete specimen. This strength is used to normalize (all stress data are devided by f'_{c0}) the stress-strain curve in order to investigate the effect of confinement of other specimens. The comparison of normalized stress-strain of this first set of test is presented in Figure 4-1 (Tavio et al., 2013; Pudjisuryadi et al., 2016). The strength gain and failure remarks are summarized in Table 4-2. CS02a which was conventionally confined with deficient volumetric ratio of stirrups in the test region has shown no significant gain in strength. The Control Specimen CS03a indicated strength gain of 1.206 due to the better confinement. The collared Specimens S02 and S04 seemed to have a little deviated strength gain. Specimens S02 indicated slightly higher strength gain of about 1.325, whereas S04 showed slightly lower strength gain of approximately 1.232. The other collared Specimens S01, S03, and S05 exhibited an expected strength gain increment of 1.085, 1.209, and 1.422, respectively. Overall, S03 performed quite well with the strength gain similar to CS03a. However, S03 has less ductility compared with CS03a. S05 demonstrated the best performance in terms of both strength and ductility gains. Eventhough two steel collars of Specimen S05 failed during the test, they only occured at relatively large axial strains of around 8.60 and 11.64 percent.
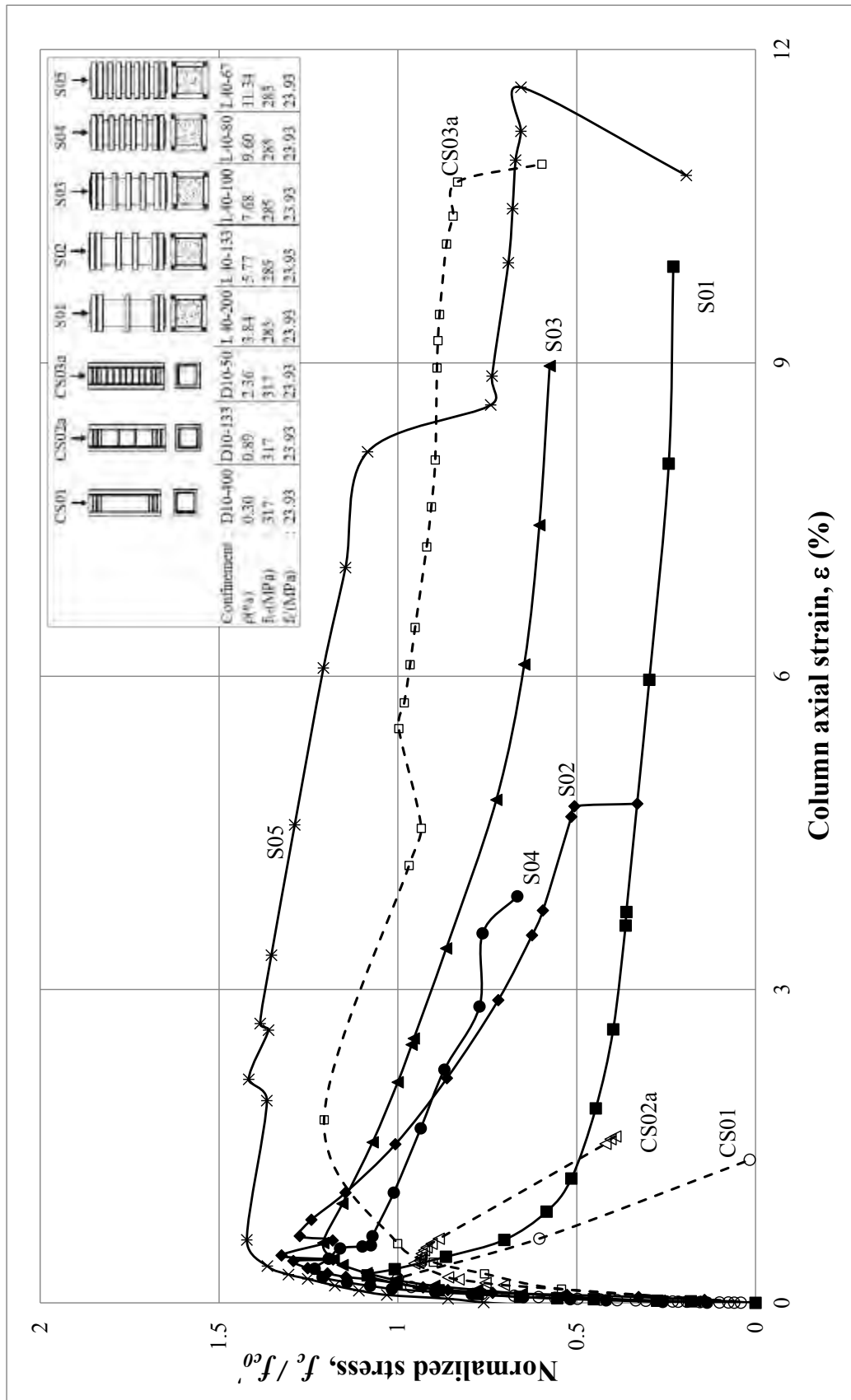
Figure 4-1 Normalized stress-strain curves of control and collared specimens

119

Table 4-2 Strength gains and failure remarks of Specimens CS01 to S05

Specimen ID	f'_{cc}/f'_{c0}	Remark for descending branch
CS01	1.000	Strength lost after descending branch dropped to 60% of peak strength (at strain 0.62%). Brittle diagonal failure and buckling of longitudinal bars were observed.
CS02a	0.954	Test was stopped after descending branch dropped below 50% of peak strength at strain about 1.5%. Excessive damages and buckling of longitudinal bars were observed.
CS03a	1.206	Test was stopped at 60% peak strength (strain 10.90%) due to LVDT limitation. It still could resist the axial force, but buckling of longitudinal bars was observed.
S01	1.085	Strength dropped below 50% at strain about 1.2 %. Brittle diagonal failure and buckling of longitudinal bars were observed.
S02	1.325	Strength dropped below 50% peak strength at strain about 3.5%. Buckling of longitudinal bars was observed.
S03	1.209	Strength dropped below 50% peak strength at strain about 7.4%. Buckling of longitudinal bars was observed.
S04	1.232	Strength dropped below 50% peak strength at strain about 3.8%. Failure of Collar 3 and buckling of longitudinal bars were observed.
S05	1.422	Two strength drops at 74% of peak strength (strain 8.60%), and at 66% of peak strength (strain 11.64%) due to broken Collars 2 and 3 respectively. Buckling of longitudinal bars was also observed.

From the strain measurement, it was evident that the stirrups as well as the steel collars acted as confinement elements. While the longitudinal bars were in compression, the stirrups and steel collars were in tension during the tests. Since the behaviors are generally the same, typical stress-strain curves for several specimens are presented here (the stresses are normalized to the strength of control Specimen CS01), and the rest of the curves are presented in Appendix B. Normalized stress-strain curve of longitudinal bars of Specimen CS01 is shown in Figure 4-2. Normalized stress-strain curve of stirrups of Specimen CS03a is shown Figure 4-3. Normalized stress-strain curve of Collar 3 of Specimen S05 is shown Figure 4-4, and the damage can be seen in Figure 4-5. The failure mechanisms suffered by the specimens are given in Figures 4-6 to 4-8. It was obvious that the absence of any confinement in CS01 has caused brittle diagonal failure of the specimen. Specimen CS02a also suffered brittle failure, but the damage was not as severe as CS01. Specimen CS03a which was confined

conventionally by stirrups required by seismic provision, could prevent the core from severe brittle failure even at very large axial strain.

For collared specimens, the confinement provided was not adequate in Specimen S01 only that the diagonal brittle failure could still be observed. Such brittle failure was completely avoided in specimens with better steel collar confinement (S02, S03, S04, and S05). It can be seen, that the concrete was protected at the regions where the steel collars were located. S04 failed to exhibit the expected performance due to early failure of the weld at the corner of one collar. Severe concrete damage was observed at the location of the failed steel collar. Specimen S05 displayed similar damage as S04, however it should be noted that the damages were occured at very later stage of the test. The complete test data, including the strains of the longitudinal bars, stirrups, and steel collars, the deformations recorded by LVDTs, as well as the photographs of the damaged concrete and steel collars are all given in Appendix B.
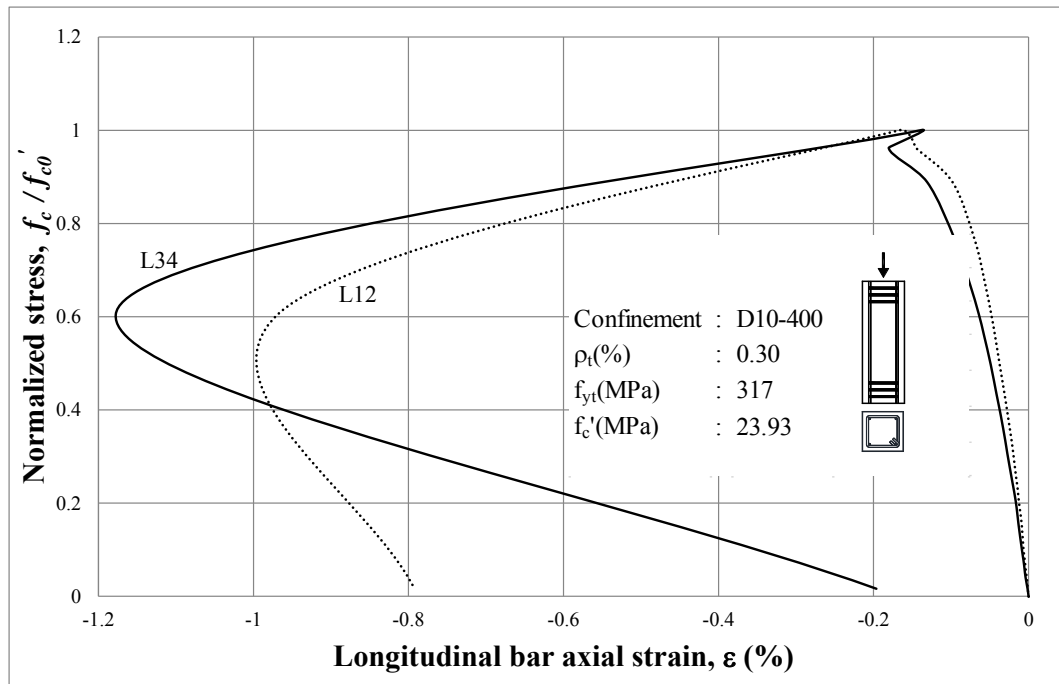
Figure 4-2 Column axial stress-longitudinal bar axial strain curves of CS01
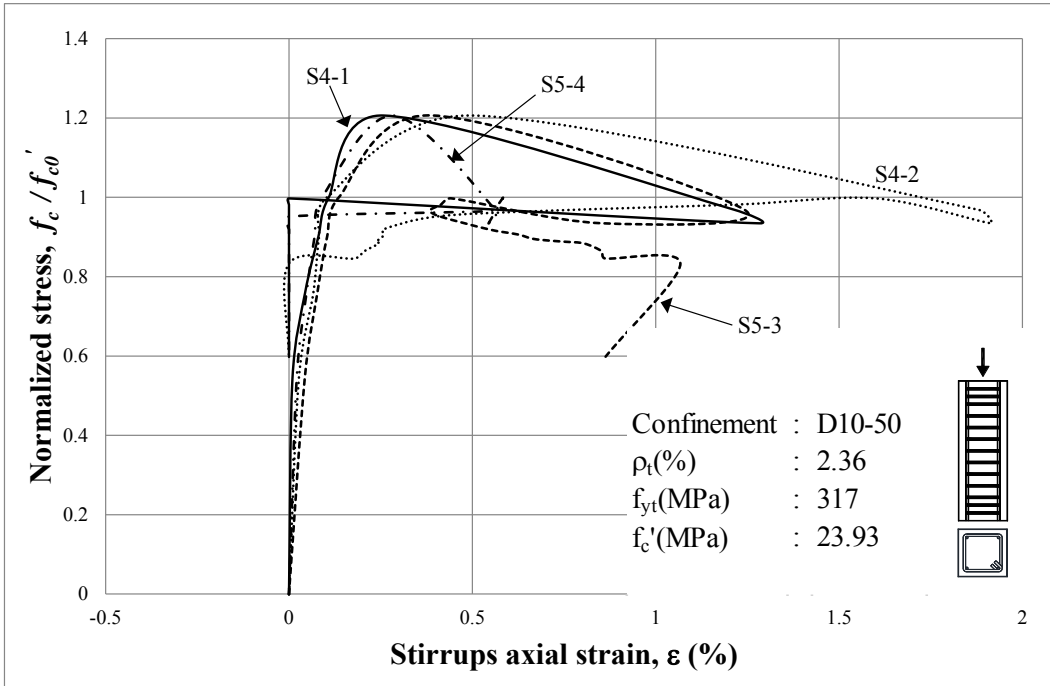
Figure 4-3 Column axial stress-stirrups strain curves of CS03a
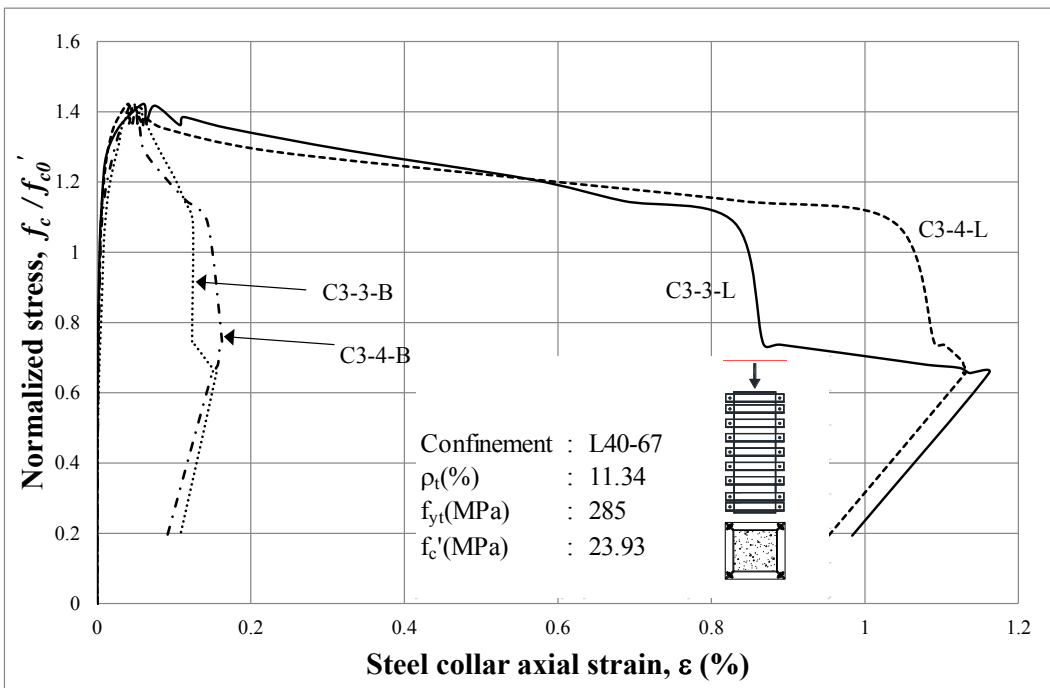
Figure 4-4 Column axial stress-steel collar axial strain curves of S05 (Collar 3)

122
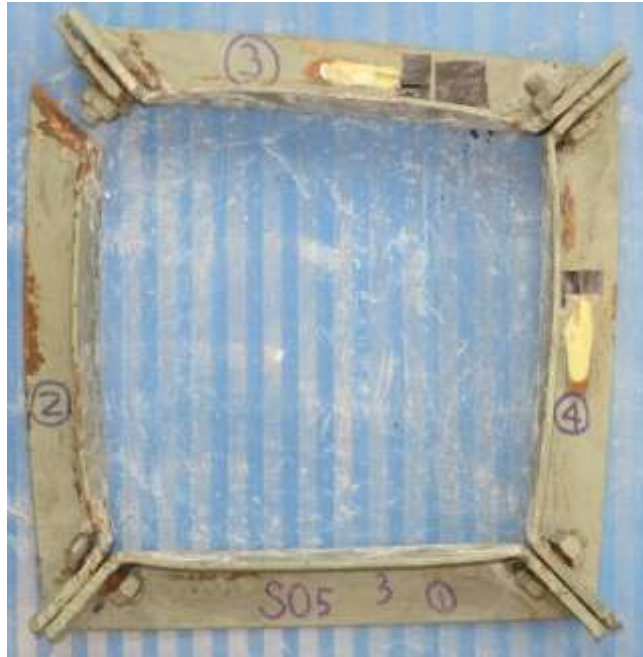
Figure 4-5 Collar 3 of S05 after the completion of the test

(a)	**(b)**	**(c)**
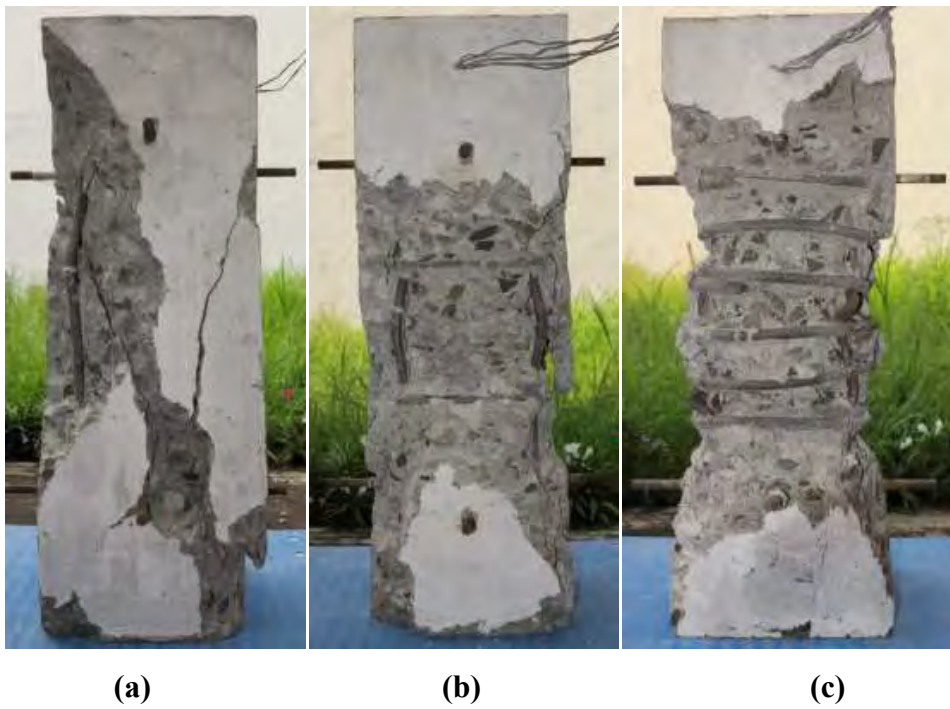
Figure 4-6 Specimens: (a) CS01; (b) CS02a; and (c) CS03a after the completion of the tests

Figure 4-7 Specimens: (a) S01; (b) S02; and (c) S03 after the completion of the tests

Figure 4-8 Specimens: (a) S04; and (b) S05 after the completion of the tests

4.2 RESULTS OF THE TEST (PART 2)

The second set of the tests was intended to explore the potential of steel collar confinement (six specimens). Specimens S04a and S04b which combined internal stirrups and steel collar were intended to verify the performance of proposed external confining technique for retrofitting works. The other four Specimens S04c, S04d, S04e, and S04f were built exactly the same as Specimen S04. Specimens S04c and S04d were confined with steel collars stiffened by web stiffeners. Steel collars were used to externally confine Specimens S04e, and S04f with dyna bolts applied to give additional attachment. Important data of the experiment are listed in Table 4-3. Normalized axial stress-strain curves of the specimens, altogether with Spesimen S04 are presented in Figure 4-9 (Tavio et al., 2014, and 2015). The strength gains and failure remarks are summarized in Table 4-4.

Table 4-3 Summary of compression test results of Specimens S04a to S04f

Parameters	S04a	S04b	S04c	S04d	S04e	S04f
P_{max} - kN	1302.96	1286.19	956.77	1012.10	1162.98	1145.51
P_{cmax} - kN	1213.09	1196.31	866.89	922.22	1073.10	1055.64
P_0 - kN	897.73	897.73	897.73	897.73	897.73	897.73
P_{0c} - kN	807.85	807.85	807.85	807.85	807.85	807.85
P_{0cc} - kN	807.85	807.85	807.85	807.85	807.85	807.85
P_{max}/P_0	1.45	1.43	1.07	1.13	1.30	1.28
P_{cmax}/P_{0c}	1.50	1.48	1.07	1.14	1.33	1.31
P_{cmax}/P_{0cc}	1.50	1.48	1.07	1.14	1.33	1.31
$\varepsilon_{p\,max}$ (%)	2.09	1.66	0.69	0.50	0.65	0.41
ε_{cc} (%)	2.09	1.66	0.69	0.50	0.65	0.41
$\varepsilon_{01}=\varepsilon_{cc}$ CS01 (%)	0.23	0.23	0.23	0.23	0.23	0.23
ε_{f85} (%)	4.92	5.24	2.57	2.43	2.87	2.19
ε_{f80} (%)	6.32	7.40	3.30	3.27	3.72	2.88
ε_{f50} (%)	still 77%	still 80%	5.01	5.88	still 59%	9.09
$\mu_{\varepsilon a}=\varepsilon_{f85}/\varepsilon_{cc}$	2.36	3.15	3.73	4.86	4.39	5.38
$\mu_{\varepsilon}=\varepsilon_{f85}/\varepsilon_{01}$	21.21	22.58	11.08	10.47	12.38	9.46
ε_{spall} theoretically (%)	0.30	0.30	0.30	0.30	0.30	0.30
ε_{spall} observed (%)	0.34	0.25	0.51	0.31	0.32	0.29
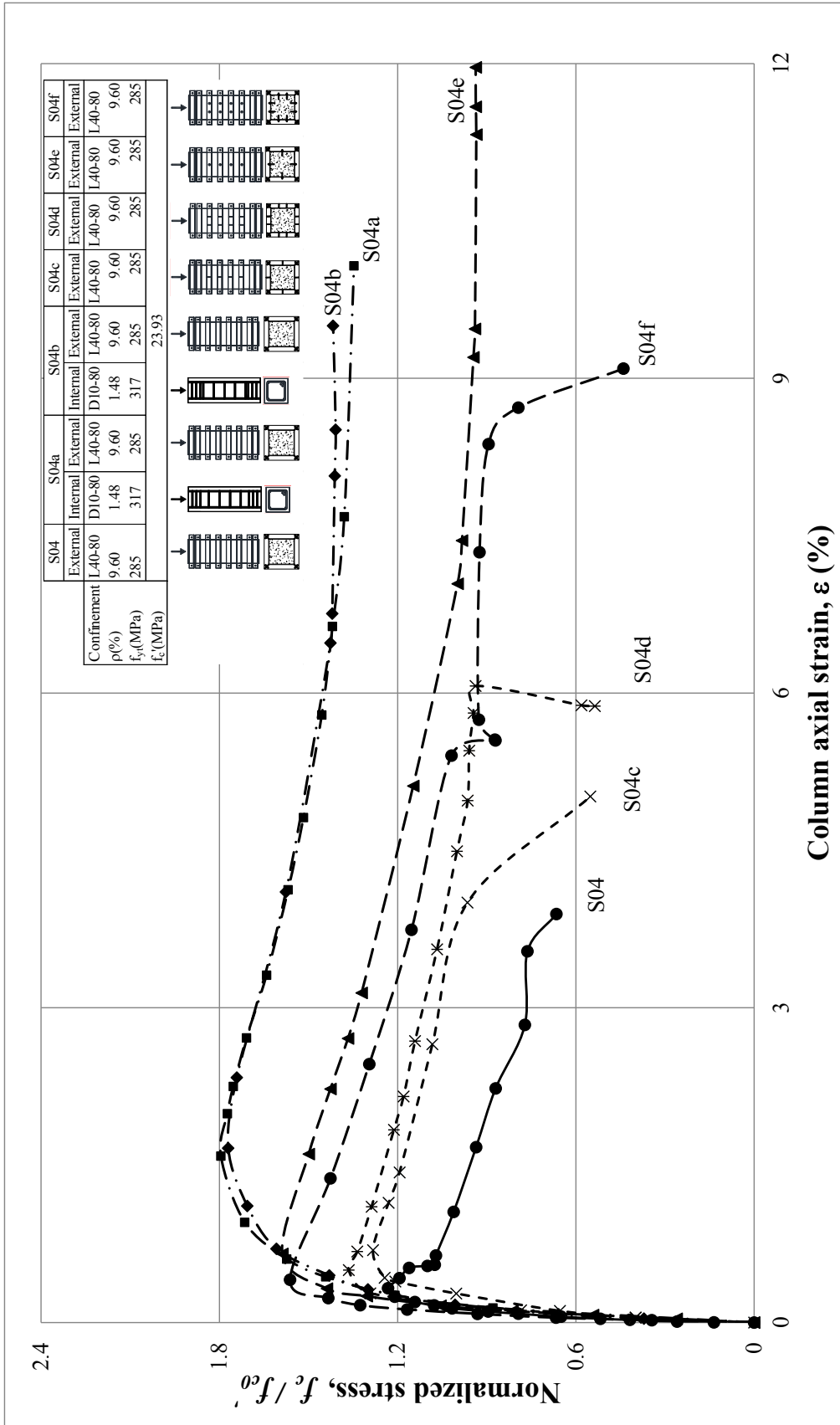
Figure 4-9 Normalized stress-strain curves of collared Specimens S04 to S04f

A very promising finding were demonstrated by the results of Specimens S04a and S04b. These two specimens performed best, and proved that the application of external steel collars could improve significantly the performance of the columns with lack internal stirrups. The strength gains of S04a and S04b were found as high as 1.795 and 1.770, respectively, while the strain ductilities (μ_ε) were found to be 21.21 and 22.58, respectively. This promises that the proposed external confinement technique is very suitable for retrofitting work of existing RC columns. The performances of the two specimens were practically similar dispite the difference of location of the internal stirrups. This might be due to the close stirrups and steel collars spacings, such that the deviation in the performances were not very evident. The initial concrete spalling occured at strains about 0.34 and 0.25 percent for Specimens S04a and S04b, respectively.

Specimens S04c and S04d showed strength improvements over S04 (1.286 and 1.365, respectively) and much improved ductilities (μ_ε=11.08 and 10.47, respectively). Noting that the standard Specimen S04 suffered earlier collar failure and the performance of S04c and S04d (strength and ductility gains) which fell between standard Specimens S03 and S05, it seemed that the influence of the web stiffeners was not very effective. This is because of the local instability of the steel collars did not occur during the tests. This was supported by the fact that the performance of specimens strengthened with two web stiffeners (S04d compared to S04c) did not show significant improvement. The strength gains of S04c and S04d were also the lowest of all six specimens. The initial spalling occured at strains about 0.51 and 0.31 percent for Specimens S04c and S04d, respectively.

Specimens S04e and S04f which collars attachment were strengthened with dyna bolts performed better peak strengths as well as ductilities. The ductilies of S04e and S04f were recorded as high as 12.38 and 9.46, respectively. The strength gains of S04e and S04f (1.588 and 1.562, respectively) were better than S04c and S04d, however, they were still below S04a and S04b. The additional attachment by using the dyna bolts has clearly improved the performance of the retrofitting technique. However, it shoud be noted that using

more bolts do not necessarily mean better performance. In this experiment, specimen with more bolts (S04f) exhibbited significantly less ductility and slightly lower strength. This might be due to the trade of between the addition of attachment points (dyna bolts) and the damage of the concrete (damage due to the drilling works prior to the bolt attachment). The initial concrete spalling occured at strains of about 0.32 and 0.29 percent for Specimens S04ce and S04f, respectively.

Similar to the first set of the tests, the strain measurement confirmed that the stirrups as well as the steel collars acted as confinement element (tension forces were detected). Large non-linear axial strains were observed in longitudinal bars when the specimen approached its peak strength. Typical deformed steel collar of the specimens after the completion of the tests are shown in Figure 4-10. The damage suffered by the specimens can be seen in Figure 4-11. Only Specimen S04c indicated diagonal splitting failure. The rest of the spesimens had similar level of damages at the final stage after the completion of the tests. However, it should be noted that those failure photographs were taken at different ultimate axial strains. The complete data are provided in Appendix C.

Table 4-4 Strength gain and failure remarks of Specimens S04a to S04f

Specimen	f'_{cc}/f'_{c0}	Remark (descending branch)
S04a	1.795	Test was stopped at 77% of peak strength (strain 10.85%) due to LVDT limitation. Buckling of longitudinal bars were observed.
S04b	1.770	Test was stopped at 80% of peak strength (strain 9.50%) due to LVDT limitation. Buckling of longitudinal bars were observed.
S04c	1.283	Strength loss after reaching 75% of peak strength on the descending branch at strain about 4.00%. Failure of Collar 2 and buckling of longitudinal bars were observed.
S04d	1.365	Strength loss after reaching 69% of peak strength on the descending branch at strain about 6.07%. Failure of Collar 3 and buckling of longitudinal bars were observed.
S04e	1.588	Test was stopped at 59% of peak strength (strain 11.96%) due to LVDT limitation. Buckling of longitudinal bars were observed.
S04f	1.562	Strength loss after reaching 51% of peak strength on the descending branch at strain about 8.72%. Failure of Collar 3 and buckling of longitudinal bars were observed.

Figure 4-10 Steel collars of Specimens S04a, S04b, S04c, S04d, S04e, and S04f after completion of the tests

Figure 4-11 Specimens S04a, S04b, S04c, S04d, S04e, and S04f after completion of the tests

CHAPTER 5.   COMBINED AXIAL COMPRESSIVE AND REVERSED CYCLIC LOAD TEST (PHASE 2)

5.1 RESULTS OF COMBINED AXIAL COMPRESSIVE AND REVERSED CYCLIC LOAD TEST

In this section, the combined axial compressive and quasi-static reversed cyclic lateral load test is presented. Important data of all specimens during the test are listed in Table 5-1.

Table 5-1 Results of quasi static cyclic combined axial and lateral load test

Parameters	CS11		CS12		S13		S14		S15	
	Push	Pull	Push	Pull	Push	Pull	Push	Pull	Push	Pull
Drift max (%)	3.5		7.0		5.0		7.0		7.0	
Cycle max	41		57		51		59		59	
P_{max} (kN)	48.2	49	52.5	48.9	48.5	61.5	65.0	70.0	65.2	66.8
Δ_{max} (mm)	21.38	21.34	43.26	42.78	32.18	39.1	42.06	44.86	42.7	43.24
Δ_y (mm)	5.46	5.45	5.38	6.35	5.46	3.25	4.47	5.23	5.14	5.99
Δ_u (mm)	18.9	16	21.9	25.1	23.9	25.8	20.3	32.7	22.8	25.1
$\mu_\Delta = \Delta_u/\Delta_y$	3.46	2.94	4.07	3.95	4.38	7.94	4.54	6.25	4.44	4.19
M_{max} (kNm)	32.1	32.4	34.1	32.6	32.6	40.9	41.7	45.5	42.6	43.9
φ_{max} (1/m)	0.233	0.335	0.465	0.241	0.369	0.386	0.463	0.458	0.592	0.564
φ_y (1/m)	0.078	0.087	0.050	0.051	0.060	0.064	0.065	0.089	0.078	0.130
φ_u (1/m)	0.261	0.214	0.418	0.240	0.234	0.194	0.388	0.424	0.431	0.435
$\mu_\varphi = \varphi_u/\varphi_y$	3.347	2.444	8.438	4.710	3.939	3.048	5.969	4.760	5.513	3.358

Notes:

   Drift max is the maximum lateral drift at the end of the test
   Cycle max is the maximum number of cycle at the end of the test
   P_{max} is the maximum lateral resistance

   Δ_{max} is the maximum lateral displacement

   Δ_y is the lateral displacement at yield point (intersection of $P - \Delta$ curve with a line connecting origin and point at $0.7P_{max}$ on the ascending branch according to ACI 374.2R-13)

   Δ_u is the lateral displacement at ultimate point (a point on descending branch where lateral resistance drops to $0.8P_{max}$ according to ACI 374.2R-13)

   μ_Δ is the displacement ductility ($= \Delta_u/\Delta_y$)

   M_{max} is the maximum bending moment resistance

   φ_{max} is the maximum curvature

φ_y is the curvature at yield point (intersection of $M - \varphi$ curve with a line connecting origin and point at $0.7M_{max}$ on the ascending branch according to ACI 374.2R-13)

φ_u is the curvature at ultimate point (a point on descending branch where moment resistance drops to $0.8M_{max}$ according to ACI 374.2R-13)

μ_φ is the curvature ductility ($= \varphi_u / \varphi_y$)

Specimens CS11 and CS12 were square RC columns with conventional internal stirrups conforming non-seismic and seismic provisions of Indonesian concrete code (SNI 2847 : 2013). The hysteretic lateral force-displacement curves of these specimens can be seen in Figures 5-1 and 5-2 (Pudjisuryadi et al., 2015). It was clearly seen from the curves that specimen with low ratio of confinement (CS11) suffered from non-ductile failure mechanism (diagonal failure of specimen at lateral drift of 3.50 percent - Cycle #41) as compared to the highly ductile CS12 (ductile flexural failure) which survived up to lateral drift of 7.00 percent. Besides the longer drift capacity possesed by CS12, more importantly, it could withstand many more drift cycles (57 cycles) without significant strength loss which leaded to much larger energy dissipation capacity. The hysteretic lateral force-displacement curves of the collared Specimens S13, S14, and S15 can be seen in Figures 5-3 to 5-5 (Pudjisuryadi et al., 2015). Spesimen S13 showed poorer performance if compared to S14 and S15 which were similar to each other. Eventhough it still indicated the diagonal crack failure pattern, Specimen S13 already had much better performance than Control Specimen CS11. It could survive until lateral drift of 5.00 percent (Cylce #51) prior to failure. Specimens S14 and S15 were indeed very similar to each other in their performances. Both specimens survived until lateral drift of 7.00 percent (Cycle #59), and showed ductile flexural failure mechanism. The tests were stopped because the lateral load resistance already dropped below 50 percent of their peaks. In order to observe the deformability of the specimens, the displacement ductilities, μ_Δ, were determined from these $P - \Delta$ curves. As expected, the Control Specimen CS11 demonstrated the least displacement ductilities (3.46 and 2.94 for push and pull modes, respectively). All other four specimens displayed better displacement ductilities (see Table 5-1). Specimens S13 and S14 showed relatively different displacement

132

ductilities at push and pull modes, indicating that the specimens suffered unsymmetric damages during the tests.
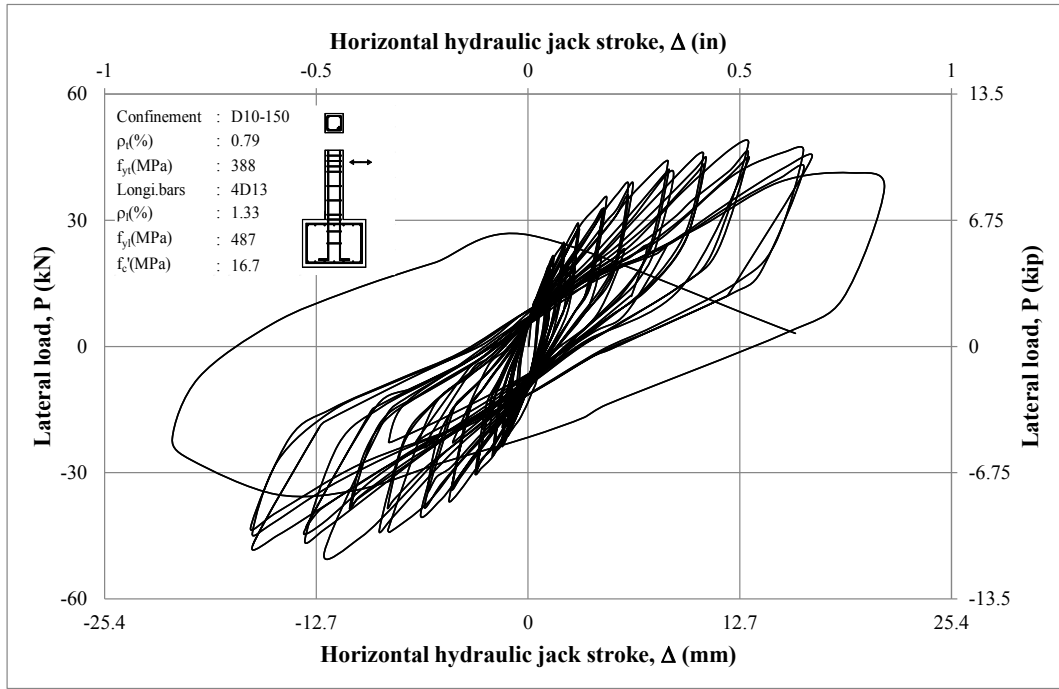
Figure 5-1 Hysteretic lateral force-displacement curve of CS11
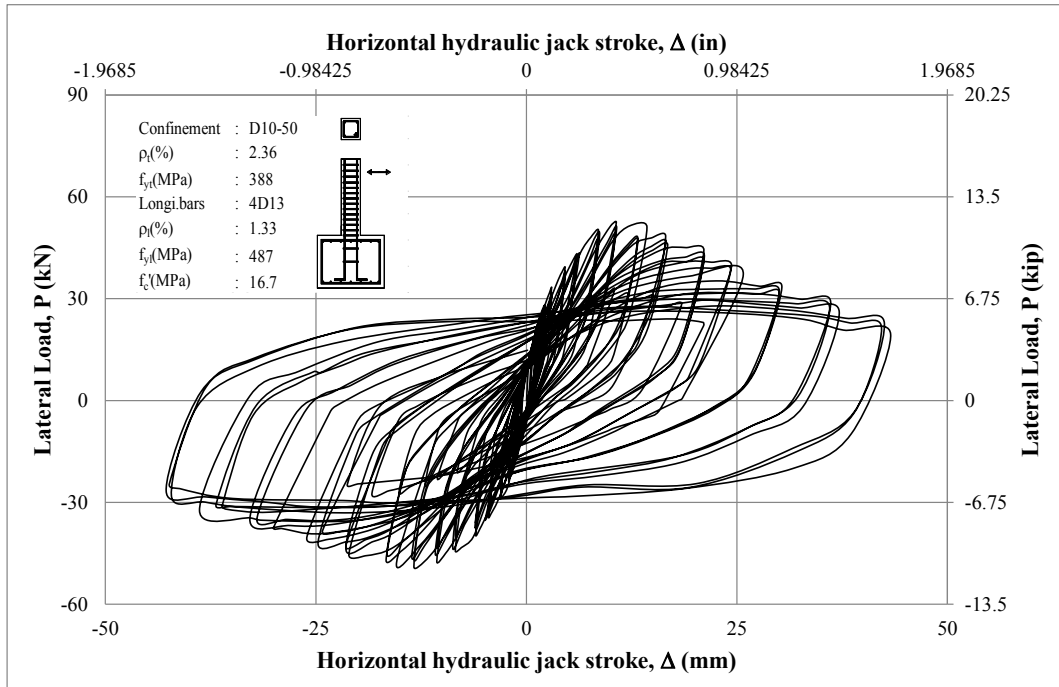
Figure 5-2 Hysteretic lateral force-displacement curve of CS12
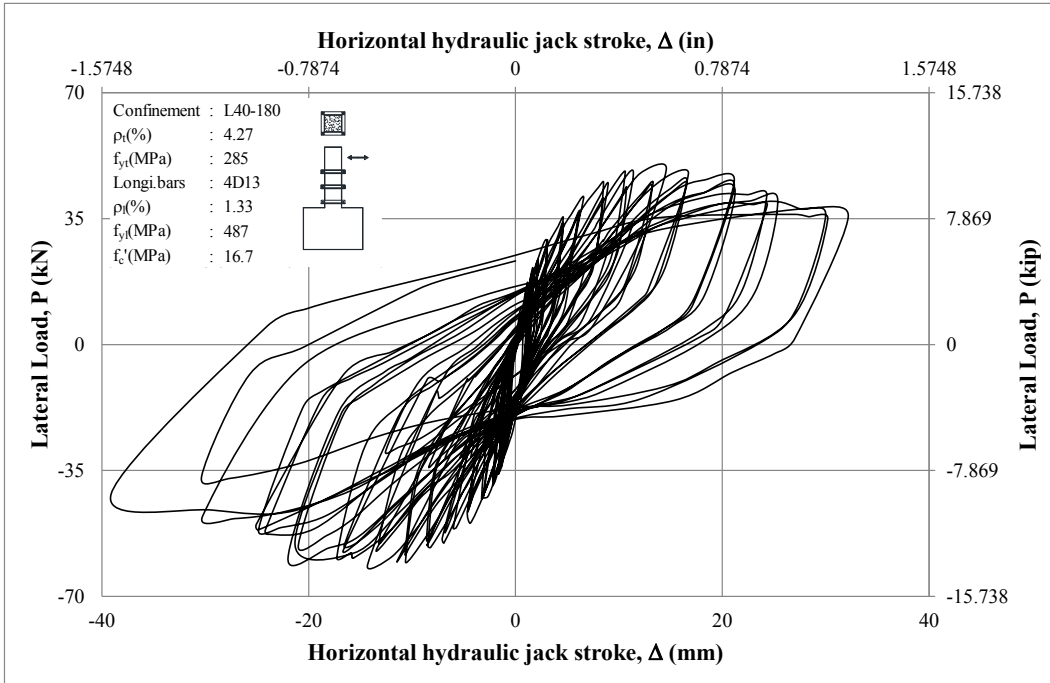
Figure 5-3 Hysteretic lateral force-displacement curve of S13
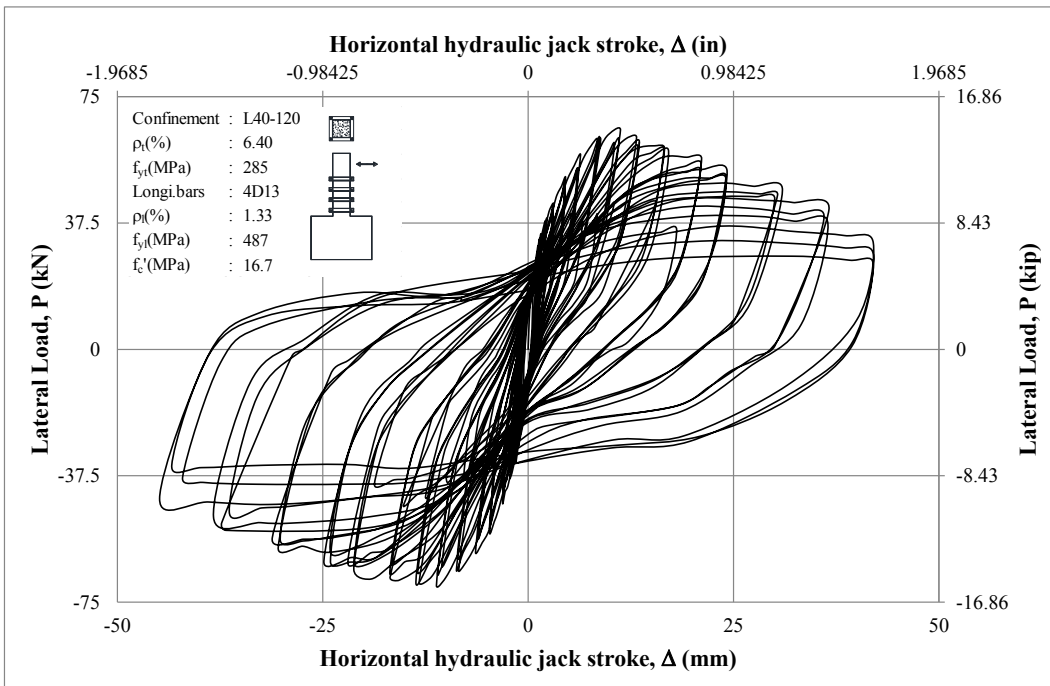
Figure 5-4 Hysteretic lateral force-displacement curve of S14

134
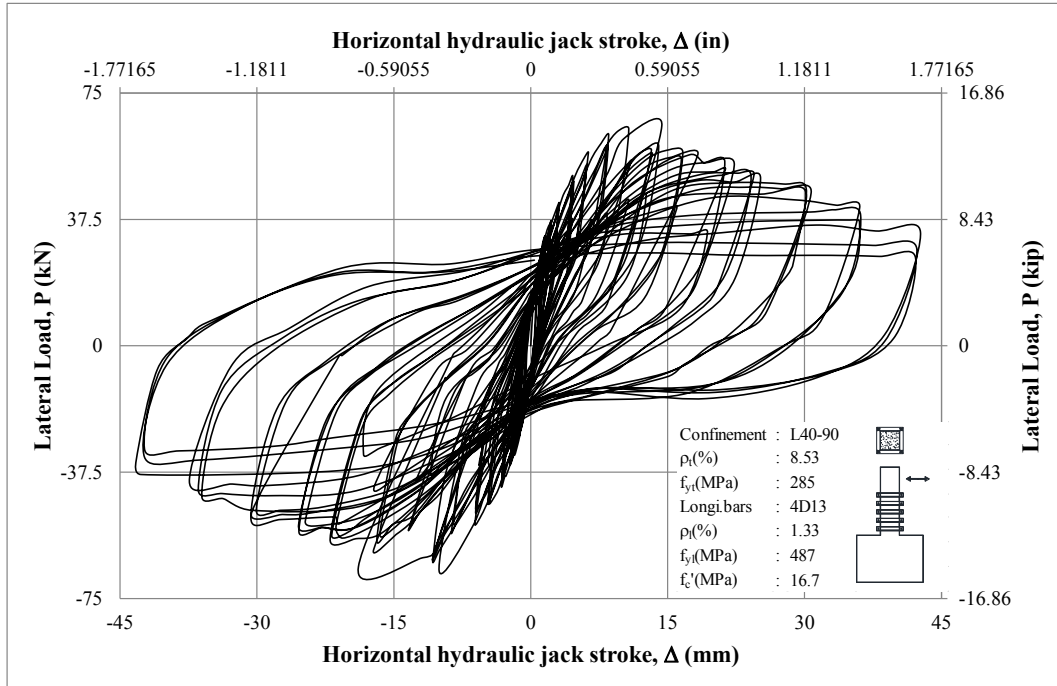
Figure 5-5 Hysteretic lateral force-displacement curve of S15

Besides the lateral force-displacement curves, it is equally important to observe the $M-\varphi$ relationships of the specimens at the plastic hinge regions. Those $M-\varphi$ curves of Specimens CS11 and CS12 are given in Figures 5-6 and 5-7. As expected, Specimen CS12 possesed much better performance than CS11. However, at later stages of the test, it could be seen that the plastic hinge damage of CS12 was very severe, that the hysteretic curve was no longer symmetric. The $M-\varphi$ curves of the collared Specimens S13, S14, and S15 are shown in Figures 5-8 to 5-10. The rotation capacities (product of curvature and the length of plastic hinge) of the specimens can be observed from the curvature ductilities, μ_{φ}, which can be determined from these $M-\varphi$ curves. It seemed to be no strong pattern of the curvature ductilities values. The values ranged widely from 2.4 to 8.4 for all specimens. However, if the maximum curvatures $\left(\varphi_{\max}\right)$ are considered instead of ultimate curvatures $\left(\varphi_u\right)$ it is clear that CS11 had the least rotational capacity ($\varphi_{\max}=0.23$ and 0.34 /m for push and pull modes, respectively). Specimen S13 showed slightly better maximum curvature than CS11 ($\varphi_{\max}=0.369$ and 0.386 /m for push and pull modes, respectively). The well confined Control Specimen

CS12 performed even better maximum curvatures, eventhough it experienced the unsymmetrical damage (φ = 0.465 and 0.241 /m for push and pull modes respectively). Most importantly, the collared Specimens S14 had the maximum curvatures of 0.463 and 0.458 /m, whereas S15 had the maximum curvatures of 0.592 and 0.564 /m for push and pull modes, respectively. These values are much higher than those of CS12.
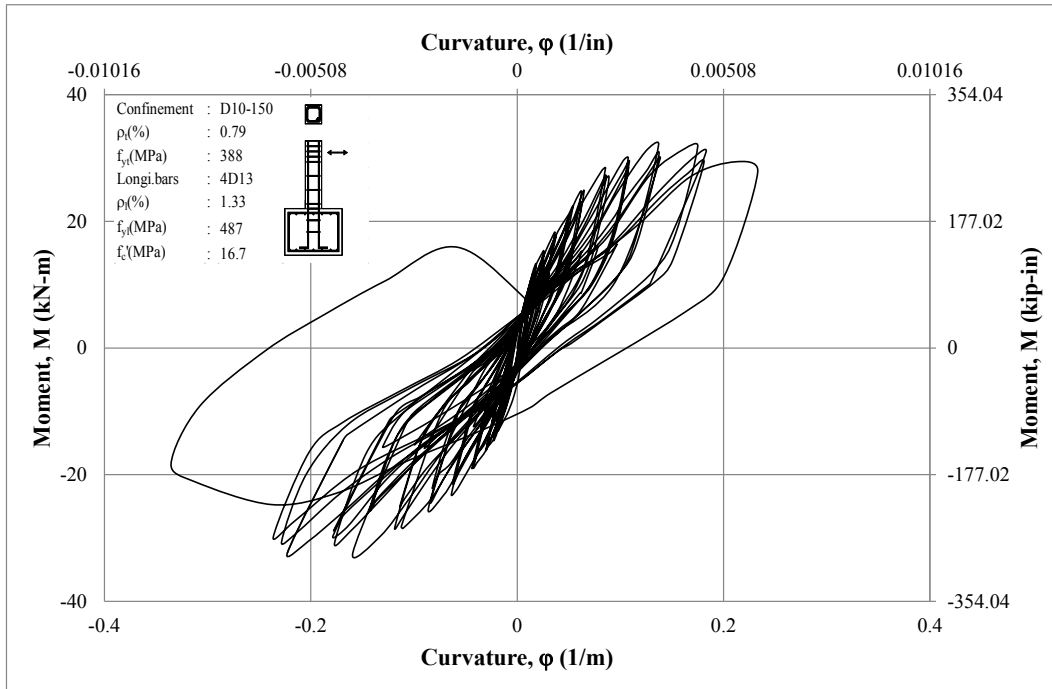
Figure 5-6 Hysteretic bending moment – curvature curve of CS11
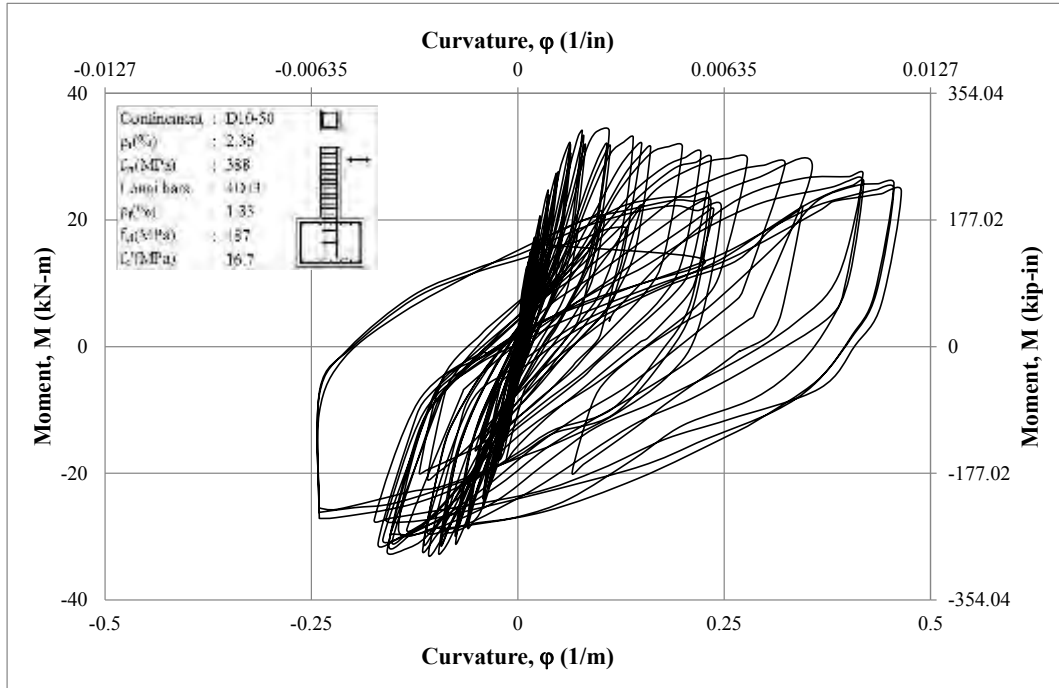
Figure 5-7 Hysteretic bending moment - curvature curve of CS12
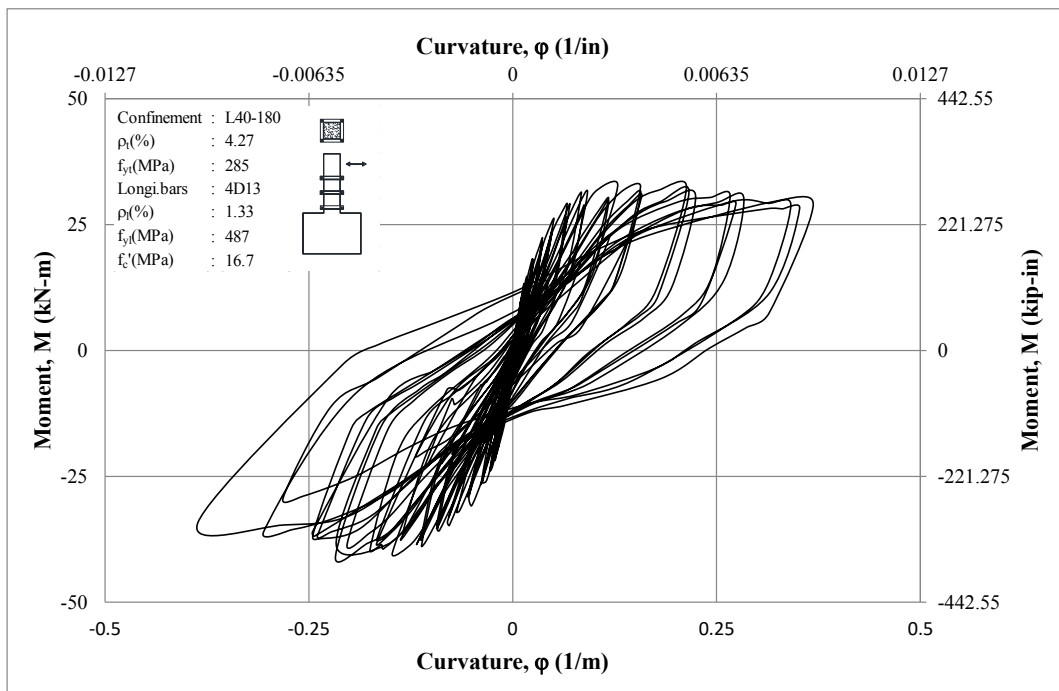
Figure 5-8 Hysteretic bending moment – curvature curve of S13

137
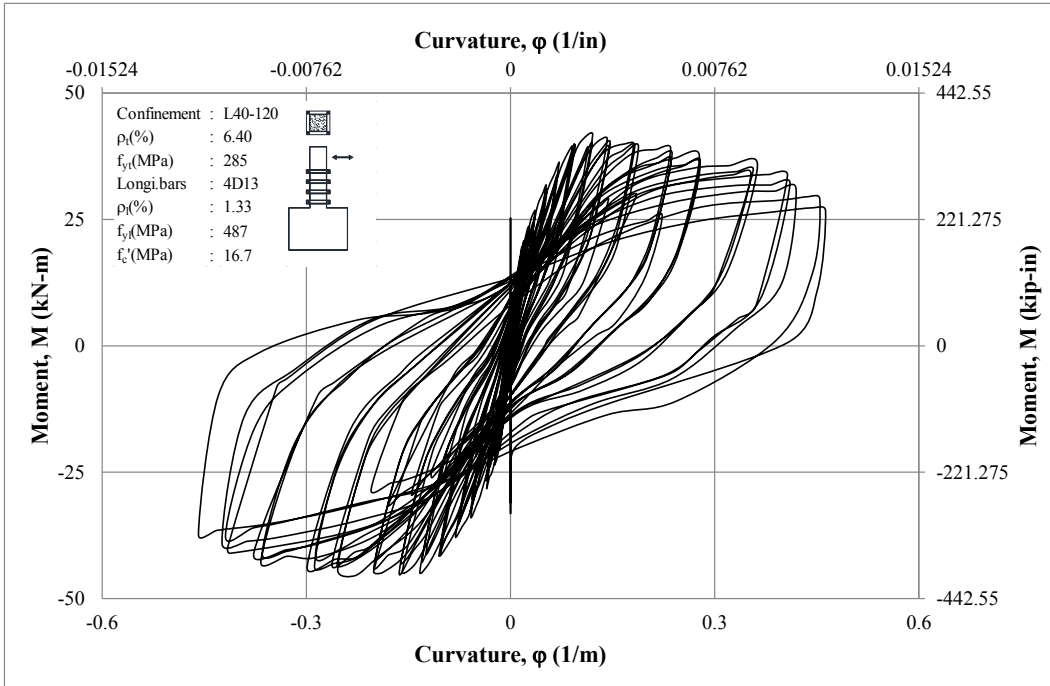
Figure 5-9 Hysteretic bending moment – curvature curve of S14
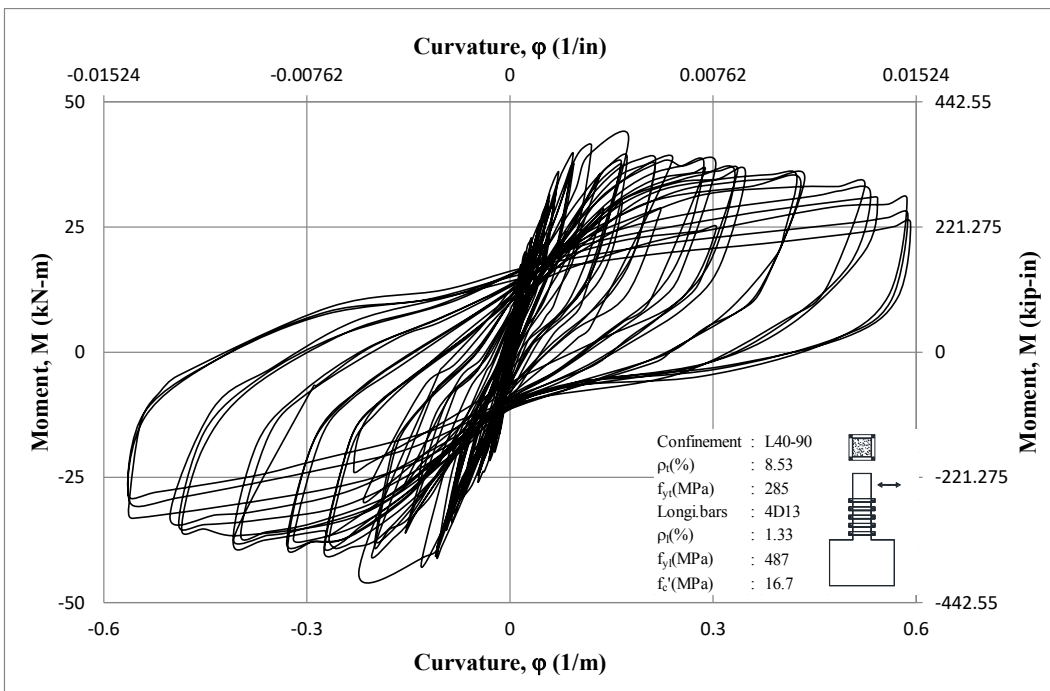
Figure 5-10 Hysteretic bending moment – curvature curve of S15

The damages of specimens after the test are shown in Figures 5-11 and 5-12. Diagonal cracks only appeared on specimens with low confinements (CS11 and S13). Specimen CS11 exhibited clear brittle diagonal split failure as shown in

138

Figure 5-11(a). Specimen S13 had better ductility than CS11, however the diagonal crack pattern as shown in Figure 5-12(a) was still found though it was not as obvious as that on CS11. Specimens CS12, S14, and S15 with better confinement, were completely free from brittle failure modes as shown in Figures 5-11(b), 5-12(b), and 5-12(c), respectively. The damages of the column specimens near the fixity points indicated the cyclic plastic bending damages as shown in Figures 5-11 and 5-12.

(a)   (b)
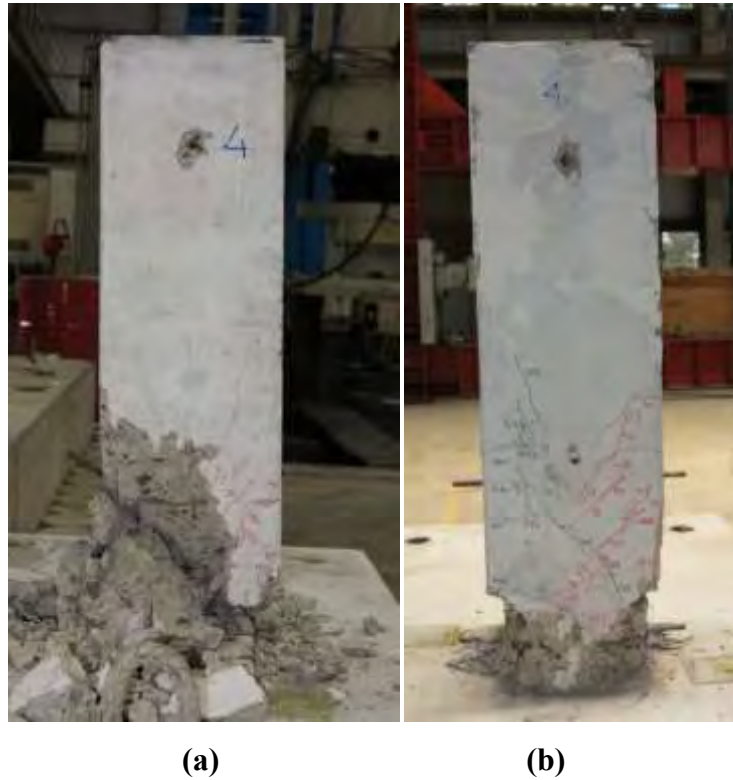
Figure 5-11 Specimens: (a) CS11; and (b) CS12 after the completion of the tests

| (a) | (b) | (c) |
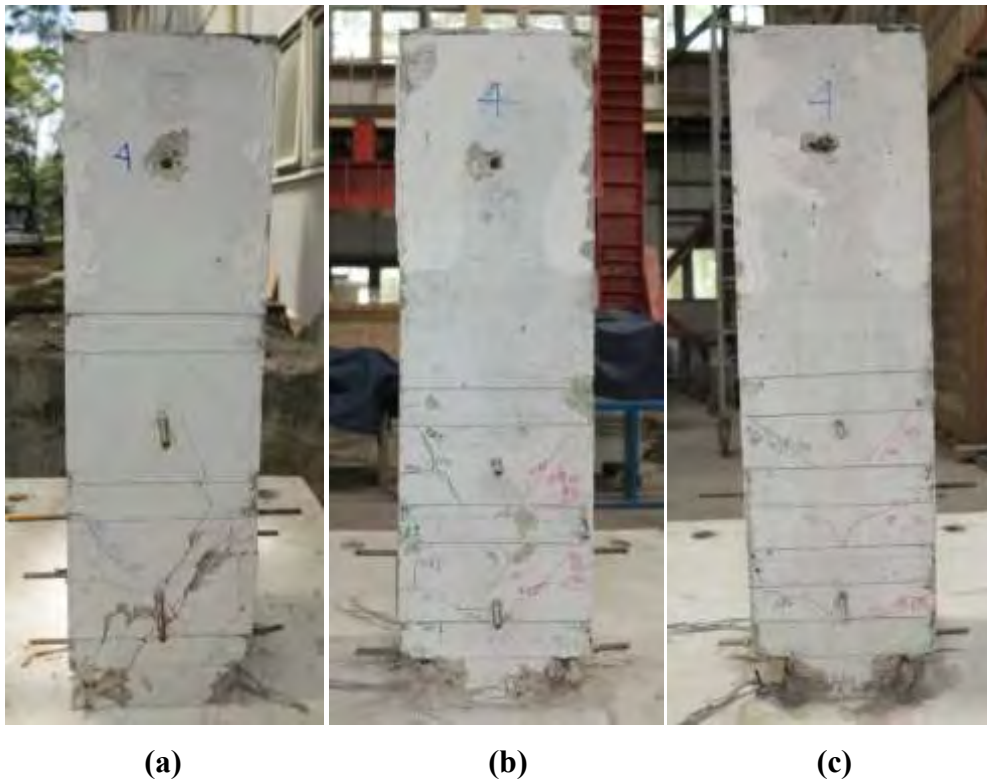
Figure 5-12 Specimens: (a) S13; (b) S14; and (c) S15 after the completion of the tests

Furthermore, the steel strains experienced by Control Specimens CS11 and CS12 are presented in Figures 5-13 to 5-16. The longitudinal bars and stirrups are expected to yield at axial strains of 0.24 and 0.19 percent, respectively (noting that the yield strength of the longitudinal bars and stirrups are 487 MPa and 388 MPa, respectively with the modulus of elasticiy assumed to be $200,000$ MPa). It was observed that all longitudinal bars and stirrups of Specimens CS11 and CS12 experienced strains beyond the yield point. Similar to the control Specimens CS11 and CS12, all longitudinal bars of collared Specimens S13, S14, and S15 also experienced strains exceeding the yield point. The typical axial strains of the longitudinal bars and stirrups of the specimens can be seen in Figures 5-13 to 5-16.
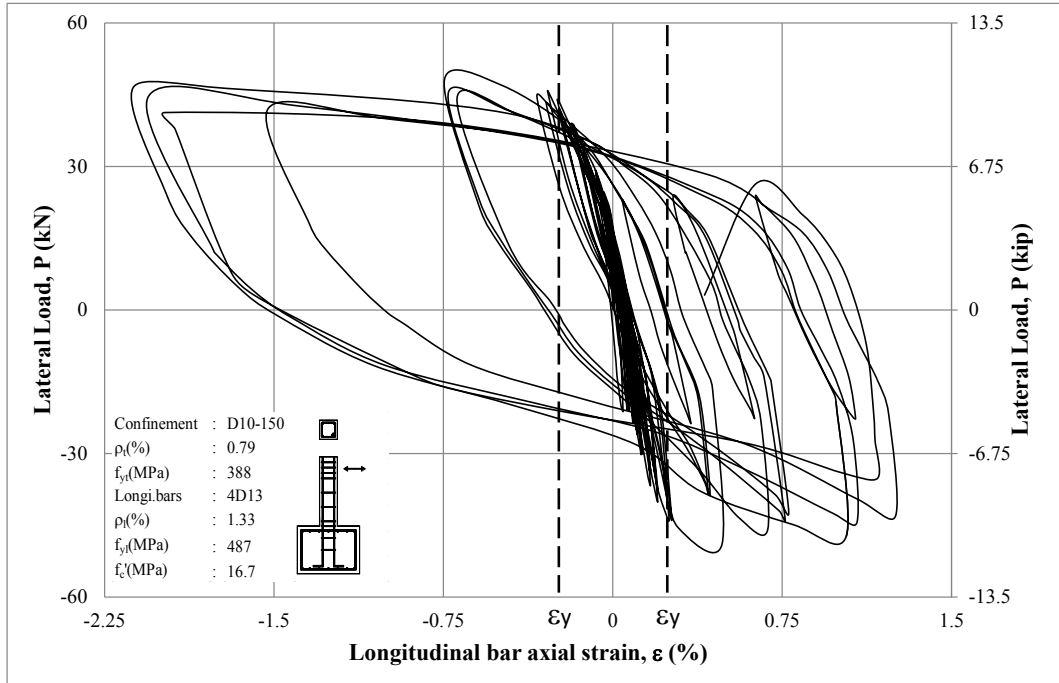
Figure 5-13 Hysteretic lateral load-longitudinal bar axial strain curve of CS11
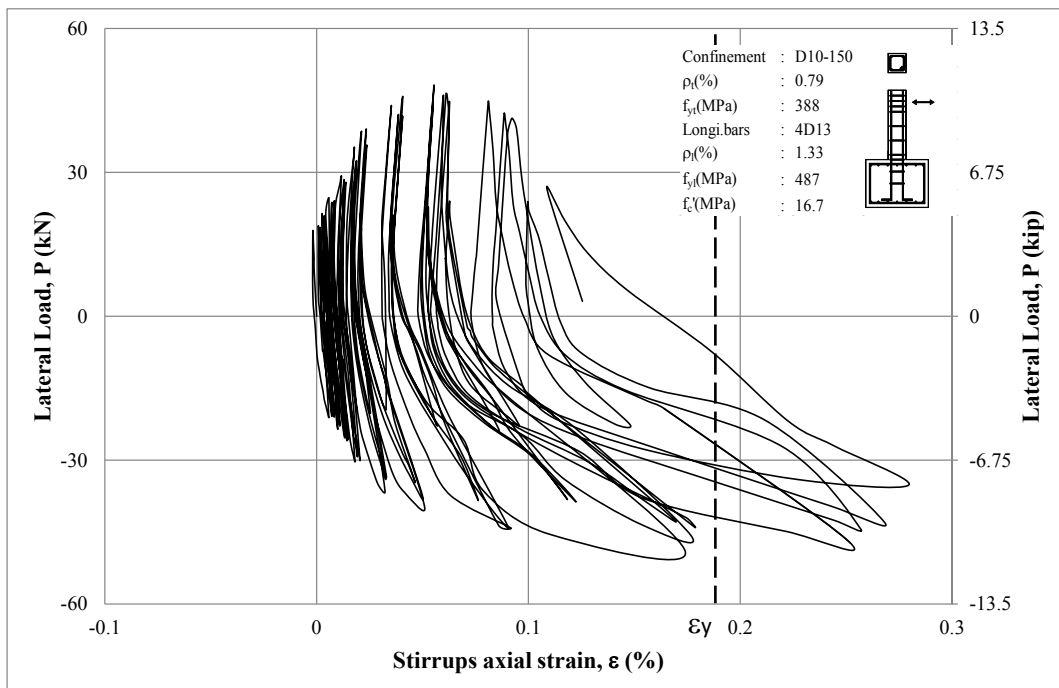
Figure 5-14 Hysteretic lateral loap-stirrups axial strain curve of CS11

141

Figure 5-15 Hysteretic lateral loap-longitudinal bar axial strain curve of CS12
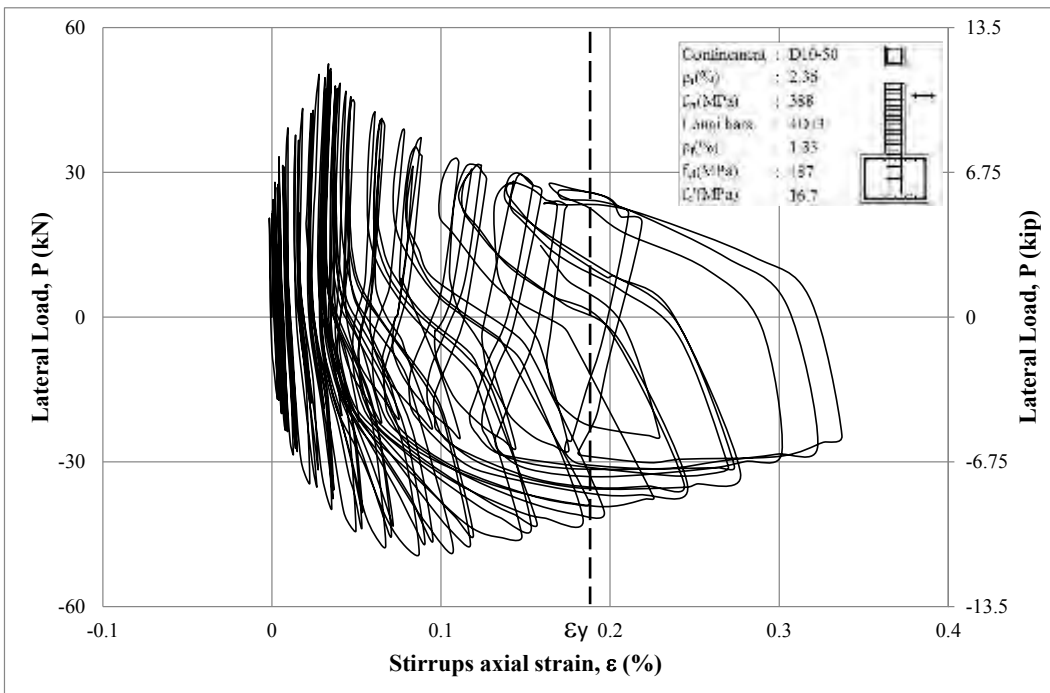
Figure 5-16 Hysteretic lateral load-stirrups axial strain curve of CS12

The axial strains on the steel collars of Specimens S13, S14, and S15 are presented in Figures 5-17 to 5-19. As expected, the steel collars effectively worked as confinement element to the column specimens as they suffered axial

142

tensile strains. However, the corresponding strains are still lower than the yield strain of 0.14 percent. This finding is different from that found in the concentric compressive tests, where all steel collars yielded. There are two possible reasons to explain this: (1) the axial load applied to the specimens (Phase 2) was much lower than that applied in the axial concentric load test (Phase 1); and (2) in this cyclic loading test, approximately only half part of the columns suffered compressions which lead to lateral expansion, while the other part received tension stress which reverse the lateral expansion. Thus, the overall lateral expansions of the specimens in the concentric load tests were much higher than those in the lateral cyclic load tests. These expansions must be resisted by the confinement elements. The deformed shapes of the steel collars after the completion of the tests can be seen in Figure 5-20. It could also be seen from the photographs that the steel collars did not experience any apparent residual or plastic deformations.
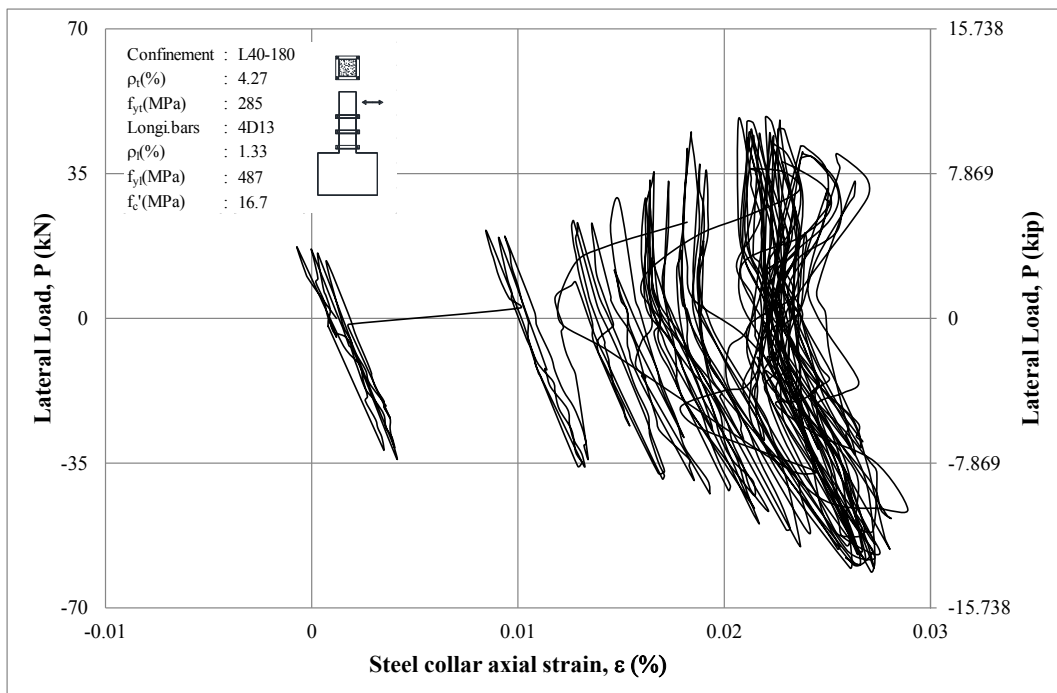
Figure 5-17 Hysteretic lateral load-steel collar axial strain of S13
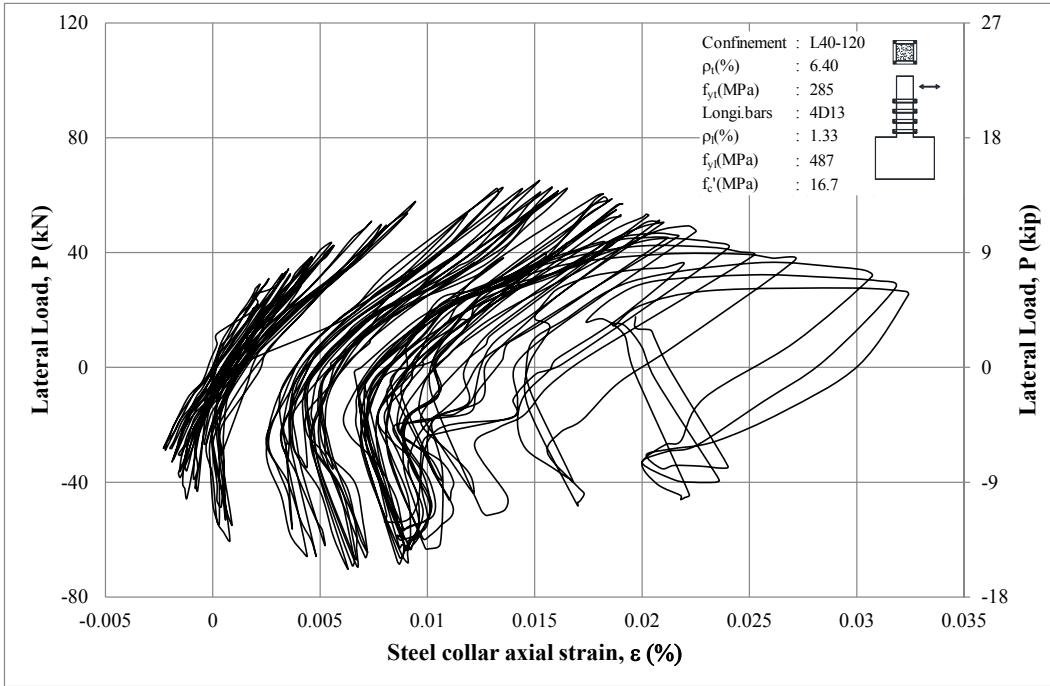
Figure 5-18 Hysteretic lateral load-steel collar axial strain of S14
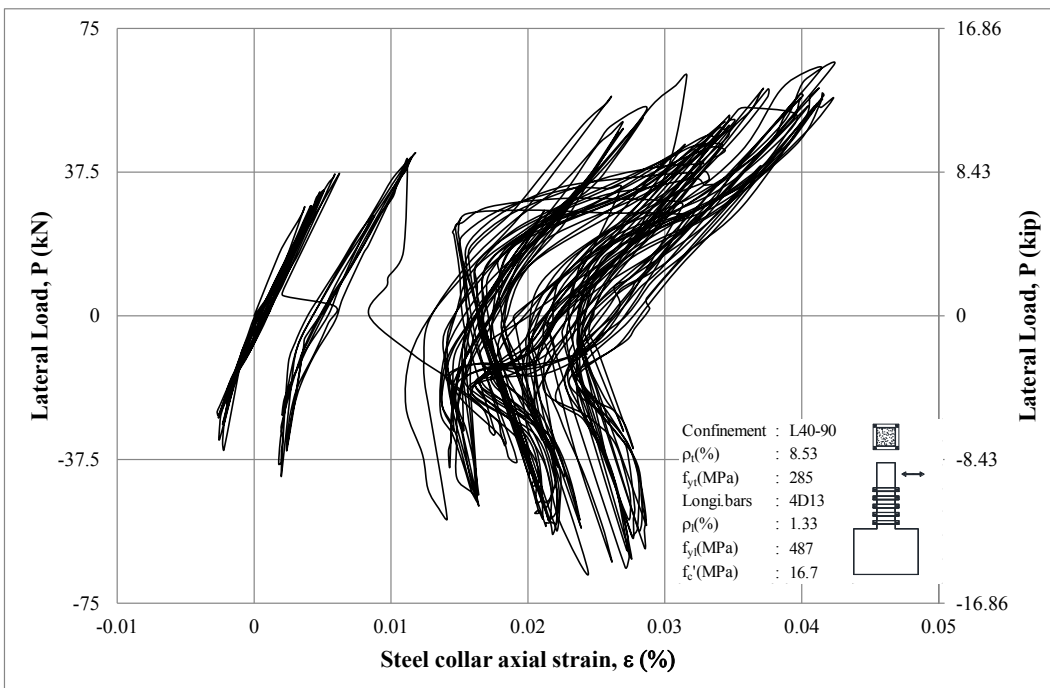
Figure 5-19 Hysteretic lateral load-steel collar axial strain of S15

144

(a)   **(b)**   **(c)**
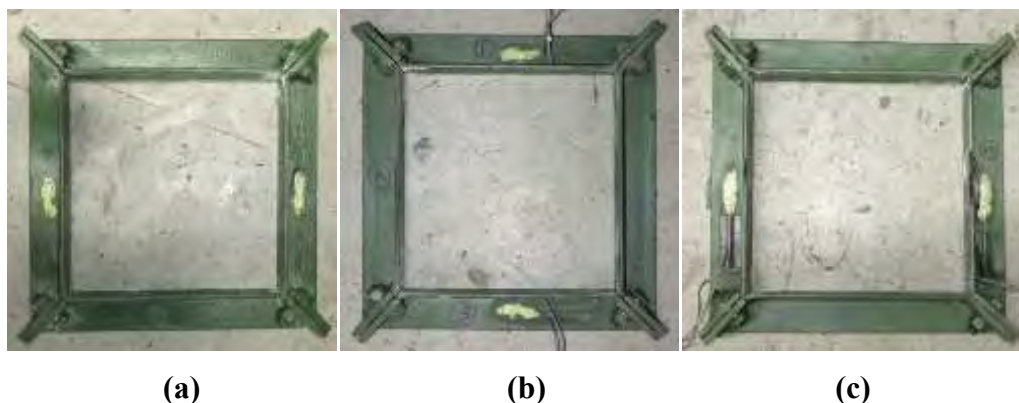
Figure 5-20 Steel collars nearest to fixity points (column footings) of Specimens : (a) S13; (b) S14; and (c) S15 after the completion of the test

Furthermore, in order to serve idea on the overall deformabilities of the seismic-resistant structural members, several parameters are normally used. In this study, the cumulative dissipation energy, displacement ductility, and curvature ductility values are listed in Table 5-2. The cumulative dissipation energies in Figure 5-21 represent the strain energies can be absorbed by the column specimens. If the specimens are analyzed up to the failure stage, it can be seen that specimens, which survive more cyclic loading sequence, logically indicate better energy capacities. Specimens CS12, S14, and S15 show about the same level of capacities, followed by Specimen S13 and CS11 with less capacities. Similar behaviors were observed in Figures 5-22 and 5-23, which present the cumulative displacement and cumulative curvature ductilities, respectively.

However, corresponding to the definition of ultimate limit condition, that is about 20 percent decay of the peak strength, the following considerations can be discussed. Specimens CS12, S14, and S15, which survived more cycles than Specimen S13, actually had similar post peak behaviors with Specimen S13. Thus, their cumulative energies up to this stage (TE_{80}) were not much greater than Specimen S13. Similarly, it is also applicable fot the cumulative displacement ductilities $(N_{\Delta 80})$, and curvature ductilities $(N_{\varphi 80})$. The cumulative energies normalized to the ideal elastoplastic energy (TE_N) of the externally collared Specimens S13, S14, and S15 ranged from 13.8 to 23.1.

Table 5-2 Energy dissipation capacity and deformability of the specimens

Parameters	CS11	CS12	S13	S14	S15
TE_f (kNm)	8.81	50.07	23.89	57.15	53.13
TE_{80} (kNm)	8.81	11.81	19.03	19.41	14.59
TE_N (kNm)	14.77	14.61	23.14	20.69	13.83
Δ_{y+} (mm)	5.46	5.38	5.46	4.47	5.14
Δ_{y-} (mm)	5.45	6.35	3.25	5.23	5.99
Δ_{ya} (mm)	5.46	5.87	4.36	4.85	5.57
$N_{\Delta f}$	44.46	136.71	105.66	152.81	137.53
$N_{\Delta 80}$	44.46	48.50	91.39	67.22	51.16
φ_{y+} (1/m)	0.08	0.05	0.06	0.07	0.08
φ_{y-} (1/m)	0.09	0.05	0.06	0.09	0.13
φ_{ya} (1/m)	0.08	0.05	0.06	0.08	0.10
$N_{\phi f}$	39.02	123.71	81.91	104.71	98.26
$N_{\phi 80}$	39.02	72.08	54.79	87.56	58.15

Notes:

TE_f is the cumulative energy up to failure of specimen

TE_{80} is the cumulative energy up to 20 percent decay of peak strength

TE_N is TE_{80} normalized by the ideal elastoplastic energy

Δ_{y+} is the yield displacement (push mode)

Δ_{y-} is the yield displacement (pull mode)

Δ_{ya} is the average yield displacement of both direction

$N_{\Delta f}$ is the cumulative displacement ductility up to failure of specimen

$N_{\Delta 80}$ is the cumulative displacement ductility up to 20 percent decay of peak strength

φ_{y+} is the yield curvature (push mode)

φ_{y-} is the yield curvature (pull mode)

φ_{ya} is the average yield curvature of both direction

$N_{\varphi f}$ is the cumulative curvature ductility up to failure of specimen

$N_{\varphi 80}$ is the cumulative curvature ductility up to 20 percent decay of peak strength
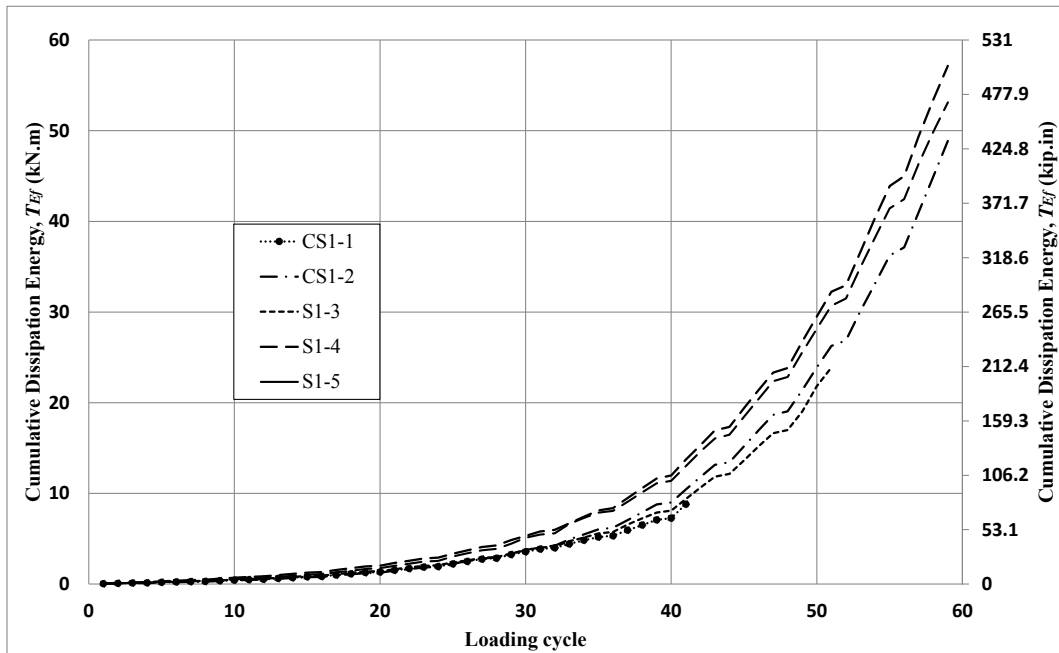
Figure 5-21 Cumulative dissipation energy vs loading cycle
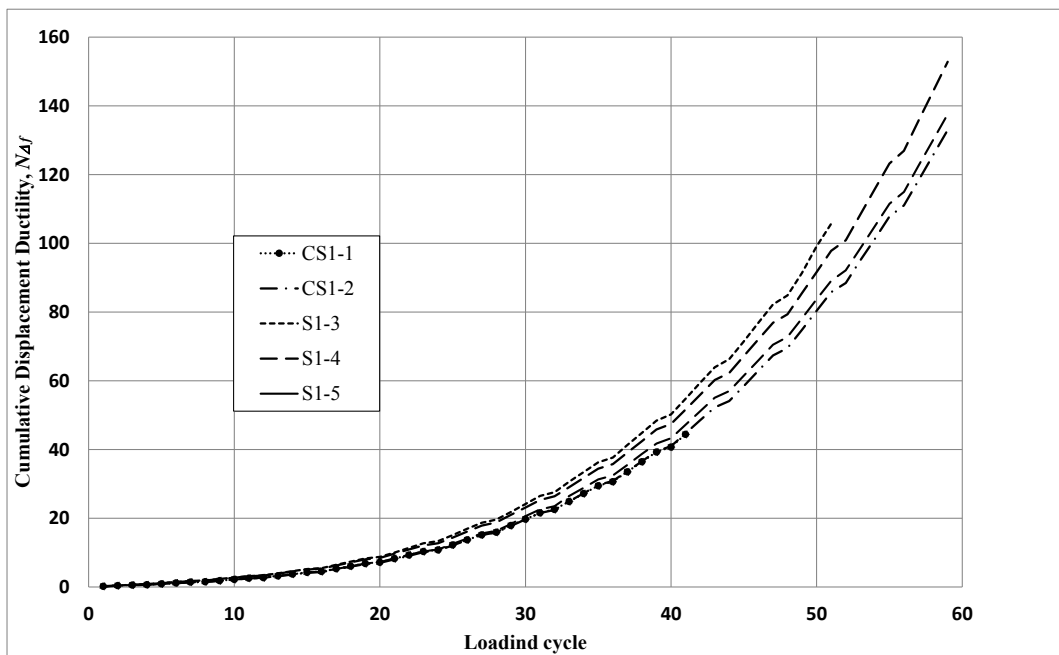
Figure 5-22 Cumulative displacement ductility vs loading cycle

147
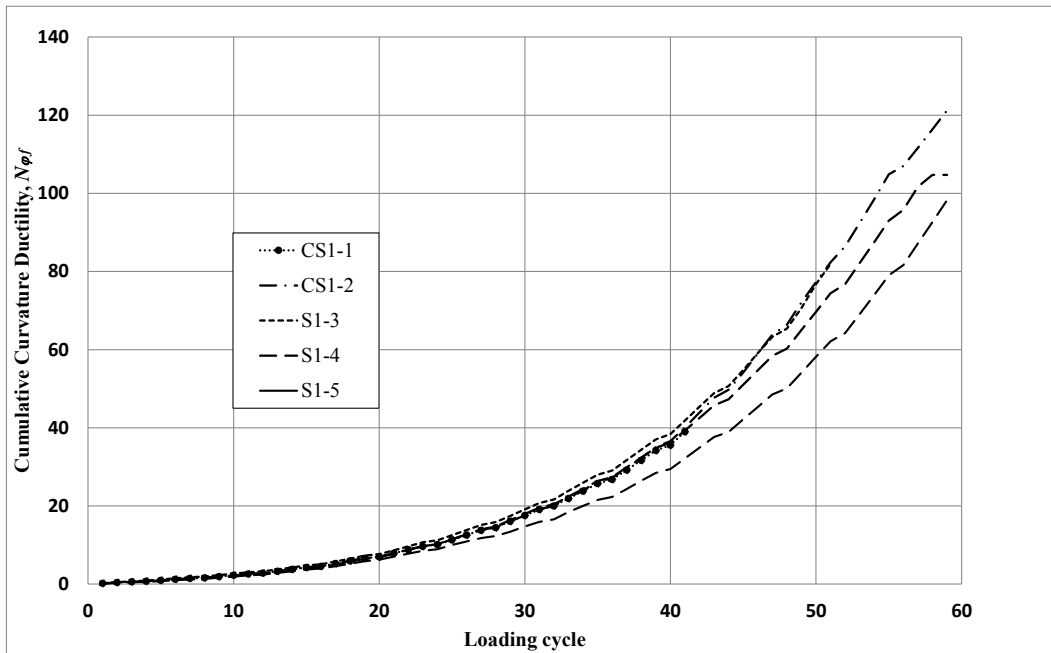
Figure 5-23 Cumulative curvature ductility vs loading cycle

In order to ensure the footing fixity, it is important to observe the possible movement of the footing. Typically (Specimen CS11 for example), by using six anchorage points (with steel rods and nuts) to the strong floor, it was adequate to provide relatively rigid fixity. The footing vertical and horizontal movements were found to be very small, and thus negligible (Figures 5-24 and 5-25). Also, the tilting angle of horizontal jack should be kept minimum during the tests. This angle was determined by installing two transducers (LVDTs) to measure vertical displacement of the horizontal jack at two points with a certain distance. Typical setup can be seen in Figures 3-66 and 3-67 presented earlier for Specimen S14. It was observed that the maximum tilting angle during the test was only about 1.7 degree, which leaded to only 2.9 percent of jacking force becoming the additional vertical force. Noting that 70 kN was the maximum lateral force in S14, the additional vertical force was equal to only about 2 kN, which was negligibly small compared to the constant axial load of 240 kN. Complete results of all measuring devices for these the specimens can be found in Appendix D.
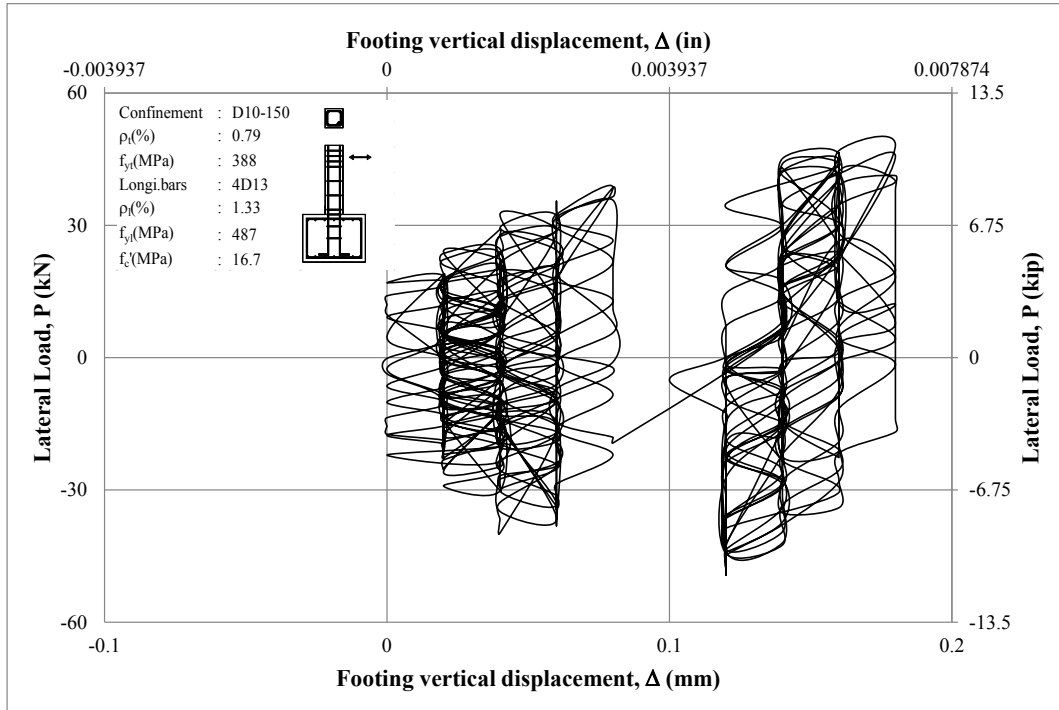
Figure 5-24 Hysteretic lateral load vs vertical movement of CS11 footing
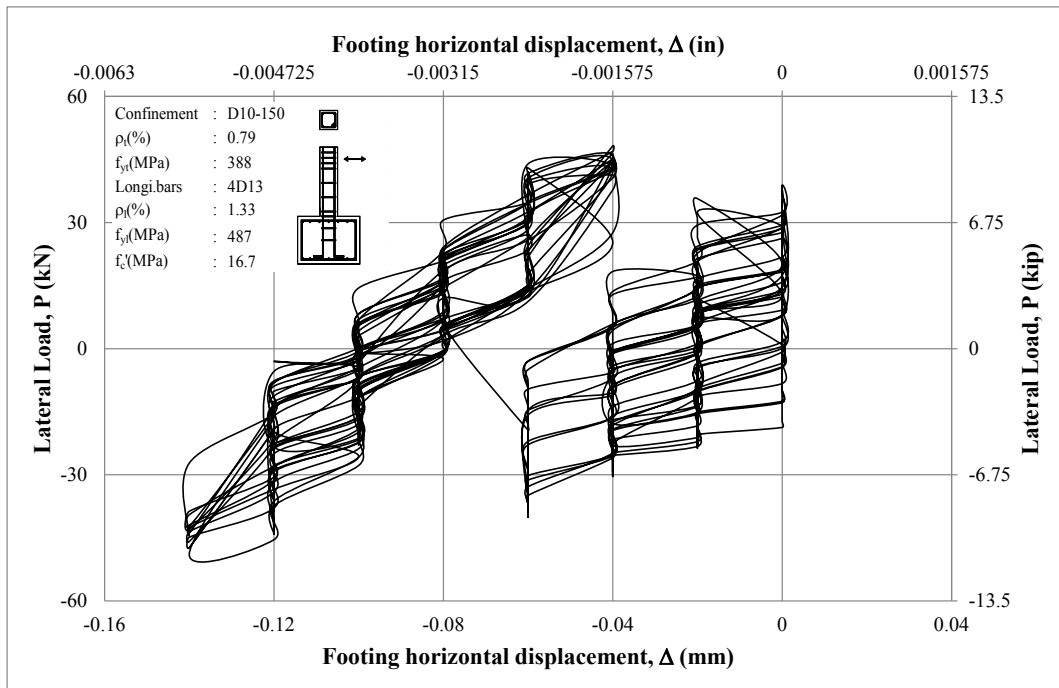
Figure 5-25 Hyteretic lateral load vs horizontal movement of CS11 footing

149

5.2 ACCEPTANCE CRITERIA ACCORDING TO ACI 374.1-05

In order to ensure the performance of a structural member under such cyclic load, some acceptance criteria are set by ACI 374.1-05. There are totally three criteria as follows:

1. The specimen shall have attained lateral resistance equal to or greater than nominal resistance (E_n) before its drift ratio exceeds the value consistent with the allowable story drift limitation specified by International Building Code (IBC).

2. Maximum resistance (E_{max}) should not exceed λE_n, where λ is the overstrength of column nominal moments with respect to beam nominal moments (= 6/5).

3. Characteristic of 3rd cycle of hysteretic loop at drift ratio 0.035 where the acceptance criteria should be checked:
   a. Peak resistance of 3rd cycle ≥ 0.75 peak resistance (all cycles)
   b. Relative Dissipation Energy (R.D.E.) $\geq 1/8$
   c. Secant stiffness from drift ratio -0.0035 to 0.0035 ≥ 5 percent of initial stiffness

As an example for checking the acceptance criteria, a complete calculation of Specimen S15 is presented here.

- **First criterion**

With the data given:

$b = h = 200\,\text{mm}$ (column sectional dimensions)

$f_c' = 16.7\,\text{MPa}$ (concrete compressive strength)

$h_{sc} = w_{sc} = 40\,\text{mm}$ (height and width of steel angle collar)

$t_{sc} = 4\,\text{mm}$ (thickness of steel angle collar)

$f_{ysc} = 284.98\,\text{MPa}$ (yield strength of steel angle collar)

$s_{sc} = 90\,\text{mm}$ (center-to-center distance of steel collar)

$n_l = 4$ (number of longitudinal steel bars)

$\phi_l = 12.8\,\text{mm}$ (nominal diameter of longitudinal steel bar)

$h_P = 600\,\text{mm}$ (height of lateral stroke from fixity point)

$f'_{cc} = 28.6\,\text{MPa}$ (peak strength of confined concrete)

The detailed calculation of f'_{cc} can be found in Section 6.2. With the calculated confined peak strength, a standard nominal axial force-bending moment interaction diagram is generated for the specimen. At an applied axial load $P_0 = 240\,\text{kN}$, the calculated nominal bending capacity, $M_n = 28.6$ kNm.

$E_n = M_n / h_P = 28.6 / 0.6 = 47.7\,\text{kN}$ (nominal lateral load resistance)

The initial drift ratio consistent with the allowable story drift limitation is equal to $\Delta_a / (\phi C_d h)$. In Table 1617.3 of IBC2000, it is given that:

$\Delta_a / h = 0.020$ for seismic group I

$\Delta_a / h = 0.015$ for seismic group II

$\Delta_a / h = 0.010$ for seismic group III

$C_d = 5.5$ for Special Moment Frame (SMF)

$C_d = 4.5$ for Intermediate Moment Frame (IMF)

$C_d = 2.5$ for Ordinary Moment Frame (OMF)

Strength reduction factor for combined axial force and bending moment, $\phi = 0.65$ for $P_0 > 0.1 f'_c A_g \rightarrow 240 kN > 0.1(16.7)(200^2) \times 10^{-3} kN \rightarrow 240 kN > 66.8 kN$.

the $\Delta_a / (\phi C_d h)$ can be calculated and shown in Table 5-3. For example, the initial drift ratio for Seismic Group I of SMF is determined as follows:

$\Delta_a / (\phi C_d h) = 0.020 / (0.65 \times 5.5) = 0.0056$

Table 5-3 Initial drift ratios for acceptance criteria according to ACI 374.1-05

	SMF $(C_d = 5.5)$	IMF $(C_d = 4.5)$	OMF $(C_d = 2.5)$
Seismic Group I	0.0056	0.0068	0.0120
Seismic Group II	0.0042	0.0051	0.0092
Seismic Group III	0.0028	0.0034	0.0062

The corresponding initial lateral displacements can be calculated by multiplying those initial drifts with the height of lateral stroke ($\delta = \Delta_a / (\phi C_d h) \times h_P$, listed in

151

Table 5-4). The real lateral resistances corresponding to the displacements could be traced from the hysteretic data during the tests, and are listed in Table 5-5.

Table 5-4 Initial displacement for acceptance criteria according to ACI 374.1-05

	SMF $\left(C_d = 5.5\right)$	IMF $\left(C_d = 4.5\right)$	OMF $\left(C_d = 2.5\right)$
Seismic Group I	3.36mm	4.10mm	7.38mm
Seismic Group II	2.52mm	3.08mm	5.54mm
Seismic Group III	1.68mm	2.05mm	3.69mm

Table 5-5 Observed lateral resistance (push/pull) for Specimen S15

	SMF $\left(C_d = 5.5\right)$	IMF $\left(C_d = 4.5\right)$	OMF $\left(C_d = 2.5\right)$
Seismic Group I	+44kN / -42kN	+50kN / -42kN	+60kN / -68kN
Seismic Group II	+37kN / -42kN	+44kN / -42kN	+50kN / -47kN
Seismic Group III	+33kN / -32kN	+37kN / -39kN	+43kN / -42kN

It should be noted that the longitudinal steel provided were only 4-D13 (ρ =1.33 percent). It is determined without consideration of real design loads specified by relevant codes, since the column specimens were designed primarily for investigating the strength gain and ductility enhancement due to the existence of the external steel collars as confinement. Therefore, this acceptance criterion cannot be used to evaluate the specimens of this study. However, if such specimen was to be evaluated with this criterion, it can be seen that Specimen S15 is only acceptable for OMRF with Seismic Group I (observed resistance $> E_n$).

- **Second criterion**

The second criteria is obviously meant for beam members, that the ratio of maximum observed strength with respect to its nominal capacity is not allowed to exceed the overstrength factor λ . This is to protect the columns from subjected to excessive action from the beam plastic hinging. This criterion also cannot be used to evaluate the specimens in this study.

- **Third criterion**

The evaluation is taken at the 3rd cycle of hyteretic loop at drift ratio 0.035, as shown in Figure 5-26.

a) Peak lateral force of that loop $\geq$ 75% peak lateral force of whole test

The peak lateral force resistances are found :

Push mode = +52 kN

Pull mode = - 56 kN

while the minimum value = 75% of peak resistance of the whole test :

Push mode = 0.75 (65.25 kN) = 48.9 kN

Pull mode = 0.75 (-66.8 kN) = -50.1 kN

→ criterion 3a) is passed.

b) Relative Dissipation Energy (R.D.E) ≥ /18

From Figure 5-26, the area enclosed by solid line, is the actual dissipation energy, while the area enclosed by the dashed line is the ideal energy. From the peak resistances of each mode, lines paralel to the corresponding initial stifnesses are drawn to intersect with horizontal axis (lines CD, and GA), and extended to the opposite peak resistances (lines DF, and AB). Lines AB and CD are paralel to initial stiffness of push mode (K+), and lines GA and DF are paralel to initial stifness of pull mode (K-). From those polygons, the energies can be calculated:

$E_{ac} = 1471.3$ kN.mm (actual energy, area enclosed by solid line)

$E_{id} = 4146.7$ kN.mm (ideal energy, area enclosed by dashed line)

$R.D.E. = E_{ac}/E_{id} = 35.5\%$ (relative dissipation energy)

→ criterion 3b) is passed

c) Secant stiffness from drift ratio -0.0035 to 0.0035 ≥ 5 percent of the initial stiffnesses

The definition of secant stiffnesses meant by the criterion can be seen in Figure 5-27, and are found to be :

$K_{sec}+ = 2.52$ kN/mm (for push mode)
$K_{sec}- = 2.04$ kN/mm (for pull mode)

while the initial stiffnesses are :

$K+ = 28.8$ kN/mm → $5\%K+ = 1.44$ kN/mm (for push mode)

$K- = 29.2$ kN/mm → $5\%K- = 1.46$ kN/mm (for pull mode)

→ criterion 3c) is passed.

Thus, the Specimen S15 is acceptable for this criterion.
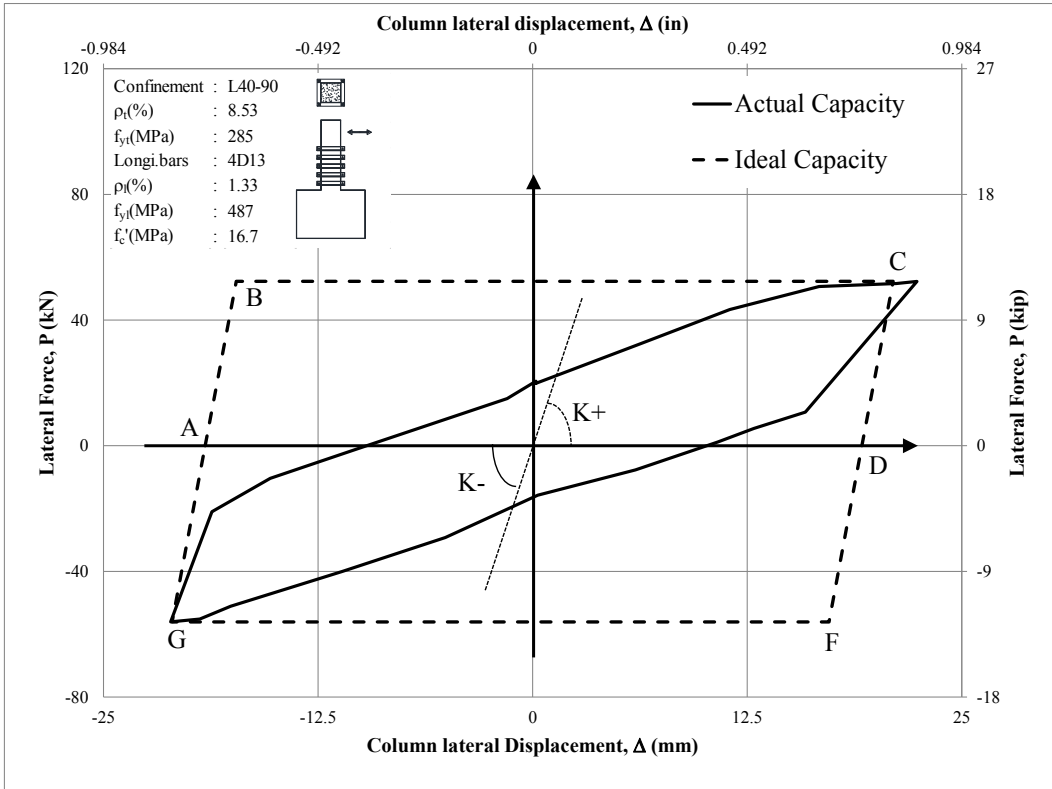
Figure 5-26 Energy dissipation capacity of Specimen S15
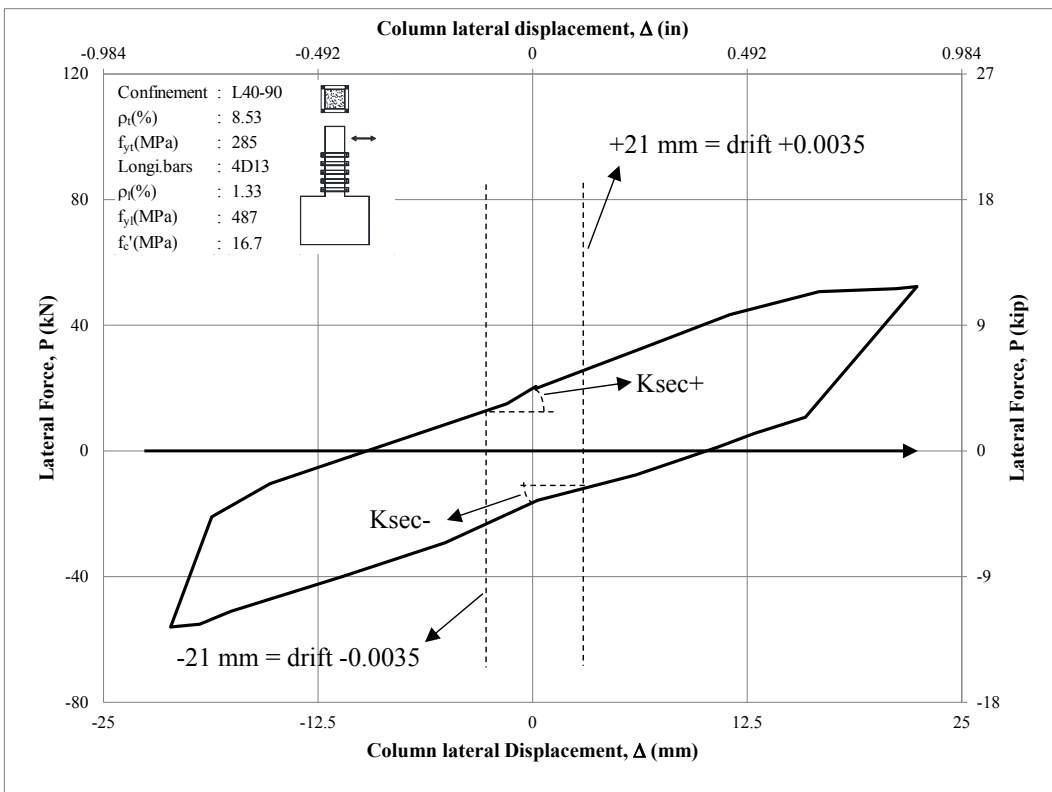
Figure 5-27 Secant stiffnesses of Specimen S15

154

With the first and second criteria excluded, the summary of the third acceptance criterion for all specimens are listed in Table 5-6. With Specimen CS11 excluded, it can be seen that all other four specimens satisfy all criteria stipulated by the ACI. This means that the proposed retrofitting method can be used to improve the deficient square RC columns in order to provide better ductility for seismic resistant structural members.

Table 5-6 Summary of third criteria of ACI 374.1-05

Specimen ID	Min Lateral resistance (kN)	Lateral resistance (kN)	Min R.D.E. (%)	R.D.E. (%)	Min.Secant stiffness (kN/mm)	Secant stiffness (kN/mm)
CS11	+36/-37	N/A	12.5	N/A	0.9/1.19	N/A
CS12	+39/-37	+41/-42	12.5	42.6	0.98/0.87	1.42/1.14
S13	+36/-46	+43/-56	12.5	32.9	0.73/1.31	1.79/1.36
S14	+49/-53	+53/-63	12.5	36.8	1.62/1.62	1.88/2.33
S15	+49/-50	+52/-56	12.5	35.5	1.44/1.46	2.52/2.04

= This Page is Intentionally Left Blank =

CHAPTER 6.   PROPOSED ANALYTICAL MODEL AND RETROFIT DESIGN APPROACH

In this Chapter, an analytical model of the proposed method is presented. This analytical model is developed based on previously established model for conventional stirrups. Modifications to accomodate the characteristic of steel collars as external confinement is presented. The enhancement of peak strength as well as the complete stress-strain relationship are proposed. Furthermore, a retrofit design approach, combining the joint effects of conventional internal stirrups and the proposed external steel collars is presented. The calculation examples of the proposed method and the design procedure are also provided.

6.1   PROPOSED ANALYTICAL MODEL

The proposed model for predicting the stress-strain curve of the externally confined concrete by the steel collars is mainly adopted from Mander et al. (1988a). The prediction of confining stress provided by the external steel collars through combined bending and axial forces is adopted from Xiao and Wu (2003). Consider a concrete column which is externally retrofitted by external steel collars (from steel angle sections) as illustrated in Figure 6-1. In the figure, the notations b, s_{sc}, and s_{scc} are the width or depth of the square column section, spacing of steel collars, and clear spacing of steel collars, respectively. The confining stress along the perimeter of column at the level of external steel collar is not uniform as seen in Figure 6-2. This condition causes some ineffectively confined regions across the column section. In Figure 6-3(a), the arching action is assumed to act in the form of second-degree parabolas with an initial tangent slope of 45 degree at the corners which results in an ineffectively confined area of $b^2/6$ for each parabola (Mander et al., 1988a; and Saatcioglu and Razvi, 1992). To take into account all parabolic regions on each side of the column section, an expression of the ineffectively confined area $\left(A_{par} \right)$, can then be calculated as shown in Equation 6-1.

$$A_{par} = \frac{2}{3}b^2$$ (6-1)

The ineffectively confined parabolic regions are also assumed vertically between adjacent confinement elements as in Figure 6-3(b).
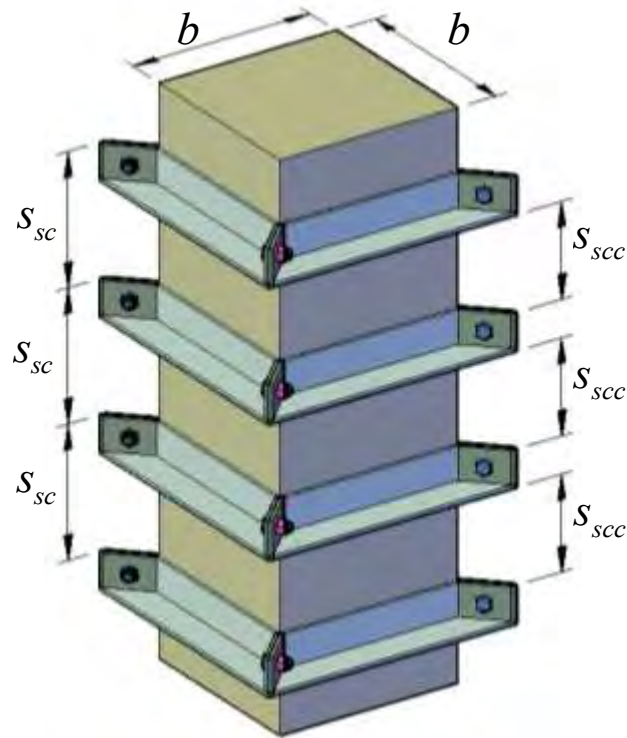
Figure 6-1 Perspective view of the illustration of the externally confined column specimen with steel collars

pressure ditribution
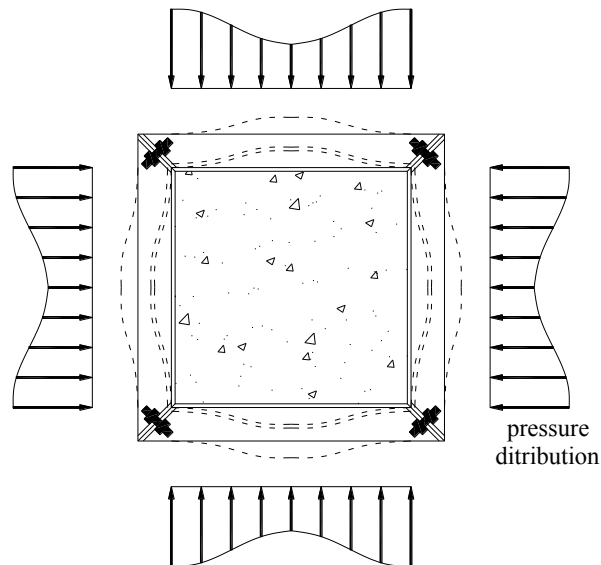
Figure 6-2 Non-uniform confining stress of square column section externally retrofitted by steel collars
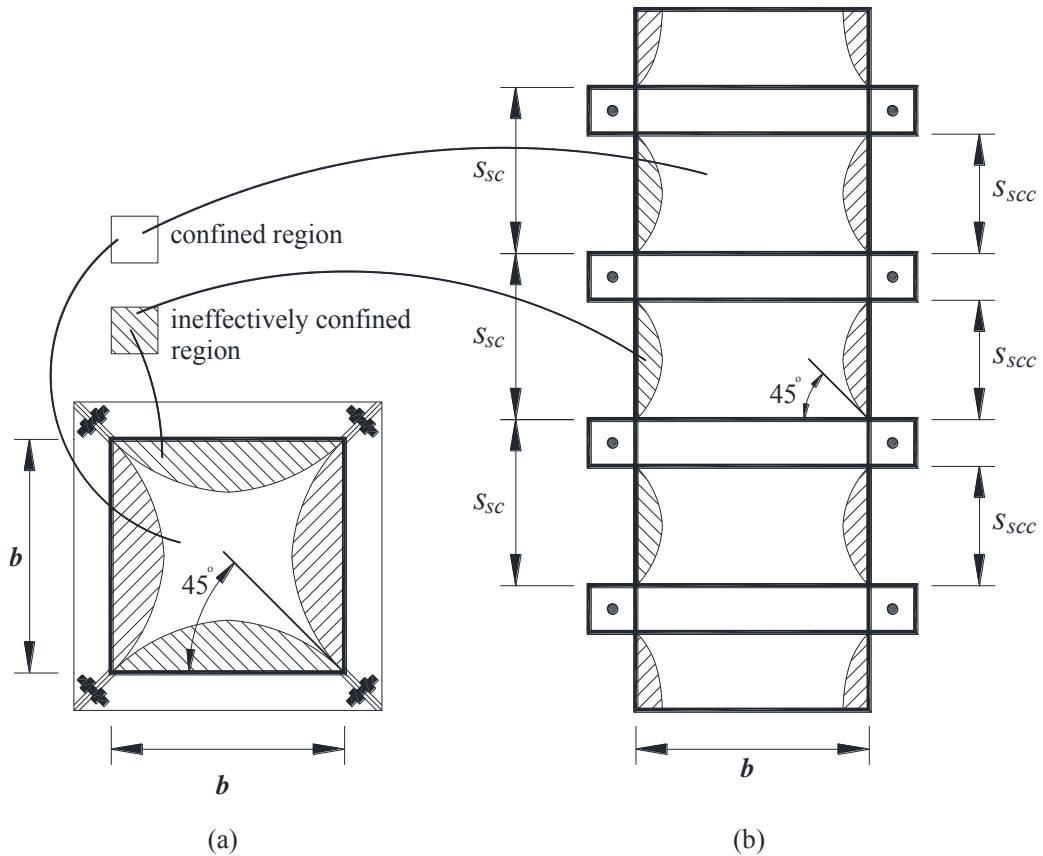
Figure 6-3 The parabolic-shaped ineffectively confined region at: (a) cross section and (b) along the height of the column

With the consideration of the ineffective regions in both horizontal and vertical directions, thus the average of the effectively confined cross sectional area (A_e) can be adopted from Mander et al. (1988a) as given in Equation 6-2.

$$A_e = A_c \left(1 - \frac{A_{par}}{A_c}\right)\left(1 - \frac{s_{scc}}{2b}\right)^2 \tag{6-2}$$

where A_c is the concrete core area, which is the gross cross sectional area of the column $(= b^2)$ in the case of externally confined columns. Further, a confinement effectiveness factor (k_e) is proposed as expressed in Equation 6-3:

$$k_e = \frac{A_e}{A_{cc}} \tag{6-3}$$

where A_{cc} is the net core area of the columns (A_c minus the area of longitudinal bars, if any). To consider the actual non-uniform lateral confining pressure, k_e is

159

introduced to modify the equivalent uniform confining pressure, f_l (which will be explained later) into the effective equivalent uniform confining pressure $\left(f_{le}\right)$ as given in Equation 6-4 (see Figure 6-4).

$$f_{le} = k_e f_l \qquad\qquad\qquad\qquad\qquad (6\text{-}4)$$
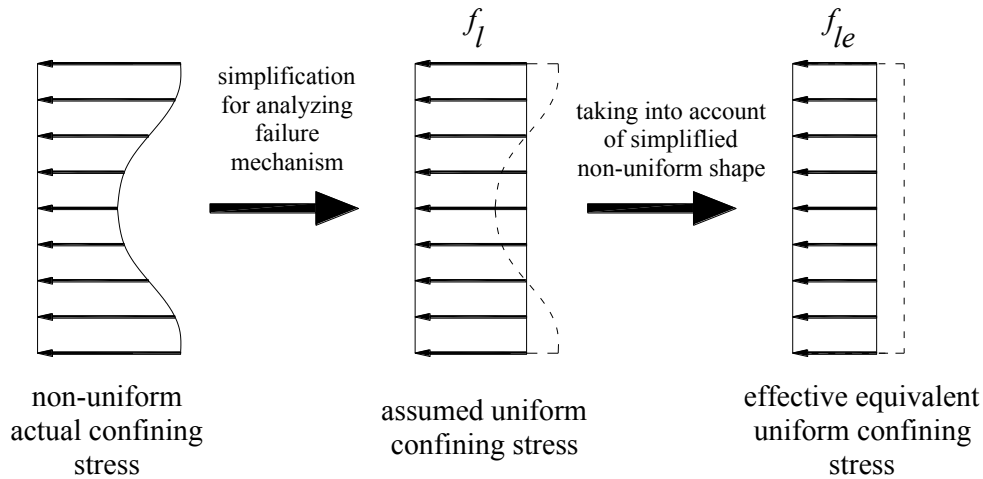
Figure 6-4 The effective equivalent uniform confining stress

The empirical expression for peak strength prediction was derived by using the regression analysis. The regression analysis was carried out to relates the normalized peak strength $\left(f'_{cc}/f'_{c0}\right)$ to the normalized effective equilvalent uniform confining pressure $\left(f_{le}/f'_{c0}\right)$ as suggested by Tavio et al. (2008b). To derive this empirical relation, experimental results of Specimen S02 and S04 were considered to be out layered data, since both specimens suffered premature failure of steel collar corner connection due to the imperfection of the manufacturing process. After the exclusion of these two specimens, the relation between the two parameters was found to be well correlated with the linear equation (coefficient of correlation $R = 0.992$) as shown in Figure 6-5. With the effective equivalent uniform confining pressure determined, the peak strength can be calculated by using empirically determined Equation 6-5.

$$f'_{cc} = f'_{c0}\left(1.0173 + 5.7558\frac{f_{le}}{f'_{c0}}\right) \qquad\qquad (6\text{-}5)$$

where :

160

f'_{cc} = compressive strength of confined concrete (MPa)

f'_{c0} = compressive strength of unconfined concrete (MPa)
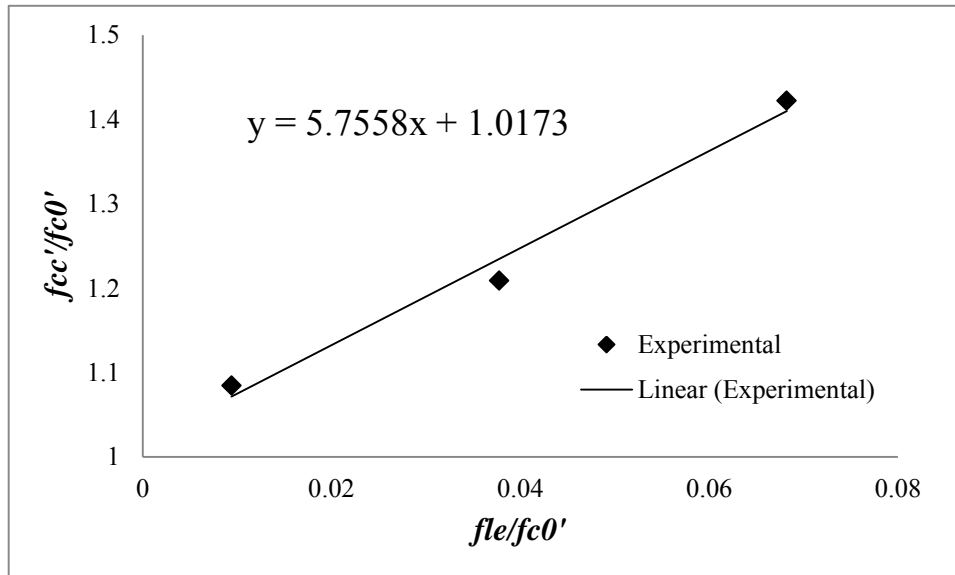
Figure 6-5 Linear relationship of peak strength and effective uniform confining pressure

The strain corresponding to the peak strength was also derived based on Mander et al. (1988a). Mander et al. (1988a) suggested that the ratio $\varepsilon'_{cc}/\varepsilon'_{c0}$ was linearly related to $\left(f'_{cc}/f'_{c0}-1\right)$ as shown in Equation 6-6. By using the same approach, the regression analysis of the experimental data reveals slightly different linear relationship (Equation 6-7). The comparison can be seen graphically in Figure 6-6. In the figure, the solid triangle marks show the experimental data, while the solid circle marks are predictions by Mander et al. (1988a). The function of fitted line of the experimental data is also shown in the figure. Due to the only slight difference, the original expression proposed by Mander et al. (1988a) is adopted in this study, since it was fitted from numerous experimental data. However, if the number of specimens of the current retrofitting approach is increased in the future, Equation 6-7 can be refined further to conform if it is different to replace the proposed equation by Mander model (Mander et al., 1988a).

$$\varepsilon'_{cc} = \varepsilon'_{c0}\left(1 + 5\left(\frac{f'_{cc}}{f'_{c0}} - 1\right)\right)$$ (6-6)

$$\varepsilon'_{cc} = \varepsilon'_{c0}\left(1.0527 + 4.2615\left(\frac{f'_{cc}}{f'_{c0}} - 1\right)\right)$$ (6-7)

y = 4.2615x + 1.0527

▲ Experimental
● Mander
— Linear (Experimental)
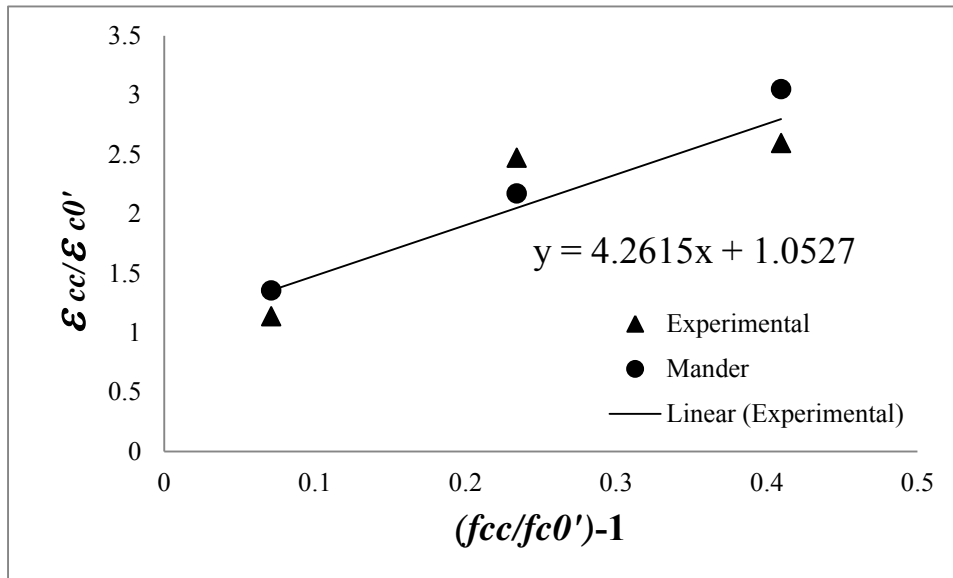
Figure 6-6 Relationship of normalized peak strength and the normalized corresponding strain

Externally confined square concrete columns tend to have more effective confinement at the corners due to stiffer parts of the confinement elements. Similar condition is also found in the conventionally confined concrete using internal transverse reinforcement. According to Xiao and Wu (2003), external steel collars provided the confining pressure through combined bending and axial mechanism. This combined bending and axial mechanism was also observed by Pudjisuryadi et al. (2011). This mechanism is different from the assumption for transverse reinforcement which only depends on axial action because of the relatively small bending stiffness.

First, consider a bulged externally retrofitted concrete column under axial compressive load as in Figure 6-7(a). The steel collars are assumed to deform such a way to maintain the compatibility of outward expansion of the concrete. This deformation is logically larger at the mid-sides than at the corners. The steel collars are assumed to fail in combined axial and bending mechanism at the

162

corners and mid-sides of the columns (plastic hinges are developed). The actual non-uniform confining pressure generated, is simplified with the assumption of uniformly generated confining pressure. The equilibrium of forces along cross sectional plane can be seen in Figure 6-7(b) (only a quarter of the model is analyzed due to the double symmetric condition).
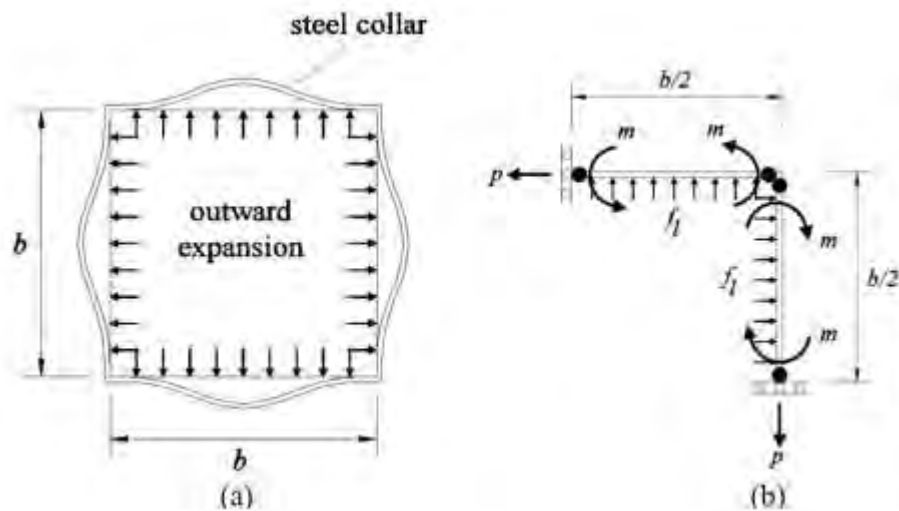
Figure 6-7 (a) Bulged steel collars due to lateral expansion of axially loaded concrete column, and (b) equilibrium of forces analyzed at a quarter of the cross section

Using equilibrium of the forces, the axial force (p) and the bending moment (m) developed in the steel collars can be expressed as a function of equivalent uniform confining pressure (f_l), depth or width of column section (b), and spacing of steel collars (s_{sc}) (Equations 6-8 and 6-9).

$$p = f_l \frac{b}{2} s_{sc} \tag{6-8}$$

$$m = f_l \frac{b^2}{16} s_{sc} \tag{6-9}$$

With the nominal axial and bending capacities (p_n and m_n, respectively) of steel collars given, and adopting the criterion of combined axial and bending failure of the steel collars (Equations 6-10 and 6-11) from the in Indonesian structural steel code (SNI Committee 1729, 2002), f_l can be determined. In calculating the

163

nominal capacity of the steel collars, the reduction factors (ϕ) should be taken as 1.0.

$$\frac{p}{\phi p_n} + \frac{8}{9}\frac{m}{\phi m_n} = 1.0 \quad \text{for} \quad \frac{p}{\phi p_n} \geq 0.2 \tag{6-10}$$

$$\frac{p}{2\phi p_n} + \frac{m}{\phi m_n} = 1.0 \quad \text{for} \quad \frac{p}{\phi p_n} < 0.2 \tag{6-11}$$

With the peak strength given by Equation 6-5, the rest of the model can adopt Mander model (Mander et al. 1988a), as described in Equations 6-12 to 6-14:

$$E_{sec} = \frac{f'_{cc}}{\varepsilon'_{cc}} \tag{6-12}$$

$$r = \frac{E_c}{E_c - E_{sec}} \tag{6-13}$$

$$f_c(\varepsilon_c) = \frac{f'_{cc}\left(\dfrac{\varepsilon_c}{\varepsilon'_{cc}}\right)r}{r - 1 + \left(\dfrac{\varepsilon_c}{\varepsilon'_{cc}}\right)^r} \tag{6-14}$$

where :

f'_{cc} = compressive strength of confined concrete (MPa)

ε'_{cc} = compressive strain of confined concrete corresponding to f'_{cc}

ε'_{c0} = compressive strain of unconfined concrete corresponding to f'_{c0}

E_{sec} = secant modulus of elasticity of confined concrete (MPa)

r = a constant

E_c = modulus of elasticity of plain concrete (MPa)

$f_c(\varepsilon_c)$ = concrete stress as a function of concrete strain (MPa)

ε_c = concrete strain

     To describe the step-by-step procedure of the proposed analytical model, a flowchart is presented in Figure 6-8. To better explain the application of the procedure, detail calculation example is also given in Section 6.2.
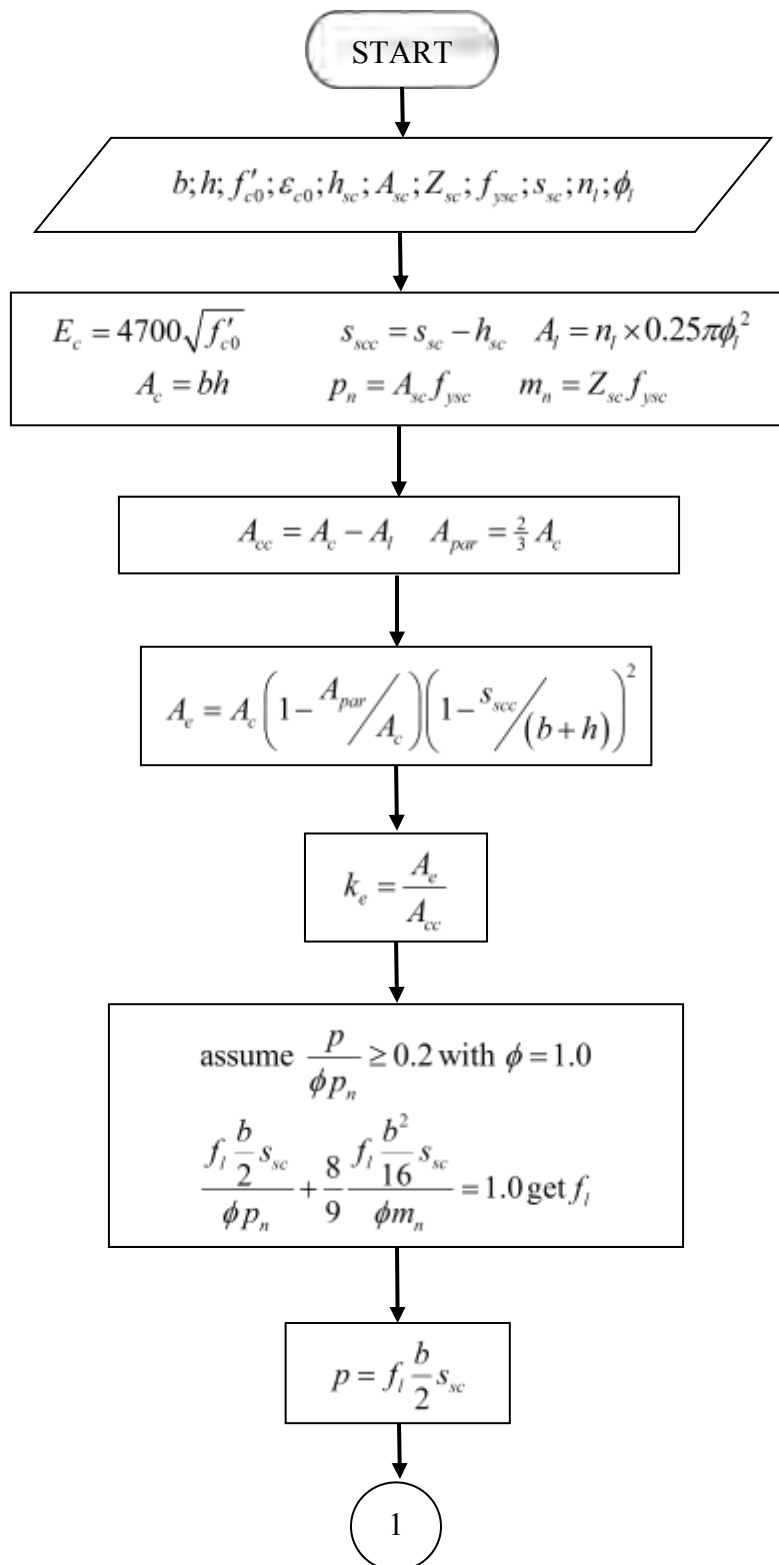
START

$$b; h; f'_{c0}; \varepsilon_{c0}; h_{sc}; A_{sc}; Z_{sc}; f_{ysc}; s_{sc}; n_l; \phi_l$$

$$E_c = 4700\sqrt{f'_{c0}} \qquad s_{scc} = s_{sc} - h_{sc} \qquad A_l = n_l \times 0.25\pi\phi_l^2$$
$$A_c = bh \qquad p_n = A_{sc}f_{ysc} \qquad m_n = Z_{sc}f_{ysc}$$

$$A_{cc} = A_c - A_l \qquad A_{par} = \tfrac{2}{3}A_c$$

$$A_e = A_c \left(1 - {A_{par}}\Big/{A_c}\right)\left(1 - {s_{scc}}\Big/{(b+h)}\right)^2$$

$$k_e = \frac{A_e}{A_{cc}}$$

$$\text{assume } \frac{p}{\phi p_n} \geq 0.2 \text{ with } \phi = 1.0$$

$$\frac{f_l \dfrac{b}{2} s_{sc}}{\phi p_n} + \frac{8}{9}\frac{f_l \dfrac{b^2}{16} s_{sc}}{\phi m_n} = 1.0 \text{ get } f_l$$

$$p = f_l \frac{b}{2} s_{sc}$$

1

Figure 6-8 Flowchart of the step-by-step proposed procedure

165
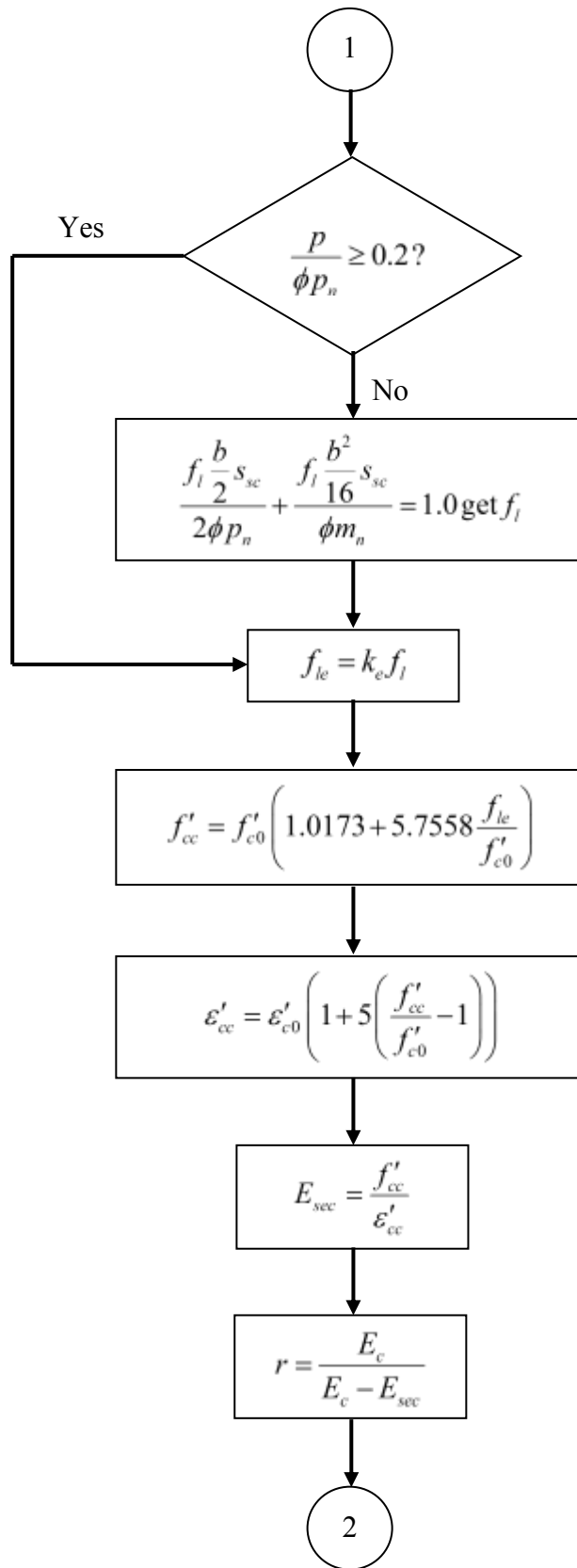
Figure 6-8 Flowchart of the step-by-step proposed procedure (Continued)
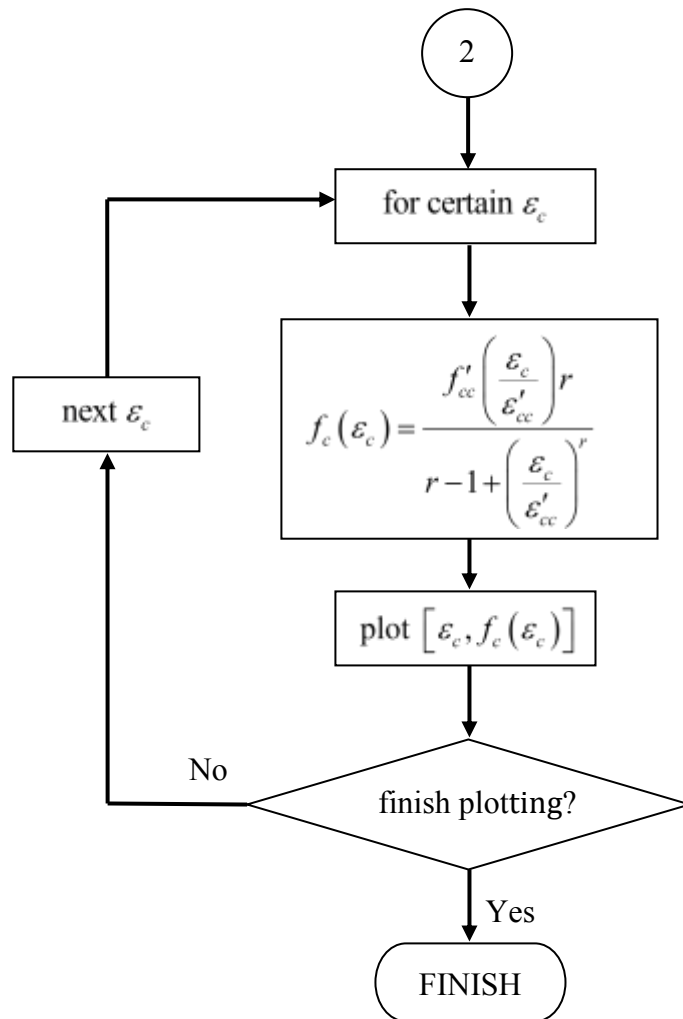
Figure 6-8 Flowchart of the step-by-step proposed procedure (Continued)

6.2 CALCULATION EXAMPLE OF THE PROPOSED ANALYTICAL PROCEDURE

In this Section, a step-by-step proposed analytical procedure for predicting the axial stress-strain of Specimen S03 (Figure 3-4) is presented with a detailed calculation example.

Given data:

$b = h = 200\,\text{mm}$ (specimen cross sectional dimensions)

- Concrete properties obtained from Phase 1 experimental program

$f'_{c0} = 17.0155\,\text{MPa}$ (compressive strength of plain concrete specimen)

$\varepsilon_{c0} = 0.00231884$ (strain corresponding to f'_{c0})

$$E_c = 4700\sqrt{f'_{c0}} = 4700\sqrt{17.0155} = 19,387 \, \text{MPa} \qquad \text{(concrete elastic modulus)}$$

$h_{sc} = w_{sc} = 40 \, \text{mm}$ (height and width of steel angle section)

$t_{sc} = 4 \, \text{mm}$ (thickness of steel angle section)

$A_{sc} = 320 \, \text{mm}^2$ (cross section area of steel angle section)

$Z_{sc} = 2910 \, \text{mm}^3$ (plastic modulus of steel angle section)

$f_{ysc} = 284.98 \, \text{MPa}$ (yield strength of steel angle section)

$s_{sc} = 100 \, \text{mm}$ (center-to-center spacing of steel angle sections)

$s_{scc} = s_{sc} - h_{sc} = 100 - 40 = 60 \, \text{mm}$ (clear spacing of steel angle sections)

$n_l = 4$ (number of longitudinal bars)

$\phi_l = 9.5 \, \text{mm}$ (nominal diameter of longitudinal bars)

- Confinement effectiveness factor, k_e

$$A_l = n_l \times 0.25\pi\phi_l^2 = 4(0.25)(3.14)(9.5^2) = 283.53 \, \text{mm}^2$$

$$A_c = bh = 200(200) = 40,000 \, \text{mm}^2$$

$$A_{cc} = A_c - A_l = 40,000 - 283.53 = 39,716.47 \, \text{mm}^2$$

$$A_{par} = \frac{2}{3}A_c = \frac{2}{3}(40,000) = 26,666.67 \, \text{mm}^2$$

$$A_e = A_c\left(1 - \frac{A_{par}}{A_c}\right)\left(1 - \frac{s_{scc}}{(b+h)}\right)^2$$

$$= 40,000\left(1 - \frac{26,666.67}{40,000}\right)\left(1 - \frac{60}{(200+200)}\right)^2 = 9,633.33 \, \text{mm}^2$$

$$k_e = \frac{A_e}{A_{cc}} = \frac{9,633.33}{39,716.47} = 0.2426$$

- Effective equivalent uniform confining pressure

$$p_n = A_{sc}f_{ysc} = 320(284.98) = 91,193.6 \, \text{N}$$

$$m_n = Z_{sc}f_{ysc} = 2910(284.98) = 829,291.8 \, \text{Nmm}$$

assume $\dfrac{p}{\phi p_n} \geq 0.2$ with $\phi = 1.0$

$$\frac{f_l \dfrac{b}{2} s_{sc}}{\phi p_n} + \frac{8}{9}\frac{f_l \dfrac{b^2}{16} s_{sc}}{\phi m_n} = 1.0$$

$$\frac{f_l \dfrac{200}{2}100}{1(91,193.6)} + \frac{8}{9}\frac{f_l \dfrac{200^2}{16}100}{1(829,291.8)} = 1.0 \rightarrow f_l = 2.648\,\text{MPa}$$

then $\dfrac{p}{\phi p_n} = \dfrac{f_l \dfrac{b}{2} s_{sc}}{1.0 p_n} = \dfrac{2.648\dfrac{200}{2}100}{1.0(91,193.6)} = 0.29 \geq 0.2$ (correct assumption)

$f_{le} = k_e f_l = 0.2426(2.648) = 0.6423\,\text{MPa}$

- Peak strength and strain at peak strength of confined concrete

$$f'_{cc} = f'_{c0}\left(1.0173 + 5.7558\frac{f_{le}}{f'_{c0}}\right) = 17.0155\left(1.0173 + 5.7558\frac{0.6423}{17.0155}\right) = 21.0013\,\text{MPa}$$

$$\varepsilon'_{cc} = \varepsilon'_{c0}\left(1 + 5\left(\frac{f'_{cc}}{f'_{c0}} - 1\right)\right) = 0.00231884\left(1 + 5\left(\frac{21.0013}{17.0155} - 1\right)\right) = 0.0050347$$

- Generate the axial stress-strain relationship

$$E_{sec} = \frac{f'_{cc}}{\varepsilon'_{cc}} = \frac{21.0013}{0.0050347} = 4172.3\,\text{MPa}$$

$$r = \frac{E_c}{E_c - E_{sec}} = 1.274$$

for example, the stress is generated at strain, $\varepsilon_c = 0.008$ on the descending branch.

$$f_c(\varepsilon_c) = \frac{f'_{cc}\left(\dfrac{\varepsilon_c}{\varepsilon'_{cc}}\right)r}{r - 1 + \left(\dfrac{\varepsilon_c}{\varepsilon'_{cc}}\right)^r} = \frac{21.0013\left(\dfrac{0.008}{0.0050347}\right)1.274}{1.274 - 1 + \left(\dfrac{0.008}{0.0050347}\right)^{1.274}} = 20.459\,\text{MPa}$$

The remaining data for developing the axial stress-strain curve can be computed by the same procedure with different strain value. The completely generated axial stress-strain curve is presented in Figure 6-9. Verification of this proposed analytical model with the experimental results is reported in Section 6.3.
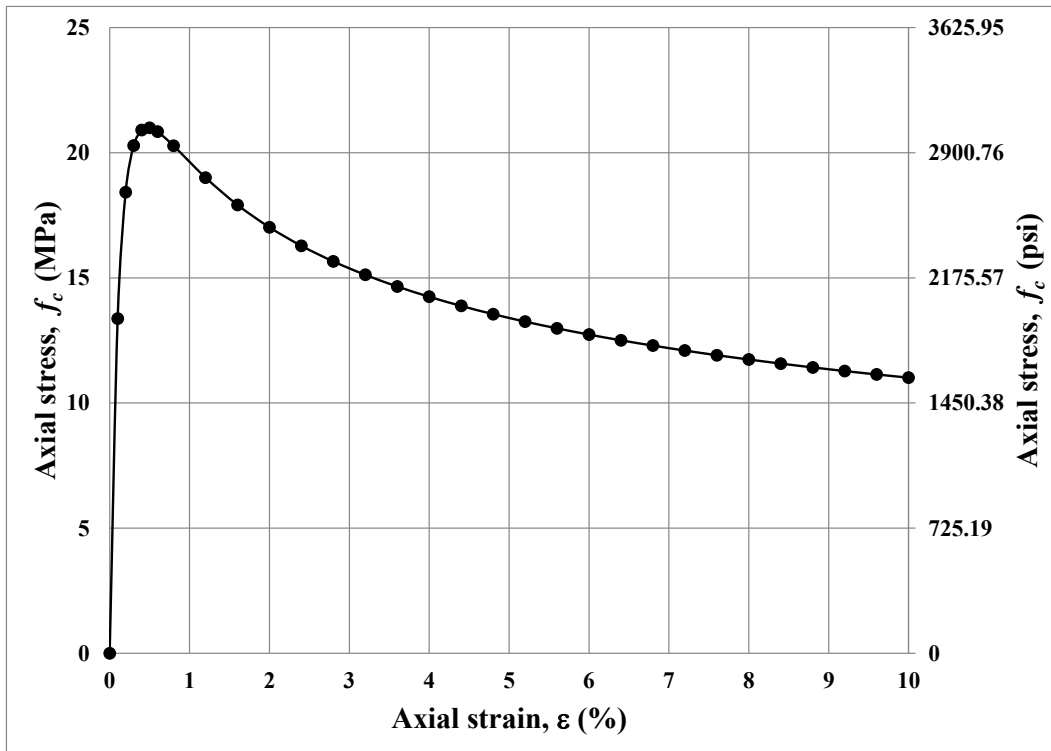
Figure 6-9 Axial stress-strain relationship of S03 (proposed analytical model).

6.3 COMPARISON OF PROPOSED ANALYTICAL MODEL WITH EXPERIMENTAL RESULTS OF MONONOTIC COMPRESSION TESTS

In order to investigate the strength gain, all stresses presented in this section are normalized to the peak strength of Control Specimen CS01, representing specimen with no confinement. Comparisons of the experimental results (S01, S03, and S05) with their analytical predictions can be seen in Figure 6-10. In the figure, the curves' legends with suffix "-Prop" indicate the proposed analytical models. It can be seen that the normalized experimental stress-strain curves of Specimen S03 can be predicted reasonably well by the proposed analytical model. The prediction of S01 is slightly overestimated by the proposed model, while for S05 it is slightly underestimated prior the first failure of a collar at a relatively high axial strain value. For the sake of discussions, the comparisons of the proposed model with Specimens S02 and S04 (which were taken out for the regression analysis as explained in Section 6.1) are also presented. In Figure 6-11, the peak strength prediction of Specimen S02 is underestimated by the proposed

170

model. However, the descending branch of the curve only deviates by reasonable margin. In Figure 6-12, both the peak strength and the descending branch of the curve of S04 are overestimated by the proposed model. This is expected since S04 suffered premature failure at the corner of a steel collar as explained earlier (Chapter 4). If Specimens S04c and S04d (which were indentified that the web stiffeners were ineffective) are included in the comparisons, it is clear that the proposed model can predict the peak strength and descending branch of the curve quite well prior to the first failure of a collar. This confirms that the proposed analytical model can predict accurately the stress-strain relationships of the externally confined columns with steel collars.

To predict the specimens with the additional bolt attachment (S04e and S04f), the proposed analytical model can be simply modified by recalculating the effectively confined region by considering the bolt attachment as additional support. This will lead to a bigger confined area since the ineffective parabolic areas become smaller. The results of the implementation of this concept, are shown by the comparisons of the measured and the predicted stress-strain curves (Figure 6-13). It can be seen that the predictions of analytical models overestimate the experimental curves. There are two possible reasons to explain this issue : (1) the attachment process of the bolts which involves the drilling process on the concrete might have cause the initial damage; and (2) the bolts are only embedded shortly from the concrete surface (if the bolt used are longer and they can pass through the section from one face to the other face of the column, they can be more effective).

Figure 6-10 Normalized stress vs axial strain of proposed analytical model and experimental results of S01, S03, and S05

Figure 6-11 Normalized stress vs axial strain of proposed analytical model and experimental results of S02
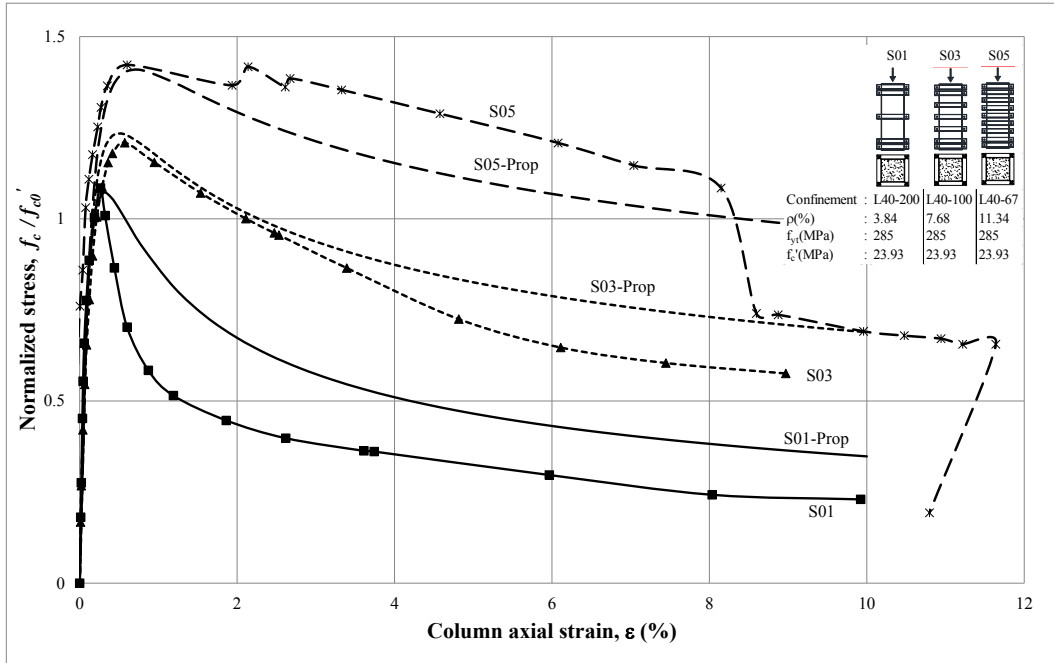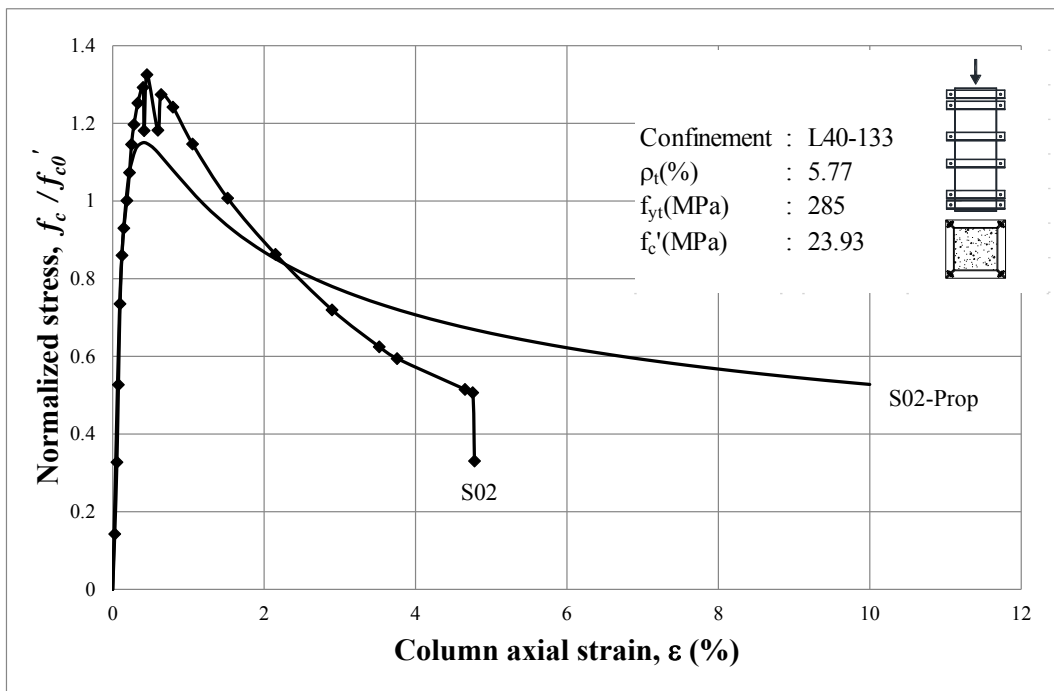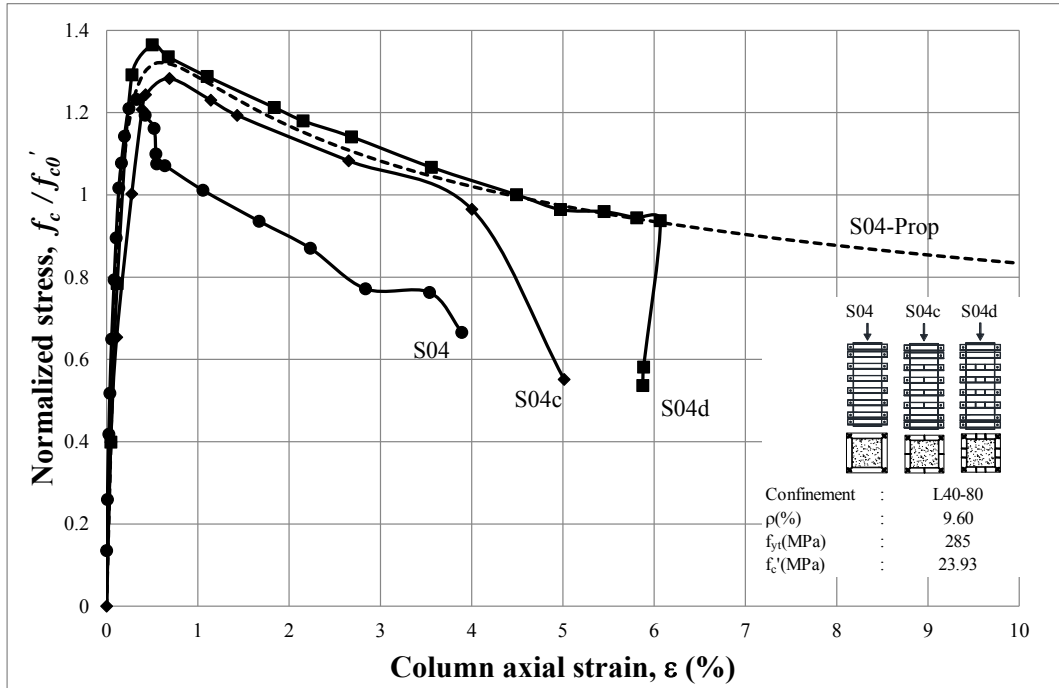
172

Figure 6-12 Normalized stress vs axial strain of proposed analytical model and experimental results of S04, S04c, and S04d
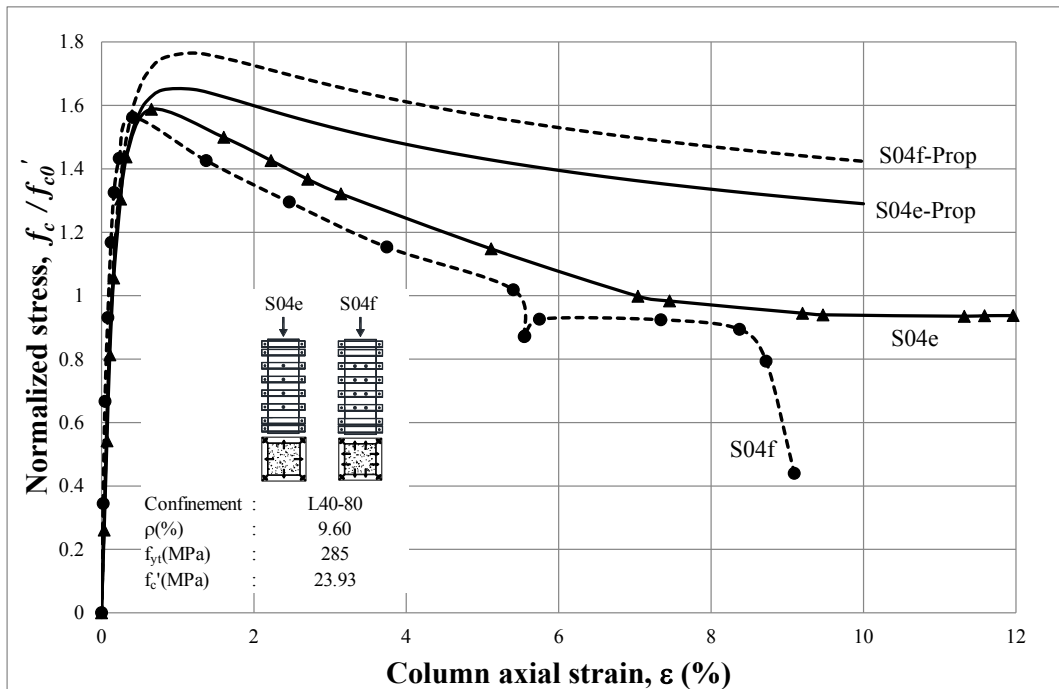

Figure 6-13 Normalized stress vs axial strain of proposed analytical model and experimental results of S04e, and S04f

173

6.4 GENERATED BACKBONES OF HYSTERETIC LOOPS BY PROPOSED ANALYTICAL AXIAL STRESS-STRAIN MODEL

In this section, the proposed analytical model of axial stress-strain is implemented in a computer algorithm to generate the backbones of $M - \varphi$ curves. The procedure to generate such curve can be summarized in following the following steps:

a. Discretize the square RC section into layers as shown in Figure 6-14.
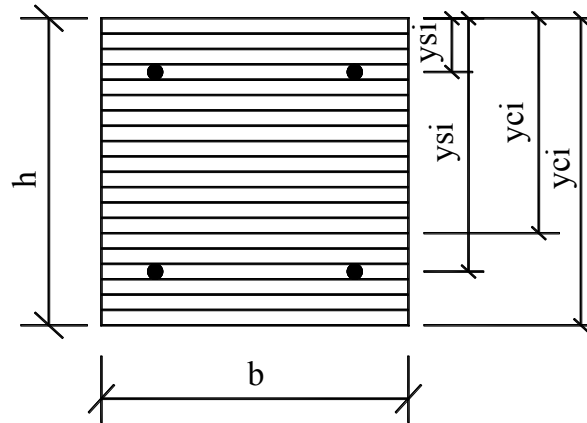
Figure 6-14 Descretization of RC section

In Figure 6-14, the section is discretized into layers of small slices. The depths to extreme fiber of the section of each concrete layers and steel centroid from the top extreme fiber of the section are recorded $\left(y_{si} \text{ and } y_{ci} \right)$. The area of concrete layers and steels at each discretization are also computed.

b. Apply the constant axial load $\left(P_0 \right)$ and find the initial values of strains and stresses in both concrete $\left(\varepsilon_{ci}, f_{ci} \right)$ and steels $\left(\varepsilon_{si}, f_{si} \right)$.

The initial strains of concrete and steel are the same at this initial stage (Figure 6-15). The strains $\left(\varepsilon_{ci} \text{ and } \varepsilon_{si} \right)$ can be calculated by using the equilibrium of the external and internal forces as in Equation 6-15.

$$P_0 = A_t f_s \left(\varepsilon_{si} \right) + A_{cc} f_c \left(\varepsilon_{ci} \right) \tag{6-15}$$

where A_l and A_{cc} are the total area of steel and net area of concrete; $f_l(\varepsilon_{si})$ and $f_c(\varepsilon_{ci})$ are the stresses of steel and concrete corresponding to the initial strain of concrete and steel.
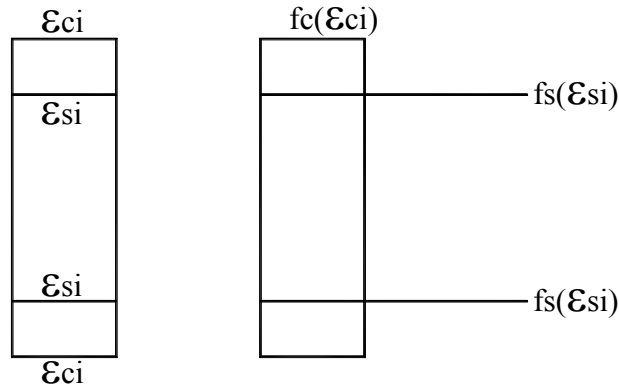
**Figure 6-15 Strains and stresses due to initial axial force P_0**

c. Apply the incremental additional strain (Δ_ε) and iterate to find the appropriate neutral axis, c (satisfy the equilibrium of forces).

Figure 6-16 shows the strain and stress distributions acrros the sectional depth after the application of the small strain increment (Δ_ε). Any strains (ε_x) at any locations (y_x) can also be calculated if the value of neutral axis (c) is assumed. In turn, every stresses in both concrete layers $(f_c(\varepsilon_c))$ and steels $(f_s(\varepsilon_s))$, can be calculated by using the proposed constitutive law of the materials (the stress-strain relationships). It should be noted, as the concrete strain (ε_c) become greater, the corresponding concrete stress $(f_c(\varepsilon_c))$ would have non-linear shape over the sectional depth. With the areas of concrete layers (A_{ci}) and steels (A_{si}) given, the neutral axis must be iterated until the sum of all internal forces almost equal to the external load $\left(\sum\left[f_{ci}(\varepsilon_{ci})A_{ci}\right]+\sum\left[f_{si}(\varepsilon_{si})A_{si}\right]-P_0=\Delta_t\right)$. Δ_t is the tolerable error which can be set near to zero with certain accuracy for solving numerical issue. The internal forces of the concrete layer can be

175

computed by multiplying the average of the discrete concrete stresses with the area of the layer (trapezoidal rule).
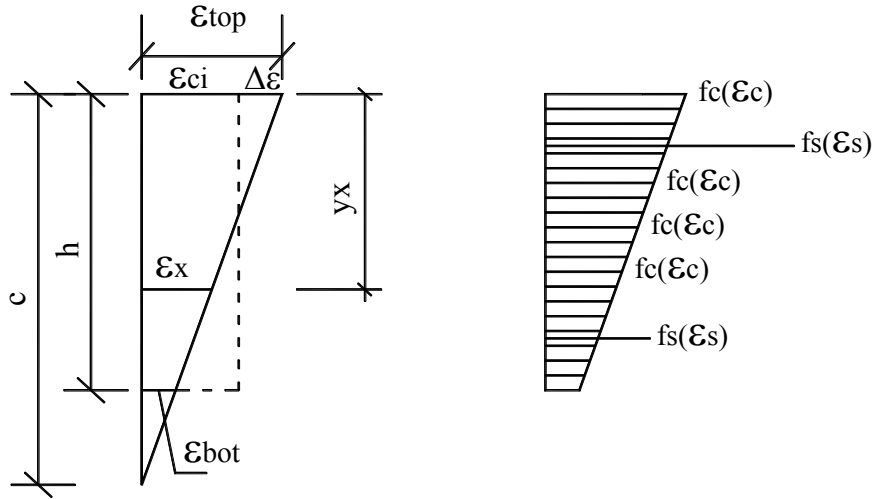
Figure 6-16 Strain and stress distributions across the sectional depth with the application of the incremental strain ($\Delta\varepsilon$) over the initial strains

d. Determine the bending moment (M) and the corresponding curvature (φ) to obtain one point (M, φ) in the curve.

Once the neutral axis (c) is found, the bending moment (M) of the section can be calculated by taking the sum of all internal forces and P_0 multiplied by their corresponding distances to a point (Equation 6-16). In Equation 6-16, the positive sign is adopted for internal forces in compression. The curvature (φ) can be calculated by using Equation 6-17.

$$M = \sum C_i y_{ci} + \sum T_i y_{si} - P_0 \frac{h}{2} \qquad (6\text{-}16)$$

C_i and T_i are the compression forces in ith layer of concrete ans steel, respectively.

$$\varphi = \frac{\varepsilon_{top} - \varepsilon_{bot}}{h} \qquad (6\text{-}17)$$

176

ε_{top} and ε_{bot} are the strains at the top and bottom fiber of the column section.

    e.   Repeat steps c and d to calculate the other points of the curve.

    f.   Finish step e at a desired maximum strain value.

The comparisons of measured and the analytical $M - \varphi$ curves (backbone) as shown in Figures 6-17 to 6-19. The solid lines represent the analytical backbone of the $M - \varphi$ curve. It can be seen from the curves, that generally the initial stiffnesses are slightly overestimated, whereas on the other hand the peak strengths are underestimated.
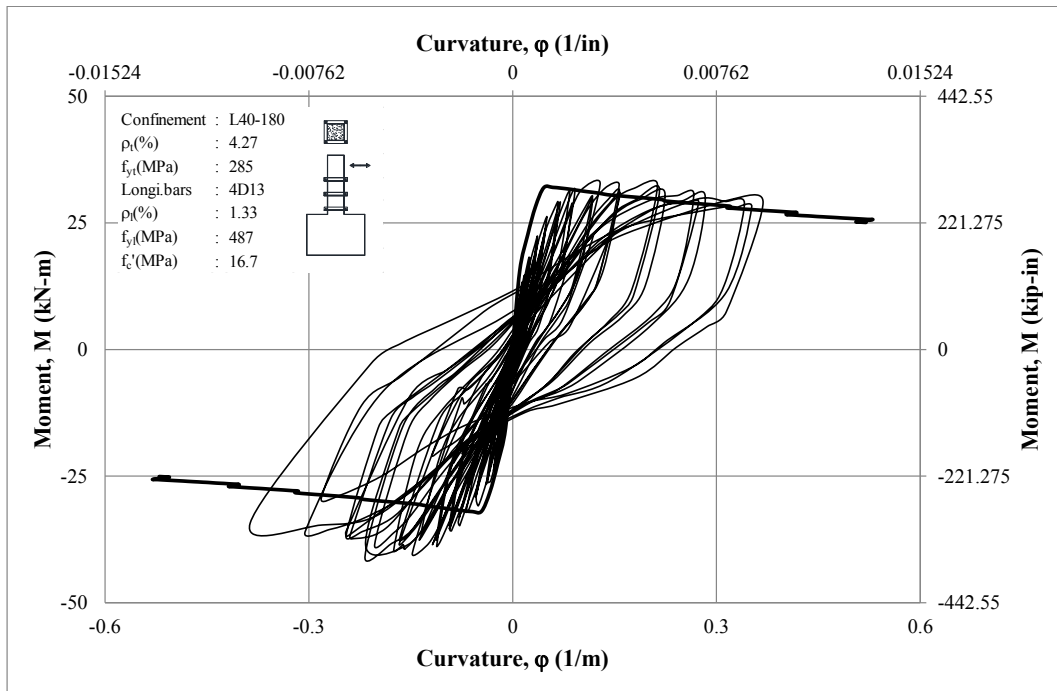

Figure 6-17 Predicted backbone of M-ϕ curve of Specimen S13

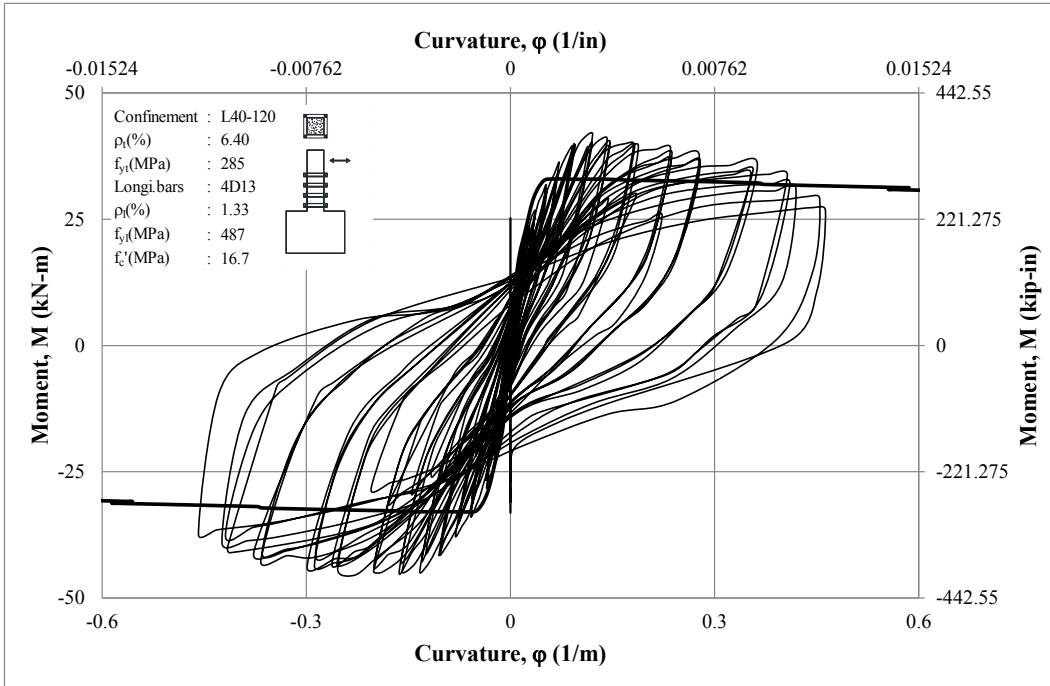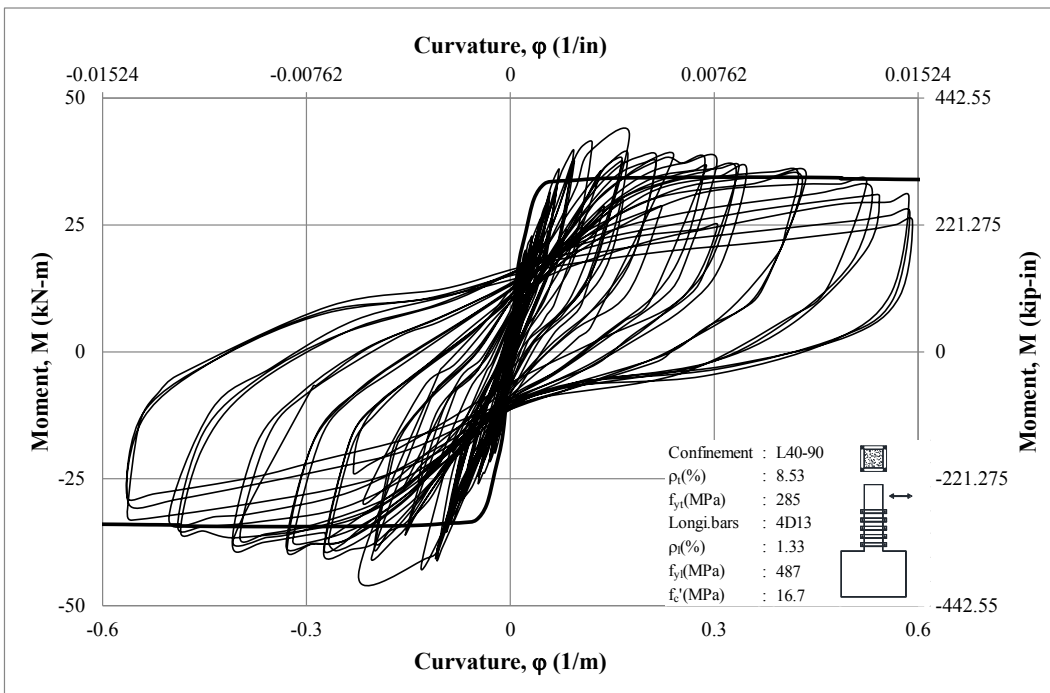**Figure 6-18 Predicted backbone of M-ϕ curve of Specimen S14**

Figure 6-19 Predicted backbone of M-ϕ curve of Specimen S15

For example, the calculation of a point at the backbone of $M - \varphi$ curve of Specimen S14 is given as follows:

Data given:

$j_s = 20$ (the number of descritization layers of the section)

$y_{s1} = 36.4\,\text{mm}$ (location of 1$^{\text{st}}$ layer of steel bars)

$y_{s2} = 163.6\,\text{mm}$ (location of 2$^{\text{nd}}$ layer of steel bars)

$b = h = 200\,\text{mm}$ (column sectional dimensions)

$f_c' = 16.7\,\text{MPa}$ (cylinder compressive strength)

$f_{yl} = 542\,\text{MPa}$ (yield strength of longitudinal bars)

$f_{su} = 648\,\text{MPa}$ (tensile strength of longitudinal bars)

$n_l = 4$ (numbers of longitudinal bars)

$\phi_l = 12.8\,\text{mm}$ (nominal diameter of longitudinal bars)

$P_0 = 240,000\,\text{N}$ (constant axial load applied)

$E_s = 200,000\,\text{MPa}$ (concrete elastic modulus)

$h_{sc} = 40\,\text{mm}$ (height of steel angle collar)

$f_{ysc} = 285\,\text{MPa}$ (yield strength of steel angle collar)

$Z_{sc} = 2,910\,\text{mm}^3$ (plastic modulus of steel angle collar)

$A_{sc} = 320\,\text{mm}^2$ (cross sectional area of steel angle collar)

$s_{sc} = 120\,\text{mm}$ (center-to-center distance of steel angle collars)

$s_{scc} = s_{sc} - h_{sc} = 120 - 40 = 80\,\text{mm}$ (clear distance of steel angle collars)

$A_l = \dfrac{n_l}{4}\,0.25\pi\phi_l^2 = \dfrac{4}{4}(0.25)(3.14)(12.8^2) = 514.7\,\text{mm}^2$ (area of longitudinal bars)

$f_{c0}' = 0.85 f_c' = 0.85(16.7) = 14.2\,\text{MPa}$ (column compressive strength)

$\varepsilon_{c0} = 0.002$ (strain corresponding to f_{c0}')

$E_c = 4700\sqrt{f_{c0}'} = 4700\sqrt{14.2} = 17,708\,\text{MPa}$ (concrete elastic modulus)

- Confinement effectiveness factor, k_e

$$A_c = bh = 200(200) = 40,000\,\text{mm}^2$$

$$A_{cc} = A_c - A_l = 40,000 - 514.7 = 39,485.3\,\text{mm}^2$$

$$A_{par} = \frac{2}{3}A_c = \frac{2}{3}(40,000) = 26,667\,\text{mm}^2$$

$$A_e = A_c\left(1 - \frac{A_{par}}{A_c}\right)\left(1 - \frac{s_{scc}}{b+h}\right)^2$$

$$= 40,000\left(1 - \frac{26,667}{40,000}\right)\left(1 - \frac{80}{200+200}\right)^2 = 8,533\,\text{mm}^2$$

$$k_e = \frac{A_e}{A_{cc}} = 0.2161$$

- Effective equivalent uniform confining pressure

$$p_n = A_{sc}f_{ysc} = 320(284.98) = 91,194\,\text{N}$$

$$m_n = Z_{sc}f_{ysc} = 2910(284.98) = 829,292\,\text{Nmm}$$

assume $\dfrac{p}{\phi p_n} \geq 0.2$ with $\phi = 1.0$

$$\frac{f_l\dfrac{b}{2}s_{sc}}{\phi p_n} + \frac{8}{9}\frac{f_l\dfrac{b^2}{16}s_{sc}}{\phi m_n} = 1.0$$

$$\frac{f_l\dfrac{200}{2}120}{1(91,194)} + \frac{8}{9}\frac{f_l\dfrac{200^2}{16}120}{1(829,292)} = 1.0 \rightarrow f_l = 2.21\,\text{MPa}$$

then $\dfrac{p}{\phi p_n} = \dfrac{f_l\dfrac{b}{2}s_{sc}}{1.0\,p_n} = \dfrac{2.21\dfrac{200}{2}120}{1.0(91,194)} = 0.29 \geq 0.2$ (correct assumption)

$$f_{le} = k_e f_l = 0.2161(2.21) = 0.4769\,\text{MPa}$$

$$f'_{cc} = f'_{c0}\left(1.0173 + 5.7558\frac{f_{le}}{f'_{c0}}\right) = 14.2\left(1.0173 + 5.7558\frac{0.4769}{14.2}\right) = 17.181\,\text{MPa}$$

$$\varepsilon'_{cc} = \varepsilon'_{c0}\left(1 + 5\left(\frac{f'_{cc}}{f'_{c0}} - 1\right)\right) = 0.002\left(1 + 5\left(\frac{17.181}{14.2} - 1\right)\right) = 0.0041$$

$$E_{sec} = \frac{f'_{cc}}{\varepsilon'_{cc}} = \frac{17.181}{0.0041} = 4,187 \, \text{MPa}$$

$$r = \frac{E_c}{E_c - E_{sec}} = \frac{17,708}{17,708 - 4,187} = 1.31$$

- Initial Condition (due to constant axial load P_0)

$$P_0 = A_l E_s \varepsilon_{cin} + A_{cc} \frac{f'_{cc}\left(\dfrac{\varepsilon_{cin}}{\varepsilon'_{cc}}\right)r}{r - 1 + \left(\dfrac{\varepsilon_{cin}}{\varepsilon'_{cc}}\right)^r}$$

$$240,000 = 514.7\,(200,000)\,\varepsilon_{cin} + 39,485.3 \frac{17.181\left(\dfrac{\varepsilon_{cin}}{0.0041}\right)1.31}{1.31 - 1 + \left(\dfrac{\varepsilon_{cin}}{0.0041}\right)^{1.31}}$$

$$\rightarrow \varepsilon_{cin} = 3.3 \times 10^{-4}$$

$$f_{cin}\left(\varepsilon_{cin}\right) = \frac{f'_{cc}\left(\dfrac{\varepsilon_{cin}}{\varepsilon'_{cc}}\right)r}{r - 1 + \left(\dfrac{\varepsilon_{cin}}{\varepsilon'_{cc}}\right)^r} = \frac{17.181\left(\dfrac{3.3\times10^{-4}}{0.0041}\right)1.31}{1.31 - 1 + \left(\dfrac{3.3\times10^{-4}}{0.0041}\right)^{1.31}} = 5.22 \, \text{MPa}$$

$$f_{si}\left(\varepsilon_{cin}\right) = E_s \varepsilon_{cin} = 200,000\left(3.3\times10^{-4}\right) = 65.9 \, \text{MPa}$$

- Condition with additional strain $\Delta_\varepsilon = 0.05$ at compression fiber

$$\varepsilon_{ctop} = \varepsilon_{cin} + \Delta_\varepsilon = 3.3\times10^{-4} + 0.05 = 0.05033$$

The neutral axis c should be calculated so that the equilibrium of forces is satisfied. This can be done by iterating the trial values of strain at the other extreme fiber.

$$\varepsilon_{cbot} = -0.0547 \quad \text{(after several trial values)}$$

$$c = \frac{\varepsilon_{ctop} h}{\varepsilon_{ctop} - \varepsilon_{cbot}} = \frac{0.05033\,(200)}{0.05033 - (-0.0547)} = 95.88 \, \text{mm}$$

With the assumption of plane section remains plane, the strains of every steel $\left(\varepsilon_{si}\right)$, and every layer of concrete $\left(\varepsilon_{ci}\right)$ can be calculated. Furthermore, the stress at each concrete layer $\left(f_{ci}\left(\varepsilon_{ci}\right)\right)$ and steels $\left(f_{si}\left(\varepsilon_{si}\right)\right)$ can also be computed.

For example, if the concrete is analyzed for the 10th layer :

$$\varepsilon_{ci} = \frac{\varepsilon_{ci} + \varepsilon_{ci+1}}{2} = \frac{0.0195 + 0.0160}{2} = 0.0178$$

$f_{ci}(\varepsilon_{ci}) = 13.67\,\text{MPa}$ (by using proposed model described in Section 6.1)

$$C_i = A_{cli} f_{ci} = 10(200)(13.67) = 27,347\,\text{N}$$

For example, if the steel is analyzed for the 1st layer (by model proposed by King et al., 1986):

$\varepsilon_{si} = 0.0378$ (steel strain at 1st layer, obtained from strain profile)
$\varepsilon_{sh} = 0.008$ (steel strain at start of hardening)
$\varepsilon_{su} = 0.12$ (ultimate steel strain)
$r = \varepsilon_{su} - \varepsilon_{sh} = 0.12 - 0.008 = 0.112$

$$m = \frac{f_{su}/f_{yl}(30r^2+1)^2 - 60r - 1}{15r^2} = \frac{648/542\left(30(0.112)^2 + 1\right)^2 - 60(0.112) - 1}{15(0.112)^2} = 81.62$$

$$f_{si} = f_{yl}\left|\frac{m(\varepsilon_s - \varepsilon_{sh}) + 2}{60(\varepsilon_s - \varepsilon_{sh}) + 2} + \frac{(\varepsilon_s - \varepsilon_{sh})(60 - m)}{2(30r+1)^2}\right|$$

$$= 542\left[\frac{81.62(0.0378 - 0.008) + 2}{60(0.0378 - 0.008) + 2} + \frac{(0.0378 - 0.008)(60 - 81.62)}{2(30(0.112)+1)^2}\right] = 625.1\,\text{MPa}$$

The forces at all concrete layers (C_i) (twenty layers) are listed in Table 6-1, while forces at the longitudinal steels bars (T_i) are given in Table 6-2.

Table 6-1 Concrete forces at all layers

Layer #	y_{ci} (mm)	ε_{ci}	$f_{ci}(\varepsilon_{ci})$ MPa	A_{cli} (mm^2)	C_i (N)
1	0	0.0503	10.40	2000	20794
2	10	0.0451	10.78	2000	21515
3	20	0.0398	11.18	2000	22352
4	30	0.0346	11.67	1742.6	20339
5	40	0.0293	12.27	2000	24543
6	50	0.0241	13.02	2000	26039
7	60	0.0188	14.00	2000	27977
8	70	0.0136	15.30	2000	30584
9	80	0.0083	16.92	2000	33830
10	90	0.0031	6.87	2000	13749
11	100	-0.0022	0	2000	0

Table 6-1 Concrete forces at all layers (Continued)

Layer #	y_{ci} (mm)	ε_{ci}	$f_{ci}(\varepsilon_{ci})$ MPa	A_{cli} (mm^2)	C_i (N)
12	110	-0.0074	0	2000	0
13	120	-0.0127	0	2000	0
14	130	-0.0179	0	2000	0
15	140	-0.0232	0	2000	0
16	150	-0.0284	0	2000	0
17	160	-0.0337	0	1742.6	0
18	170	-0.0389	0	2000	0
19	180	-0.0442	0	2000	0
20	190	-0.0494	0	2000	0
	200	-0.0547	0	$\sum C_c = 241,724$N	

Table 6-2 Steel forces at longitudinal bars

y_{si} (mm)	ε_{si}	$f_{si}(\varepsilon_{si})$ MPa	A_{si} (mm^2)	T_i (N)
36.4	0.0312	615.04	257.4	158287
163.6	-0.0356	-621.90	257.4	-160051
			$\sum T = -1,763.8$N	

The Equilibrium of forces (external and internal forces) :

$\sum C_c + \sum T - P_0 = 241.724 - 1.7638 - 240.000 = -0.0403\,\text{kN} \cong 0$ (the interval of iteration in computer algorithm to find the neutral axis can be refined to obtain the error value closer to zero, if necessary). The curvature and the corresponding moment are finally can be computed.

$$\varphi = \frac{\varepsilon_{top} - \varepsilon_{bot}}{h} = \frac{0.05033 - (-0.0547)}{200} = 5.25 \times 10^{-4}\,\text{mm}^{-1}$$

$$M = \sum C_i y_{ci} + \sum T_i y_{si} - P_0\,{h}/{2} = 31.895\,\text{kNm}$$

6.5 PROPOSED DESIGN PROCEDURE FOR RETROFITTING DEFICIENT SQUARE RC COLUMNS WITH EXTERNAL STEEL COLLAR

In this section, a retrofitting design procedure by adopting the proposed external retrofit method is presented. To ensure the rotational deformability of the potential plastic hinges near the column ends, the minimum confinement requirement of RC columns in seismic area are expressed in Equations 6-18 and 6-19 (Xiao et al., 2003; and SNI 2847 : 2013).

$$A_{sh1} = 0.09 \left(sb_c \frac{f_c'}{f_{yh}} \right)$$ (6-18),

or :

$$A_{sh2} = 0.3 \left(sb_c \frac{f_c'}{f_{yh}} \right) \left(\frac{A_g}{A_{ch}} - 1 \right)$$ (6-19).

Those expressions are based on the premise that confined columns should maintain their axial capacities after the spalling of concrete cover. In short, the confincement should be provided such that the strength in concrete cover be equal to the strength gain in concrete core (Saatcioglu and Razvi, 2002).

For retrofit design, it is suggested that the equivalent confinement pressure should be provided to a column under consideration (Xiao et al., 2003). In this proposed retrofitting method, providing the targeted equivalent confinement pressure is not an easy task since it involves the combined axial and bending mechanism of the steel collar elements (see Equations 6-10 and 6-11). This difficulty was already considered by Xiao et al. (2003). They suggested to neglect the tensile force in the confinement element in order come up with a simple expression in calculating the thickness of the external steel plates. Furthermore, the mathematical expressions will be more complex since the retrofitting method is normally implemented to the existing deficiently confined columns that already have conventional stirrups. The main issue is the existance of two combined internal and external confinement. However, with the availability of computer aid, it is much simpler to develop an algorithm to calculate the combined effects of internal and external confinements. Thus, the retrofit design can be simply simulated to satisfy the confinement required by the code (SNI 2847 : 2013).

A step-by-step procedure is presented here to serve the idea of the proposed steel collar retrofit design. The main idea is to superpose the available confinement effects of available internal confinement with the additional external confinement. Supposed that the effectively confined areas affected by the internal and external confinements be A_{ei} and A_{ee}, respectively as illustrated in Figure 6-20.

184
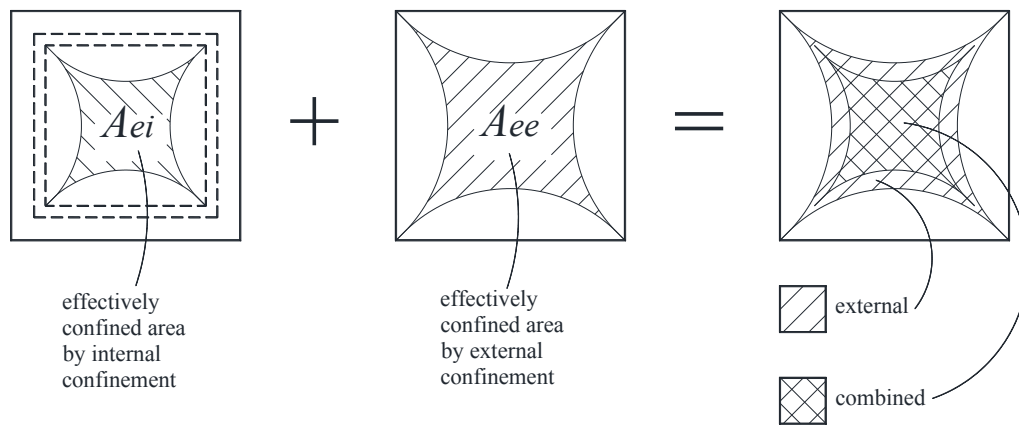
Figure 6-20 Effectively confined areas due to the internal and external confinements

The area A_{ei} experiences the confining pressure from both internal and external confinements, whereas area $A_{ee} - A_{ei}$ only experiences the confining pressure from the external confinement. The confining pressure from the internal confinement (f_{li}) can be determined by using the classic model suggested by Mander et al. (1988a), while that from the external confinement (f_{le}) can be determined by the proposed analytical model described earlier in Section 6.1 (Equation 6-4). To combine these effects, it is proposed to adopt the average confining pressure (f_{lcomb}), that is proportional to their affected areas as expressed in Equation 6-20.

$$f_{lcomb} = \frac{\left(f_{li} + f_{le}\right)A_{ei} + f_{l_e}\left(A_{ee} - A_{ei}\right)}{A_{ee}}$$

(6-20)

This average confining pressure can be used along with the proposed analytical model (Section 6.1) to generate the axial stress-strain relationship due to effects of both internal and external confinements. The flowchart of the step-by-step procedure of this design retrofit apporach is presented in Figure 6-21. The calculation example of this procedure is presented in Section 6.4.

START

$b; h; f'_{c0}; \varepsilon_{c0}; h_{sc}; A_{sc}; Z_{sc}; f_{ysc}; s_{sc}; n_l; \phi_l; d_{cover}; \phi_s; f_{yst}; s$

$E_c = 4700\sqrt{f'_{c0}}$ $A_l = n_l \times 0.25\pi\phi_l^2$

$A_v = \frac{2}{4}\pi\phi_s^2$ $s'' = s - 2(0.5)\phi_s$
$b_c = h_c = b - 2d_{cover} - 2(0.5)\phi_s$

$f_l = \dfrac{f_{yt}A_v}{sb_c}$ $A_{ci} = b_c h_c$
$w' = b_c - 2(0.5)\phi_s - 2\phi_l$

$A_{cci} = A_{ci} - A_l$
$A_{ei} = \left(A_{ci} - \frac{2}{3}w'^2\right)\left(1 - \frac{s'}{2b_c}\right)^2$

$k_{ei} = \dfrac{A_{ei}}{A_{cci}}$

$f_{li} = k_{ei}f_l$

1

$s_{scc} = s_{sc} - h_{sc}$ $p_n = A_{sc}f_{ysc}$
$m_n = Z_{sc}f_{ysc}$ $A_{ce} = bh$ $A_{par} = \frac{2}{3}A_{ce}$

$A_{cce} = A_{ce} - A_l$
$A_{ee} = A_{ce}\left(1 - \dfrac{A_{par}}{A_{ce}}\right)\left(1 - \dfrac{s_{scc}}{(b+h)}\right)^2$

$k_{ee} = \dfrac{A_{ee}}{A_{cce}}$

assume $\dfrac{p}{\phi p_n} \geq 0.2$ with $\phi = 1.0$
$\dfrac{f_l\frac{b}{2}s_{sc}}{\phi p_n} + \dfrac{8}{9}\dfrac{f_l\frac{b^2}{16}s_{sc}}{\phi m_n} = 1.0 \text{ get } f_l$

$p = f_l\dfrac{b}{2}s_{sc}$

2

Figure 6-21 Flowchart of the proposed retrofit design approach

① ②

$$f'_{cci} = f'_{c0}\left(-1.254 + 2.254\sqrt{\left(1 + \frac{7.94 f_{li}}{f'_{c0}}\right)} - 2\frac{f_{li}}{f'_{c0}}\right)$$

$$\frac{p}{\phi p_n} \geq 0.2?$$

Yes

No

$$\varepsilon'_{cci} = \varepsilon'_{c0}\left(1 + 5\left(\frac{f'_{cci}}{f'_{c0}} - 1\right)\right)$$

$$\frac{f_l \frac{b}{2} s_{sc}}{2\phi p_n} + \frac{f_l \frac{b^2}{16} s_{sc}}{\phi m_n} = 1.0 \, \text{get} \, f_l$$

$$E_{seci} = \frac{f'_{cci}}{\varepsilon'_{cci}}$$

$$f_{le} = k_{ee} f_l$$

$$r_i = \frac{E_c}{E_c - E_{seci}}$$

$$f'_{cce} = f'_{c0}\left(1.0173 + 5.7558\frac{f_{le}}{f'_{c0}}\right)$$

for certain ε_c get

$$f_{ci}(\varepsilon_c) = \frac{f'_{cci}\left(\frac{\varepsilon_c}{\varepsilon'_{cci}}\right) r_i}{r_i - 1 + \left(\frac{\varepsilon_c}{\varepsilon'_{cci}}\right)^{r_i}}$$

$$\varepsilon'_{cce} = \varepsilon'_{c0}\left(1 + 5\left(\frac{f'_{cce}}{f'_{c0}} - 1\right)\right)$$

$$E_{sece} = \frac{f'_{cce}}{\varepsilon'_{cce}}$$

plot $\left[\varepsilon_c, f_{ci}(\varepsilon_c)\right]$

$$r_e = \frac{E_c}{E_c - E_{sece}}$$

③ ④

Figure 6-21 Flowchart of the proposed retrofit design approach (Continued)

187

③

④

for certain ε_c get

$$f_{ce}\left(\varepsilon_c\right)=\frac{f'_{cce}\left(\dfrac{\varepsilon_c}{\varepsilon'_{cce}}\right)r_e}{r_e-1+\left(\dfrac{\varepsilon_c}{\varepsilon'_{cce}}\right)^{r_e}}$$

plot $\left[\varepsilon_c,f_{ce}\left(\varepsilon_c\right)\right]$

$$f_{lcomb}=\frac{\left(f_{li}+f_{le}\right)A_{ei}+f_{l_e}\left(A_{ee}-A_{ei}\right)}{A_{ee}}$$

$$f'_{cccomb}=f'_{c0}\left(1.0173+5.7558\frac{f_{lcomb}}{f'_{c0}}\right)$$

$$\varepsilon'_{cccomb}=\varepsilon'_{c0}\left(1+5\left(\frac{f'_{cccomb}}{f'_{c0}}-1\right)\right)$$

$$E_{seccomb}=\frac{f'_{cccomb}}{\varepsilon'_{cccomb}}$$

$$r_{comb}=\frac{E_c}{E_c-E_{seccomb}}$$

⑤

Figure 6-21 Flowchart of the proposed retrofit design approach (Continued)
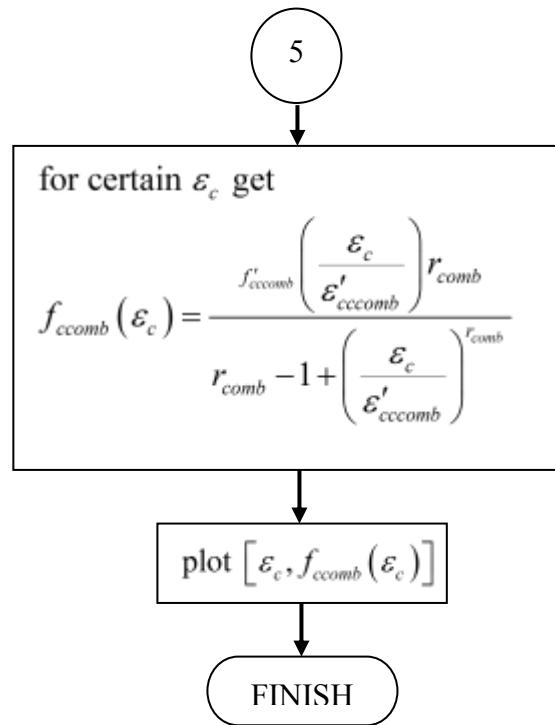
Figure 6-21 Flowchart of the proposed retrofit design approach (Continued)

The flowchart in Figure 6-21 presents the procedure for computing the effect of retrofit approach (combined internal and external confinement) on the axial stress-strain relationship of confined square concrete column only. Similar approach (by averaging the confining stresses proportional to their affected areas) can also be used to predict the combined effects on other parameters, such as the enhancement of flexural strength, displacement ductility, and curvature ductility. The expressions for calculating those parameters can be obtained from the regression analysis of the experimental data. Figure 6-22 shows the relationship of flexural strength enhancement with the confinement index by using the data of Specimens S13 and S14 (S15 is excluded from the analysis due to the anomaly of its data). The equation for predicting the flexural strength enhancement from the confinement index is also given (Equation 6-21).

$$\frac{M_{max}}{M_n} = 21.86\left(\frac{f_{le}}{f'_c}\right) + 0.9802 \tag{6-21}$$

189

Figure 6-23 shows the relationship of curvature ductility and confinement index. The equation for predicting the flexural strength increment from the confinement index is also provided (Equation 6-22).

$$\mu_\phi = 117.05\left(\frac{f_{le}}{f_c'}\right) + 2.0218 \qquad (6\text{-}22)$$
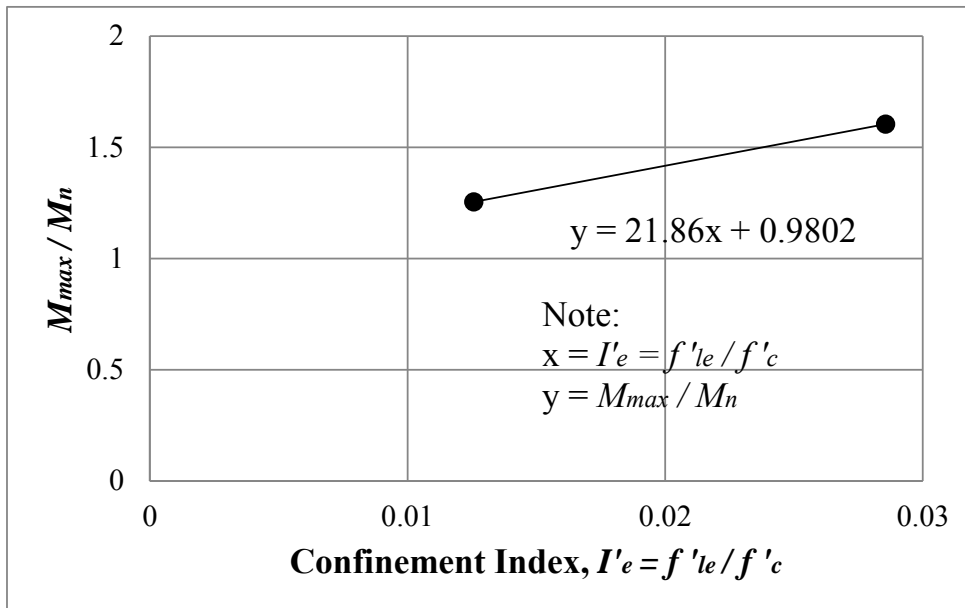
Figure 6-22 Relationship of flexural strength increment and confinement index
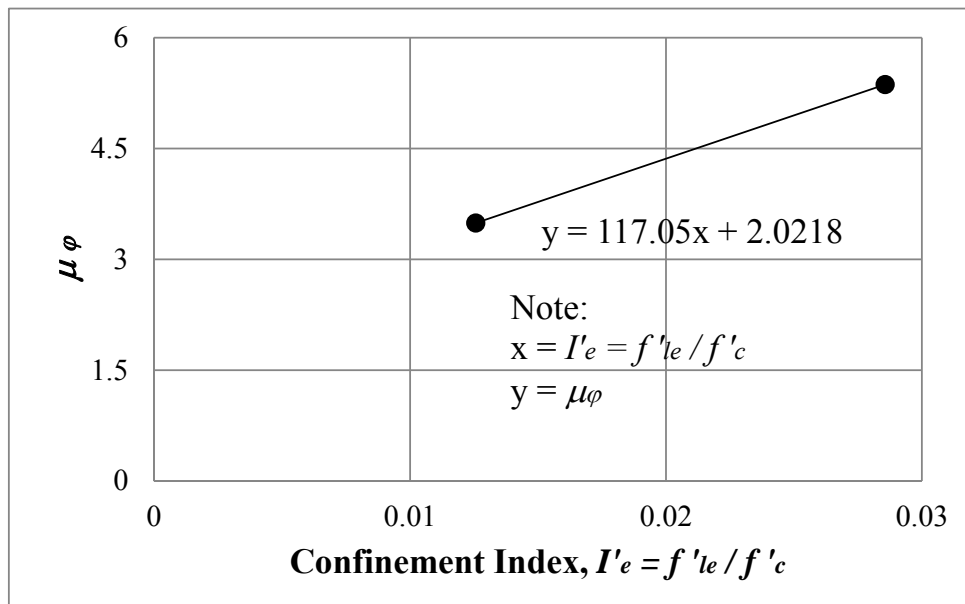
Figure 6-23 Relationship of curvature ductility and confinement index

190

Unfortunately, the displacement ductility did not show any apparent trend when correlated to the confinement index (see Table 5-1). It should be noted that at this moment Equations 6-21 and 6-22 have to be used very carefully since they were derived from only two specimens. With additional experimental data in the future, those equations can possibly be improved. However, there is another possible approach that can be taken. The calculations of those parameters can be adopted from the more established expressions (e.g. Kusuma et al., 2015b) derived for the internal confinement. An equivalent internal confining stress (with combinatoin of external confinement) can be used to substitute the original internal confining stress. The modification to get the equivalent internal confining stress is by substituting denominator of Equation 6-20 with effectively confined core area by internal confinement (A_{ei}) instead of the original effectively confined area by external confinement (A_{ee}). An example of the complete calculation exercise is given in Section 6.6.

6.6 CALCULATION EXAMPLE OF THE PROPOSED DESIGN RETROFIT APPROACH

In this section, Specimen S04a shown in Figure 6-24 is selected for verifying the proposed design procedure as it has both internal and external confinements. The concrete compressive strength (f'_{c0}) and steel yield strength (f_{yt}) of the specimen are 17.0155 and 317 MPa, respectively. The RC column is externally confined with the steel angle collars (L40.40.4) with uniform spacing at 80 mm. The steel yield strength of the collar is $f_{ysc} = 284.98 \, \text{MPa}$.

Determine the enhancement effects of retrofitting method in terms of:
1. Compressive Strength
2. Flexural Strength
3. Curvature Ductility
4. Displacement Ductiliy
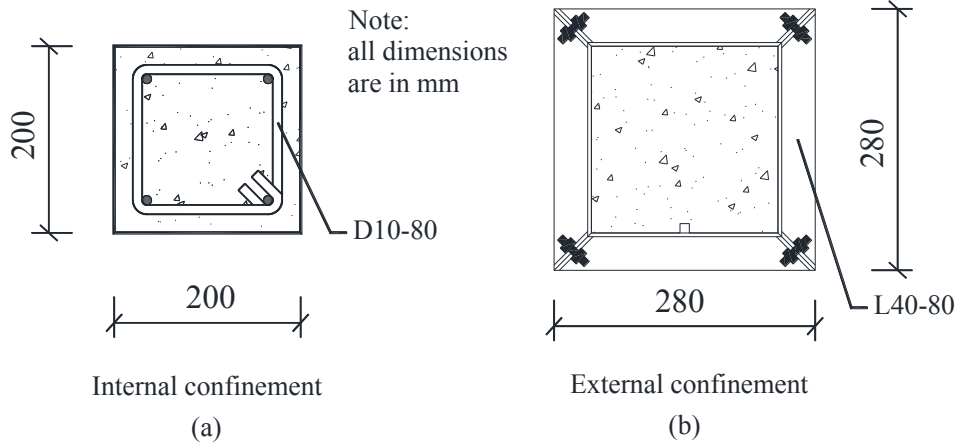
Figure 6-24 Confinements of Specimen S04a : (a) internal; and (b) external

Data given:

$b = h = 200\,\text{mm}$ (column sectional dimension)

$f'_{c0} = 17.0155\,\text{MPa}$ (compressive strength of plain concrete specimen)

$\varepsilon_{c0} = 0.00231884$ (strain corresponding to f'_{c0})

$E_c = 4700\sqrt{f'_{c0}} = 4700\sqrt{17.0155} = 19{,}387\,\text{MPa}$ (concrete elastic modulus)

$h_{sc} = w_{sc} = 40\,\text{mm}$ (height and width of steel collar)

$t_{sc} = 4\,\text{mm}$ (thickness of steel collar)

$A_{sc} = 320\,\text{mm}^2$ (cross section area of steel collar)

$Z_{sc} = 2{,}910\,\text{mm}^3$ (plastic modulus of steel collar)

$f_{ysc} = 284.98\,\text{MPa}$ (yield strength of steel collar)

$s_{sc} = 80\,\text{mm}$ (center-to-center spacing of steel collars)

$s_{sc} = s_{cc} - h_{sc} = 40\,\text{mm}$ (clear distance spacing of steel collars)

$n_l = 4$ (number of longitudinal steel bars)

$\phi_l = 9.5\,\text{mm}$ (nominal diameter of longitudinal steel bars)

$A_l = n_l \times 0.25\pi\phi_l^2 = 4 \times 0.25(3.14)(9.5)^2 = 283.53\,\text{mm}^2$

$d_{cover} = 20\,\text{mm}$ (deck cover)

$\phi_s = 10\,\text{mm}$ (diameter of stirrups)

$f_{yt} = 317\,\text{MPa}$ (yield strength of stirrups)

$s = 80 \, \text{mm}$ (spacing of stirrups)

- Contribution of internal stirrups

$A_v = 2 \times 0.25 \pi \phi_s^{\;2} = 2 \times 0.25 (3.14)(10)^2 = 157.08 \, \text{mm}^2$

$s' = s - 2(0.5)\phi_s = 80 - 2(0.5)(10) = 70 \, \text{mm}$

$b_c = h_c = b - 2d_{cover} - 2(0.5)\phi_s = 200 - 2(20) - 2(0.5)(10) = 150 \, \text{mm}$

$f_l = \dfrac{f_{yt} A_v}{s b_c} = \dfrac{317(157.08)}{80(150)} = 4.1495 \, \text{MPa}$

$w' = b_c - 2(0.5)\phi_s - 2\phi_l = 150 - 2(0.5)(10) - 2(9.5) = 121 \, \text{mm}$

$A_{ci} = b_c h_c = 150(150) = 22,500 \, \text{mm}^2$

$A_{ei} = \left(A_{ci} - \dfrac{2}{3} w'^2 \right)\left(1 - \dfrac{s'}{2 b_c} \right)^2 = \left(22,500 - \dfrac{2}{3} 121^2 \right)\left(1 - \dfrac{70}{2(150)} \right)^2 = 7,487.9 \, \text{mm}^2$

$A_{cci} = A_{ci} - A_l = 22,500 - 283.53 = 22,216.47 \, \text{mm}^2$

$k_{ei} = \dfrac{A_{ei}}{A_{cci}} = \dfrac{7,487.9}{22,216.47} = 0.337$

$f_{li} = k_{ei} f_l = 0.337(4.1495) = 1.3986 \, \text{MPa}$

$f'_{cci} = f'_{c0}\left(-1.254 + 2.254 \sqrt{\left(1 + 7.94 \dfrac{f_{li}}{f'_{c0}}\right)} - 2 \dfrac{f_{li}}{f'_{c0}} \right)$

$\qquad = 17.0155 \left(-1.254 + 2.254 \sqrt{\left(1 + 7.94 \dfrac{1.3986}{17.0155}\right)} - 2 \dfrac{1.3986}{17.0155} \right) = 25.1697 \, \text{MPa}$

$\varepsilon'_{cci} = \varepsilon'_{c0}\left(1 + 5\left(\dfrac{f'_{cci}}{f'_{c0}} - 1 \right) \right) = 0.00231884 \left(1 + 5 \left(\dfrac{25.1697}{17.0155} - 1 \right) \right) = 0.0079$

$E_{seci} = \dfrac{f'_{cci}}{\varepsilon'_{cci}} = \dfrac{25.1697}{0.0079} = 3,196.1 \, \text{MPa}$

$r_i = \dfrac{E_c}{E_c - E_{seci}} = \dfrac{19,387}{19,387 - 3,196.1} = 1.1974$

For example, if the stress is generated at a strain, $\varepsilon_c = 0.012$ on the descending branch:

$$f_{ci}(\varepsilon_c) = \frac{f'_{cci}\left(\dfrac{\varepsilon_c}{\varepsilon'_{cci}}\right)r_i}{r_i - 1 + \left(\dfrac{\varepsilon_c}{\varepsilon'_{cci}}\right)^{r_i}} = \frac{25.1697\left(\dfrac{0.012}{0.0079}\right)1.1974}{1.1974 - 1 + \left(\dfrac{0.012}{0.0079}\right)^{1.1974}} = 24.7797\,\text{MPa}$$

Similarly, the remaining or the next of the f_{ci} can be generated from the next increment of ε_c. Thus the axial stress-strain curve can be developed for the internally confined column.

- Contribution of external steel collars

$$A_{ce} = bh = 200(200) = 40,000\,\text{mm}^2$$

$$A_{cce} = A_{ce} - A_l = 40,000 - 283.53 = 39,716.47\,\text{mm}^2$$

$$A_{par} = \frac{2}{3}A_{ce} = \frac{2}{3}40,000 = 26,666.67\,\text{mm}^2$$

$$A_{ee} = A_{ce}\left(1 - \frac{A_{par}}{A_{ce}}\right)\left(1 - \frac{s_{scc}}{(b+h)}\right)^2$$

$$= 40,000\left(1 - \frac{26,666.67}{39,716.47}\right)\left(1 - \frac{40}{(200+200)}\right)^2 = 10,800\,\text{mm}^2$$

$$k_{ee} = \frac{A_{ee}}{A_{cce}} = \frac{10,800}{39,716.47} = 0.2719$$

$$p_n = A_{sc}f_{ysc} = 320(284.98) = 91,193.6\,\text{N}$$

$$m_n = Z_{sc}f_{ysc} = 2,910(284.98) = 829,291.8\,\text{Nmm}$$

assume $\dfrac{p}{\phi p_n} \geq 0.2$ with $\phi = 1.0$

$$\frac{f_l\dfrac{b}{2}s_{sc}}{\phi p_n} + \frac{8}{9}\frac{f_l\dfrac{b^2}{16}s_{sc}}{\phi m_n} = 1.0$$

$$\frac{f_l\dfrac{200}{2}80}{1(91,193.6)} + \frac{8}{9}\frac{f_l\dfrac{200^2}{16}80}{1(829,291.8)} = 1.0 \rightarrow f_l = 3.3102\,\text{MPa}$$

then $\dfrac{p}{\phi p_n} = \dfrac{f_l\dfrac{b}{2}s_{sc}}{1.0p_n} = \dfrac{3.3102\dfrac{200}{2}80}{1.0(91,193.6)} = 0.2904 \geq 0.2$ (assumption is correct)

$$f_{le} = k_{ee}f_l = 0.2719(3.3102) = 0.9001 \, \text{MPa}$$

$$f'_{cce} = f'_{c0}\left(1.0173 + 5.7558\frac{f_{le}}{f'_{c0}}\right)$$

$$= 17.0155\left(1.0173 + 5.7558\frac{0.9001}{17.0155}\right) = 22.485 \, \text{MPa}$$

$$\varepsilon'_{cce} = \varepsilon'_{c0}\left(1 + 5\left(\frac{f'_{cce}}{f'_{c0}} - 1\right)\right) = 0.00231884\left(1 + 5\left(\frac{22.485}{17.0155} - 1\right)\right) = 0.006$$

$$E_{sece} = \frac{f'_{cce}}{\varepsilon'_{cce}} = \frac{22.485}{0.006} = 3,719.2 \, \text{MPa}$$

$$r_e = \frac{E_c}{E_c - E_{sece}} = \frac{19,387}{19,387 - 3,719.2} = 1.237$$

$$f_{ce}(\varepsilon_c) = \frac{f'_{cce}\left(\dfrac{\varepsilon_c}{\varepsilon'_{cce}}\right)r_e}{r_e - 1 + \left(\dfrac{\varepsilon_c}{\varepsilon'_{cce}}\right)^{r_e}} = \frac{22.485\left(\dfrac{0.012}{0.006}\right)1.237}{1.237 - 1 + \left(\dfrac{0.012}{0.006}\right)^{1.237}} = 21.4627 \, \text{MPa}$$

Similarly, the remaining or the next of the f_{ce} can be generated from the next increment of ε_c. Thus the axial stress-strain curve can be developed for the externally confined column.

- Combined effect of internal stirrups and external steel collars

$$f_{lcomb} = \frac{(f_{li} + f_{le})A_{ei} + f_{l_e}(A_{ee} - A_{ei})}{A_{ee}}$$

$$= \frac{(1.3986 + 0.9001)7,487.9 + 0.9001(10,800 - 7,487.9)}{10,800} = 1.8698 \, \text{MPa}$$

$$f'_{cccomb} = f'_{c0}\left(1.0173 + 5.7558\frac{f_{lcomb}}{f'_{c0}}\right)$$

$$= 17.0155\left(1.0173 + 5.7558\frac{1.8698}{17.0155}\right) = 28.0654 \, \text{MPa}$$

$$\varepsilon'_{cccomb} = \varepsilon'_{c0}\left(1 + 5\left(\frac{f'_{cccomb}}{f'_{c0}} - 1\right)\right) = 0.00231884\left(1 + 5\left(\frac{27.9761}{17.0155} - 1\right)\right) = 0.0098$$

$$E_{seccomb} = \frac{f'_{cccomb}}{\varepsilon'_{cccomb}} = \frac{28.0654}{0.0098} = 2,849.8 \, \text{MPa}$$

$$r_{comb} = \frac{E_c}{E_c - E_{seccomb}} = \frac{19,387}{19,387 - 2,849.8} = 1.1723$$

$$f_{ccomb}(\varepsilon_c) = \frac{f'_{cccomb}\left(\dfrac{\varepsilon_c}{\varepsilon'_{cccomb}}\right)r_{comb}}{r_{comb} - 1 + \left(\dfrac{\varepsilon_c}{\varepsilon'_{cccomb}}\right)^{r_{comb}}}$$

$$= \frac{28.0654\left(\dfrac{0.012}{0.0098}\right)1.1723}{1.1723 - 1 + \left(\dfrac{0.012}{0.0098}\right)^{1.1723}} = 27.9761\,\text{MPa}$$

Similarly, the remaining or the next of the f_{cccomb} can be generated from the next increment of ε_c. Thus the axial stress-strain curve can be developed for the combined confinement effect. The curve of individual effect as well as the combined effect of internal and external confinement, is presented in Figure 6-25.
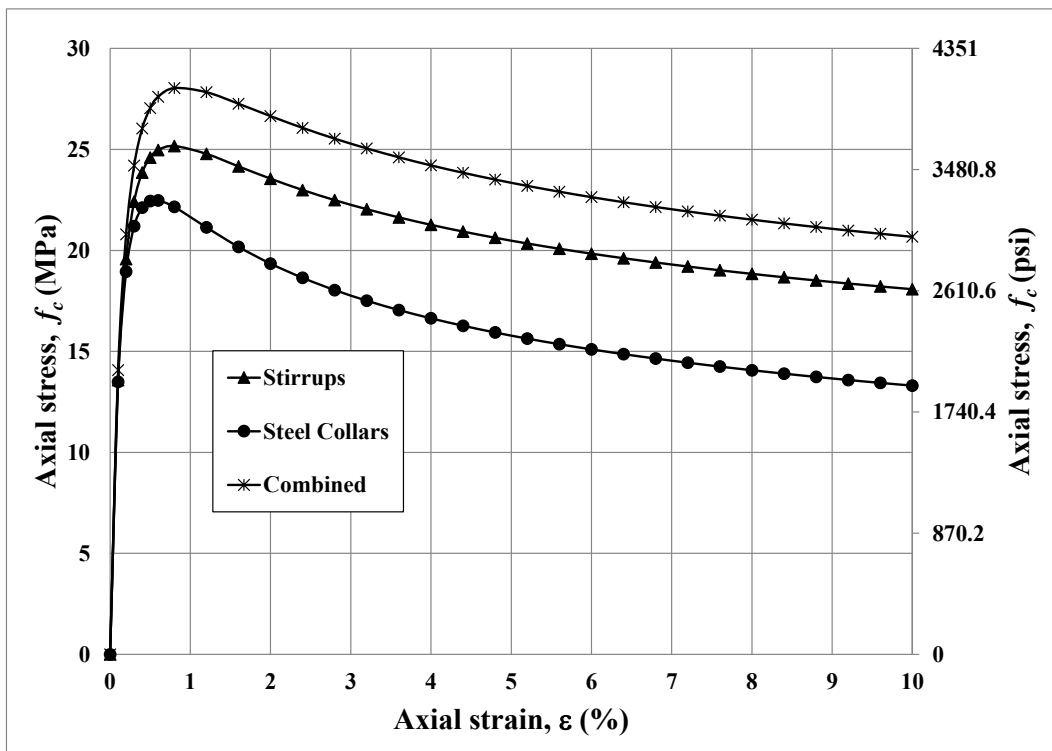
Figure 6-25 Stress-strain relationship of S04a (retrofit design approach)

- Compressive Strength Enhancement

From the existing internal stirrups:

$$\frac{f'_{cci}}{f'_{c0}} = \frac{25.1697}{17.0155} = 1.4563$$

After retrofit:

$$\frac{f'_{cccomb}}{f'_{c0}} = \frac{28.0654}{17.0155} = 1.6494$$

- Flexural Strength Enhancement

From the existing internal stirrups:

$$\frac{M_{max}}{M_n} = 1.26 + 6\left(\frac{f'_{li}}{f'_{c0}}\right)^{0.35}\left(\frac{P}{A_g f'_{c0}} - 0.1\right)^2$$

$$= 1.26 + 6\left(\frac{1.3986}{17.0155}\right)^{0.35}\left(\frac{240,000}{200(200)(17.0155)} - 0.1\right)^2 = 1.42$$

It should be noted that in the calculation of flexural strength enhancement, any well established expressions based on the effect of internal confinement can be used. As example, the model proposed by Kusuma et al. (2015b) is used.

After retrofit:

$$\frac{M_{max}}{M_n} = 21.86\left(\frac{f_{lcomb}}{f'_{c0}}\right) + 0.9802 = 21.86\left(\frac{1.8698}{17.0155}\right) + 0.9802 = 3.38$$

Alternatively, similar expression can also be adopted from the model developed from specimens with internal confinement such as that suggested by Kusuma et al. (2015b). However, a modification should be made for the combined confining pressure, that it should be averaged over the internal core area instead of the gross area.

$$f_{lcomb} = \frac{(f_{li} + f_{le})A_{ei} + f_{l_e}(A_{ee} - A_{ei})}{A_{ei}}$$

$$= \frac{(1.3986 + 0.9001)7,487.9 + 0.9001(10,800 - 7,487.9)}{7,487.9} = 2.6969\,\text{MPa}$$

After retrofit (alternative approach):

$$\frac{M_{\max}}{M_n} = 1.26 + 6\left(\frac{f'_{lcomb}}{f'_{c0}}\right)^{0.35}\left(\frac{P}{A_g f'_{c0}} - 0.1\right)^2$$

$$= 1.26 + 6\left(\frac{2.6969}{17.0155}\right)^{0.35}\left(\frac{240,000}{200(200)(17.0155)} - 0.1\right)^2 = 1.46$$

- Curvature Ductility Enhancement

From the existing internal stirrups:

$$\mu_\varphi = 8 + 77.6\frac{f_{li}}{\left(f'_{c0}\right)^{1.5}\left(\dfrac{P}{A_g f'_{c0}}\right)^{0.55}}$$

$$= 8 + 77.6\frac{1.3986}{\left(17.0155\right)^{1.5}\left(\dfrac{240,000}{200(200)(17.0155)}\right)^{0.55}} = 10.74$$

The expression is also adopted from the model proposed by Kusuma et al. (2015b) for internal confinement.

After retrofit:

$$\mu_\phi = 117.05\left(\frac{f_{lcomb}}{f'_{c0}}\right) + 2.0218 = 117.05\left(\frac{1.8698}{17.0155}\right) + 2.0218 = 14.88$$

Again, similar expression can be adopted from Kusuma et al. (2015b) as an option.

$$\mu_\varphi = 8 + 77.6\frac{f_{li}}{\left(f'_{c0}\right)^{1.5}\left(\dfrac{P}{A_g f'_{c0}}\right)^{0.55}}$$

$$= 8 + 77.6\frac{2.6969}{\left(17.0155\right)^{1.5}\left(\dfrac{240,000}{200(200)(17.0155)}\right)^{0.55}} = 13.28$$

- Displacement Ductility Enhancement (Kusuma et al. 2016)

From the existing internal stirrups:

$$\mu_\Delta = 10.6 \frac{f_{li}^{0.19}}{\left(f_{c0}'\right)^{0.29}\left(\dfrac{P}{A_g f_{c0}'}\right)^{0.1}} = 10.6 \frac{1.3986^{0.19}}{\left(17.0155\right)^{0.29}\left(\dfrac{240,000}{200(200)(17.0155)}\right)^{0.1}} = 5.51$$

After retrofit:

$$\mu_\Delta = 10.6 \frac{f_{lcomb}^{0.19}}{\left(f_{c0}'\right)^{0.29}\left(\dfrac{P}{A_g f_{c0}'}\right)^{0.1}} = 10.6 \frac{2.6969^{0.19}}{\left(17.0155\right)^{0.29}\left(\dfrac{240,000}{200(200)(17.0155)}\right)^{0.1}} = 6.24$$

Further, the calculation of the proposed retrofit design approach can be compared to the experimental results. Figure 6-26 compares the normalized stress-strain curves of Specimens S04a and S04b obtained from the experimental results and the proposed retrofit design model. The result shows that the analytical model can predict the observed behavior reasonably well. Even though, it is found that the results from proposed method underestimates experimental data, it is still acceptable since it means that the design is in the safe / conservative side. The legends for the proposed analytical model curves are labeled as "S04ab-x-Prop". The index 'x' indicates the effects of the internal, external, and combined confinements for "i", "e", and "c" respectively.

As presented in the detail calculation example (Section 6.6), the confined concrete column strength is logically influenced by the existing internal stirrups and the designed external steel collars. Since the confining pressure generated by the steel collars is influenced by both axial force and bending moment, the determination of steel collar spacing required to strengthen the existing deficient column is difficult. It depends on both the axial and bending capacities of the steel collars. However, it is easier to design the need of the external confinement by iteration. The spacing of steel collars can be iterated until the combined peak strength meets a certain target value (might be the strength generated by minimum internal stirrups required by the code, e.g. SNI 2847 : 2013). This approach can be easily employed in a computer algorithm. In the study, the algorithm was developed using MATLAB environment.
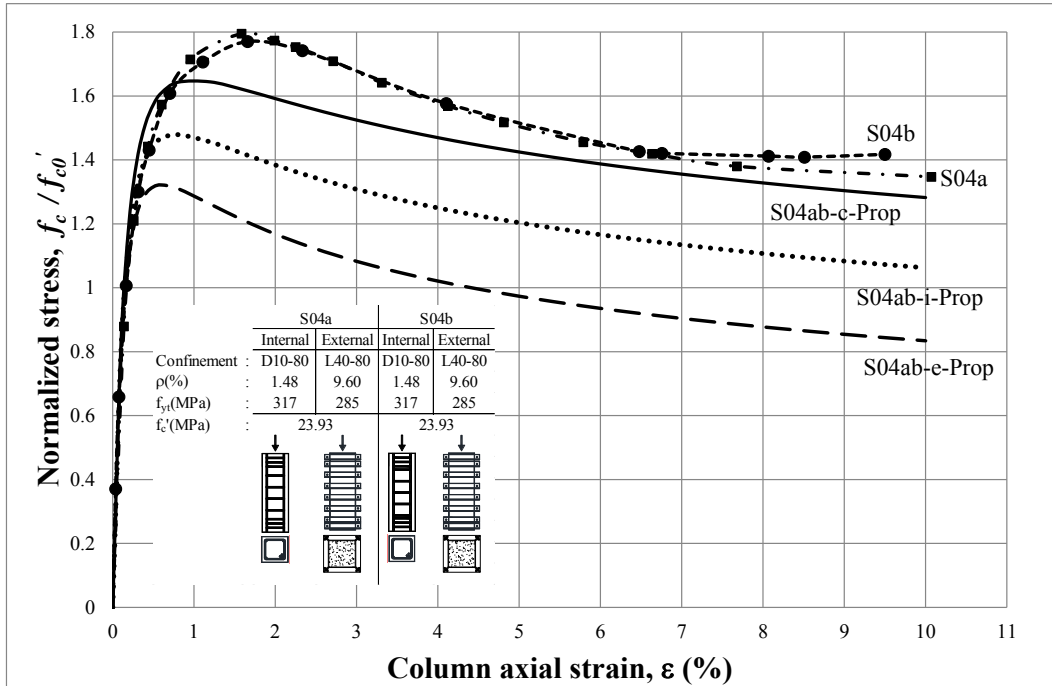
Figure 6-26 Normalized stress vs axial strain of combined effect of internal and external confinement and experimental results of Specimens S04a and S04b

For example, a specimen with the same stirrups as S04a is targeted to have a performance equals to the ordinary RC columns with stirrup spacing at 50 mm (required target). The targeted stirrups spacing at 50 mm above comes from the provisions of maximum spacing allowed (SNI 2847 : 2013 Section 21.6.4.3), as explained in Chapter 3 for Specimen CS03a. Since the existing stirrups spacing is only 80 mm in Specimen S04a, which is less than the target, the specimen needs to be retrofitted. By using Mander model (Mander et al., 1988a), the program can simulate the performance deviations between the targeted and the existing column as shown in Figure 6-27. It can also easily simulate the effect of a required retrofit. For example, the spacing of the steel collars is taken as 80 mm (as in Specimen S04a), then the performance (stress-strain curve) of the retrofitted specimen can easily be generated as shown in Figure 6-28. It can also be seen in the figure that the performance of the retrofitted specimen still under the target. With a subsequent trial, the required steel collars can be easily determined. In this case, it is found that the required steel collar spacing is approximately 55 mm, such that the targeted and retrofitted stress-strain curves coincide to each other as shown in Figure 6-29.

200
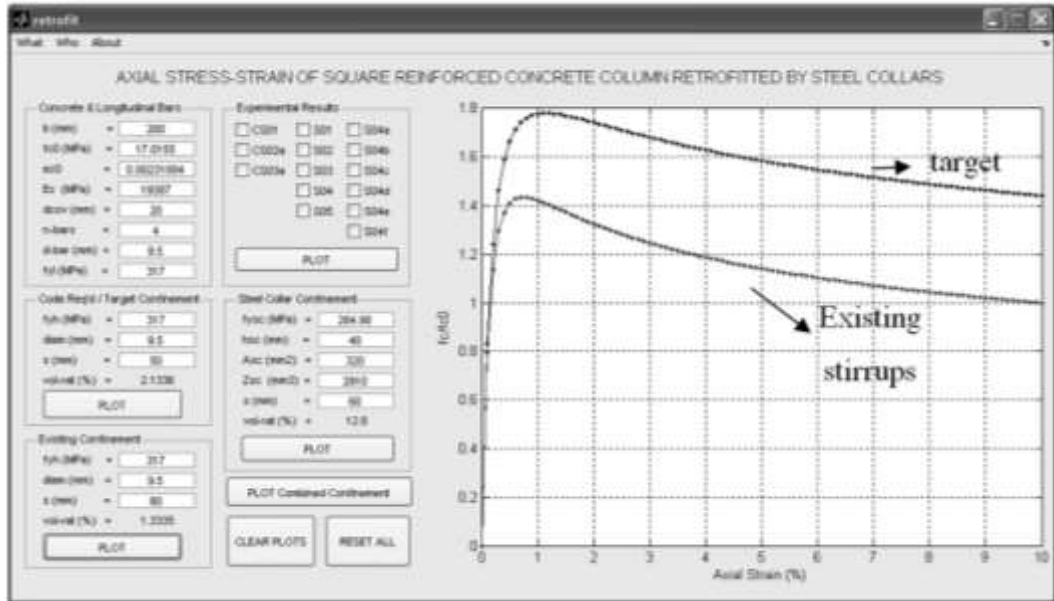
Figure 6-27 Performances (stress-strain curve) of deficient and targeted RC columns
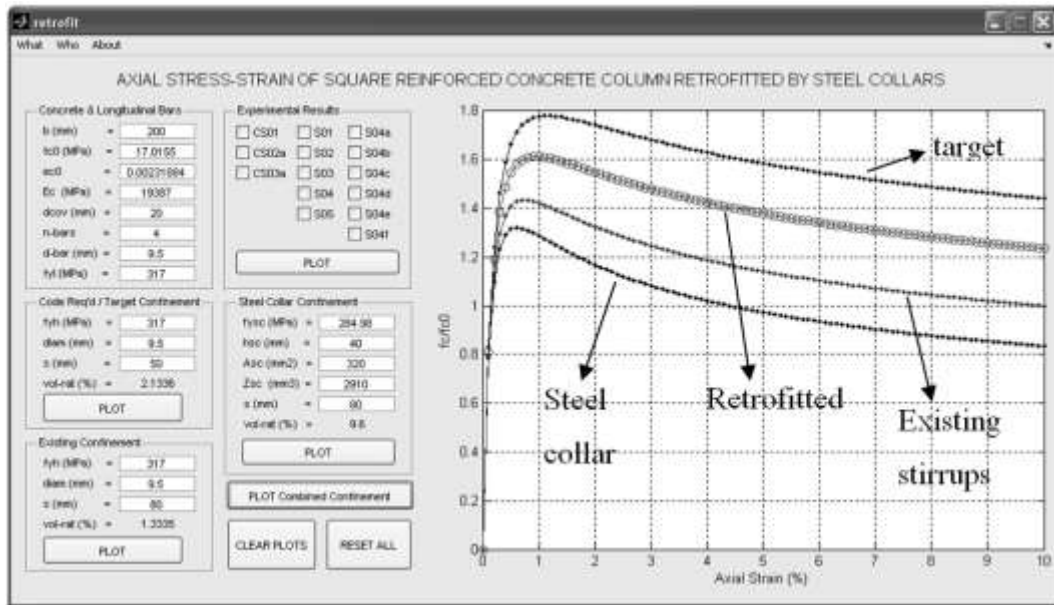
Figure 6-28 Performance (stress-strain curves) of deficient and targeted RC columns (first trial)

201
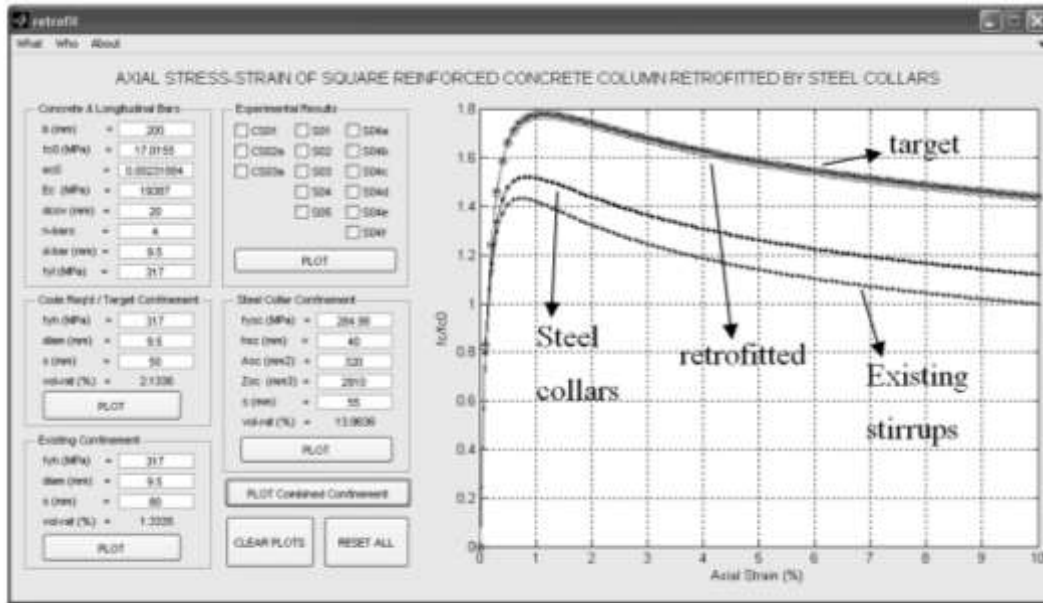
Figure 6-29 Performance (stress-strain curves) of deficient and targeted RC columns (final attempt)

6.7   DISCUSSION 1: MINIMUM AMOUNT OF CONFINING STEEL

In designing the confining steel, a minimum amount is specified by the codes, including Indonesian concrete code (SNI 2847 : 2013) as expressed in Equations 6-18 and 6-19. The idea of providing such minimum confinement is to preserve the axial capacity of the column sections after the spalling of concrete cover. Ideally, the proposed external retrofitting method using a set of steel collars also has such expressions. However, due to some differences of the method compared to that of the conventional internal stirrups, some concerns need to be raised. In order to address this matter, the following sub-sections are discussed : (1) summary of the current proposed design approach; (2) new approach proposed by Paultre and Legeron (2008); (3) implementation of the new approach for external steel collars confinement.

6.7.1   Summary of current proposed design approach

The proposed analytical model to account for the effect of external steel collar confinement on concrete columns is described in Section 6.1. The derivation of confining pressure provided by the steel collars is presented in the

section. It is clear from Equations 6-10 and 6-11 that both axial and bending capacities of the collar sections play very important role in providing the lateral pressure (different from the case of conventional confining steel bars that relies only from the axial capacity as seen in Equations 2-11 to 2-13). With the determined lateral pressure, the confined strength of the column can be expressed in Equation 6-5.

Further in Section 6.5, an approach to predict the combined effect of internal and external confinements on the confined column strength is proposed. The idea is to superpose the lateral confining pressure by simply taking the average confining pressure proportional to their affected areas, as expressed in Equation 6-20 (see Figure 6-20). With any targeted confined concrete strengths of internally confined concrete column given, the requirement of steel collars can be determined to achieve the same confined concrete column strength. If the targeted confined concrete column strength is derived from the minimum amount of confining steel according the code (SNI 2847 : 2013), logically the calculated amount of steel collars can be considered as the requirement to meet the same performance specified (that is meant for preserving the axial capacity of the concrete section).

6.7.2 New approach proposed by Paultre and Legeron

Paultre and Legeron (2008) mentioned that Equations 6-18 and 6-19 (expressions for confinement steel requirement in SNI 2847 : 2013) had some limitations that they did not take into account the effect of axial load level, high strength concrete, and curvature ductility demand. They have taken into account the effect of high strength steel, but only in a limited way. New equations for determining the confinement steel requirement were proposed to overcome the limitations. Important ideas in developing the equations are summarized in this sub-section.

Legeron and Paultre (2003) model related the increases of strength and ductility of confined concrete to the effective confinement index I'_e which was defined as:

$$I'_e = \frac{f'_{le}}{f'_c} \tag{6-23}$$

where f'_{le} and f'_c are the effective confinement pressure and the unconfined concrete strength, respectively. The effective confinement pressure was derived from only the axial strength of the hoop, and defined as:

$$f'_{le} = K_e \frac{A_{shy} f'_h}{c_y s} \tag{6-24}$$

where K_e is the geometric geometric confinement effectiveness coefficient that varies from 1.0 for continuous tube (perfectly confined) to 0.0 for ties which are spaced more than half of the core cross section minimum dimension (some parts of the columns between spacing of ties are not confined at all). A_{shy}, c_y, s, and f'_h are the area of confining steel bars, core dimension, spacing of confining steel bars, and effective hoop stress, respectively.

Legeron and Paultre (2003) then conducted a parametric numerical study of more than 200 column sections. Variables included in the study were the longitudinal reinforcement ratio, axial load level, effective confinement index (I'_e), and concrete strength. It was found that the most important parameters controlling ductility (μ_φ) were the effective confinement index (I'_e) and the relative level of axial load $(k_p = P/P_0)$ (ratio of axial load with respect to nominal axial capacity of the column), which was expressed in the following empirical equation:

$$I'_e = 0.0111 k_p \mu_\varphi \tag{6-25}$$

For different level of curvature ductility demands μ_φ, Equation 6-25 could further be expressed as Equations 6-26 and 6-27:

$$I'_e = 0.178 k_p \quad \text{for} \quad \mu_\varphi = 16 \tag{6-26}$$

$$I'_e = 0.111 k_p \quad \text{for} \quad \mu_\varphi = 10 \tag{6-27}$$

204

The curvature ductility demands of 10 and 16 corresponded to moderate ductile and ductile levels (force reduction factor of 2.5 and 4.0).

The geometric confinement effectiveness coefficient K_e, mentioned earlier, is a product of two coefficients, K_h and K_v, which correspond to arching in the horizontal and vertical directions, respectively. For the design purposes, a simplified and conservative expression of K_h is given in Equation 6-28:

$$K_h = 1 - \frac{2}{n_l} \tag{6-28}$$

where n_l is the number of longitudinal bars laterally supported by hoop corner or by seismic cross tie hooks. A conservative expressions of K_v are given in Equations 6-29 and 6-30:

$$K_v = 1.05 \left(\frac{A_{ch}}{A_g} \right) \quad \text{for} \quad \mu_\varphi = 16 \tag{6-29}$$

$$K_v = 0.95 \left(\frac{A_{ch}}{A_g} \right) \quad \text{for} \quad \mu_\varphi = 10 \tag{6-30}$$

where A_{ch} and A_g are the concrete core and gross areas, respectively.

In calculating the effective hoop stress, Legeron and Paultre (2003) proposed the following equations for rectangular sections:

$$f_h' = 0.83 f_{yh} \quad \text{for} \quad \mu_\varphi = 16 \tag{6-31}$$

$$f_h' = 0.68 f_{yh} \quad \text{for} \quad \mu_\varphi = 10 \tag{6-32}$$

Using Equations 6-23 to 6-32 all together, finally the requirement of confining steel A_{sh} steel could be expressed as a functions of $k_p, f_c', c_y, s, k_n, f_{yh}, A_g$, and A_{ch} as follows:

$$A_{sh} = 0.20 k_p k_n c_y s \frac{f_c'}{f_{yh}} \frac{A_g}{A_{ch}} \quad \text{for} \quad \mu_\varphi = 16 \tag{6-33}$$

$$A_{sh} = 0.17 k_p k_n c_y s \frac{f_c'}{f_{yh}} \frac{A_g}{A_{ch}} \quad \text{for} \quad \mu_\varphi = 10 \tag{6-34}$$

where $k_n = 1/K_h$.

Equation 6-33 was also adopted in the latest ACI 318M-14 (Table 18.7.5.4) accompanying the previous two equations in earlier edition of ACI 318M-11 (also adopted in Indonesian concrete code (SNI 2847 : 2013) as expressed in Equations 6-18 and 6-19) for confinement steel requirements in a very similar expression as follows:

$$\frac{A_{sh}}{sb_c} = 0.20 k_f k_n \frac{P_u}{f_{yh} A_{ch}} \tag{6-35}$$

where b_c is the core dimension (equals to c_y), P_u is the factored axial load, k_f is a term to increase the required confinement for concrete with $f_c' > 68.9 \, \text{MPa}$ to avoid brittle failure.

6.7.3 Implementation of Paultre and Legeron (2008) approach for external steel collars confinement

It is logical if minimum confining steel requirement arises as one of interests of a new proposed confining method. The proposed external confining method by using a set of steel angle collars also need to consider this minimum requirement. Even though its primary use is for retrofitting the existing deficient RC columns, it is stiil interesting to examine how the minimum confining requirement is derived (with neglecting the effect of existing conventional internal confinement for this kind of retrofitting technique). This section presents a brief explanation on what are the current problems and what can be improved in the future research if the approach suggested by Paultre and Legeron (2008) is adopted to determine the minimum external steel collars confinement.

The basic difference of the external confinement by using the steel angle collars and the conventional internal rectilinier hoop is the mechanism assumption in determining the lateral pressure provided by the steel. While the later utilizes

the axial capacity of the steel bar, the former utilizes the combined capacities of axial force and bending moment of the steel angle section. By adopting the expressions for axial force-bending moment interaction (Equations 6-10 and 6-11) from the Indonesian steel code (SNI 1729 : 2002), the lateral pressure can be calculated. With the definition of axial force and bending moment as expressed in Equations 6-8 and 6-9, the axial force-bending moment interaction expressions can be re-writen in these following forms (ϕ is set as 1.0):

$$\frac{f_l\left(b/2\right)s_{sc}}{A_{sc}f_{ysc}} + \frac{8}{9}\frac{f_l\left(b^2/16\right)s_{sc}}{Z_{sc}f_{ysc}} = 1 \quad \text{for} \quad \frac{p}{p_n} \geq 0.2 \tag{6-36}$$

$$\frac{f_l\left(b/2\right)s_{sc}}{2A_{sc}f_{ysc}} + \frac{f_l\left(b^2/16\right)s_{sc}}{Z_{sc}f_{ysc}} = 1 \quad \text{for} \quad \frac{p}{p_n} < 0.2 \tag{6-37}$$

Since Equations 6-36 and 6-37 are basically similar to each other, the mathematical derivation of the two equations will be the same. Thus, the derivation is only carried out for Equation 6-36. Equation 6-37 will follow similar procedure and only need to be slightly adjusted. Noting that the effective uniform lateral pressure $\left(f_{le}\right)$ is a product of confinement effectiveness factor (k_e defined in Equation 6-3) and uniform lateral pressure $\left(f_l\right)$, thus Equation 6-36 can be expressed as:

$$\frac{f_{le}\left(b/2\right)s_{sc}}{k_e A_{sc}f_{ysc}} + \frac{8}{9}\frac{f_{le}\left(b^2/16\right)s_{sc}}{k_e Z_{sc}f_{ysc}} = 1 \tag{6-38}$$

As mentioned by Paultre and Legeron (2008), the stresses developed in steel during confining action were not necessarily fully utilized as high as its yield strength. The same fact was found in this research, that in the combined axial and cyclic lateral loads that the steel collar only experienced a stress lower than its yield stress. By inspecting only two specimens (S13 and S14), it was found that the effective stresses $\left(f_{sc}\right)$ are about 0.175 and 0.197 of its yield strength $\left(f_{ysc}\right)$ for the ductility demands, μ_φ of 3.5 and 5.3, respectively (see also Table 5-1). A coefficient c_1 is introduced to define an effective stress of steel collars, that is a

part of its yield strength $\left(f_{sc} = c_1 f_{ysc}\right)$. It should also be noted that Specimen S15 is excluded in the current discussion since the data obtained from the experiment was considered an outlier (see Table 5-1). By taking into account the effective stress of steel collars, Equation 6-38 can be rewritten as:

$$\frac{f_{le}\left(\frac{b}{2}\right)s_{sc}}{k_e A_{sc} c_1 f_{ysc}} + \frac{8}{9}\frac{f_{le}\left(\frac{b^2}{16}\right)s_{sc}}{k_e Z_{sc} c_1 f_{ysc}} = 1 \tag{6-39}$$

From Equation 6-39, an expression for the effective lateral pressure can be derived as:

$$f_{le} = \frac{9 k_e A_{sc} Z_{sc} c_1 f_{ysc}}{9\left(\frac{b}{2}\right)s_{sc} Z_{sc} + 8\left(\frac{b^2}{16}\right)s_{sc} A_{sc}} \tag{6-40}$$

With the analytical model proposed in Section 6.1, the effective uniform confining pressure $\left(f_{le}\right)$ can be calculated for specific steel collared specimens, namely Specimens S13 and S14. With the concrete strength $\left(f_c'\right)$ given, the effective confinement index $\left(I_e' = f_{le}'/f_c'\right)$ can be calculated. With $k_p = 0.3$ during the experimental test, the effective confinement index can be expressed in terms of k_p. With the experimental data of both Specimens S13, and S14 (recorded μ_φ is about 3.5 and 5.3, respectively as shown in Table 5-1), this following expression can be derived:

$$I_e' = c_2 k_p \tag{6-41}$$

where c_2 is a coefficient which depends on the ductility demand (equals to 0.0047 and 0.0105 for μ_φ of 3.5 and 5.3, respectively). For example, the derivation for Specimen S1-3 is described as follows:

$f_c' = 16.7$ MPa
$f_{le} = 0.0223$ MPa (using expression described in Section 6.1)

$$I'_e = f_{le}/f'_c = 0.0223/16.7 = 0.0014$$

$$= 0.0047(0.3) = 0.0047 k_p$$

$c_2 = 0.0047$ for $\mu_\varphi = 3.5$ (see Table 5-1 for Specimen S1-3)

Finally, by substituting Equations 6-40 and 6-41 into the definition of effective confinement index $\left(I'_e = f'_{le}/f'_c \right)$, the following expression can be obtained.

$$f'_c c_2 k_p = \frac{9 k_e A_{sc} Z_{sc} c_1 f_{ysc}}{9 \left(b/2 \right) s_{sc} Z_{sc} + 8 \left(b^2/16 \right) s_{sc} A_{sc}} \tag{6-42}$$

If the effect of bending moment is neglected, then the second term of the denominator can be set to zero. Rearranging the Equation 4-2, then it becomes:

$$\frac{A_{sc}}{b s_{sc}} = 0.5 \frac{c_2}{c_1} \frac{k_p}{k_e} \frac{f'_c}{f_{ysc}} \tag{6-43}$$

By considering Equations 6-2 and 6-3, in the case of external steel collars, the confinement effectiveness factor can be expressed as:

$$k_e = \frac{A_{ch}}{A_g} \left(1 - \frac{A_{par}}{A_c} \right) \left(1 - \frac{s_{scc}}{2b} \right)^2 \tag{6-44}$$

By substituting Equation 6-44 into Equation 6-43, the following equation can be found:

$$\frac{A_{sc}}{b s_{sc}} = 0.5 \frac{c_2}{c_1} k_p k_n \frac{f'_c}{f_{ysc}} \frac{A_g}{A_{ch}} \tag{6-45}$$

which is very similar to the expressions proposed by Paultre and Legeron (2008) in Equations 6-33 and 6-34. It should be noted that in the particular case of external steel collar confinement, $\dfrac{A_g}{A_{ch}} = 1$, and $k_n = 1 \bigg/ \left(1 - \dfrac{A_{par}}{A_c} \right) \left(1 - \dfrac{s_{scc}}{2b} \right)^2$.

But, since the contribution of bending effect can not be simply neglected, it is more proper to use Equation 6-42 to calculate the requirement for steel collar confinement rather than Equation 6-45 (with bending effect considered). With all design parameters given, a certain steel angle collar can be designed (A_{sc} and Z_{sc}

are selected) and hence, the required spacing (s_{sc}) can be calculated. However, it should be noted that the calculation may require an iterative procedure since the clear spacing of the collar (s_{scc}) is needed in calculating the spacing (s_{sc}). Then, the assumption of $\dfrac{p}{p_n} = \dfrac{f_l \, b/2 \, s_{sc}}{A_{sc} f_{ysc}} \geq 0.2$ should be checked, and recalculation should also be conducted by using the other expression if the assumption is not correct. Equation 6-42 can be rearranged to derive Equation 6-46 for expression for calculating the required confinement spacing. Similarly, when $\dfrac{p}{p_n} < 0.2$, Equation 6-47 can also be obtained.

$$s_{sc} = \frac{9 k_e A_{sc} Z_{sc} c_1 f_{ysc}}{\left[9\left(b/2\right) Z_{sc} + 8\left(b^2/16\right) A_{sc} \right]\left(f_c' c_2 k_p \right)} \quad \text{for} \quad \frac{p}{p_n} \geq 0.2 \qquad (6\text{-}46)$$

$$s_{sc} = \frac{2 k_e A_{sc} Z_{sc} c_1 f_{ysc}}{\left[\left(b/2\right) Z_{sc} + 2\left(b^2/16\right) A_{sc} \right]\left(f_c' c_2 k_p \right)} \quad \text{for} \quad \frac{p}{p_n} < 0.2 \qquad (6\text{-}47)$$

6.7.4 Design example of required minimum steel collar confinement

The following is an example of the calculation of the required minimum steel collar confinement.

Data given :

$b = h = 200\,\text{mm}$ (column sectional dimensions)

$f_c' = 17\,\text{MPa}$ (concrete compressive strength)

$h_{sc} = w_{sc} = 40\,\text{mm}$ (height and width of steel angle collar)

$t_{sc} = 4\,\text{mm}$ (thickness of steel angle collar)

$A_{sc} = 320\,\text{mm}^2$ (cross sectional area of steel angle collar)

$Z_{sc} = 2{,}910\,\text{mm}^3$ (plastic modulus of steel angle collar)

$f_{ysc} = 284.98\,\text{MPa}$ (yield strength of steel angle collar)

$s_{sc} = 60\,\text{mm}$ (assumed center-to-center distance of steel collar)

$s_{scc} = s_{sc} - h_{sc} = 60 - 40 = 20$ mm   (clear spacing of steel collar)

- With a selected target ductility demand value of 5.30

$c_1 = 0.197$ and $c_2 = 0.0105$

- With the estimated level of axial load equals to 30 percent of the column axial capacity

$k_p = 0.3$

$A_c = bh = 200(200) = 40,000$ mm^2

$A_{cc} = A_c$ (concrete without longitudinal bars)

$A_{par} = \dfrac{2}{3} A_c = \dfrac{2}{3} 40,000 = 26,666.67$ mm^2

$A_e = A_c \left(1 - \dfrac{A_{par}}{A_c}\right)\left(1 - \dfrac{s_{scc}}{2b}\right)^2$

$ = 40,000 \left(1 - \dfrac{26,666.67}{40,000}\right)\left(1 - \dfrac{20}{2(200)}\right)^2 = 12,033$ mm^2

$k_e = \dfrac{A_e}{A_{cc}} = \dfrac{12,033}{40,000} = 0.3008$

- Assuming $\dfrac{p}{p_n} < 0.2$

$s_{sc} = \dfrac{2k_e A_{sc} Z_{sc} c_1 f_{ysc}}{\left[\left(b/2\right)Z_{sc} + 2\left(b^2/16\right)A_{sc}\right]\left(f_c' c_2 k_p\right)}$

$s_{sc} = \dfrac{2(0.3008)(320)(2,910)(0.197)(284.98)}{\left[\left(200/2\right)(2,910) + 2\left(200^2/16\right)(320)\right]\left((17)(0.0105)(0.3)\right)} = 310.6$ mm

- Since the calculated and assumed spacings deviate significantly, the iterative procedure should be carried out until the values of the two is within the defined tolerable error value. Through the iterative procedure, it can be found that the required spacing is 163.9 mm.

- Checking the assumption that $\dfrac{p}{p_n} < 0.2$

$p_n = A_{sc} f_{ysc} = 320(284.98) = 91,193.6$ N

$$m_n = Z_{sc} f_{ysc} = 2{,}910(284.98) = 829{,}291.8 \text{ Nmm}$$

$$\frac{f_l\left(\sfrac{b}{2}\right) s_{sc}}{2 p_n} + \frac{f_l\left(\sfrac{b^2}{16}\right) s_{sc}}{m_n} = 1.0$$

$$\frac{f_l\left(\sfrac{200}{2}\right) 163.9}{2(91{,}193.6)} + \frac{f_l\left(\sfrac{200^2}{16}\right) 163.9}{829{,}291.8} = 1.0 \rightarrow f_l = 1.713 \text{ MPa}$$

$$\frac{p}{p_n} = \frac{f_l\left(\sfrac{b}{2}\right) s_{sc}}{p_n} = \frac{1.713\left(\sfrac{200}{2}\right) 163.9}{91{,}193.6} = 0.308 > 0.2, \text{ means that the assumption}$$
is incorrect

- The calculation should be repeated by assuming $\dfrac{p}{p_n} \geq 0.2$, and the expression to calculate s_{sc} is:

$$s_{sc} = \frac{9 k_e A_{sc} Z_{sc} c_1 f_{ysc}}{\left[9\left(\sfrac{b}{2}\right) Z_{sc} + 8\left(\sfrac{b^2}{16}\right) A_{sc} \right]\left(f_c' c_2 k_p \right)}$$

By using the iterative procedure, it is found that the required spacing is 159.6 mm.

- Checking the assumption that $\dfrac{p}{p_n} \geq 0.2$

$$\frac{f_l\left(\sfrac{b}{2}\right) s_{sc}}{p_n} + \frac{8}{9} \frac{f_l\left(\sfrac{b^2}{16}\right) s_{sc}}{m_n} = 1.0$$

$$\frac{f_l\left(\sfrac{200}{2}\right) 159.6}{91{,}193.6} + \frac{8}{9} \frac{f_l\left(\sfrac{200^2}{16}\right) 159.6}{829{,}291.8} = 1.0 \rightarrow f_l = 1.66 \text{ MPa}$$

$$\frac{p}{p_n} = \frac{f_l\left(\sfrac{b}{2}\right) s_{sc}}{p_n} = \frac{1.66\left(\sfrac{200}{2}\right) 159.6}{91{,}193.6} = 0.29 > 0.2, \text{ means that the assumption is}$$
true

- Thus, to fulfill the minimum confinement requirement the selected steel angle section of L40.40.4 should be spaced at a minimum of 159.6 mm.

It can be seen in the above example, that the required spacing is 159.6 mm. This required spacing lies in between Specimens S01 and S02 (Phase 1

experiment) which have spacings of 200 and 133 mm, respectively. However, the specimen which conforms to seismic provision, CS03a is comparable to Specimen S03 which had steel collars confinement at 100 mm spacing. It is clear that the derived expression is not very accurate. It should be emphasized that the derivation the minimum confinement requirement presented in this section has some limitations. Some empirical coefficients $(c_1$ and $c_2)$ are derived from very limited numbers of specimens (two specimens). However, the derivation presented in this section can be used as a good starting point for determining the required minimum confinement steel. It is suggested that further experiment should be conducted in the near future. More specimens with wide parameter variations are needed to appropriately refine the derivation of the expression for minimum confining steel collars.

For the actual retrofit application, it should be noted that the existing internal confinement has already experienced some stresses due to the acting internal forces (axial force and bending moment from the gravity load), and the external confinement only resists the additional stresses due to the seismic load. However, for retrofitting purposes of the existing columns which have not suffered from a major earthquake, the deformations of the columns due to the gravity load are relatively small. The external steel collar retrofitting method proposed in this study is ap assive confinement technique, that it starts to be effective when there is large lateral expansion. Thus, the behavior of the retrofitted specimens observed in this study should be approximately the same as the actual retrofitting application.

6.8   DISCUSSION 2: COMPARISON WITH OTHER EXTERNAL RETROFITTING METHODS

Due to many available alternatives for external retrofitting methods, it is interesting to compare the performances of each other. In this section, the performance of the proposed retrofitting technique as well as the selected other methods are summarized and discussed (Saafi et al., 1999; Saatcioglu and Yalcin, 2003; Xiao and Wu, 2003; Hussain and Driver, 2005; and Choi et al., 2010). The

summary covers the important sectional data as well as their performance highlights. The dimensions and shapes; concrete compressive strengths; amount and grades of reinforcement steel; type of external retrofitting methods; and type of loadings of the selected specimens are the primary data which is summarized. Moreover, the commonly used ratios which represent the degree of confinement are also presented. They are the volumetric ratio (ρ_s) and the effective confinement index $(I'_e = f_{le}/f'_c)$. All of the axial compression tests were conducted until the specimen failures unless otherwie stated. The level of constant axial load $\left[k_p = P/(A_g f'_c) \right]$ in the combined axial and lateral loadings are also listed in the table. In order to examine the performances of each methods, both strength and strain enhancement at peak strength relative to that of the plain concrete specimen are presented for axial loading tests. While the peak resistance and several points on the descending branch of $P - \Delta$ hysteretic curves are presented for the combined axial and lateral loading tests.

The summarized studies from literatures (see Table 6-3) include the external retrofitting methods with: (1) Fibre Reinforced Polymer (FRP) jacketing (Saafi et al., 2010); (2) prestressing strands (Saatcioglu and Yalcin, 2003); steel sheet jacketing and with stiffening elements (Xiao and Wu, 2003; Choi et al, 2010); and steel collars jacketing (Hussain and Driver, 2005; Pudjisuryadi et al., 2015, and 2016). The volumetric ratio of confinement element (ρ_s) can be taken one of the important parameter to judge the effectiveness of each method (provided in Columns 10 and 15 in Table 6-3). However, it should be noted that ρ_s alone cannot be used to determine the economical value of the methods since the actual economical value is still affected by the unit price of confining materials and also the labor cost as well as other expenses involved for different application methods.

It can be seen from the table for the studies of column axial load tests, that the FRP jacketing method (Saafi et al., 1999) performed very well with ρ_s only about 6.3 percent could increase the peak strength and peak strain (compared to the plain concrete) about 137 and 1100 percent, respectively. Methods involving

214

steel materials, such as Hussain and Driver (2005) and the current study required higher ρ_s of confining elements. The best performing specimen tested by Hussain and Driver possessed ρ_s of about 18.9 percent and indicated strength and strain increment about 131 and 688 percent, respectively. While the the most heavily confined specimen with ρ_s of about 11.46 percent tested in current study (Pudjisuryadi et al., 2016) only indicated strength and strain increments about 42 and 1700 percent, respectively. However, for specimens confined with combination of internal stirrups (ρ_s = 2.62 percent) and external steel collars (ρ_s = 9.6 percent) improved the behavior significantly (strength and strain increment about 80 and 1480 percent, respectively).

Since the strengths of confining element could be different, it might also interesting to take into account the strengths in comparing the performances. For this purpose, parameter $\rho_s \times f_c'/f_y$ is also provided in Columns 11 and 16 of Table 6-3. Lastly, an indicator which commonly considered as most directly related to the performance, the effective confinement index $\left(I_e' = f_{le}/f_c'\right)$ is given in Columns 12 and 17 of Table 6-3. However, to calculate the effective lateral pressure f_{le} involves analytical calculations which only available for some methods. Thus, these parameter could not be calculated (marked as "unknown" in Table 6-3) for the methods which still have not published their analytical model.

Furthermore, comparing the performances of retrofitting methods in combined axial and cyclic lateral loadings test is rather difficult. The different variables involved increased since the researches used different ρ_s of internal confinement and also different level of constant axial loads $\left(k_p\right)$. Some researches also applied initial stressing of external confining element which made this comparison more complex. Best specimen tested $\left(k_p = 14\,\text{percent}\right)$ by Saatcioglu and Yalcin (2003) with internal stirrups (ρ_s = 0.196 percent) retrofitted by prestressing strand (ρ_s = 0.24 percent with initial stressing of 300 MPa) indicated that the peak strength was reach at drift ratio (DR) of 4 percent. At drift ratio of 5 percent, the resistance showed about 25 percent decay, and finally failed (decay

more than 50 percent) at drift ratio of 6 percent. Xiao and Wu (2003) used constant axial load level (k_p) equal to 30 percent in the test. The most heavily confined specimen used internal stirrups (ρ_s = 0.236 percent), retrofitted by double steel sheet jacketing (ρ_s = 5+25 percent). The performance was spectacular that at very large drift ratio level of 8 percent, the lateral resistance only decay as much as 7 percent of its peak resistance. Choi et al. (2010) used prestressed steel sheet jacketing to retrofit their specimens. The specimens already had internal stirrups with ρ_s = 0.27 percent installed inside. The best performing specimen used steel sheet jacket with ρ_s = 1 percent with initial stressing value of 20 MPa. With constant axial load level (k_p) of 10 percent, the specimen reached its peak strength, and failed at drift ratio level of 3 and 6 percent, respectively. The current study (Pudjisuryadi et al., 2015) used specimens without any internal stirrups in the combined axial and lateral cyclic loading test. With constant axial load level (k_p) of 30 percent, the specimen with external confinement (ρ_s = 6.4 percent) reached its peak strength at drift ratio of 1.75 percent. Observation indicated that the specimen experienced strength decay of about 22 percent and 57 percent at drift ratio level of 4 and 7 percent, respectively.

In conclusion, the proposed retrofitting method in this study has comparable performances with similar methods by other. In the axial load test, Specimen S05 is comparable to Specimen C09 of Hussain and Driver (2005). In the combined axial and lateral load test, Specimens S13, S14, and S15 are comparable to Specimen RC-2R of Xiao and Wu (2003).

Table 6-3 Comparison of performances of external retrofitting methods from literatures

No.	Research by	Specimen	Shape	Size (mm)	fc' (MPa)	Longi.bars ρ(%)	Internal Confinement				
							steel	fy (MPa)	ρs (%)	ρs.fc'/fy	Ie'=fle/fc'
[1]	[2]	[3]	[4]	[5]	[6]	[7]	[8]	[9]	[10]	[11]	[12]
1	Saafi et al. (1999)	GE1 GE2 GE3 C1 C2 C3	Circle	152	38	none	none				
2	Saatcioglu & Yalcin (2003)	BR-S1	Square	550	45	12D25 (1.98)	D11.3-300	400	0.305	0.027	0.0033
		BR-S2									
		BR-C1	Circle	610		12D25 (2.05)			0.196	0.017	0.0119
		BR-C2									
		BR-C3									
		BR-C4									
		BR-C5									
3	Xiao & Wu (2003)	RC-1A	Square	254	45	8D16 (2.50)	D6.5-254	449	0.236	0.024	0.0024
		RC-2R			57					0.019	0.0019
		RC-3R			57						
		RC-4R			57						
		RC-5R			60					0.018	0.0018
4	Hussain & Driver (2005)	C00A	Square	300	34.4	4D20 (1.33)	D10-267	450	0.70	0.092	0.0048
		C00B			35		D15-70	453	5.19	0.672	0.0275
		C01			37.9		none				
		C02			38.7						
		C03			37.8						
		C04			37.8						
		C05			36.4						
		C06			34.8						
		C07			47						
		C08			52.8						
		C09			36.3						
5	Choi et al. (2010)	SP00-NUB SP50-NUB SP50-UB1 SP50-UB2	Circle	400	24	16D13 (1.61)	D6-130	325	0.27	0.037	0.0147
6	Pudjisuryadi et al. (2015, 2016)	CS01	Square	200	24	4D10 (0.78)	none	317			
		CS02a					D10-133		1.57	0.208	0.0780
		CS03a					D10-50		4.19	0.553	0.2075
		S01					none				
		S02									
		S03									
		S04									
		S05									
		S04a					D10-80a	317	2.62	0.346	0.1297
		S04b					D10-80b				
		CS11			17	4D13 (1.33)	D10-150		1.40	0.260	0.0976
		CS12					D10-50		4.19	0.781	0.2929
		S13					none				
		S14									
		S15									

Table 6-3 Comparison of performances of external retrofitting methods from literatures (Continued)

No.	Specimen	External Confinement					Loading	Results
		type	fy (MPa)	ρs (%)	ρs.fc'/fy	Ie'=fle/fc'		
[1]	[3]	[13]	[14]	[15]	[16]	[17]	[18]	[19]
1	GE1	FRP	450	2.105	0.249	unknown	Axial	Strength Incr. 51%, Strain Inc. 660%
	GE2		505	4.211	0.560			Strength Incr. 89%, Strain Inc. 880%
	GE3		560	6.316	0.931			Strength Incr. 137%, Strain Inc. 1100%
	C1		3300	0.289	0.251			Strength Incr. 57%, Strain Inc. 300%
	C2		3550	0.605	0.565			Strength Incr. 94%, Strain Inc. 540%
	C3		3700	1.447	1.409			Strength Incr. 177%, Strain Inc. 788%
2	BR-S1	none					Cyclic kp 13%	Drift Ratio (DR) 1% ,2% - peak,fail
	BR-S2	strand 54.8mm2-150 initial stressing (IS) 300 MPa	1860	0.285	0.118	unknown		DR 4%,5%,6% - peak,decay 20%,fail
	BR-C1	none					Cyclic kp 14%	DR 1% ,2% - peak,fail
	BR-C2	strand 54.8mm2-150 IS 300 MPa	1860	0.240	0.099	unknown		DR 4%,5%,6% - peak,decay 25%,>50%
	BR-C3	strand 54.8mm2-150 IS 50 MPa						DR 4%,5% - peak,decay >40%
	BR-C4	strand 54.8mm2-300 IS 300 MPa		0.120	0.050			DR 2%,3% - peak,diagonal crack
	BR-C5	steel strap 1.12x19mm2-150 IS 50 MPa	950	0.093	0.020			DR 3% - peak & diagonal crack
3	RC-1A	none					Cyclic kp 30%	DR 1.5% - brittle shear failure
	RC-2R	steel sheet 3.175mm	393	5.000	0.345	0.172		DR 3%,4% - decay 27%,rupture
	RC-3R	steel sheet 3.175mm	393	5.000	0.345	0.172		DR 8%, decay 7%
		steel sheet 15.9mm	328	25.039	1.441	0.720		
	RC-4R	steel sheet 3.175mm	393	5.000	0.345	0.172		DR 8%, decay 17%
		steel angle L32.32.6,4-51	367	14.241	0.917	unknown		
	RC-5R	steel sheet 3.175mm	393	5.000	0.328	0.164		DR 8%, decay 22%
		steel HSS 32.32.6,4-64	491	22.697	1.857	unknown		
4	C00A	none					Axial	Strength Incr. 13%, Strain Inc. 0%
	C00B							Strength Incr. 8%, Strain Inc. 1256%
	C01	HSS 51.51.6,35-122	497	13.920	1.825	unknown		Strength Incr. 46%, Strain Inc. 1234%
	C02	HSS 76.51.6,35-122 65.1 kN bolt force	445	18.900	2.173			Strength Incr. 56%, Strain Inc. 1243%
	C03	HSS 76.51.6,35-122 145.9 kN bolt force			2.225			Strength Incr. 89%, Strain Inc. 1010%
	C04	HSS 76.51.6,35-170 68.9 kN bolt force		13.500	1.589			Strength Incr. 27%, Strain Inc. 322%
	C05	HSS 76.51.6,35-95 90.2 kN bolt force		24.160	2.954			Strength Incr. 115%, Strain Inc. >632%
	C06	Welded HSS 51.51.6,35-122	497	13.920	1.988			Strength Incr. 118%, Strain Inc. 861%
	C07	Welded HSS 76.51.6,35-122	445	18.900	1.789			Strength Incr. 131%, Strain Inc. 688%
	C08	Welded HSS 102.51.6,35-122	410	25.480	1.979			Strength Incr. 128%, Strain Inc. 715%
	C09	Welded HSS 76.51.6,35-170	445	13.500	1.655			Strength Incr. 63%, Strain Inc. 751%
5	SP00-NUB	none					Cyclic kp 10%	DR 4%,6% - peak, fail(decay>50%)
	SP50-NUB							DR 1.5%,2.5% - peak, fail
	SP50-UB1	steel sheet 1mm, IS 40MPa	236.7	0.500	4.931	0.049		DR 2%,5% - peak, fail(decay>40%)
	SP50-UB2	steel sheet 2mm, IS 20MPa		1.000	9.863	0.099		DR 3%,6% - peak, fail(decay>40%)
6	CS01	none					Axial	Strength Incr. 0%, Strain Inc. 0%
	CS02a							Strength Incr. -5%, Strain Inc. 113%
	CS03a							Strength Incr. 21%, Strain Inc. 955%
	S01	steel angle L40.40.4-200	285	3.840	0.456	0.007		Strength Incr. 9%, Strain Inc. 53%
	S02	steel angle L40.40.4-133	285	5.774	0.686	0.012		Strength Incr. 33%, Strain Inc. 235%
	S03	steel angle L40.40.4-100	285	7.680	0.912	0.027		Strength Incr. 21%, Strain Inc. 505%
	S04	steel angle L40.40.4-80	285	9.600	1.140	0.038		Strength Incr. 23%, Strain Inc. 215%
	S05	steel angle L40.40.4-67	285	11.463	1.361	0.048		Strength Incr. 42%, Strain Inc. 1700%
	S04a	steel angle L40.40.4-80	285	9.600	1.140	0.038		Strength Incr. 80%, Strain Inc. 1480%
	S04b							Strength Incr. 77%, Strain Inc. 1750%
	CS11	none					Cyclic kp 30%	DR 2.2%,2.75%,3.5% - peak,decay 13%,fail
	CS12							DR 1.75%,4%,7% - peak,decay 29%,51%
	S13	steel angle L40.40.4-180	285	4.267	0.715	0.012		DR 2.2%,4%,6% - peak,decay 20%,fail
	S14	steel angle L40.40.4-120	285	6.400	1.073	0.028		DR 1.75%,4%,7% - peak,decay 22%,57%
	S15	steel angle L40.40.4-90	285	8.533	1.431	0.045		DR 1.75%,4%,7% - peak,decay 25%,59%

CHAPTER 7. CONCLUSIONS AND RECOMMENDATIONS

From the results of the analytical and experimental studies on RC columns retrofitted by external steel angle collars, the following conclusions which are divided into general, monotonic axial compression load test, and quasi-static combined axial compression and reversed cyclic lateral load test findings, can be drawn.

7.1 GENERAL FINDINGS

After conducting a series of literature reviews and experimental testing, some general conclusions can be drawn from this study as follows:

1. Proposed retrofit method of square RC columns externally confined by steel angle collars has been successfully developed. Experimental tests indicated significant performance improvement of retrofitted specimens.

2. An analytical model to predict full axial stress-strain relationship of concrete column retrofitted by external steel angle collars, has been successfully developed. This model can predict both enhancement due to the external confinement only as well as the combined confinement effect of conventional internal and proposed external confinements.

3. A retrofit design procedure is developed by simulating the combined effect of internal and external confinement (implemented in computer algorithm) to achieve a certain target strength (e.g. according to code requirement). Comparisons with experimental data indicated that the proposed retrofit design can predict the results with reasonable margin on the conservative side.

7.2 MONOTONIC COMPRESSION LOAD TEST FINDINGS

A set of fourteen column specimens were tested under monotonic compressive load to investigate the performance of the proposed external confining method. By observing the experimental results, some conclusions can be made as follows:

1. Improved axial stress-strain behavior is achieved by specimens externally confined by the proposed method as compared to the plain concrete Control Specimen CS01.

2. Specimens with less amount of steel collars suffered brittle failure, whereas ductile behaviors were observed in specimens with larger amount of steel collars.

3. From damaged patterns observation, it is clear that the steel collars work as confining element. Strips of concrete regions covered by the confining steel collars showed less damages than other regions.

4. Behavior of Control Specimen CS03a with internal confinement (2.36 percent volumetric ratio of confining element) comforming to the seismic provisions (SNI 2847 : 2013) is comparable to Specimen S03 (specimen using three steel collars with 7.68 percent volumetric ratio). Both specimens could reach peak strength about 1.2 times of CS01's strength, and showed axial strain at 50 percent of peak strength on the descending curve $\left(\varepsilon_{f50}\right)$ more than 8.00 percent.

5. The most heavily confined specimen with five steel collars (S05 with 11.46 percent volumetric ratio of confining element) could reach peak strength of 1.422 times of CS01 strength, and demonstrated ε_{f50} more than 10.00 percent.

6. Specimens confined by modified steel collars (with web stiffeners), namely Specimens S04c and S04d indicated negligibly improved performances (strength and ductility enhancements). Their performances were well predicted with the analytical model of S04 (retrofitted with steel collars without any stiffeners). Due to short length of the steel angle section, no local instability of the sections governed the failure mechanism, hence the effect of the web stiffeners were not apparent.

7. Specimens with strengthened steel collars (by applying dyna bolts for additional attachment points), namely Specimens S04e and S04f (with volumetric ratio of 9.60 percent) demonstrated good improvement. However, the effect of the improvement was ineffective. If the bolts pass through the columns, they will provide more effective additional supports to the steel

220

collars. The analytical predictions showed the overestimations if the effective bolt supports were assumed.

8. Most importantly, this proposed external retrofitting method is proven to be effective in retrofitting the existing deficient square RC columns. The combined effect of conventional internal stirrups and external steel collars demonstrated significant strength and ductility improvement through Specimens S04a and S04b. Both specimens reached peak strengths almost 1.8 times of CS01's strength with very large axial deformability. This behavior could be well predicted by the proposed retrofitting design approach.

7.3 QUASI-STATIC COMBINED AXIAL COMPRESSION AND REVERSED CYCLIC LATERAL LOAD TEST FINDINGS

A set of five column specimens were tested under quasi-static combined axial and reversed cyclic lateral load. By observing the experimental results, some conclusions can be made as follows:

1. In line with the findings from the monotonic compressive tests, specimens with external steel collars as confining elements showed promising results. Both lateral hysteretic load-displacement and moment-curvature curves of retrofitted specimens with three, four, and five collars within test regions (S13, S14, and S15, respectively) exhibited significantly improved behavior compared to deficiently confined Control Specimen CS11 with internal confinement which did not comform to the seismic provisions (SNI 2847 : 2013).

2. CS11 failed at 3.5 percent lateral drift with brittle diagonal failure. The least collared Specimen S13 failed at 5.0 percent lateral drift with slightly ductile behavior, but the diagonal crack pattern was still observed. This could probably due to the clear spacing of steel collars is about 140 mm which is still greater than half of specimen dimension of 100 mm.

3. The Control Specimen CS12 which was confined by internal stirrups conforming to the seismic provisions indicated very ductile behavior. It survived until 7.00 percent lateral drift, and the damage was characterized by the ductile flexural failure mechanism at the fixity region. This behavior was

generally similar to that of Specimens S14 and S15. Both specimens also survived until 7.00 percent lateral drift with ductile flexural failure mechanism.

4. The cumulative energy dissipation energy, cumulative displacement ductility, and cumulative curvature ductility are used to determine the overall seismic resistant capacity of the column. All the three parameters indicated that the proposed confining method are very effective in confining the columns. The specimens with more steel collars (S14 and S15) revealed larger seismic resistant capacities.

5. However, with definition of ultimate state which corresponds to 20 percent decay of peak strength, actually Specimens CS12, S14, and S15 had about the similar post peak behaviors as Specimen S13. Thus, their cumulative energies up to this ultimate state (TE_{80}) are not significantly greater than that of S13. Similarly, the above can also be mentioned for the other two parameters, namely the cumulative displacement ductility ($N_{\Delta 80}$) and the curvature ductility ($N_{\varphi 80}$). Moreover, the normalized cumulative energies (TE_{80} devided by the elasto plastic energy) of the retrofitted specimens range from 13.8 to 23.1.

7.4 RECOMMENDATIONS

In order to improve the study, the following important notes are given:

1. The author realizes that the number of test specimens was still very limited. More specimens should be tested to further verify the already observed behavior and proposed analytical model. Adequate parameter variations are needed to appropriately derived the expression for the minimum requirement of confining steel collars.

2. In order to further investigate the retrofit method economically, numerical finite element study can be used as alternative approach. Constitutive law of concrete from triaxial test of concrete cylinder, and adaptive redefinition of problem domain due to unstable elements due to large deformations / damages are two of many modeling problems that should be taken into attentions.

REFERENCES

ACI Committee 318 (2014), *Building Code Requirements for Structural Concrete*, American Concrete Institute, Detroit, 519 pp.

ACI Committee 374 (2005), *Acceptance Criteria for Moment Frames Based on Structural Testing and Commentary (ACI 374.1-05)*, Farmington Hills – Michigan.

ACI Committee 374 (2005), *Guide for Testing Reinforced Concrete Structural Elements under Slowly Applied Simulated Seismic Load (ACI 374.2R-13)*, Farmington Hills – Michigan.

Azizinamini, A.; Kuska, S.S.B.; Brungardt, P.; and Hatfield, E. (1994), "Seismic Behavior of Square High-Strength Concrete Columns," *ACI Structural Journal*, Vol. 91., No.3, pp. 336-345.

Barros, J.A.O.; Ferriera, D.R.S.M.; and Varma, R.K. (2008), "CFRP-Confined Reinforced Concrete Elements Subjected to Cyclic Compressive Loading," *ACI Special Publication*, Vol. 258, pp. 85-104.

Carey, S.A.; and Harries, K.A. (2005), "Axial Behavior and Modeling of Confined Small-, Medium-, and Large-Scale Circular Sections with Carbon Fiber-Reinforced Polymer Jackets," *ACI Structural Journal*, Vol. 102, No. 4, pp. 596-604.

Chai, Y.H.; Priestley, M.J.N; and Seible, F. (1994), "Analytical Model For Steel Jacketed RC Circular Bridge Columns," *Journal of Structural Engineering*, ASCE, Vol. 120, No. 8, pp. 2358-2376.

Chan, W.W.L. (1955), "The Ultimate Strength and Deformation of Plastic Hinges in Reinforced Concrete Frameworks," *Magazine of Concrete Research* (London), Vol. 7., No. 21, pp. 121-132.

Chapman, J.R.; and Driver, R.G. (2006), *Behaviour of Collared Concrete Columns Under Concentric and Eccentric Loads*, Structural Engineering

Report 263, Department of Civil & Environmental Engineering, University of Alberta, 140 pp.

Choi, E.; Chung, Y.S.; Park, J.; and Cho, B.S. (2010), "Behavior Of Reinforced Concrete Columns Confined By New Steel-Jacketing Method," *ACI Structural Journal*, Vol. 107, No.6, pp. 654-662.

Cusson, D.; and Paultre, P. (1995), "Stress Strain Model for Confined High-Strength Concrete," *Journal of Structural Engineering*, ASCE, Vol. 121., No. 3, pp. 468-477.

Fam, A.Z.; and Rizkalla, S.H. (2001), "Confinement Model for Axially Loaded Concrete Confined by Circular Fiber-Reinforced Polymer Tubes," *ACI Structural Journal*, Vol. 98, No. 4, pp. 451-461.

Guo, Z.X.; Zhang, J.; and Yun, Z. (2006), "Experimental Study On A New Retrofitted Scheme For Seismically Deficient Rc Columns," *Proceedings : 4th International Conference on Earthquake Engineering*, Taipe, Taiwan, paper no. 109.

Hoshikusuma, J.; Kawashima, K.; Nagaya, K.; and Taylor, A.W. (1997), "Stress-Strain Model for Confined Reinforced Concrete in Bridges Piers," *Journal of Structural Engineering*, Vol. 123, No. 5, pp. 624-633.

Hussain M.A.; and Driver, R.G (2005), "Experimental Investigation of External Confinement of Reinforced Concrete Columns by HSS Collars," *ACI Structural Journal*, Vol. 102, No. 2, pp. 242-251.

Kent, D.C.; and Park, R. (1971), "Flexural Members with Confined Concrete," *Journal of Structural Division*, ASCE, Vol. 97, No. 7, pp. 1969-1990.

Kusuma, B.; and Tavio (2007), "Usulan Kurva Tegangan-Regangan Beton Mutu Tinggi Terkekang Welded Wire Reinforcement," *Seminar HAKI*, Indonesia.

Kusuma, B.; and Tavio (2008), "Unified Stress-Strain Model for Confined Columns of Any Concrete and Steel Strengths," *Proceeding of the International Conference on Earthquake Engineering and Disaster Mitigation (ICEEDM-I)*, April 14th-15th, Jakarta, Indonesia, pp. 502-509.

Kusuma, B.; and Tavio (2009), "A Comparative Study of Models for Confinement of Concrete by Welded Wire Mesh," *Proceeding of the 1st International Conference Rehabilitation and Maintenance in Civil Engineering (ICRMCE)*, March 21th-22nd 2009, Solo, Indonesia, pp. 90-101.

Kusuma, B.; Tavio; and Suprobo, P. (2011a), "Axial Load Behavior of Concrete Columns with Welded Wire Fabric as Transverse Reinforcement," *Procedia Engineering*, V. 14, pp. 2039-2047.

Kusuma, B.; Tavio; and Suprobo, P. (2011b), "Prediction of Peak Stress for Concrete Confined with Welded Wire Fabric," *Proceedings: The 2nd International Conference on Earthquake Engineering and Disaster Mitigation (ICEEDM-II)*, July 19th-20th, Surabaya, Indonesia, pp. F117-F131.

Kusuma, B.; Tavio; and Suprobo, P. (2015a), "Behavior of Concentrically Loaded Welded Wire Fabric Reinforced Concrete Columns with Varying Reinforcement Grids and Ratios," *International Journal of ICT-aided Architecture and Civil Engineering (IJIACE)*, Vol. 2, No. 1, pp. 1-15.

Kusuma, B.; Tavio; and Suprobo, P. (2015b), *Behavior of Reinforced Concrete Columns Confined with Welded Reinforcement Grid under Axial Compression and Combined Axial Compression and Reversed Cyclic Loading*, Structural Engineering Dissertation, Department of Civil Engineering, Sepuluh Nopember Institute of Technology, 632 pp.

Legeron, F.; and Paultre, P. (2003), "Uniaxial Confinement Model for Normal-and High-Strength Concrete Columns," *Journal of Structural Engineering*, Vol. 129, No. 2, pp. 241-252.

Lee, C.S.; Hegemier, G.A.; and Phillipi, D.J. (2010), "Analytical Model for Fiber-Reinforced Polymer-Jacketed Square Concrete Columns in Axial Compression," *ACI Structural Journal*, Vol. 107, No. 2, pp. 208-217.

Liu, J.; Driver, R.G.; and Lubell, A.S. (2008), *Rehabilitation and Repair of Reinforced Concrete Short Columns with External Steel Collars*, Structural Engineering Report No. 281, Department of Civil & Environmental Engineering, University of Alberta, 303 pp.

Mander, J.; Priestley, M.J.N.; and Park, R. (1988a), "Theoretical Stress-Strain Model For Confined Concrete," *Journal of Structural Engineering*, ASCE, Vol. 114, No. 8, pp. 1804-1826.

Mander, J.; Priestley, M.J.N.; and Park, R. (1988b), "Observed Stress-Strain Model For Confined Concrete," *Journal of Structural Engineering*, ASCE, Vol. 114, No.8, pp. 1827-1849.

Muruguma, H.; Nishiyama, M.; and Watanabe, F. (1993), "Stress-Strain Curve Model for Concrete with a Wide-Range of Compressive Strength," *Proceeding High Strength Concrete*, Lillehammer, Norway, pp. 314-321.

Nesheli, K.N.; and Meguro, K. "External Prestressing Concrete Columns with Fibrous Composite Belts," *FRPRCS-7*, SP-230-92, pp. 1631-1645.

Paultre, P.; and Legeron, F. (2008), "Confinement Reinforcement Design for Reinforced Concrete Columns," *Journal of Structural Engineering*, Vol. 134, No. 5, pp. 738-749.

Priestley, M.J.N.; Seible, F.; Xiao, Y.; and Verma, R. (1994a), "Steel Jacket Retrofitting Of Reinforced Concrete Bridge Columns For Enhanced Shear Strength – Part 1: Theoretical Consideration And Test Design," *ACI Structural Journal*, Vol. 91, No. 4, pp. 394-405.

Priestley, M.J.N.; Seible, F.; Xiao, Y.; and Verma, R. (1994b), "Steel Jacket Retrofitting Of Reinforced Concrete Bridge Columns For Enhanced Shear

226

Strength – Part 2: Test Results And Comparison With Theory," *ACI Structural Journal*, Vol. 91., No. 5, pp. 537-551.

Pudjisuryadi, P.; and Tavio (2013), "Compressive Strength Prediction of Square Concrete Columns Retrofitted with External Steel Collars," *Civil Engineering Dimension*, Vol. 15., No. 1, pp. 18-24.

Pudjisuryadi, P.; Tavio; and Suprobo, P. (2011), "Transverse Stress Distribution in Concrete Columns Externally Confined by Steel Angle Collars," *Proceedings: The 3ʳᵈ International Conference on Earthquake Engineering and Disaster Mitigation (ICEEDM-II)*, Surabaya, pp. H139-H143.

Pudjisuryadi, P.; Tavio; and Suprobo, P. (2014), "Analytical Confining Model of Square Reinforced Concrete Columns using External Steel Collars," *International Journal of ICT-aided Architechture and Civil Engineering*, Vol. 1, No. 1, pp. 1-18.

Pudjisuryadi P.; Tavio; and Suprobo P. (2015),"Performance of square reinforced concrete columns externally confined by steel angle collars under combined axial and lateral load," *Procedia Engineering: The 5th International Conference of Euro Asia Civil Engineering Forum* (EACEF-5). Surabaya-Indonesia, September 2015, v.125, pp.1043-1049.

Pudjisuryadi, P.; Tavio; and Suprobo, P. (2016), "Axial Compressive Behavior of Square Concrete Columns Externally Collared by Light Structural Steel Angle Sections," International Journal of Applied Engineering Research, vol.11. no.7, India, ISSN:0973-4562, pp. 4655-4666.

Razvi, S.R.; and Saatcioglu, M. (1994), "Strength and Deformability of Confined High-Strength Concrete Columns," *ACI Structural Journal*, Vol. 91, No. 6, pp. 678-687.

Razvi, S.R.; and Saatcioglu, M. (1999), "Confinement Model for High-Strength Concrete," *Journal of Structural Engineering*, ASCE, Vol. 125, No. 3, pp. 281-289.

Roy, H.E.H.; and Sozen, M.A. (1965), "Ductility of Concrete," *Flexural Mechanics of Reinforced Concrete*, SP-12, American Concrete Institute/American Society of Civil Engineers, Detroit, pp. 213-224.

Saafi, M.; Toutanji, H.A.; and Li, Z. (1999), "Behavior of Concrete Columns Confined with Fiber-Reinforced Polymer Tubes," *ACI Material Journal*, Vol. 96, No. 4, pp. 500-509.

Saatcioglu, M.; and Razvi, S.R. (1992), "Strength And Ductility Of Confined Concrete," *Journal of Structural Engineering*, ASCE, Vol. 118., No. 6, pp. 1590-1607.

Saatcioglu, M.; and Razvi, S.R. (2002), "Displacement-Based Design of Reinforced Concrete Columns for Confinement," *ACI Structural Journal*, Vol. 99, No. 1, pp. 3-11.

Saatcioglu, M.; and Yalcin, C. (2003), "External Prestressing Concrete Columns for Improved Seismic Shear Resistance," *Journal of Structural Engineering*, ASCE, Vol. 129, No.8, pp. 1057-1070.

Sakai, K.; and Sheikh, S.A. (1989), "What Do We Know about Confinement of Reinforced Concrete Columns? (A Critical Review of Previous Work and Concrete Provisions)," *ACI Structural Journal*, Vol. 86, No. 2, pp. 192-207.

Sargin, M. (1971), *Stress-Strain Relationships for Concrete and the Analysis of Structural Concrete Sections*, Study No. 4, Solid Mechanics Division, University of Waterloo, 167 pp.

Sargin, M.; Ghosh, S.K.; and Handa, V.K., "Effects of Lateral Reinforcement upon the Strength and Deformation Properties of Concrete," *Magazine of Concrete Research*, 23(75-76), 99-110.

Sheikh, S.A.; and Uzumeri S.M. (1980), "Strength and Ductility of Tied Concrete Columns," *Proceedings*, ASCE, Vol. 106, ST5, pp. 1079-1102.

Sheikh, S.A. (1982), "A Comparative Study of Confinement Models," *ACI Journal*, Vol. 79, No. 4, pp. 296-306.

Sheikh, S.A.; and Yeh, C.C. (1986), "Flexural Behavior of Confined Concrete Columns," *ACI Journal*, 1986, pp. 389-404.

Sheikh, S.A.; and Khoury, S.S. (1993), "Confined Concrete Columns with Stubs," *ACI Structural Journal*, Vol. 90, No. 4, pp. 414-431.

SNI-1729 Committee (2002), *Structural Steel Requirements for Buildings (SNI 03-1729-2002),* National Standardization Board (BSN), Jakarta, Indonesia, 184 pp. (in Indonesian).

SNI-2847 Committee (2013), *Structural Concrete Requirements for Buildings (SNI 2847:2013)*, National Standardization Board (BSN), Jakarta, Indonesia, 264 pp. (in Indonesian).

Soliman, M.T.M.; and Yu, C.W. (1967), "The Flexural Stress-Strain Relationship of Concrete Confined by Rectangular Transverse Reinforcement," *Magazine of Concrete Research (London)*, Vol. 19, No. 61, pp. 223-238.

Tabsh, S.W. (2007), "Stress-Strain Model for High-Strength Concrete Confiend by Welded Wire Fabric," *Journal of Materials in Civil Engineering*, ASCE, Vol. 19, No. 4, pp. 286-294.

Tavio; Budiantara, I.N.; and Kusuma, B. (2008a), "Spline Nonparametric Regression Analysis of Stress-Strain Curve of Confined Concrete," *Civil Engineering Dimension*, Vol. 10, No. 1, pp. 14-27.

Tavio; and Kusuma, B. (2009), "Stress-Strain Model for High-Strength Concrete Confined by Welded Wire Fabric," *Discussion, Journal of Materials in Civil Engineering*, American Society of Civil Engineers (ASCE), Reston, Virginia, USA, Vol. 21, No. 1, 2009, pp. 40-45.

Tavio; and Kusuma, B. (2014), "A Model of Confinement Effect on Stress-Strain Relation of Reinforced Concrete Columns Confined with Welded Wire Fabric," *Proceeding of the 6th International Conference of Asian Concrete Federation*, Sept. 21th-24th, Asian Concrete Federation (ACF), Seoul, Korea, pp. 599-605.

Tavio; and Kusuma, B. (2015), "Analytical Model for Axial Stress-Strain Behavior of Welded Reinforcement Grid Confined Concrete Columns," *Journal of Asian Concrete Federation*, Vol. 1, No. 1, pp. 1-10.

Tavio; Kusuma, B.; and Suprobo, P. (2012), "Experimental Behavior of Concrete Columns Confined by Welded Wire Fabric as Transverse Reinforcement under Axial Compression,"*ACI Structural Journal, American Concrete Institute (ACI)*, Farmington Hills, Michigan, USA, Vol. 109, No. 3, pp. 339-348.

Tavio; Pudjisuryadi, P.; and Suprobo, P. (2014), "Experimental Behavior of RC Columns Externally Confined by Steel Collars Subjected to Axial Compression," *Proceeding of the 6th International Conference of Asian Concrete Federation*, Sept. 21th-24th, Asian Concrete Federation (ACF), Seoul, Korea, pp. 606-613.

Tavio; Pudjisuryadi, P.; and Suprobo, P. (2013), "L-Shaped Steel Collars: An Alternative External Confining Retrofit for Improving Ductility and Strength of Rectangular Concrete Columns," *The International Seminar on Concrete Technology: Green Concrete Technology Innovation*, June 4th-5th, Diponegoro University, Semarang, Indonesia, pp. 36-50.

Tavio; Pudjisuryadi, P.; and Suprobo, P. (2015), "Strength and Ductility of External Steel Collared Concrete Columns under Compressive Loading," *Journal of Asian Concrete Federation*, Vol. 1, No. 1, pp. 47-56.

Tavio; Suprobo, P.; and Kusuma, B. (2008b), "Strength and Ductility Enhancement of Reinforced HSC Columns Confined with High-Strength

Transverse Steel," *Proceedings : Eleventh East Asia-Pacific Conference on Structural Engineering and Construction* , Taipei-Taiwan.

Tavio; Suprobo, P.; and Kusuma, B. (2011), "Investigation of Stress-Strain Models for Confinement of Concrete by Welded Wire Fabric," *Procedia Engineering*, Vol. 14, 2011, pp. 2031-2038.

Tegola, A.L.; and Manni, O. (1999), "Experimental Investigation on Concrete confined by Fiber Reinforced Polymer and Comparison with Theoretical Model," *ACI Special Publication*, Vol. 188, pp. 243-253.

Vallenas, J.; Bertero, V.V.; and Popov, E.P. (1977), *Concrete Confined by Rectangular Hoops and Subjected to Axial Loads*, Report No. UCB/EERC-77/13, Earthquake Engineering Research Center, University of California, Berkeley, 114 pp.

Xiao, Y.; Priestley, M.J.N.; and Seible, F. (1993), *Steel Jacket Retrofit For Enhancing Shear Strength Of Short Rectangular Reinforced Concrete Bridge Columns*, Structural system research project, Rep. No. SSRP-92/07, Dept. Of Applied Mechanics and Engineering Sciences, 192 pp.

Xiao, Y.; and Wu, H. (2003), "Retrofit Of Reinforced Concrete Columns Using Partially Stiffened Steel Jacket," *Journal of Structural Engineering*, Vol. 129, No. 6, pp. 725-732.

Yong, Y. K.; Nour, M.G.; and Nawy, E.G. (1988), "Behavior of Laterally Confined High-Strength Concrete under Axial Loads," *Journal of the Structural Division*, ASCE, Vol. 114, No. ST2, pp. 332-351.

= This Page is Intentionally Left Blank =

APPENDIX A. DATA LOGGER CHANNEL NUMBERS FOR COMBINED AXIAL COMPRESSIVE AND REVERSED CYCLIC LOAD TEST

(a) East view / Side 1

(b) South view / Side 2

(c) West view / Side 3

(d) North view / Side 4

Figure A-1 Data logger channel numbers of Specimen CS11 : (a) East view / Side 1; (b) South view / Side 2; (c) West view / Side 3; and (d) North view / Side 4
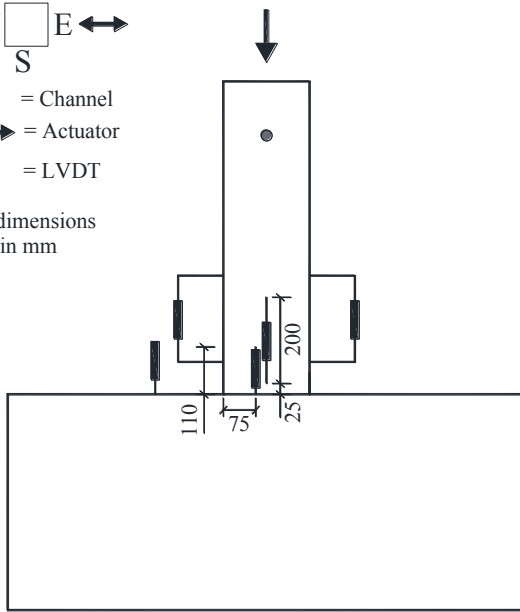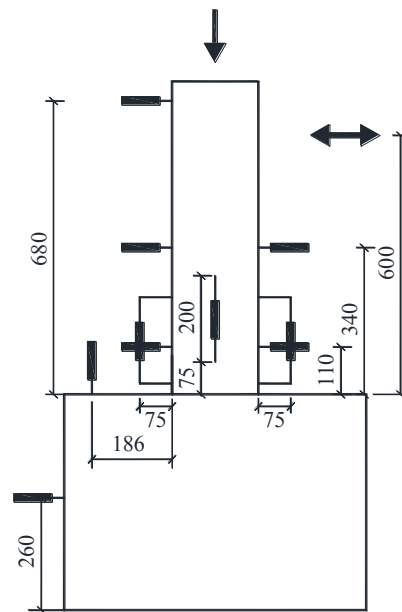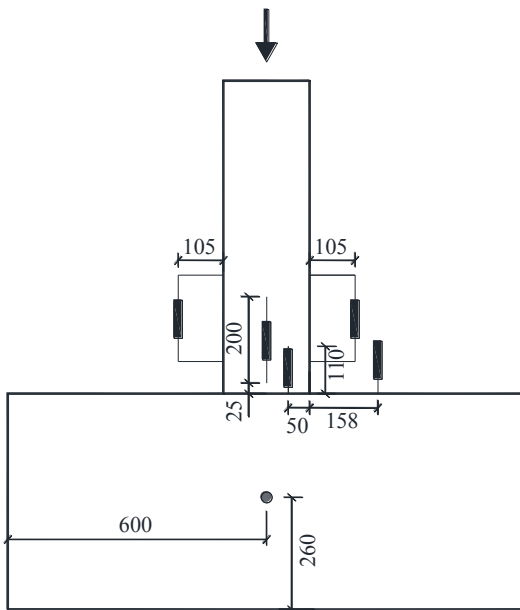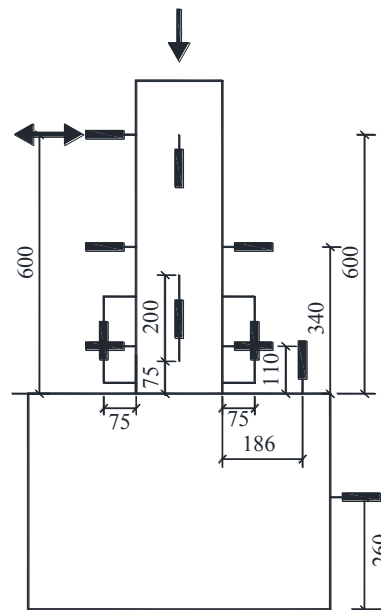
Figure A-2 Locations of each data logger channel of Specimen CS11 : (a) East view / Side 1; (b) South view / Side 2; (c) West view / Side 3; and (d) North view / Side 4

234

Table A-1 Channel numbers data of CS11

Channel	TR/SG	Note
0	A	Vertical Load
1	V	Horizontal Load
2	WR/TR-1	dH, hz jack (wire), H=60cm
3	TR-2	dH, hz jack, H=60cm
4	TR-3	dV, side 4, H=60cm
5	TR-4	dH, side 3, H=34cm
6	TR-5	dH, side 1, H=34cm
7	TR-6	dH, side 1, H=11cm
8	TR-7	dH, side 3, H=11cm
9	TR-8	dV, footing, side 3
10	TR-9	dH, footing, side 3 (H=26cm)
11	TR-10	dV, side 2, L0=20 cm (H1=7.5cm, H2=27.5cm)
12	TR-11	dV, side 4, L0=20 cm (H1=7.5cm, H2=27.5cm)
13	TR-12	dV, side 3, L0=20 cm (H1=2.5cm, H2=22.5cm)
14	TR-13	dV, side 1, L0=20 cm (H1=2.5cm, H2=22.5cm)
15	TR-14	dV, side 1, H=11cm
16	TR-15	dV, side 3, H=11cm
17	TR-16	dH, side 3, H=68cm
18	SG-1	L12-1 (longitudinal bar, corner 12, H=5cm)
19	SG-2	L23-1 (longitudinal bar, corner 23, H=5cm)
20	SG-3	L12-2 (longitudinal bar, corner 12, H=15cm)
21	SG-4	L23-2 (longitudinal bar, corner 23, H=15cm)
22	SG-5	L41-1 (longitudinal bar, corner 41, H=5cm)
23	SG-6	L34-1 (longitudinal bar, corner 34, H=5cm)
24	SG-7	L41-2 (longitudinal bar, corner 41, H=15cm)
25	SG-8	L34-2 (longitudinal bar, corner 34, H=15cm)
26	SG-9	S1-1 (stirrup side 1, h=5cm)
27	SG-10	S3-1 (stirrup side 3, h=5cm)
28	SG-11	S1-2 (stirrup side 1, h=20cm)
29	SG-12	S3-2 (stirrup side 3, h=20cm)
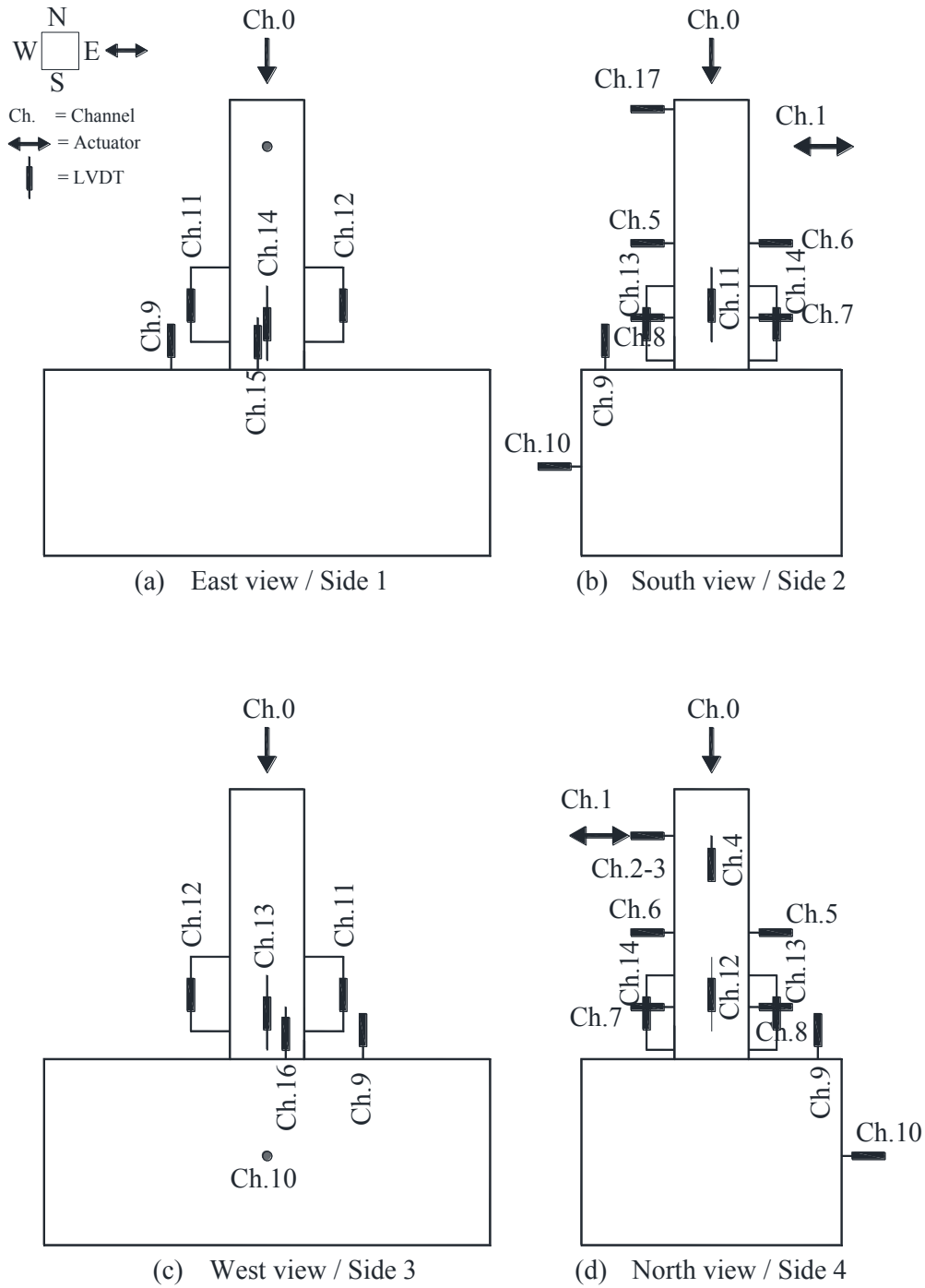
Figure A-3 Data logger channel numbers of Specimen CS12 : (a) East view / Side 1; (b) South view / Side 2; (c) West view / Side 3; and (d) North view / Side 4
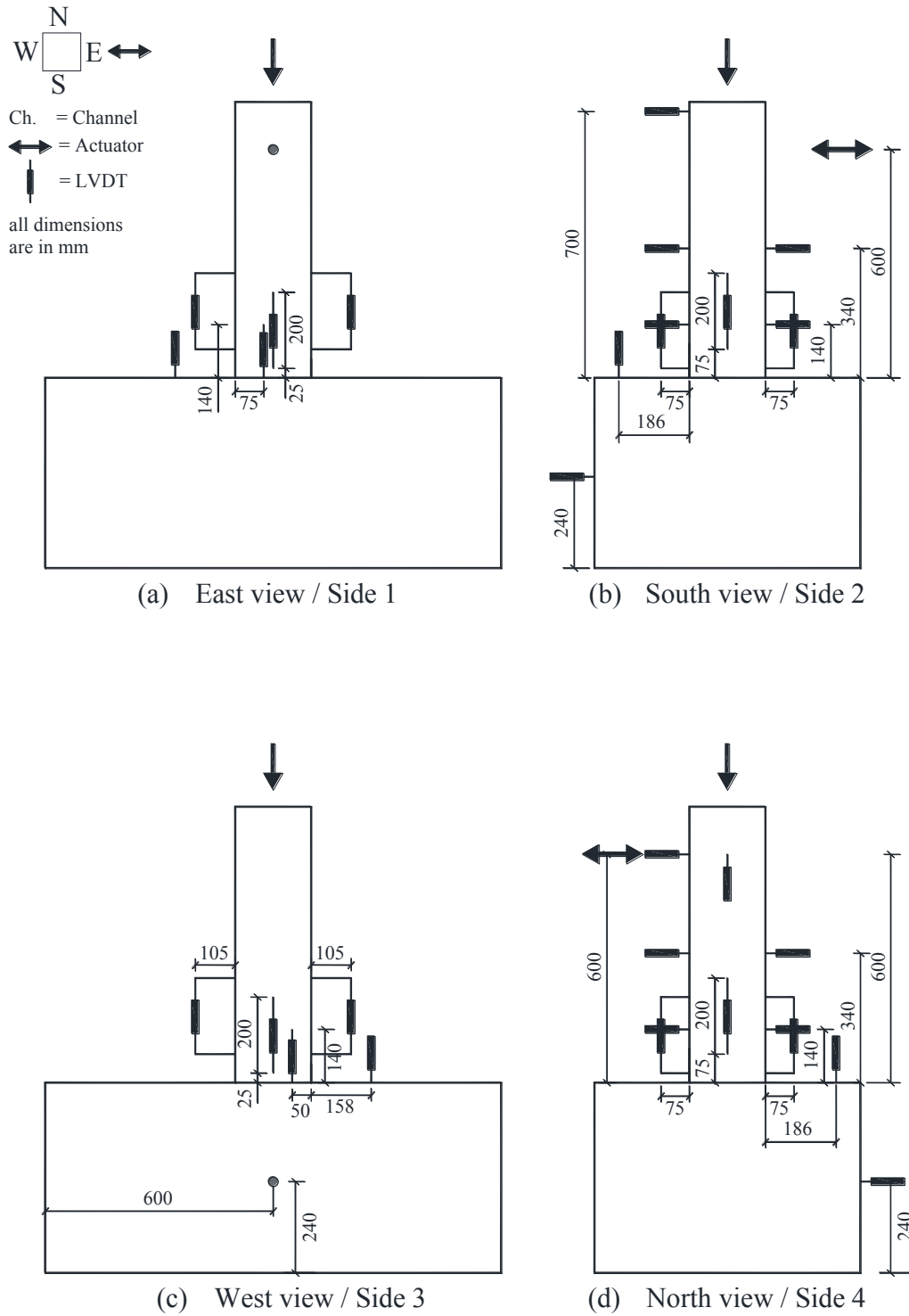
Figure A-4 Locations of each data logger channel of Specimen CS12 : (a) East view / Side 1; (b) South view / Side 2; (c) West view / Side 3; and (d) North view / Side 4

237

Table A-2 Channel numbers data of CS12

Channel	TR/SG	Note
0	A	Vertical Load
1	V	Horizontal Load
2	WR/TR-1	dH, hz jack (wire), H=60cm
3	TR-2	dH, hz jack, H=60cm
4	TR-3	dV, side 4, H=60cm
5	TR-4	dH, side 3, H=34cm
6	TR-5	dH, side 1, H=34cm
7	TR-6	dH, side 1, H=14cm
8	TR-7	dH, side 3, H=14cm
9	TR-8	dV, footing, side 3
10	TR-9	dH, footing, side 3 (H=24cm)
11	TR-10	dV, side 2, L0=20 cm (H1=7.5cm, H2=27.5cm)
12	TR-11	dV, side 4, L0=20 cm (H1=7.5cm, H2=27.5cm)
13	TR-12	dV, side 3, L0=20 cm (H1=2.5cm, H2=22.5cm)
14	TR-13	dV, side 1, L0=20 cm (H1=2.5cm, H2=22.5cm)
15	TR-14	dV, side 1, H=14cm
16	TR-15	dV, side 3, H=14cm
17	TR-16	dH, side 3, H=70cm
18	SG-1	L12-1 (longitudinal bar, corner 12, H=5cm)
19	SG-2	L23-1 (longitudinal bar, corner 23, H=5cm)
20	SG-3	L12-2 (longitudinal bar, corner 12, H=15cm)
21	SG-4	L23-2 (longitudinal bar, corner 23, H=15cm)
22	SG-5	L41-1 (longitudinal bar, corner 41, H=5cm)
23	SG-6	L34-1 (longitudinal bar, corner 34, H=5cm)
24	SG-7	L41-2 (longitudinal bar, corner 41, H=15cm)
25	SG-8	L34-2 (longitudinal bar, corner 34, H=15cm)
26	SG-9	S1-1 (stirrup side 1, h=5cm)
27	SG-10	S3-1 (stirrup side 3, h=5cm)
28	SG-11	S1-2 (stirrup side 1, h=15cm)
29	SG-12	S3-2 (stirrup side 3, h=15cm)
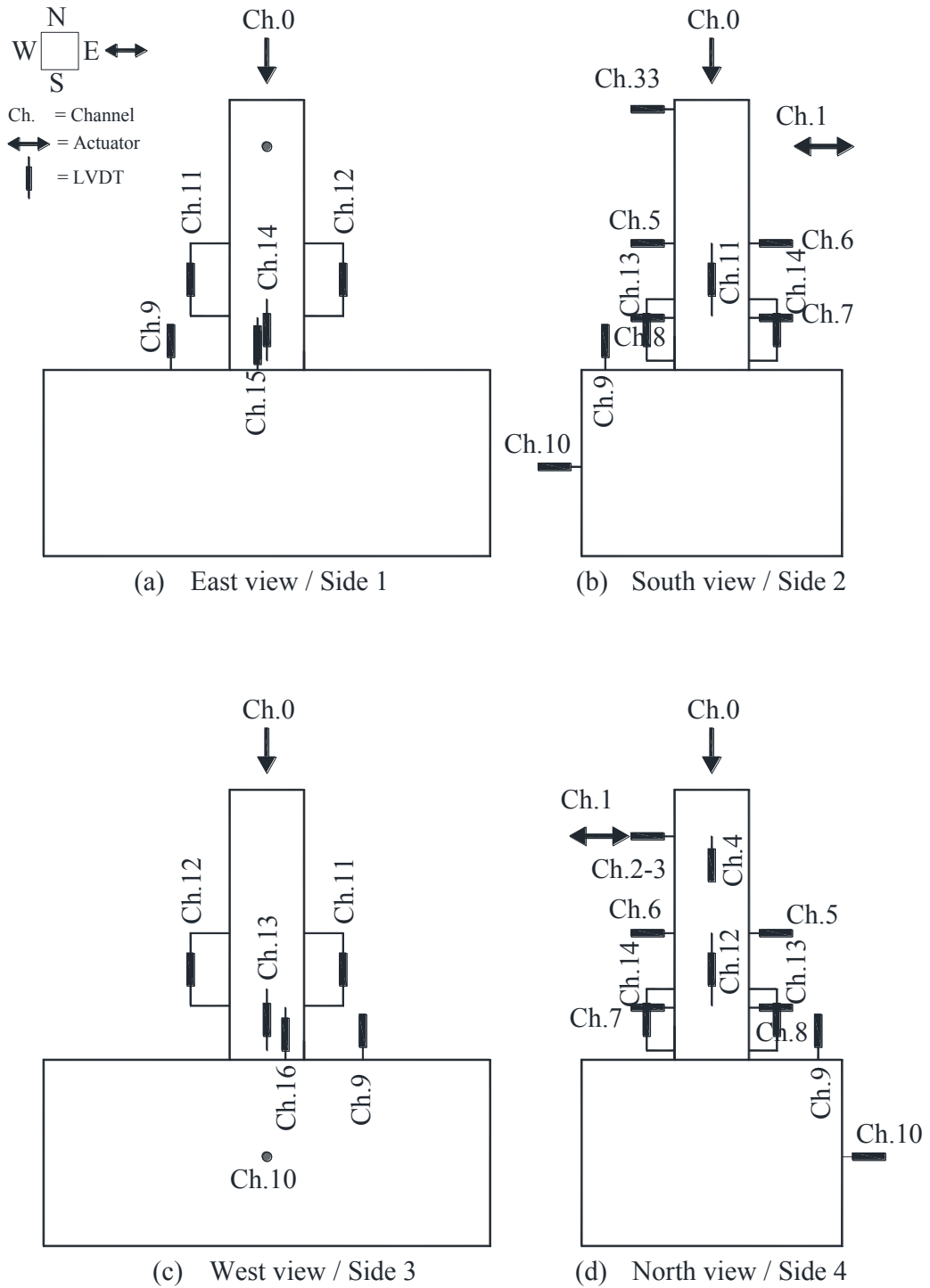
Figure A-5 Data logger channel numbers of Specimen S13 : (a) East view / Side 1; (b) South view / Side 2; (c) West view / Side 3; and (d) North view / Side 4

239

Figure A-6 Locations of each data logger channel of Specimen S13 : (a) East view / Side 1; (b) South view / Side 2; (c) West view / Side 3; and (d) North view / Side 4

Table A-3 Channel numbers data of S13

Channel	TR/SG	Note
0	A	Vertical Load
1	V	Horizontal Load
2	WR/TR-1	dH, hz jack (wire), H=60cm
3	TR-2	dH, hz jack, H=60cm
4	TR-3	dV, side 4, H=60cm
5	TR-4	dH, side 3, H=34cm
6	TR-5	dH, side 1, H=34cm
7	TR-6	dH, side 1, H=14cm
8	TR-7	dH, side 3, H=14cm
9	TR-8	dV, footing, side 3
10	TR-9	dH, footing, side 3 (H=24cm)
11	TR-10	dV, side 2, L0=19.5cm (H1=14.5cm, H2=34cm)
12	TR-11	dV, side 4, L0=19.5cm (H1=14.5cm, H2=34cm)
13	TR-12	dV, side 3, L0=16.5cm (H1=2.5cm, H2=19cm)
14	TR-13	dV, side 1, L0=16.5cm (H1=2.5cm, H2=19cm)
15	TR-14	dV, side 1, H=14cm
16	TR-15	dV, side 3, H=14cm
17	SG-1	L34-1 (longitudinal bar, corner 34, H=5cm)
18	SG-2	L41-1 (longitudinal bar, corner 41, H=5cm)
19	SG-3	L34-2 (longitudinal bar, corner 34, H=15cm)
20	SG-4	L41-2 (longitudinal bar, corner 41, H=15cm)
21	SG-5	L23-1 (longitudinal bar, corner 23, H=5cm)
22	SG-6	L12-1 (longitudinal bar, corner 12, H=5cm)
23	SG-7	L23-2 (longitudinal bar, corner 23, H=15cm)
24	SG-8	L12-2 (longitudinal bar, corner 12, H=15cm)
25	SG-9	C3-L-1 (collar side 3, Leg/hz, hb=5cm)
26	SG-10	C1-L-1 (collar side 1, Leg/hz, hb=5cm)
27	SG-11	C3-B-1 (collar side 3, Back/vt, hb=5cm)
28	SG-12	C1-B-1 (collar side 1, Back/vt, hb=5cm)
29	SG-13	C3-L-2 (collar side 3, Leg/hz, hb=23cm)
30	SG-14	C1-L-2 (collar side 1, Leg/hz, hb=23cm)
31	SG-15	C3-B-2 (collar side 3, Back/vt, hb=2cm)
32	SG-16	C1-B-2 (collar side 1, Back/vt, hb=23cm)
33	TR-16	dH, side 3, H=70cm

Figure A-7 Data logger channel numbers of Specimen S14 : (a) East view / Side 1; (b) South view / Side 2; (c) West view / Side 3; and (d) North view / Side 4

N
W □ E ↔
S

Ch. = Channel
↔ = Actuator
▯ = LVDT

all dimensions
are in mm

(a) East view / Side 1

(b) South view / Side 2

(c) West view / Side 3
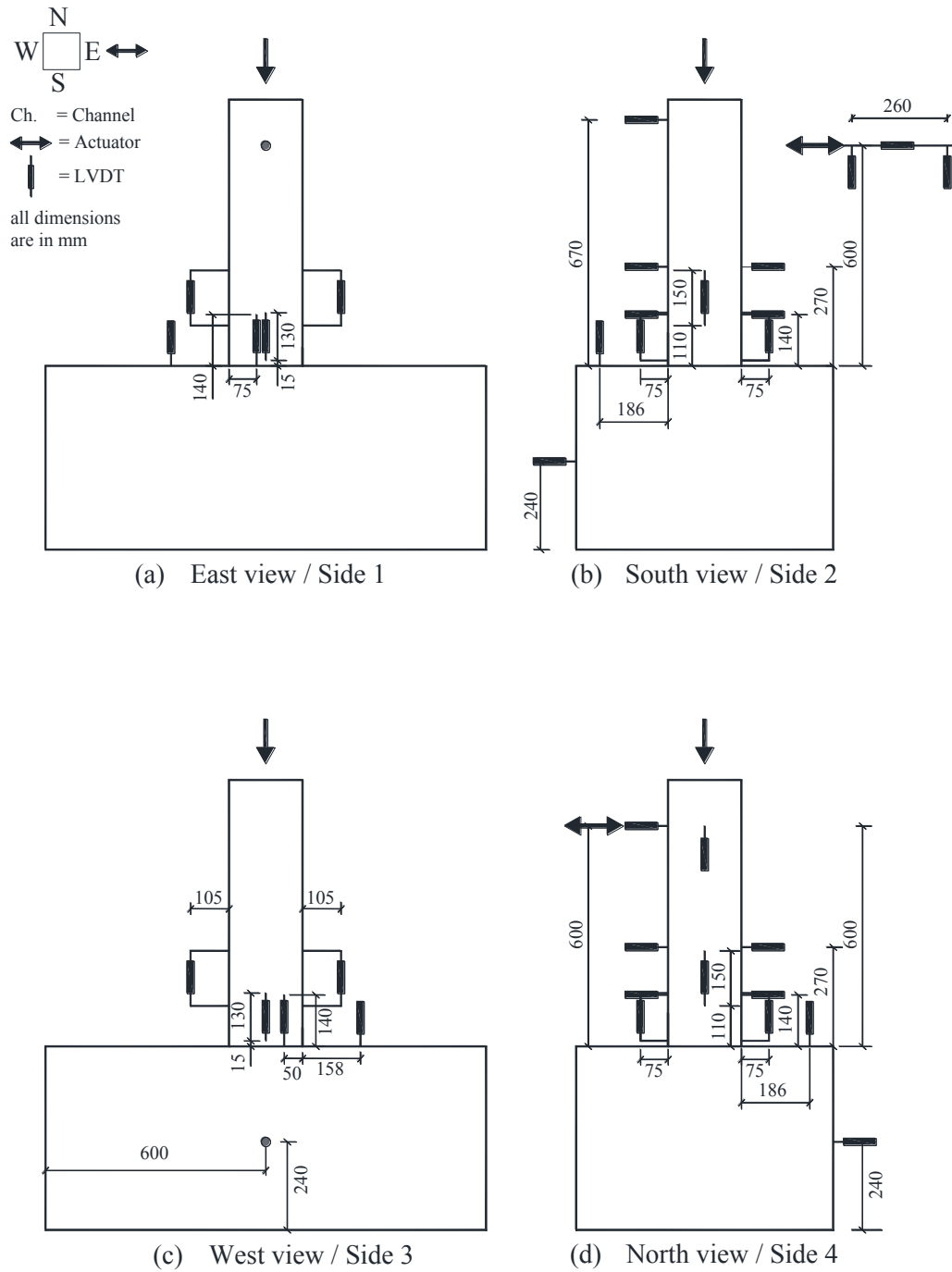
(d) North view / Side 4

Figure A-8 Locations of each data logger channel of Specimen S14 : (a) East view / Side 1; (b) South view / Side 2; (c) West view / Side 3; and (d) North view / Side 4

243

Table A-4 Channel numbers data of S14

Channel	TR/SG	Note
0	A	Vertical Load
1	V	Horizontal Load
2	WR/TR-1	dH, hz jack (wire), H=60cm
3	TR-2	dH, hz jack, H=60cm
4	TR-3	dV, side 4, H=60cm
5	TR-4	dH, side 3, H=27cm
6	TR-5	dH, side 1, H=27cm
7	TR-6	dH, side 1, H=14cm
8	TR-7	dH, side 3, H=14cm
9	TR-8	dV, footing, side 3
10	TR-9	dH, footing, side 3 (H=24cm)
11	TR-10	dV, side 2, L0=15 cm (H1=11cm, H2=26cm)
12	TR-11	dV, side 4, L0=15 cm (H1=11cm, H2=26cm)
13	TR-12	dV, side 3, L0=13 cm (H1=1.5cm, H2=14.5cm)
14	TR-13	dV, side 1, L0=13 cm (H1=1.5cm, H2=14.5cm)
15	TR-14	dV, side 3, H=14cm
16	TR-15	dV, side 1, H=14cm
17	TR-16	dH, side 3, H=67cm
18	WR/TR-17	dH, hz jack (wire), H=60cm
19	SG-1	L12-1 (longitudinal bar, corner 12, H=5cm)
20	SG-2	L23-1 (longitudinal bar, corner 23, H=5cm)
21	SG-3	L12-2 (longitudinal bar, corner 12, H=15cm)
22	SG-4	L23-2 (longitudinal bar, corner 23, H=15cm)
23	SG-5	L41-1 (longitudinal bar, corner 41, H=5cm)
24	SG-6	L34-1 (longitudinal bar, corner 34, H=5cm)
25	SG-7	L41-2 (longitudinal bar, corner 41, H=15cm)
26	SG-8	L34-2 (longitudinal bar, corner 34, H=15cm)
27	SG-9	C1-L-1 (collar side 1, Leg/hz, hb=5cm)
28	SG-10	C3-L-1 (collar side 3, Leg/hz, hb=5cm)
29	SG-11	C1-B-1 (collar side 1, Back/vt, hb=5cm)
30	SG-12	C3-B-1 (collar side 3, Back/vt, hb=5cm)
31	SG-13	C1-L-2 (collar side 1, Leg/hz, hb=17cm)
32	SG-14	C3-L-2 (collar side 3, Leg/hz, hb=17cm)
33	SG-15	C1-B-2 (collar side 1, Back/vt, hb=17cm)
34	SG-16	C3-B-2 (collar side 3, Back/vt, hb=17cm)
35	TR-18	dV, hz jack, point 1 (near support), D12=26cm
36	TR-19	dv, hz jack, point 2 (near hinge), D12=26cm

Figure A-9 Data logger channel numbers of Specimen S15 : (a) East view / Side 1; (b) South view / Side 2; (c) West view / Side 3; and (d) North view / Side 4
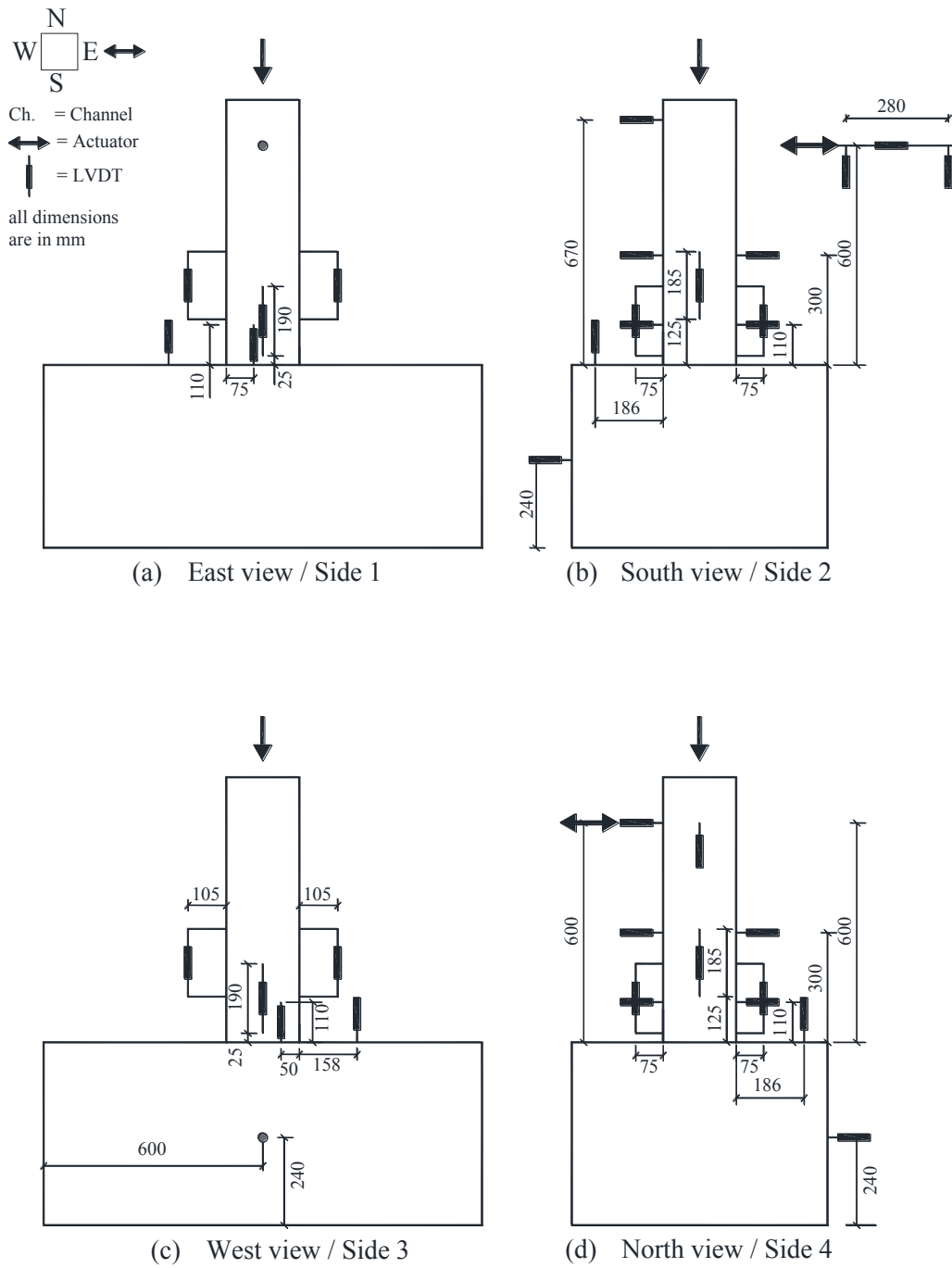
Figure A-10 Locations of each data logger channel of Specimen S15 : (a) East view / Side 1; (b) South view / Side 2; (c) West view / Side 3; and (d) North view / Side 4

246

Table A-5 Channel numbers data of S15

Channel	TR/SG	Note
0	A	Vertical Load
1	V	Horizontal Load
2	WR/TR-1	dH, hz jack (wire), H=60cm
3	TR-2	dH, hz jack, H=60cm
4	TR-3	dV, side 4, H=60cm
5	TR-4	dH, side 3, H=30cm
6	TR-5	dH, side 1, H=30cm
7	TR-6	dH, side 1, H=11cm
8	TR-7	dH, side 3, H=11cm
9	TR-8	dV, footing, side 3
10	TR-9	dH, footing, side 3 (H=24cm)
11	TR-10	dV, side 2, L0=18.5 cm (H1=12.5cm, H2=31cm)
12	TR-11	dV, side 4, L0=18.5 cm (H1=12.5cm, H2=31cm)
13	TR-12	dV, side 3, L0=19 cm (H1=2.5cm, H2=21.5cm)
14	TR-13	dV, side 1, L0=19 cm (H1=2.5cm, H2=21.5cm)
15	TR-14	dV, side 3, H=11cm
16	TR-15	dV, side 1, H=11cm
17	TR-16	dH, side 3, H=67cm
18	WR/TR-17	dH, hz jack (wire), H=60cm
19	TR-18	dV, hz jack, point 1 (near hinge), D12=28cm
20	TR-19	dv, hz jack, point 2 (near support), D12=28cm
21	SG-1	L12-1 (longitudinal bar, corner 12, H=5cm)
22	SG-2	L23-1 (longitudinal bar, corner 23, H=5cm)
23	SG-3	L12-2 (longitudinal bar, corner 12, H=15cm)
24	SG-4	L23-2 (longitudinal bar, corner 23, H=15cm)
25	SG-5	L41-1 (longitudinal bar, corner 41, H=5cm)
26	SG-6	L34-1 (longitudinal bar, corner 34, H=5cm)
27	SG-7	L41-2 (longitudinal bar, corner 41, H=15cm)
28	SG-8	L34-2 (longitudinal bar, corner 34, H=15cm)
29	SG-9	C1-L-1 (collar side 1, Leg, hb=5cm)
30	SG-10	C3-L-1 (collar side 3, Leg, hb=5cm)
31	SG-11	C1-B-1 (collar side 1, Back, hb=5cm)
32	SG-12	C3-B-1 (collar side 3, Back, hb=5cm)
33	SG-13	C1-L-2 (collar side 1, Leg, hb=14cm)
34	SG-14	C3-L-2 (collar side 3, Leg, hb=14cm)
35	SG-15	C1-B-2 (collar side 1, Back, hb=14cm)
36	SG-16	C3-B-2 (collar side 3, Back, hb=14cm)

= This Page is Intentionally Left Blank =

APPENDIX B. RESULTS OF MONONOTIC AXIAL COMPRESSIVE TEST PART-1
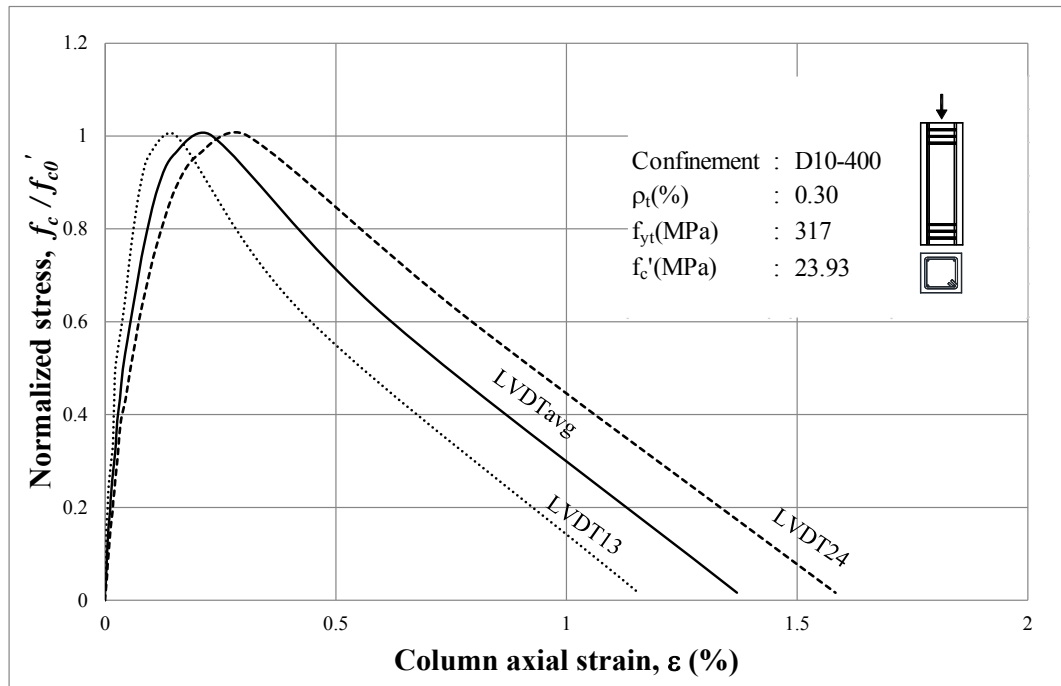
Figure B-1 Column axial stress-strain curves of CS01
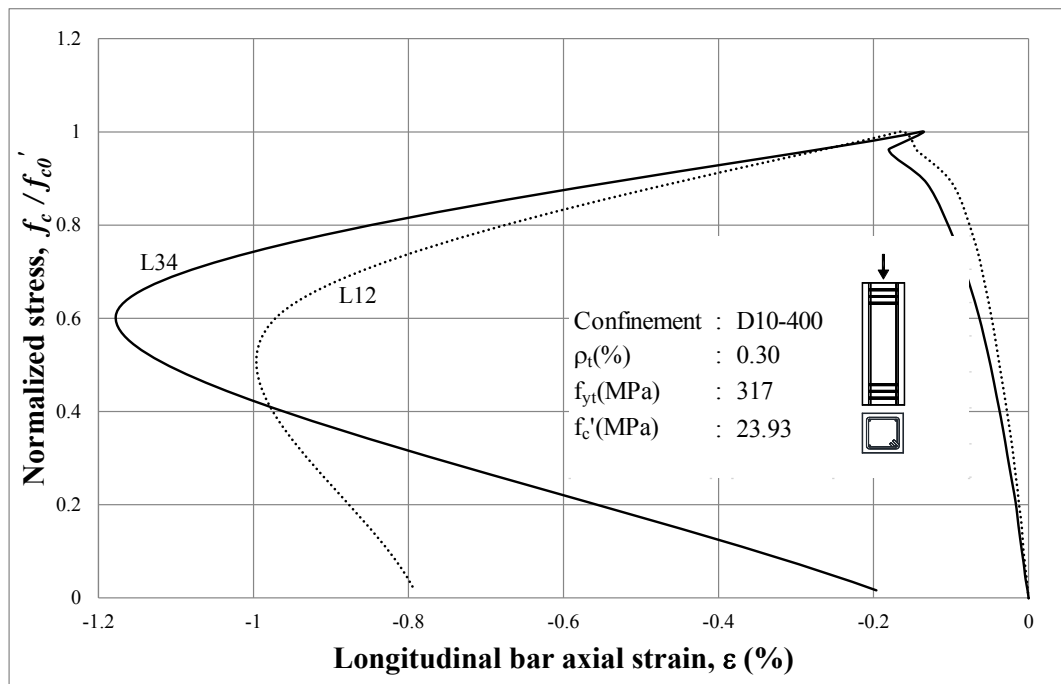
Figure B-2 Column axial stress-longitudinal bar axial strain curves of CS01

(a)   **(b)**

Figure B-3 Specimen CS01: (a) side 1; and (b) side 2 after the completion of the test

(a)   **(b)**

Figure B-4 Specimen CS01: (a) side 3; and (b) side 4 after the completion of the test
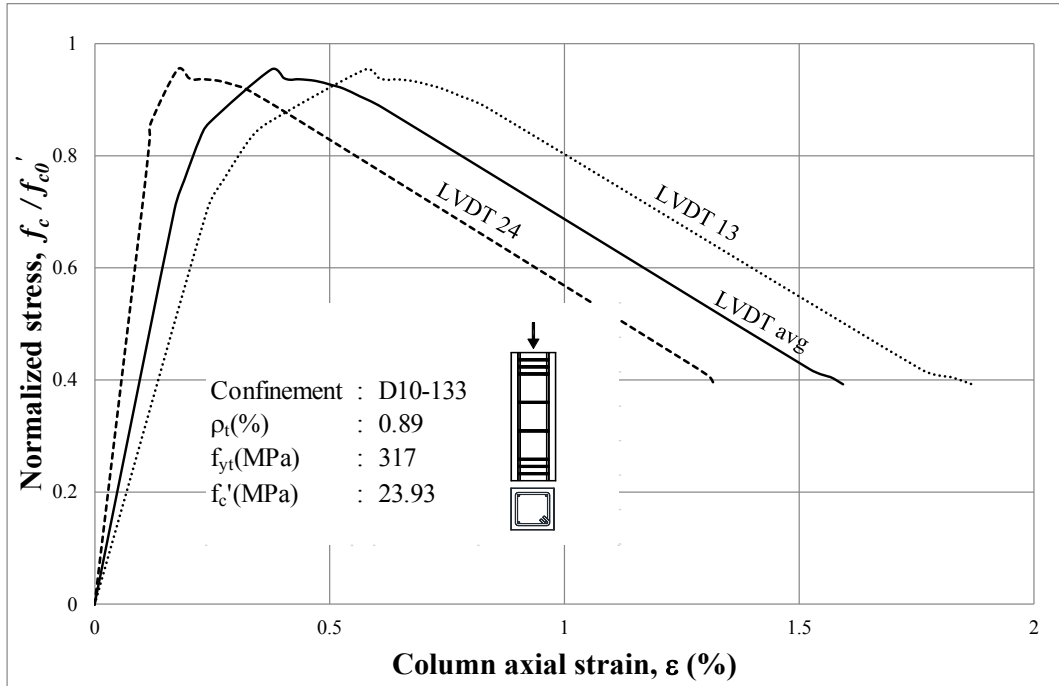
Figure B-5 Column axial stress-strain curves of CS02a
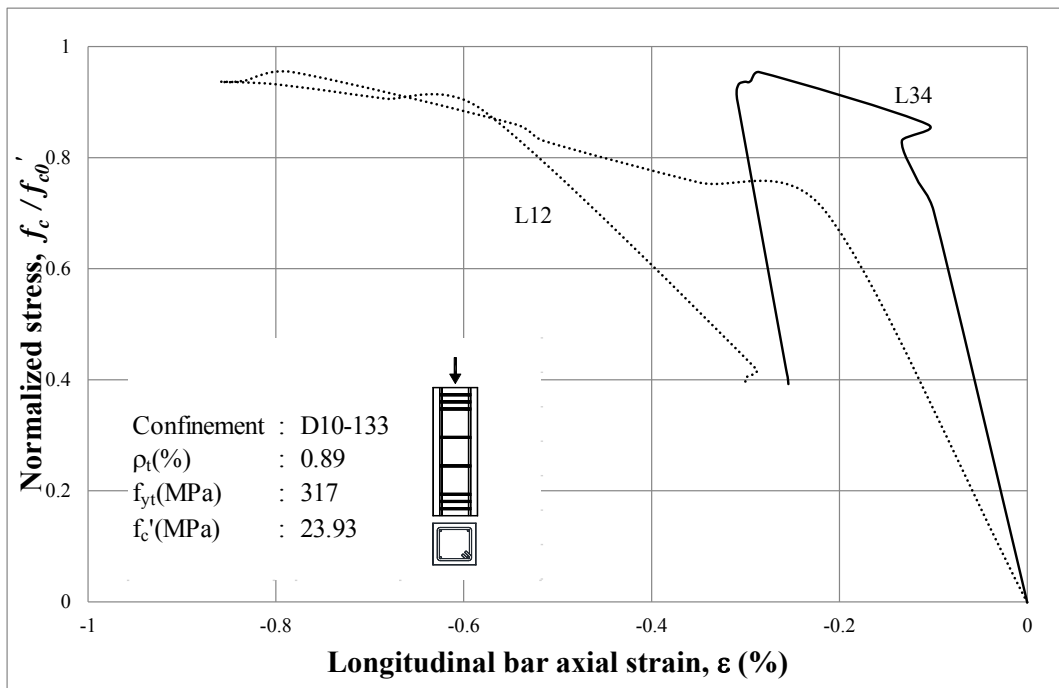
Figure B-6 Column axial stress-longitudinal bar axial strain curves CS02a

251
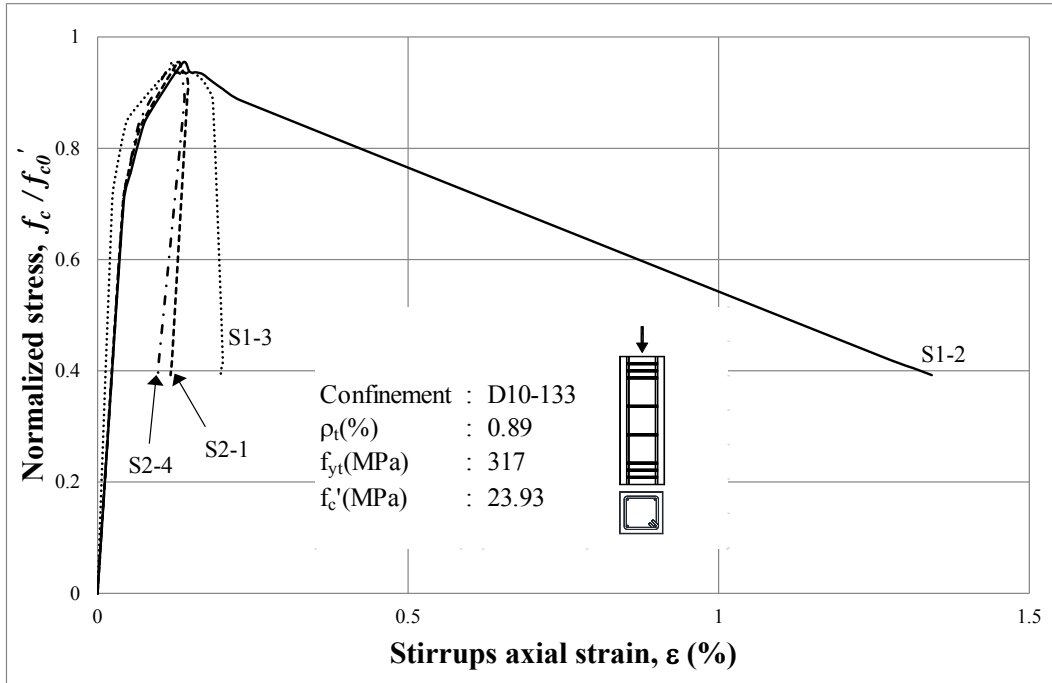
Figure B-7 Column axial stress-stirrups axial strain curves of CS02a

(a)   **(b)**

Figure B-8 Specimen CS02a: (a) side 1; and (b) side 2 after the completion of the test

(a)   **(b)**

Figure B-9 Specimen CS02a: (a) side 3; and (b) side 4 after the completion of the test

Confinement : D10-50
ρ_t(%)   : 2.36
f_{yt}(MPa)   : 317
f_c'(MPa)   : 23.93
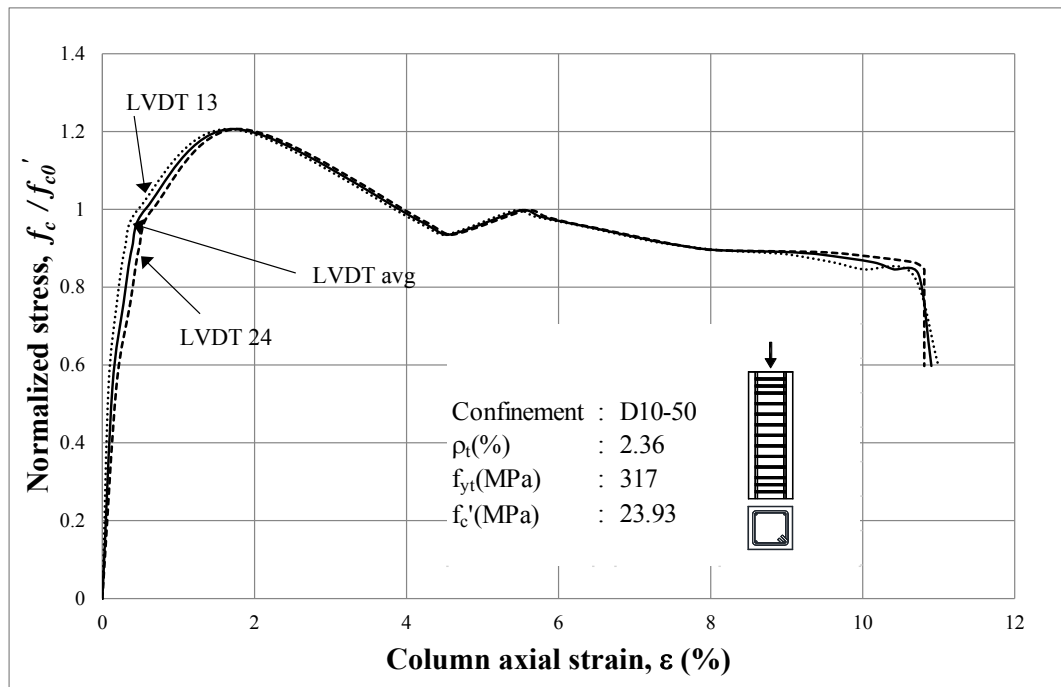
Figure B-10 Column axial stress-strain curves of CS03a
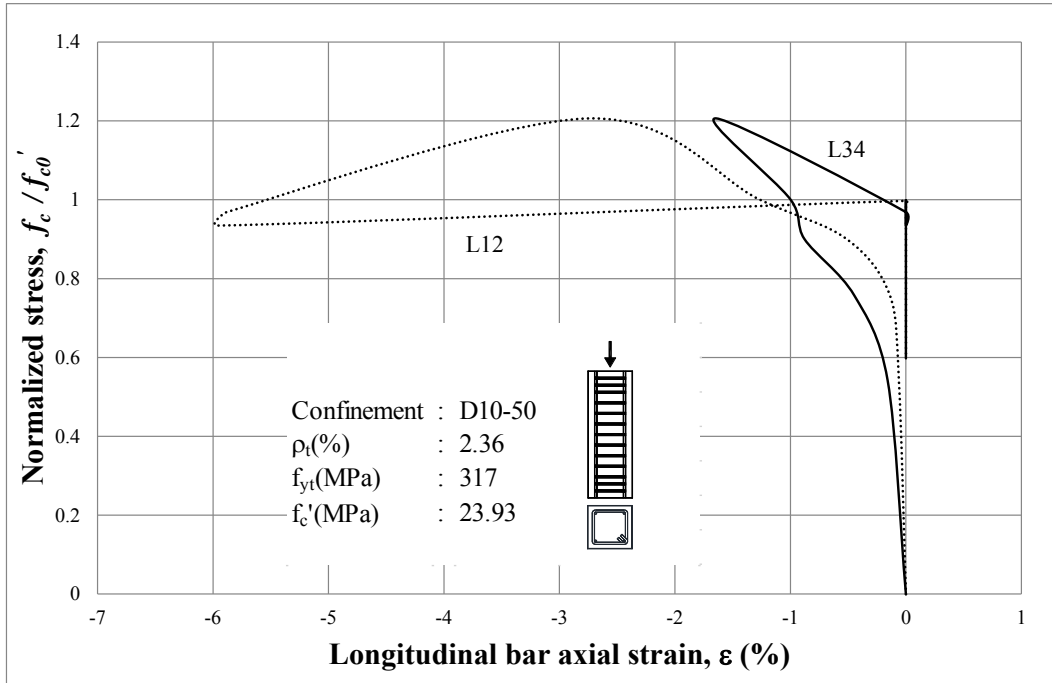
Figure B-11 Column axial stress-longitudinal bar axial strain curves of CS03a

(a)   **(b)**

Figure B-12 Specimen CS03a: (a) side 1; and (b) side 2 after the completion of the test

(a)   **(b)**

Figure B-13 Specimen CS03a: (a) side 3; and (b) side 4 after the completion of the test
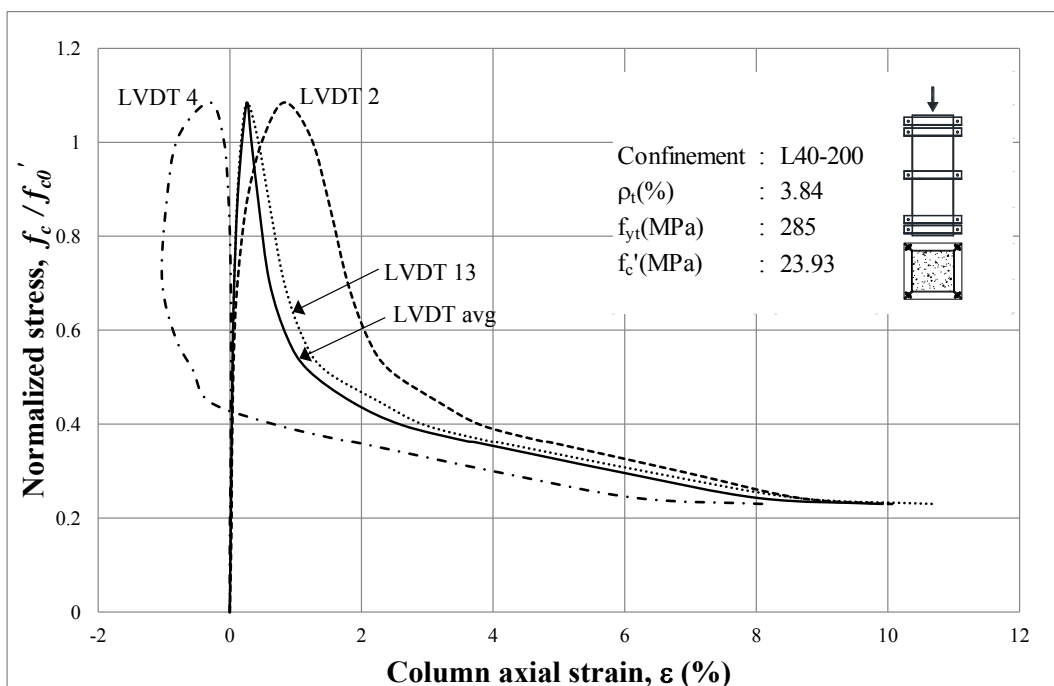
Figure B-14 Column axial stress-strain curves of S01
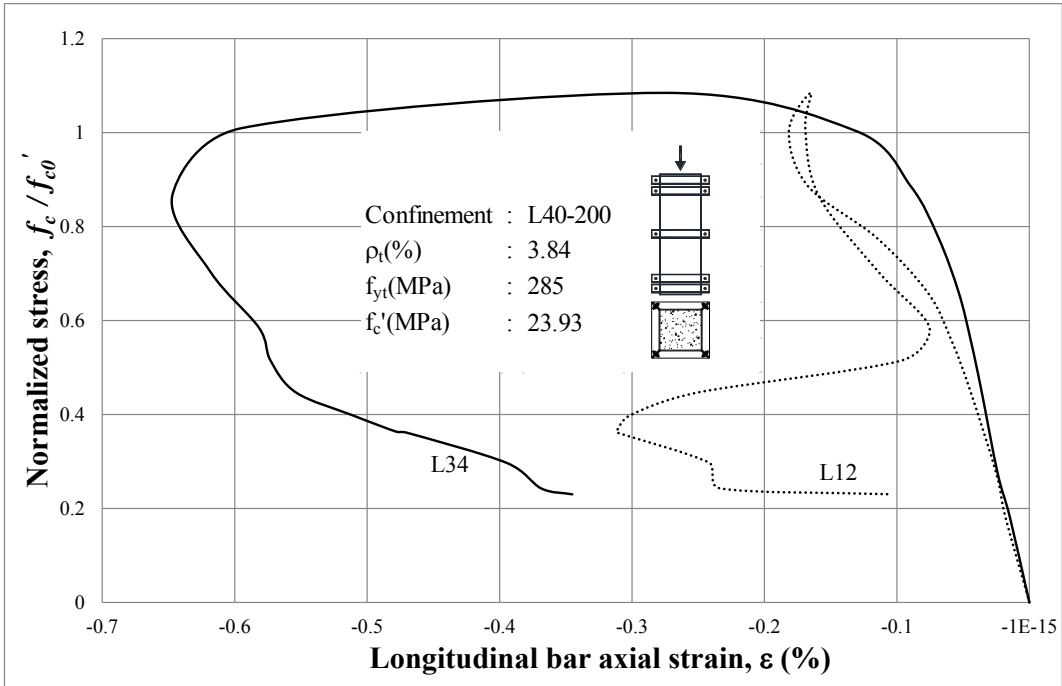
Figure B-15 Column axial stress-longitudinal bar axial strain curves of S01
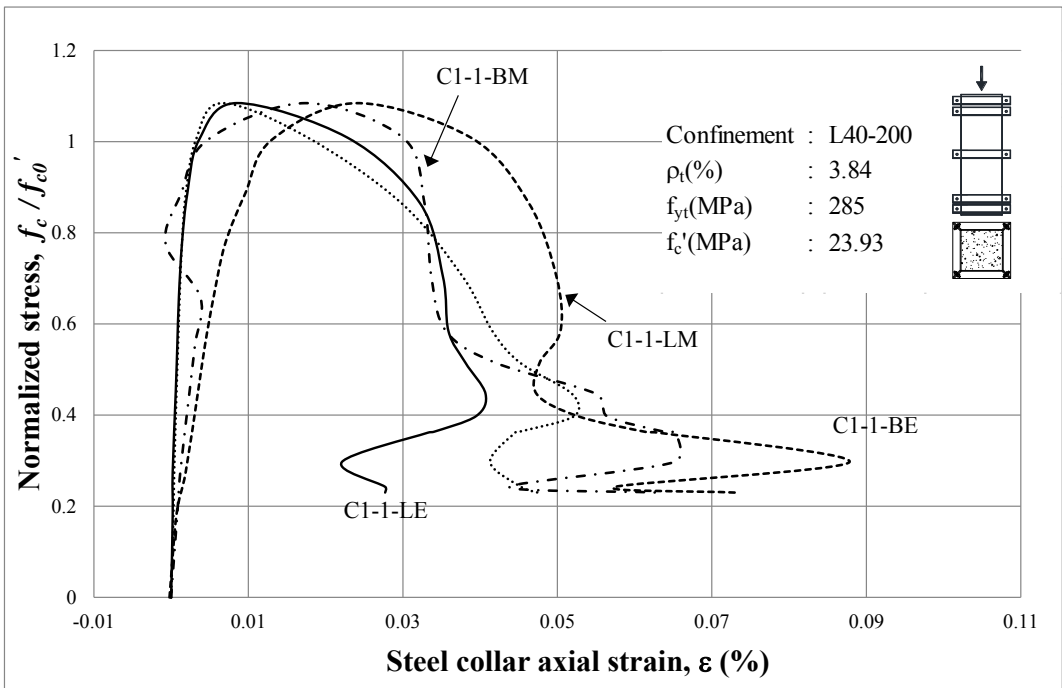
Figure B-16 Column axial stress-steel collar axial strain curves of S01 (Collar 1 Side 1)

256

The graph shows:
- Y-axis: Normalized stress, f_c / f_{c0}', ranging from 0 to 1.2
- X-axis: Steel collar axial strain, ε (%), ranging from -0.1 to 0.8

Curve labels: C1-2-BE, C1-2-LM, C1-2-BM, C1-2-LE

Legend:
Confinement	:	L40-200
ρ_t(%)	:	3.84
f_{yt}(MPa)	:	285
f_c'(MPa)	:	23.93
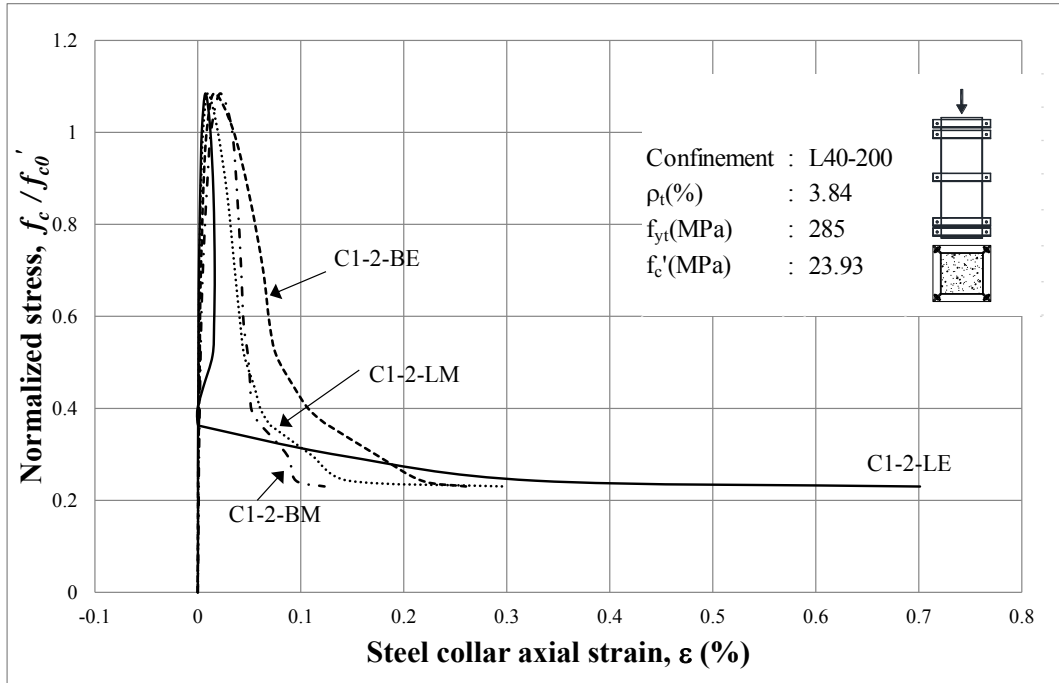
Figure B-17 Column axial stress-steel collar axial strain curves of S01 (Collar 1 Side 2)

(a)   **(b)**
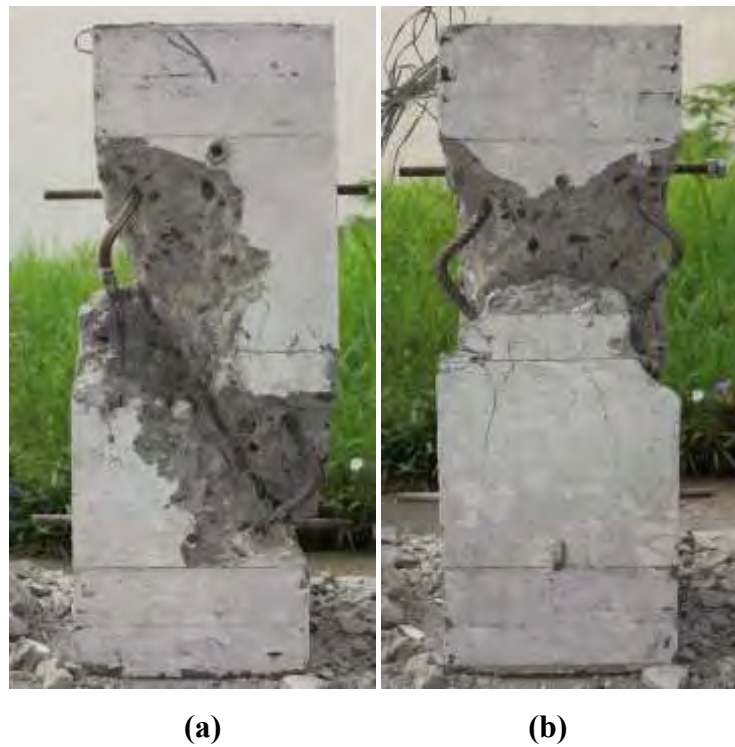
Figure B-18 Specimen S01: (a) side 1; and (b) side 2 after the completion of the test

(a)   (b)

Figure B-19 Specimen S01: (a) side 3; and (b) side 4 after the completion of the test
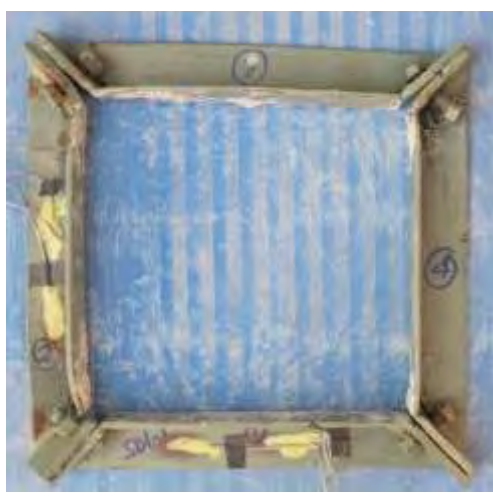
Figure B-20 Collar 1 of S01 after the completion of the test
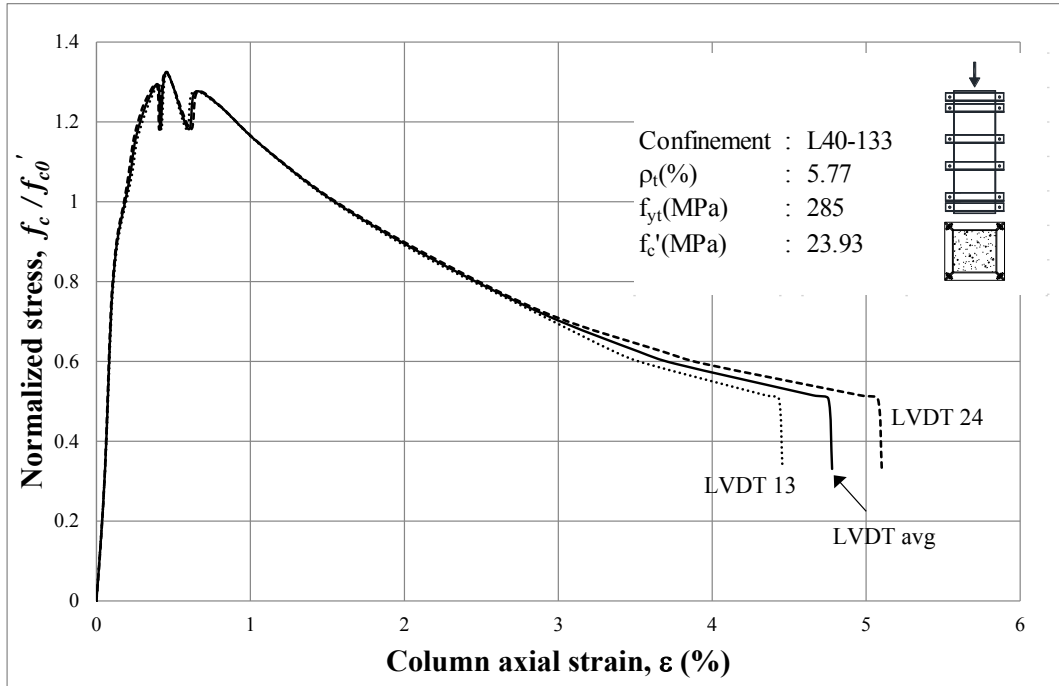
Figure B-21 Column axial stress-strain curves of S02
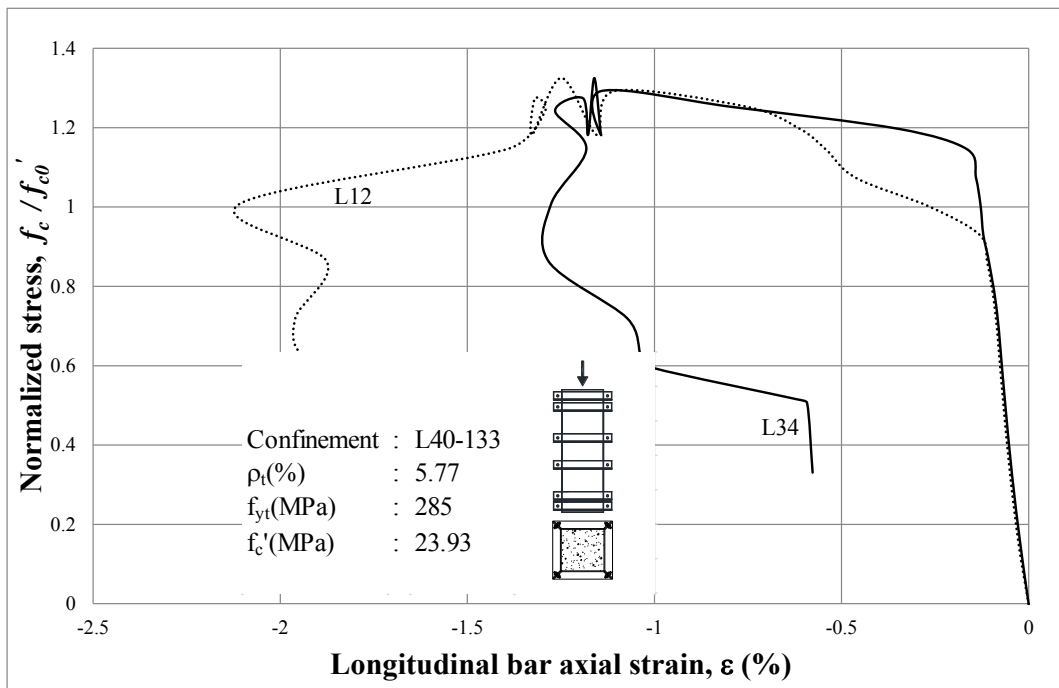
Figure B-22 Column axial stress-longitudinal bar axial strain curves of S02

259
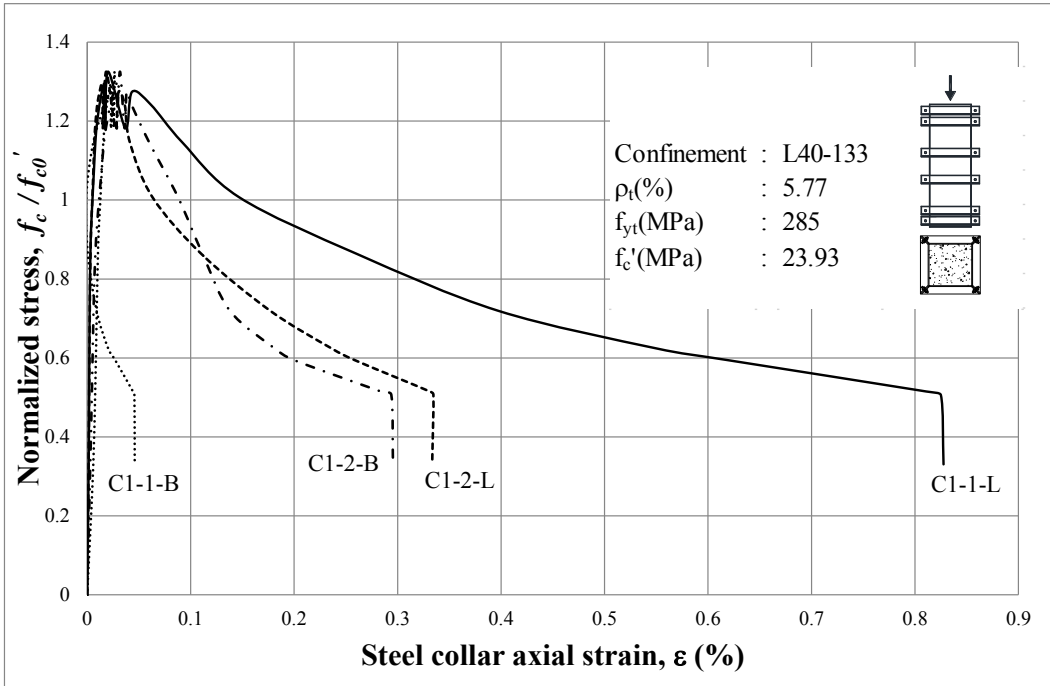
Figure B-23 Column axial stress-steel collar axial strain curves of S02 (Collar 1)
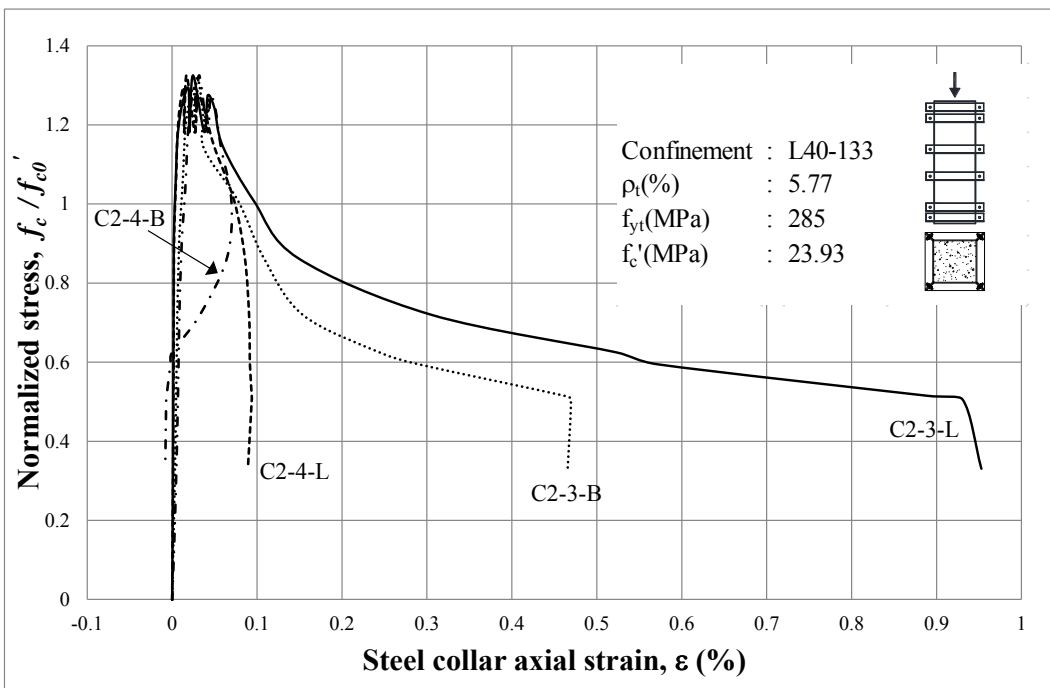
Figure B-24 Column axial stress-steel collar axial strain curves of S02 (Collar 2)

260

Figure B-25 Specimen S02 after the completion of the test

(a)   (b)

Figure B-26 Specimen S02: (a) side 1; and (b) side 2 after the completion of the test

(a)   (b)

Figure B-27 Specimen S02: (a) side 3; and (b) side 4 after the completion of the test
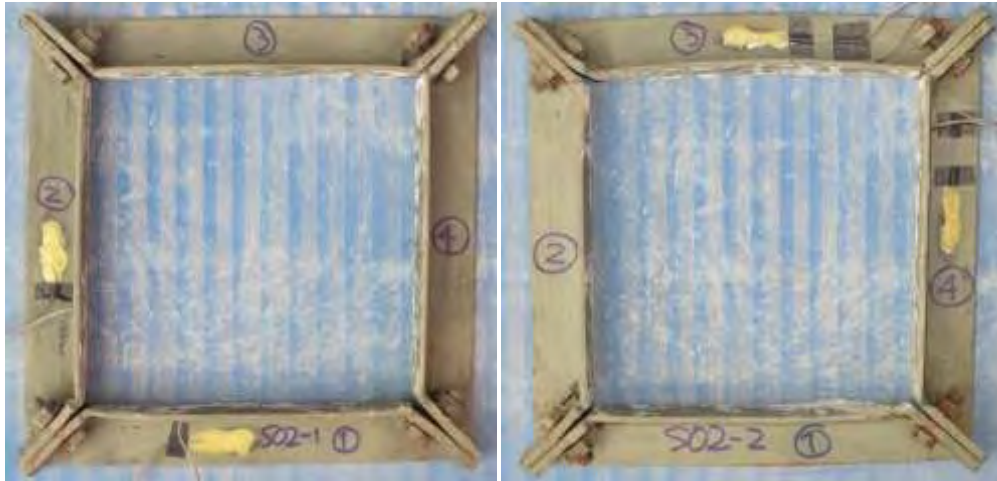
(a)   (b)

Figure B-28 Collars: (a)1; and (b)2 of S02 after the completion of the test
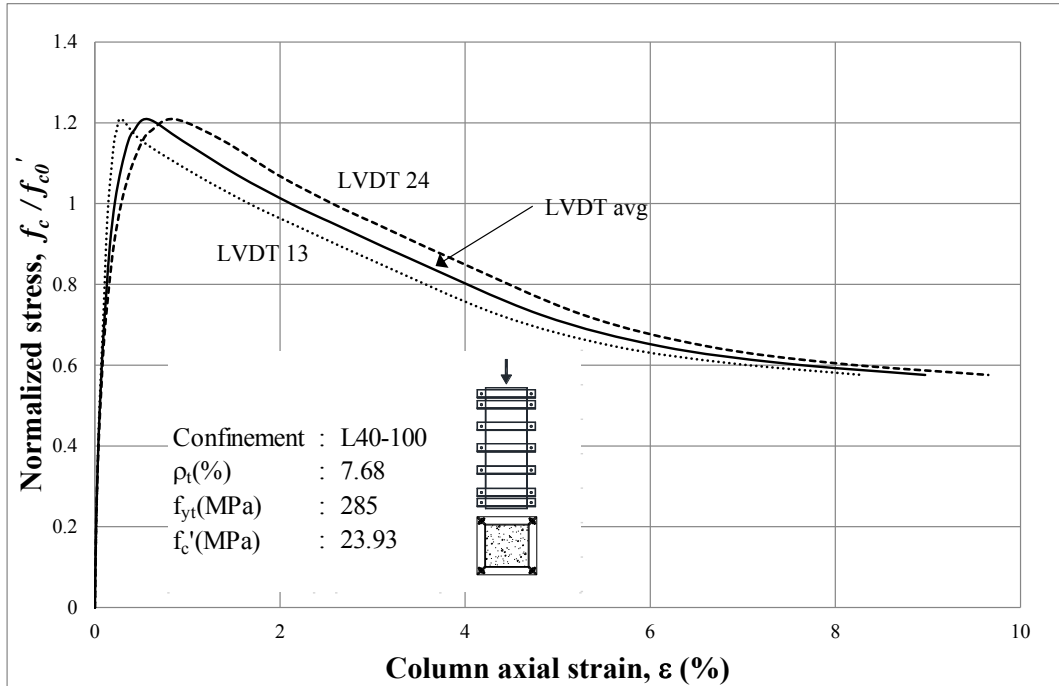
Figure B-29 Column axial stress-strain curves of S03
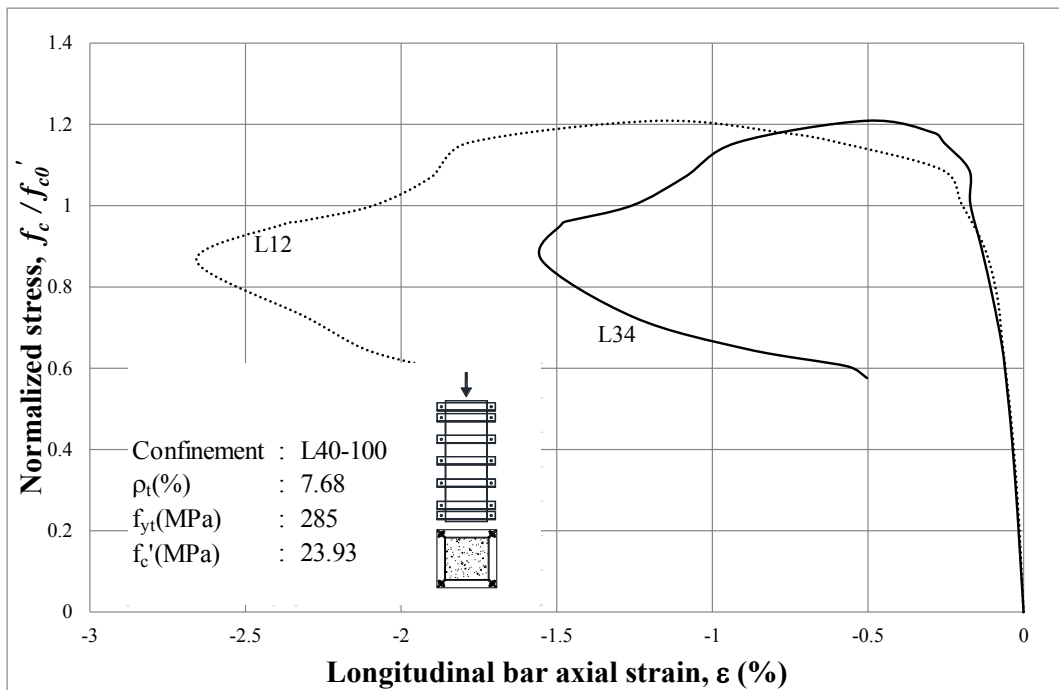
Figure B-30 Column axial stress-longitudinal bar axial strain curves of S03

263
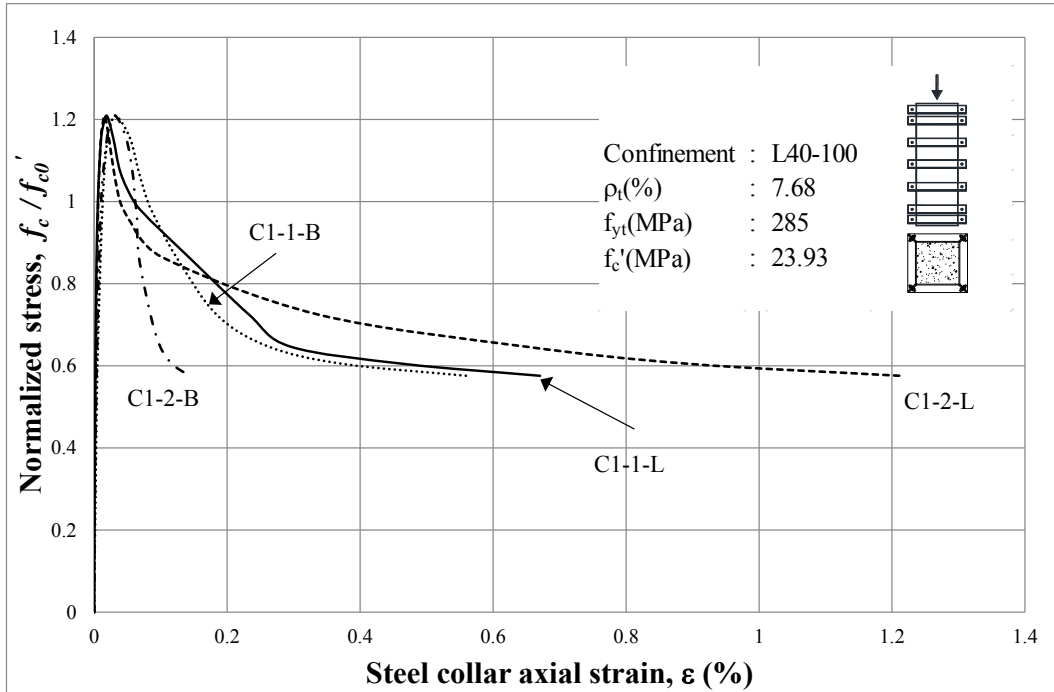
Figure B-31 Column axial stress-steel collar axial strain curves of S03 (Collar 1)
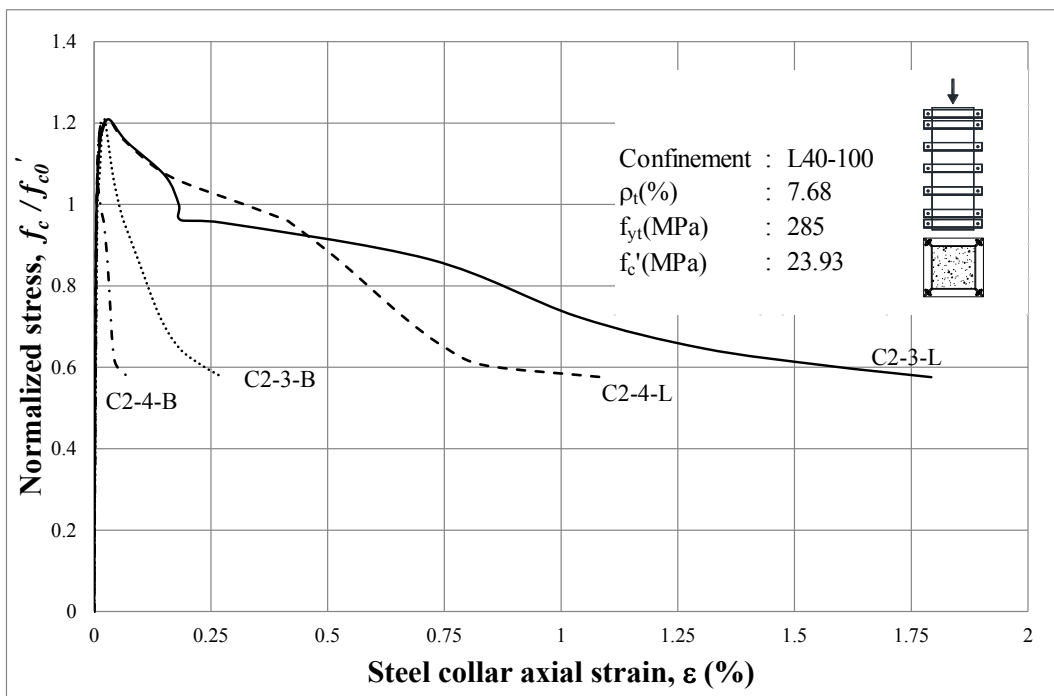
Figure B-32 Column axial stress-steel collar axial strain curves of S03 (Collar 2)

264

(a)   (b)

Figure B-33 Specimen S03: (a) side 1; and (b) side 2 after the completion of the test

(a)   (b)

Figure B-34 Specimen S03: (a) side 3; and (b) side 4 after the completion of the test
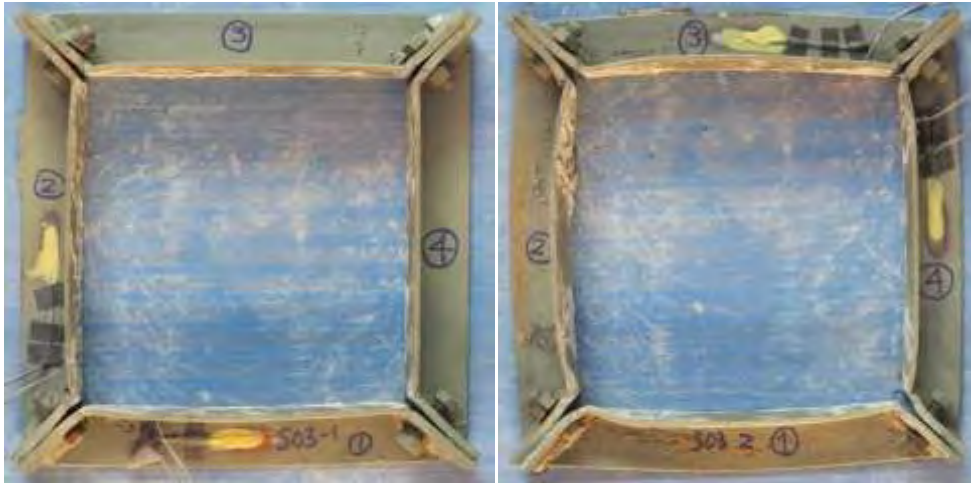
(a)   (b)

Figure B-35 Collars: (a) 1; and (b) 2 of S03 after the completion of the test

Figure B-36 Collar 3 of S03 after the completion of the test
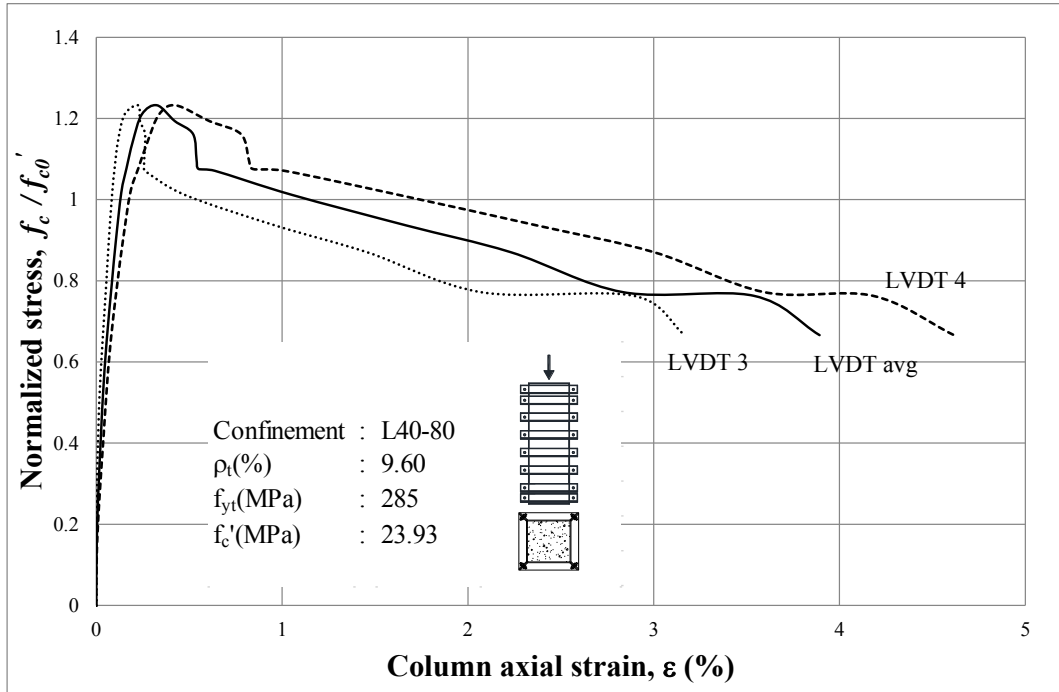
Figure B-37 Column axial stress-strain curves of S04
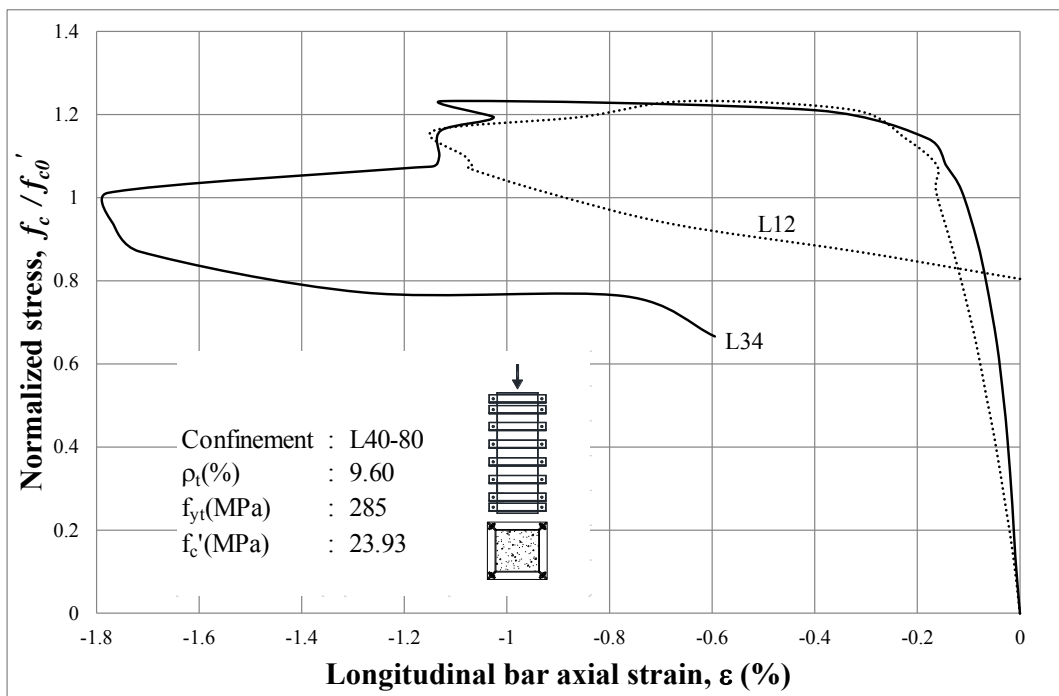
Figure B-38 Column axial stress-longitudinal bar axial strain curves of S04

267
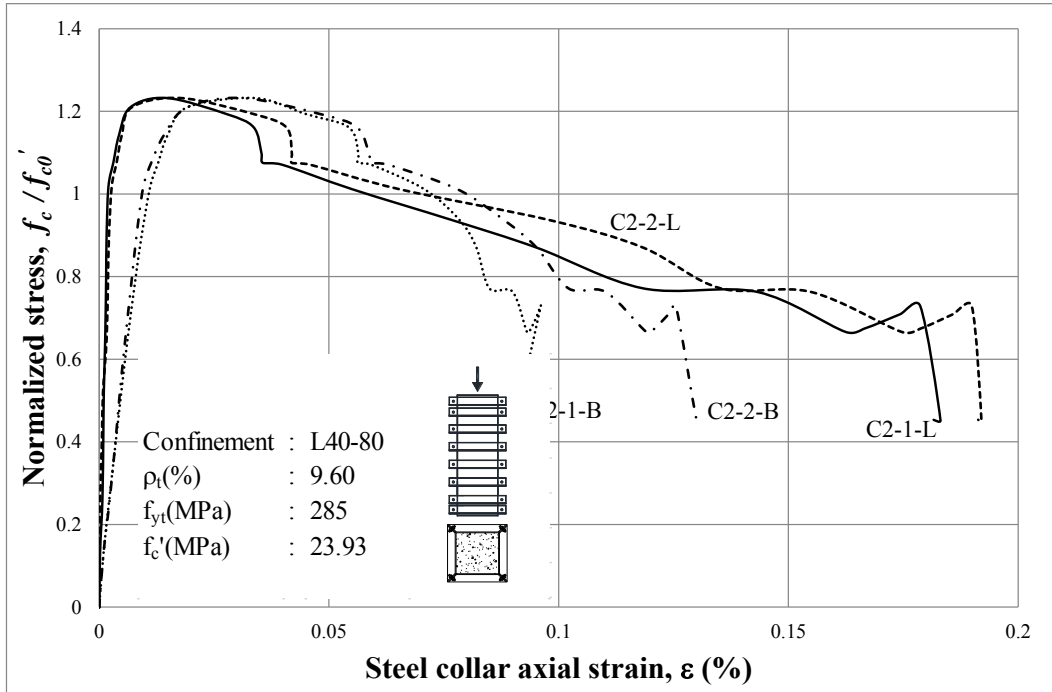
Figure B-39 Column axial stress-steel collar axial strain curves of S04 (Collar 2)
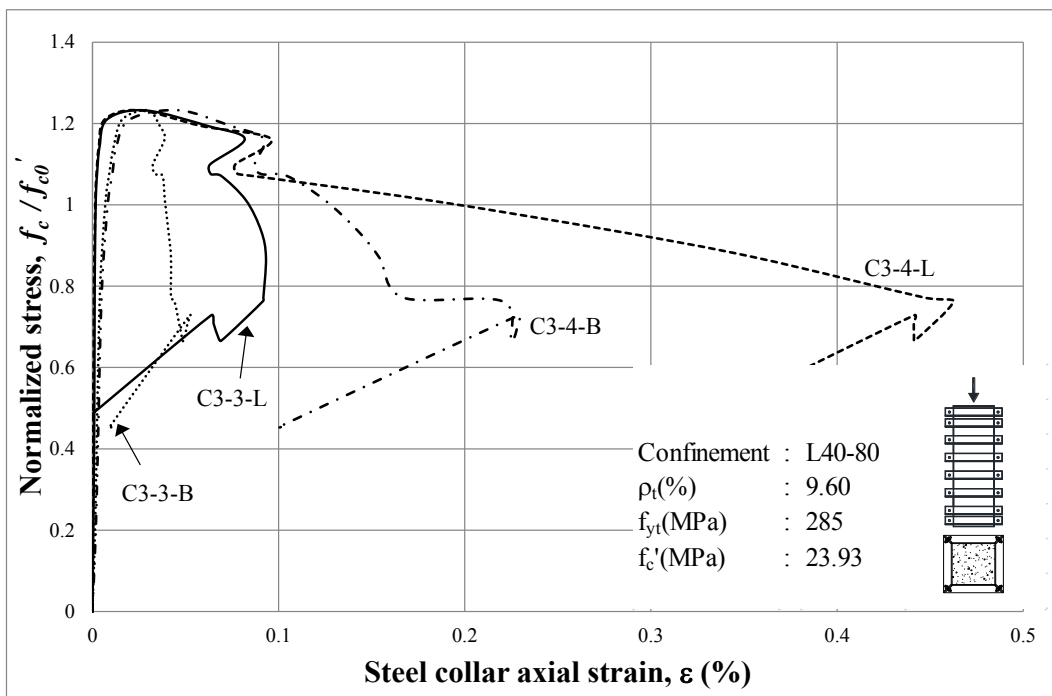
Figure B-40 Column axial stress-steel collar axial strain curves of S04 (Collar 3)

268

(a)   (b)

Figure B-41 Specimen S04: (a) side 1; and (b) side 2 after the completion of the test

(a)   (b)

Figure B-42 Specimen S04: (a) side 3; and (b) side 4 after the completion of the test
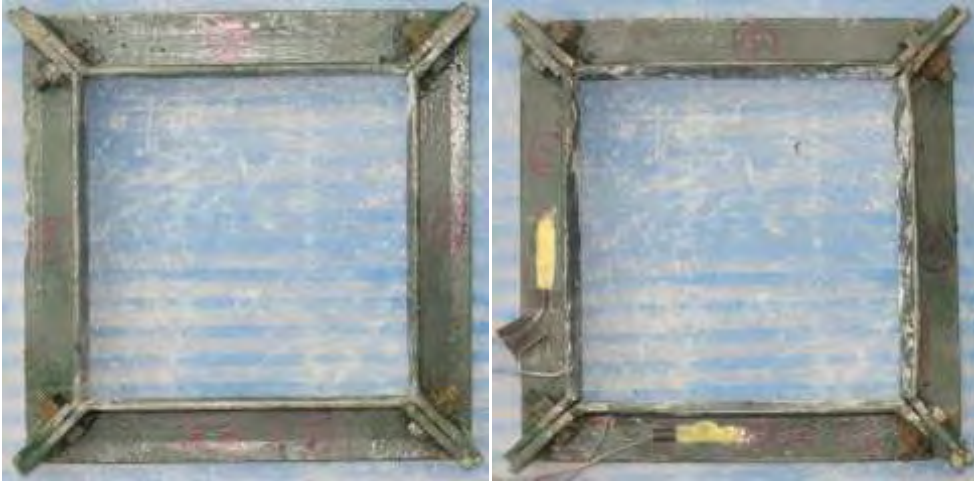
(a)   (b)

Figure B-43 Collars: (a) 1; and (b) 2 of S04 after the completion of the test

(a)   (b)

Figure B-44 Collars: (a) 3; and (b) 4 of S04 after the completion of the test
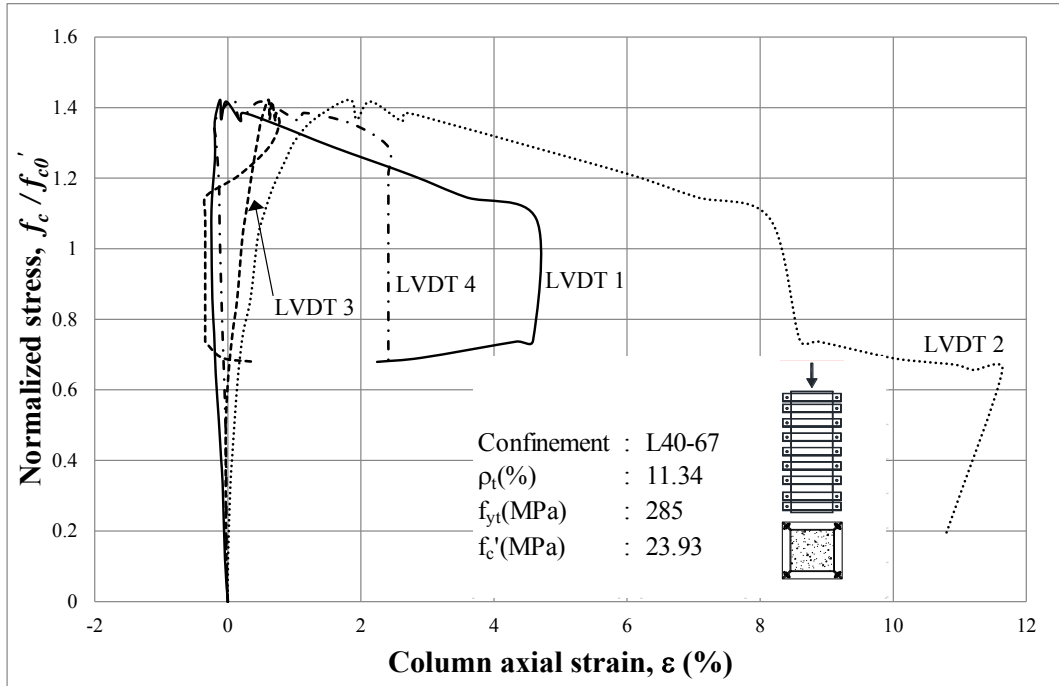
Figure B-45 Column axial stress-strain curves of S05
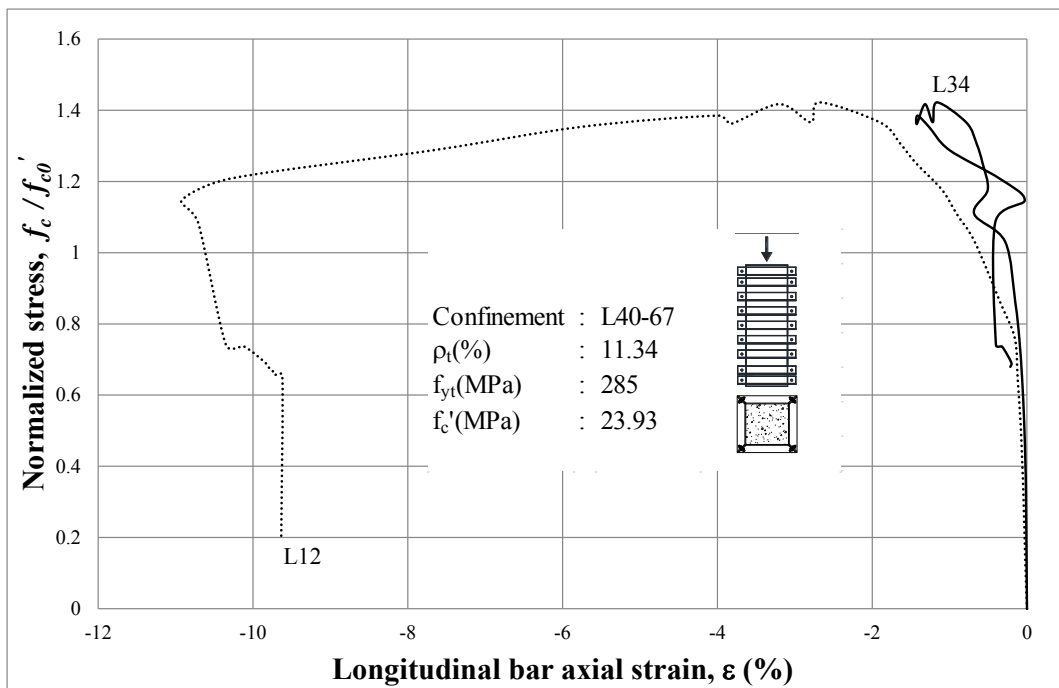
Figure B-46 Column axial stress-longitudinal bar axial strain curves of S05

271
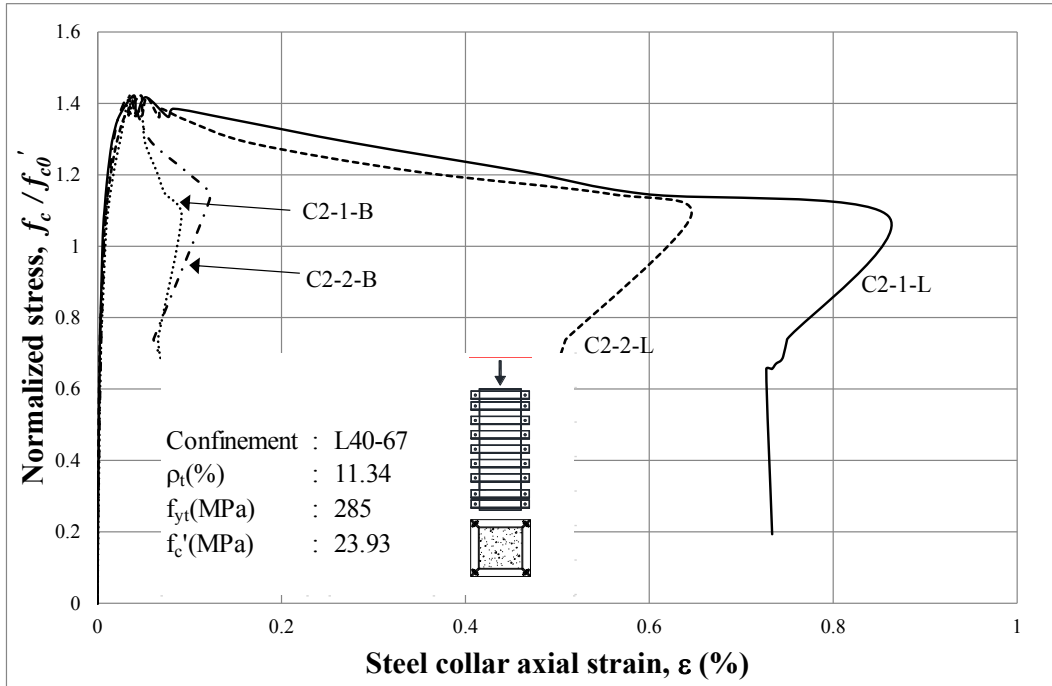
Figure B-47 Column axial stress-steel collar axial strain curves of S05 (Collar 2)

(a)   **(b)**

Figure B-48 Specimen S05: (a) side 1; and (b) side 2 after the completion of the test

(a)   **(b)**

Figure B-49 Specimen S05: (a) side 3; and (b) side 4 after the completion of the test
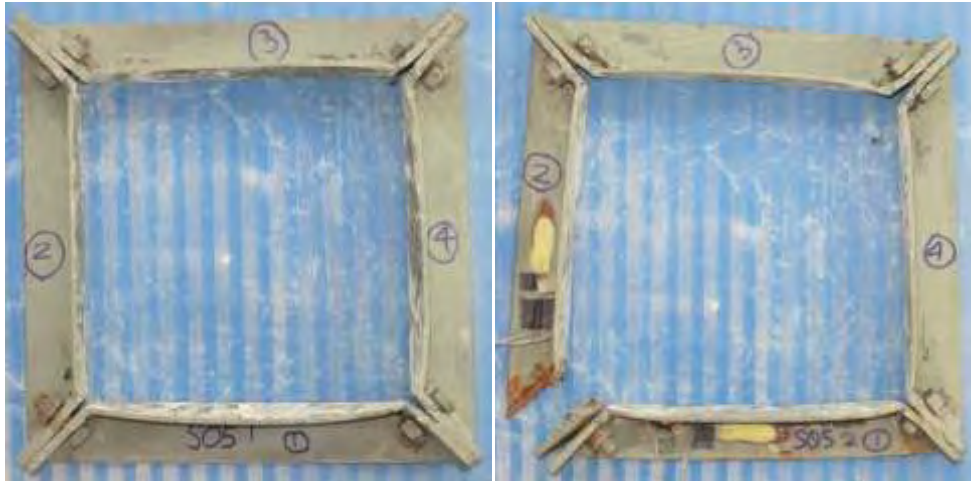
(a)   **(b)**

Figure B-50 Collars: (a) 1; and (b) 2 of S05 after the completion of the test
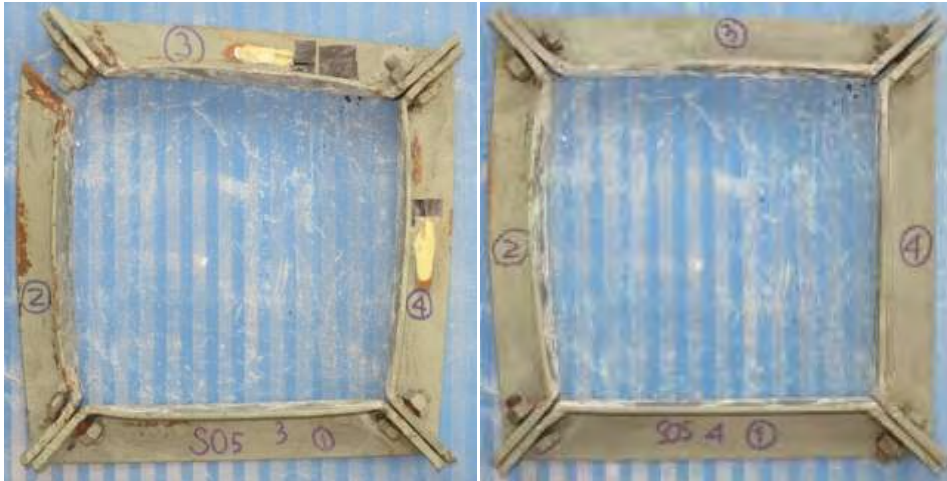
(a)   (b)

Figure B-51 Collars: (a) 3; and (b) 4 of S05 after the completion of the test

Figure B-52 Collar 5 of S05 after the completion of the test

APPENDIX C. RESULTS OF MONONOTIC AXIAL COMPRESSIVE TEST PART-2
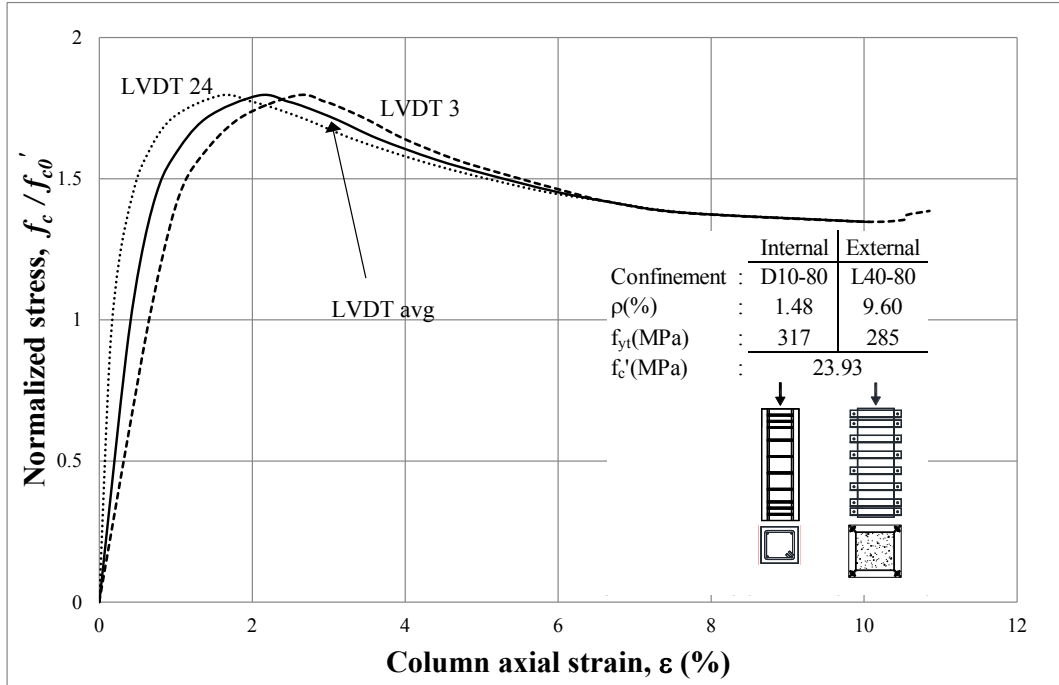
Figure C-1 Column axial stress-strain curves of S04a
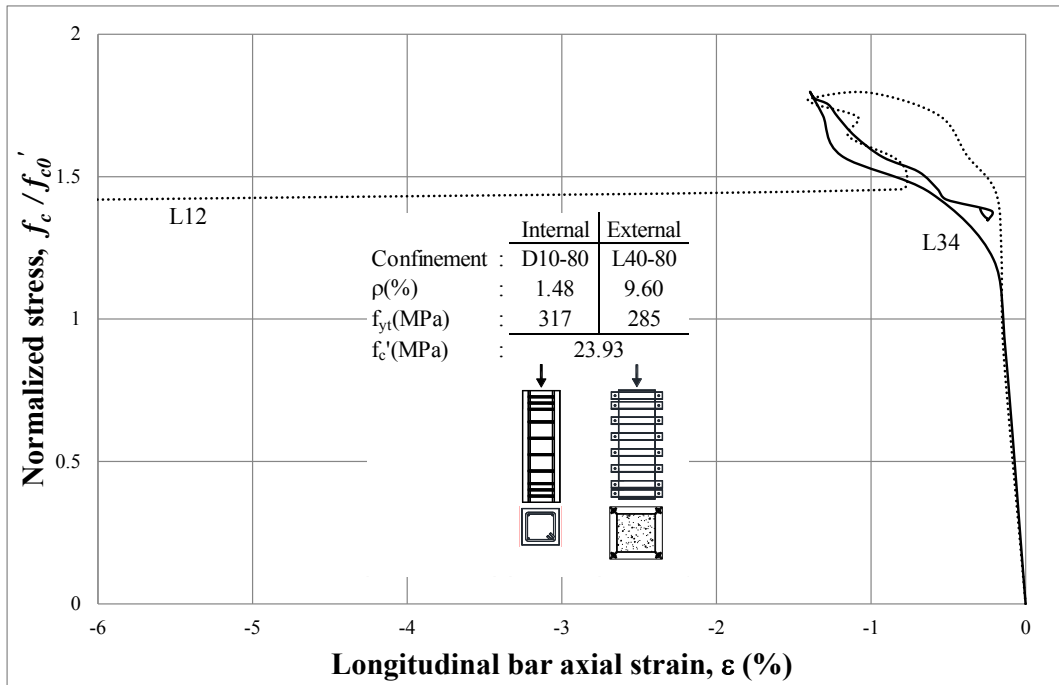
Figure C-2 Column axial stress-longitudinal bar axial strain curves of S04a
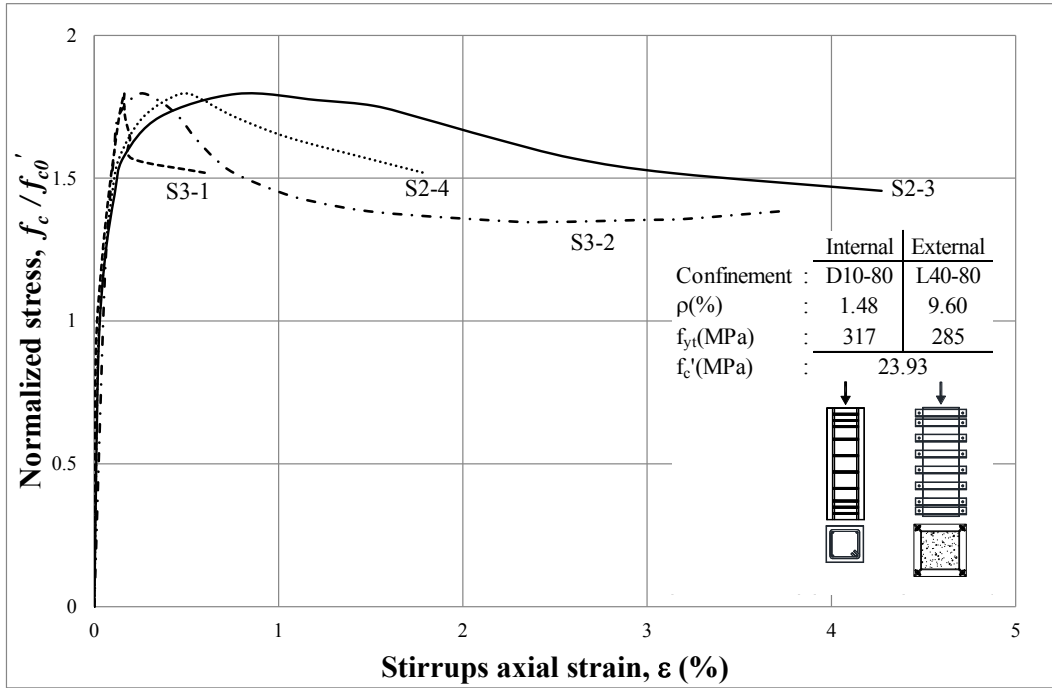
Figure C-3 Column axial stress-stirrups axial strain curves of S04a
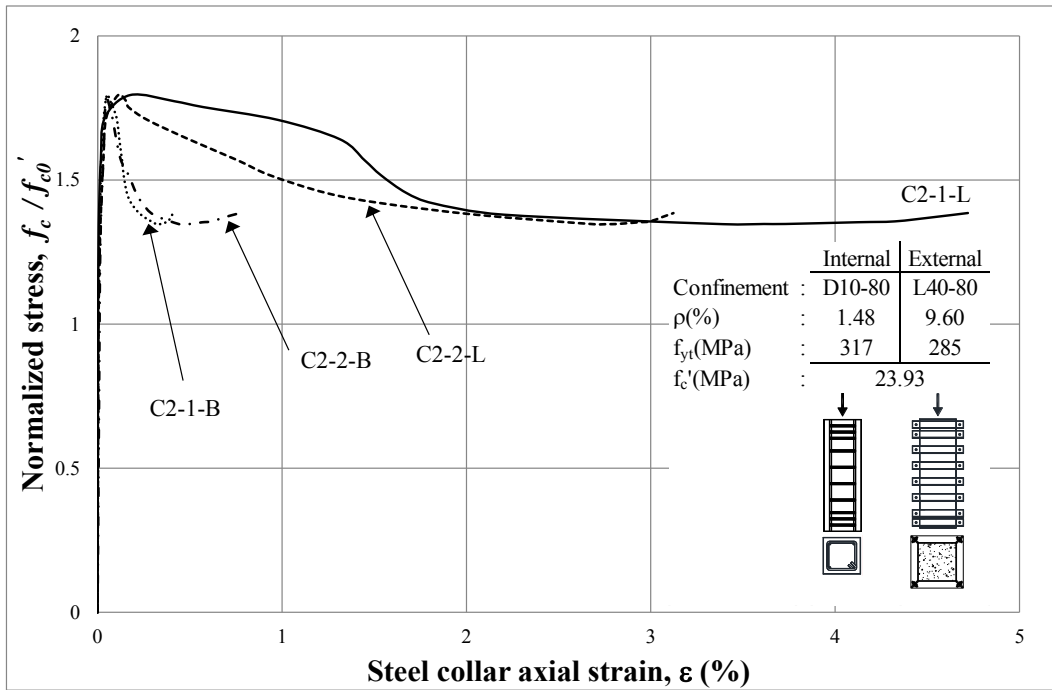
Figure C-4 Column axial stress-steel collar axial strain curves of S04a (Collar 2)

276
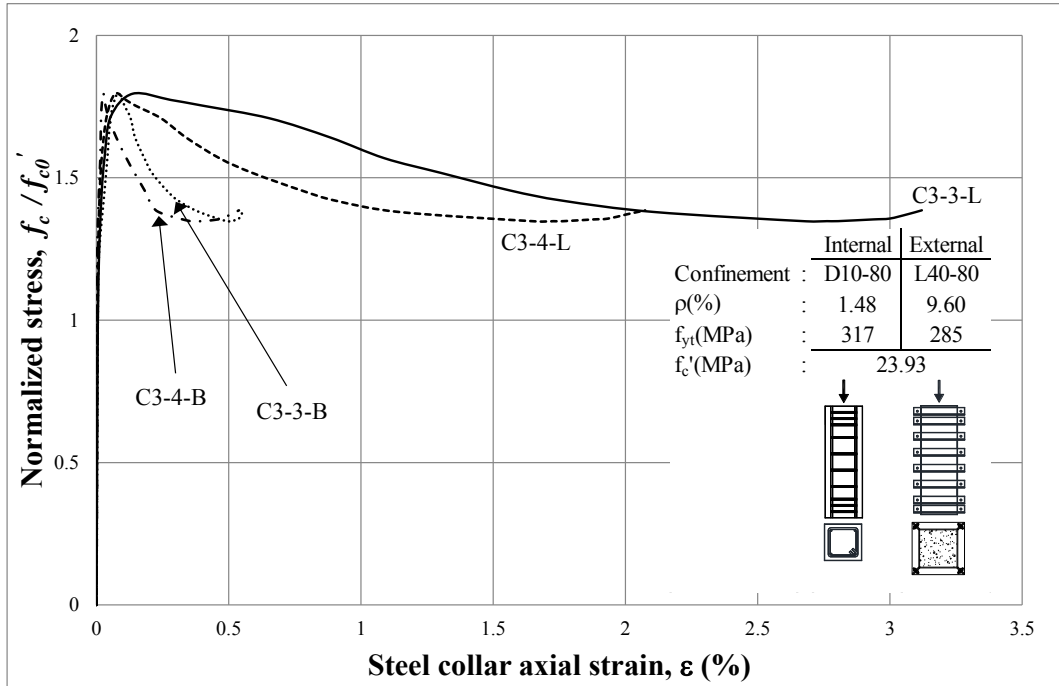
Figure C-5 Column axial stress-steel collar axial strain curves of S04a (Collar 3)

(a)	**(b)**
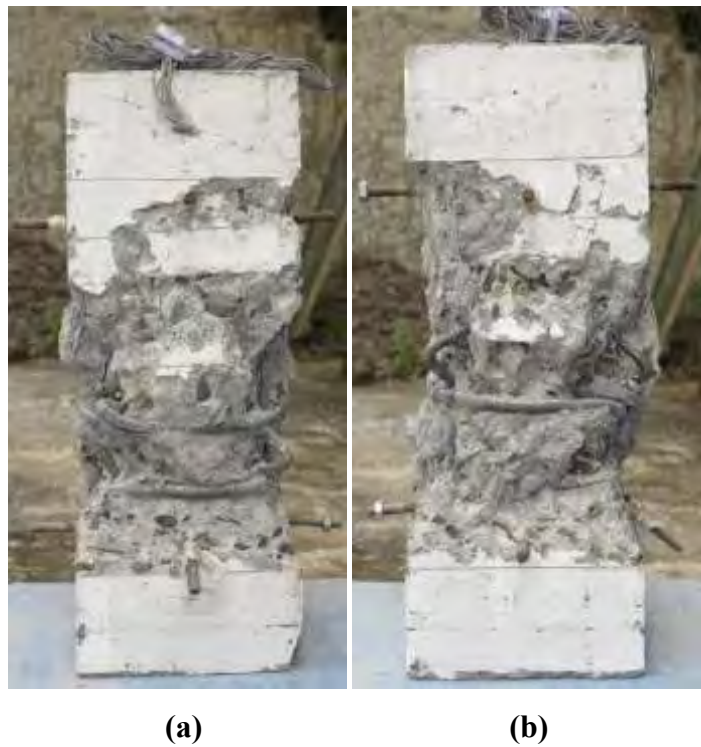
Figure C-6 Specimen S04a: (a) side 1; and (b) side 2 after the completion of the test

(a)   **(b)**

Figure C-7 Specimen S04a: (a) side 3; and (b) side 4 after the completion of the test
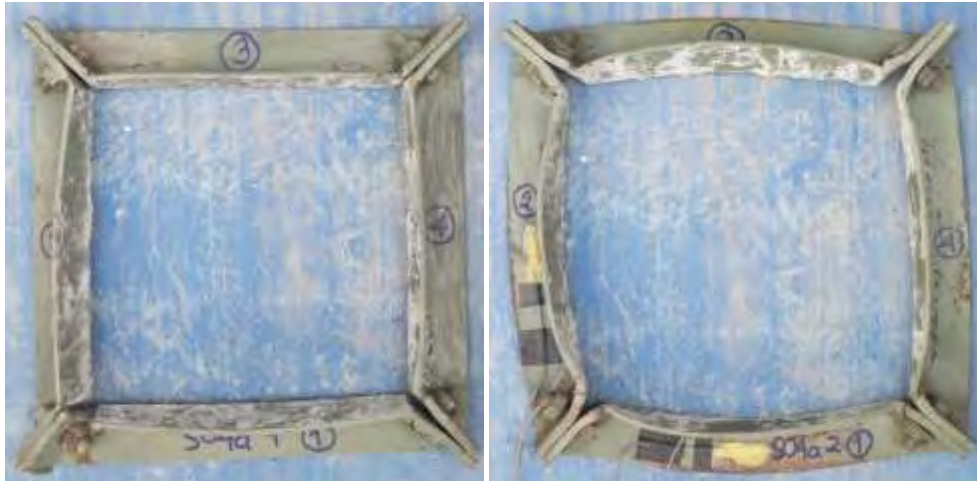
(a)   **(b)**

Figure C-8 Collars: (a) 1; and (b) 2 of S04a after the completion of the test

(a) **(b)**
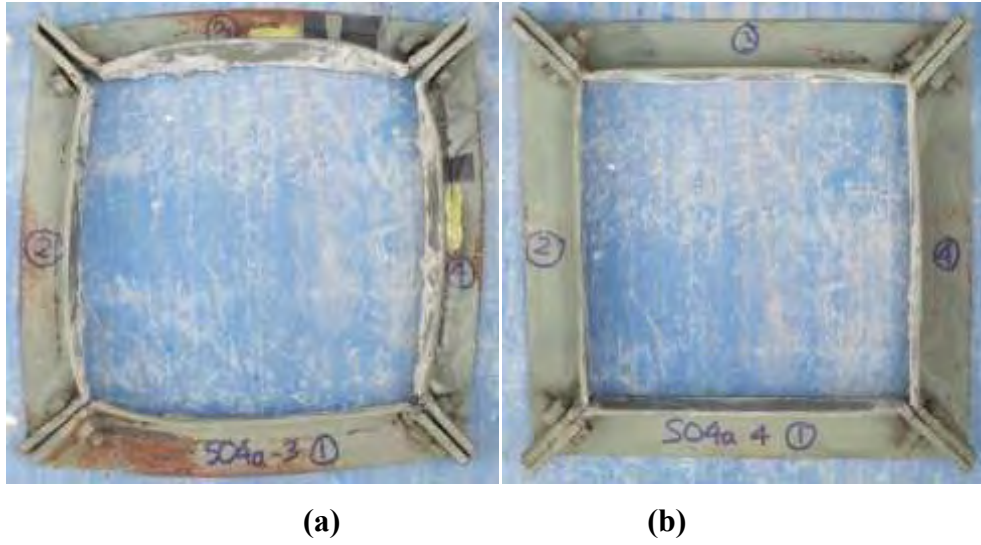
Figure C-9 Collars: (a) 3; and (b) 4 of S04a after the completion of the test
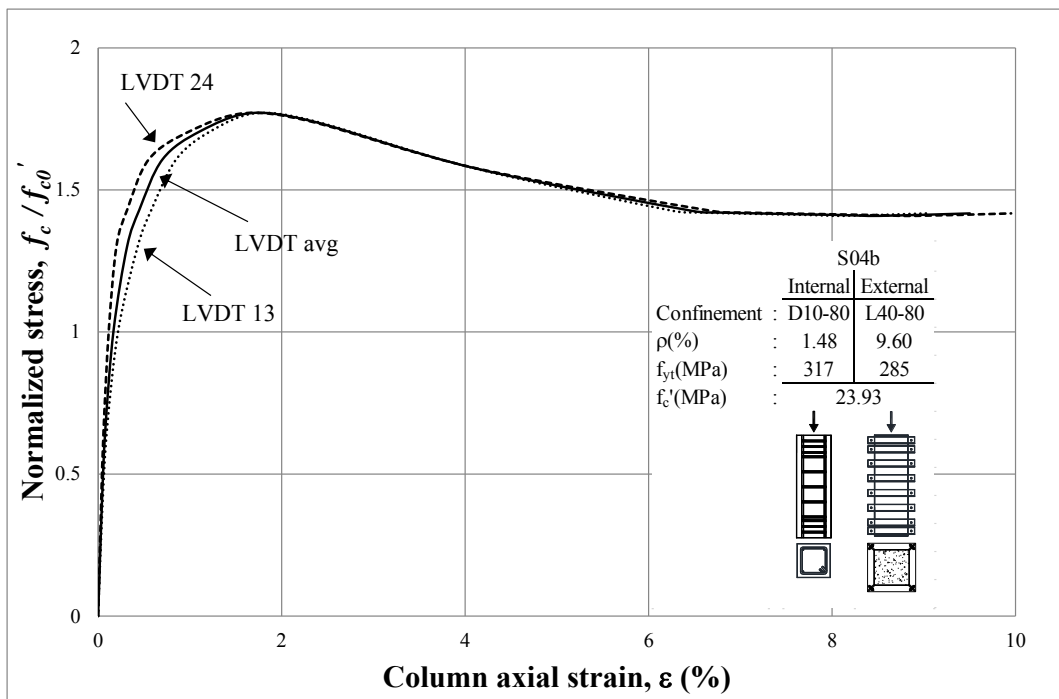
Figure C-10 Column axial stress-strain curves of S04b
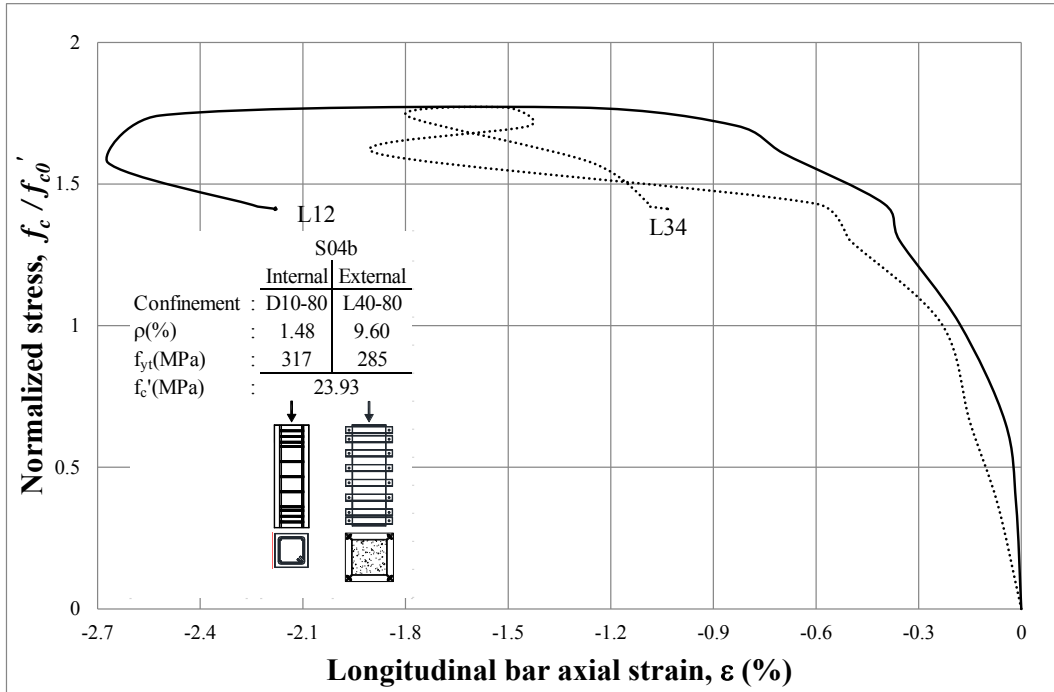
Figure C-11 Column axial stress-longitudinal bar axial strain curves of S04b
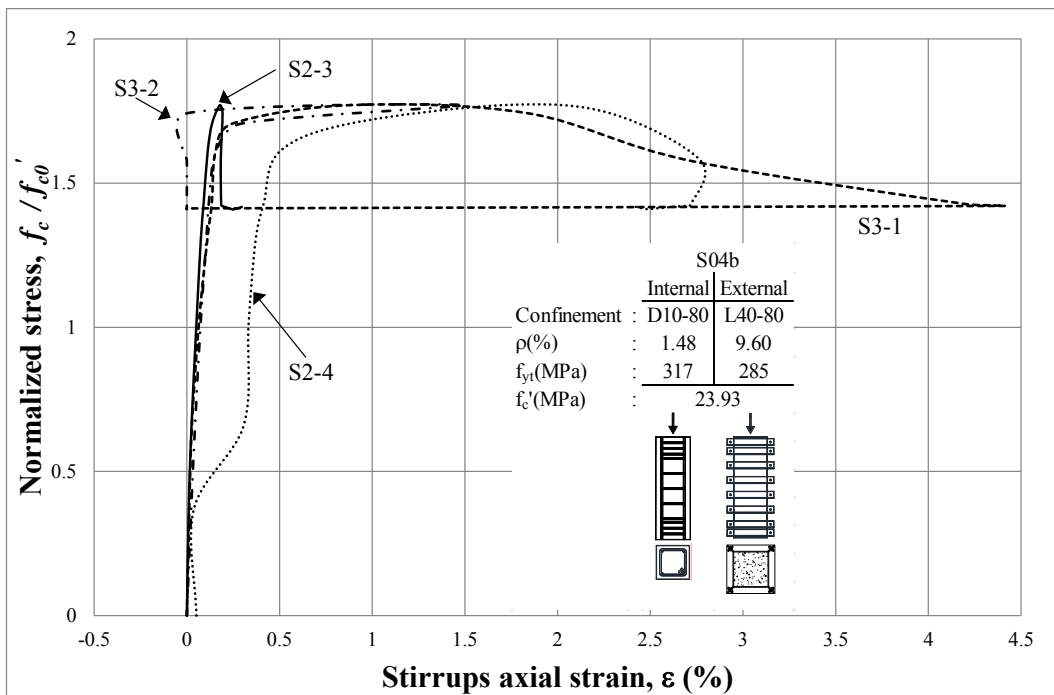
Figure C-12 Column axial stress-stirrups axial strain curves of S04b
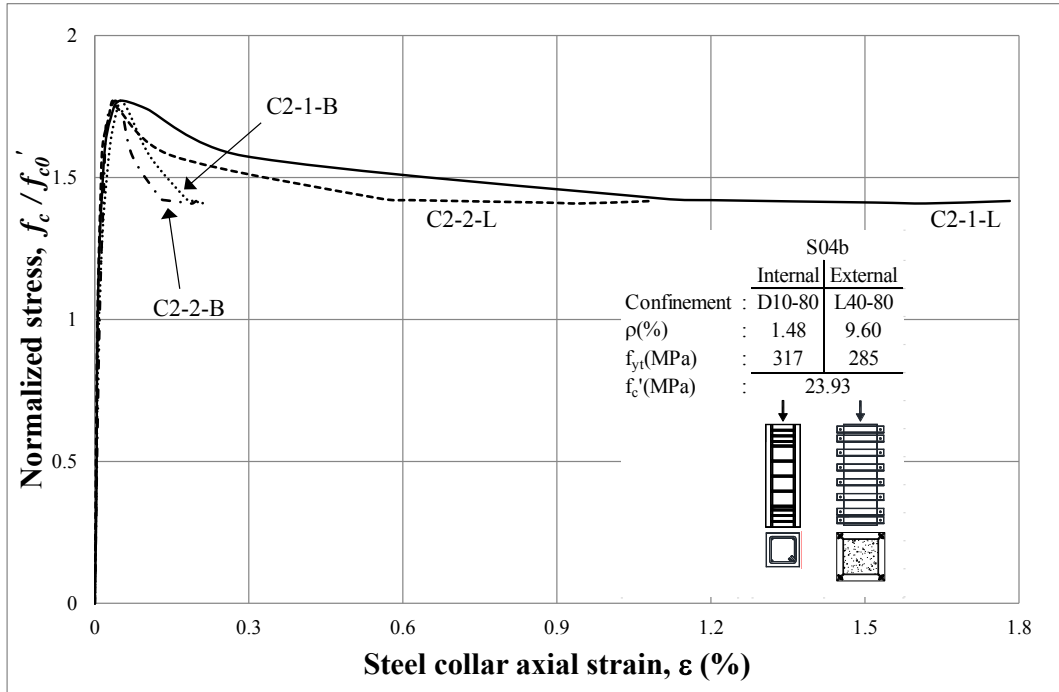
Figure C-13 Column axial stress-steel collar axial strain curves of S04b (Collar 2)
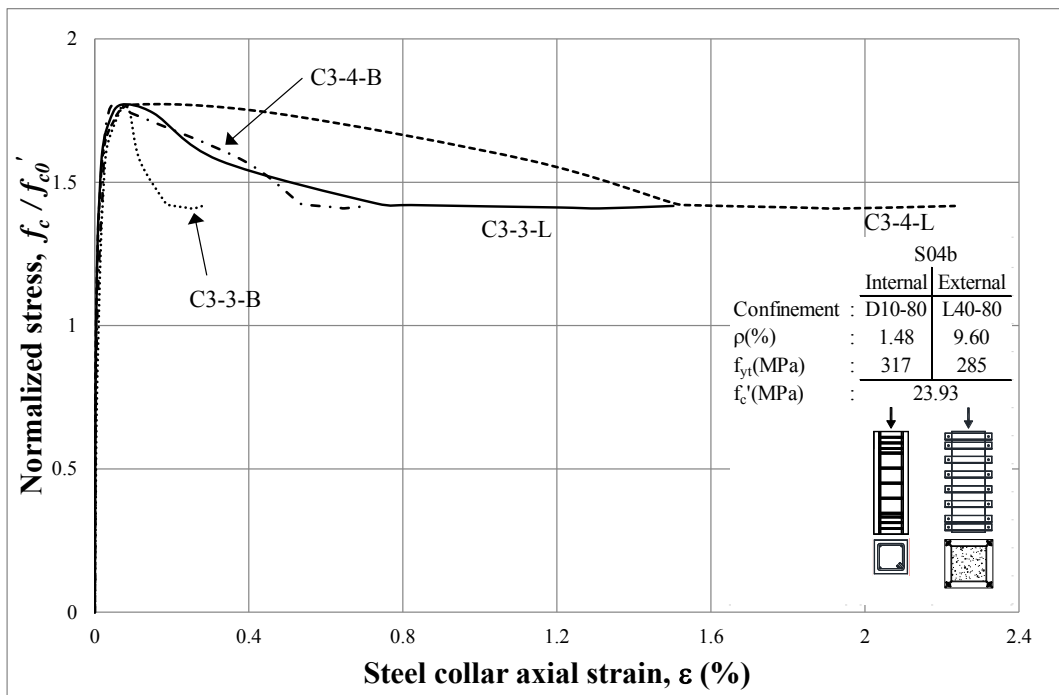
Figure C-14 Column axial stress-steel collar axial strain curves of S04b (Collar 3)

281

(a)   (b)

Figure C-15 Specimen S04b: (a) side 1; and (b) side 2 after the completion of the test

(a)   (b)

Figure C-16 Specimen S04b: (a) side 3; and (b) side 4 after the completion of the test
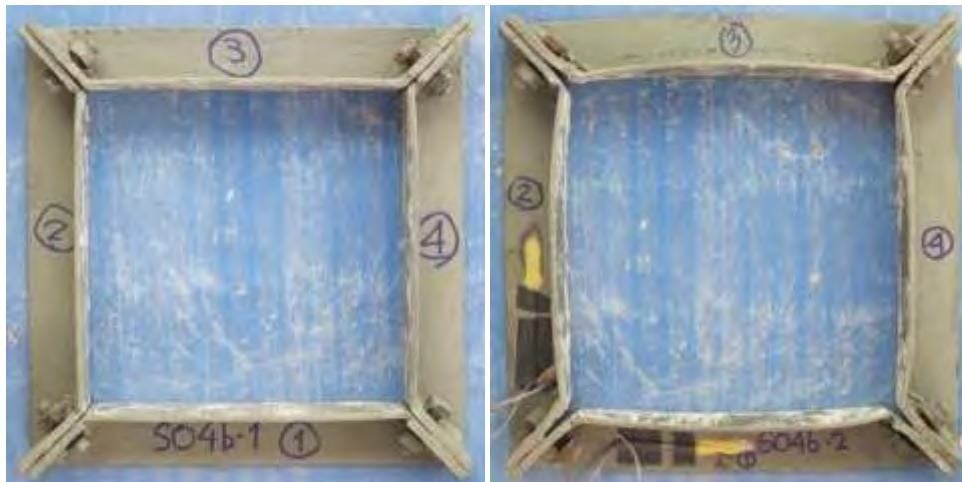
(a)

(b)

Figure C-17 Collars: (a) 1; and (b) 2 of S04b after the completion of the test
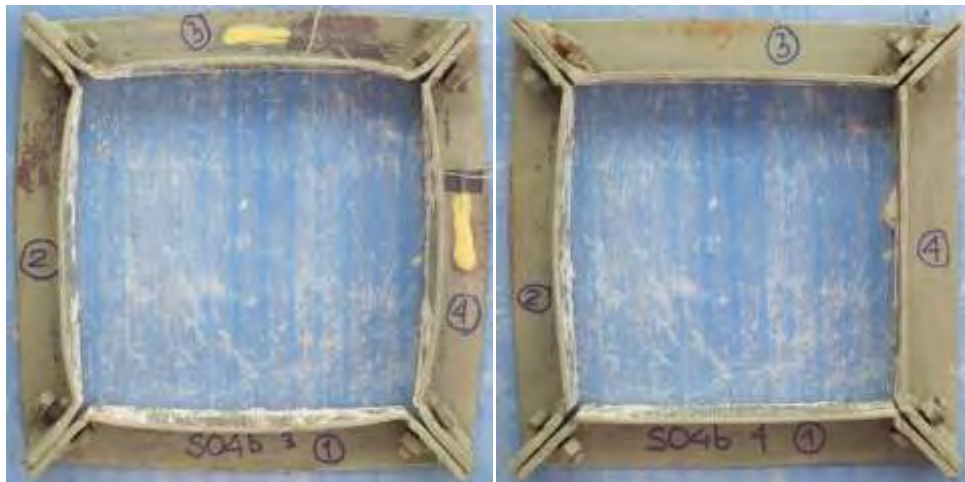
(a)

(b)

Figure C-18 Collars: (a) 3; and (b) 4 of S04b after the completion of the test
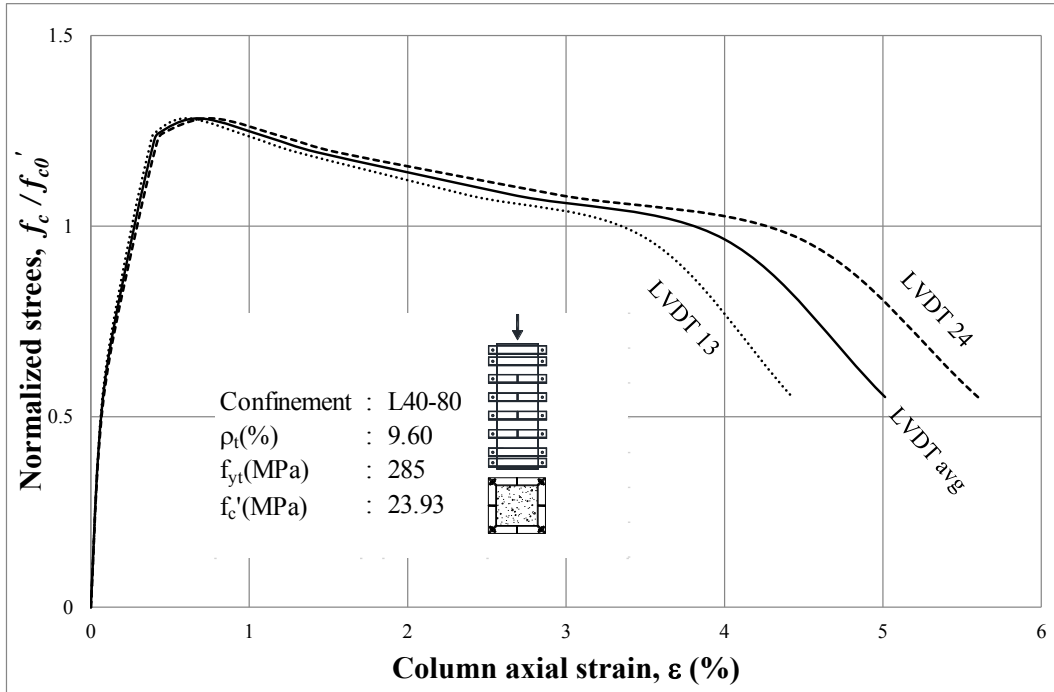
Figure C-19 Column axial stress-strain curves of S04c
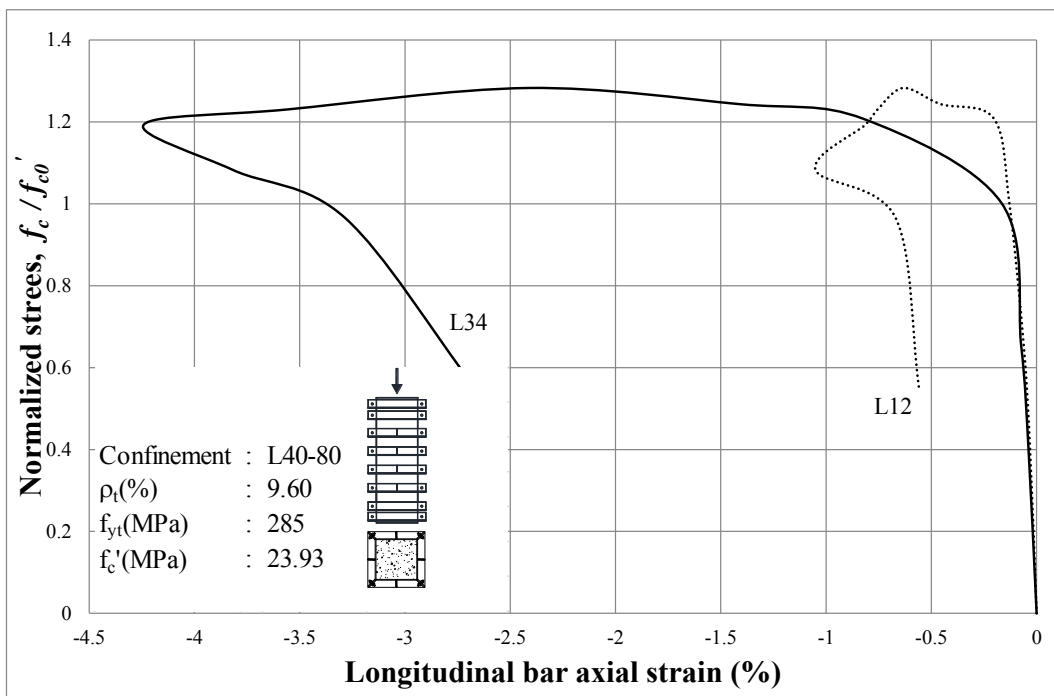
Figure C-20 Column axial stress-longitudinal bar axial strain curves of S04c

284
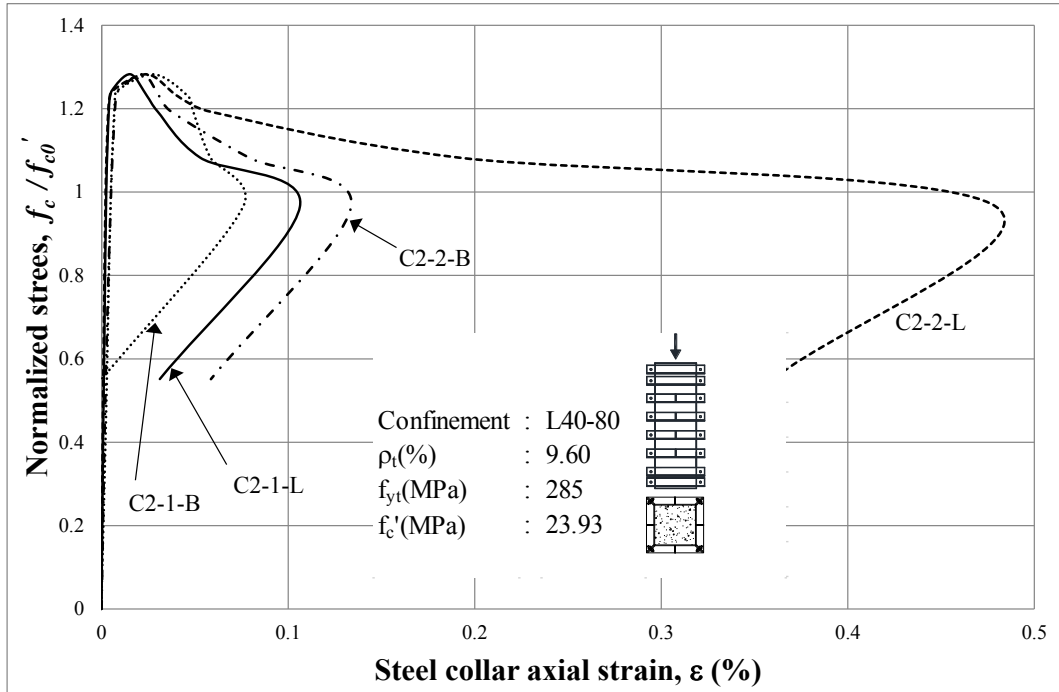
Figure C-21 Column axial stress-steel collar axial strain curves of S04c (Collar 2)
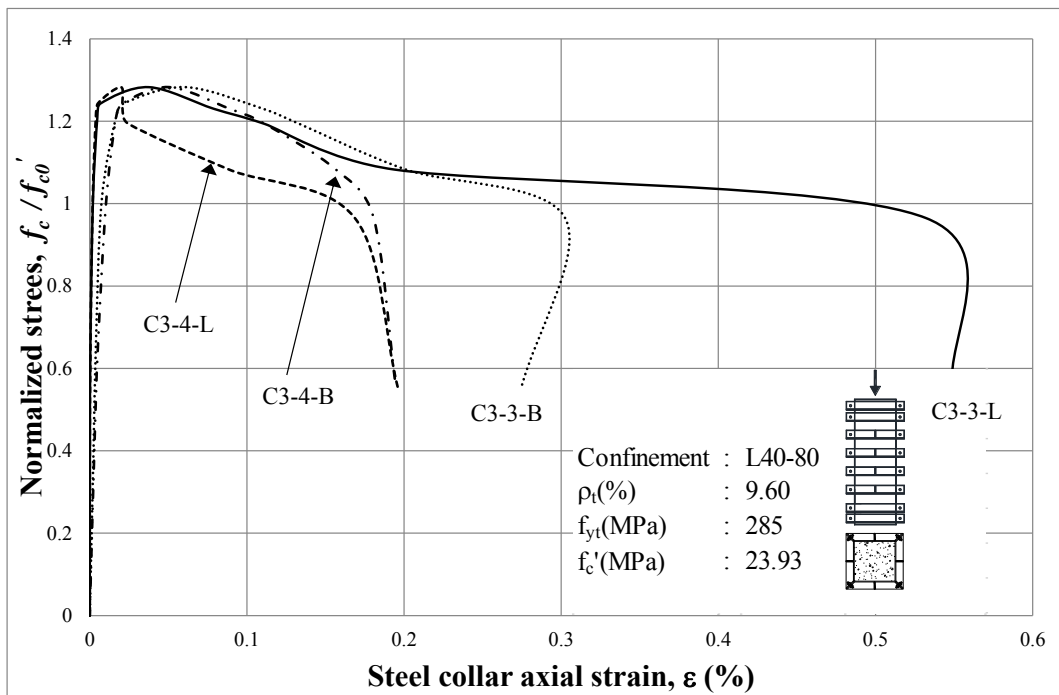
Figure C-22 Column axial stress-steel collar axial strain curves of S04c (Collar 3)

285

(a)   (b)

Figure C-23 Specimen S04c: (a) side 1; and (b) side 2 after the completion of the test

(a)   (b)

Figure C-24 Specimen S04c: (a) side 3; and (b) side 4 after the completion of the test
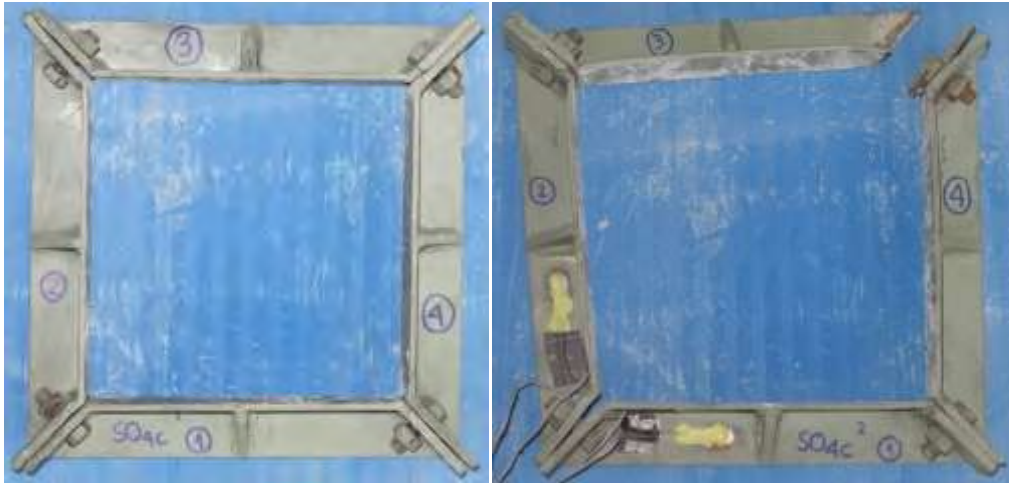
(a)   (b)

Figure C-25 Collars: (a) 1; and (b) 2 of S04c after the completion of the test
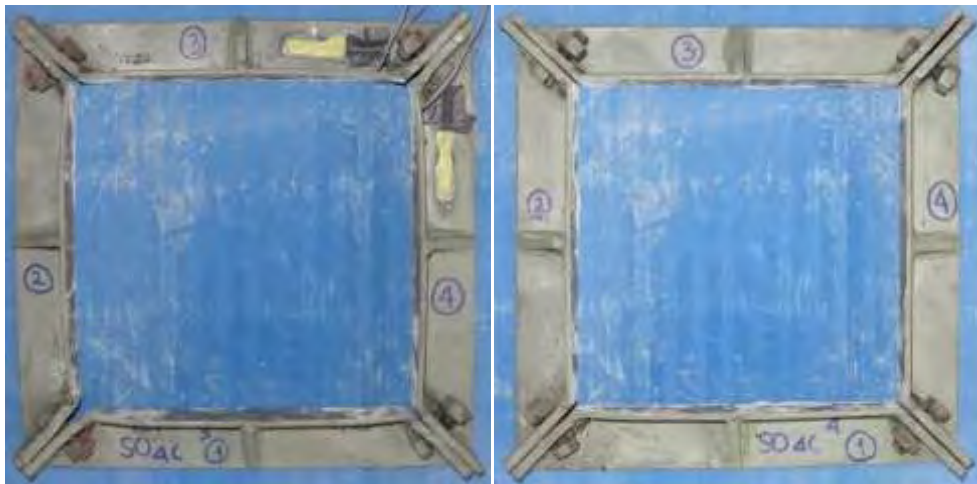
(a)   (b)

Figure C-26 Collars: (a) 3; and (b) 4 of S04c after the completion of the test
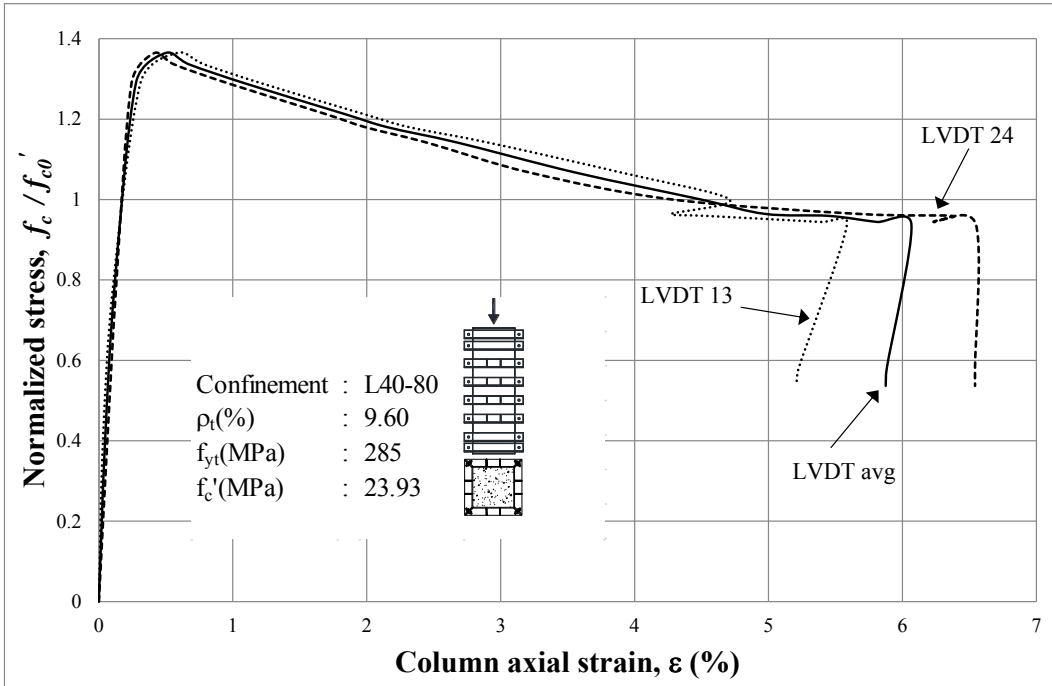
Figure C-27 Column axial stress-strain curves of S04d
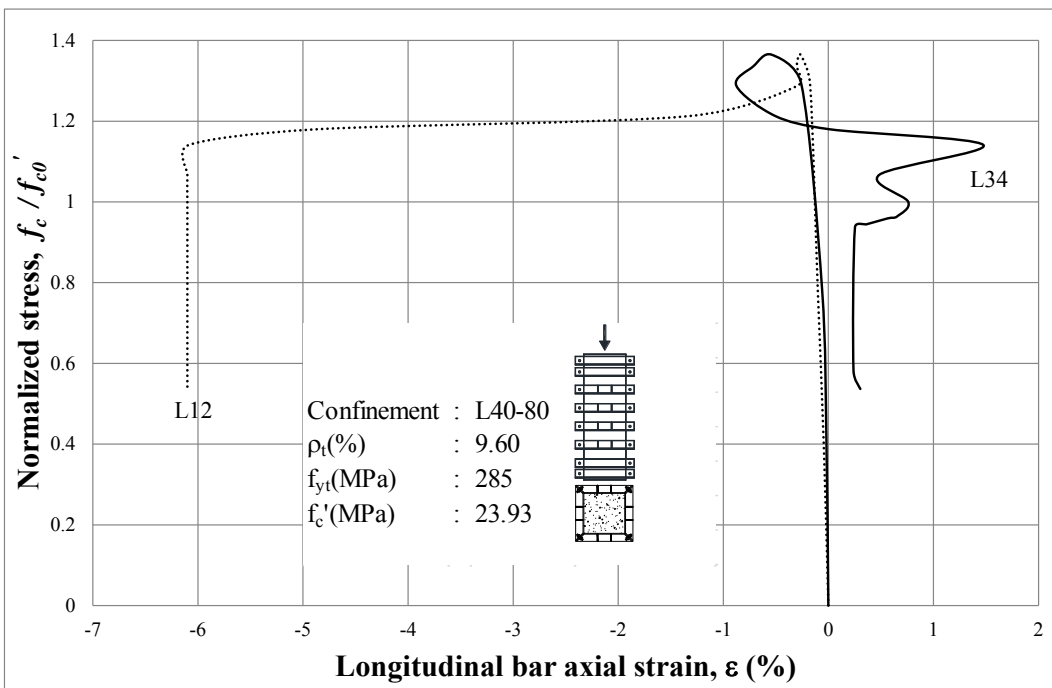
Figure C-28 Column axial stress-longitudinal bar axial strain curves of S04d
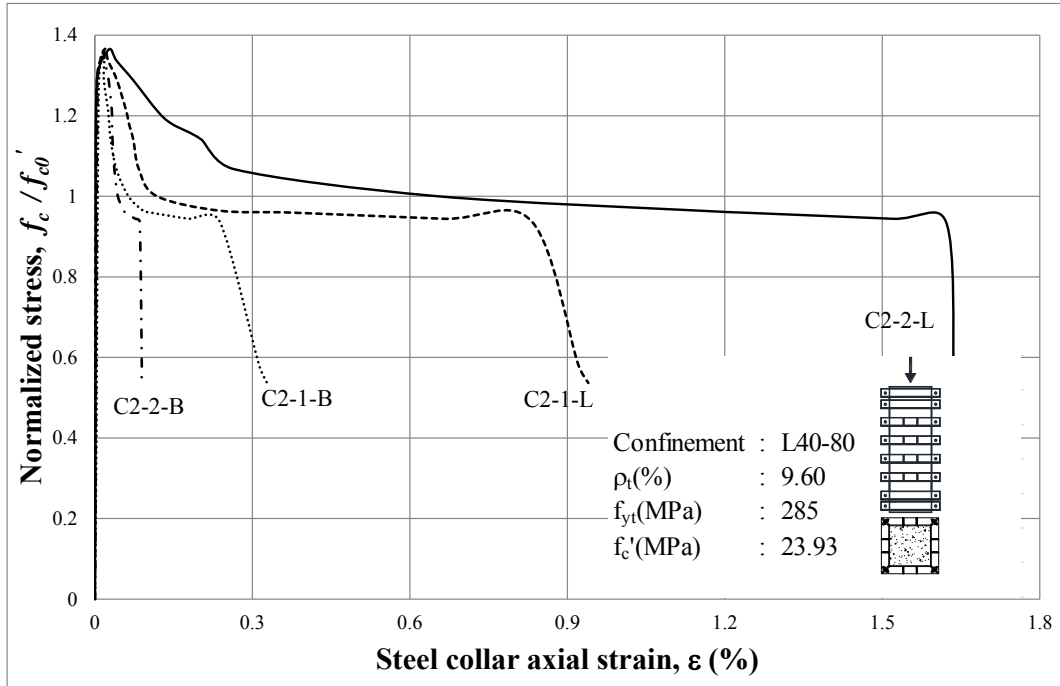
Figure C-29 Column axial stress-steel collar axial strain curves of S04d (Collar 2)
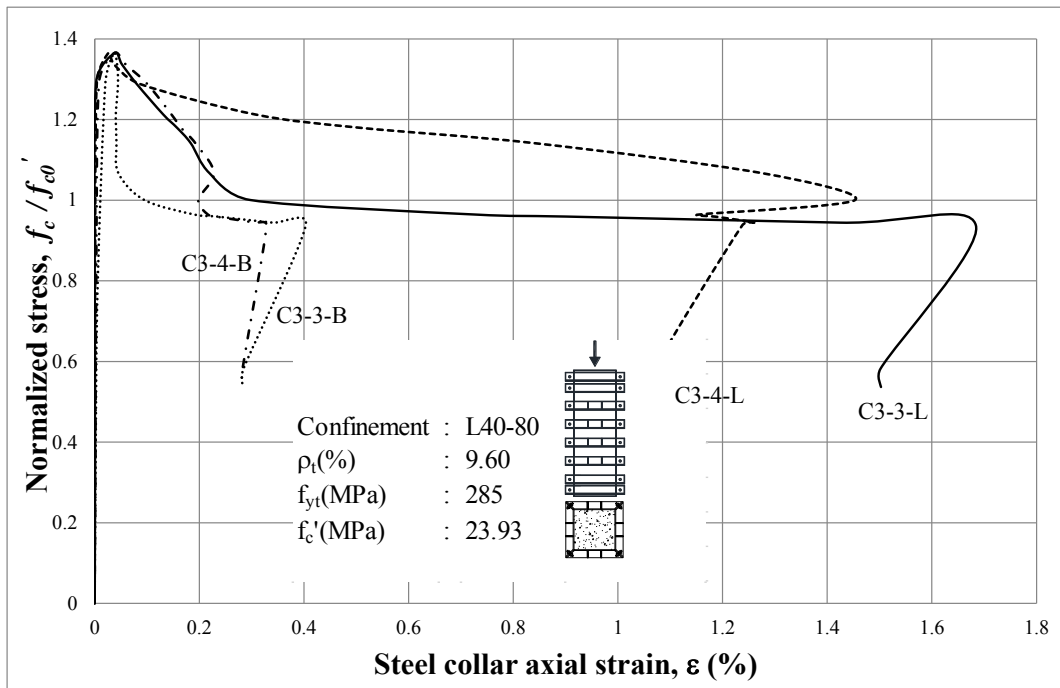
Figure C-30 Column axial stress-steel collar axial strain curves of S04d (Collar 3)

289

<center>(a)   (b)</center>

Figure C-31 Specimen S04d: (a) side 1; and (b) side 2 after the completion of the test

<center>(a)   (b)</center>

Figure C-32 Specimen S04d: (a) side 3; and (b) side 4 after the completion of the test

(a)   (b)

Figure C-33 Collars: (a)1; and (b)2 of S04d after the completion of the test
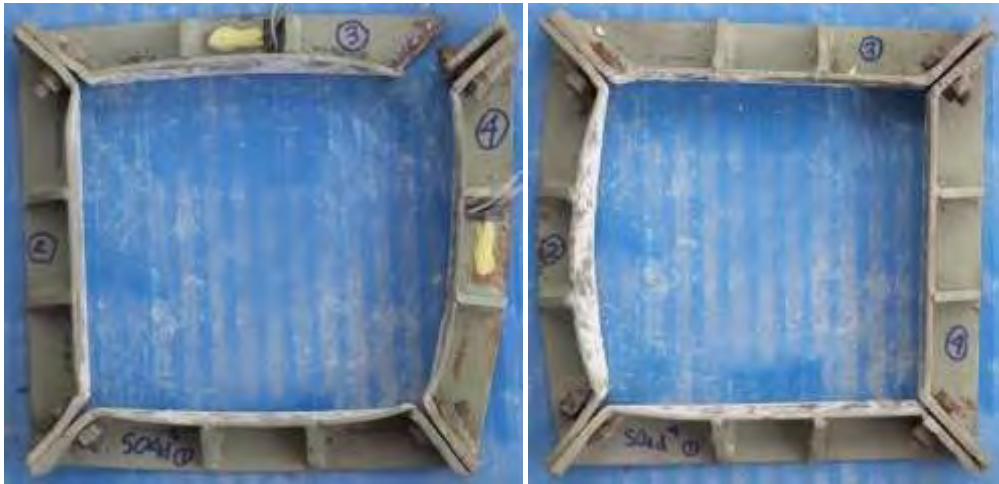
(a)   (b)

Figure C-34 Collars: (a) 3; and (b) 4 of S04d after the completion of the test
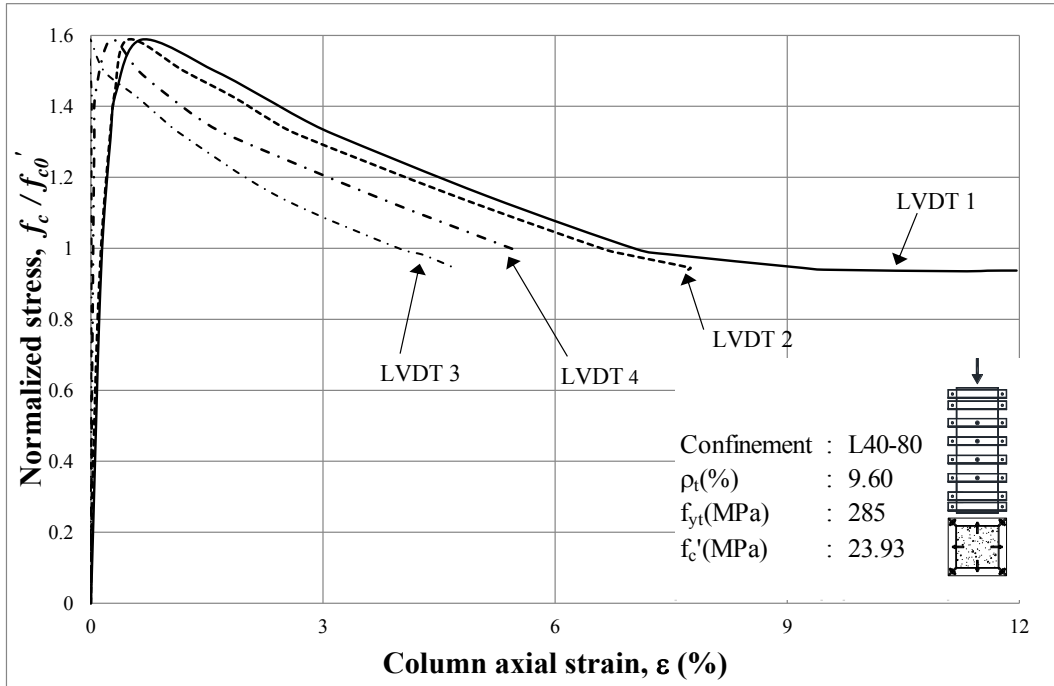
Figure C-35 Column axial stress-strain curves of S04e
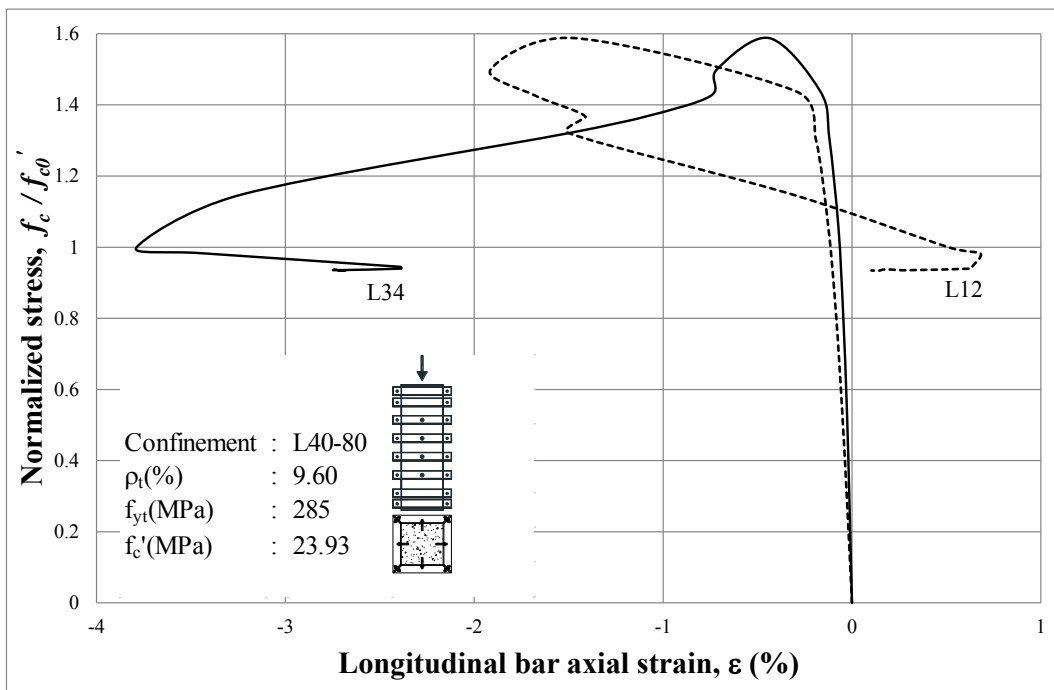
Figure C-36 Column axial stress-longitudinal bar axial strain curves of S04e
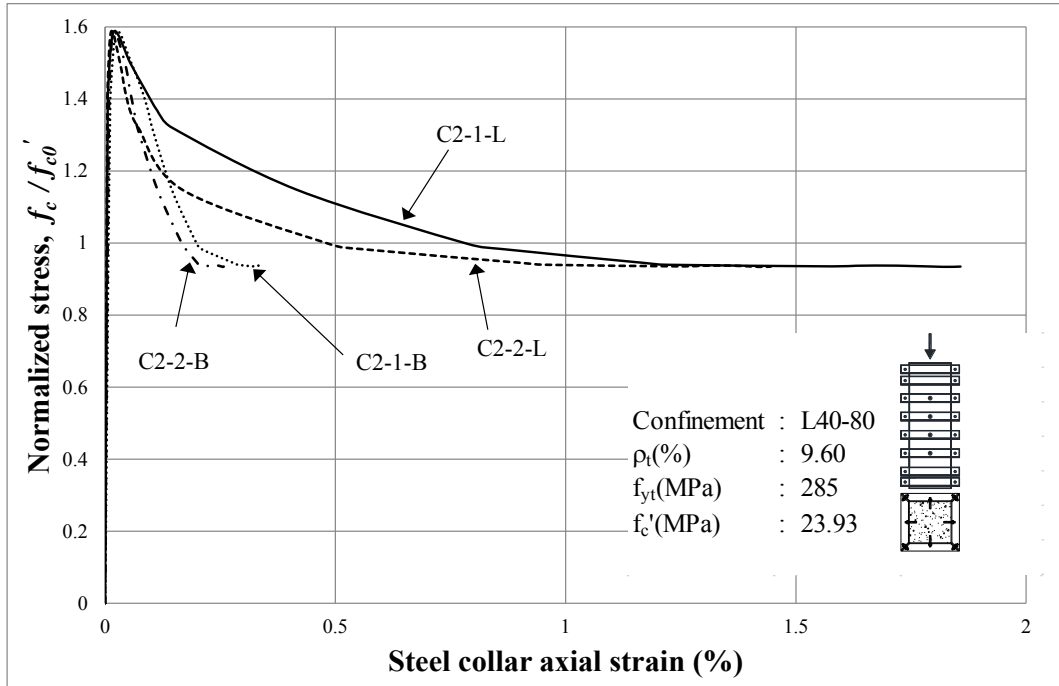
Figure C-37 Column axial stress-steel collar axial strain curves of S04e (Collar 2)
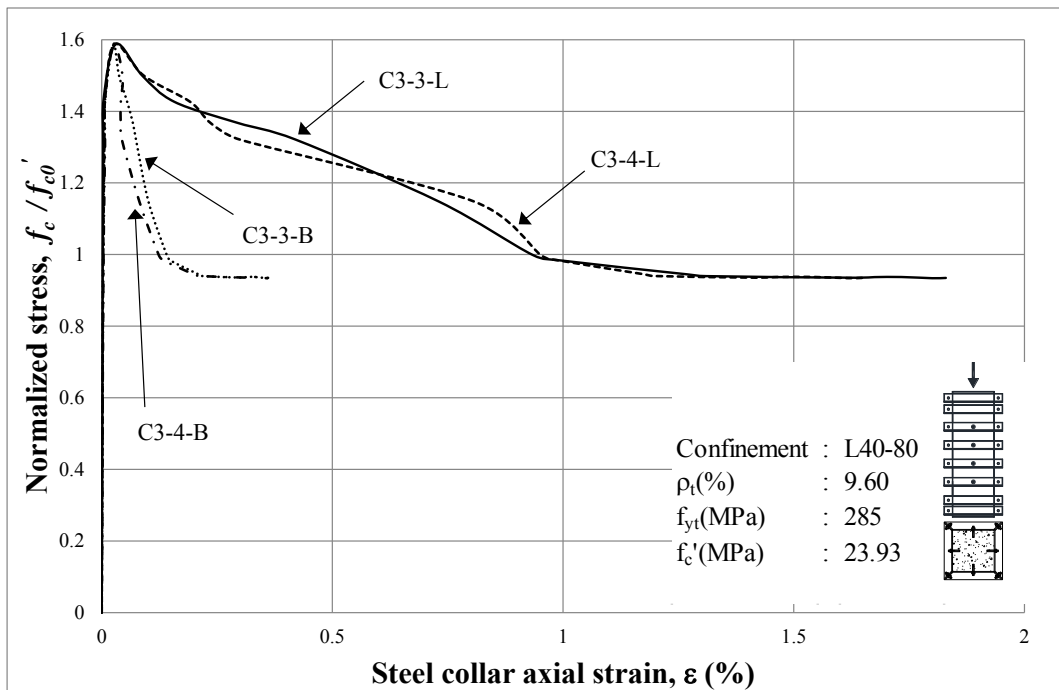
Figure C-38 Column axial stress-steel collar axial strain curves of S04e (Collar 3)

293

<div align="center">(a)   (b)</div>

Figure C-39 Specimen S04e: (a) side 1; and (b) side 2 after the completion of the test

<div align="center">(a)   (b)</div>

Figure C-40 Specimen S04e: (a) side 3; and (b) side 4 after the completion of the test
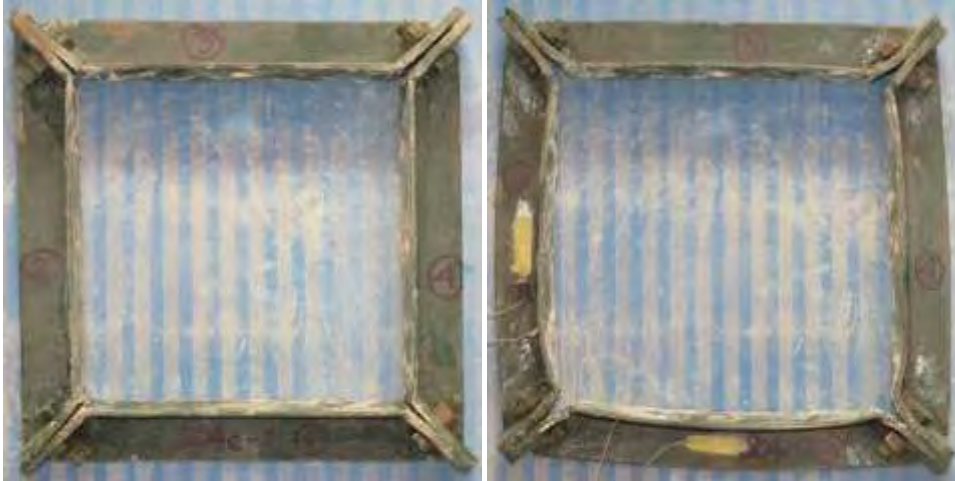
(a)   **(b)**

Figure C-41 Collars: (a) 1; and (b) 2 of S04e after the completion of the test

(a)   **(b)**

Figure C-42 Collars: (a) 3; and (b) 4 of S04e after the completion of the test
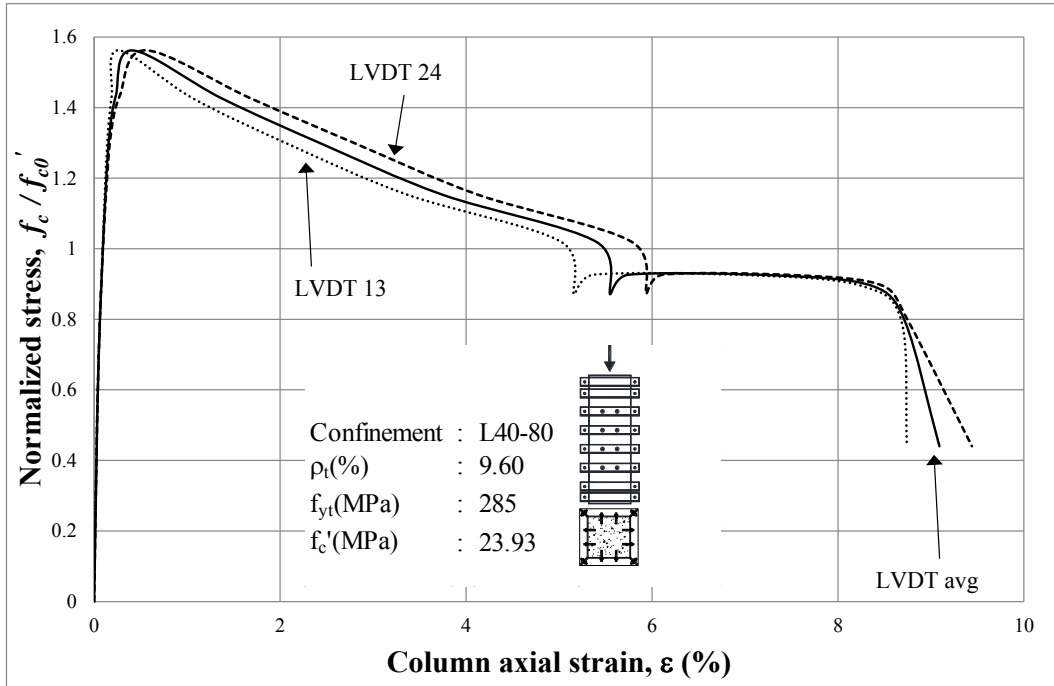
Figure C-43 Column axial stress-strain curves of S04f
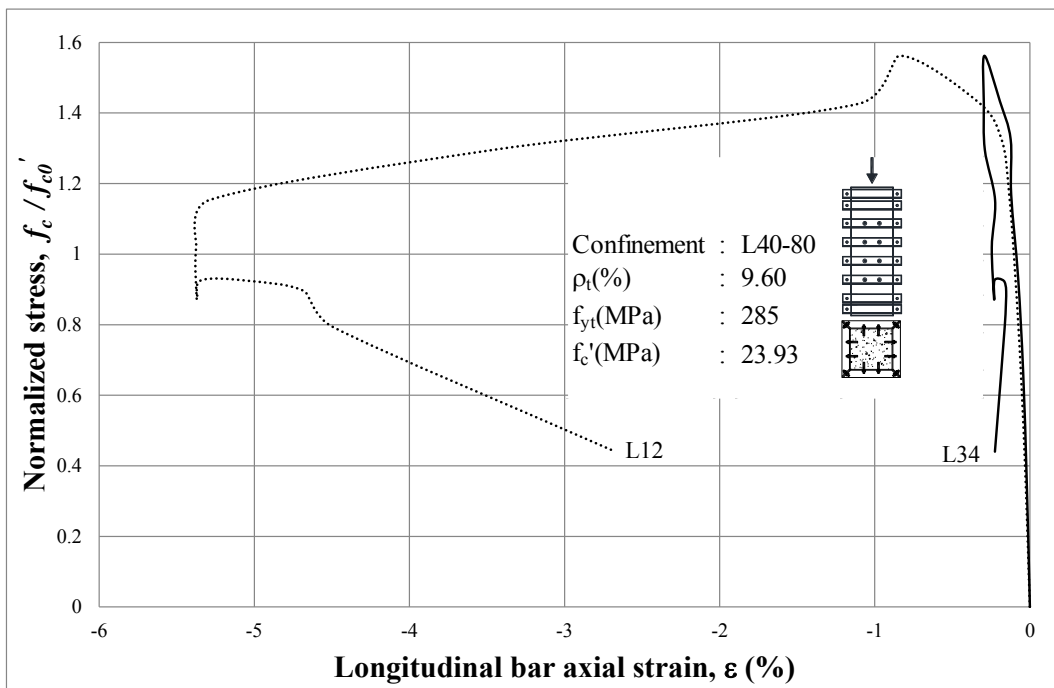
Figure C-44 Column axial stress-longitudinal bar axial strain curves of S04f

296
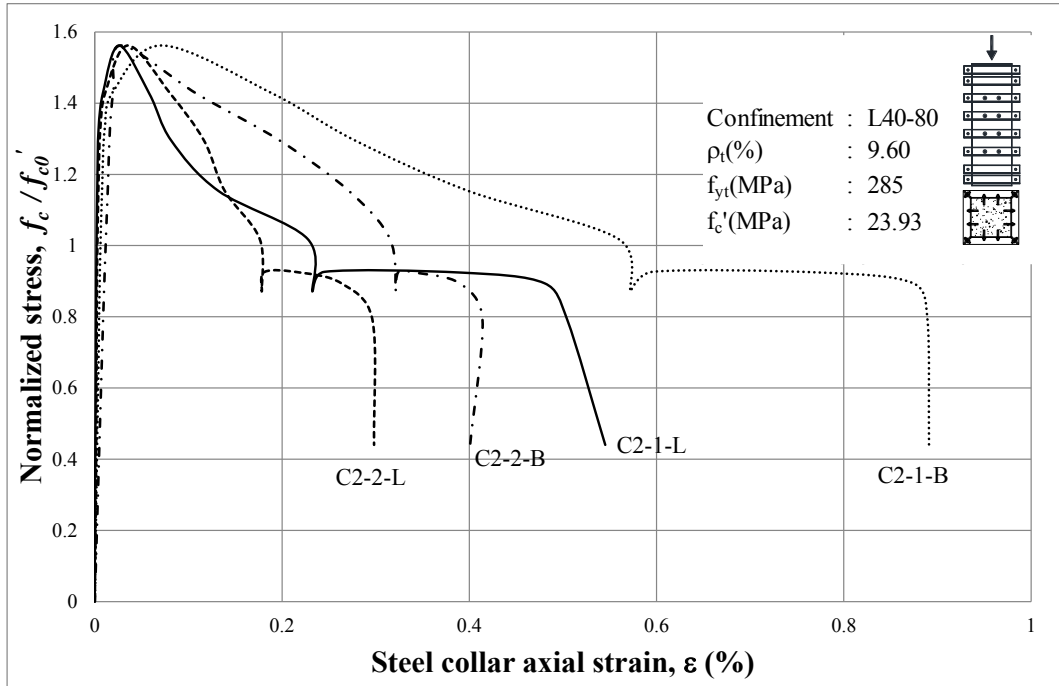
Figure C-45 Column axial stress-steel collar axial strain curves of S04f (Collar 2)
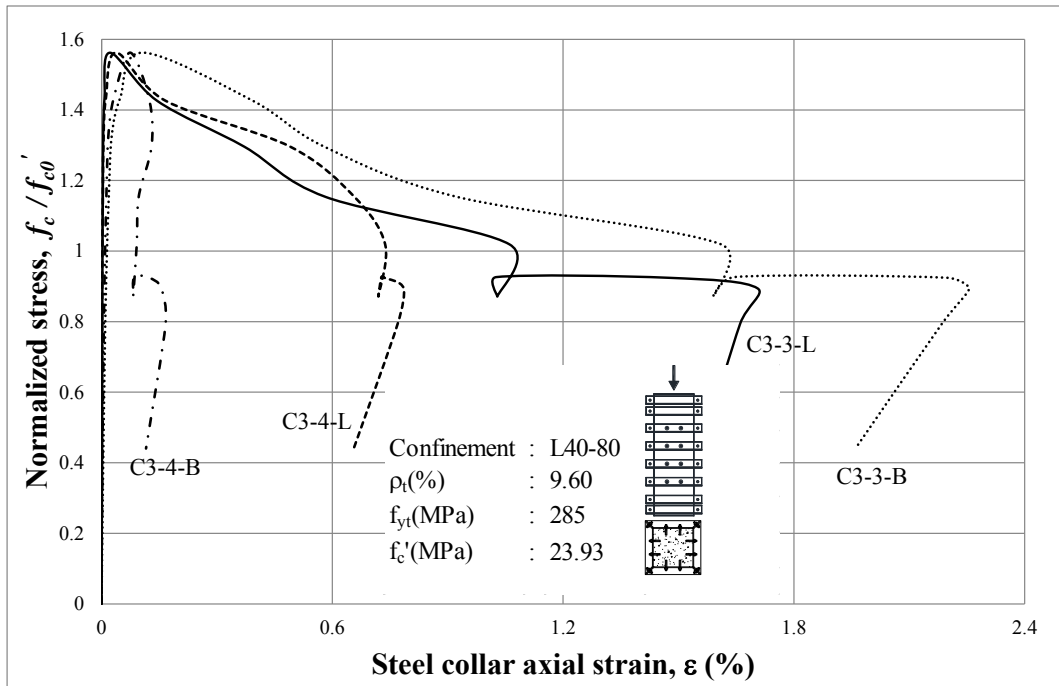
Figure C-46 Column axial stress-steel collar axial strain curves of S04f (Collar 3)

297

(a)   (b)

Figure C-47 Specimen S04f: (a) side 1; and (b) side 2 after the completion of the test

(a)   (b)

Figure C-48 Specimen S04f: (a) side 3; and (b) side 4 after the completion of the test
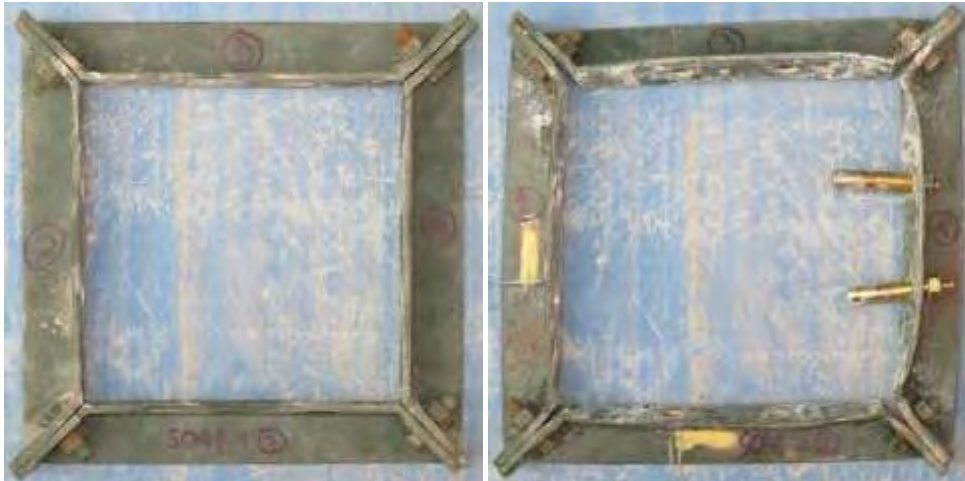
| (a) | (b) |

Figure C-49 Collars: (a) 1; and (b) 2 of S04f after the completion of the test

| (a) | (b) |

Figure C-50 Collars: (a) 3; and (b) 4 of S04f after the completion of the test

= This Page is Intentionally Left Blank =

# APPENDIX D. RESULTS OF COMBINED AXIAL COMPRESSIVE AND REVERSED CYCLIC LOADING TEST
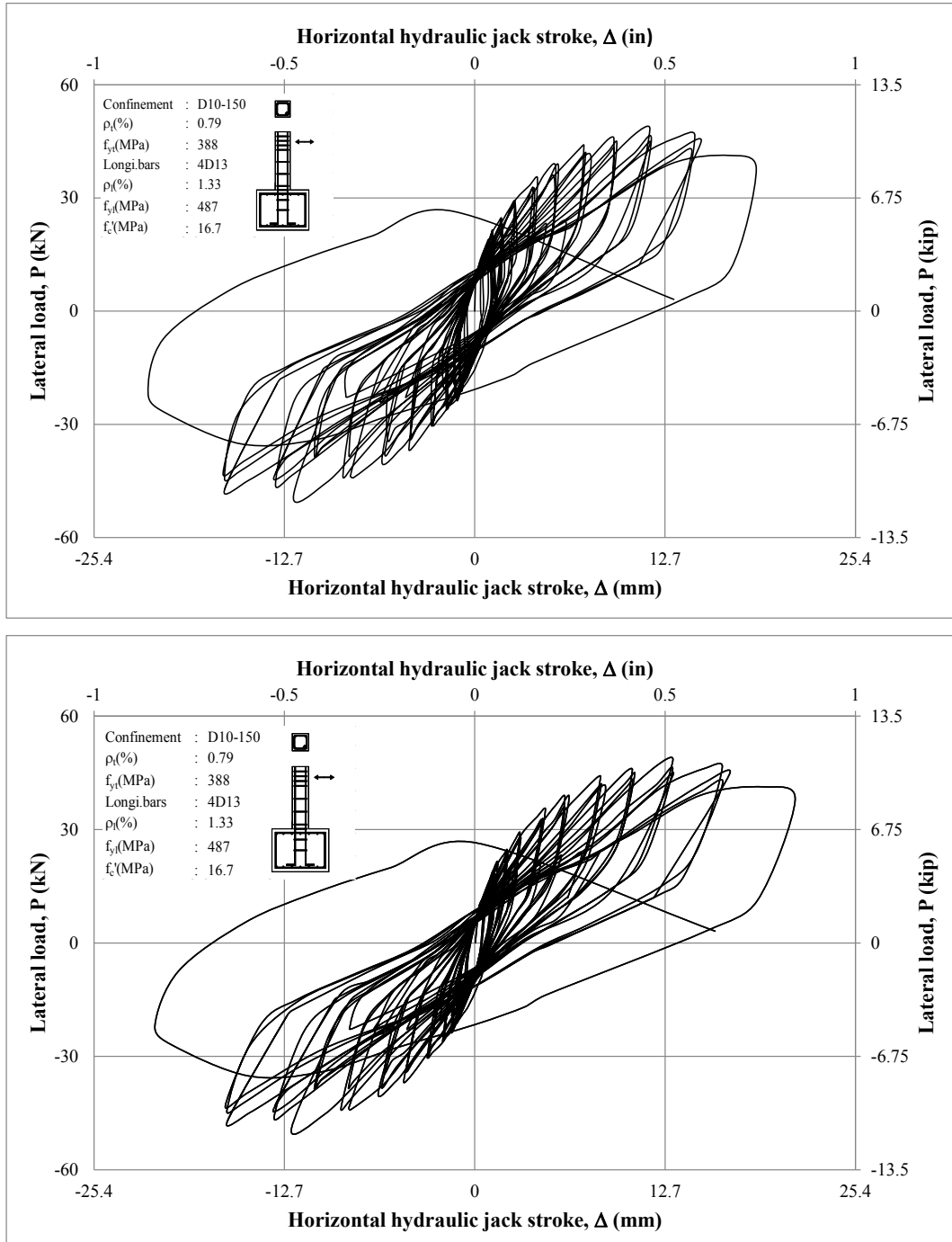
Figure D-1 Lateral load vs measurement of Channels 2 and 3 of CS11

The first chart shows Column vertical displacement, Δ (in) on the top axis ranging from -0.108 to 0.108, and Column vertical displacement, Δ (mm) on the bottom axis ranging from -2.75 to 2.75. The vertical axis shows Lateral Load, P (kN) from -60 to 60 on the left and Lateral Load, P (kip) from -13.5 to 13.5 on the right.

Legend for first chart:
Confinement : D10-150
ρ_t(%) : 0.79
f_{yt}(MPa) : 388
Longi.bars : 4D13
ρ_l(%) : 1.33
f_{yl}(MPa) : 487
f_c'(MPa) : 16.7

The second chart shows Column horizontal displacement, Δ (in) on the top axis ranging from -1 to 1, and Column horizontal displacement, Δ (mm) on the bottom axis ranging from -25.4 to 25.4. The vertical axis shows Lateral Load, P (kN) from -60 to 60 on the left and Lateral Load, P (kip) from -13.5 to 13.5 on the right.

Legend for second chart:
Confinement : D10-150
ρ_t(%) : 0.79
f_{yt}(MPa) : 388
Longi.bars : 4D13
ρ_l(%) : 1.33
f_{yl}(MPa) : 487
f_c'(MPa) : 16.7

Figure D-2 Lateral load vs measurement of Channels 4 and 5 of CS11

302
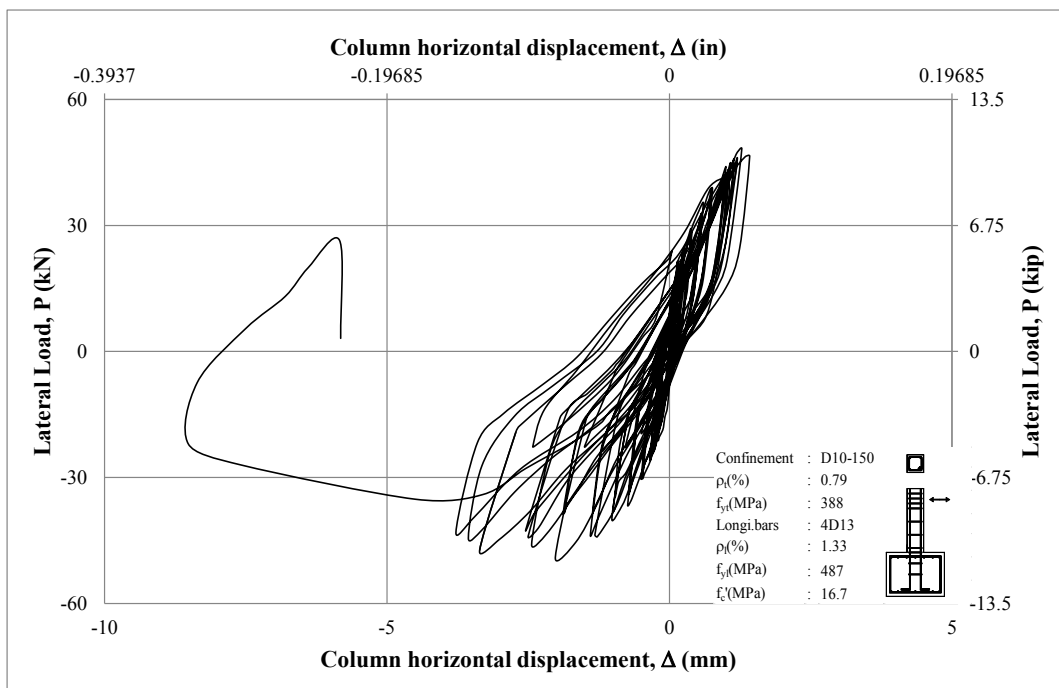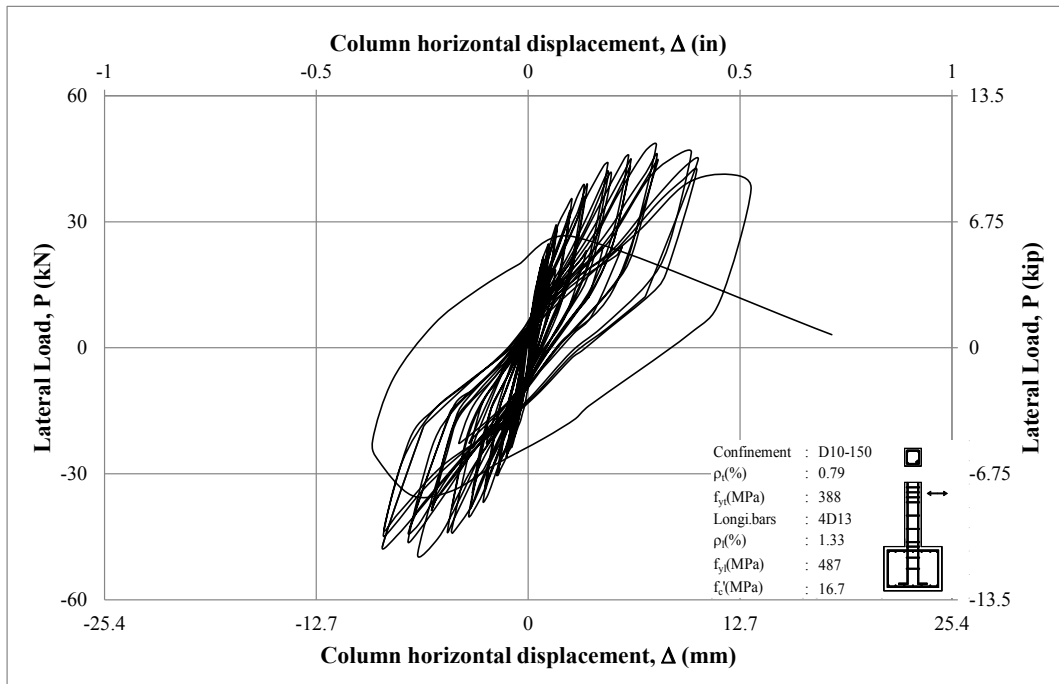
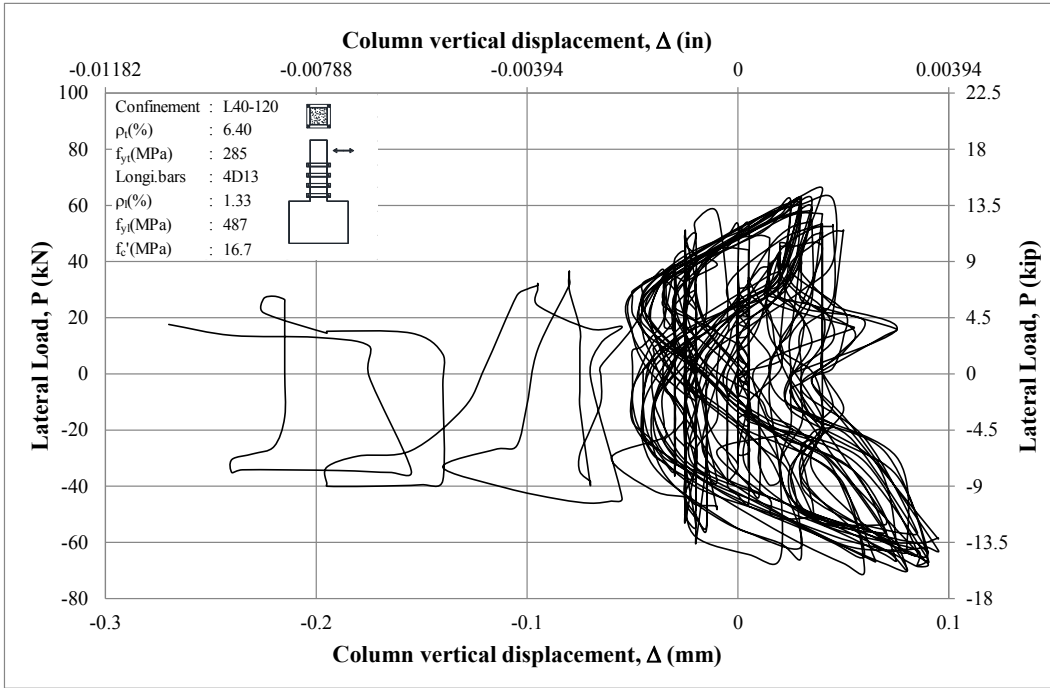**Figure D-3 Lateral load vs measurement of Channels 6 and 7 of CS11**
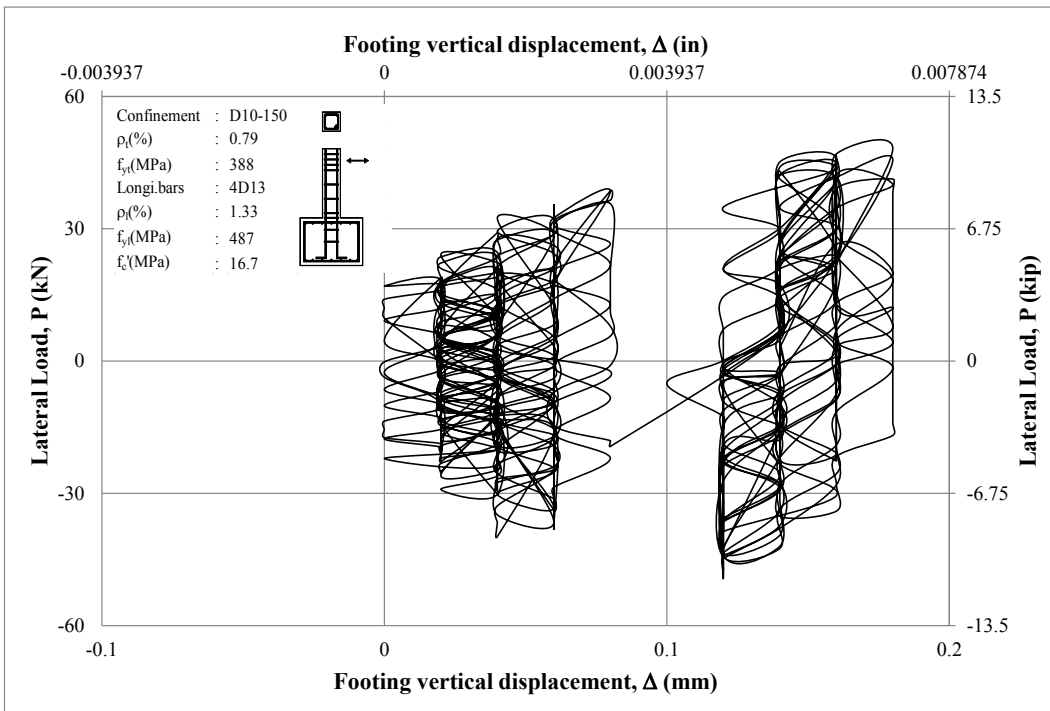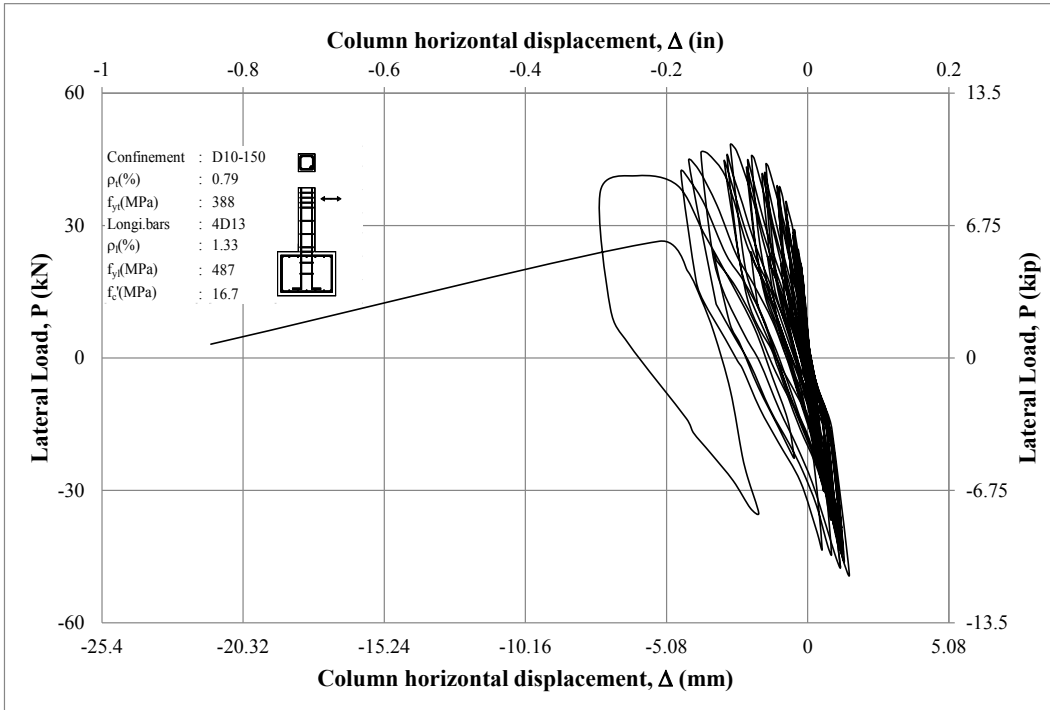
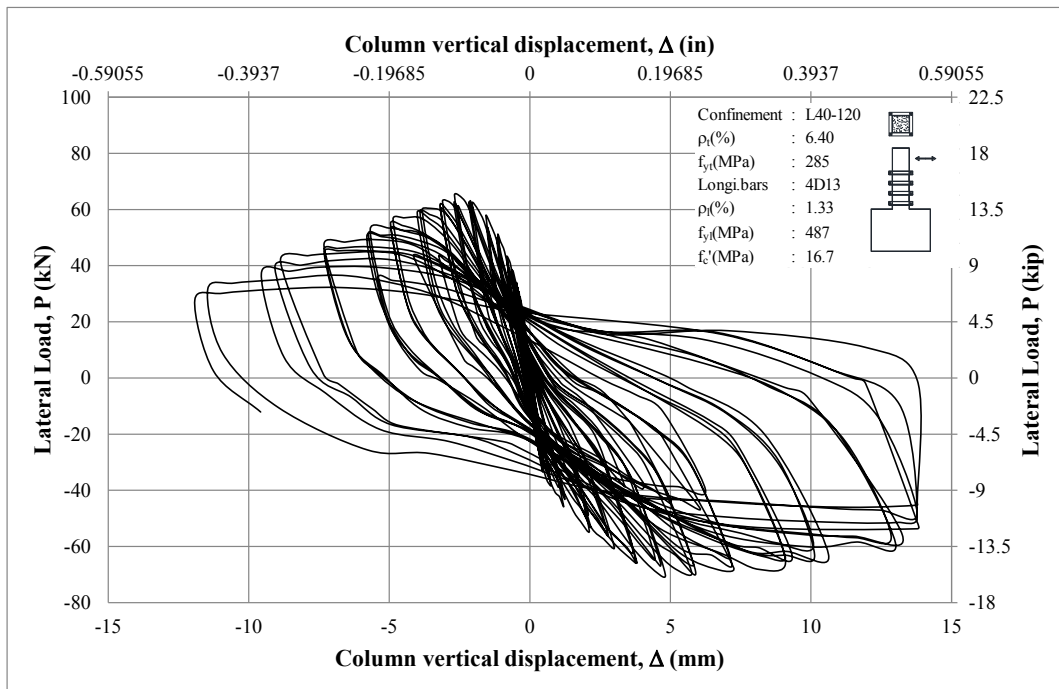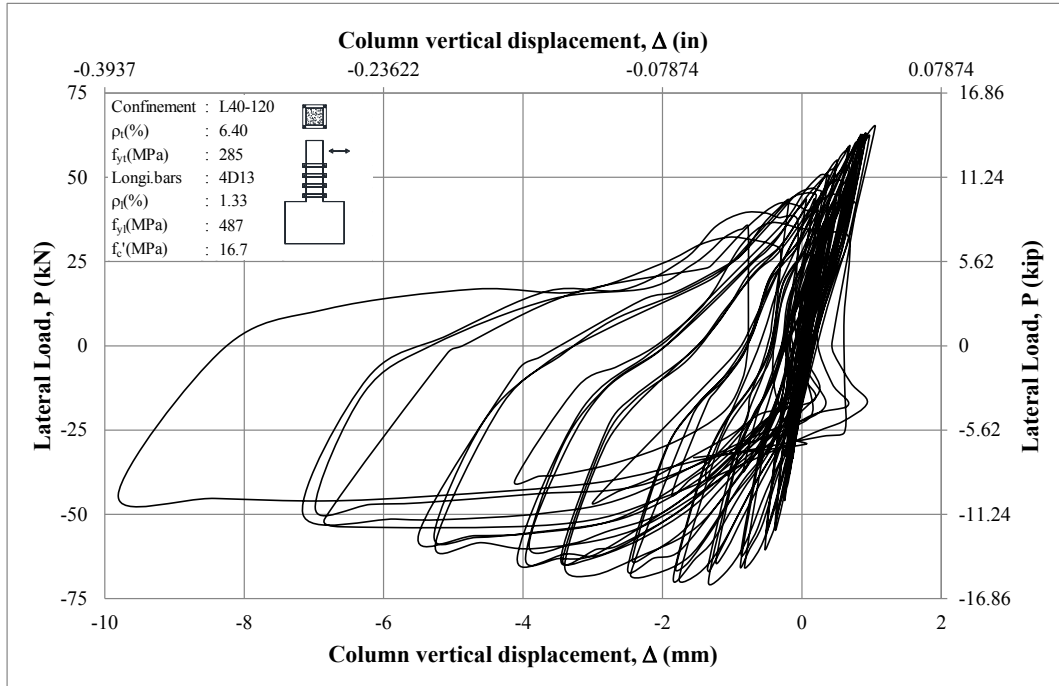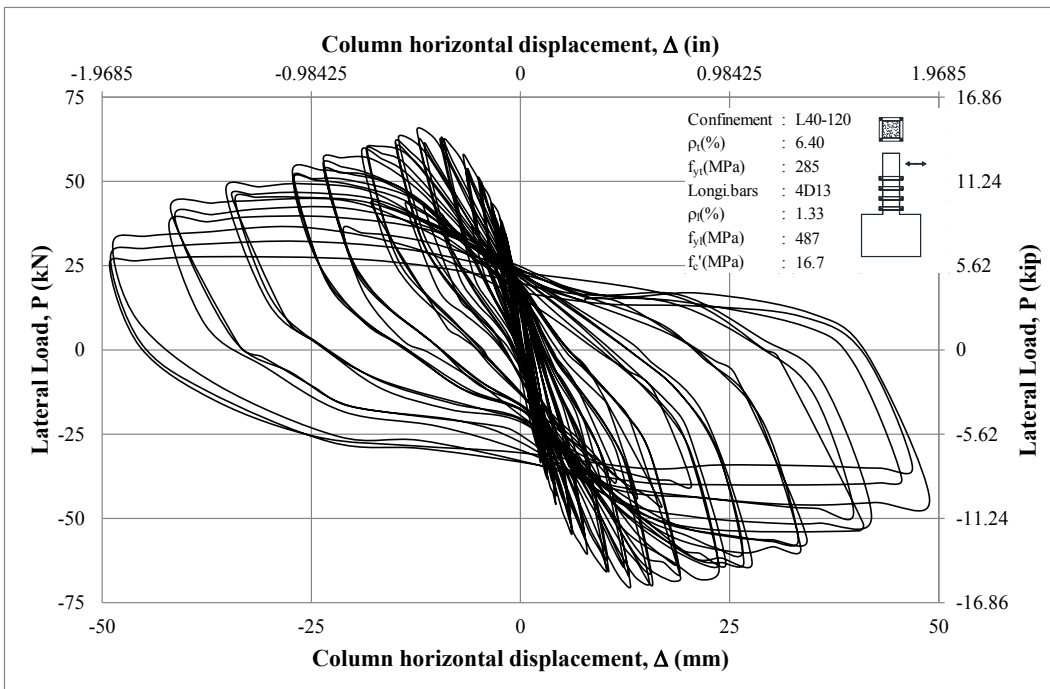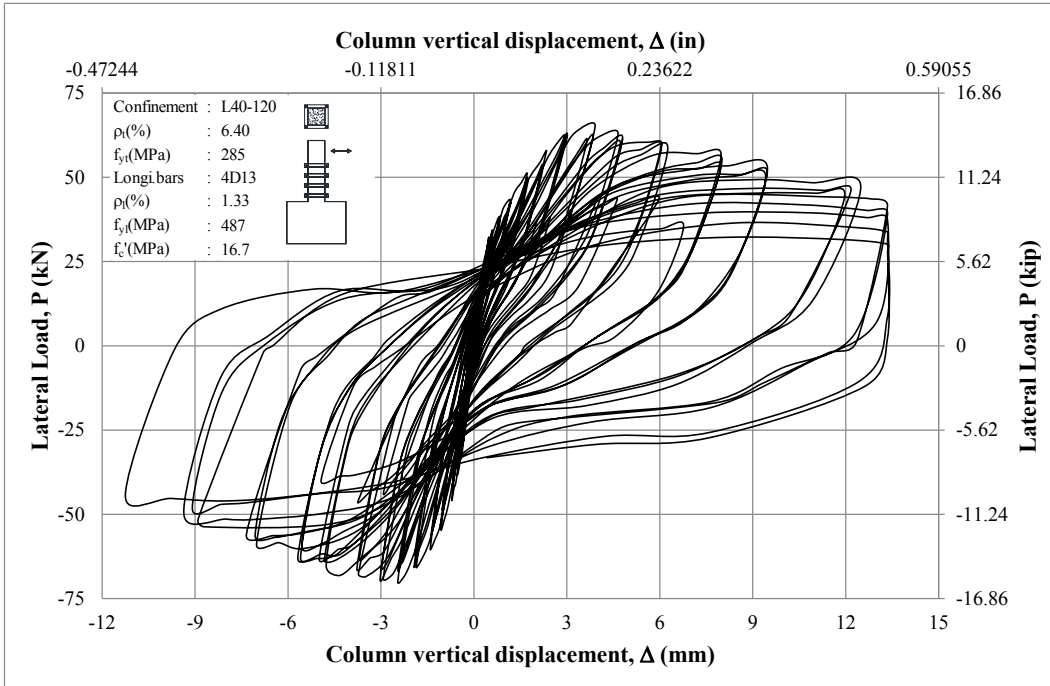**Figure D-4 Lateral load vs measurement of Channels 8 and 9 of CS11**
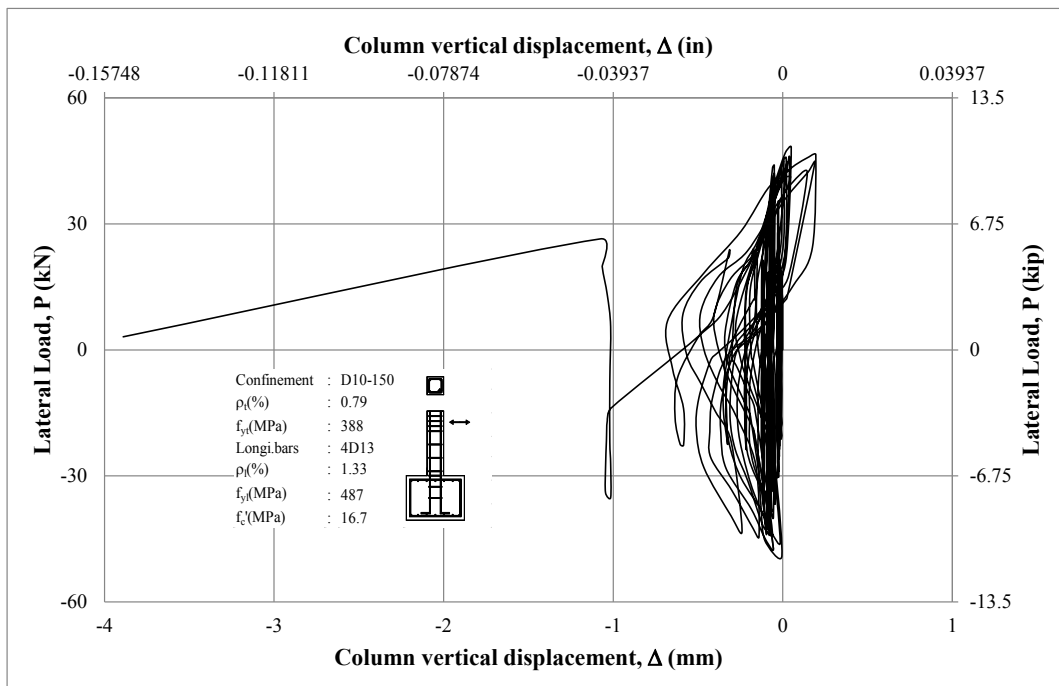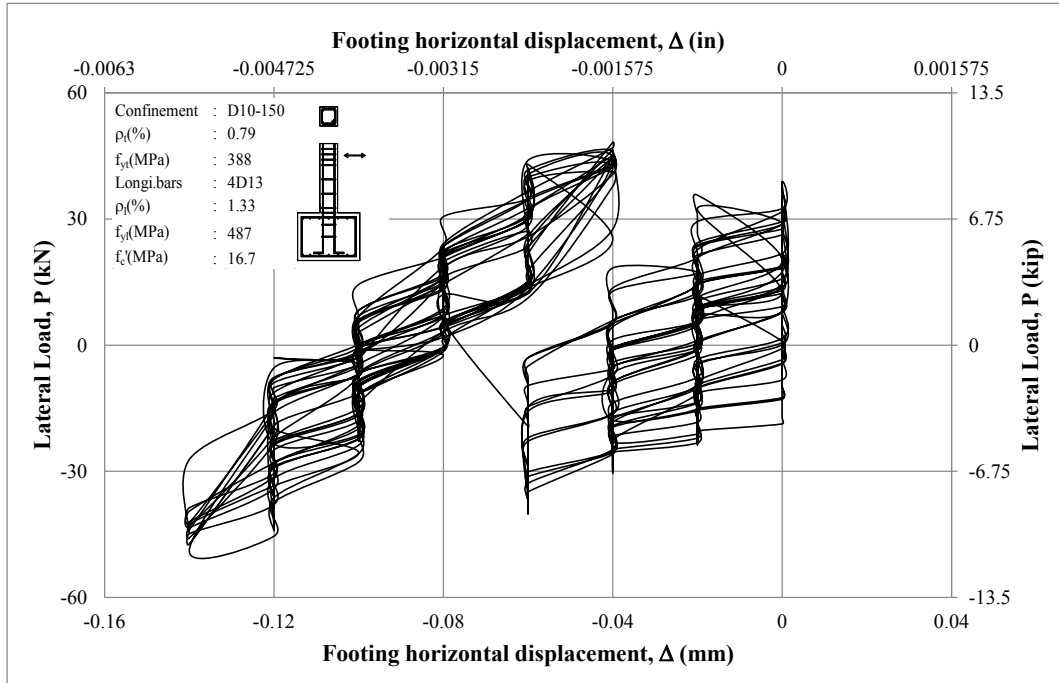
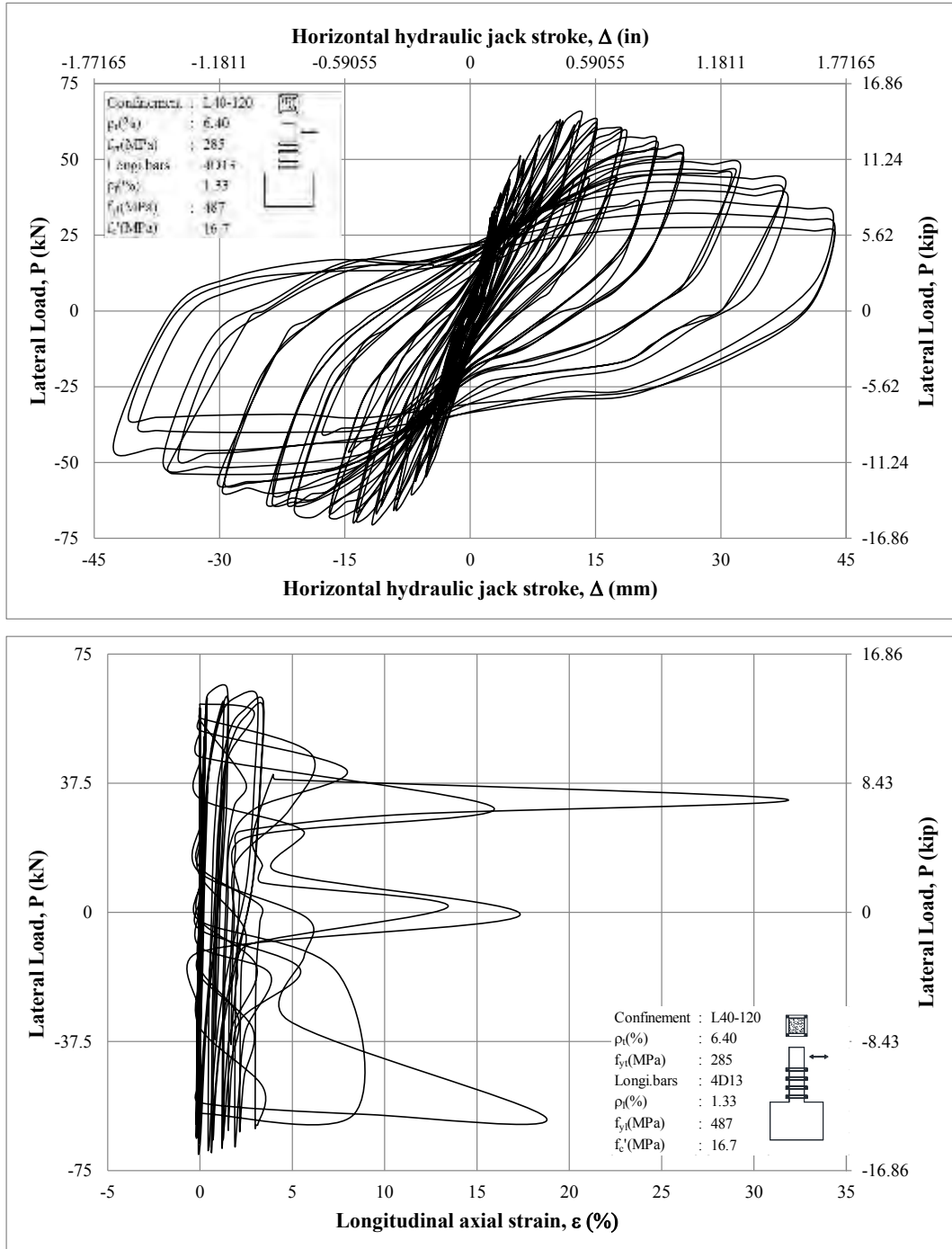**Figure D-5 Lateral load vs measurement of Channels 10 and 11 of CS11**
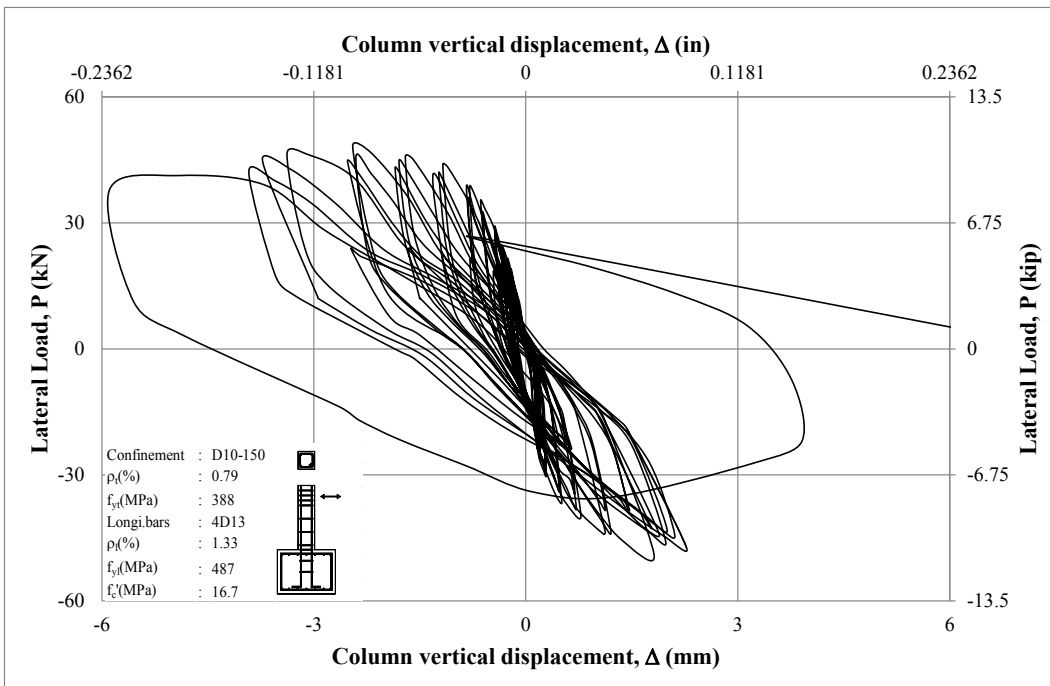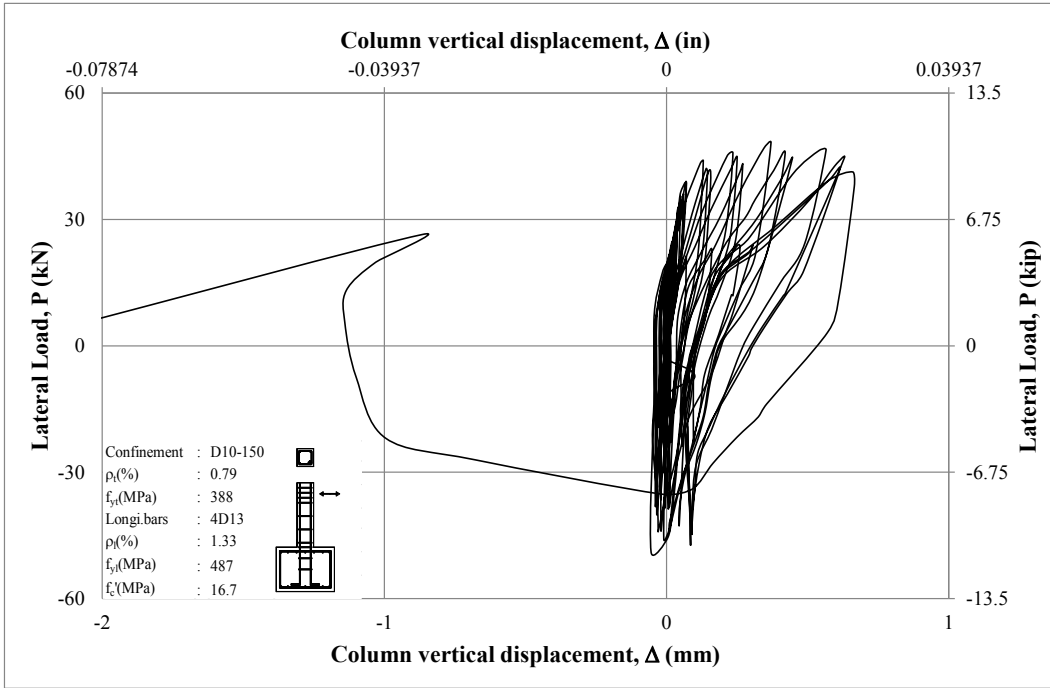
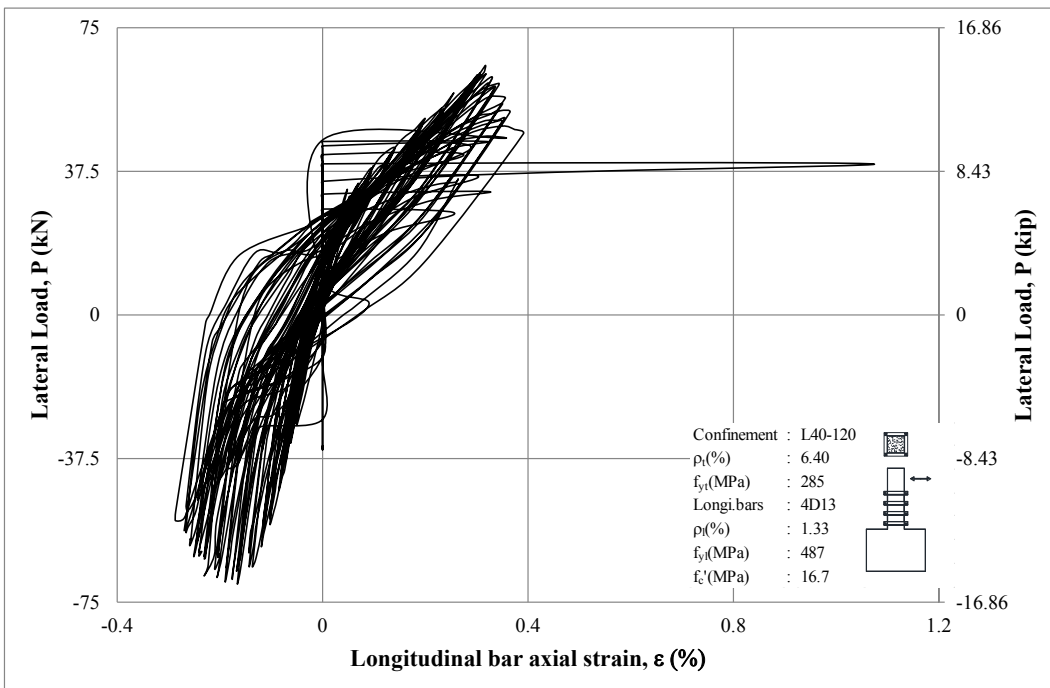**Figure D-6 Lateral load vs measurement of Channels 12 and 13 of CS11**

306
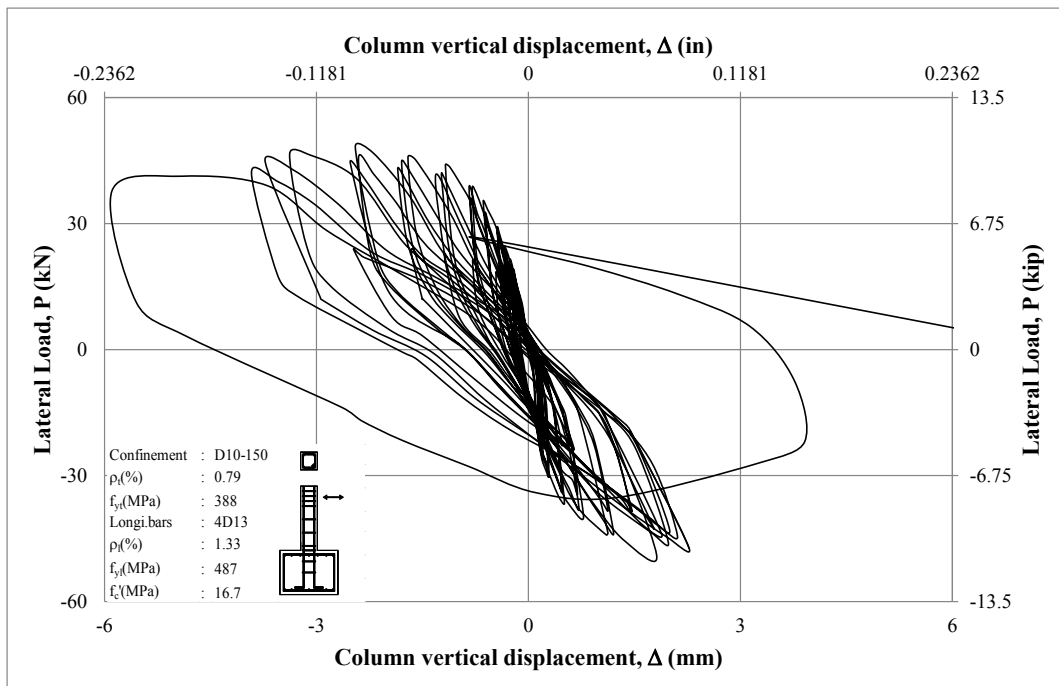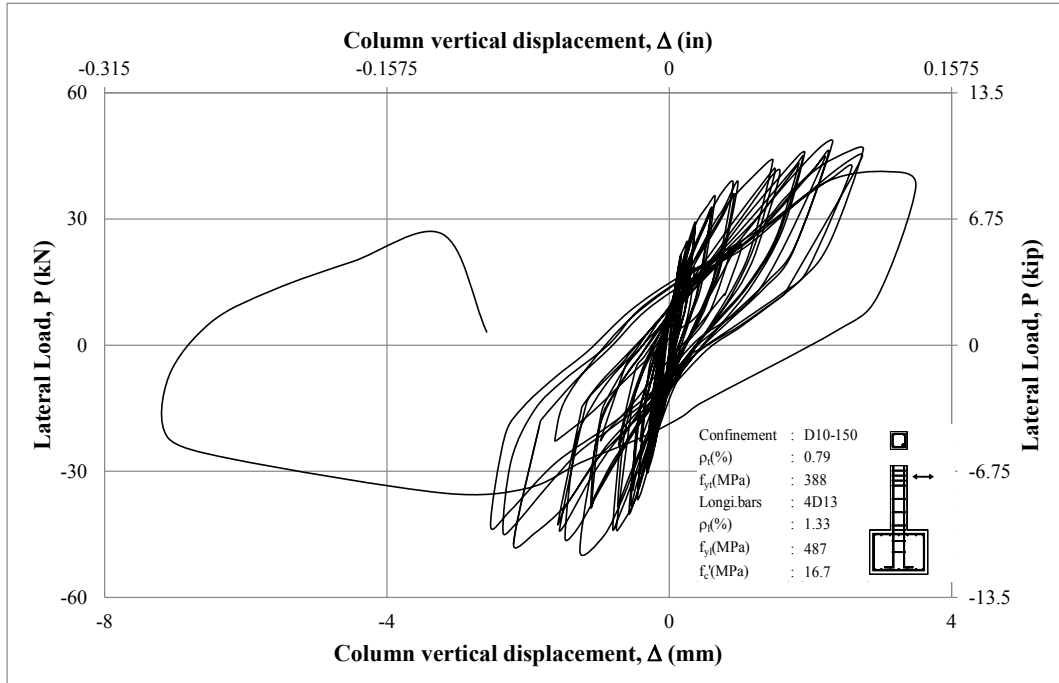
Figure D-7 Lateral load vs measurement of Channels 14 and 15 of CS11
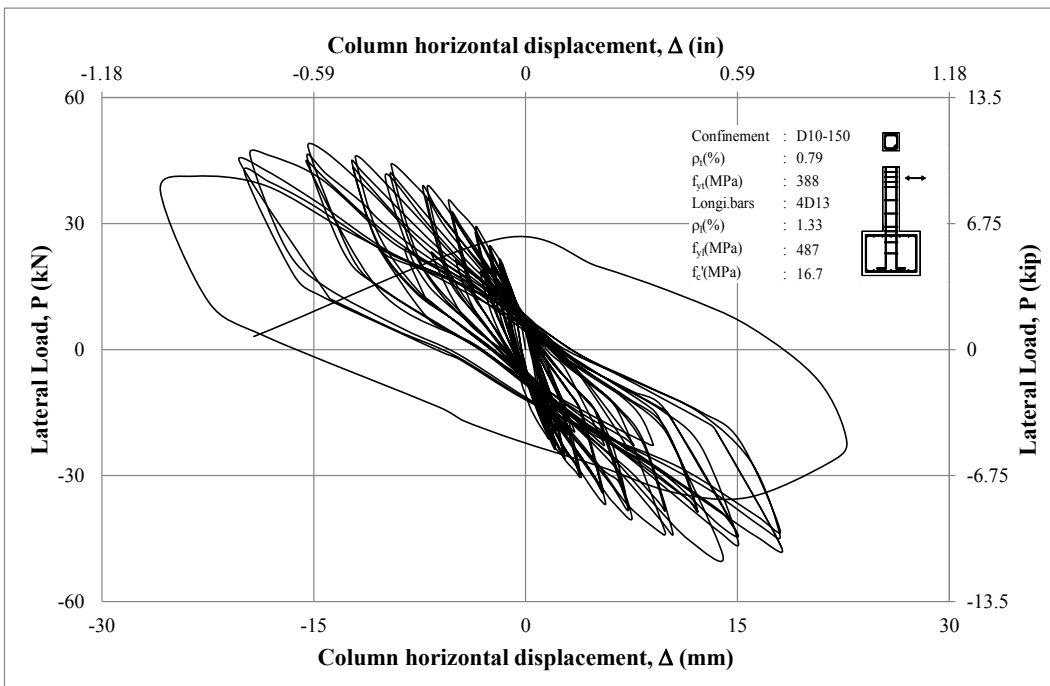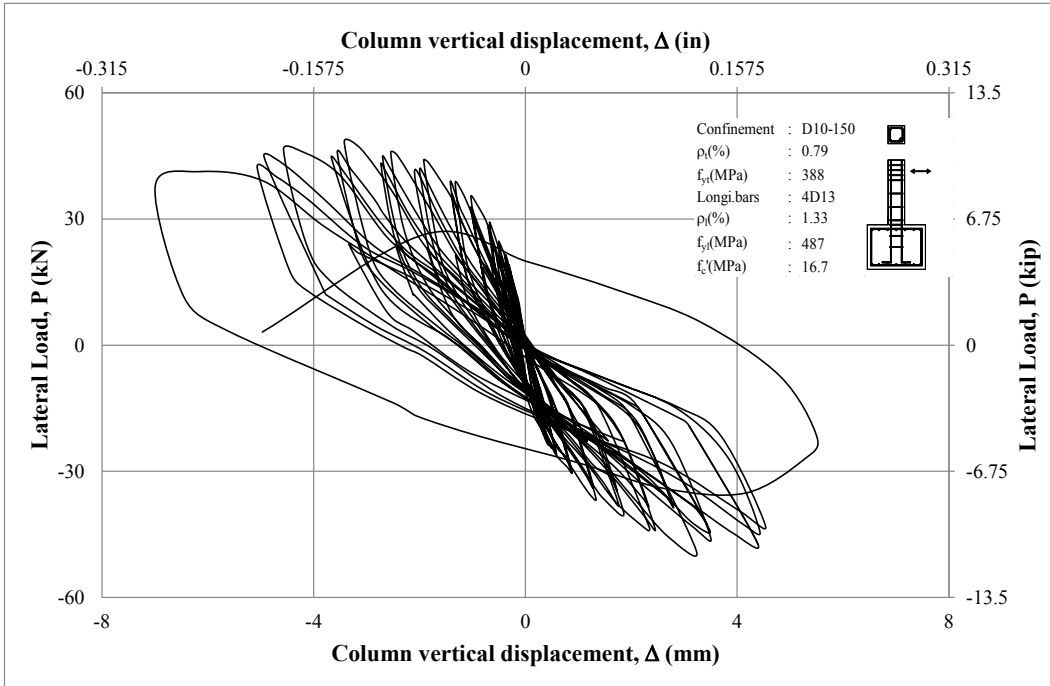
Figure D-8 Lateral load vs measurement of Channels 16 and 17 of CS11
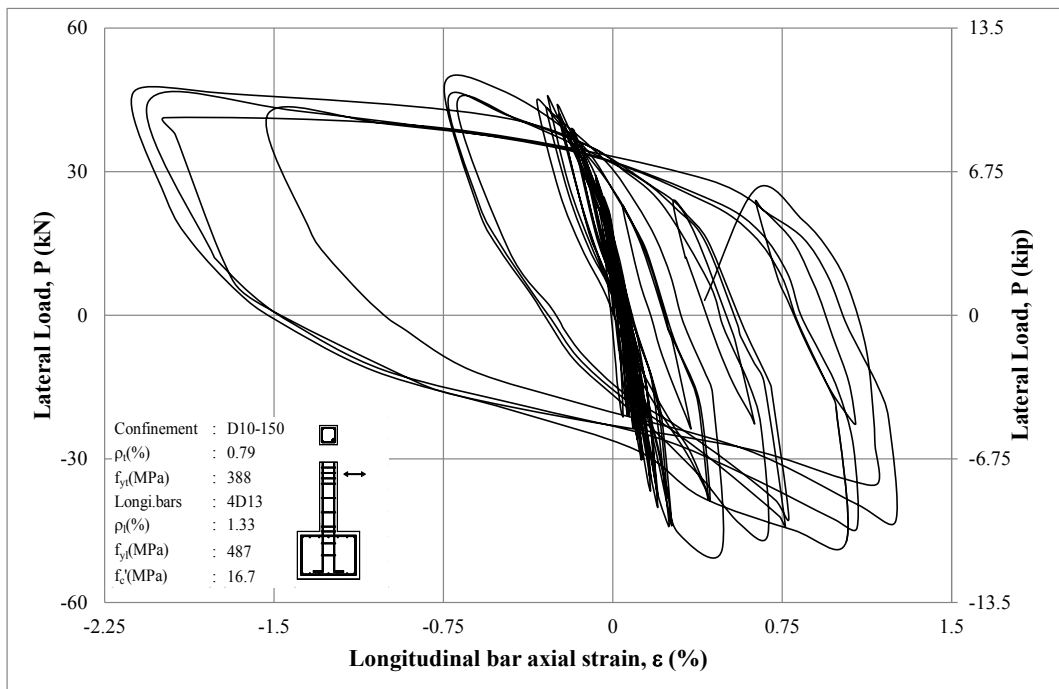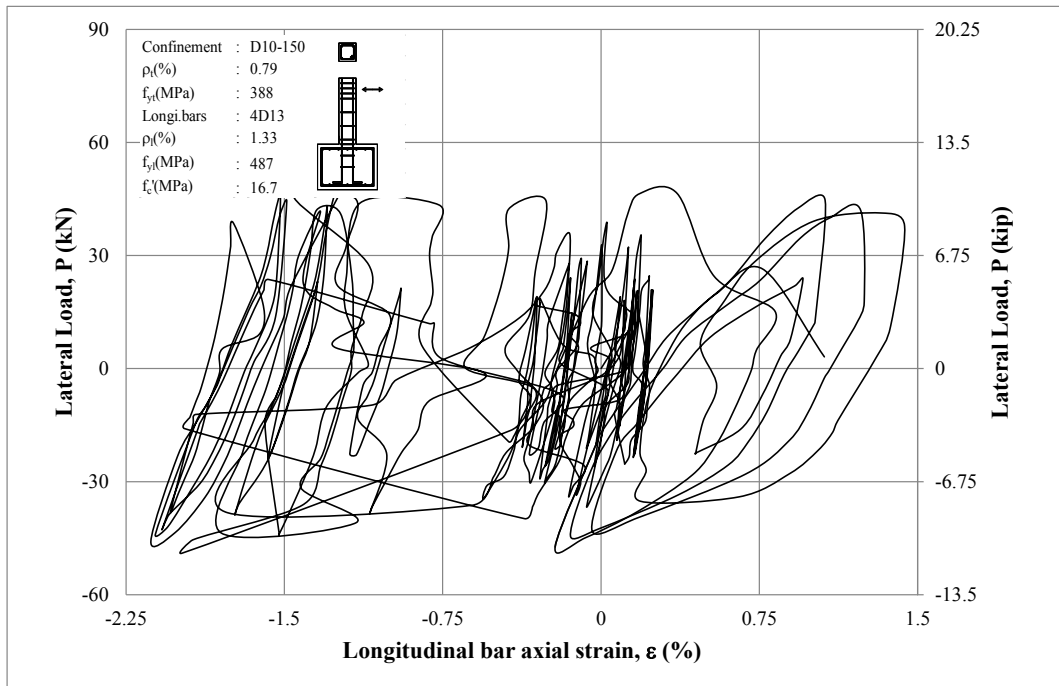
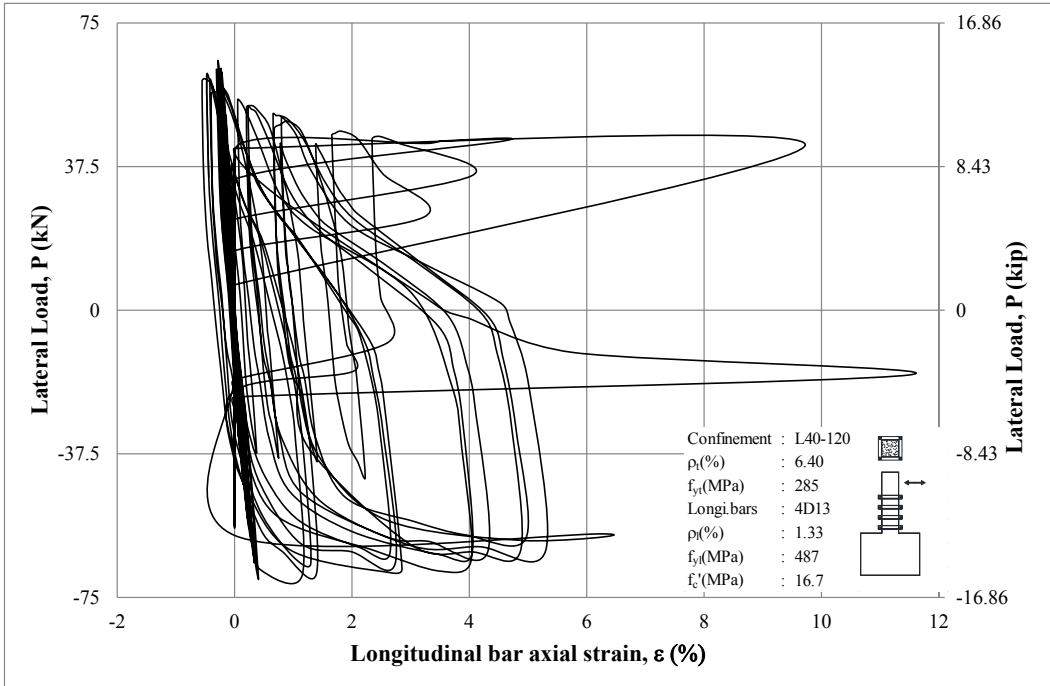**Figure D-9 Lateral load vs measurement of Channels 18 and 19 of CS11**

309
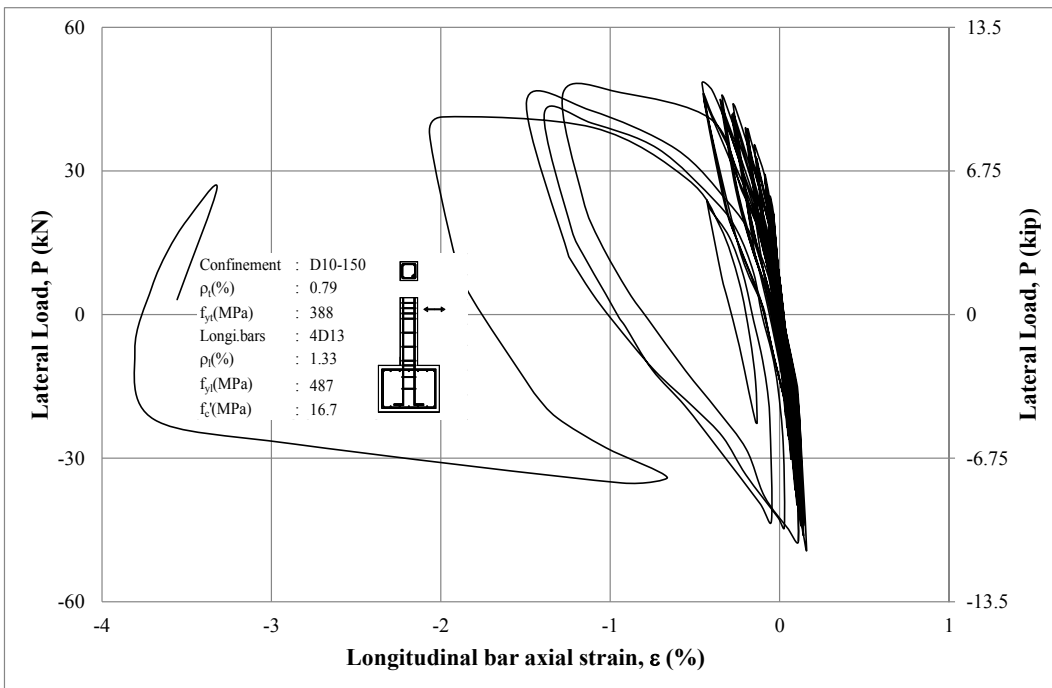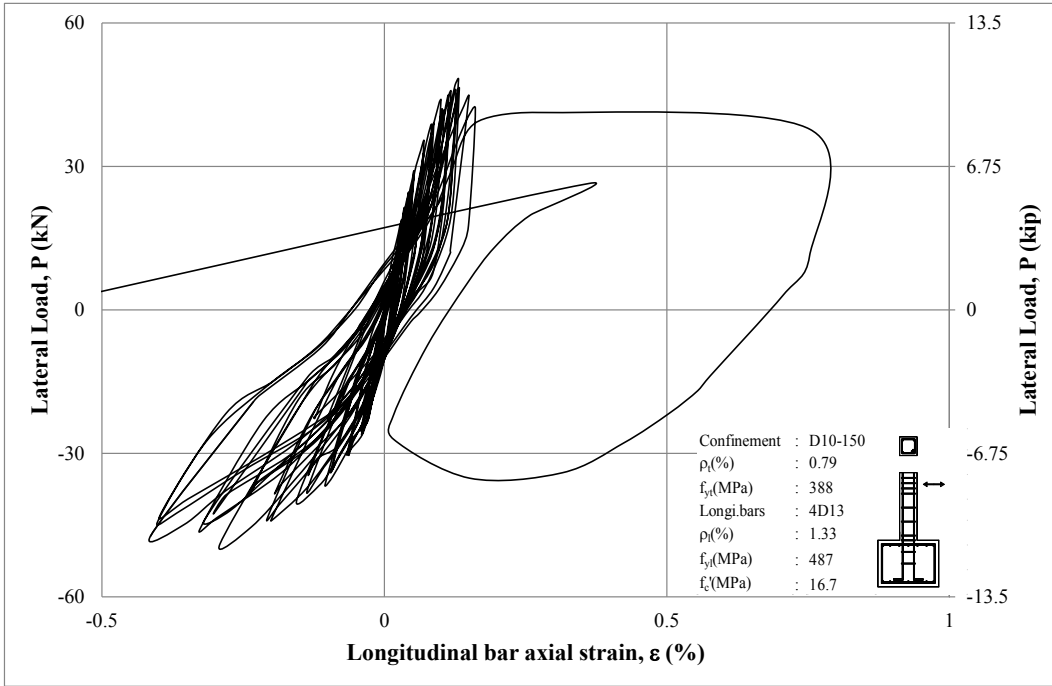
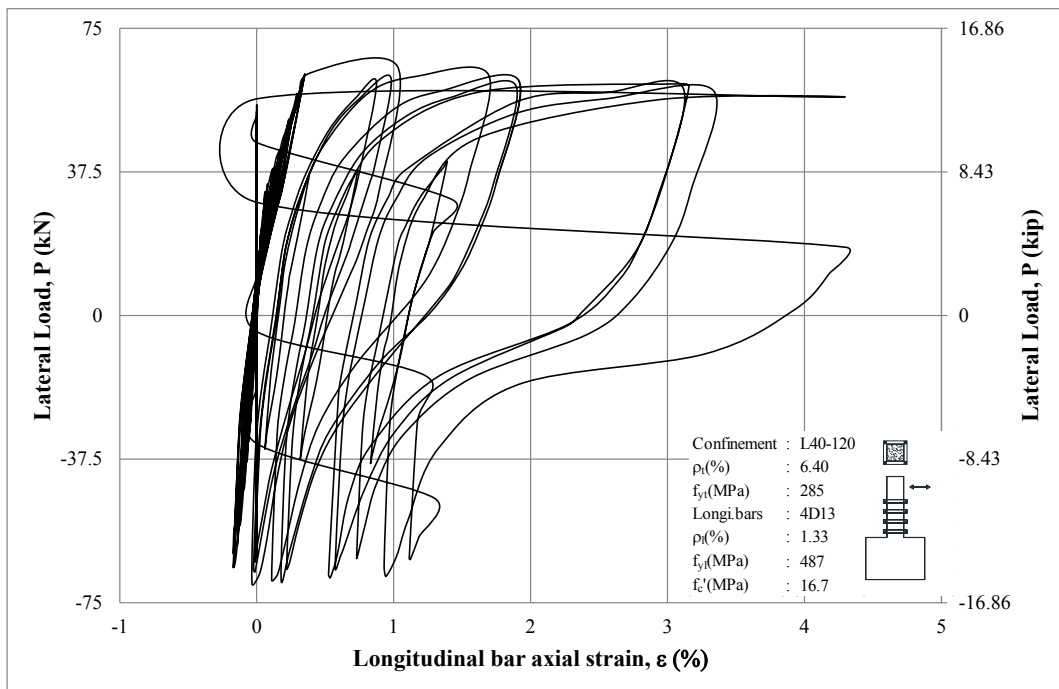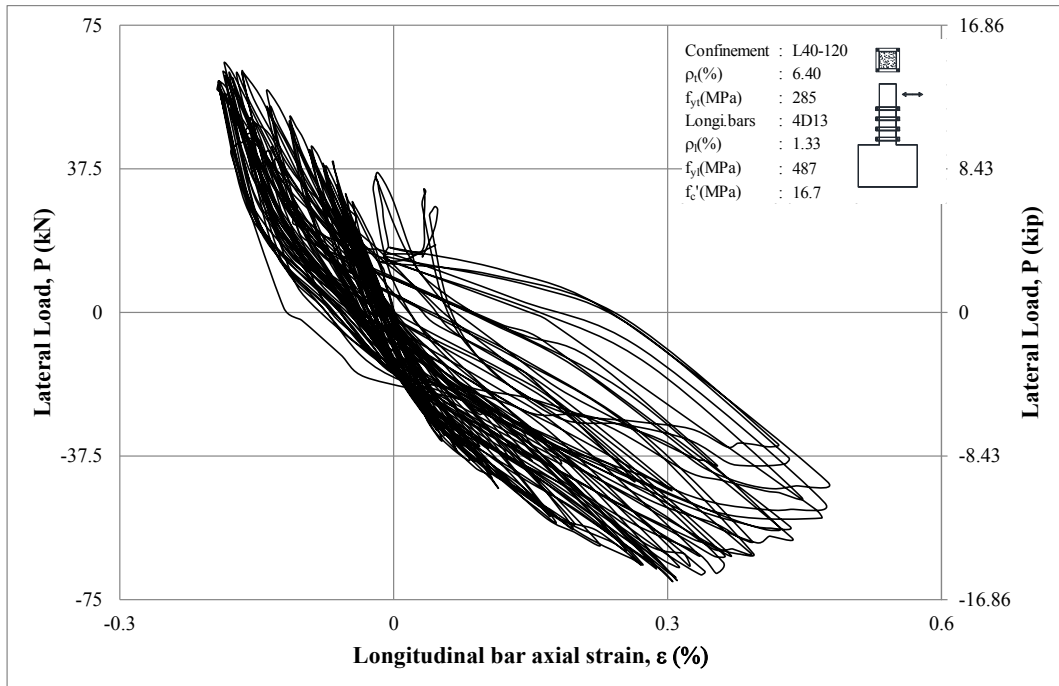**Figure D-10 Lateral load vs measurement of Channels 20 and 21 of CS11**

310
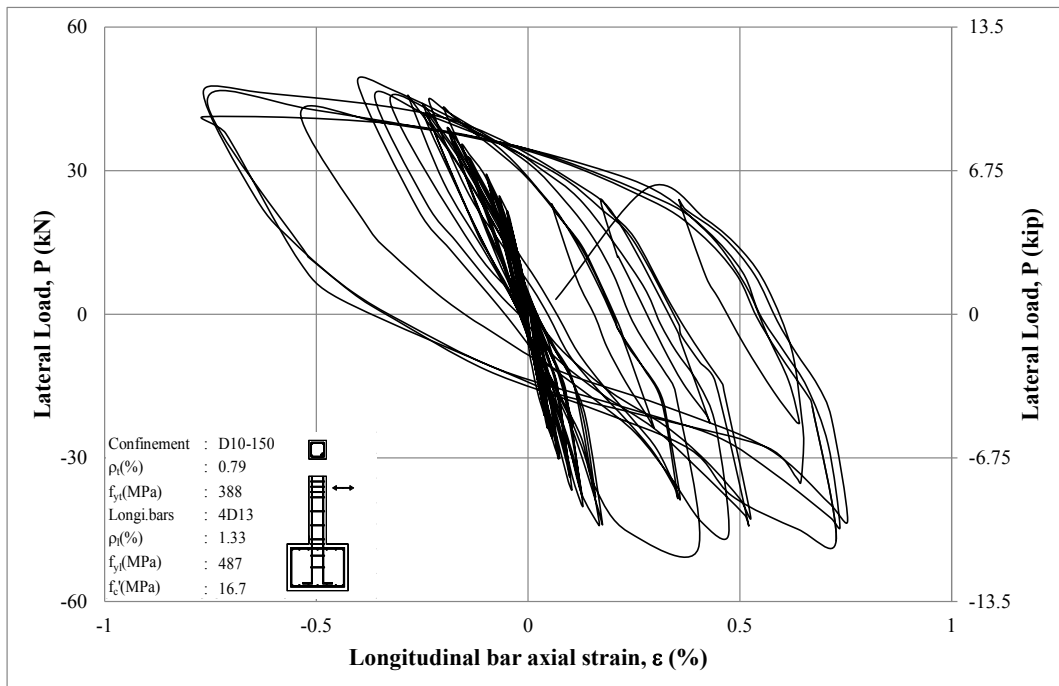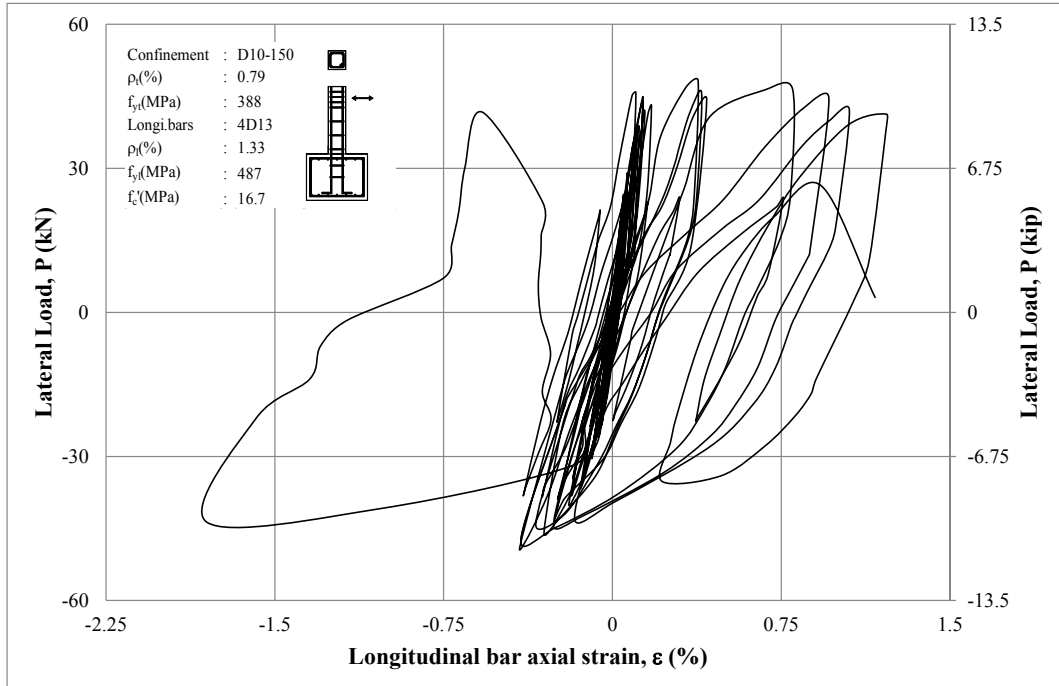
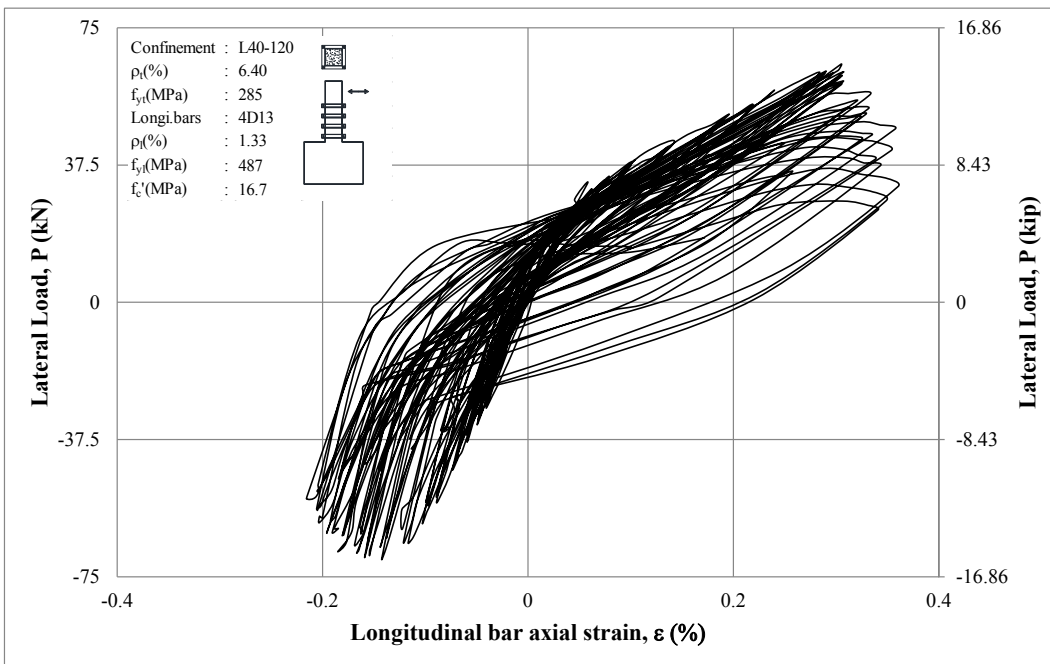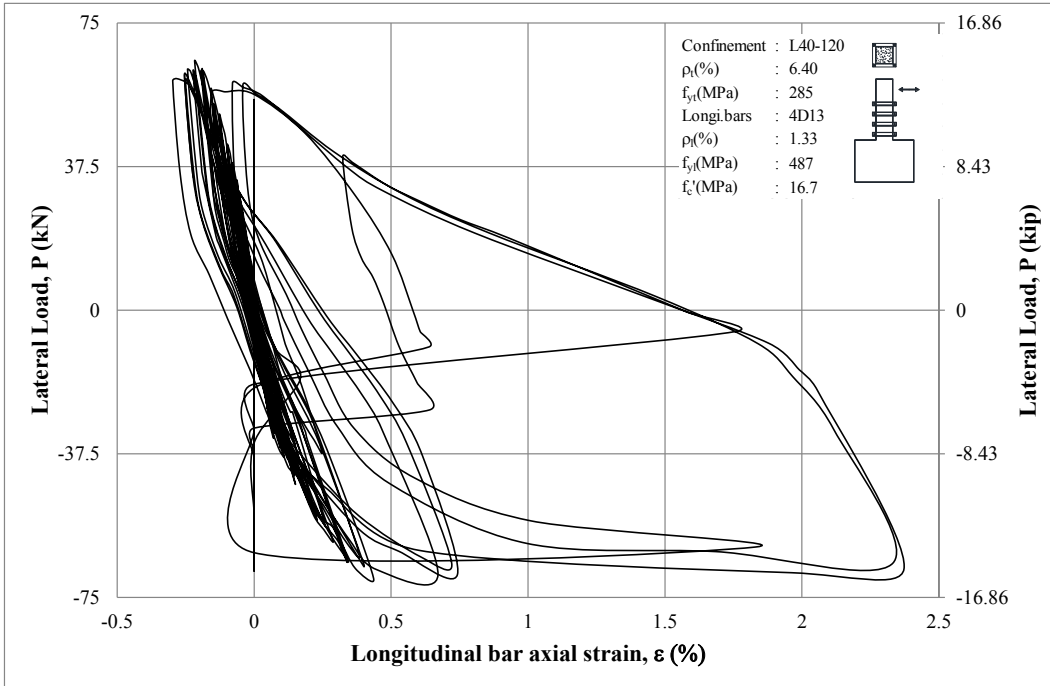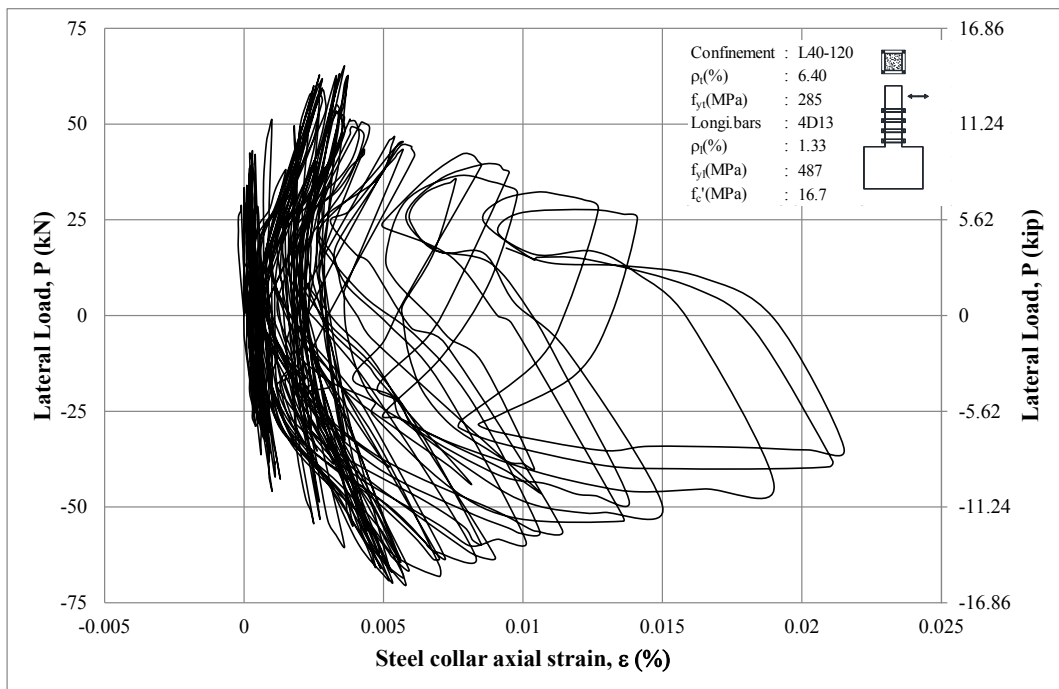**Figure D-11 Lateral load vs measurement of Channels 22 and 23 of CS11**

311

The chart (top) has axes:
- Left vertical axis: **Lateral Load, P (kN)** with values 60, 30, 0, -30, -60
- Right vertical axis: **Lateral Load, P (kip)** with values 13.5, 6.75, 0, -6.75, -13.5
- Horizontal axis: **Longitudinal bar axial strain, ε (%)** with values -2, -1.5, -1, -0.5, 0, 0.5

Inset text:
Confinement : D10-150
ρ_t(%)   : 0.79
f_{yt}(MPa)   : 388
Longi.bars   : 4D13
ρ_f(%)   : 1.33
f_{yf}(MPa)   : 487
f_c'(MPa)   : 16.7

The chart (bottom) has axes:
- Left vertical axis: **Lateral Load, P (kN)** with values 60, 30, 0, -30, -60
- Right vertical axis: **Lateral Load, P (kip)** with values 13.5, 6.75, 0, -6.75, -13.5
- Horizontal axis: **Longitudinal bar axial strain, ε (%)** with values -4, -3, -2, -1, 0, 1

Inset text:
Confinement : D10-150
ρ_t(%)   : 0.79
f_{yt}(MPa)   : 388
Longi.bars   : 4D13
ρ_f(%)   : 1.33
f_{yf}(MPa)   : 487
f_c'(MPa)   : 16.7

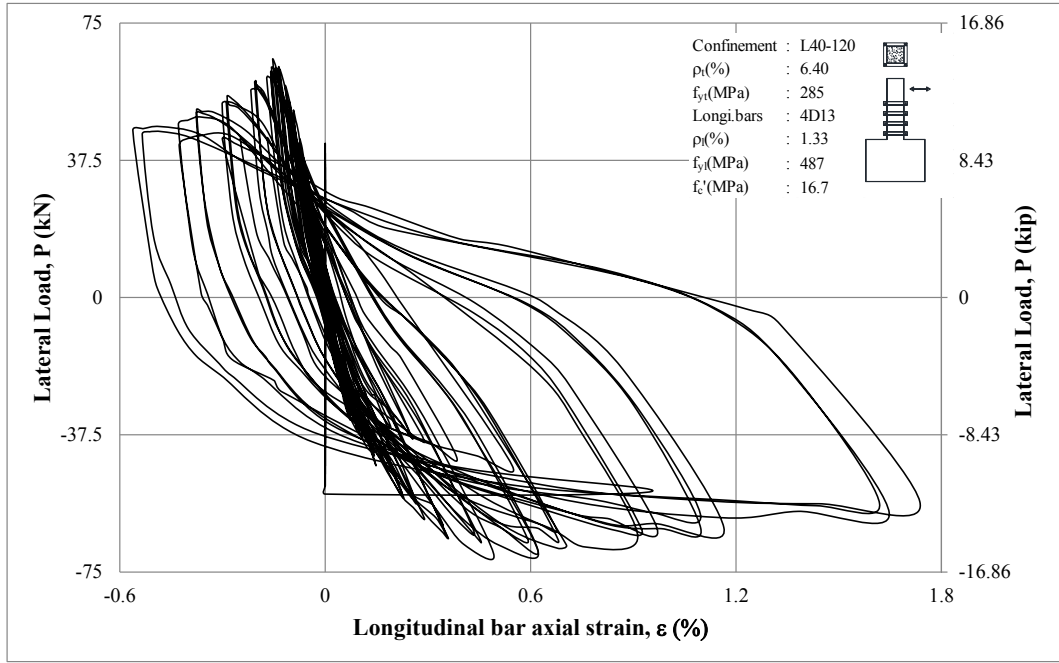**Figure D-12 Lateral load vs measurement of Channels 24 and 25 of CS11**

312
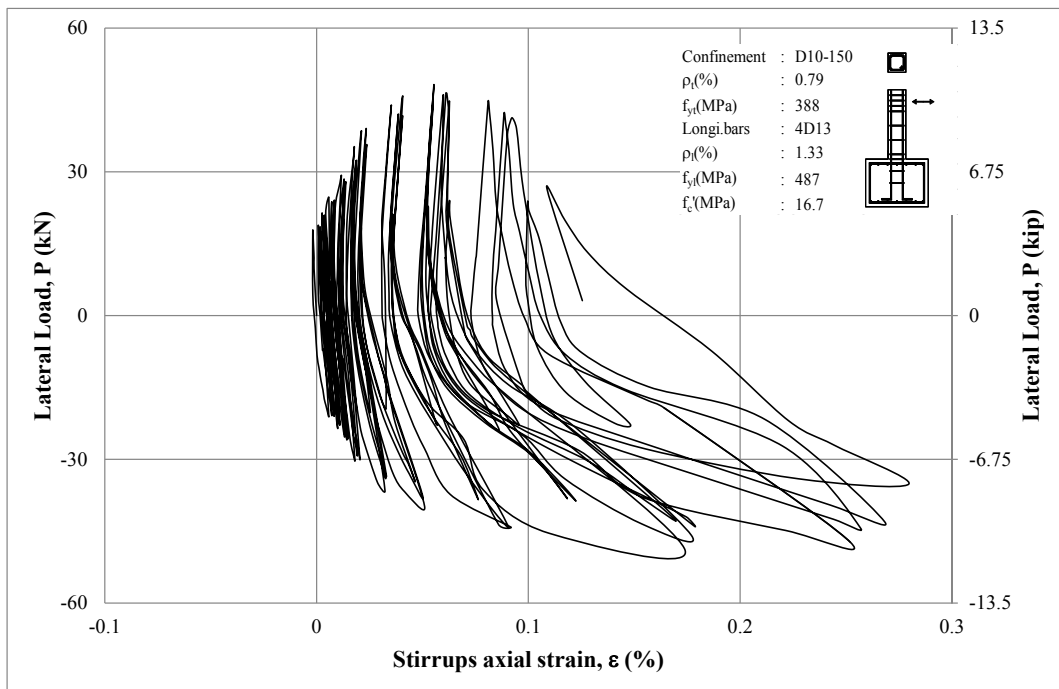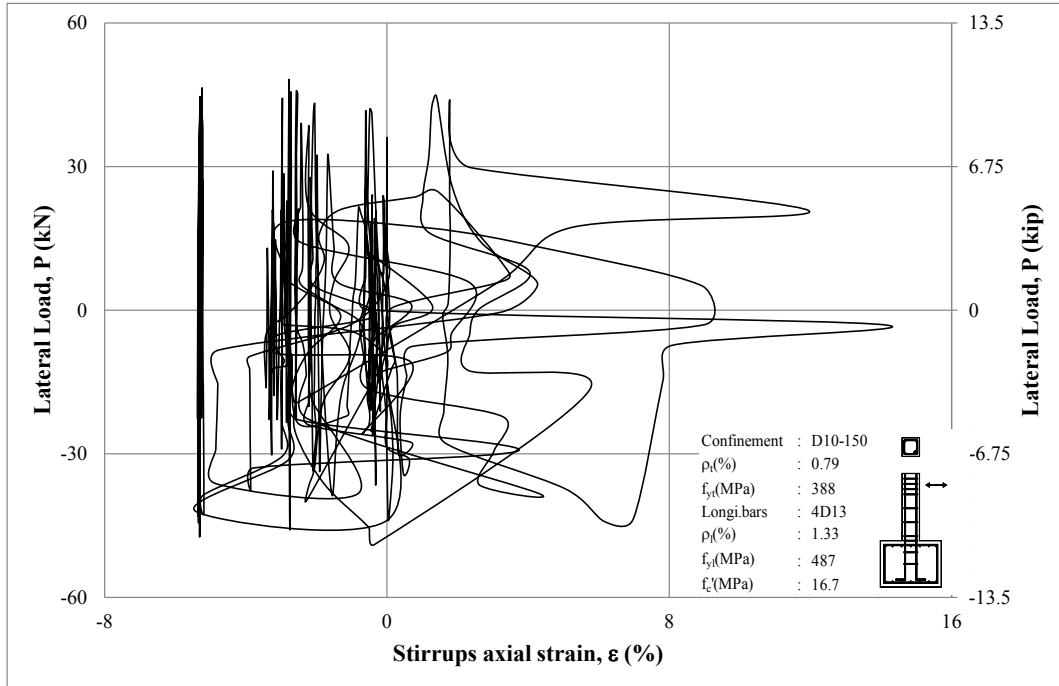
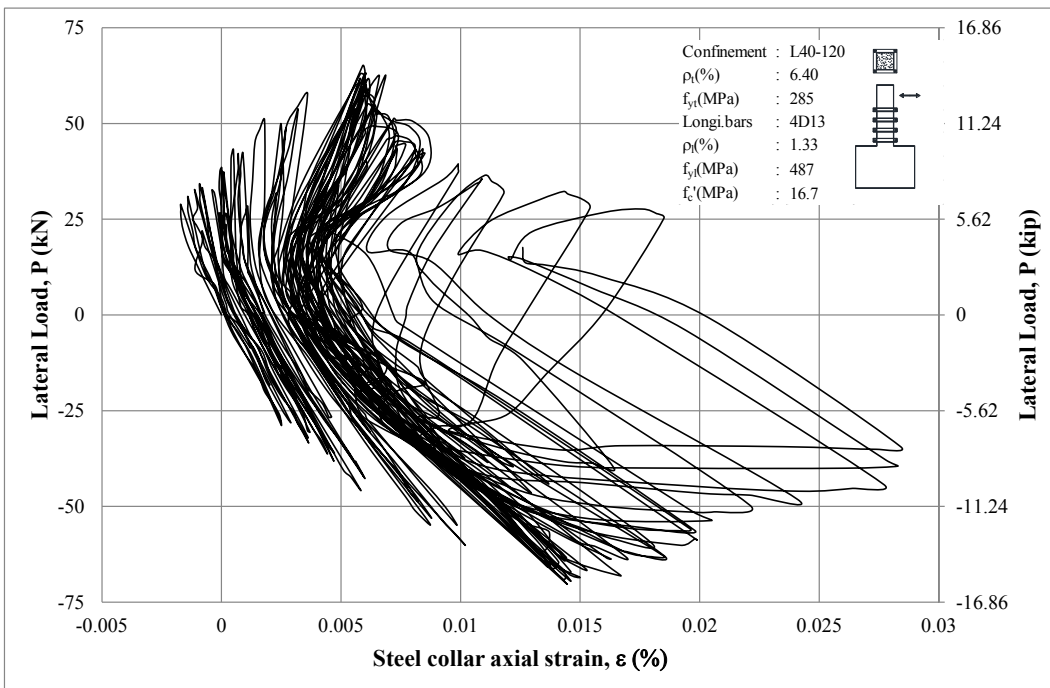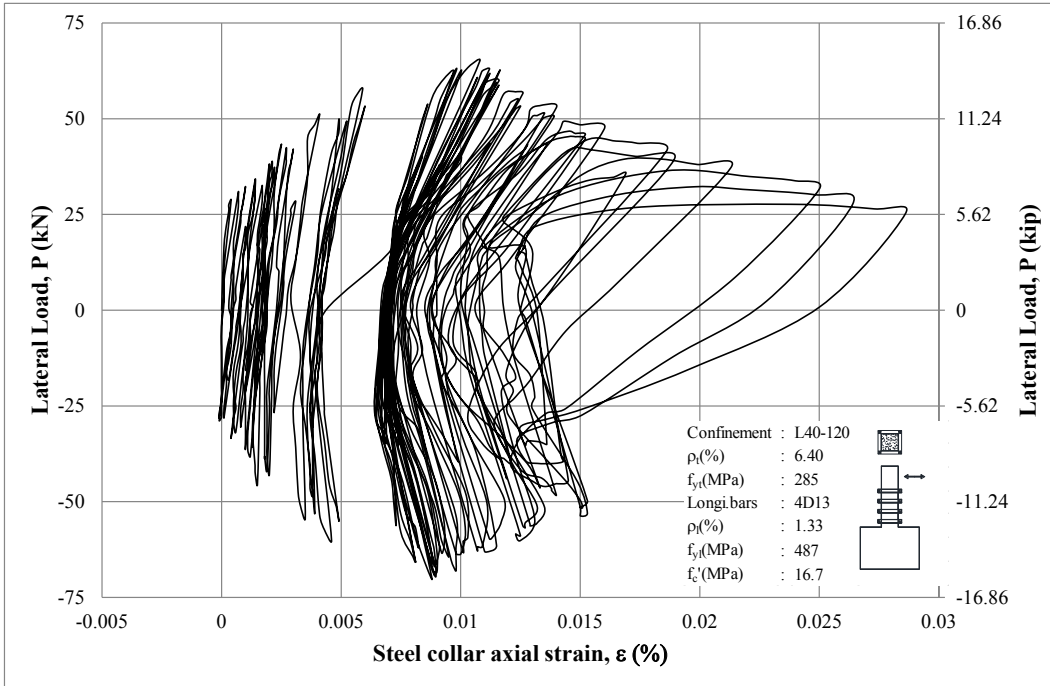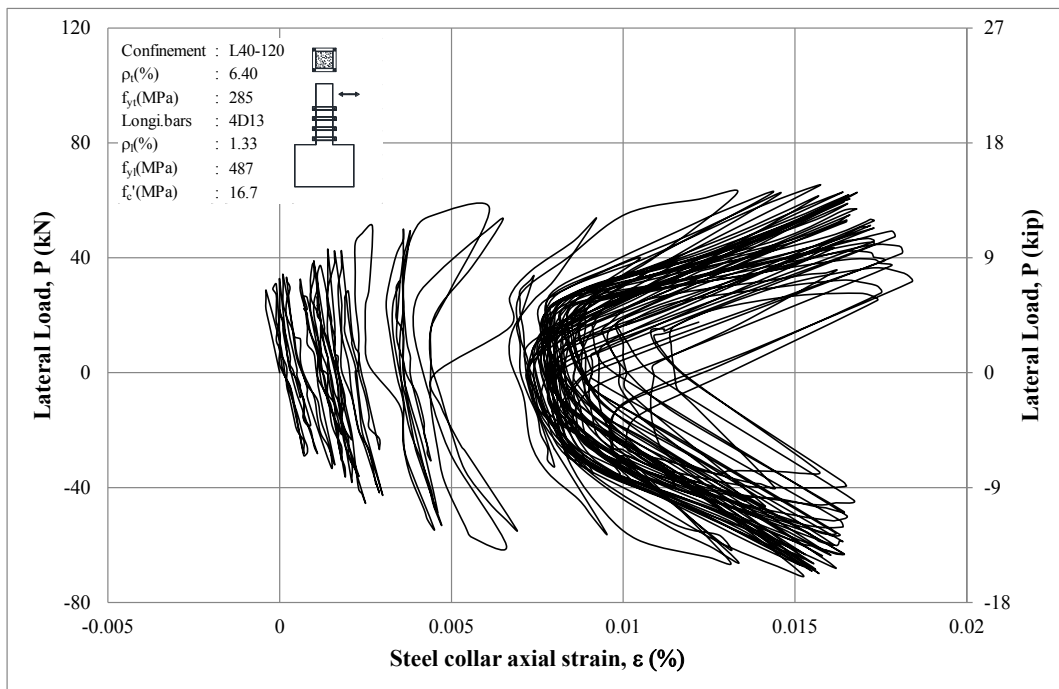**Figure D-13 Lateral load vs measurement of Channels 26 and 27 of CS11**
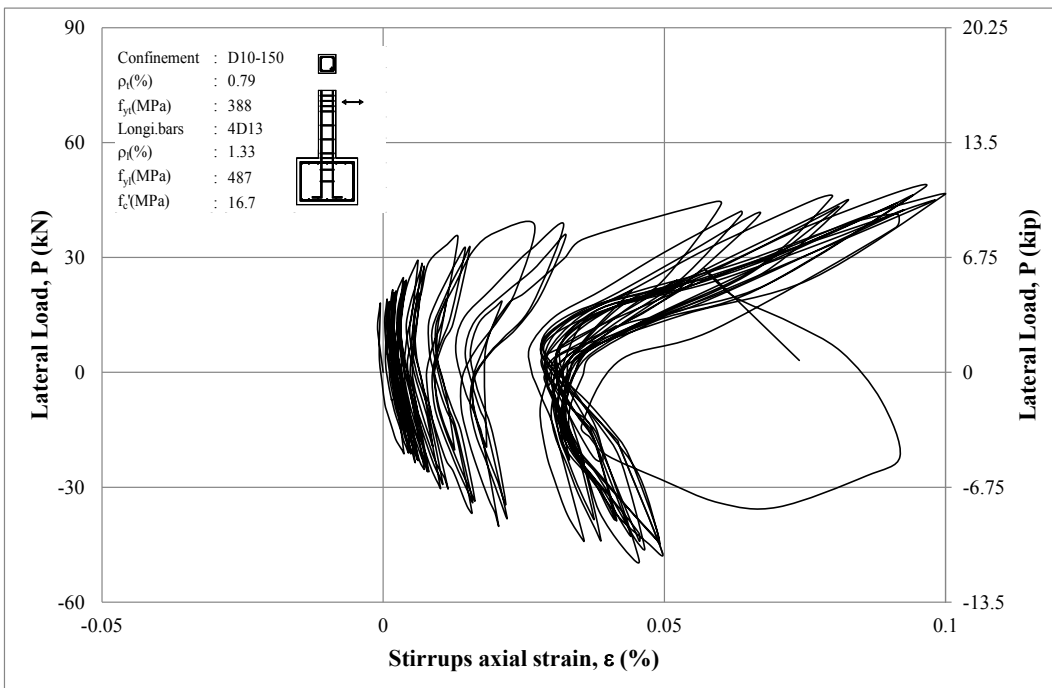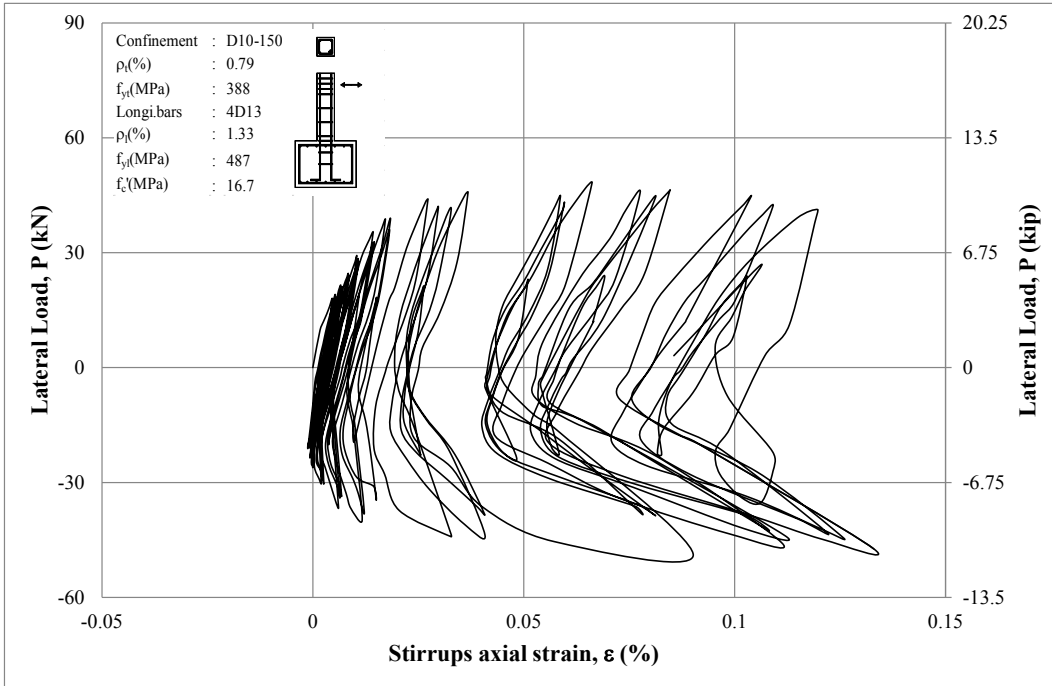
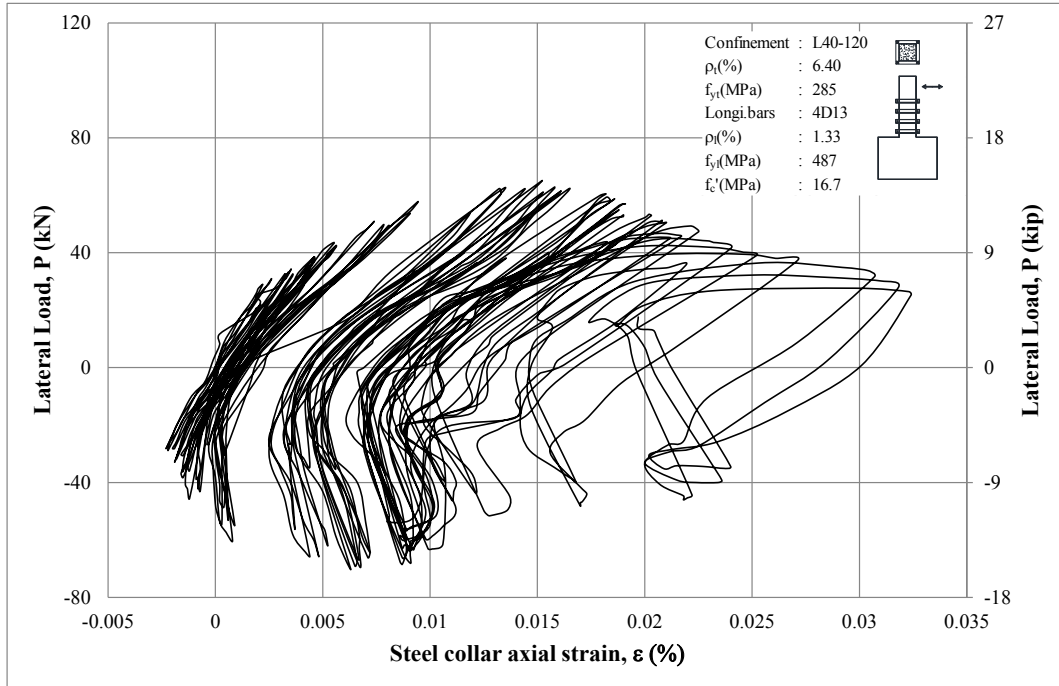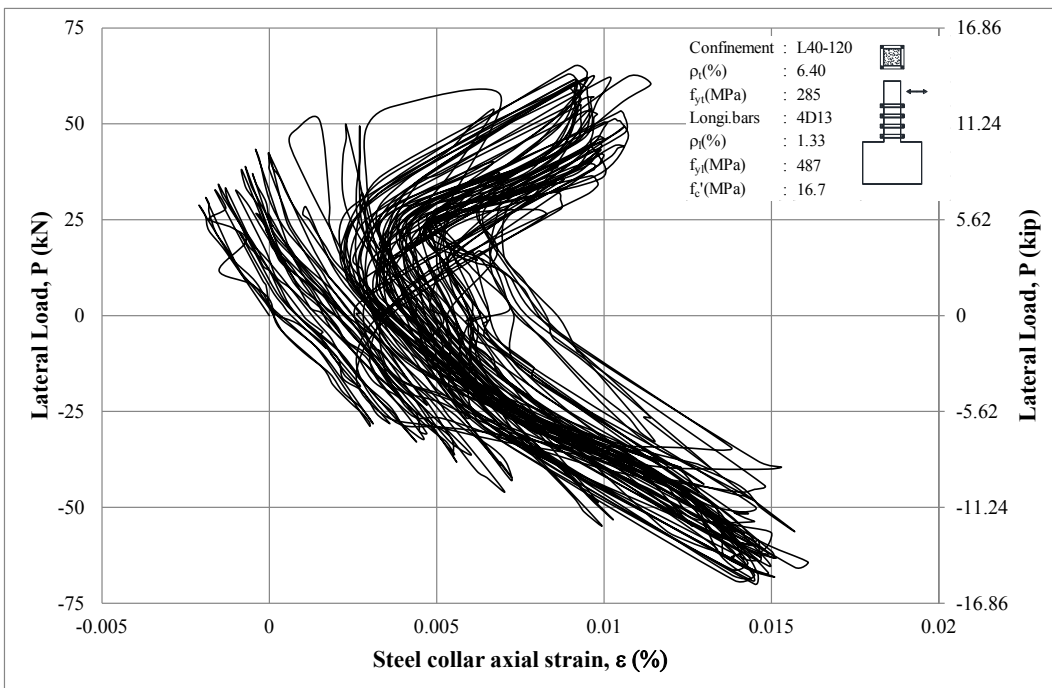**Figure D-14 Lateral load vs measurement of Channels 28 and 29 of CS11**

314

Top chart:

Horizontal hydraulic jack stroke, Δ (in)

-1.9685 -0.98425 0 0.98425 1.9685

Lateral Load, P (kN): 90, 60, 30, 0, -30, -60

Lateral Load, P (kip): 20.25, 13.5, 6.75, 0, -6.75, -13.5

Confinement : D10-50
ρ_t(%) : 2.36
f_{yt}(MPa) : 388
Longi.bars : 4D13
ρ_l(%) : 1.33
f_{yl}(MPa) : 487
f_c'(MPa) : 16.7

Horizontal hydraulic jack stroke, Δ (mm)

-50 -25 0 25 50

Bottom chart:

Horizontal hydraulic jack stroke, Δ (in)

-1.9685 -0.98425 0 0.98425 1.9685

Lateral Load, P (kN): 90, 60, 30, 0, -30, -60

Lateral Load, P (kip): 20.25, 13.5, 6.75, 0, -6.75, -13.5

Confinement : D10-50
ρ_t(%) : 2.36
f_{yt}(MPa) : 388
Longi.bars : 4D13
ρ_l(%) : 1.33
f_{yl}(MPa) : 487
f_c'(MPa) : 16.7

Horizontal hydraulic jack stroke, Δ (mm)

-50 -25 0 25 50

Figure D-15 Lateral load vs measurement of Channels 2 and 3 of CS12
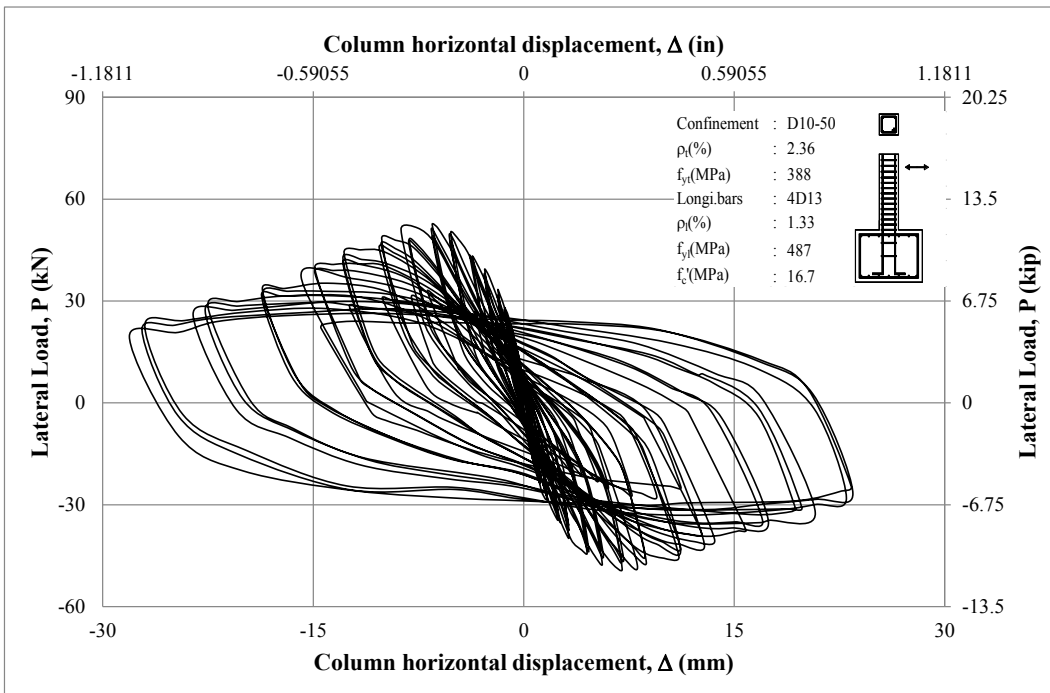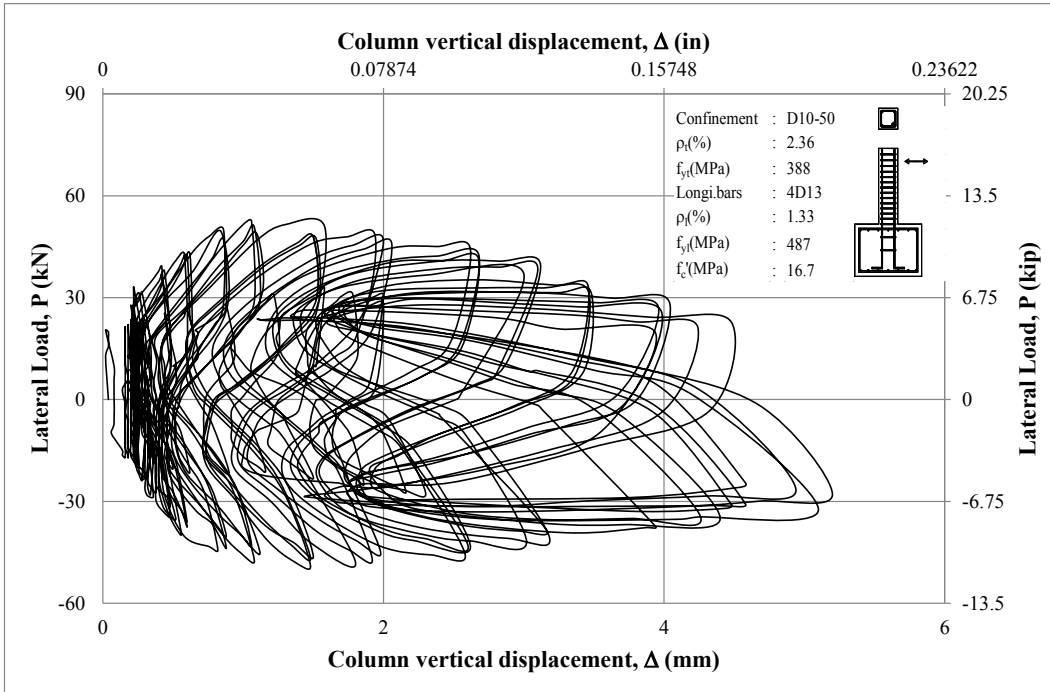
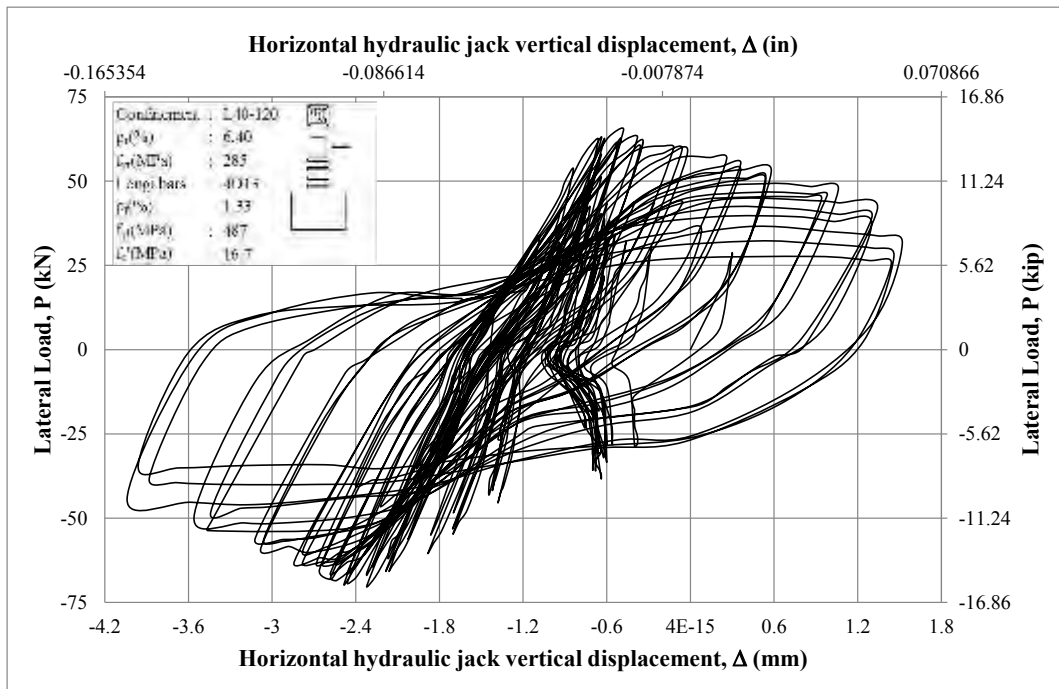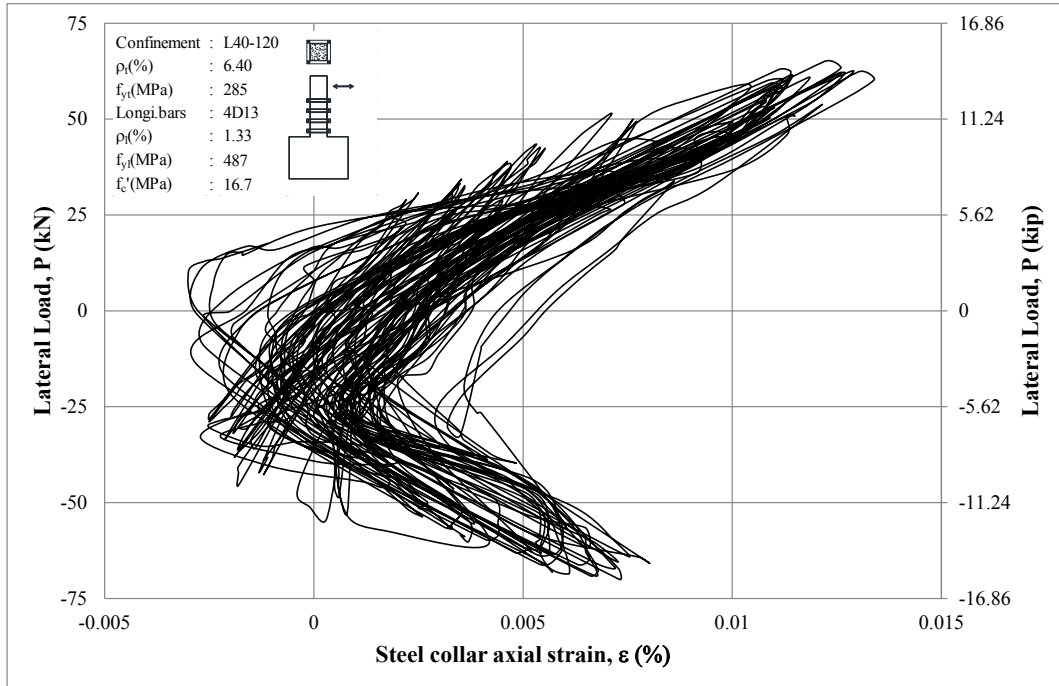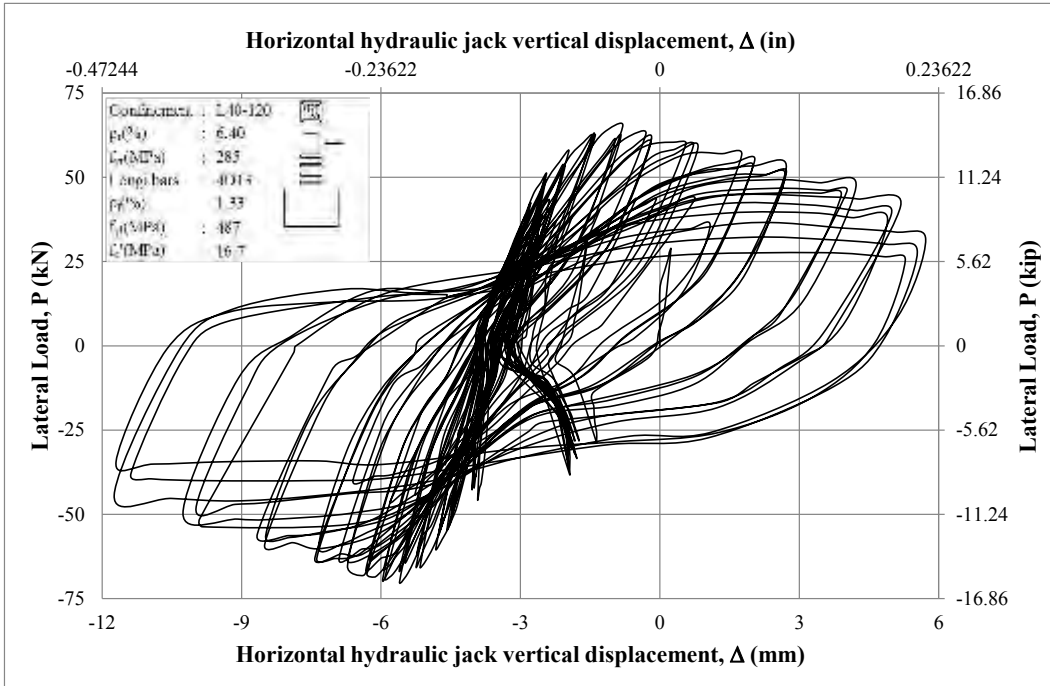**Figure D-16 Lateral load vs measurement of Channels 4 and 5 of CS12**
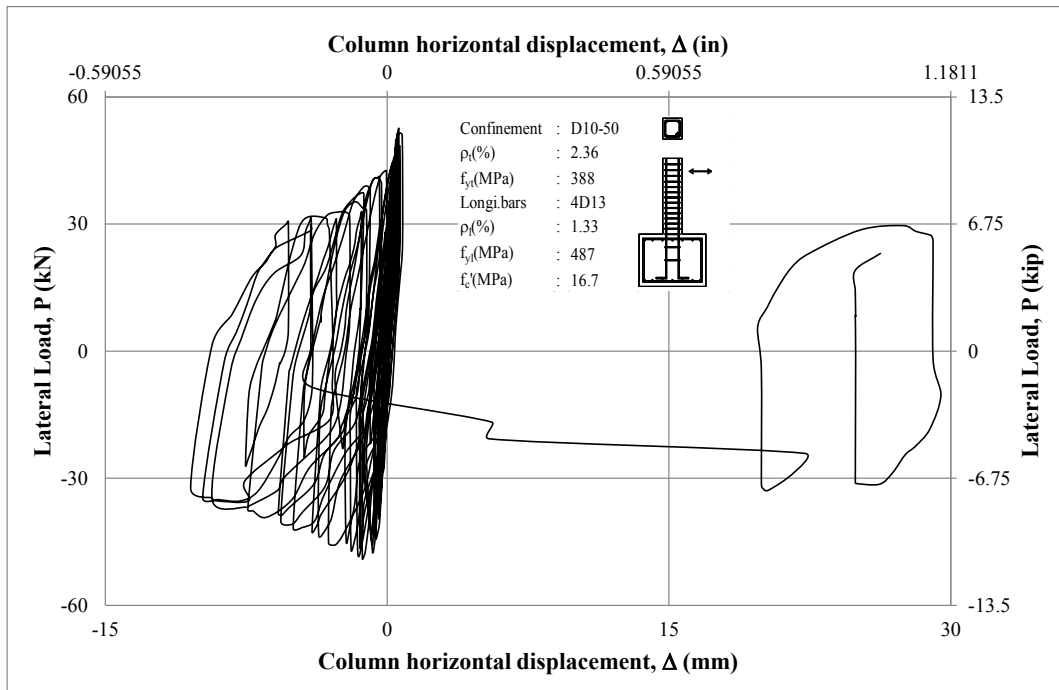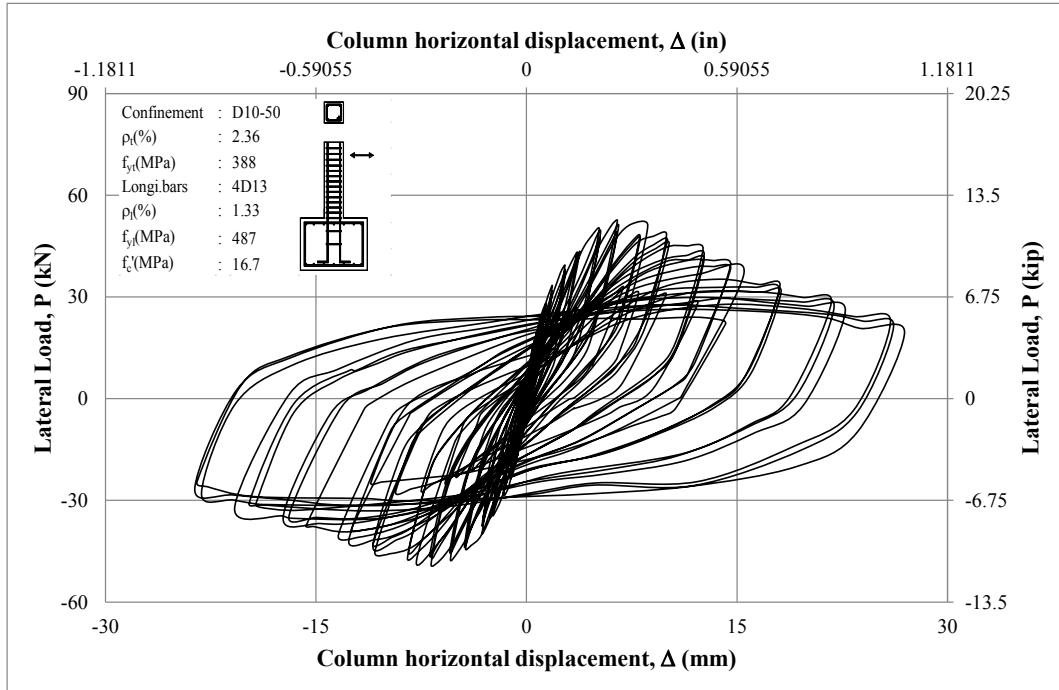
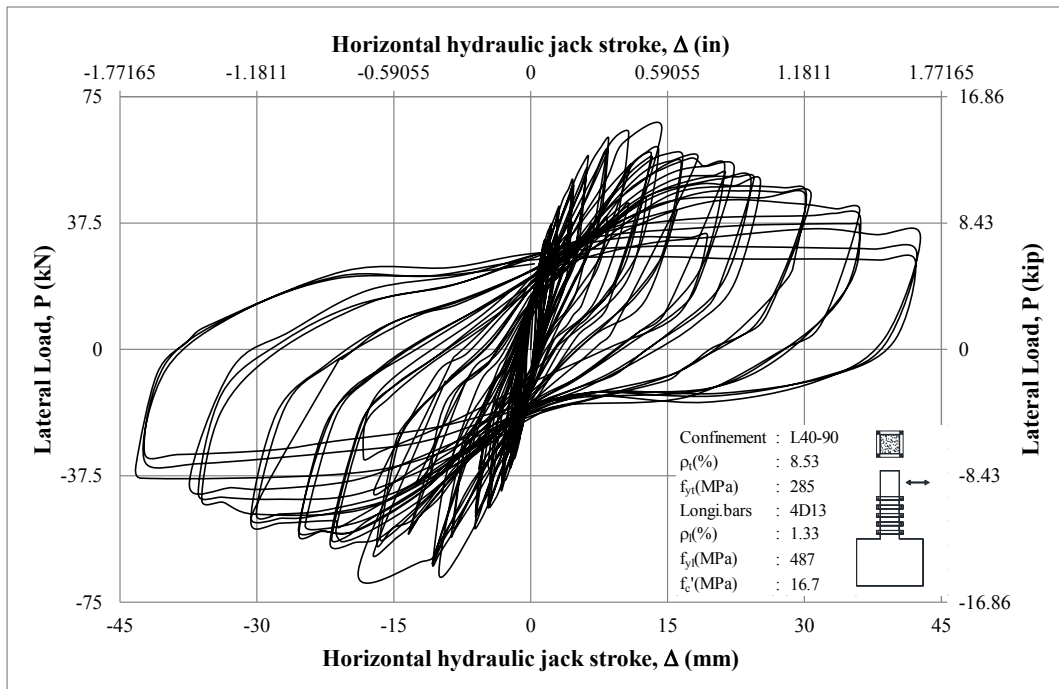**Figure D-17 Lateral load vs measurement of Channels 6 and 7 of CS12**

317
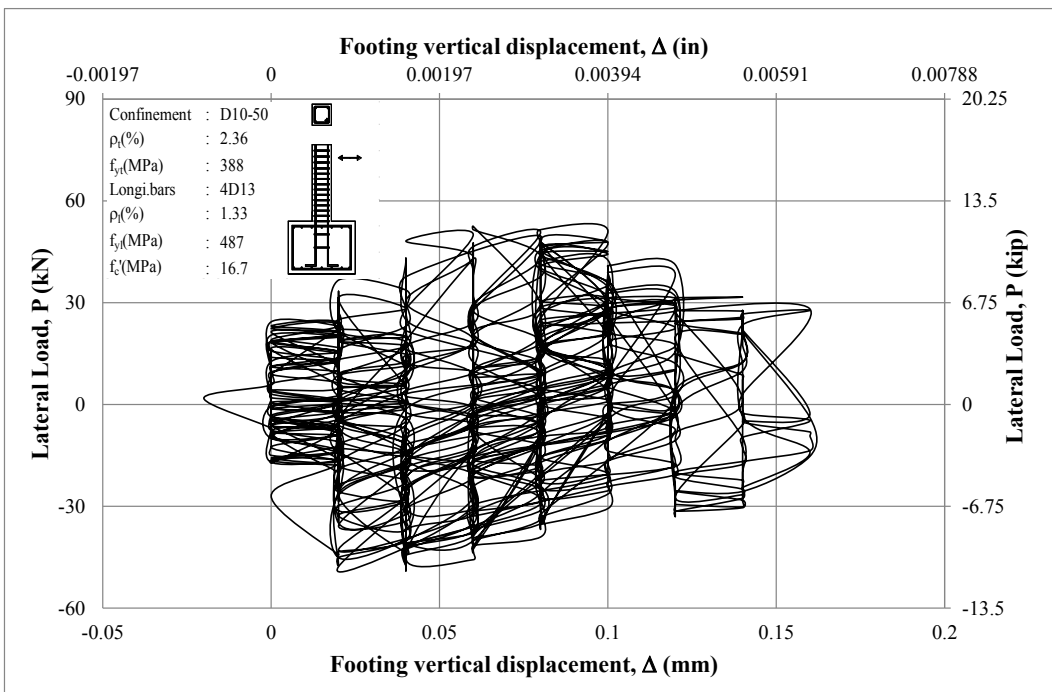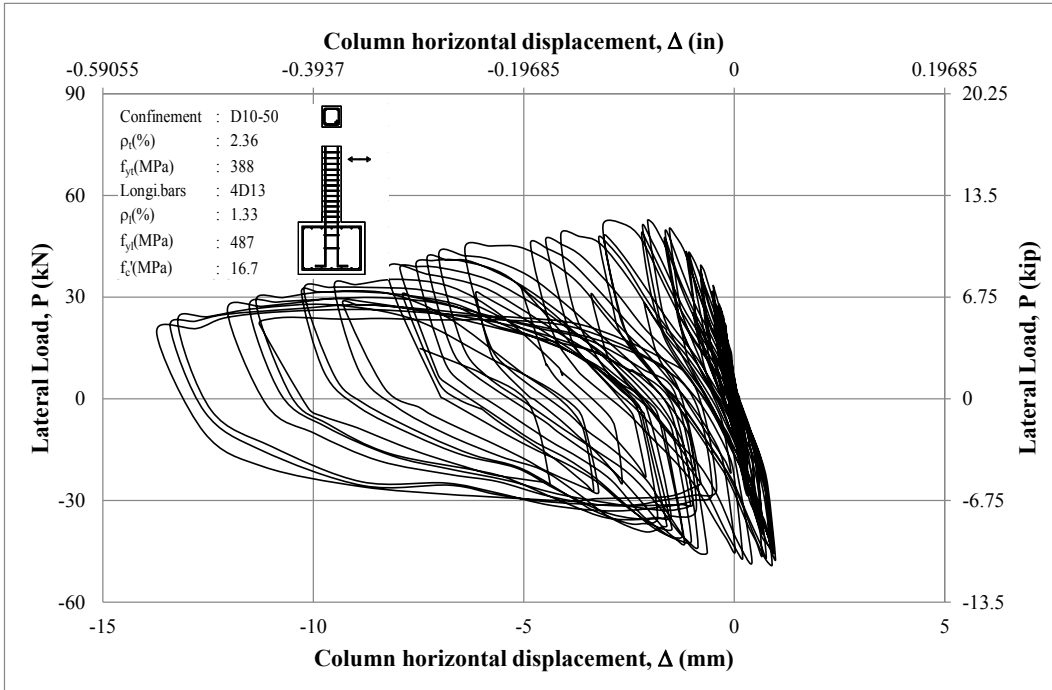
Figure D-18 Lateral load vs measurement of Channels 8 and 9 of CS12
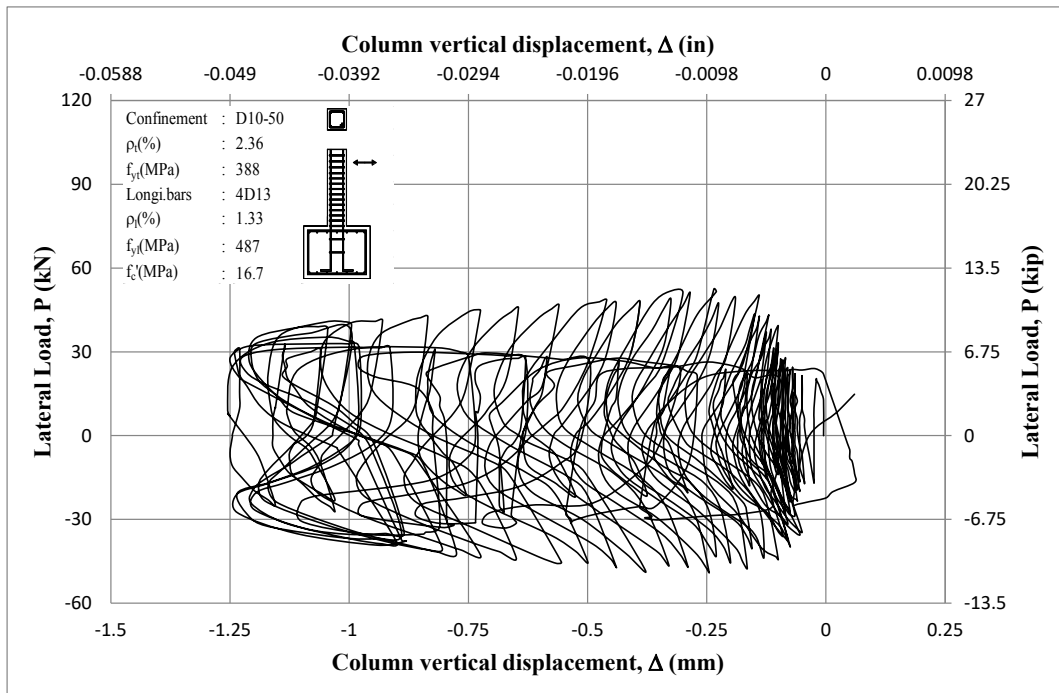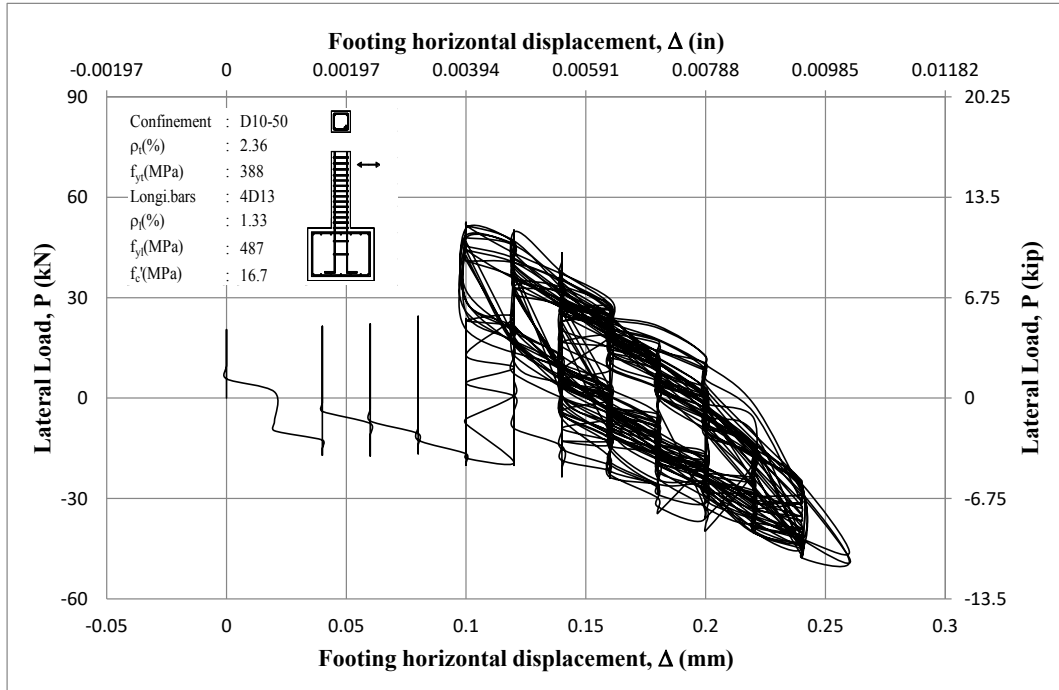
Figure D-19 Lateral load vs measurement of Channels 10 and 11 of CS12

319
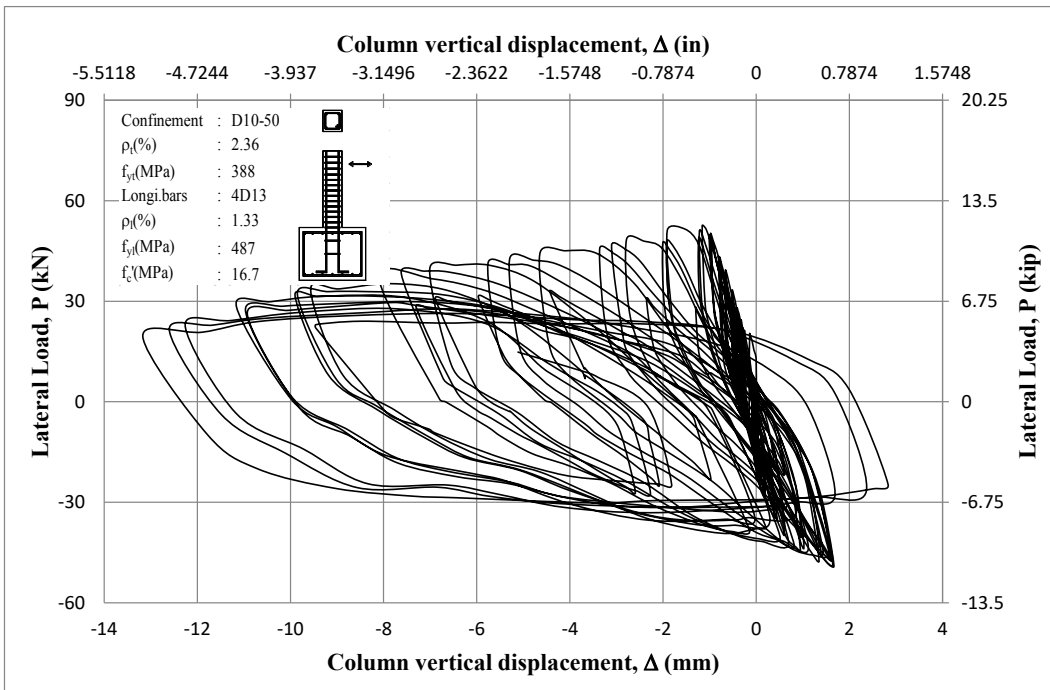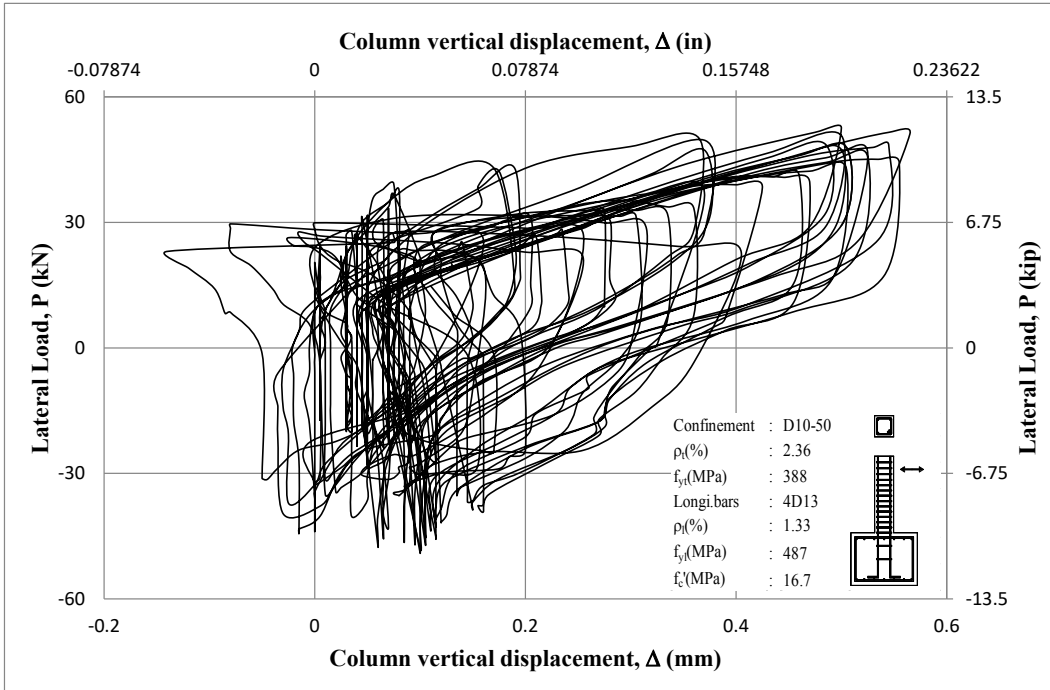
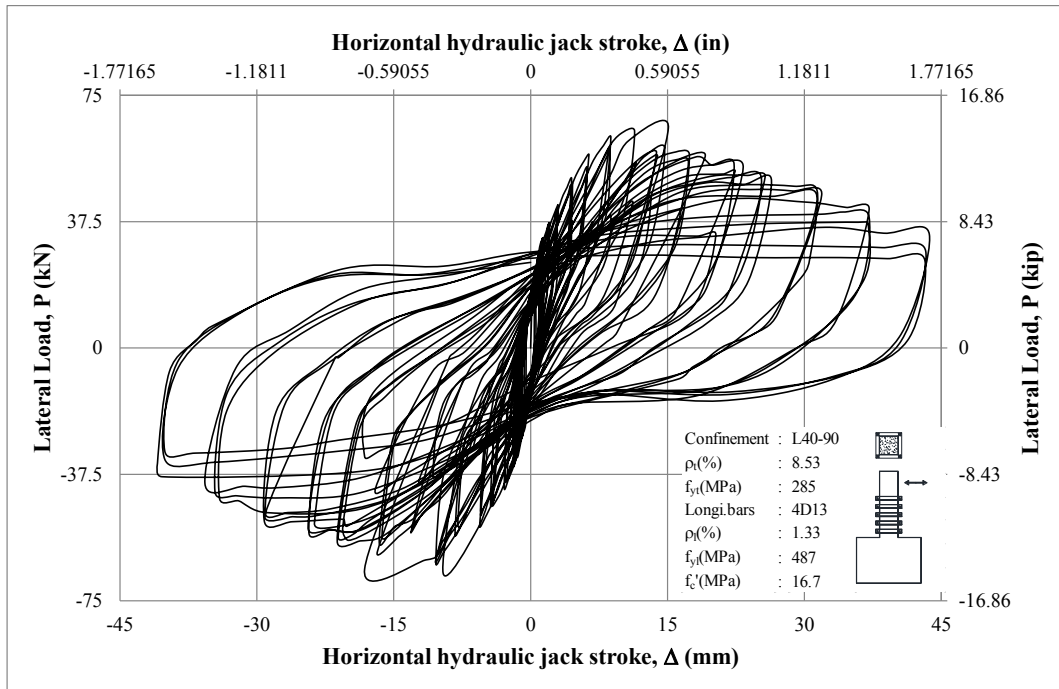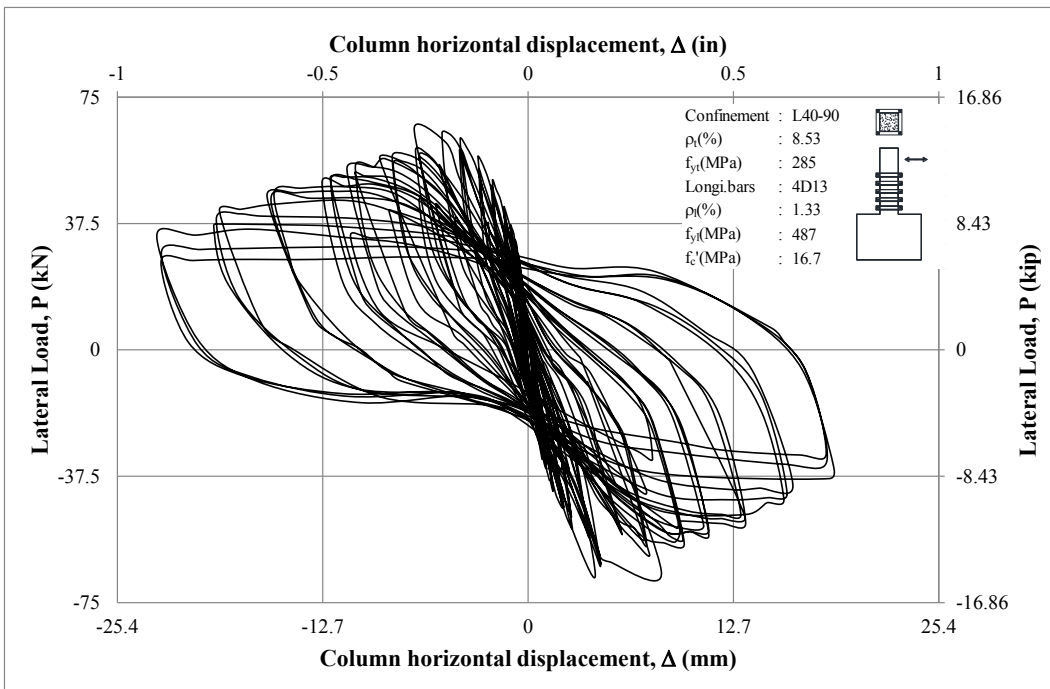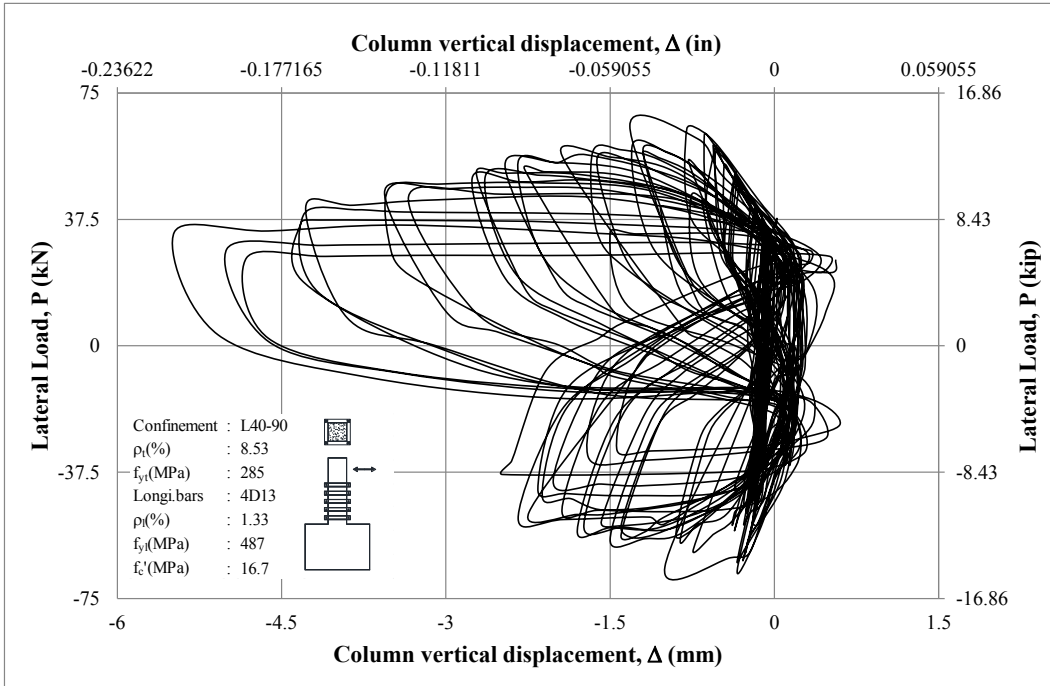Figure D-20 Lateral load vs measurement of Channels 12 and 13 of CS12

320
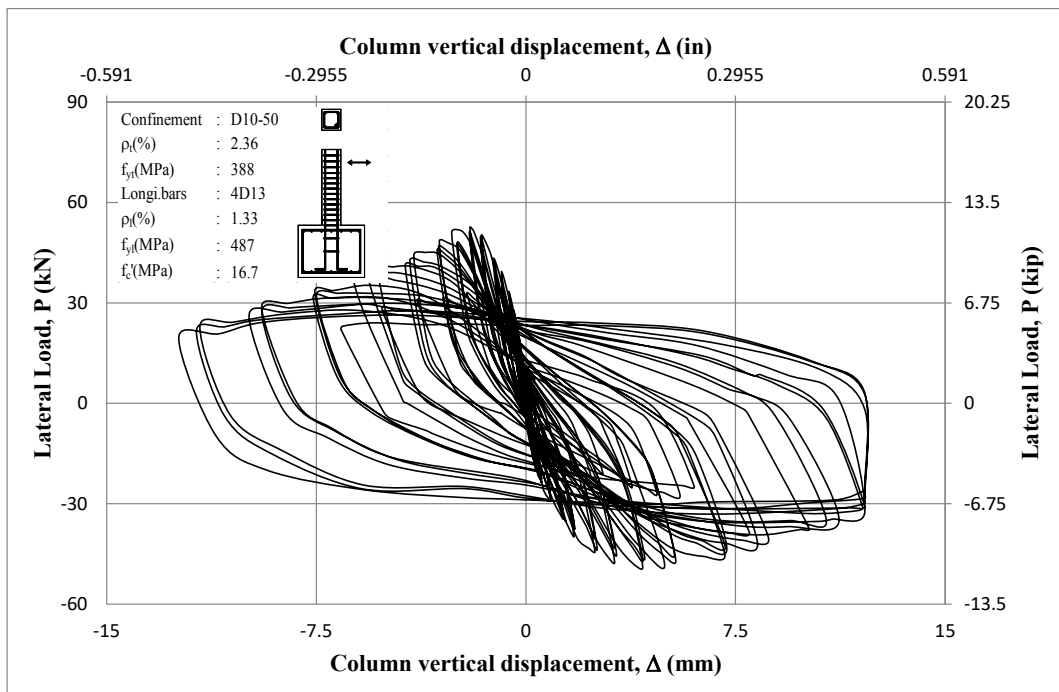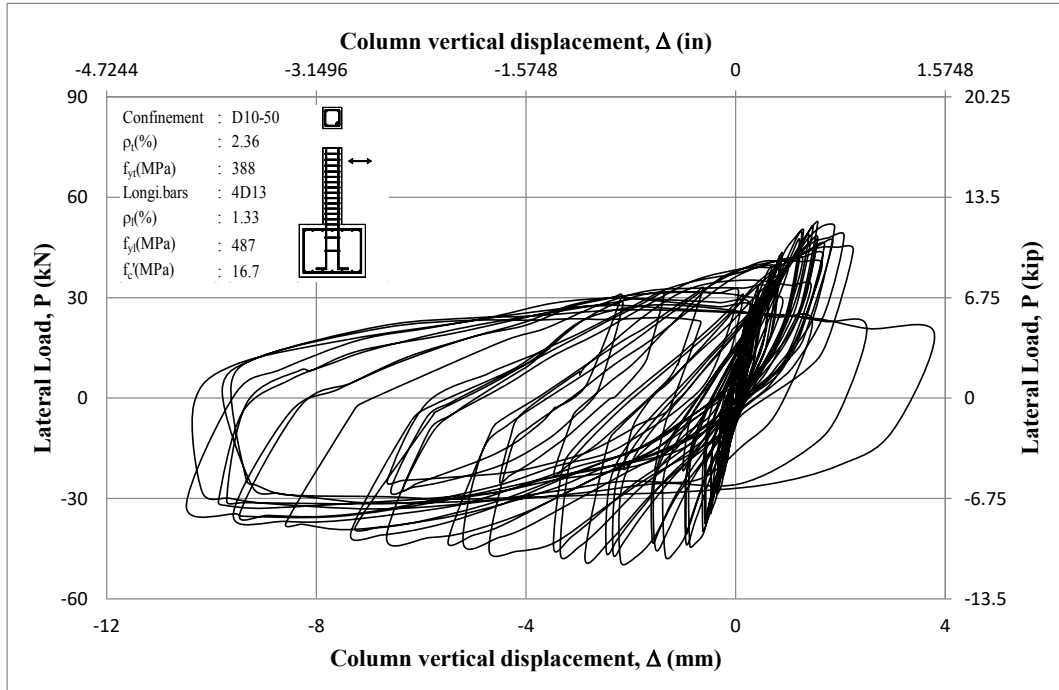
Figure D-21 Lateral load vs measurement of Channels 14 and 15 of CS12
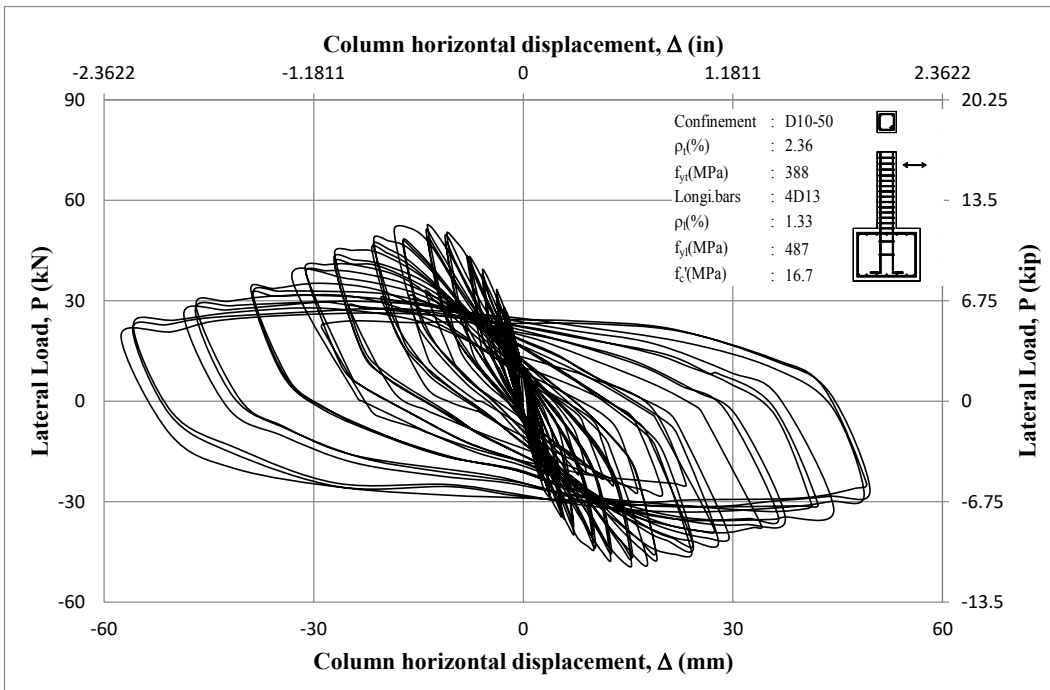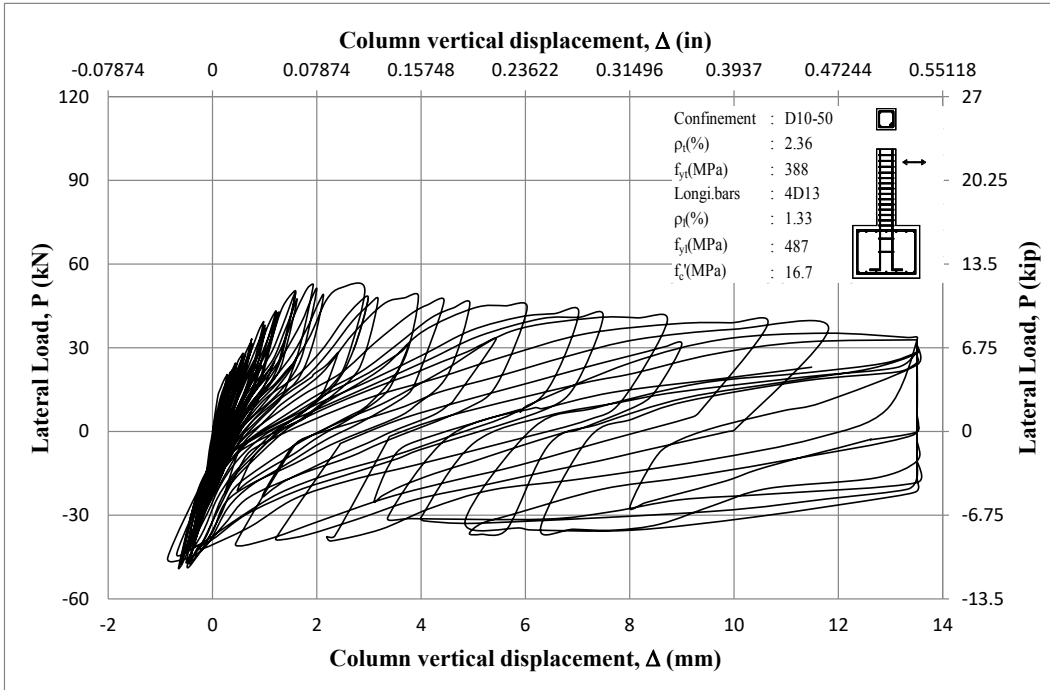
Figure D-22 Lateral load vs measurement of Channels 16 and 17 of CS12

322
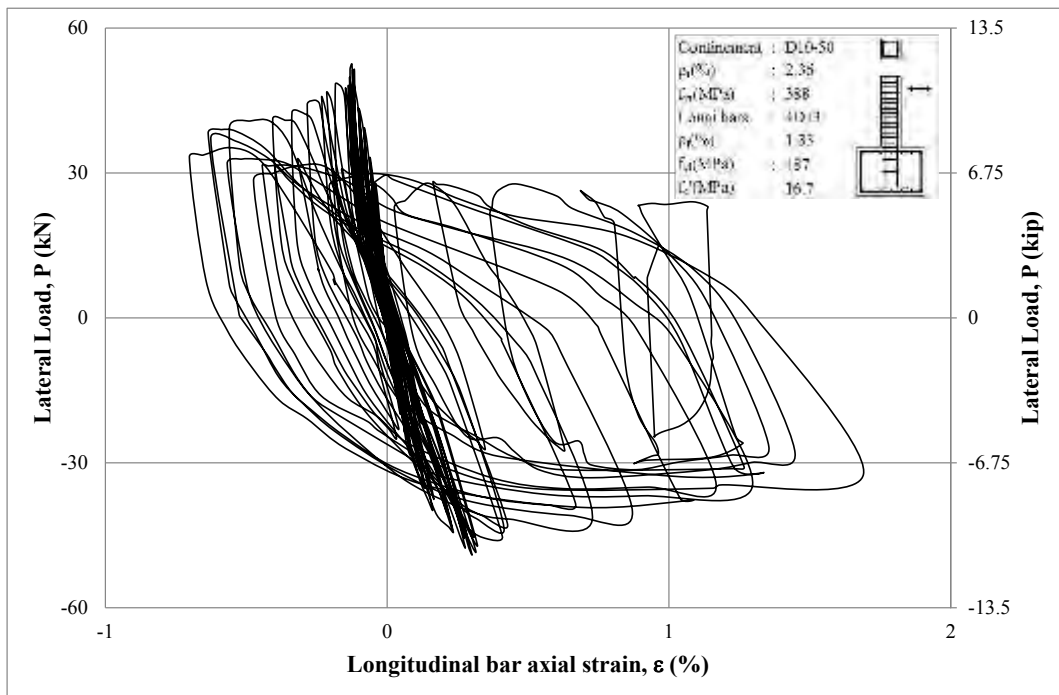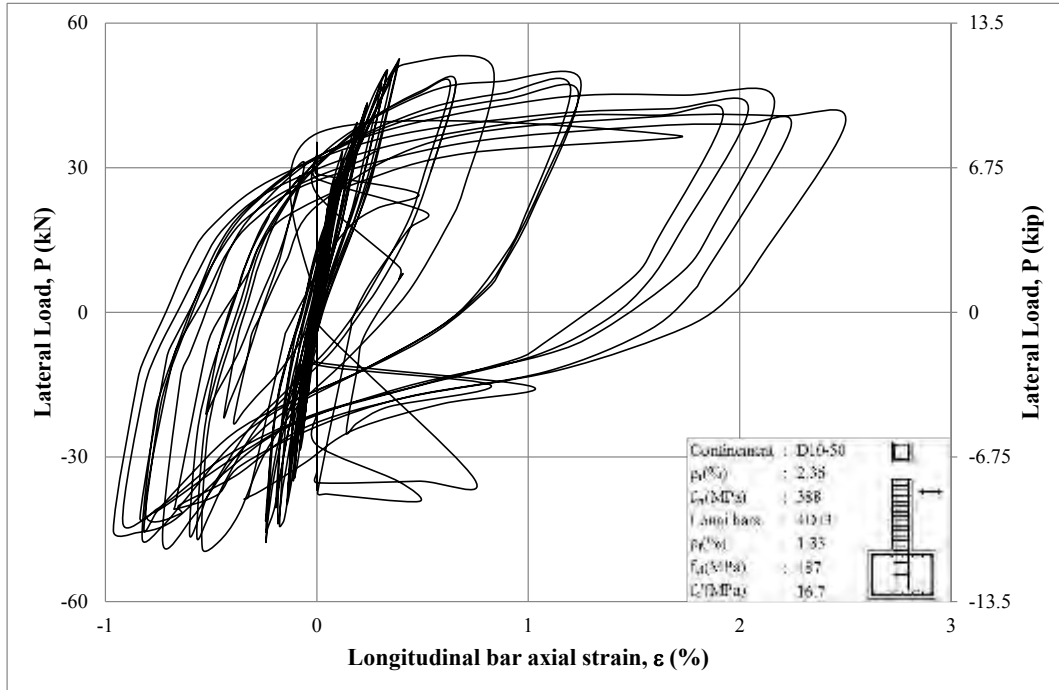
Figure D-23 Lateral load vs measurement of Channels 18 and 19 of CS12
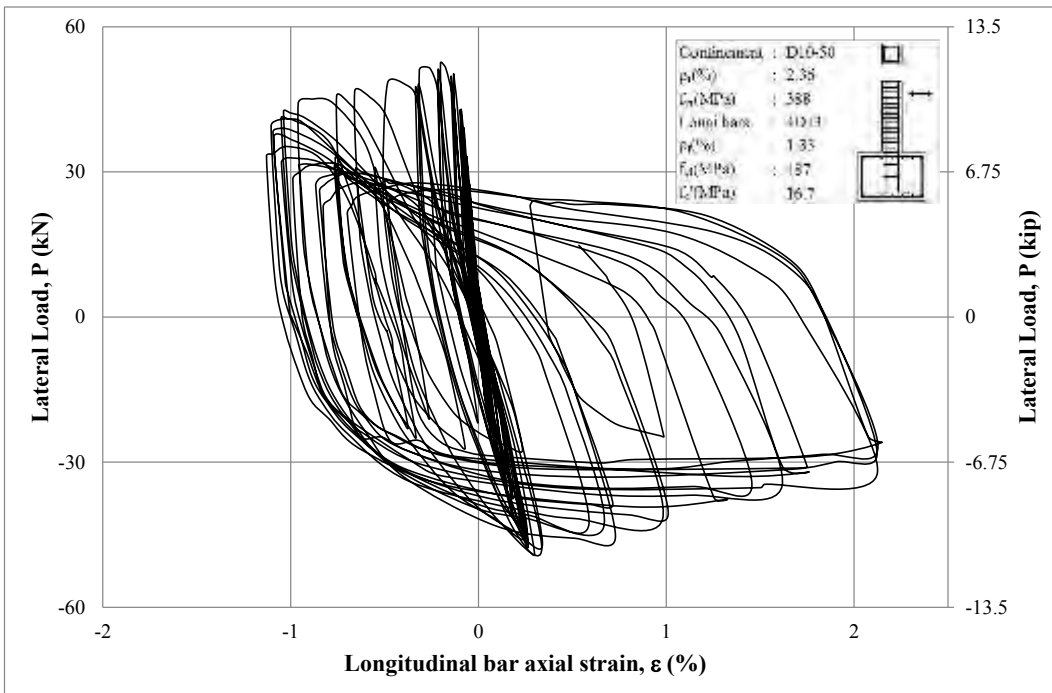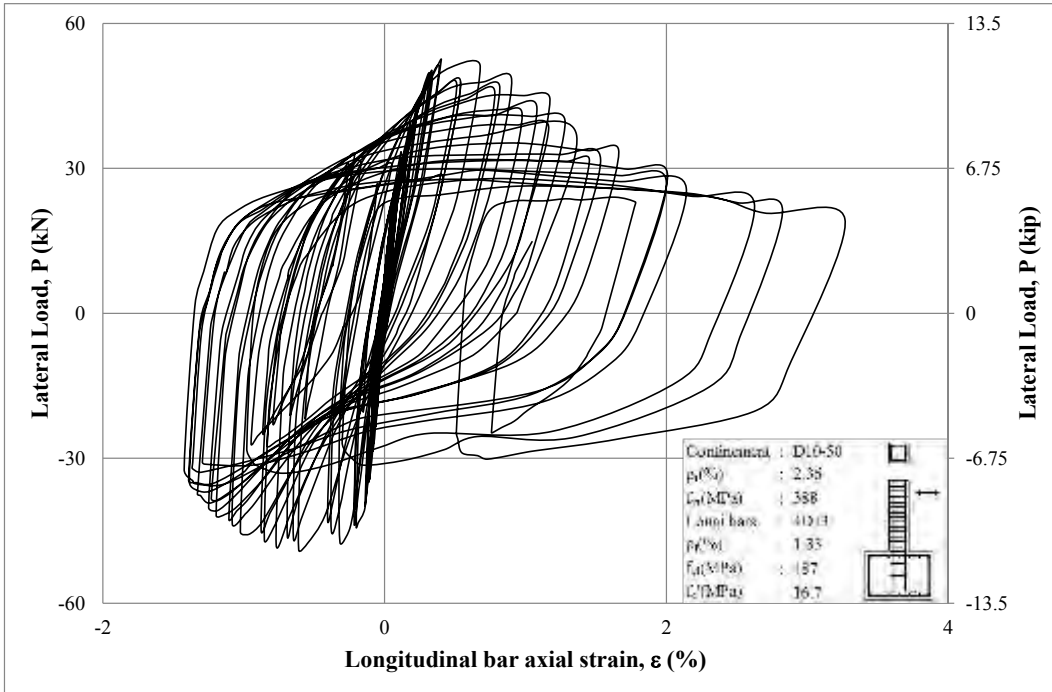
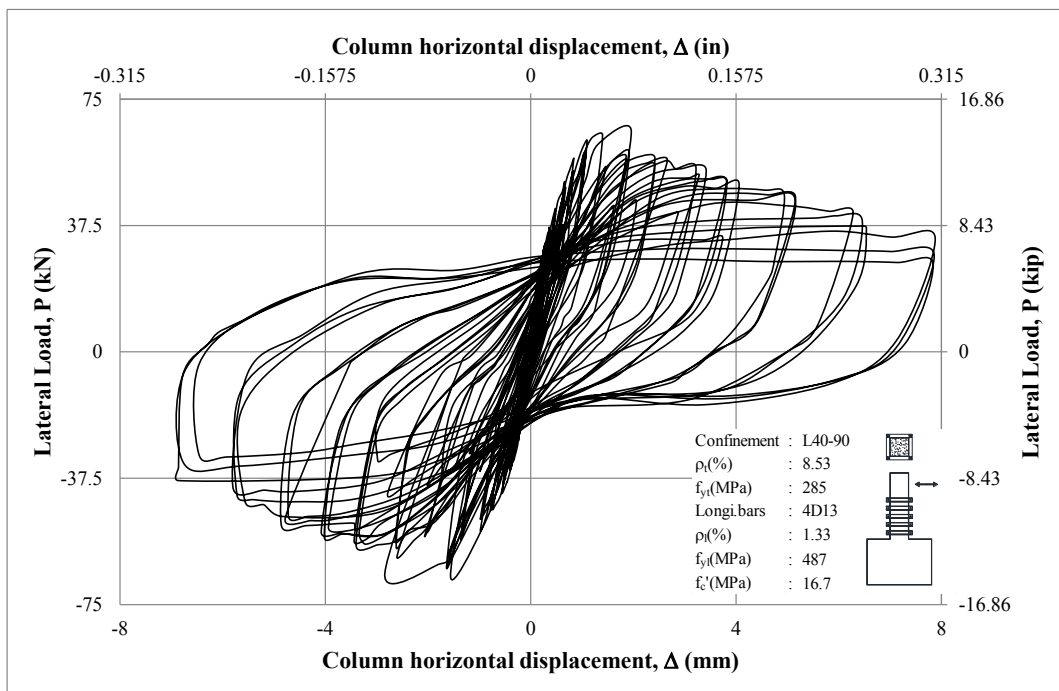**Figure D-24 Lateral load vs measurement of Channels 20 and 21 of CS12**
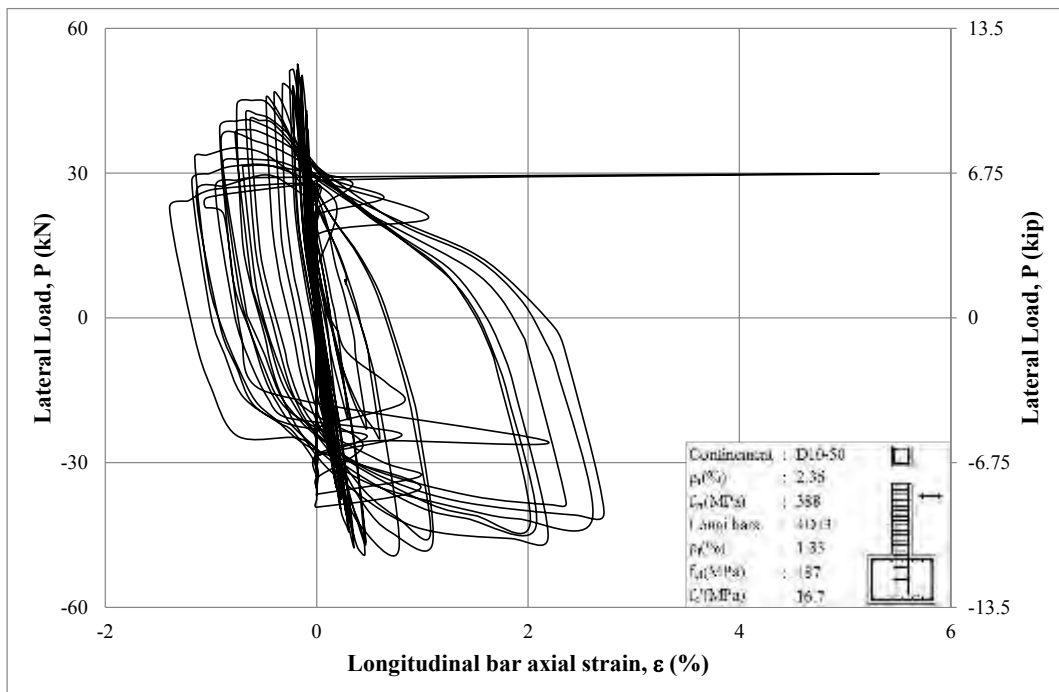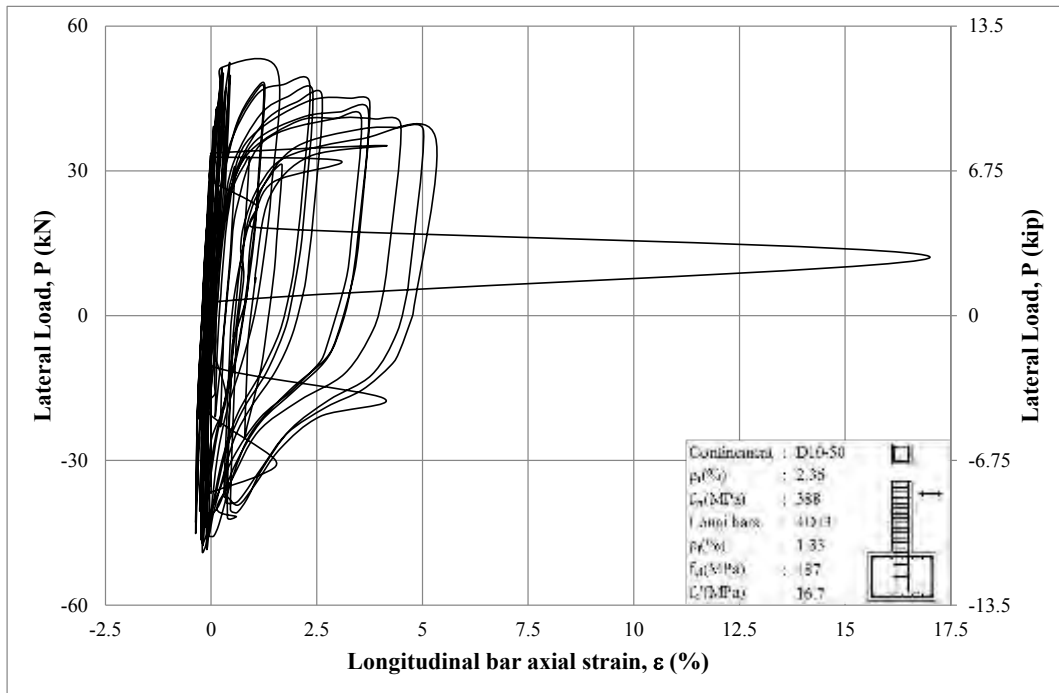
Figure D-25 Lateral load vs measurement of Channels 22 and 23 of CS12
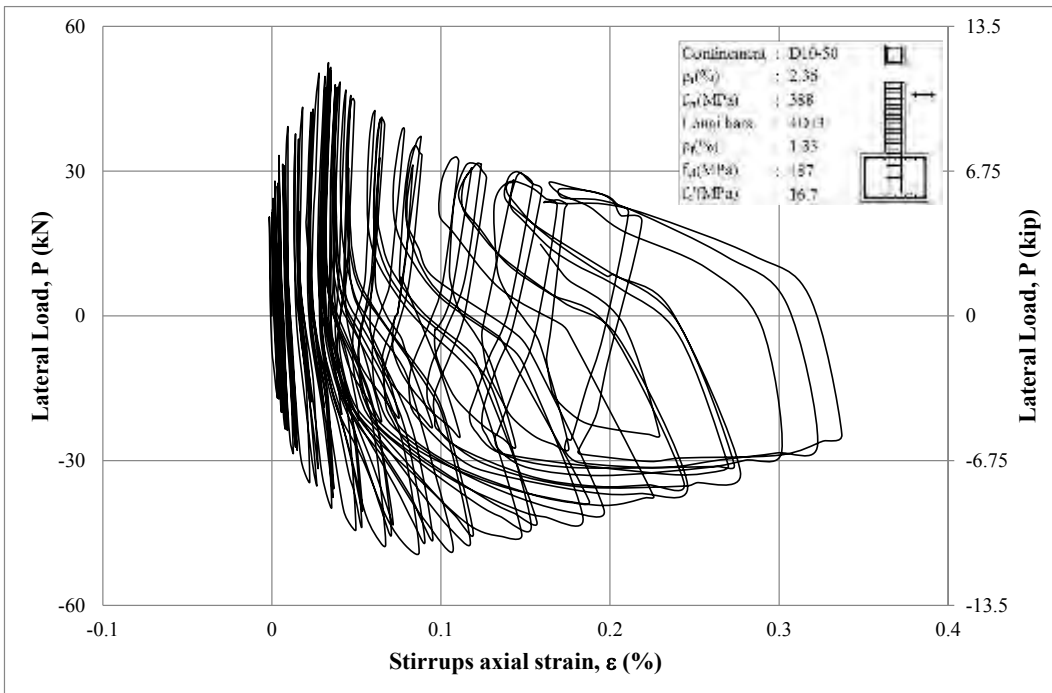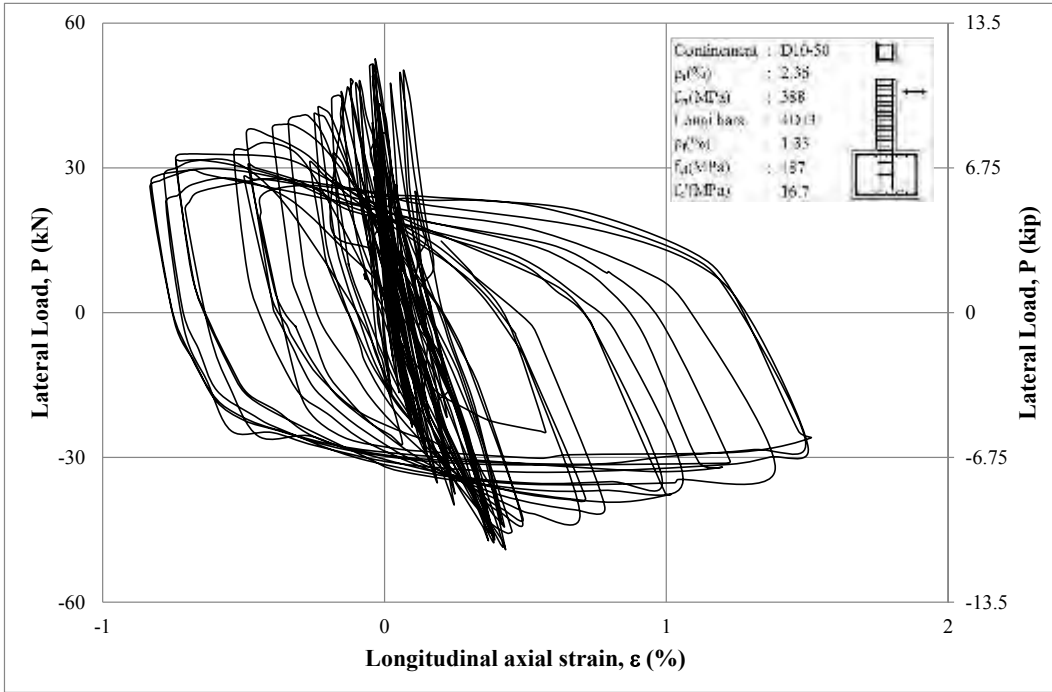
Figure D-26 Lateral load vs measurement of Channels 25 and 26 of CS12
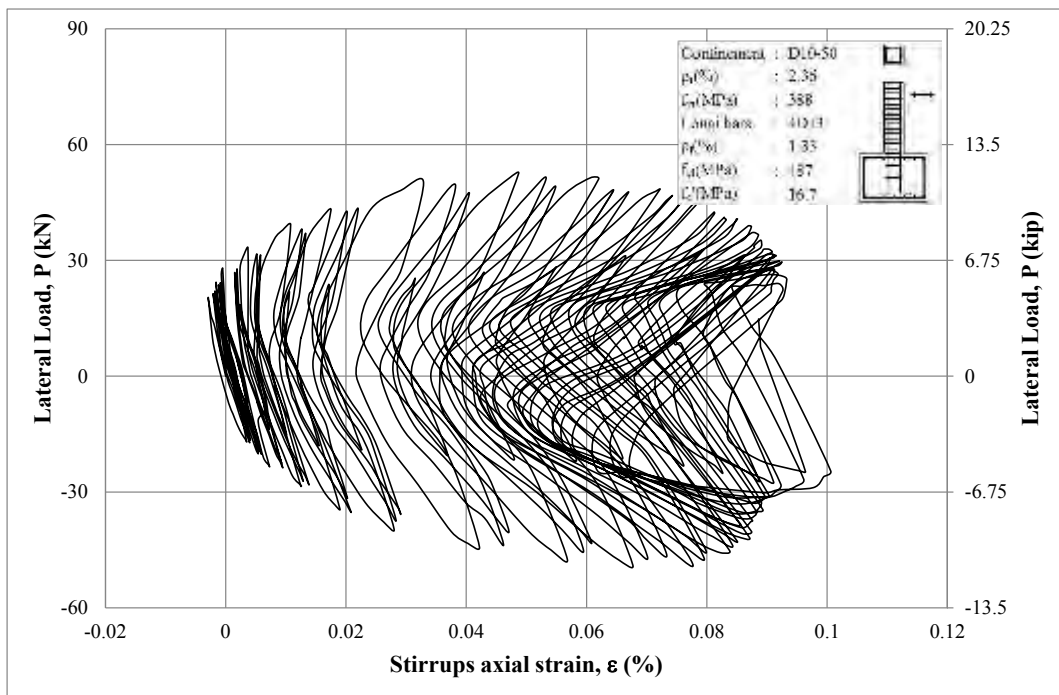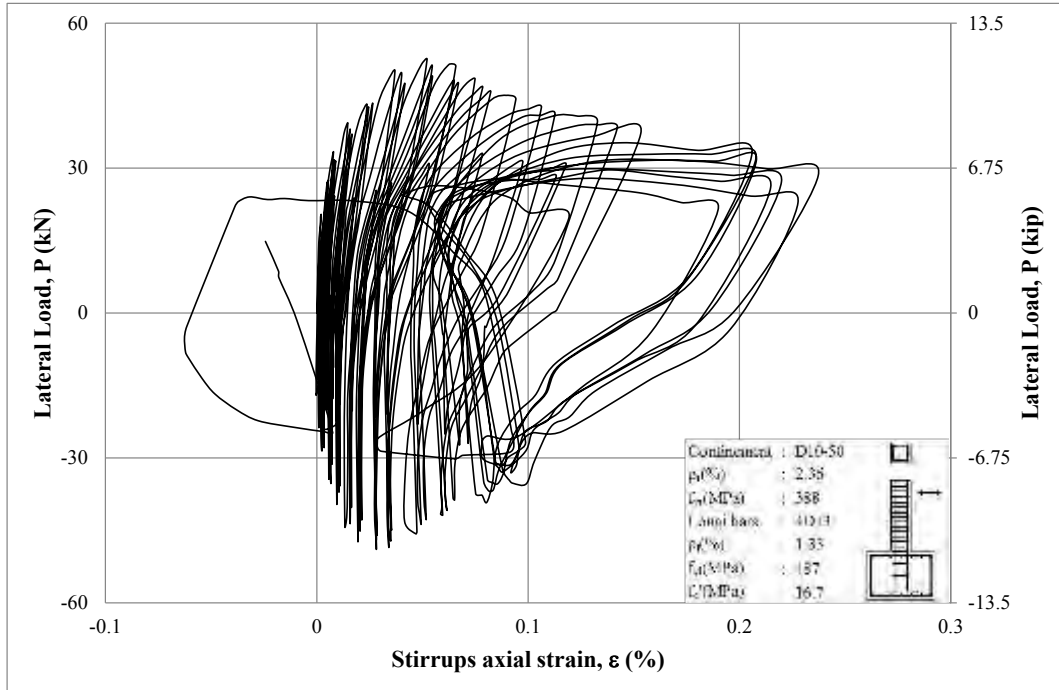
Figure D-27 Lateral load vs measurement of Channels 27 and 28 of CS12
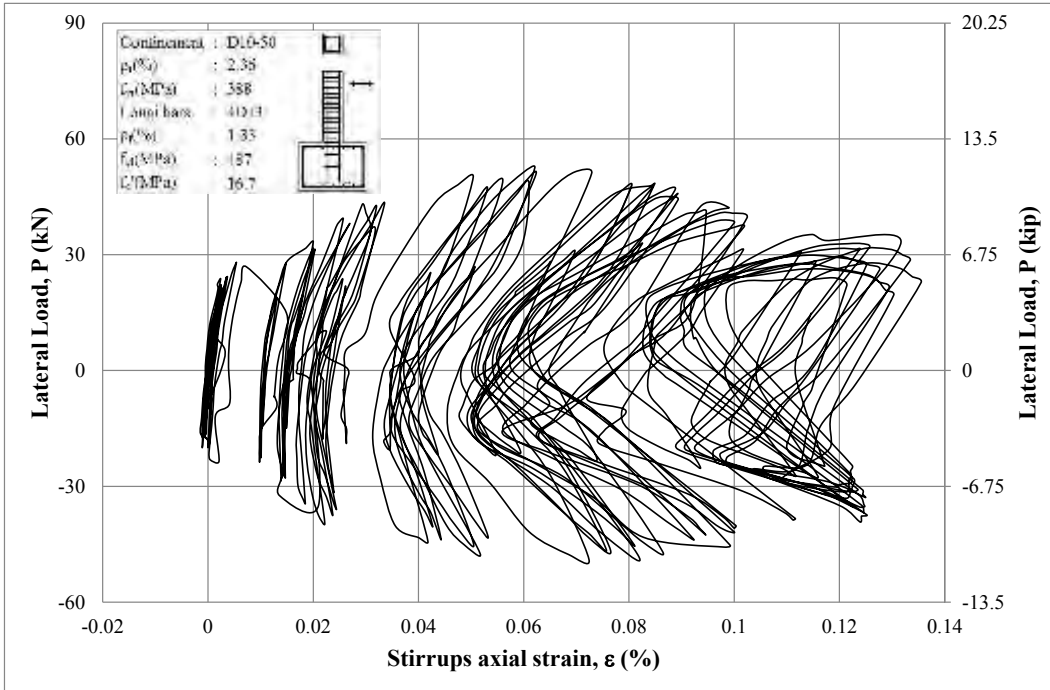
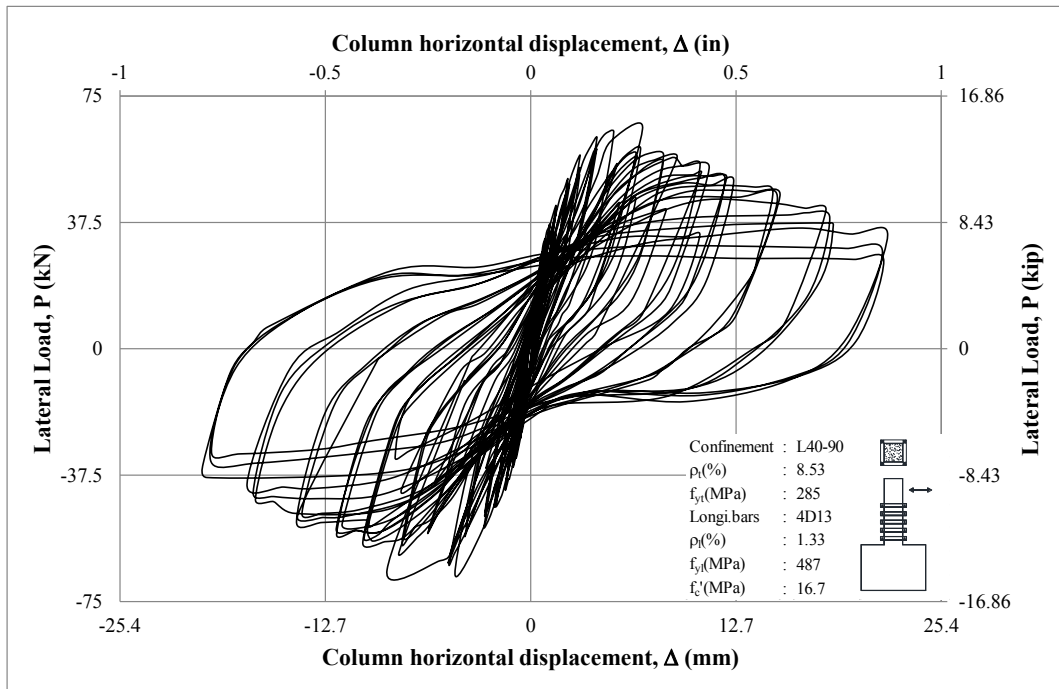**Figure D-28 Lateral load vs measurement of Channel 29 of CS12**
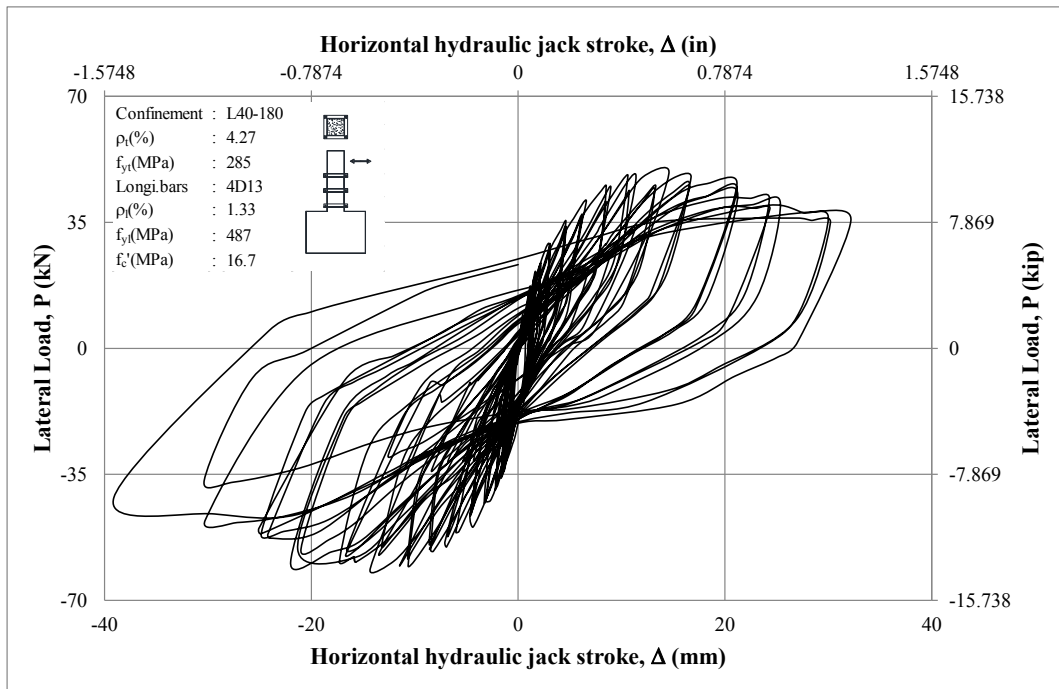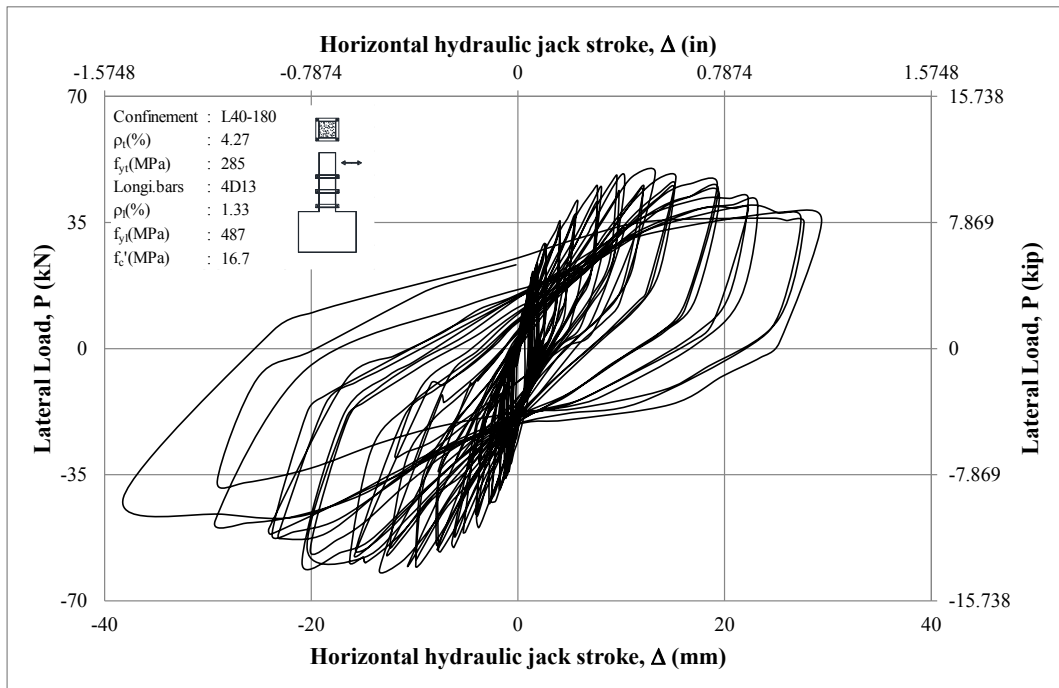
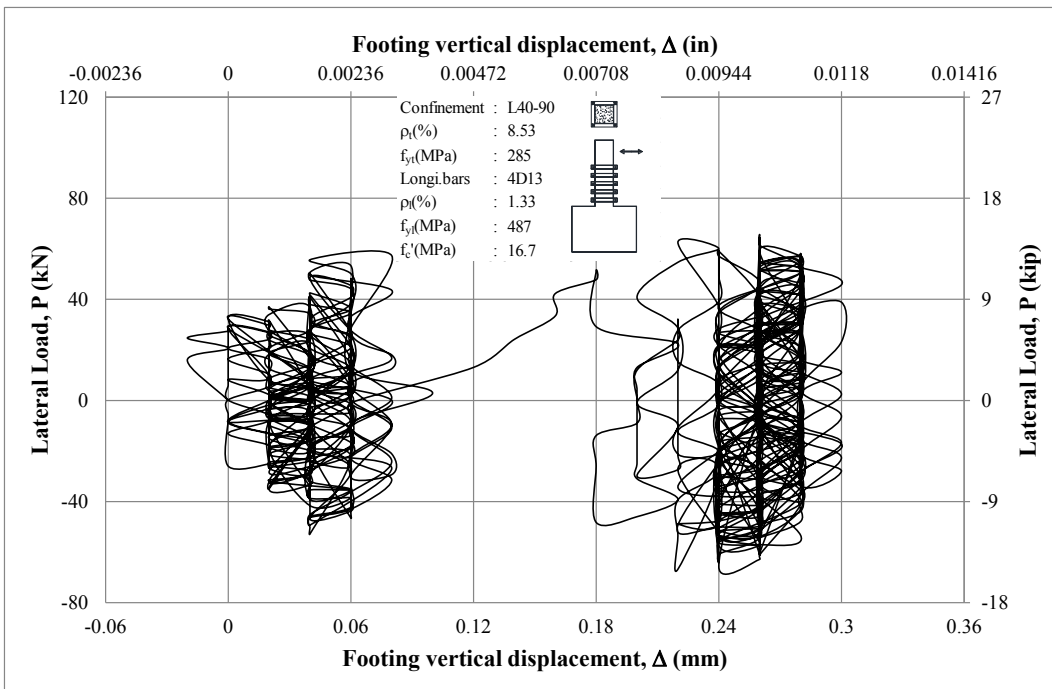**Figure D-29 Lateral load vs measurement of Channels 2 and 3 of S13**

329
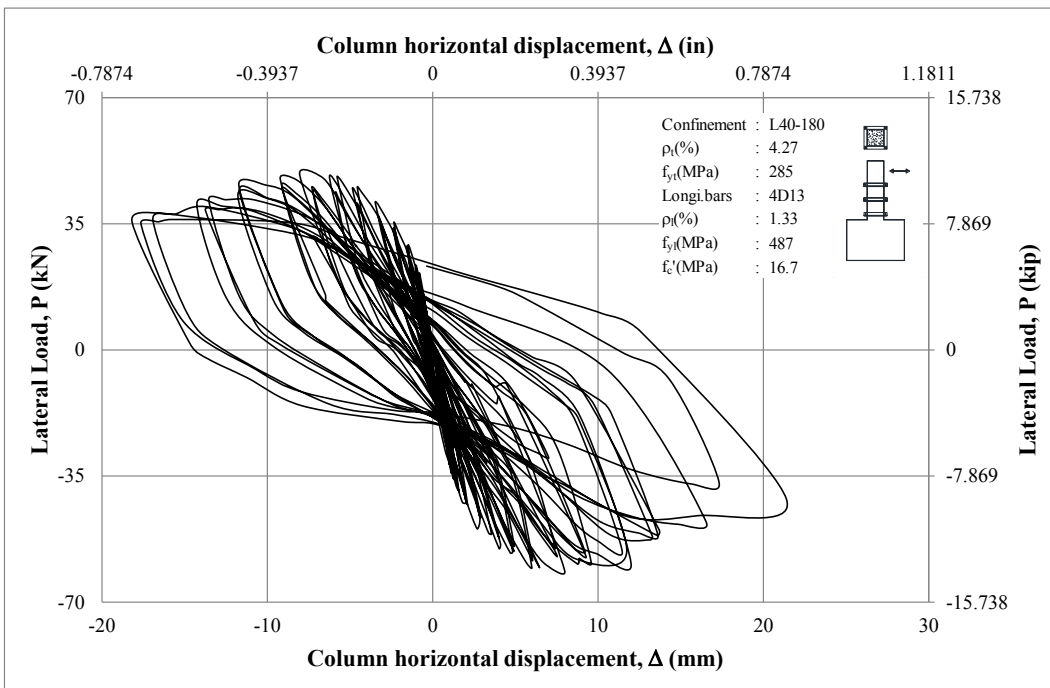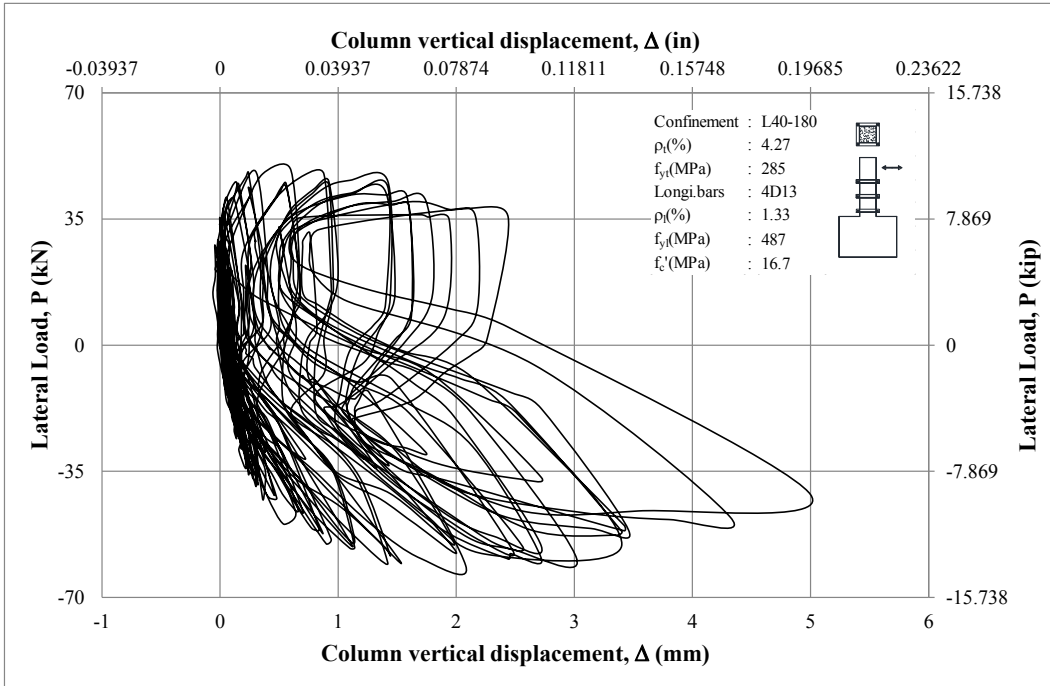
Figure D-30 Lateral load vs measurement of Channels 4 and 5 of S13
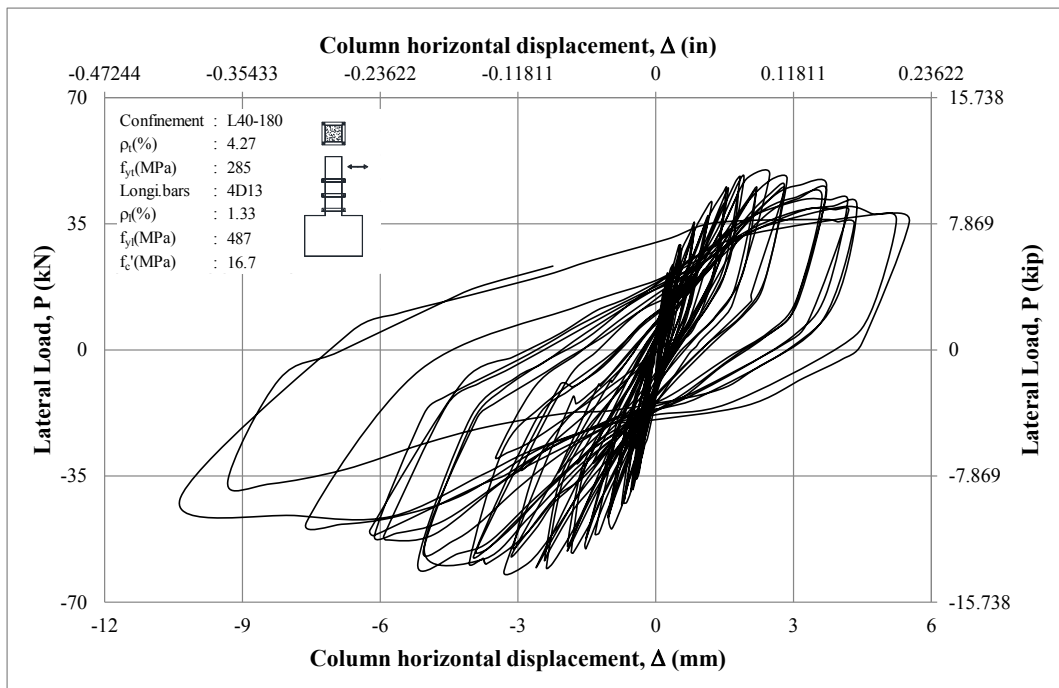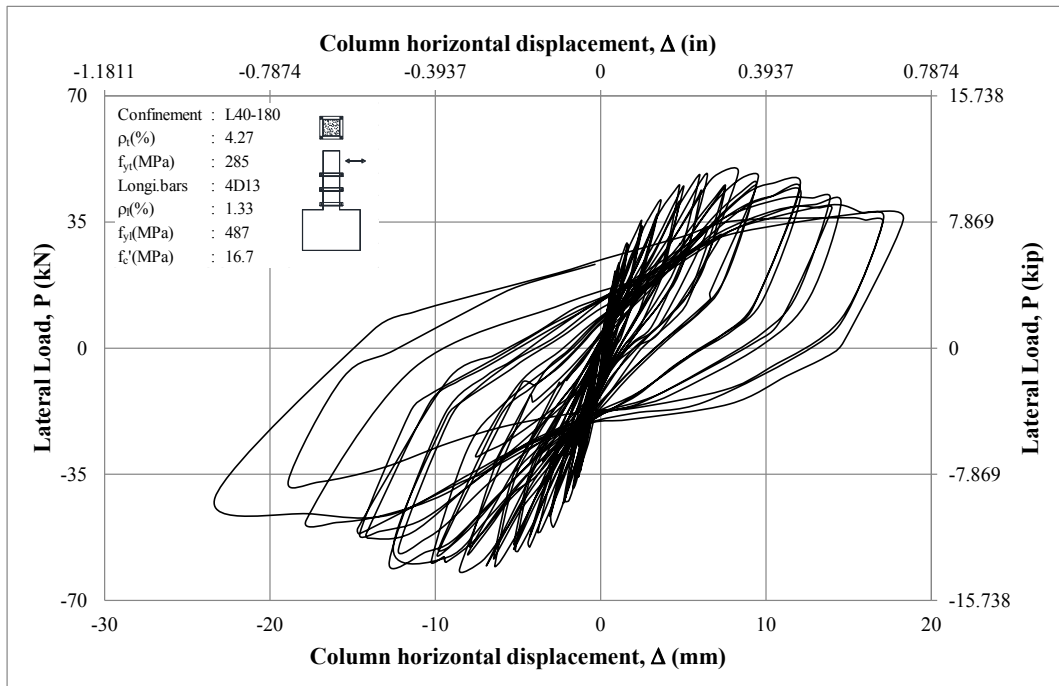
Figure D-31 Lateral load vs measurement of Channels 6 and 7 of S13
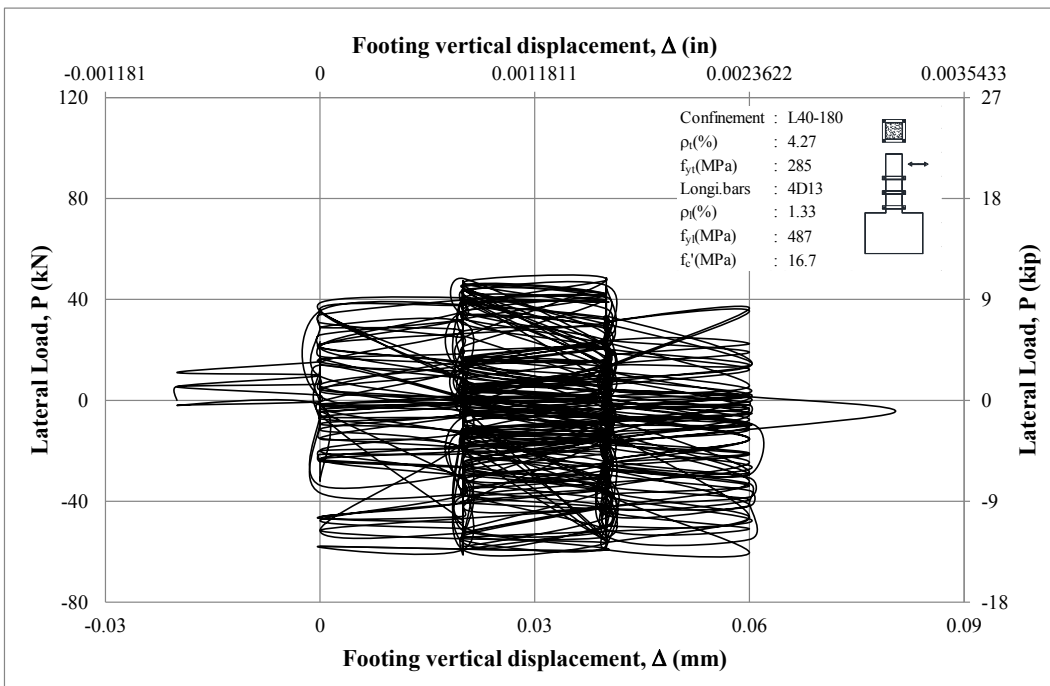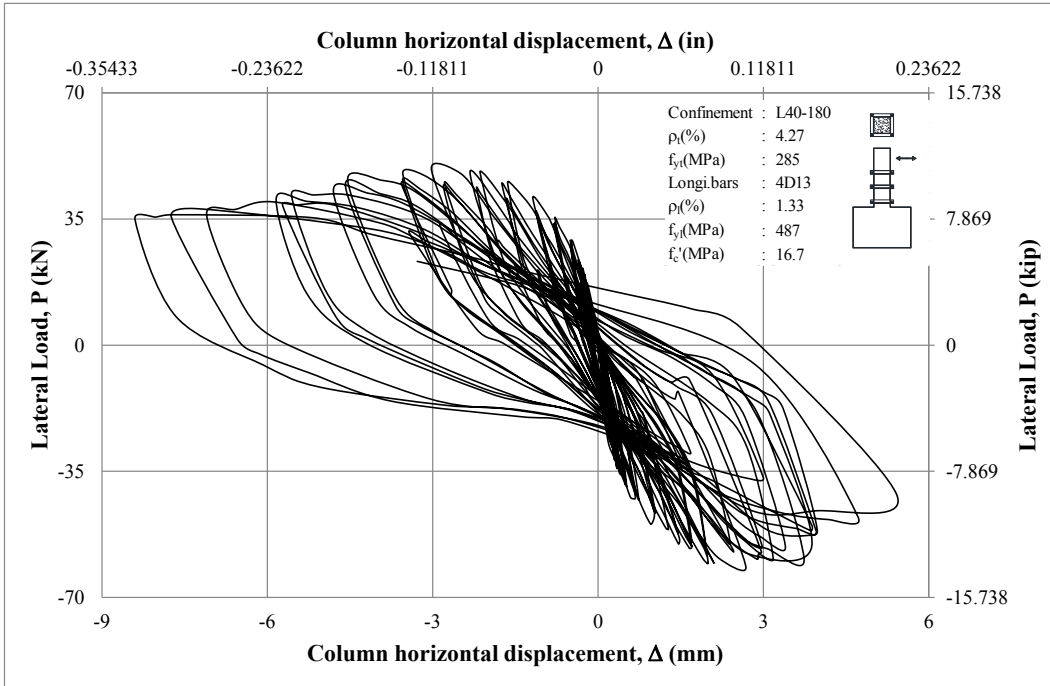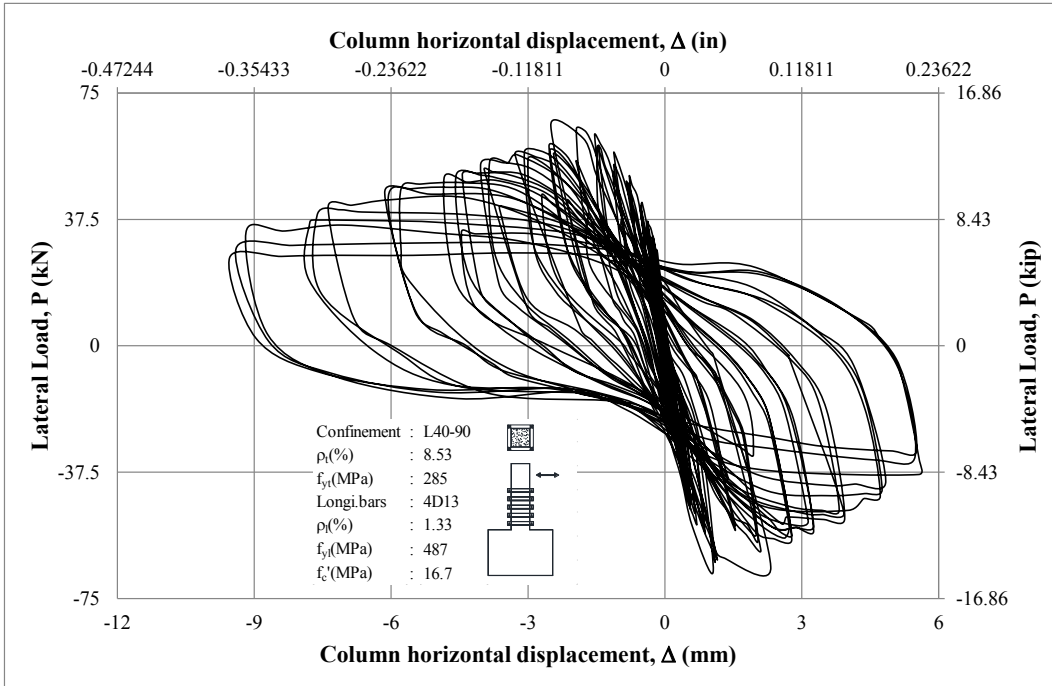
Figure D-32 Lateral load vs measurement of Channels 8 and 9 of S13
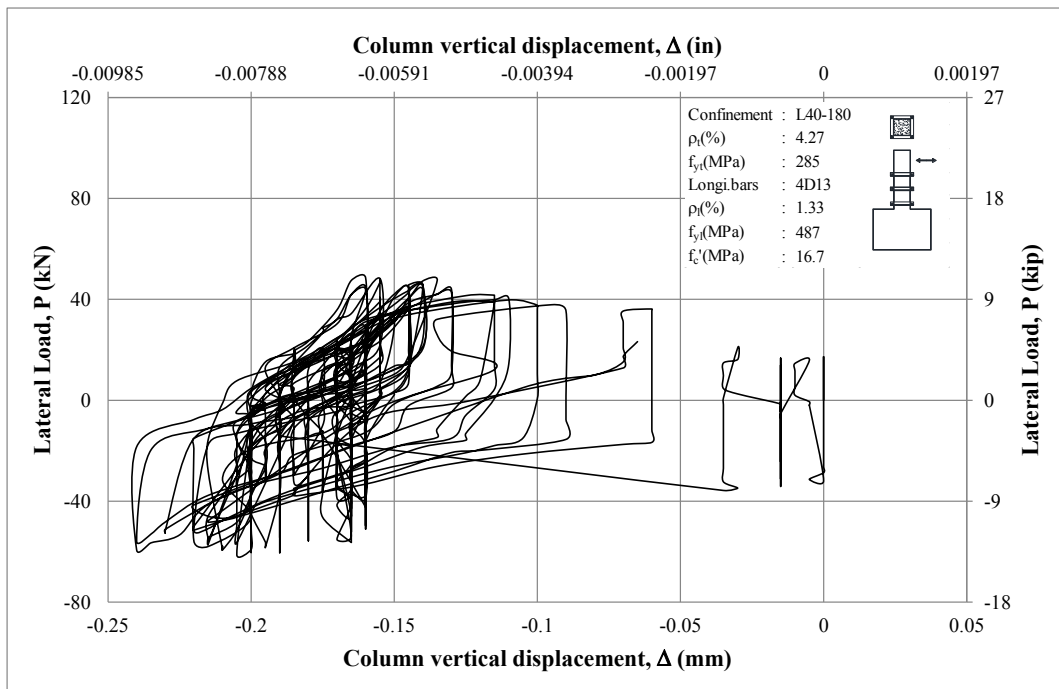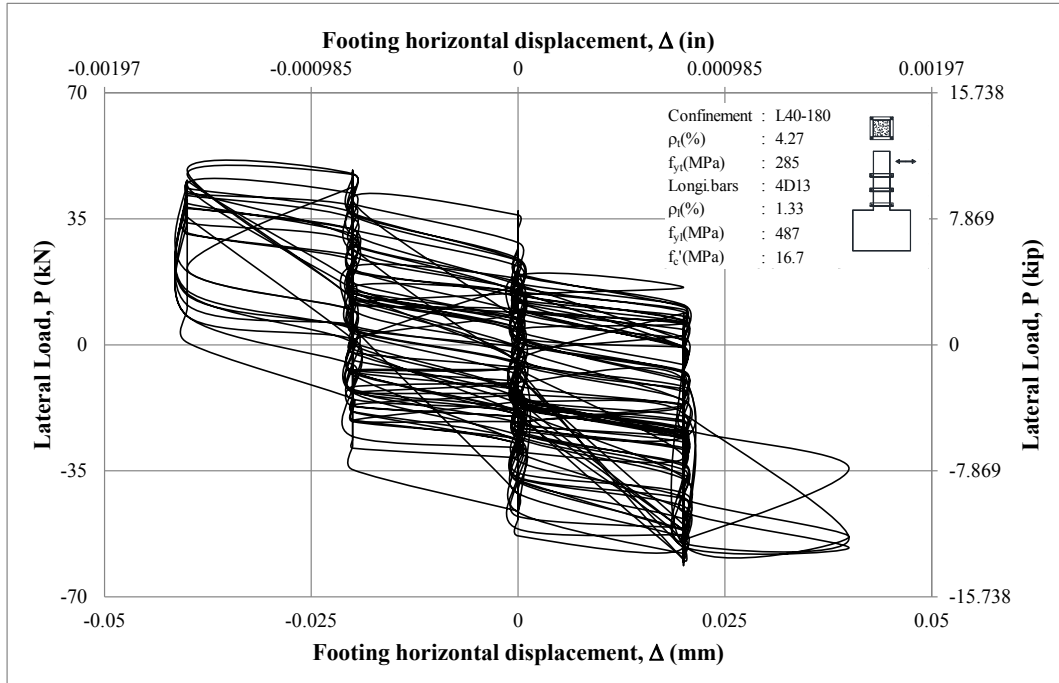
Figure D-33 Lateral load vs measurement of Channels 10 and 11 of S13

333
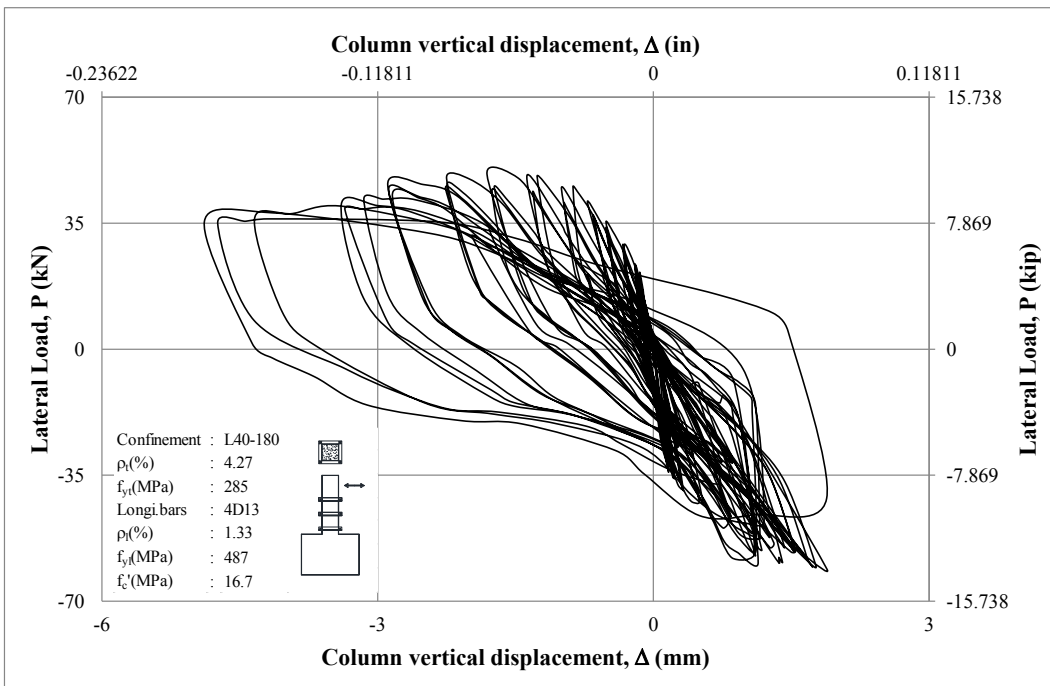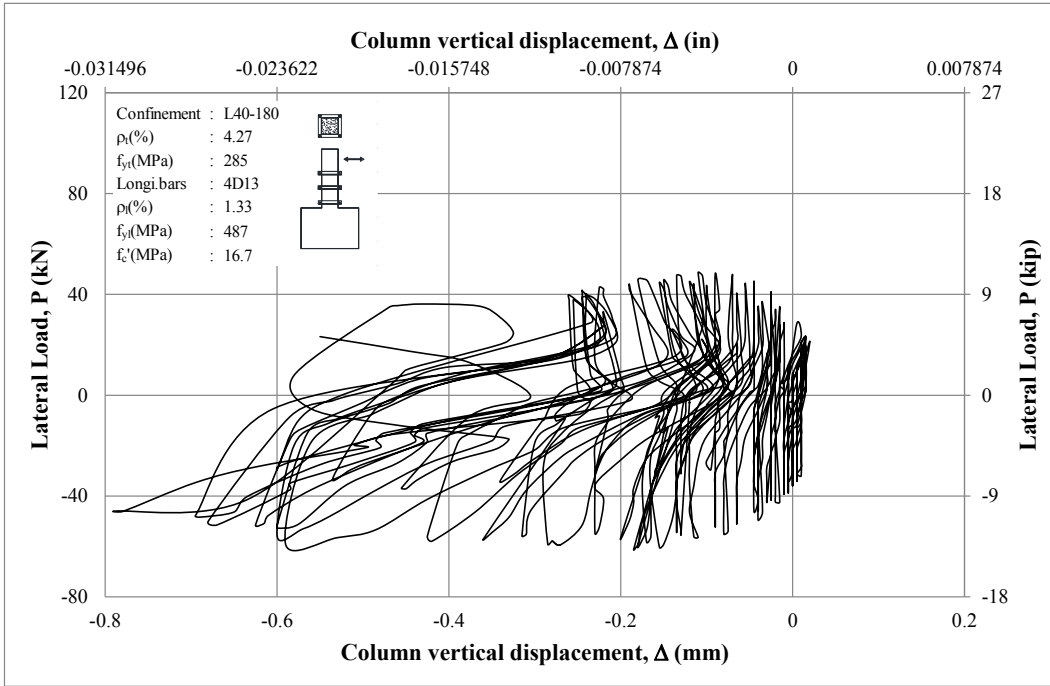
Figure D-34 Lateral load vs measurement of Channels 12 and 13 of S13

334
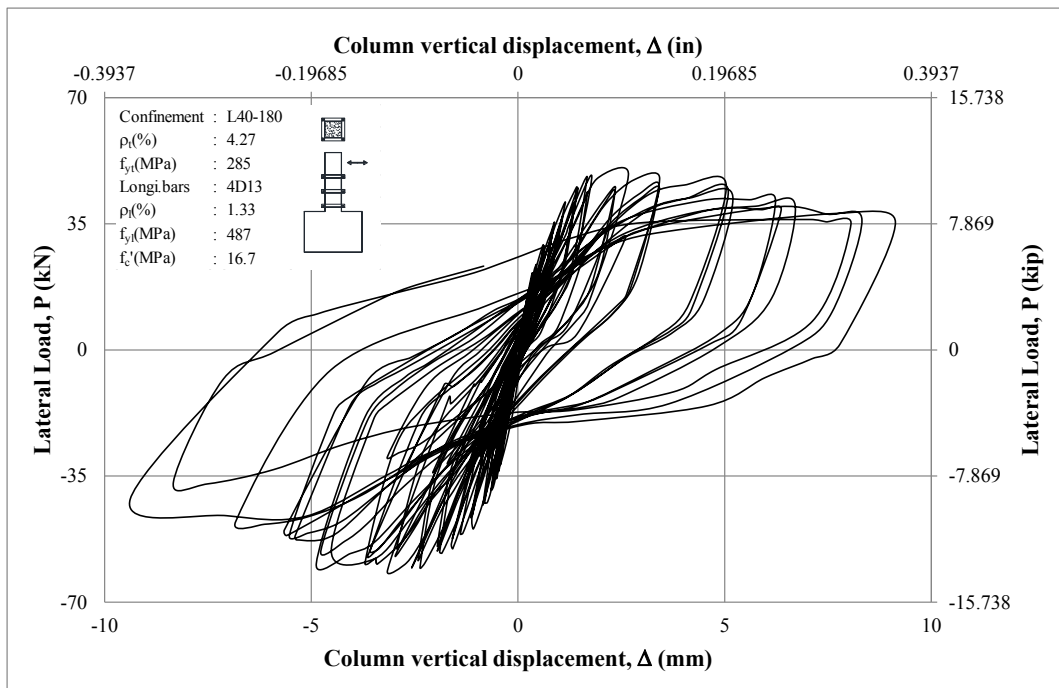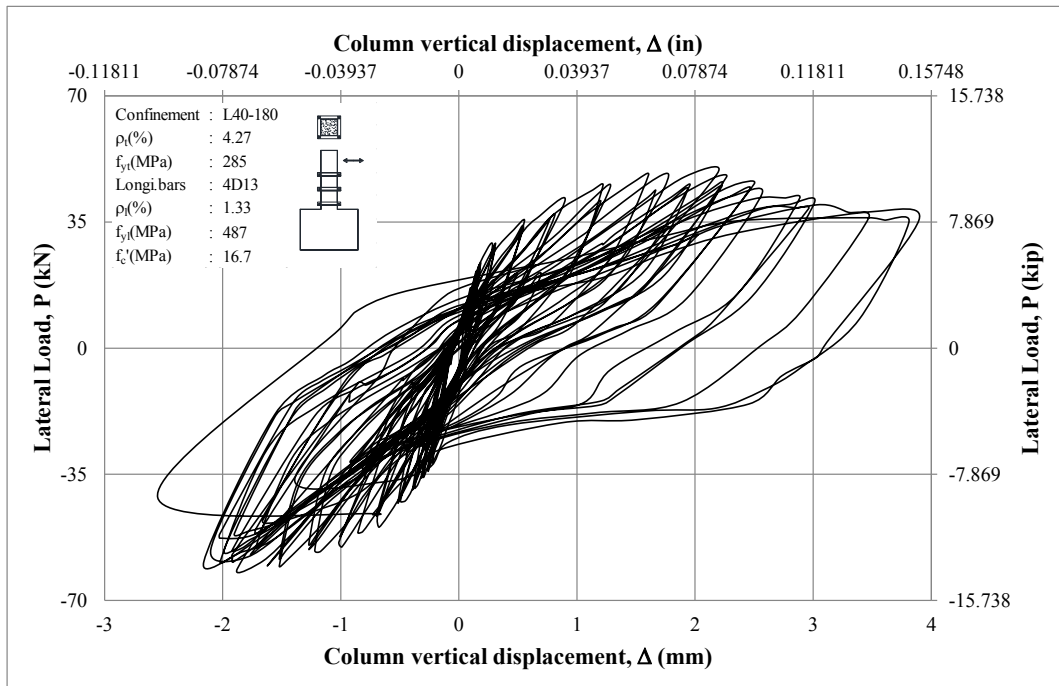
Figure D-35 Lateral load vs measurement of Channels 14 and 15 of S13
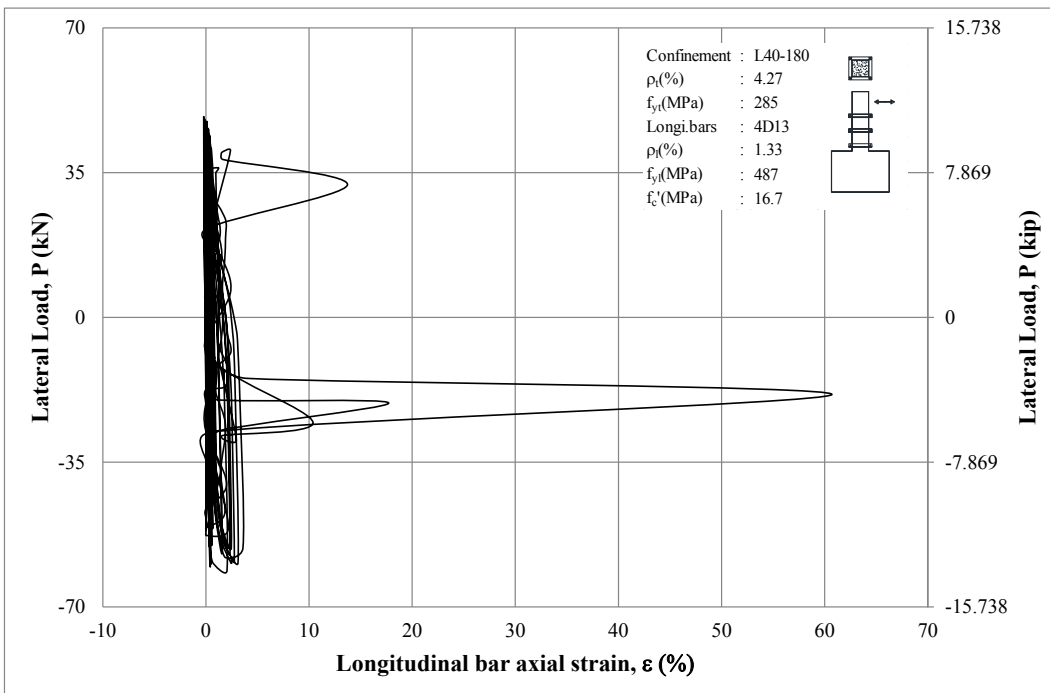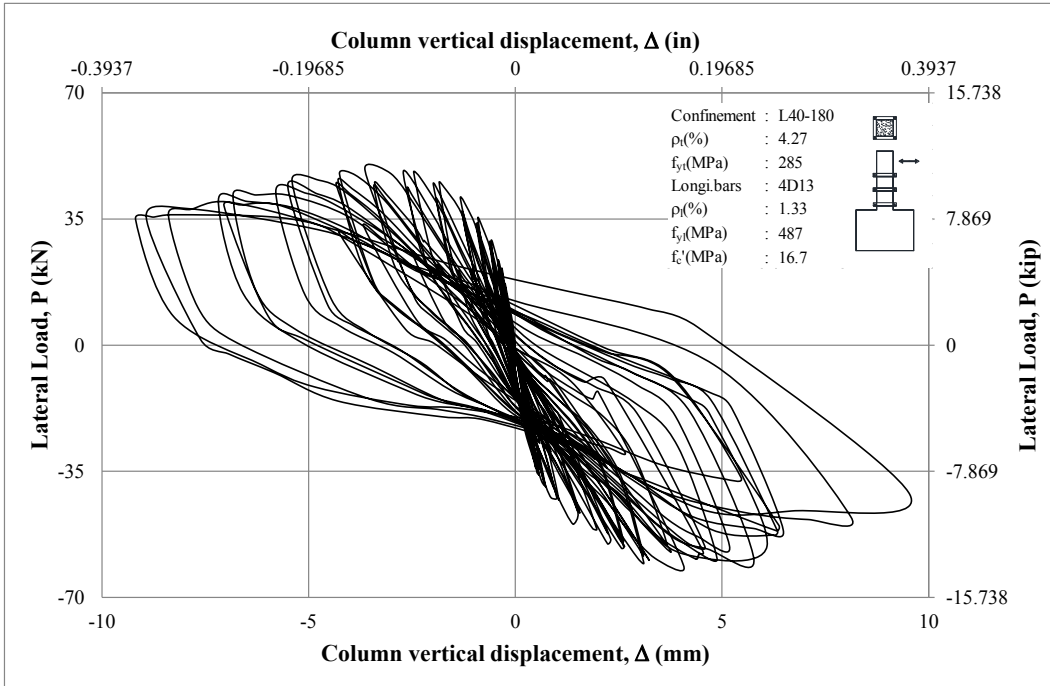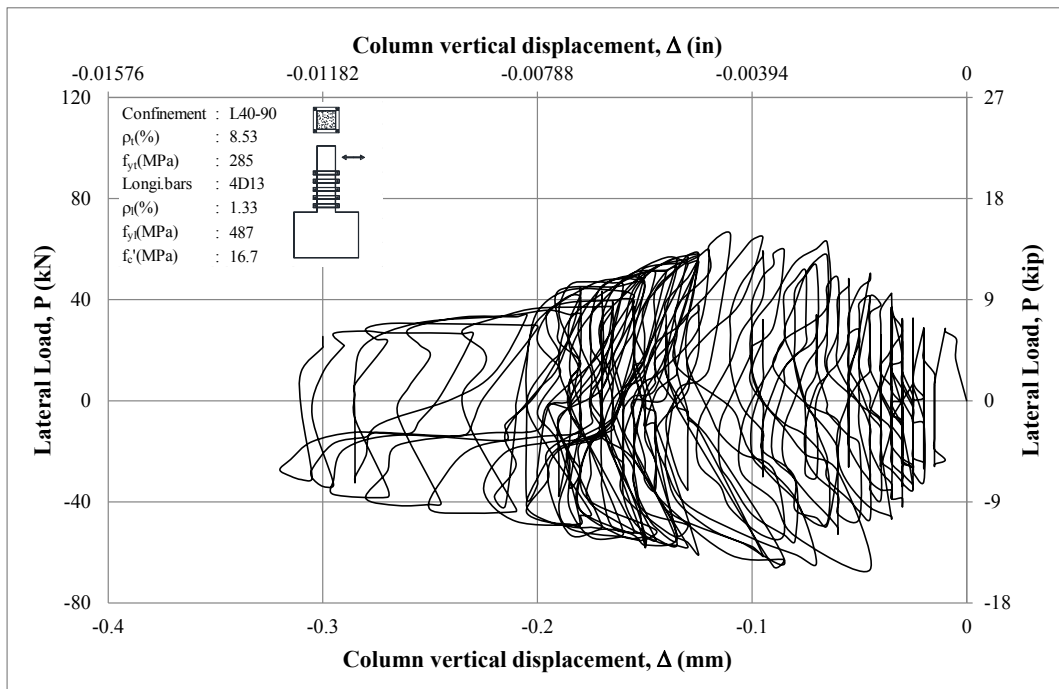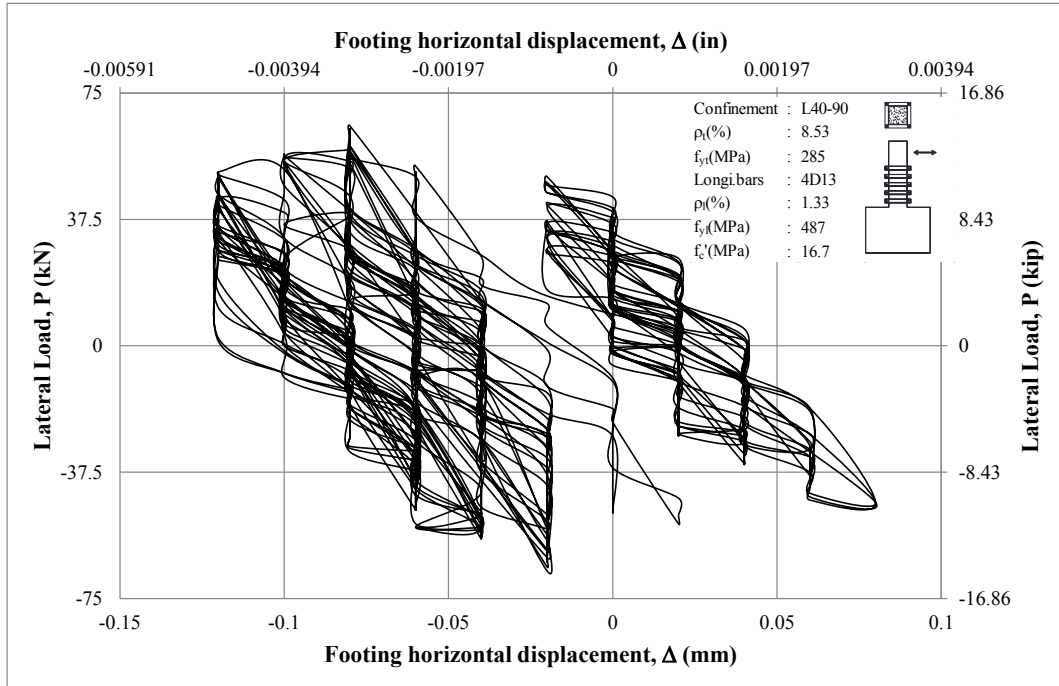
Figure D-36 Lateral load vs measurement of Channels 16 and 17 of S13
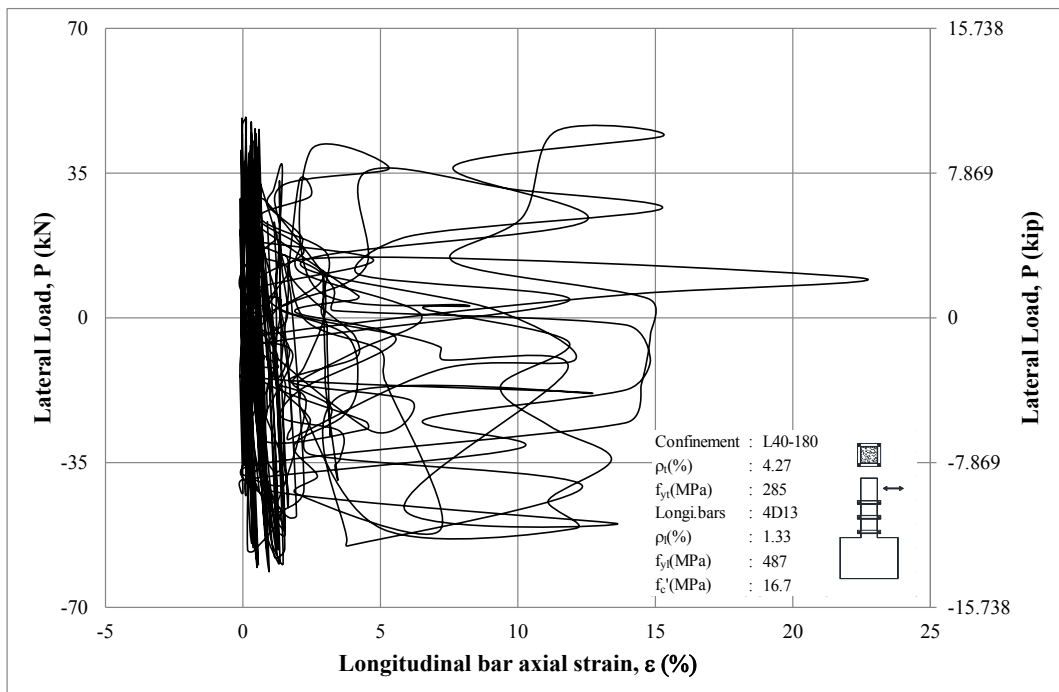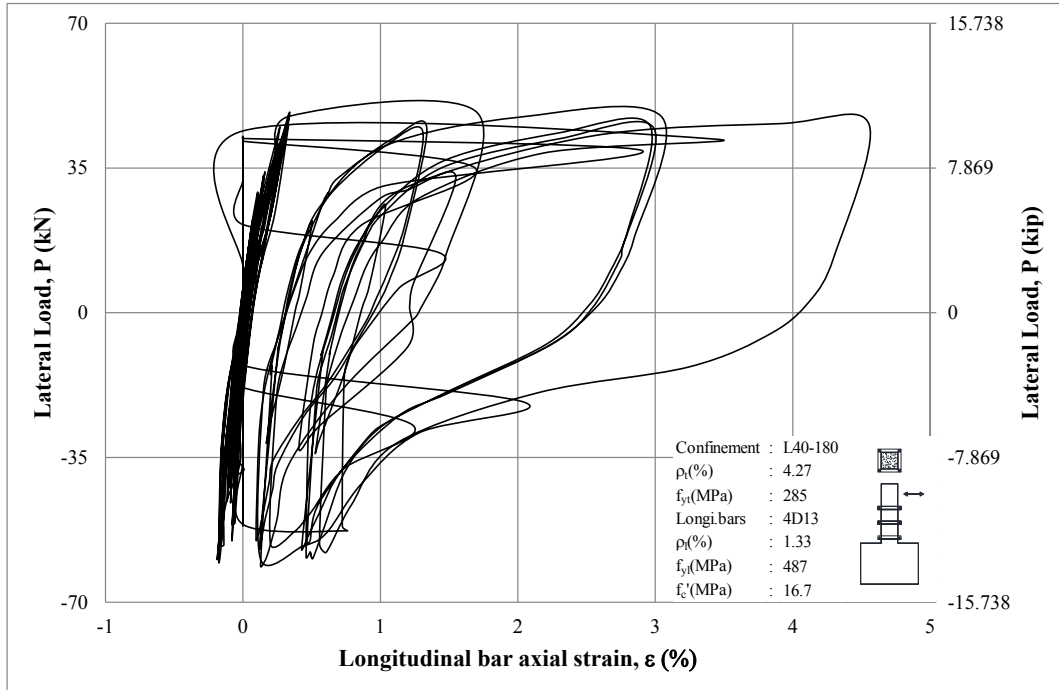
Figure D-37 Lateral load vs measurement of Channels 18 and 19 of S13
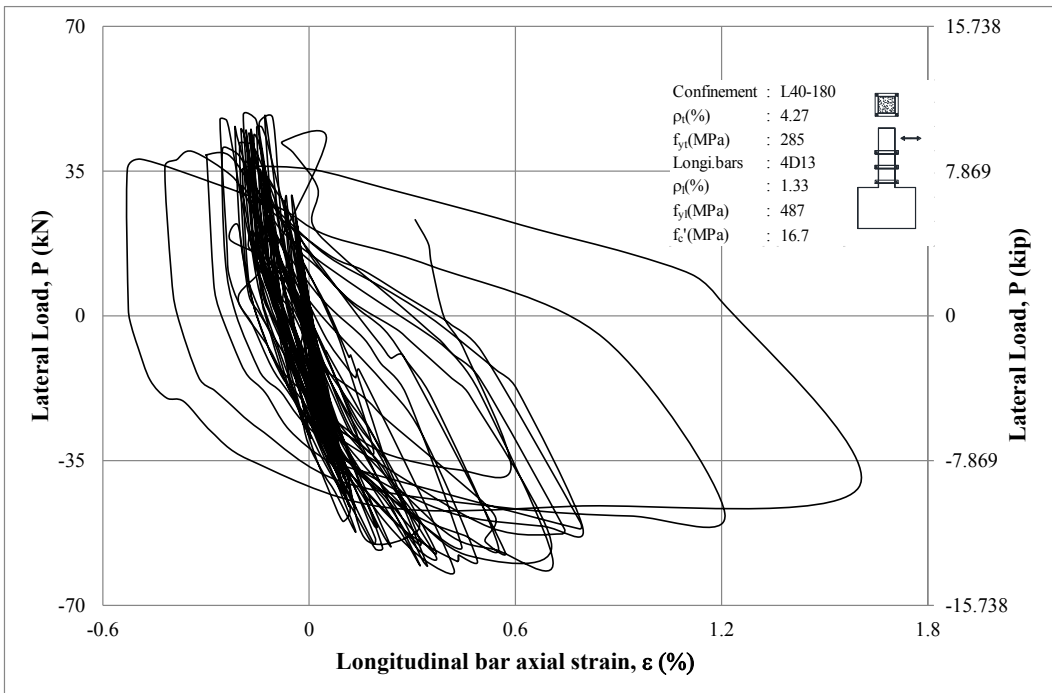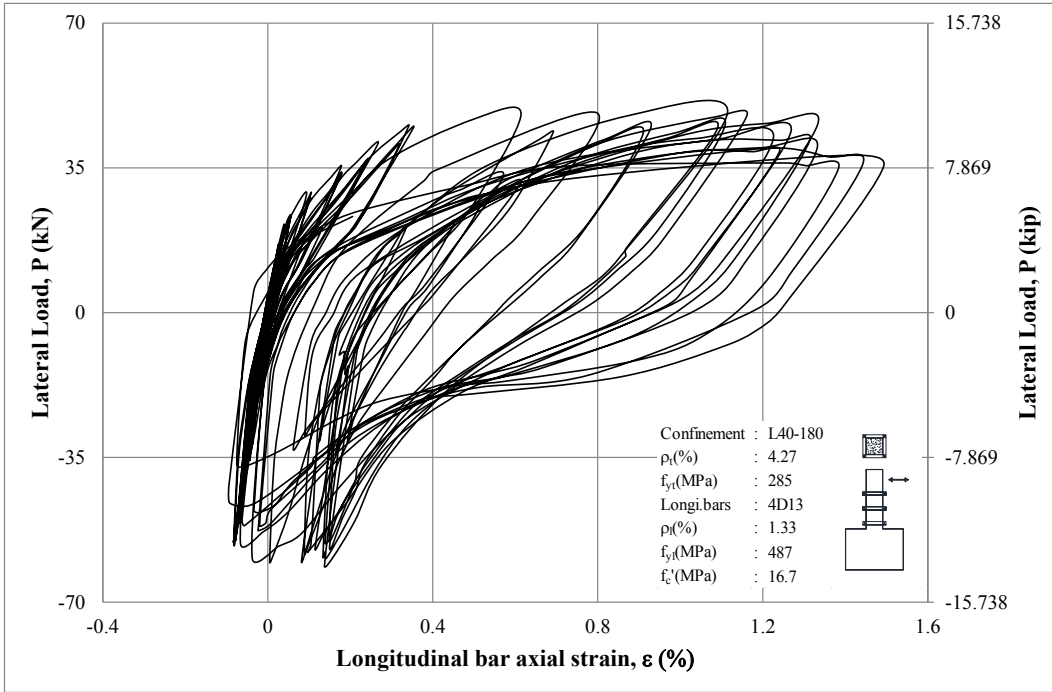
Figure D-38 Lateral load vs measurement of Channels 20 and 21 of S13

338
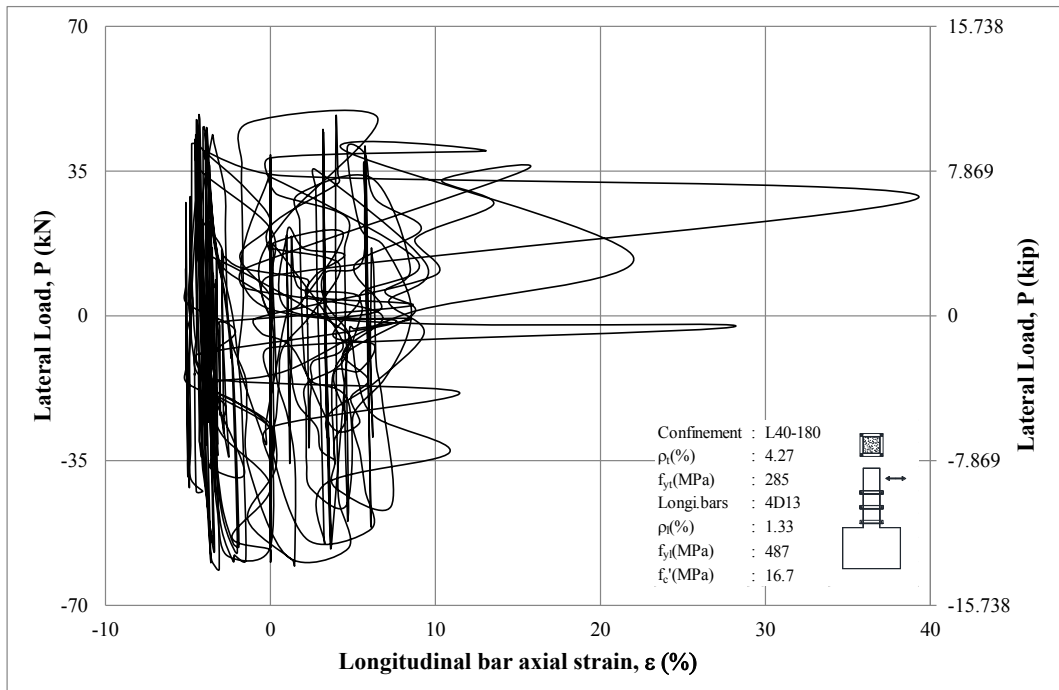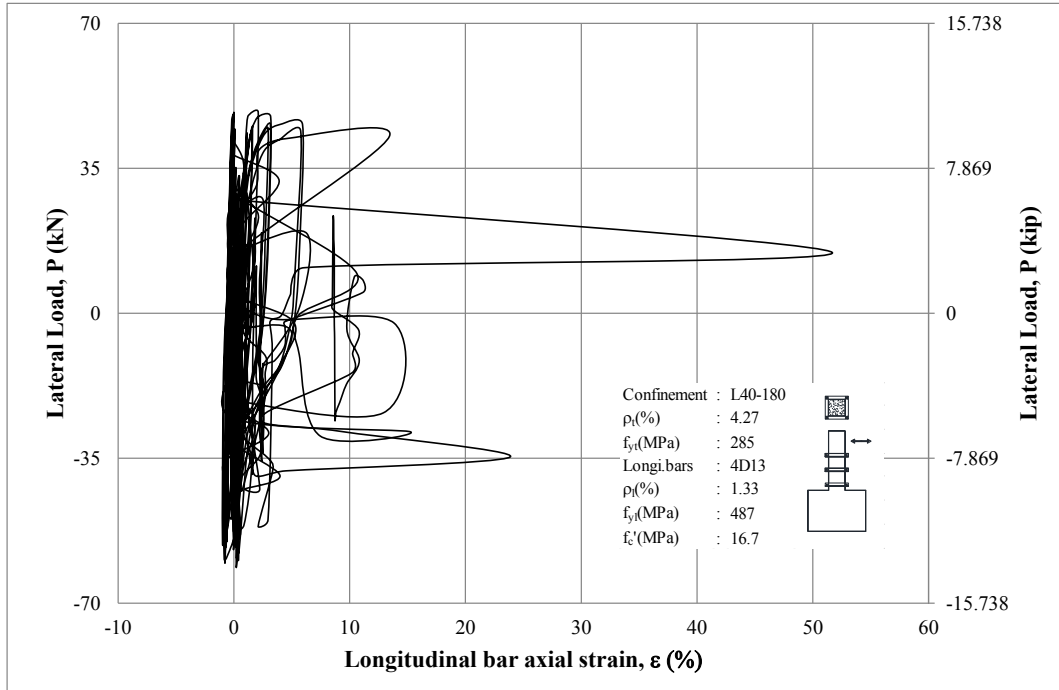
Figure D-39 Lateral load vs measurement of Channels 22 and 23 of S13

339
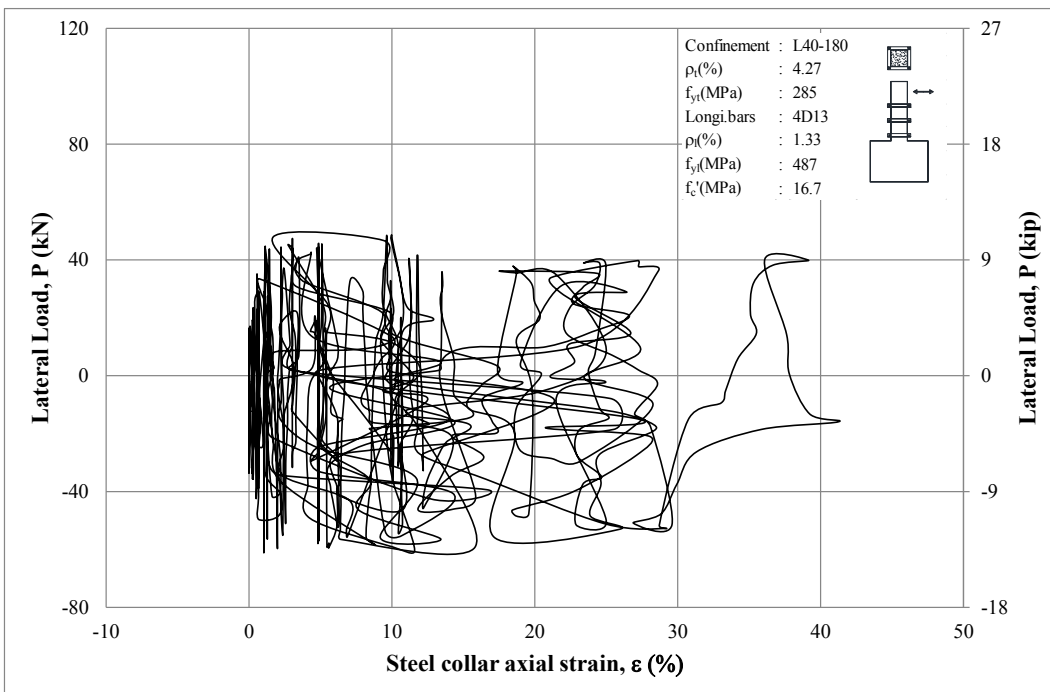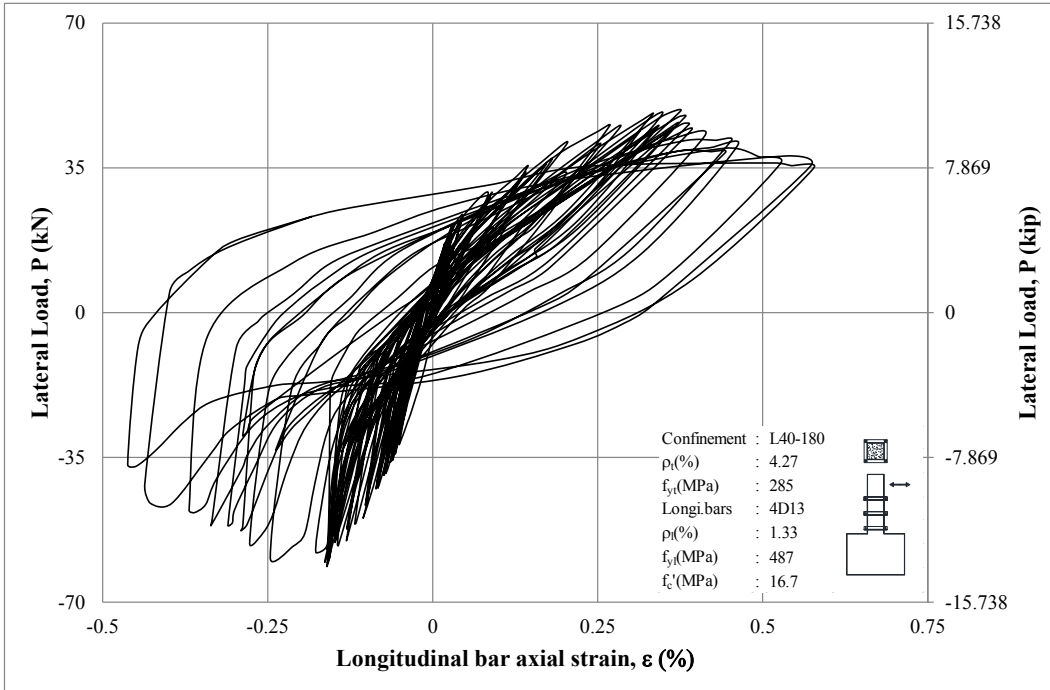
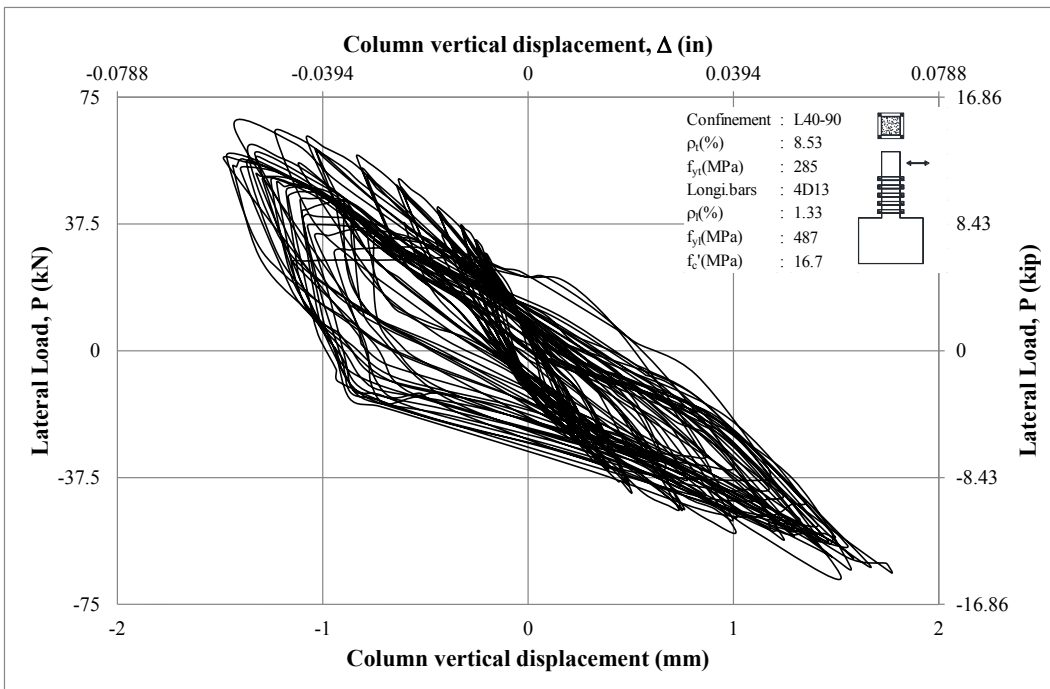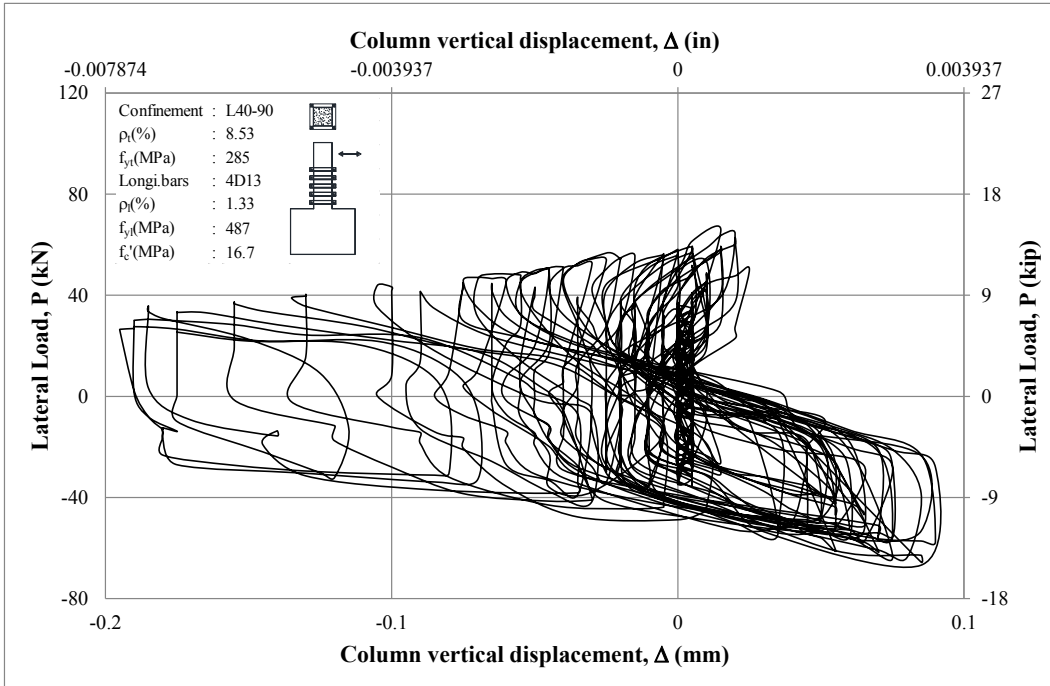**Figure D-40 Lateral load vs measurement of Channels 24 and 25 of S13**

340
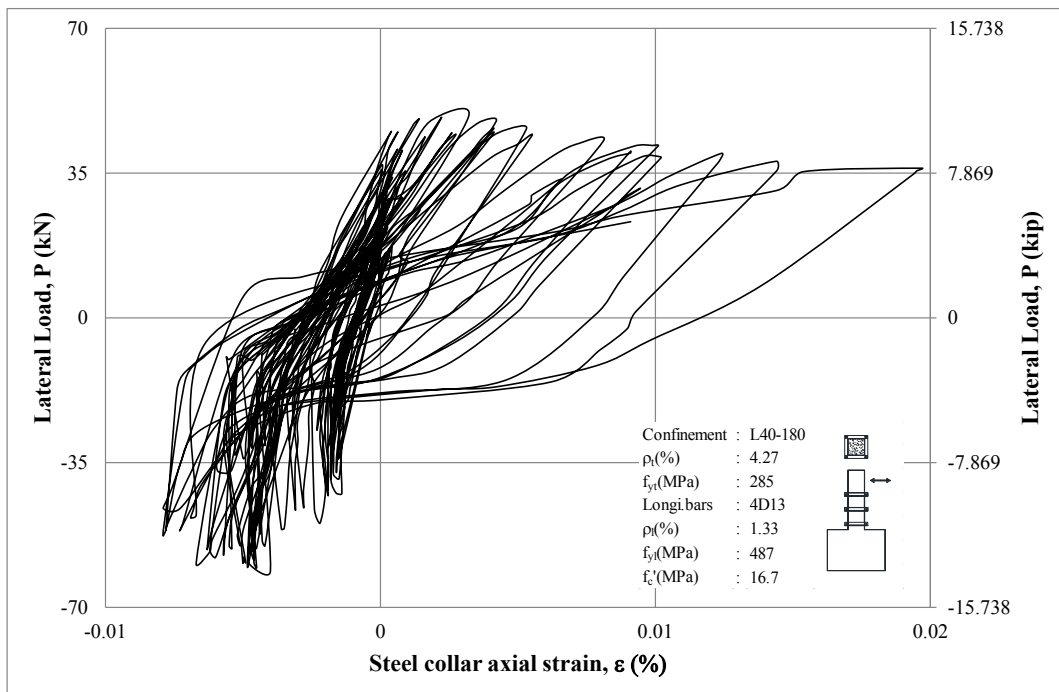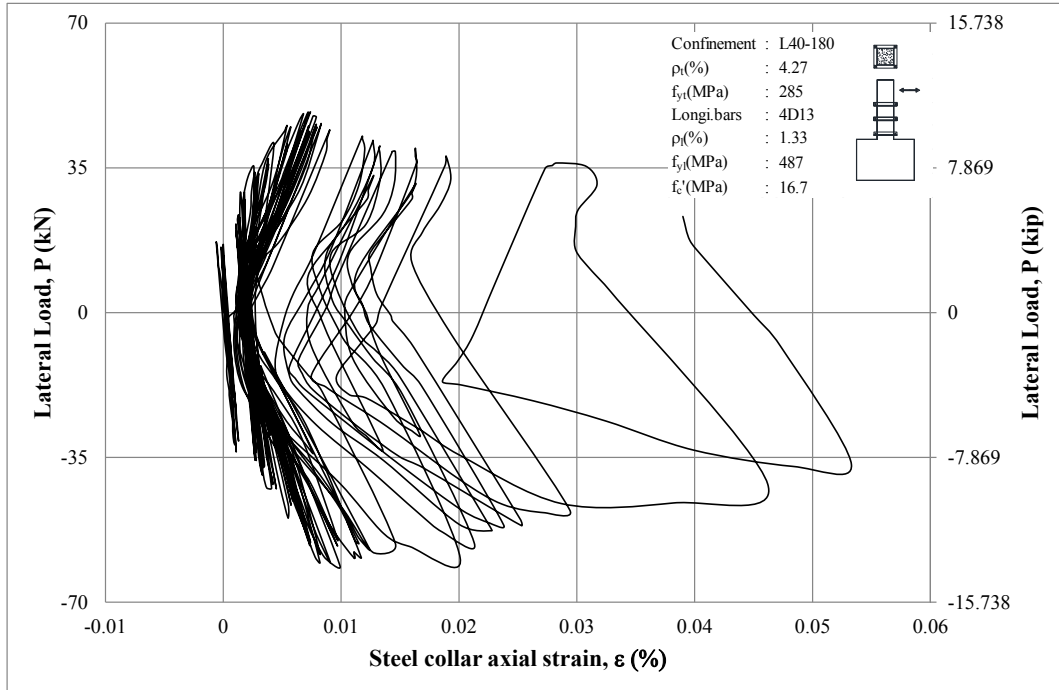
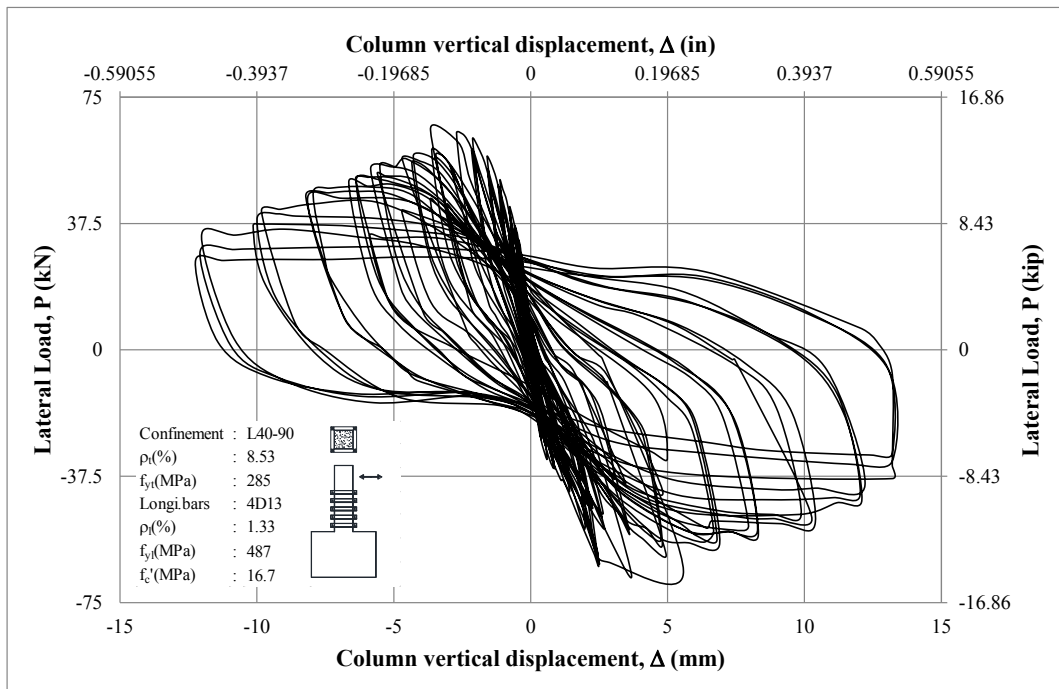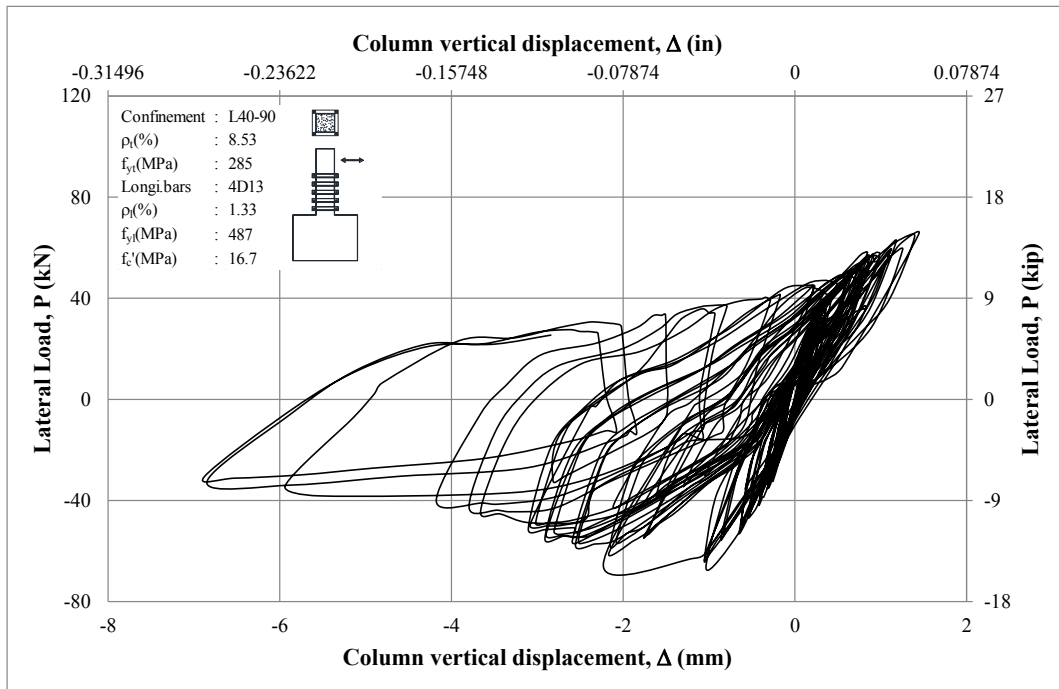**Figure D-41 Lateral load vs measurement of Channels 26 and 27 of S13**
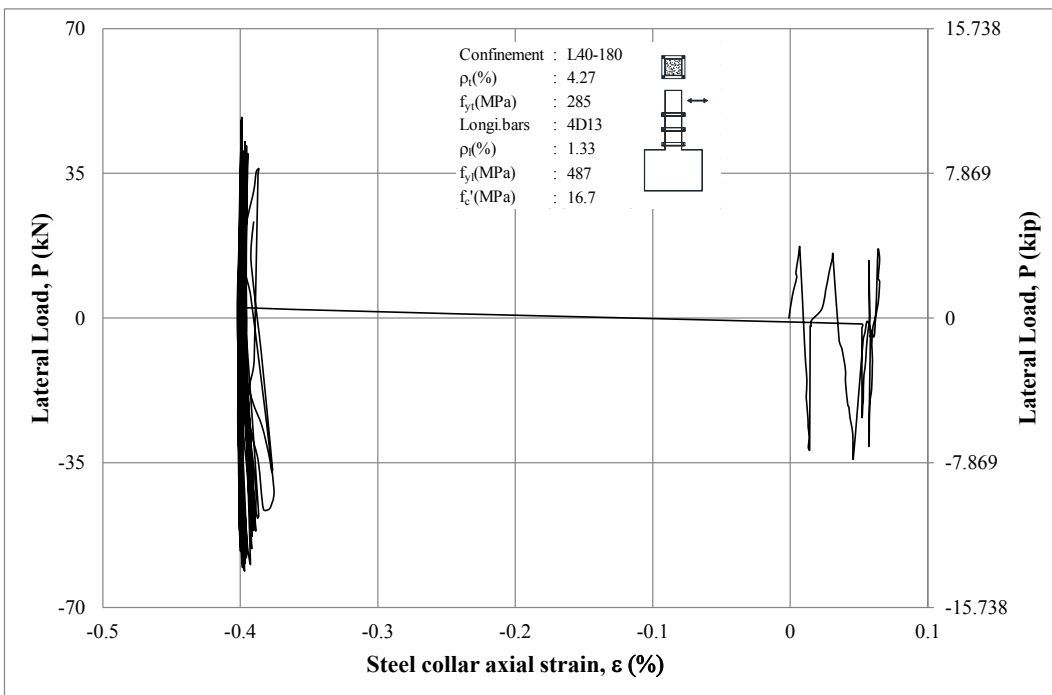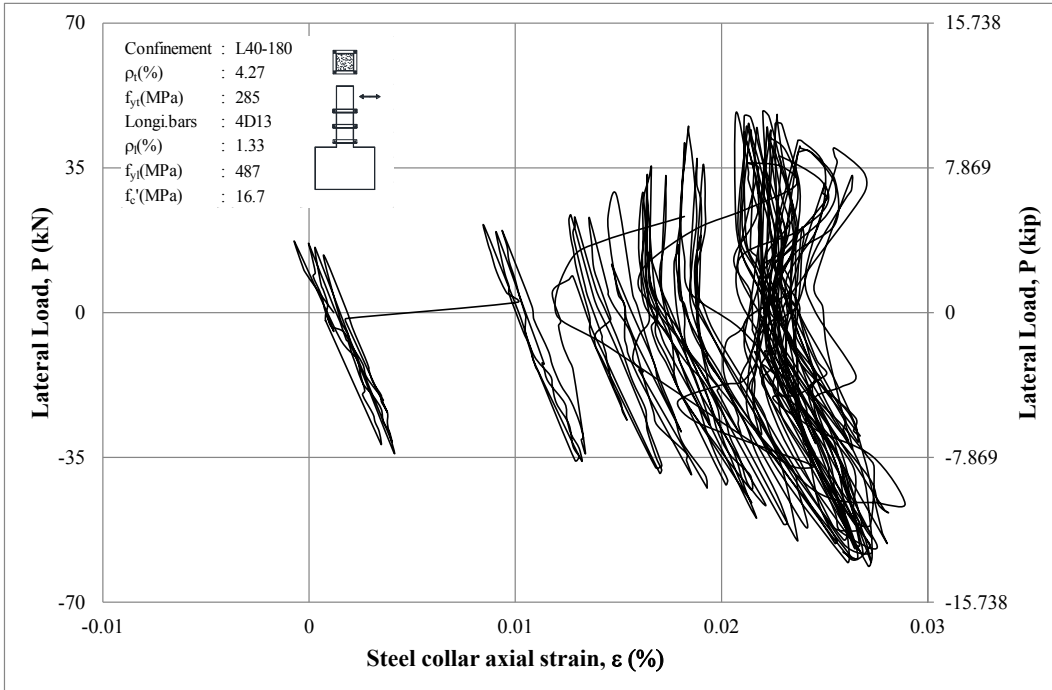
Figure D-42 Lateral load vs measurement of Channels 28 and 29 of S13
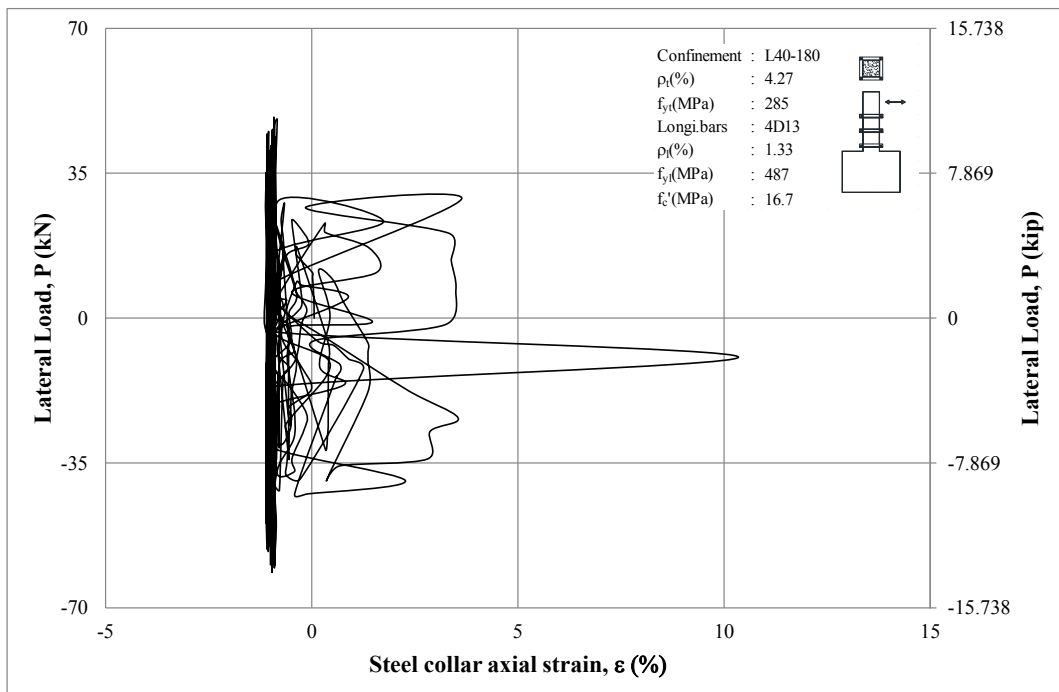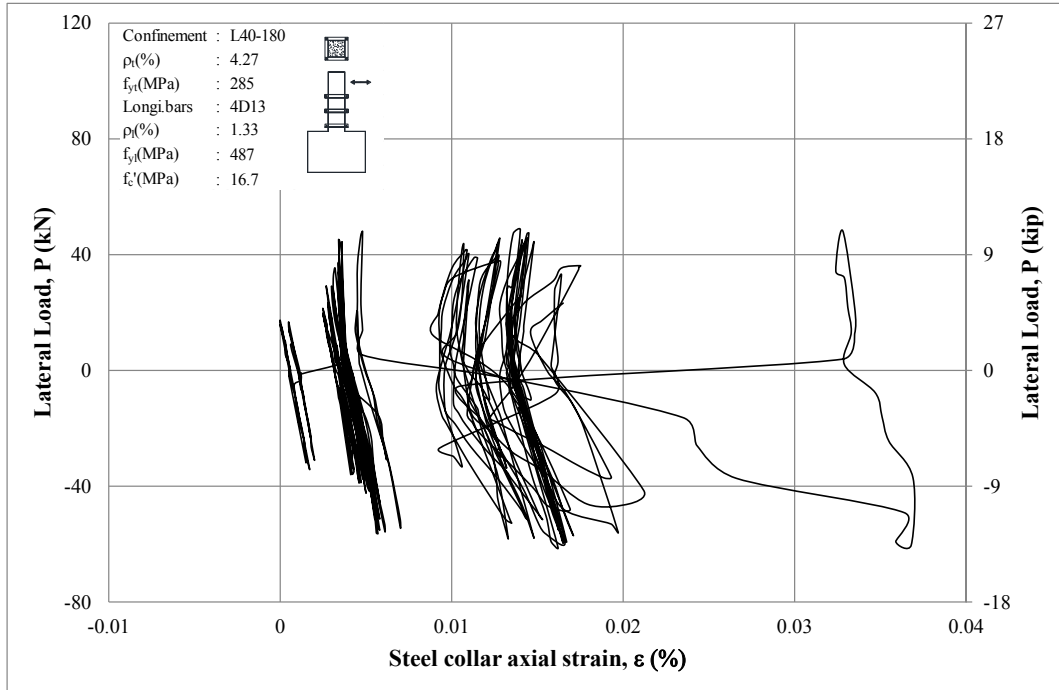
Figure D-43 Lateral load vs measurement of Channels 30 and 31 of S13
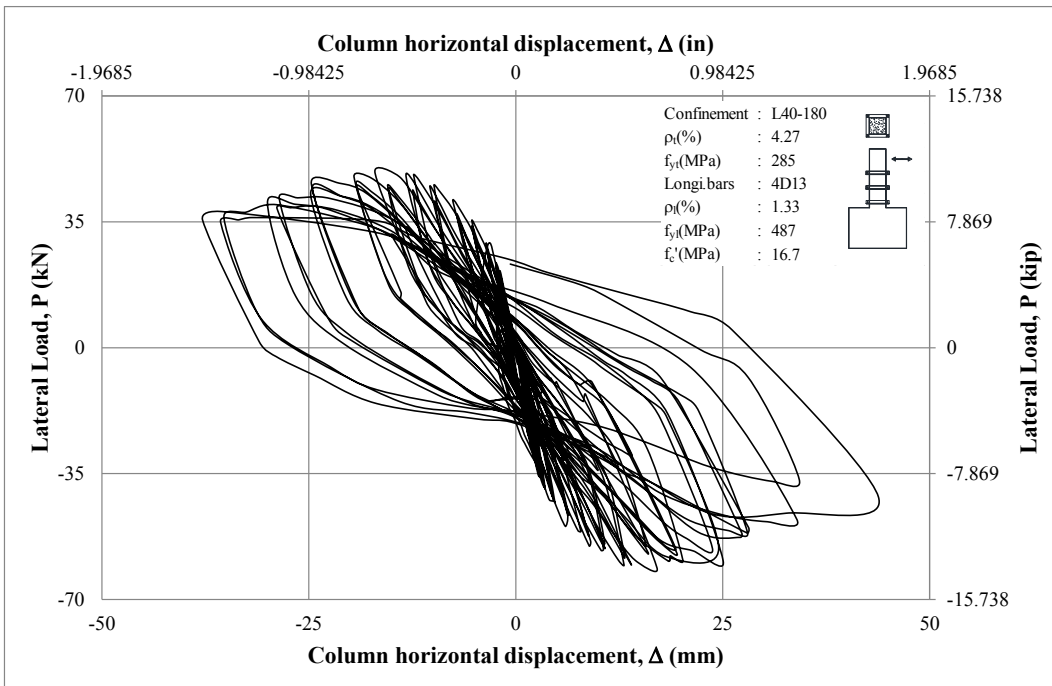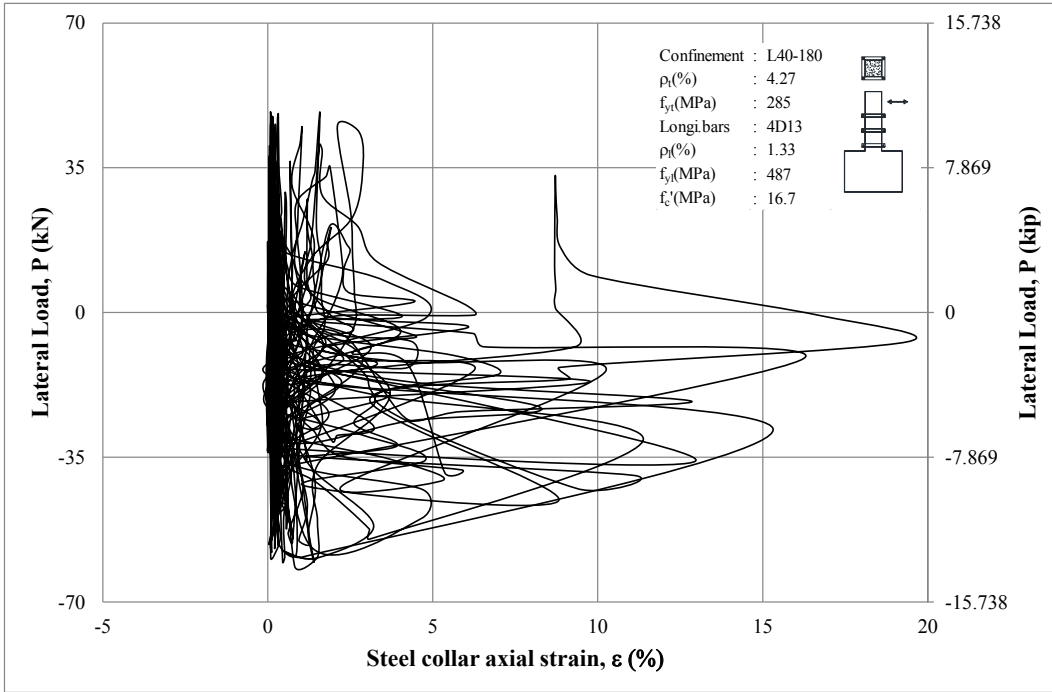
Figure D-44 Lateral load vs measurement of Channels 32 and 33 of S13

344
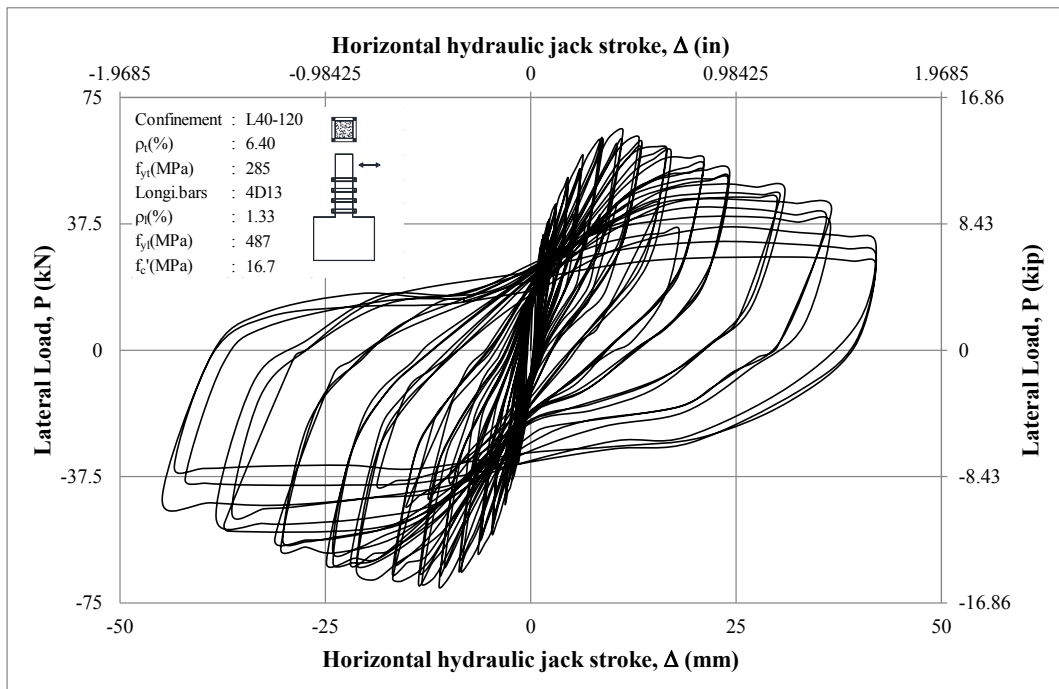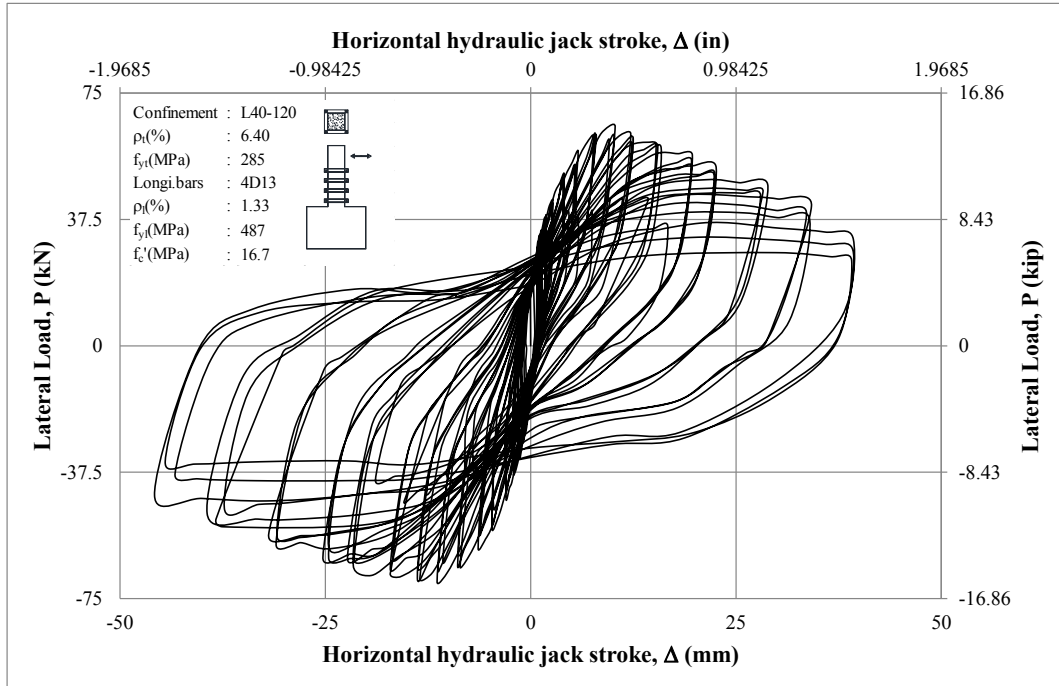
Figure D-45 Lateral load vs measurement of Channels 2 and 3 of S14

345
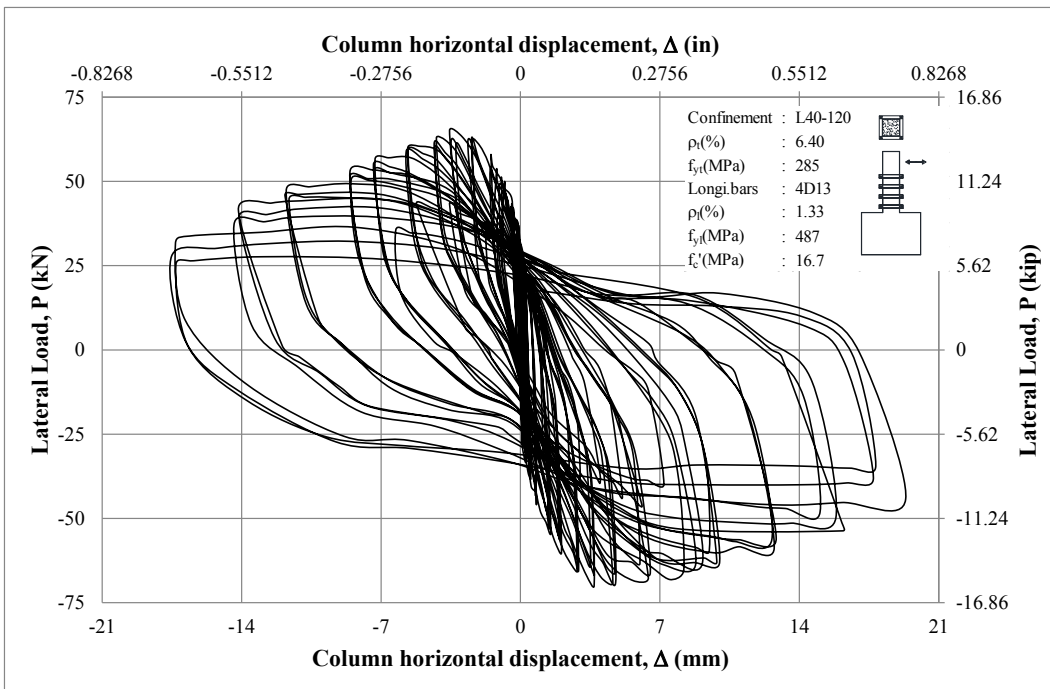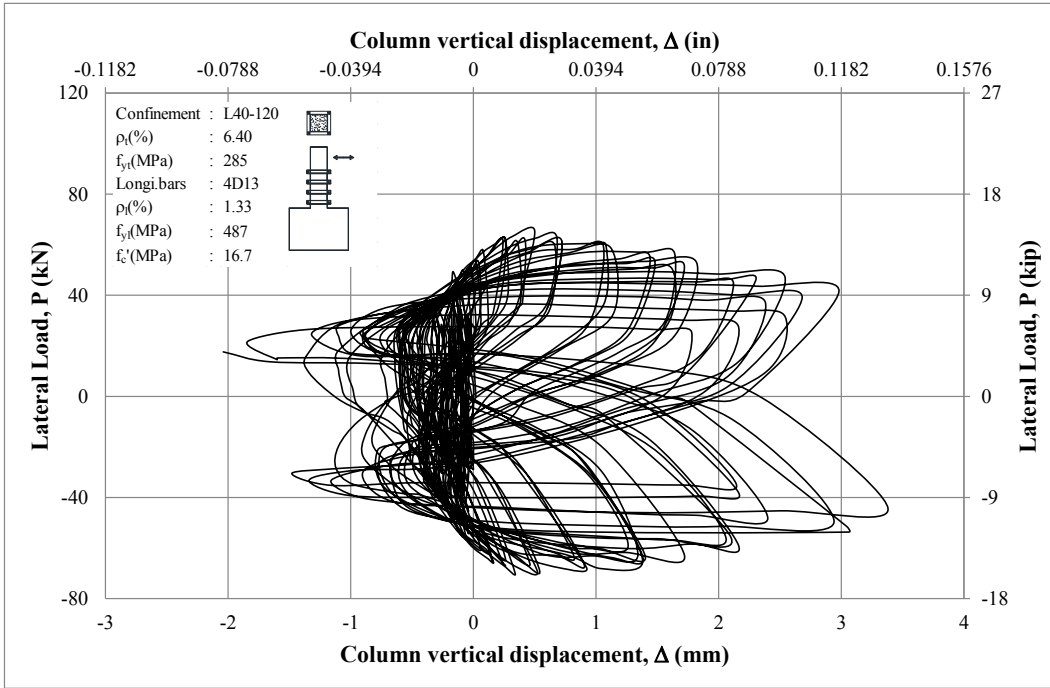
Figure D-46 Lateral load vs measurement of Channels 4 and 5 of S14

346
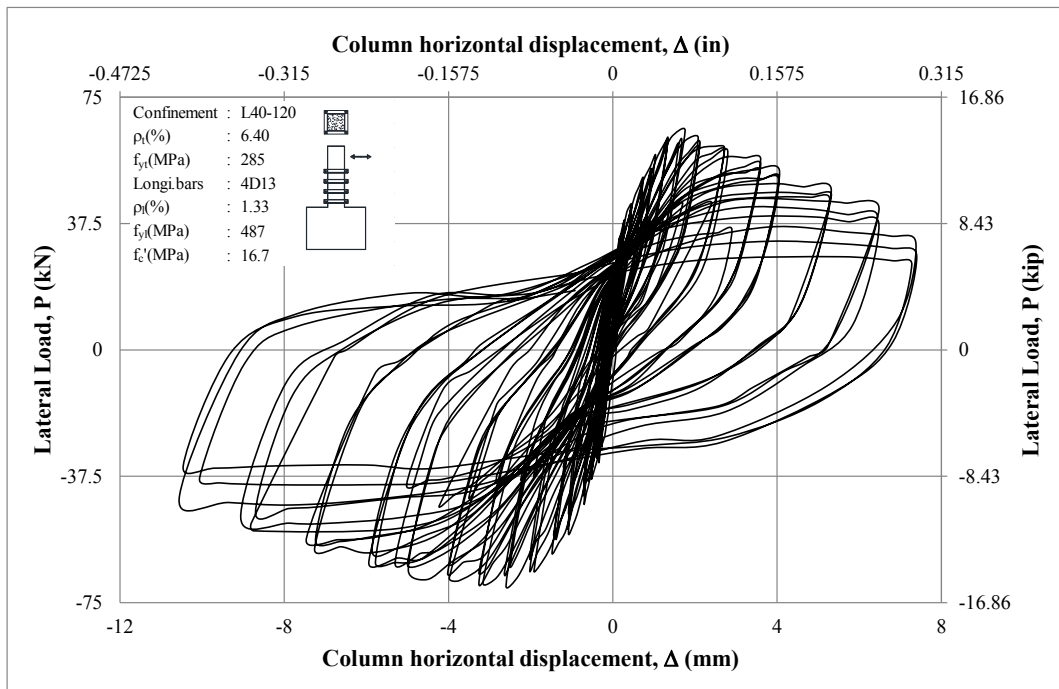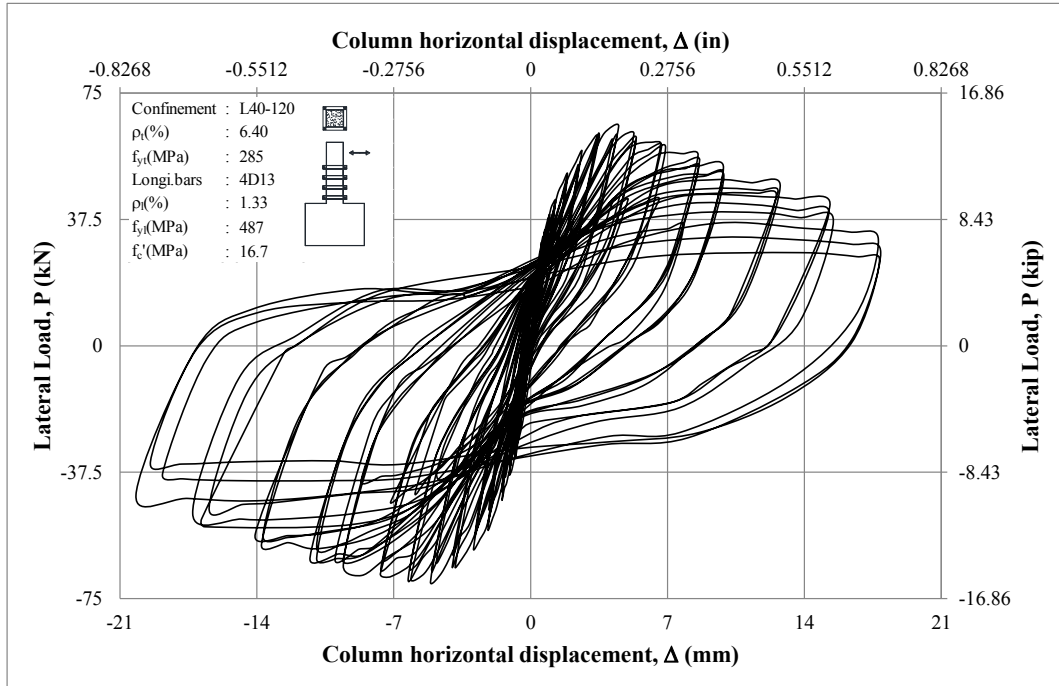
Figure D-47 Lateral load vs measurement of Channels 6 and 7 of S14

347
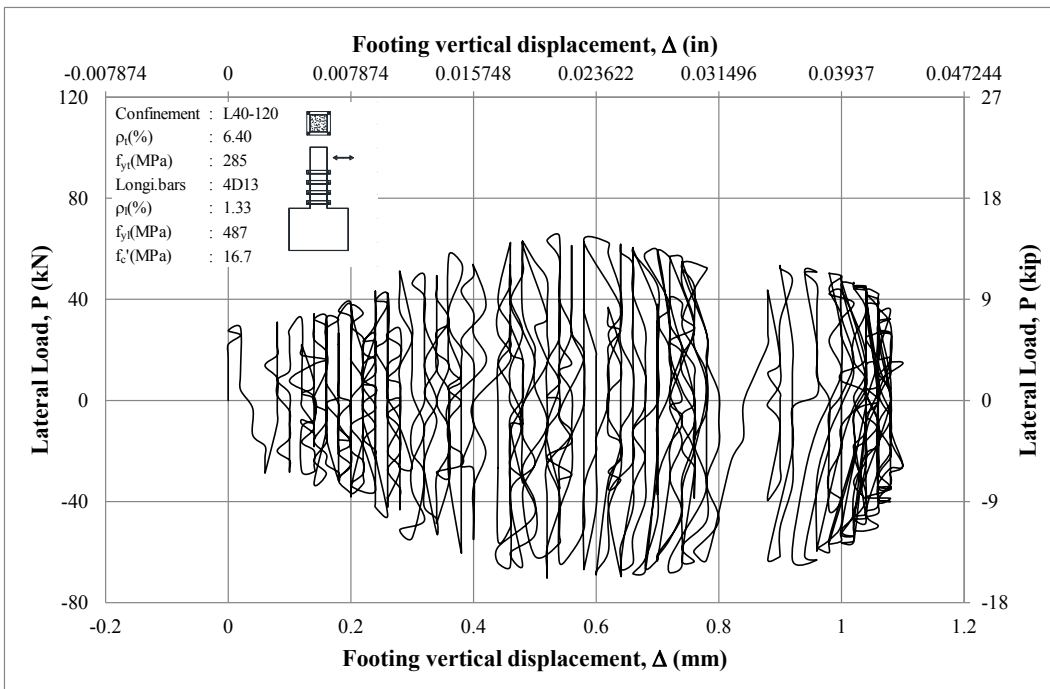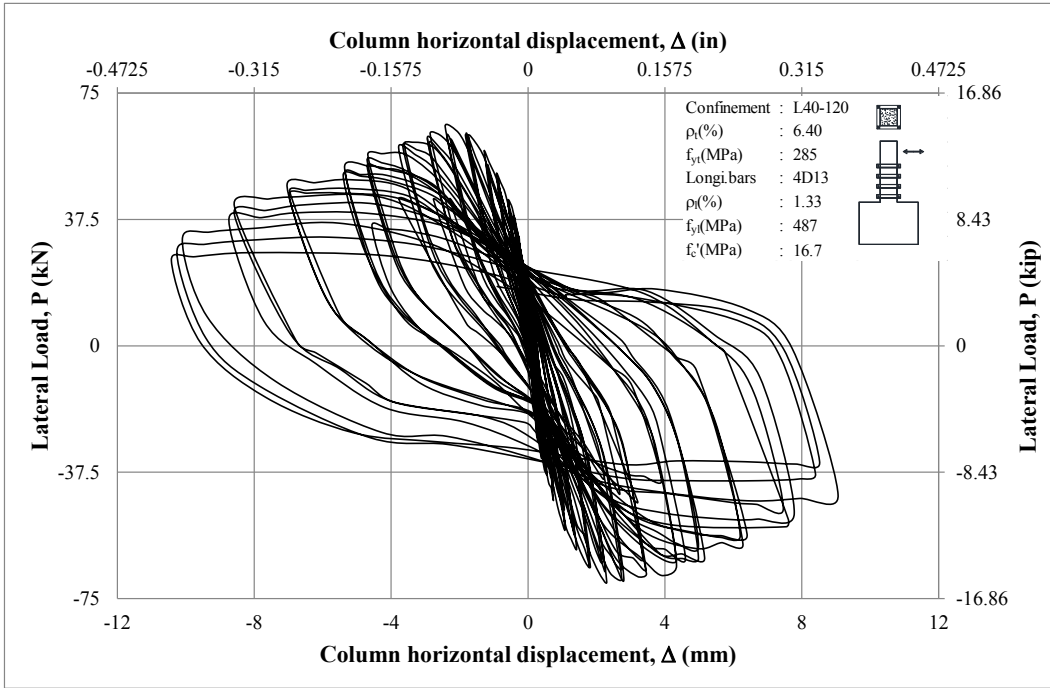
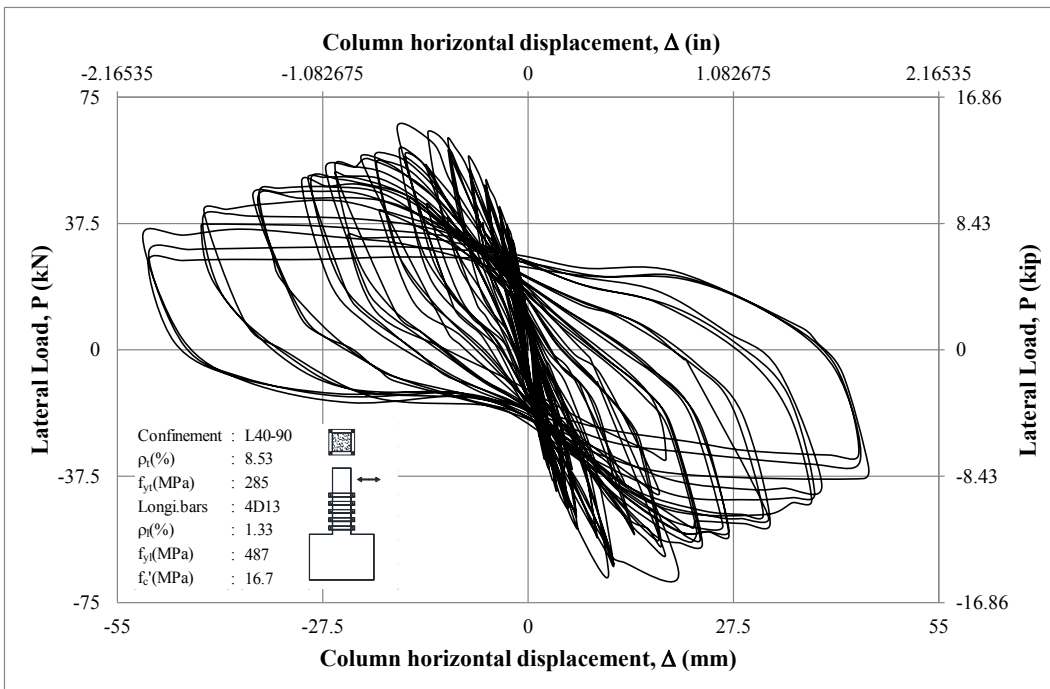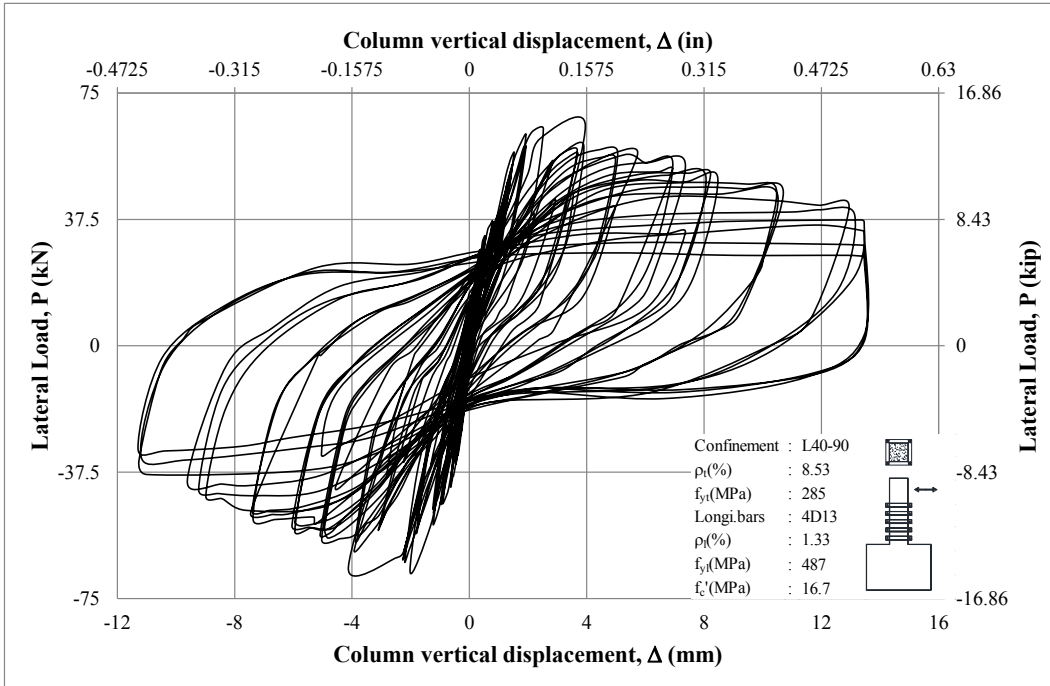**Figure D-48 Lateral load vs measurement of Channels 8 and 9 of S14**

348
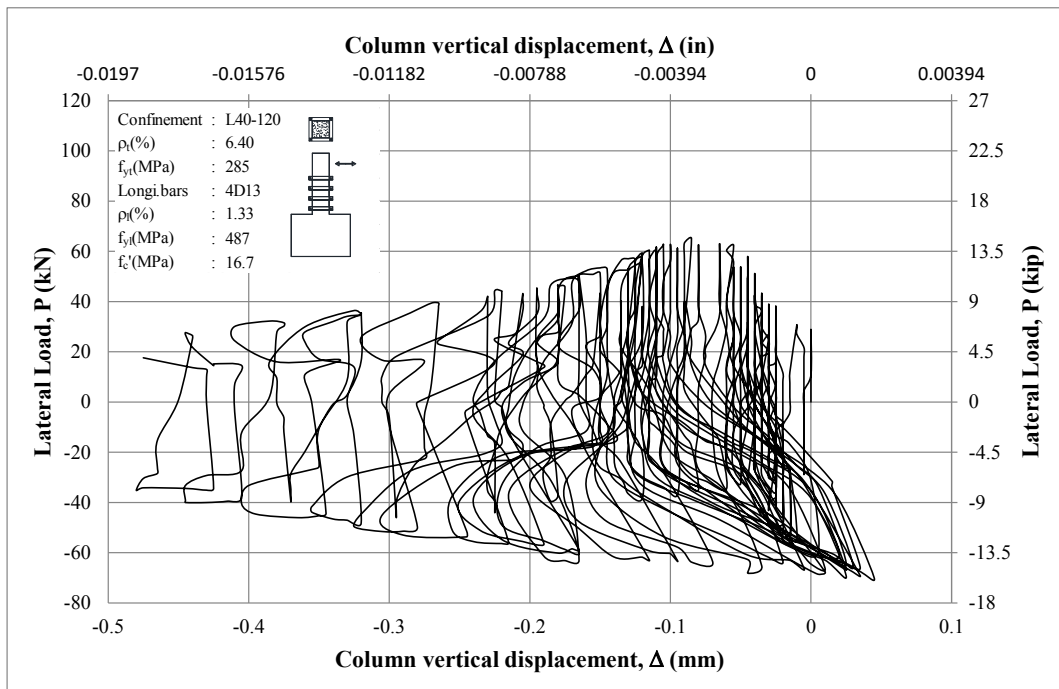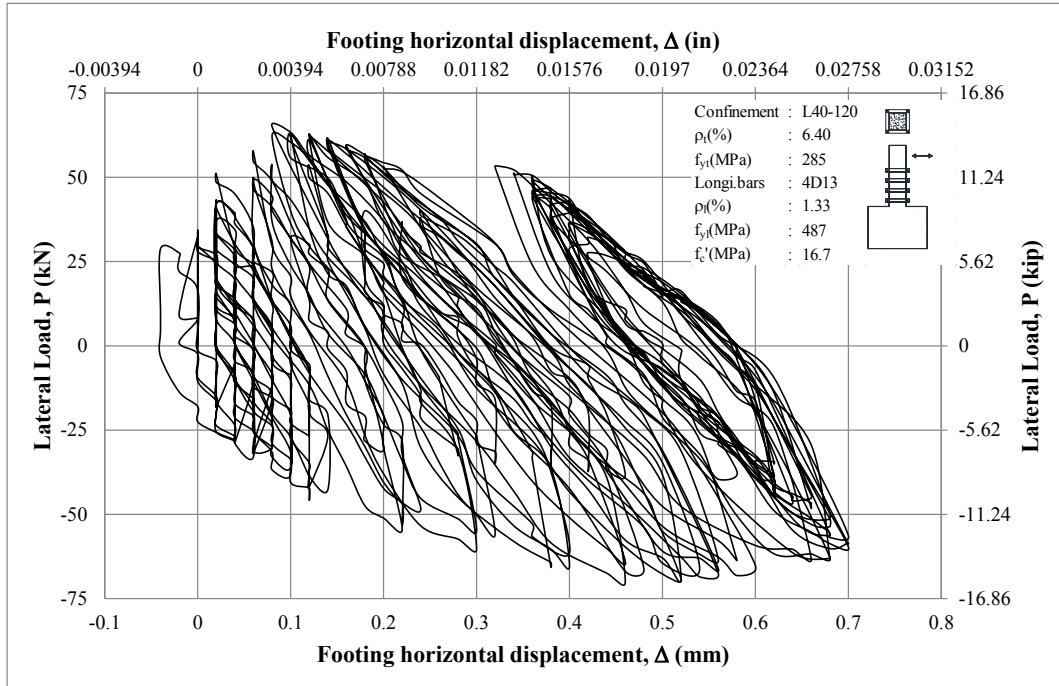
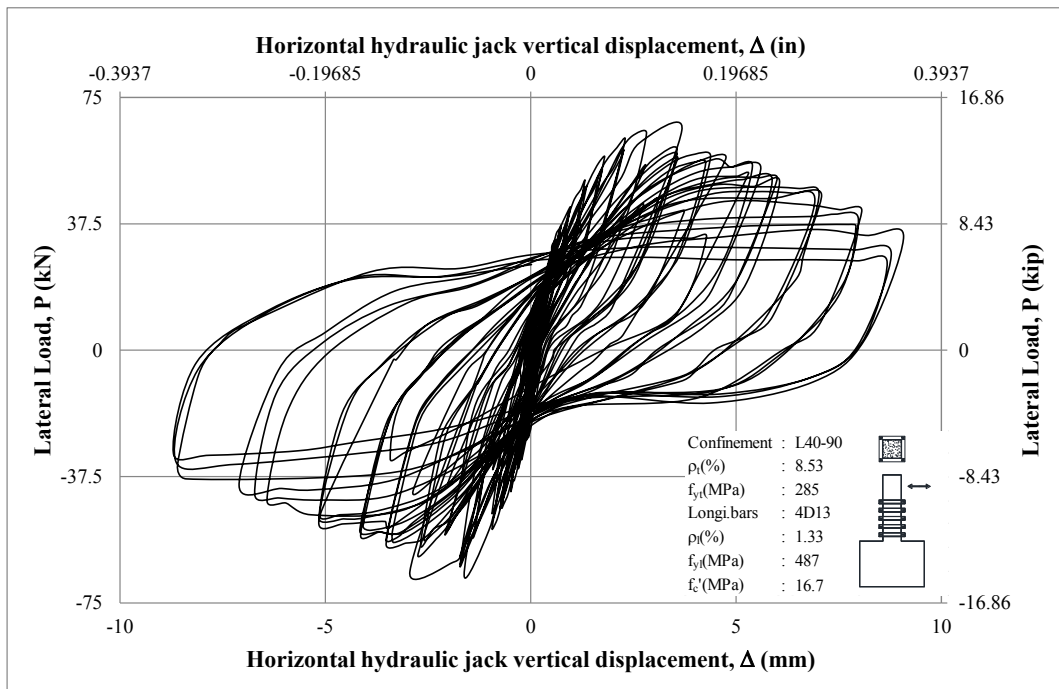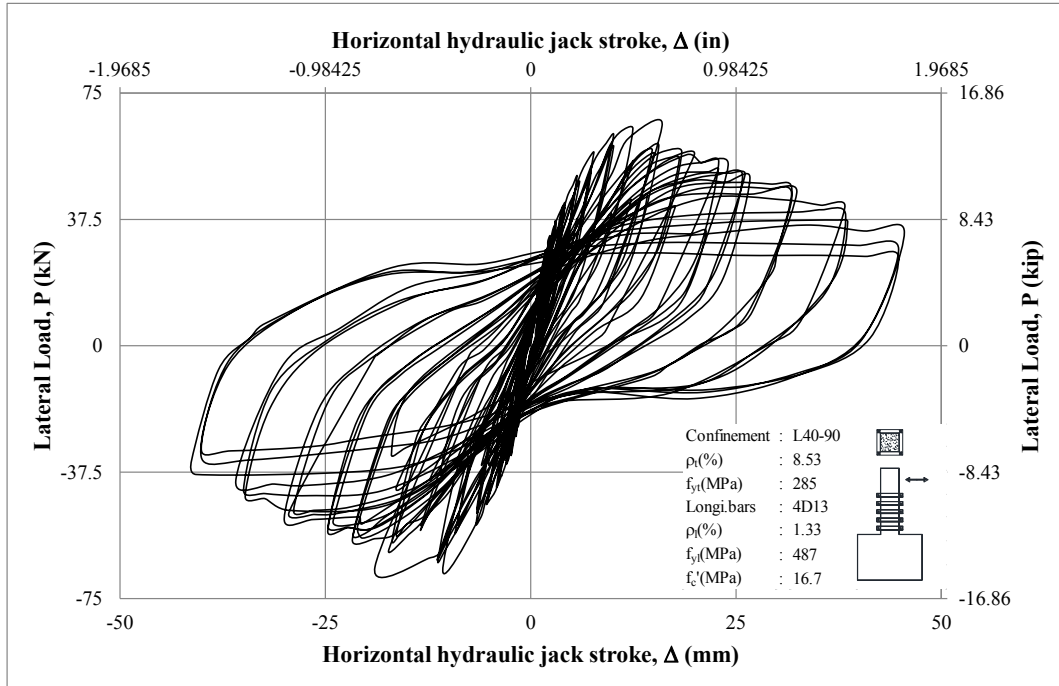**Figure D-49 Lateral load vs measurement of Channels 10 and 11 of S14**
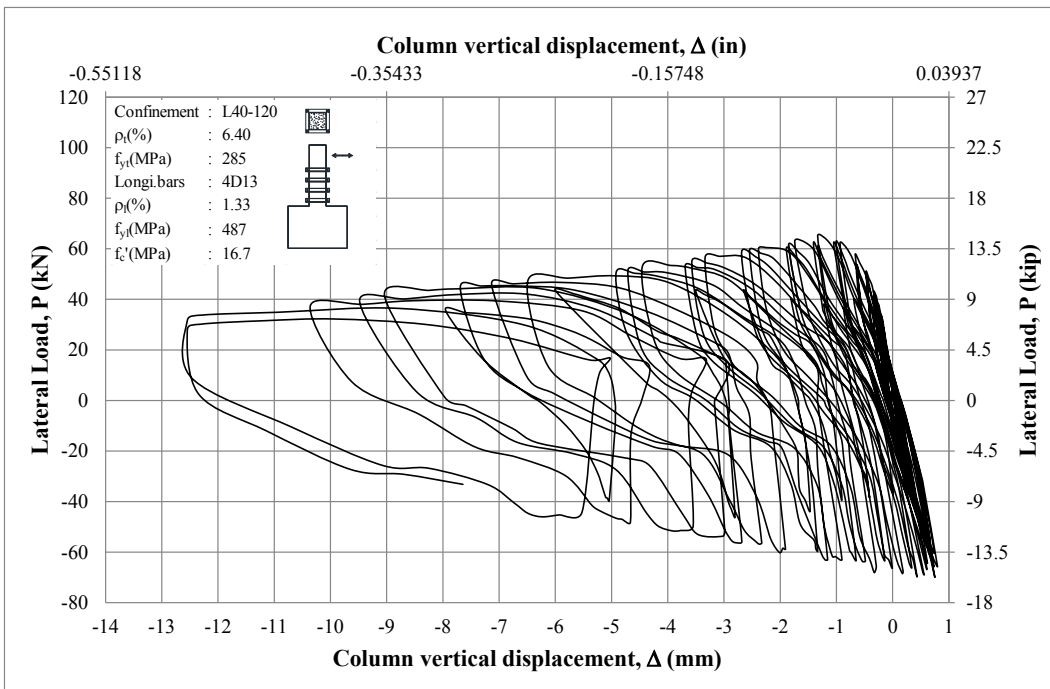
Figure D-50 Lateral load vs measurement of Channels 12 and 13 of S14

350

Figure D-51 Lateral load vs measurement of Channels 14 and 15 of S14

Figure D-52 Lateral load vs measurement of Channels 16 and 17 of S14

352

Figure D-53 Lateral load vs measurement of Channels 18 and 19 of S14

Figure D-54 Lateral load vs measurement of Channels 20 and 21 of S14

354

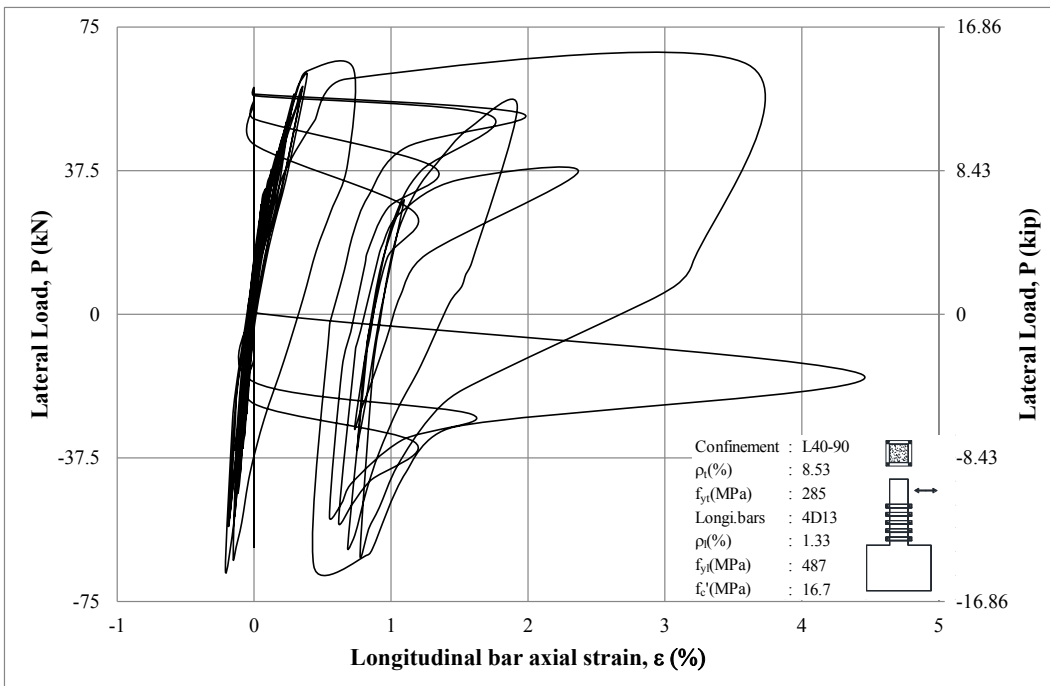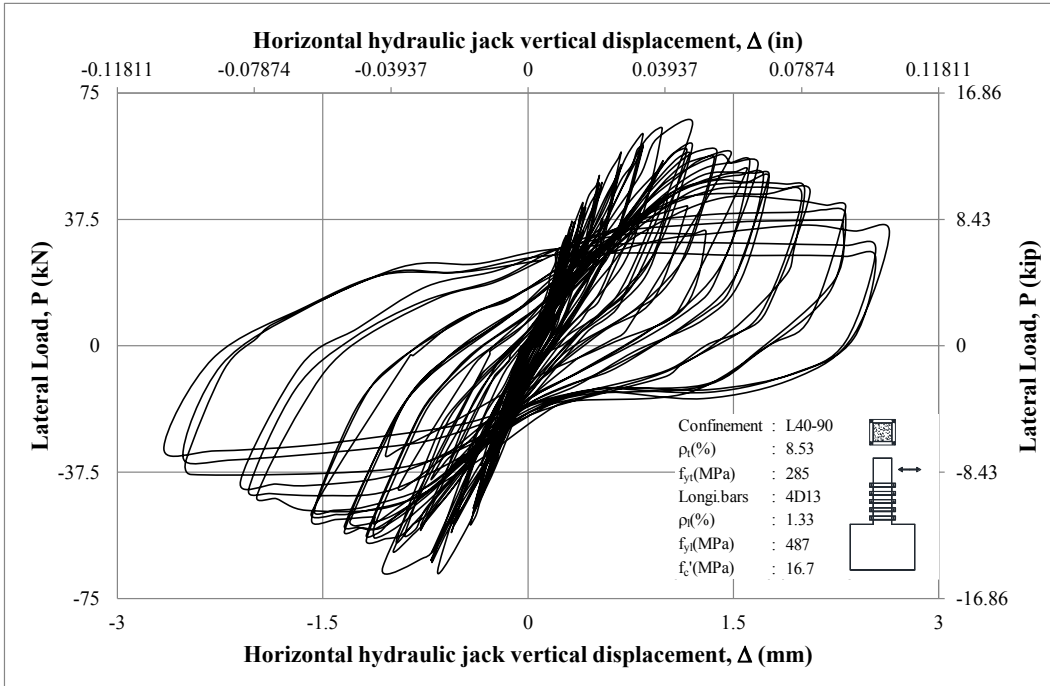**Figure D-55 Lateral load vs measurement of Channels 22 and 23 of S14**

Figure D-56 Lateral load vs measurement of Channels 24 and 25 of S14

Figure D-57 Lateral load vs measurement of Channels 26 and 27 of S14

357

Figure D-58 Lateral load vs measurement of Channels 28 and 29 of S14

358

Figure D-59 Lateral load vs measurement of Channels 30 and 31 of S14
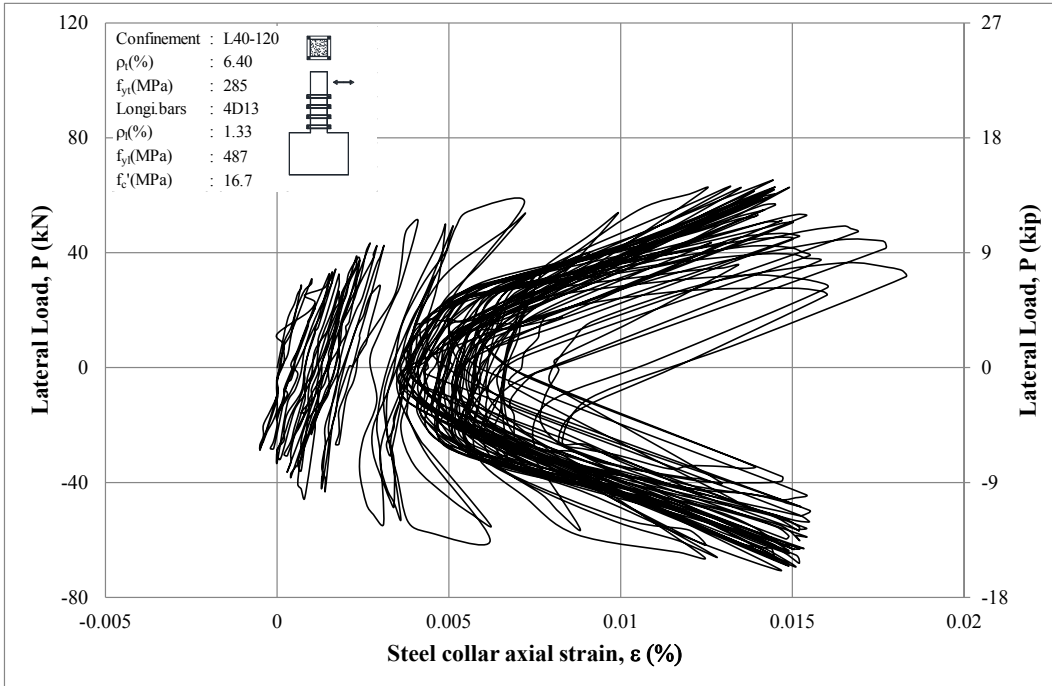
Figure D-60 Lateral load vs measurement of Channels 32 and 33 of S14

360

Figure D-61 Lateral load vs measurement of Channels 34 and 35 of S14

Figure D-62 Lateral load vs measurement of Channel 36 of S14

Figure D-63 Lateral load vs measurement of Channels 2 and 3 of S15
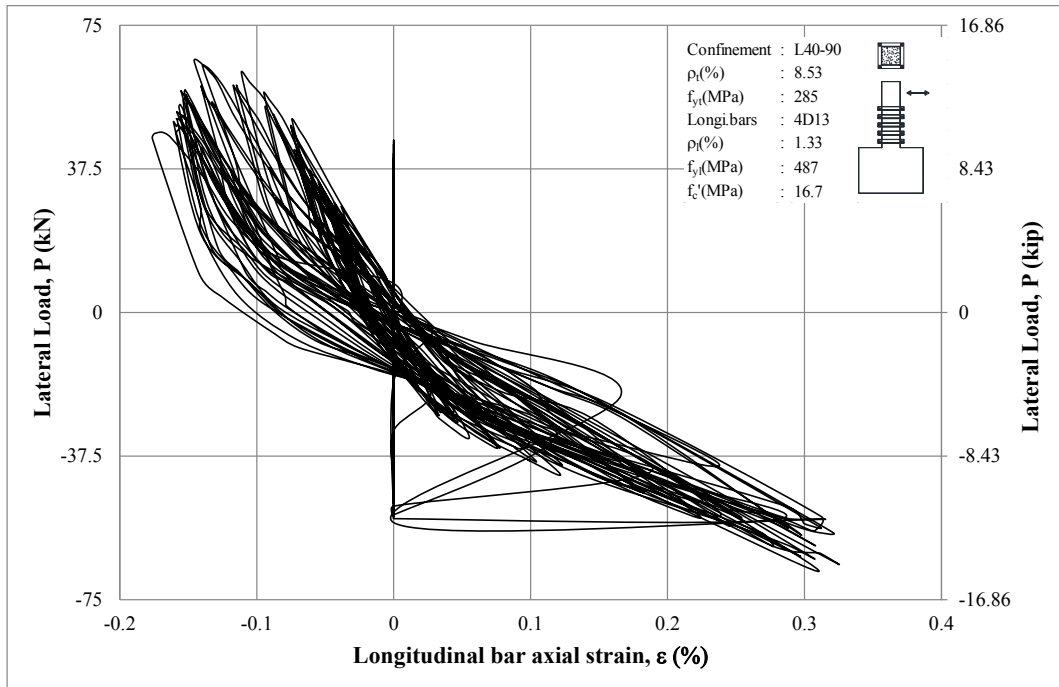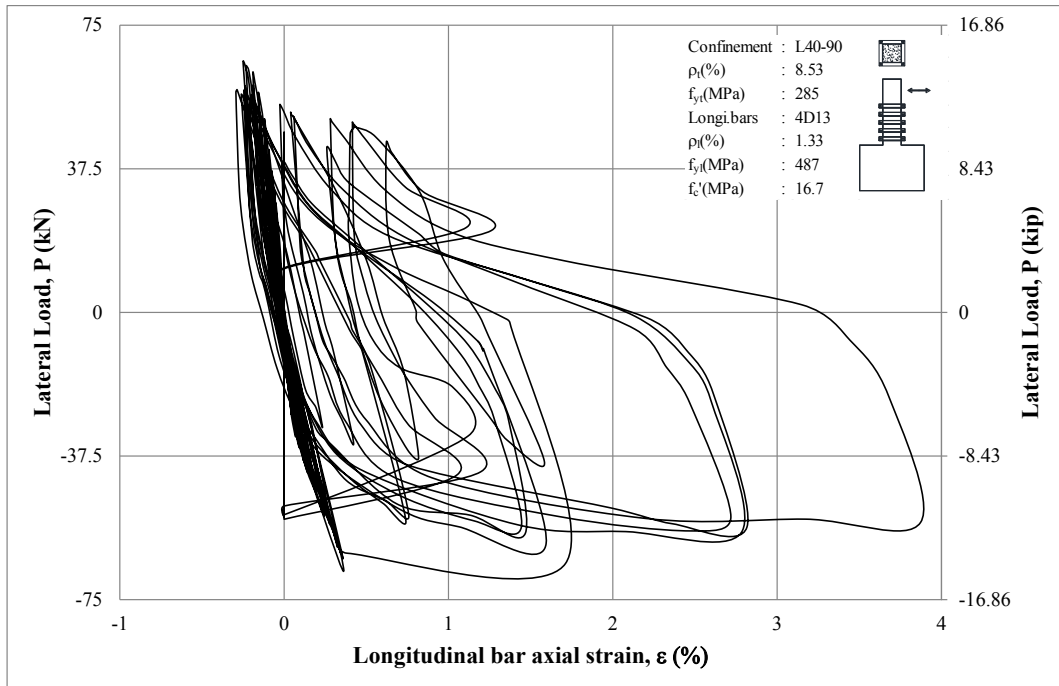
363
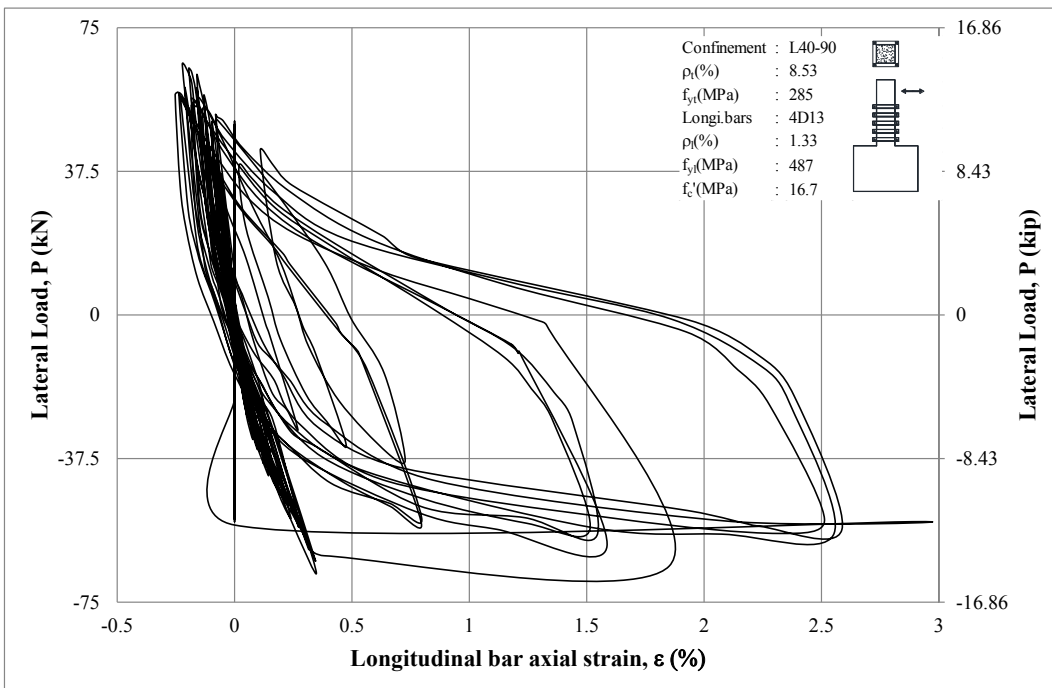
Figure D-64 Lateral load vs measurement of Channels 4 and 5 of S15

Figure D-65 Lateral load vs measurement of Channels 6 and 7 of S15

365

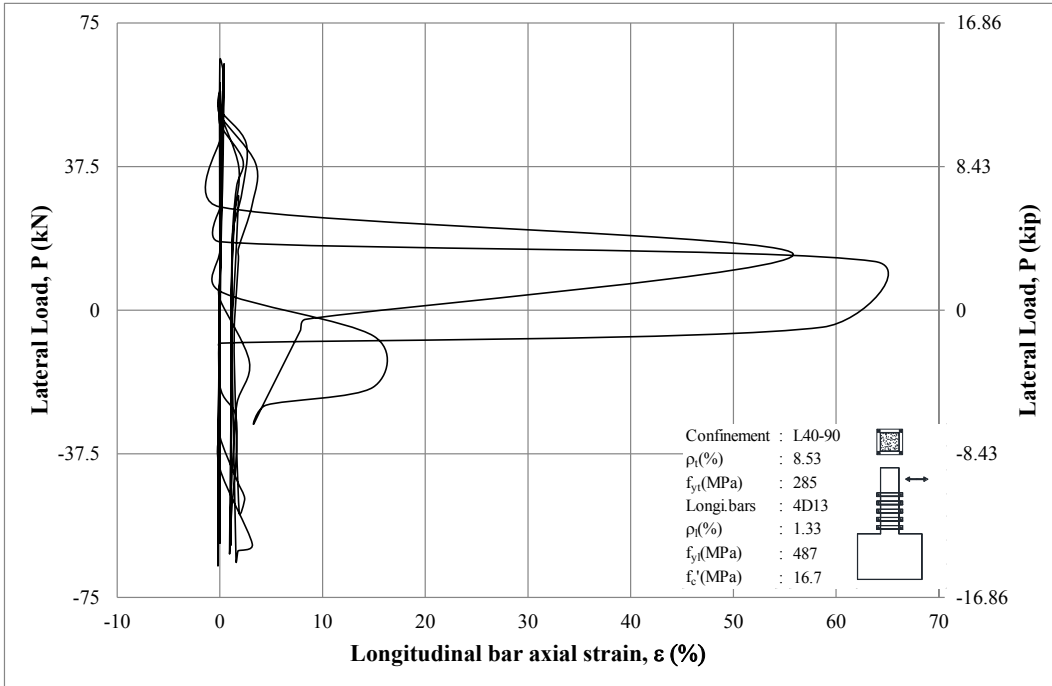Figure D-66 Lateral load vs measurement of Channels 8 and 9 of S15

Figure D-67 Lateral load vs measurement of Channels 10 and 11 of S15

Figure D-68 Lateral load vs measurement of Channels 12 and 13 of S15

368

Figure D-69 Lateral load vs measurement of Channels 14 and 15 of S15

Figure D-70 Lateral load vs measurement of Channels 16 and 17 of S15

Figure D-71 Lateral load vs measurement of Channels 18 and 19 of S15

371

Figure D-72 Lateral load vs measurement of Channels 20 and 21 of S15

Figure D-73 Lateral load vs measurement of Channels 22 and 24 of S15

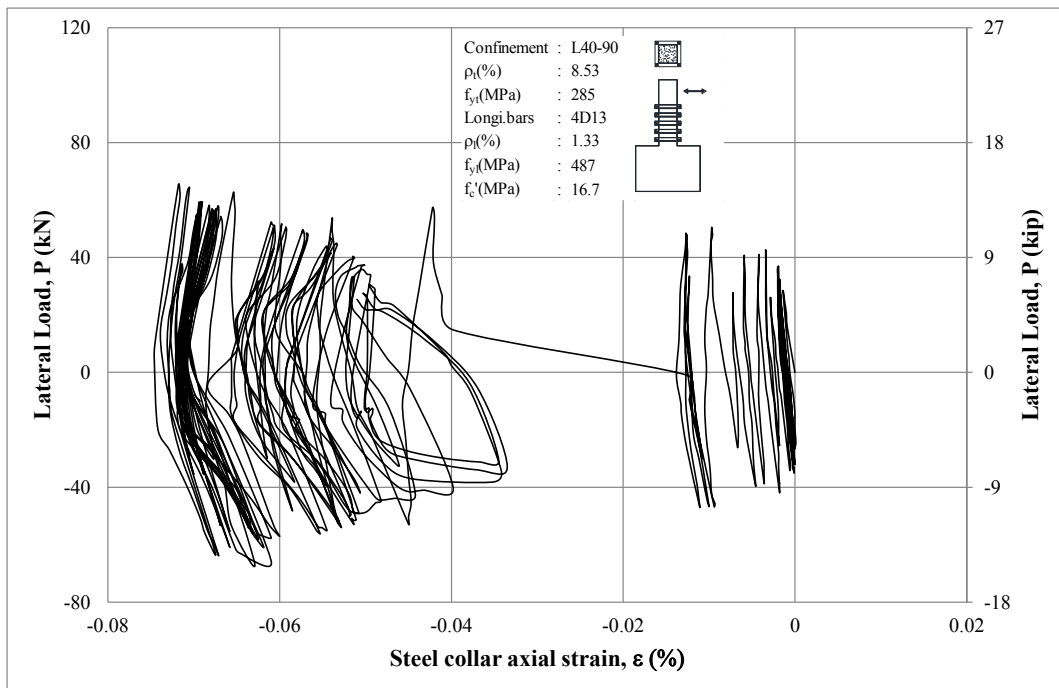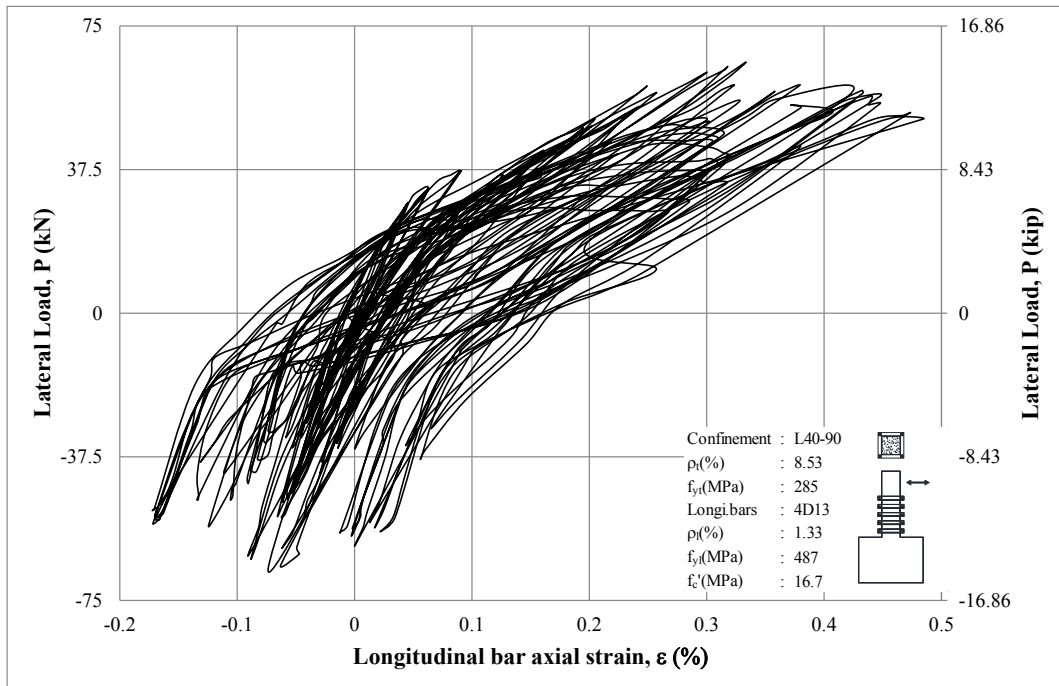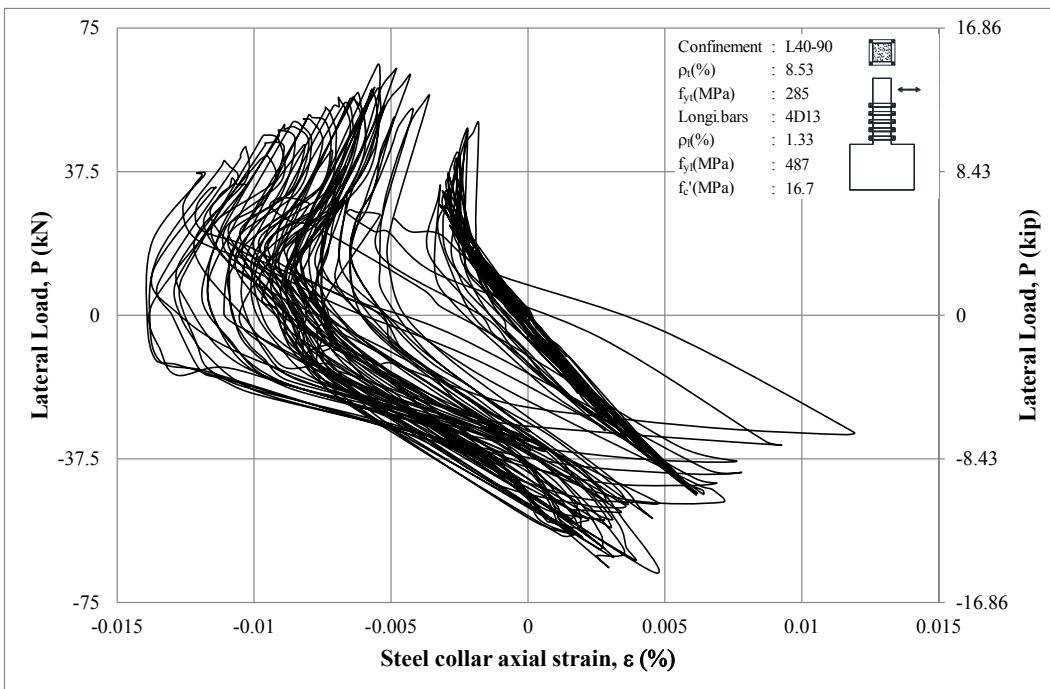**Figure D-74 Lateral load vs measurement of Channels 25 and 26 of S15**
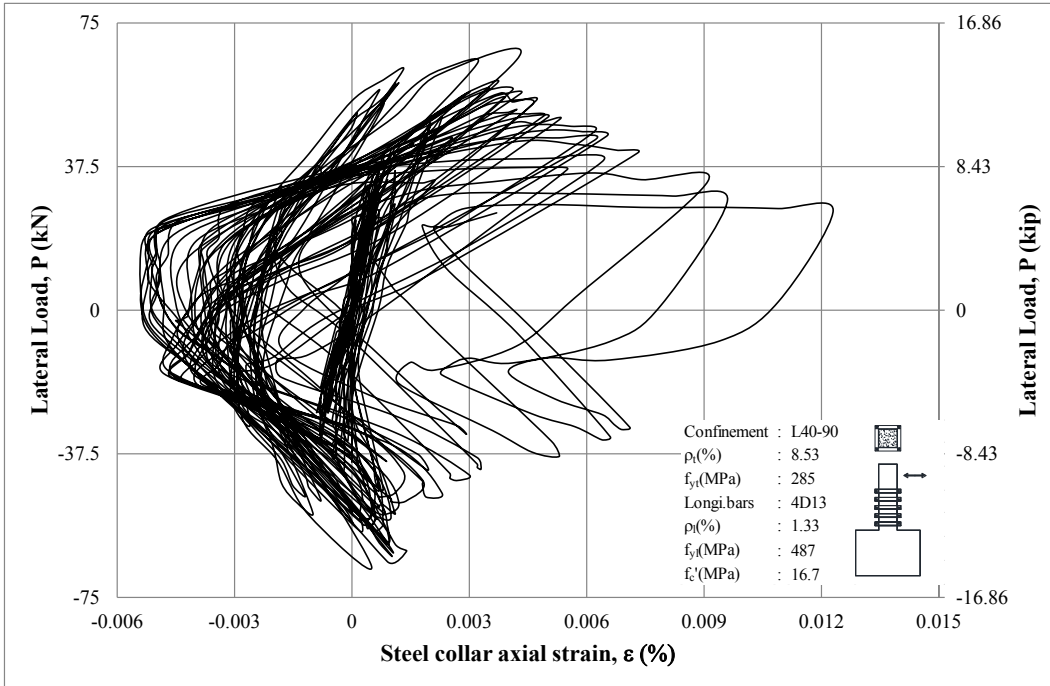
374

Figure D-75 Lateral load vs measurement of Channels 27 and 29 of S15

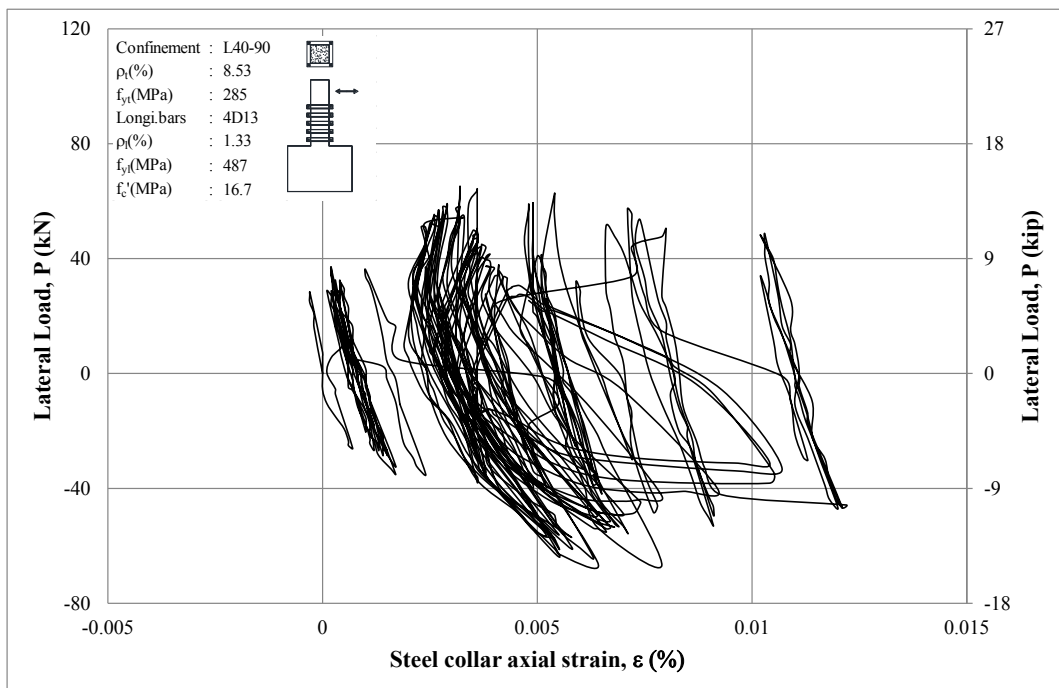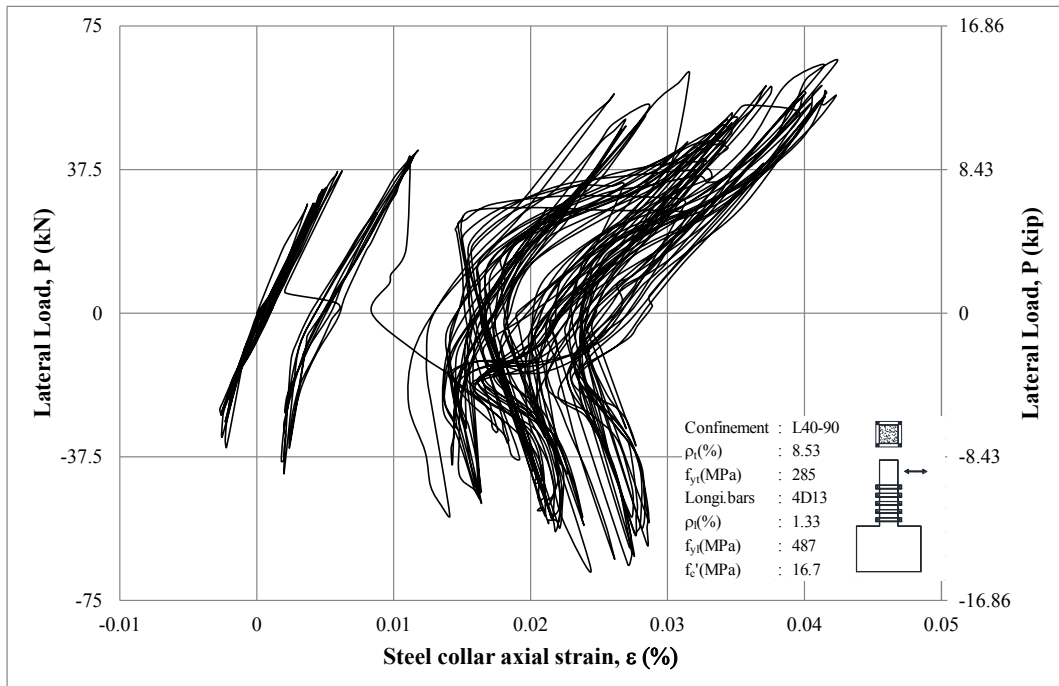**Figure D-76 Lateral load vs measurement of Channels 30 and 31 of S15**

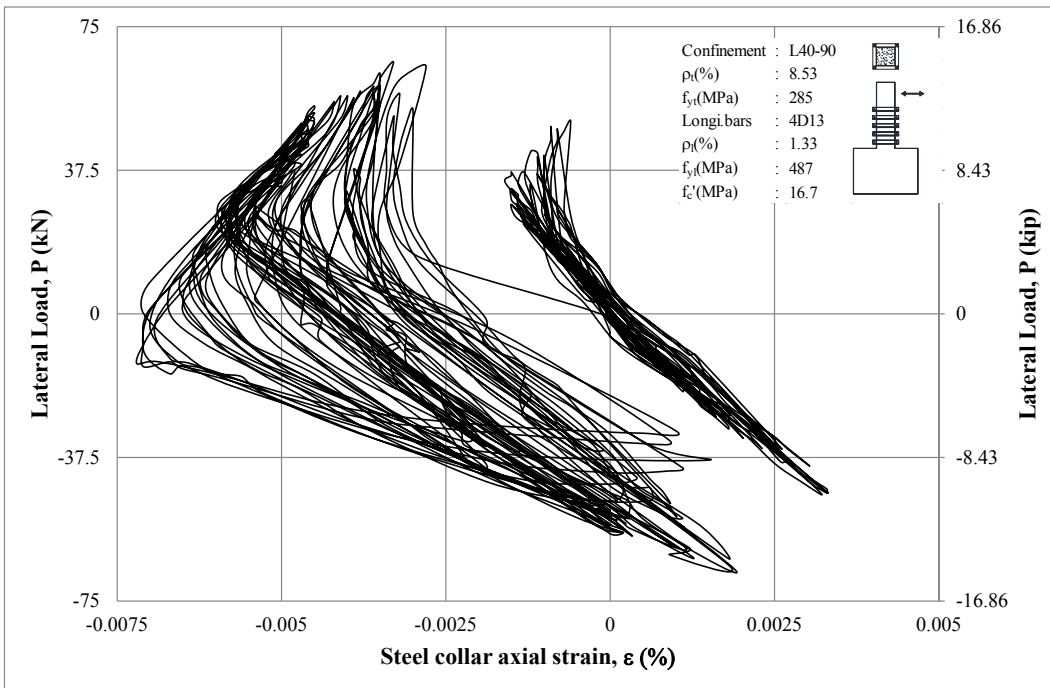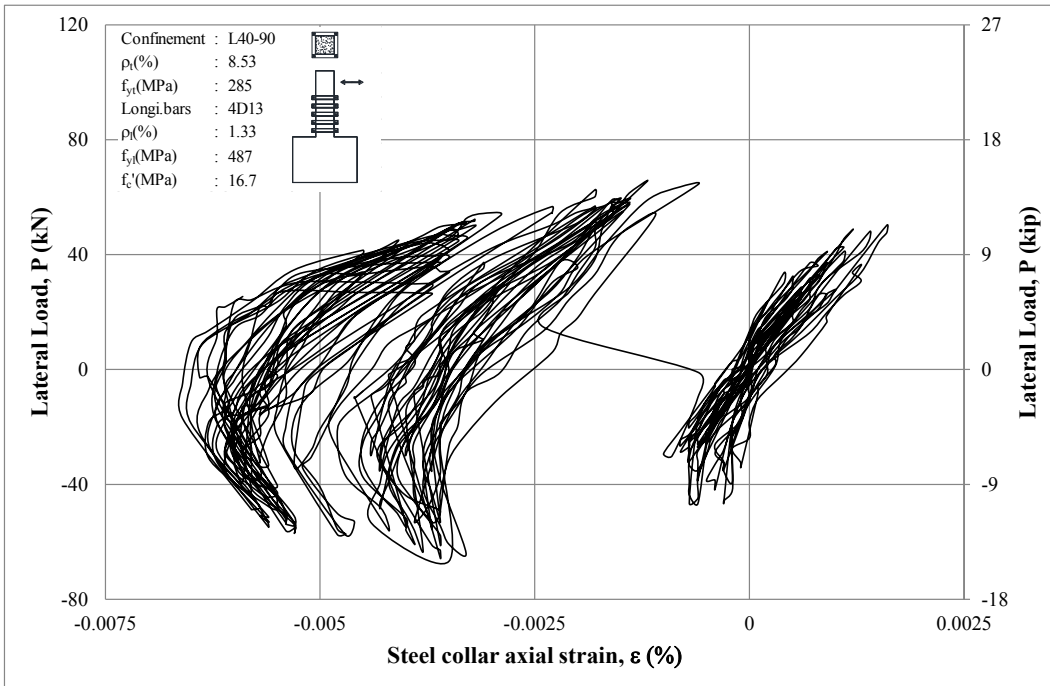**Figure D-77 Lateral load vs measurement of Channels 32 and 33 of S15**
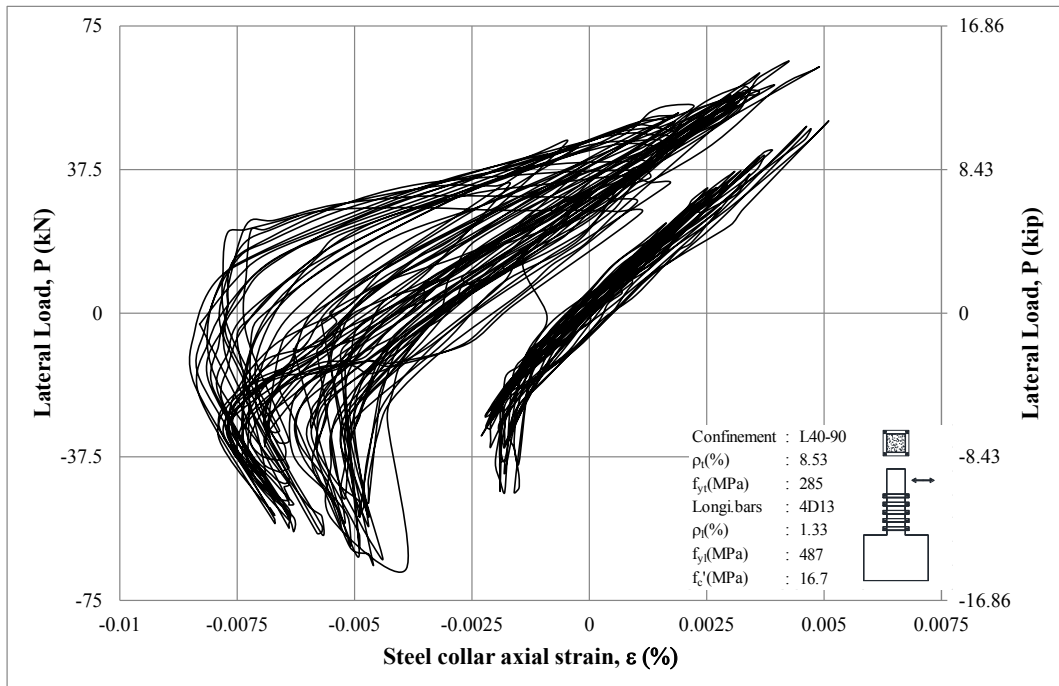
Figure D-78 Lateral load vs measurement of Channels 34 and 35 of S15

378

Figure D-79 Lateral load vs measurement of Channel 36 of S15

= This Page is Intentionally Left Blank =

BIOGRAPHY

Name   : Pamuda Pudjisuryadi

Place / Date of birth   : Surabaya / October 28th 1975

Occupation   : Lecturer

Rank / Level   : IV / A

Academic Rank   : Associate Professor

Office Address   : Siwalankerto 121-131, Petra Christian University
                            Surabaya

Home Address   : Graha Indah H/20-B, Gayung Kebonsari
                            Surabaya

A. Formal Education

    1. Elementary School   : SDK St. Yosef, Surabaya (1982-1988)

    2. Junior High School   : SMPK St. Yosef, Surabaya (1988-1991)

    3. Senior High School   : SMAK St. Louis I, Surabaya (1991-1994)

    4. Bachelor Degree   : Petra Christian Univerisy, Surabaya (1994-1999)

    5. Master Degree   : Asian Institute of Technology, Bangkok (1999-2001)

    6. Doctoral Degree   : Sepuluh Nopember Institue of Technology, Surabaya (2010-2017)

B. Working Histories

    1. Petra Christian University (1999-on going)

C. Research Activities

1. Rehabilitasi Kolom Beton Bertulang Persegi yang tidak Memenuhi Syarat Gempa dengan Besi Siku, Program Desentralisasi Pengelolaan Penelitian Ditlitabnas Tahun Anggaran 2012, ITS (Member of Research Team).

2. Kinerja Baja Siku Sebagai Elemen Pengekang Eksternal Kolom Beton Bertulang Persegi, Program Penelitian Hibah Bersaing 2012-2013, Universitas Kristen Petra (Head of Research Team).

D. Publications during Doctoral Program

1. International Journal

- Pudjisuryadi, P.; Tavio; and Suprobo, P., (2014), "Analytical Confining Model of Square Reinforced Concrete Columns using External Steel Collars", International Journal of ICT-aided Architectural and Civil Engineering, vol.1. no.1, Australia, ISSN:2383-4773, pp. 1-18.

- Pudjisuryadi, P.; Tavio; and Suprobo, P., (2016), "Axial Compressive Behavior of Square Concrete Columns Externally Collared by Light Structural Steel Angle Sections", International Journal of Applied Engineering Research, vol.11. no.7, India, ISSN:0973-4562, pp. 4655-4666.

- Tavio; Pudjisuryadi, P.; and Suprobo, P. (2015), "Strength and Ductility of External Steel Collared Concrete Columns under Compressive Loading," *Journal of Asian Concrete Federation*, Vol. 1, No. 1, pp. 47-56.

2. Accredited National Journal

- Pudjisuryadi, P.; and Tavio, (2013), "Compressive Strength Prediction of Square Concrete Columns Retrofitted with External Steel Collars", Civil Engineering Dimension, vol.15. no.1, March 2013, Surabaya, ISSN:1410-9530, pp. 18-24.